US Army Corps of Engineers

AD-A198 760



GEOTECHNICAL LABORATORY

TECHNICAL REPORT GL-88-9

(4)

RETROGRESSIVE FAILURES IN SAND DEPOSITS OF THE MISSISSIPPI RIVER

Report 1

FIELD INVESTIGATIONS, LABORATORY STUDIES AND ANALYSIS OF THE HYPOTHESIZED FAILURE MECHANISM

by

Victor H. Torrey III, Joseph B. Dunbar, Richard W. Peterson

Geotechnical Laboratory

DEPARTMENT OF THE ARMY
Waterways Experiment Station, Corps of Engineers
PO Box 631, Vicksburg, Mississippi 39180-0631

U.S. ARMY ENGINEER WATERWAYS EXPERIMENT STATION

DTIC
AUG 15 1988
S
H

June 1988
Report 1 of a Series

Approved for Public Release; Distribution Unlimited

Prepared for US Army Engineer Division, Lower Mississippi Valley
PO Box 80, Vicksburg, Mississippi 39180-0080

88 8 15 026

Destroy this report when no longer needed. Do not return
it to the originator.

The findings in this report are not to be construed as an official Department of the Army position unless so designated by other authorized documents.

The use of trade names or manufacturers' names in this report does not constitute an official endorsement or approval of the use of such commercial products.

Unclassified

SECURITY CLASSIFICATION OF THIS PAGE

REPORT DOCUMENTATION PAGE

Form Approved
OMB No. 0704-0188

1a REPORT SECURITY CLASSIFICATION Unclassified	1b RESTRICTIVE MARKINGS
2a SECURITY CLASSIFICATION AUTHORITY	3 DISTRIBUTION/AVAILABILITY OF REPORT Approved for public release; distribution unlimited.
2b DECLASSIFICATION/DOWNGRADING SCHEDULE	
4 PERFORMING ORGANIZATION REPORT NUMBER(S) Technical Report GL-88-9	5 MONITORING ORGANIZATION REPORT NUMBER(S)
6a NAME OF PERFORMING ORGANIZATION USAEWES Geotechnical Laboratory 6b OFFICE SYMBOL (If applicable) CEWES-GA	7a NAME OF MONITORING ORGANIZATION
6c ADDRESS (City, State, and ZIP Code) PO Box 631 Vicksburg, MS [illegible]	7b ADDRESS (City, State, and ZIP Code)
8a NAME OF FUNDING/SPONSORING ORGANIZATION [illegible] Mississippi Valley 8b OFFICE SYMBOL (If applicable)	9 PROCUREMENT INSTRUMENT IDENTIFICATION NUMBER
8c ADDRESS (City, State, and ZIP Code) PO Box [illegible] Vicksburg, MS [illegible]	10 SOURCE OF FUNDING NUMBERS PROGRAM ELEMENT NO PROJECT NO TASK NO WORK UNIT ACCESSION NO

11 TITLE (Include Security Classification)
Retrogressive Failures in Sand Deposits of the Mississippi River, Report 1: Field Investigations, Laboratory Studies, and Analysis of the Hypothesized Failure Mechanism

12 PERSONAL AUTHOR(S)
Torrey, Victor H. III; Dunbar, Joseph B; Peterson, Richard W.

13a TYPE OF REPORT	13b TIME COVERED	14 DATE OF REPORT (Year Month Day)	15 PAGE COUNT
Final report	FROM _____ TO _____	June 1988	493

16 SUPPLEMENTARY NOTATION
Available from National Technical Information Service, 5285 Port Royal Road, Springfield, VA 22161.

17 COSATI CODES		
FIELD	GROUP	SUB-GROUP

18 SUBJECT TERMS (Continue on reverse if necessary and identify by block number)
In situ tests; Riverbank stability
Retrogressive failure; Sand flow mechanism

19 ABSTRACT (Continue on reverse if necessary and identify by block number)

This report is the first of a series documenting recent studies directed at determining the causes of, understanding the mechanism of, and developing defenses against retrogressive failures (flow slides) in sand deposits of the Mississippi River which threaten the safety of mainline flood protection levees below Baton Rouge, LA. A review of the literature tracing the progress of associated antecedent studies since their inception in the late 1930's is presented. Recent field and laboratory investigations relative to the Montz and Bonnet Carre Point, LA failure sites are described and analyzed to infer the in situ character of the sand deposits. Results obtained form several in situ investigation techniques including fixed-piston undisturbed sampling, standard penetration testing, cone penetration testing, piezocone penetration testing, and Delft resistivity cone penetration testing are presented and compared. Geologic and historic hydrographic studies of the two sites are also included. A special series of hydrographic surveys to study river

(Continued)

20 DISTRIBUTION/AVAILABILITY OF ABSTRACT	21 ABSTRACT SECURITY CLASSIFICATION
☐ UNCLASSIFIED/UNLIMITED ☐ SAME AS RPT ☐ DTIC USERS	Unclassified
22a NAME OF RESPONSIBLE INDIVIDUAL	22b TELEPHONE (Include Area Code) / 22c OFFICE SYMBOL

DD Form 1473, JUN 86 Previous editions are obsolete

19. ABSTRACT (Continued).

attack on the bank and performed along the Eighty-One Mile Point, Forty-Eight Mile Point, Bonnet Carre Point, and Montz bank reaches during each of the four periods in 1979 is presented. The weight of information gained is used to hypothesize a failure mechanism of retrogression in dilatant sand. The hypothetical mechanism is numerically analyzed and presented to fit reasonably a failure case history.

Accession For
NTIS GRA&I
DTIC TAB
Unannounced
Justification
By
Distribution/
Availability Codes
Dist Special
A-1

QUALITY INSPECTED 2

PREFACE

This report provides the results of field and laboratory investigations pertaining to two Mississippi River point bar sites conducted by the US Army Engineer Waterways Experiment Station (WES) under the Lower Mississippi Valley Division (LMVD) study, "Investigation of Liquefaction and Methods of Preventing Flow Slides in Mississippi Riverbanks." The study was under the immediate purview of Mr. Frank J. Weaver, Chief, LMVD.

The report was prepared by Dr. Victor H. Torrey III, Research Group, Soil Mechanics Division (SMD), Messrs. Joseph B. Dunbar, Site Characterization Unit, Engineering Geology and Rock Mechanics Division (EGRMD), and Richard W. Peterson, Soils Research Facility, Soils Research Center, SMD, Geotechnical Laboratory (GL).

Centrifuge model tests of overburden behavior and analytical treatment of an alternate flow slide failure mechanism were performed during 1976-1978 by Dr. Christopher Padfield, then PhD candidate, University of Cambridge, England, under funding by the Corps of Engineers, European Research Office, London, England. Portions of Dr. Padfield's dissertation are presented herein.

Field investigations at the Montz and Bonnet Carre Point, LA, sites were conducted from 1978 to 1980 by crews and drilling rigs of the Explorations Group, EGRMD, GL, WES; by Fugro-Gulf, Inc., Houston, TX (WES Contract DACW39-80-C-0084); by the Laboratorium voor Grond Mechanica, Delft, The Netherlands (under subcontract to Fugro-Gulf, Inc.); and by Ardaman and Associates, Orlando, FL, (WES Contract DACW39-80-C-0102). Dr. Torrey, assisted by Ms. Marian E. Poindexter and Mr. Richard W. Peterson, directed and monitored these field investigations. Laboratory studies were also conducted by Dr. Torrey, Ms. Poindexter, and Mr. Peterson.

Hydrographic surveys were performed in 1979 along four point bar bank reaches below Baton Rouge, LA, by contract surveyors under the administration of the New Orleans District (LMN). Mr. Jay Joseph, New Orleans District, acted as liaison in obtaining the surveys as well as assisted with other aspects of the work. Mr. Roy E. Leach, Analysis and Evaluation Unit, Engineering Group, SMD, GL, WES, monitored the survey operations in the field.

This work was performed under the supervision of Mr. Clifford L. McAnear, Chief, SMD, and Dr. William F. Marcuson III, Chief, GL, WES.

Ms. Odell F. Allen, Information Products Division, Information Technology Laboratory, edited the report.

COL Dwayne G. Lee, CE, was Commander and Director of WES during the preparation of this report. Dr. Robert W. Whalin was Technical Director.

CONTENTS

	Page
PREFACE	1
CONVERSION FACTORS, NON-SI TO SI (METRIC) UNITS OF MEASUREMENT	5
PART I: INTRODUCTION	6
Background	6
The Empirical Criteria	8
Improvements in Technique	10
Findings of the Investigations	11
Purpose and Scope	13
PART II: GEOTECHNICAL FIELD INVESTIGATIONS	14
General	14
Reconnaissance Explorations	14
Detailed Site Investigations	17
Results of Geotechnical Field Investigations	25
PART III: GEOTECHNICAL LABORATORY INVESTIGATIONS	35
General	35
Undisturbed Sample Data	35
Critical Void Ratio Test Series	41
Pertinent Findings of Earlier Potamology Investigations	42
PART IV: GEOLOGIC AND HYDROGRAPHIC STUDIES OF THE MONTZ AND BONNET CARRE POINT SITES	48
Purpose and Scope	48
Geology and Historical Setting	48
Depositional Environments and Deposits	50
River Migration and Failure Development	55
Characteristics of Failure Site Development	56
PART V: HYDROGRAPHIC SURVEYS ALONG FOUR POINT BAR REACHES, 1979	58
PART VI: FLOW FAILURE MECHANISM	60
General	60
Behavior of the Overburden	62
Liquefaction and Flow of Sand	65
PART VII: SUMMARY	83
General Dutch Hypothesis	84
Hvorslev's Modified Hypothesis	85
Undermining and Tipping	86
Blocked Failures	86
PART VIII: CONCLUSIONS AND RECOMMENDATIONS	90
Conclusions	90
Recommendations	92
REFERENCES	95

Page

TABLES 1-2

FIGURES 1-105

APPENDIX A: LIST OF POTAMOLOGY INVESTIGATIONS REPORTS AND ASSOCIATED REPORTS..... A1

APPENDIX B: SPT AND GRADATIONS DATA, MONTZ RECONNAISSANCE BORINGS..... B1

APPENDIX C: SPT AND GRADATION DATA, BONNET CARRE POINT RECONNAISSANCE BORINGS..... C1

APPENDIX D: RIVER STAGE AND PIEZOMETER DATA..... D1

APPENDIX E: SPT DATA, MONTZ AND BONNET CARRE POINT DETAILED SITES..... E1

APPENDIX F: ELECTRICAL CONE PENETRATION TESTS; FUGRO-GULF CONTRACT REPORT..... F1

APPENDIX G: ELECTRICAL RESISTIVITY CONE PENETRATION TESTS; DELFT SOIL MECHANICS LABORATORY, CONTRACT REPORT..... G1

APPENDIX H: ELECTRICAL PIEZOCONE PENETRATION TESTS; ARDAMAN AND ASSOCIATES, CONTRACT REPORT..... H1

APPENDIX I: FRESH DEPOSITS, IN SITU DENSITIES BY NUCLEAR GAGE..... I1

APPENDIX J: PHOTOGRAPHS OF DEPOSITIONAL FABRICS IN SANDS AND SILTY SANDS, FRESH DEPOSITS, AND MONTZ SITE..... J1

APPENDIX K: TRIAXIAL TEST RESULTS ON UNDISTURBED SAMPLES, MONTZ AND BONNET CARRE POINT SITES..... K1

APPENDIX L: GRADATIONS CURVES FOR TESTED UNDISTURBED SAMPLES, MONTZ AND BONNET CARRE POINT SITES..... L1

APPENDIX M: POTAMOLOGY METHODS FOR OBTAINING LABORATORY MAXIMUM AND MINIMUM DENSITIES..... M1

APPENDIX N: CRITICAL VOID RATIO TRIAXIAL TEST SERIES, MONTZ COMPOSITE SAND..... N1

APPENDIX O: BANK CONTOURS FROM 1979 HYDROGRAPHIC SURVEYS ALONG FOUR BANK REACHES BELOW BATON ROUGE, LA..... O1

CONVERSION FACTORS, NON-SI TO SI (METRIC)
UNITS OF MEASUREMENT

Non-SI units of measurement used in this report can be converted to SI (metric) units as follows:

Multiply	By	To Obtain
cubic yard	0.7645549	cubic metres
degrees (angle)	0.01745329	radians
feet	0.3048	metres
inches	2.54	centimetres
miles (US statute)	1.609347	kilometres
pounds (force) per square inch	6.894757	kilopascals
pounds (mass)	0.4535924	kilograms
pounds (mass) per cubic foot	16.01846	kilograms per cubic metre
pounds (mass) per square foot	4.882428	kilograms per square metre
tons (force) per square foot	95.76052	kilopascals
tons (2,000 pounds, mass)	907.1847	kilograms

RETROGRESSIVE FAILURES IN SAND DEPOSITS OF THE MISSISSIPPI RIVER

REPORT 1

Field Investigations, Laboratory Studies, and Analysis of the Hypothesized Failure Mechanism

PART I: INTRODUCTION

Background

1. The problem of reducing bank regression and the meander tendencies of the Mississippi River are indeed an old story for the Lower Mississippi Valley Division (LMVD). The first protection work performed under the direction of the Mississippi River Commission (MRC) was initiated in the latter part of 1881. Thereafter, various versions of revetments were developed in the interest of navigation. Stabilization work was conducted until 1933, when a program of cutoffs of several long river meander loops was initiated. Bank protection work was essentially suspended at that time and remained suspended through World War II. With the completion of 16 cutoffs by 1940, serious, accelerated bank caving problems developed which posed threats to mainline levee reaches. In 1944 the MRC submitted a report to Congress stating the belief that the time had arrived in the development of the alluvial valley to hold the river meander within as narrow limits as rapidly possible between Cairo, IL, and Baton Rouge, LA. At that time (US Army Engineer Waterways Experiment Station 1951a), it was estimated that about 97 miles* of effective revetment or stabilized banks by means of structures along the 737 river miles in the reach of interest existed. By the end of Fiscal Year 1949, there were 150 miles of revetment in place, and it was estimated that an additional 254 miles of work would be required.

2. With the advent of the major revetment/bank stabilization program, the MRC realized the need to obtain a broader understanding of the hydraulic, potamological, and geotechnical factors conducive to successful and durable

---

* A table of factors for converting Non-SI units of measurement to SI (metric) units is presented on page 5.

bank stabilization. These studies became the extensive series under the title "Potamology Investigations." The US Army Engineer Waterways Experiment Station (WES) was the principal investigative organization. The wide range of topics addressed is shown in Appendix A.

3. As best as the authors can determine, the thinking that riverbank failures in sand deposits might be "flow failures" attributable to liquefaction began to develop subsequent to field investigations of two major revetted bank failures which occurred along Reid Bedford Bend just downriver from Vicksburg, MS, in January and February of 1947. A report of those investigations stated that one of the possible modes of failure was that of liquefaction of the fine sands (US Army Engineer Waterways Experiment Station 1948). In March 1949 a major bank failure at Wilkinson Point (MRC 1950) on the right descending bank just above Baton Rouge crevasse the mainline levee. Professor Arthur Casagrande was consulted concerning the slide. His opinion was that the mechanism was liquefaction/partial liquefaction of the fine sands underlying the relatively thin top stratum. In the Potamology Investigations conference report of 6-7 October 1949 (US Army Engineer Waterways Experiment Station 1951a) two consultants, Professors Arthur Casagrande and Donald W. Taylor, were specifically asked to express their opinions on the mode of failure in sand deposits of the Mississippi River. They both cited a flow mechanism, "probably" attributable to liquefaction. It is noted that the state of the art was not sufficient at that time to achieve liquefaction in a laboratory specimen or to obtain relatively undisturbed samples of sand below the water table.

4. The early 1950's saw an impressive series of significant events such as the first achievement of liquefaction in laboratory specimens (US Army Engineer Waterways Experiment Station 1950a), standard penetration testing (US Army Engineer Waterways Experiment Station 1950b), undisturbed sampling and rotary cone penetration tests (US Army Engineer Waterways Experiment Station 1951b), determination of density changes caused by sampling (US Army Engineer Waterways Experiment Station 1952a), and the study of variability of sand deposits (US Army Engineer Waterways Experiment Station 1952b). Also during this period was the development of empirical criteria for predicting susceptibility to flow failure based on the study of many case histories and bank caving field investigations at several sites. However, after 1952 the geotechnical and hydraulic efforts devoted to the Potamology Investigations

became very modest. In 1954 the long series (ending with the 1977 data report, Gann 1981) of annual revetment boring and hydrographic survey data studies to verify the empirical criteria began. In 1981 it was decided to declare the criteria verified and end the annual data reports.

The Empirical Criteria

5. The empirical criteria for determining riverbank stability with respect to flow failure were developed from the revetment data base over the years. There was no major revetment program in the New Orleans District (NOD) until the mid-1960's. Therefore, the original criteria did not address special conditions typical of the lower river. The criteria were modified in 1974 to accommodate those situations as will be described below after presentation of the original version applicable to the river near Natchez, MS.

6. Several basic soil conditions found to be associated with flow slides were as follows:

a. Flow failures occur in point bar deposits.

b. Point bar deposits usually contain three distinct strata: a somewhat cohesive top stratum called "overburden soils" underlying fine sands called the "upper sand series", and underlying coarse sands and gravels called the "lower sand series."

c. Flow failures have never been known to extend into the lower sand series.

d. The susceptibility of a given slope is dependent upon the relative thickness of the overburden soil and a zone of fine sand (designated Zone A) in the upper sand series.

7. The upper sand series was subdivided into two zones (A and B) on the basis of variations in grain size. Where failures have occurred, the boundary between Zones A and B has roughly corresponded to the depth of failure. Predictions of susceptibility to flow failure made through 1958 were based on gradation criteria developed in October 1952 (with initiation of the annual verification studies). However, a performance evaluation made during 1958 indicated that the gradation classification criteria for overburden soils (Zone A and B sands) should be modified. A comparison of the original and modified criteria is presented in Table 1.

8. In determining zoning of soil conditions from boring data, it should be noted that Zone B sands may contain occasional thin strata of sands as fine

as Zone A sands, but Zone B contains predominantly coarser and denser material than Zone A. Conversely, the occurrence of strata of medium or coarse sand not exceeding 5 ft thick within a zone of fine sand greater than 20 ft thick is not considered a sufficient reason to classify the zone other than a Zone A. In determining the overburden thickness, the thickness of all strata overlying Zone A sand governing thickness (i.e., thickness greater than 20 ft) is included. Thus, the overburden zone may include not only cohesive top stratum material but also strata of silts and relatively thin strata of sands (even Zone A sands when separated from underlying Zone A sands by more than 5 ft of other soils).

9. It has been found that where flow failures have occurred, Zone A sands were at least 20 ft thick. This was established as a minimum thickness for any location considered as potentially unstable with respect to flow failure. The ratio of overburden thickness to Zone A sand thickness, called the R value, was also found to be significant. An R value of 0.85 or less and a Zone A sand thickness of 20 ft or more indicated an unstable condition. However an R value greater than 0.85 or a Zone A sand thickness less than 20 ft indicated a stable condition with regard to flow failure.

10. Investigations showed that the thickness of Zone A sand may vary considerably in borings spaced as close as 250 ft (US Army Engineer Waterways Experiment Station 1952b). Because of the wide spacing of revetment borings at the sites studied, usually 1,000 ft or more, it was considered reasonable to assume that appreciable changes in soil conditions would occur between borings. Therefore, predictions were made for individual boring locations rather than for entire revetment reaches.

11. Inclusion of boring data from the NOD began in 1974. That data revealed a problem associated with the modified empirical criteria. The borings made by the NOD for revetment work often extended to or slightly below the river thalweg elevation but still did not completely penetrate Zone A sands. In addition, borings also failed to extend sufficiently far into Zone A considering potential deepening of the river to permit a prediction as to the susceptibility of flow slides under the criteria suited to the upper river. A criterion limiting the depth considered in making predictions was developed for borings made by the NOD. The limiting depth taken for a given boring location was based on the assumption that the mass of soil that might be involved in a flow failure would be that between the ground surface and the

elevation of the thalweg plus an additional 50 ft to allow for any normal range deepening of the river.

12. For the total period (1954 to 1977) of the empirical method verification studies, more than 2,300 boring locations were classified according to susceptibility to flow slides. Some 204 flow failures were identified with 87 percent within the Vicksburg District and the remainder in the Memphis District. With only 19 exceptions, all flow failures occurred either near locations predicted to be susceptible or, in a few instances, where the full depth of Zone A sand had not been determined. However, since only 36 percent of the locations in the Vicksburg and Memphis Districts predicted to be susceptible to flow failure actually experienced such failures, it is apparent that the criteria define only a part of the conditions indicative of the probability of failure. The most likely missing ingredient was the ability to enter severity of river attack in considerations of susceptibility.

13. In 1956 Dr. M. J. Hvorslev made an objective review of the soils phase of the Potamology Investigations (Hvorslev 1956). He summarized the principal accomplishments over the years (with Torrey's comments in parentheses) as follows.

Improvements in Technique

14. The following new or improved methods and equipment for field and laboratory investigations were developed:

a. Equipment was developed for static sounding to depths of 200 ft in sand operated by standard rotary drilling rig. This method (rotary cone penetrometer) furnishes continuous and very detailed profiles and is faster and more economical than sampling and testing.

b. A simple, economical, and reliable method for obtaining practically undisturbed samples of saturated sand, utilizing a piston sampler (Hvorslev sampler) and stabilization of the sand with drilling fluid was developed.

c. Improved methods were devised for handling and transporting samples and for determination of the natural densities of sample sections.

d. Changes in density of sands during sampling, using the improved method (Hvorslev sampler), were determined for limited depths or pressures. The results permit greater accuracy in determination of in situ densities of sand deposits.

e. Simplification and improvement of methods were achieved for the determination of relative densities resulting in smaller sample requirements and greater efficiency and reproducibility (this method was used in the studies reported herein and found to be excellent in comparison to current Corps of Engineers methods).

f. Improvements were made in operating techniques for triaxial tests with the result that flow failures in loose sands, for the first time, can be produced in such tests and furnished approximate values of lower or limiting critical density (after hypotheses of Geuze 1948, described herein).

g. The distribution of volume changes in triaxial test specimens of sand for various stress and density conditions was determined. The nonuniformity of this distribution was found to be much greater than formerly known or anticipated, a negative but very important result.

Findings of the Investigations

15. Extensive soundings and borings were made in all areas of major bank failures and in some areas where the banks are essentially stable, and samples obtained were subjected to classification and other laboratory tests. The following significant results were obtained:

a. It was found possible to characterize the point bar sands by their peak grain diameter (defined later herein) and to correlate this diameter with the natural, maximum, minimum, and relative densities. These correlations have extended the usefulness of otherwise incomplete data and test results for disturbed samples.

b. Results of laboratory tests to determine the strength characteristics and critical densities of the principal types of sand in failure areas were not conclusive, but were helpful in explaining the major bank failures and establishing criteria for potentially unstable soil conditions.

c. By utilizing the results of the above-mentioned tests, supplemented by direct comparisons of soils in failed and stable areas, it was found possible to subdivide the upper sand series in point bars into a potentially unstable section of fine and loose (loose by criteria of that day confused by Geuze approach to critical density, not loose in current terms) sands, Zone A, underlain by an essentially stable section of coarser and denser sands, Zone B. Very simple tests for recognizing the two zones were established.

Although the mechanics of the initiation and progress of major bank failures were not fully and satisfactorily determined from the field and laboratory investigations mentioned above, the following general conclusions may be drawn

on the basis of these investigations and direct comparison of data available on conditions in failed and stable areas:

a. All major failures have occurred in point bar deposits and are practically confined to the more or less cohesive overburden materials and Zone A of the upper sand series. The failures take place during high-water periods and generally, but not always, during a falling river stage.

b. Factual data on the initiation of major failures are fragmentary, but local scour and oversteepening of the bank are probably the principal causes combined with exposure of potentially unstable strata.

c. Most, and probably all, of the major bank failures are progressive rather than instantaneous in character. The flat outer slopes of the failures can be explained only by partial liquefaction of Zone A sands, at least during later stages of a failure cycle.

d. It is probable that excess pore-water pressures are developed in the bank prior to failure of individual sections and contribute to the failure, but it is also possible that such excess pressures are confined to strata of subcritical density and that partial liquefaction of the remaining parts of A sands is caused by disturbance after actual failure of a section.

e. The overburden materials in a failed section may block further progress of the failure when the ratio (R) between the overburden thickness and the thickness of Zone A sand is large. It was found that a bank is essentially stable or subject to only normal caving when R is greater than 1.4, but conditions are potentially unstable and major failures may develop when R is less than 0.85 and the thickness of Zone A sands is greater than 25 ft.

The above summary proved that the early Potamology Investigations yielded several major contributions to the geotechnical profession of truly classic nature, a fact unknown by most practitioners today.

16. Banks and Strohm (1965) updated the material and references presented in Dr. Hvorslev's review and suggested methods of stabilizing potentially unstable deposits. Also, Dr. Krinitzsky (1965) reported on geological influences on bank erosion.

17. In 1982 the important work of Dr. Kolb was completed which revealed the fact that point bar deposits with thin top strata and very thick Zone A sand strata were common in occurrence below Baton Rouge. In 1969, in light of these findings, WES geotechnical personnel approached LMVD Engineering Division contending that the probability of the occurrence of flow slides below Baton Rouge was significant. The river reach had never been addressed because

the revetment program had not included it and because there was no record of such failures other than the one at Wilkinson Point which breached the levee in 1949. The absence of a record of flow failures below Baton Rouge was probably because such failures had not regularly threatened the levees, been investigated, and consequently been identified. Also, regular revetment boring and survey data were nonexistent. The LMVD authorized WES to proceed to assess conditions below Baton Rouge on the basis of considerable boring data available as a result of the major revetment program in progress at that time. WES proceeded under modest funding to attack the task.

18. During the flood of 1973 four large flow failures occurred below Baton Rouge at Plaquemine Bend, Montz, Stanton, and Nairn, LA. Levee setbacks were required at all four locations. WES had already designated the bank reaches suffering failure as susceptible according to the empirical criteria. The authors, WES principal investigators, were detailed to LMVD Geology, Soils, and Materials Branch during the flood period to study the four case histories. As a result of the flood experience, LMVD authorized and expanded WES investigation under the title of this report.

Purpose and Scope

19. In April Torrey and Strohm (1976) submitted a major report to LMVD which presented the findings with respect to conditions below Baton Rouge and results of laboratory critical void ratio triaxial tests on Reid Bedford sand performed after the techniques of Castro (1969). That report was so voluminous that publication costs were prohibited in light of the important tasks yet to be addressed. As LMVD reviewed that report, it was decided to reorient the study toward comprehensive field investigations of point bar characteristics and documentation of river attack at several sites below Baton Rouge rather than concentrate on laboratory investigations. This report presents the results of those multifaceted field investigations, associated laboratory work, and major work performed by the University of Cambridge, England (at no cost to LMVD). The conclusions drawn from the recent work are compatible with the earlier work prior to 1952, but the conclusions suggest a failure mechanism other than that of liquefaction.

PART II: GEOTECHNICAL FIELD INVESTIGATIONS

General

20. The objective of the geotechnical field investigations was to apply current state-of-the-art knowledge and methods to assessing the in situ characteristics of susceptible point bar deposits below Baton Rouge. To achieve this objective, two point bar bank reaches were selected on the basis of their susceptibility to flow slides under the existing empirical criteria (Gann 1981): the fact that both reaches have suffered flow failures in the past and their proximity to each other. The reach receiving greater investigative effort was at Montz, LA, in the vicinity of the large flow slide (Figures 1 and 2) which occurred during the flood of 1973 at about mile 130.1 A.H.P.* on the left descending bank. The secondary reach selected was on Bonnet Carre Point (Lucy revetment) in the vicinity of the older failure which occurred at the downstream end of revetment mattress placed in 1969 at about mile 134.5 A.H.P. on the right descending bank. These two reaches are located on the vicinity map of Figure 3. These were the general reaches selected; it remained to perform reconnaissance explorations as described below to locate the small sites which would be investigated in detail.

Reconnaissance Explorations

Montz reach

21. In order to determine the best location or the detail site, the area on the top of the bank behind the existing failure scar was explored with an array of split-spoon borings during July to September 1978, as shown in Figure 4. WES drill rigs and crews performed this work. The north-south line of borings, including hole Nos. 10M, 13M, 16M, and 22M, was the center line of the array and lay along the alignment of the riverside toe of the old levee (degraded after the 1973 setback) and about 200 ft from the top of the bank. The other two lines of holes were 100 ft to the east and west of the centerline group. The upstream limit of the array was set on Montz Revetment survey range D-114 (Record Map, Montz, LA, Mile 132.5-L, 1962, survey of 8-15-75,

---

* A.H.P. = Above head of passes.

File No. H-13-27501, Sheet 9 of 10) which was also at the approximate upstream limit of the failure scar. The boring program proceeded from upstream to downstream. The first hole (1M) revealed about 100 ft of overburden over sands and silty sands (stable with respect to flow failure by the empirical criteria). In view of the absence of shallow Zone A sands at location 1M, it was decided to move downstream about 200 ft to location 8M. This boring showed about 60 ft of overburden over substratum sands exhibiting occasional strata or lenses of silt and clay. The next boring at location 10M encountered substratum sands at about 70 ft, but the top stratum did contain appreciable downstream, the sand and silty sand strata or lenses became more prevalent below a depth of about 35 ft. It is somewhat arbitrary, but from revetment range D-117 to D-119, the overburden depth was from 40 to 50 ft thick including those frequent thin (less than 5 ft) lenses of sand and silty sand below 35 ft. From revetment range D-119 to range D-122 (downstream limit of the array), the overburden thickness was clearly and consistently about 35 ft. In addition, from about revetment range D-118 thence downstream, the overburden thickness appeared to decrease gradually toward the top of the bank. An open-riser piezometer was set in the substratum sands (tip el -60 msl) in hole 17M. This location was chosen in anticipation that the detailed site would be nearby and to conceal the riser (to avoid vandalism) from the local traffic on the access road from the levee to the riverbank. The standard penetration tests (SPT) records for the reconnaissance holes (2M through 17M, 9M not drilled) are given in Appendix B. The blow counts shown are corrected values after the method described in subsequent paragraphs. Also shown in Appendix B are gradation data with depth for holes 13M, 15M, 19M, 22M, and 24M.

22. To select the detail investigation site location within the reconnaissance array, reference was made to Plan and Profile Map Gypsy Levee Setback, NOD File No. H-8-263-75, dated March 31, 1973, which showed top of bank lines at intervals from 1896 through 1949. The pertinent portion of that map is given in Figure 5. An overall picture of bank regression over the years is evident from Figure 5 and discussed in more detail in Part IV of this report. The older bank line surveys together with the 1973 failure location clearly indicate a trend in direction of localized bank failures over the years toward the reconnaissance array. Judging the general direction of the historical bank failure trend and also wishing to work near the top of the bank close to

the 1973 failure location, it was decided to position the detailed site over the location of reconnaissance hole 21M as shown in Figure 4. Oblique and vertical aerial photographs of the Montz area and detail site are shown in Figures 6 and 7.

Bonnet Carre Point reach

23. General site reconnaissance at Bonnet Carre Point was complicated by limited access, heavy vegetation, and the presence of a flooded borrow pit near the top of the bank. Since this was to be the secondary site, funds did not permit extensive and time-consuming efforts in locating a detail exploration site. Therefore, on the basis of stratigraphy indicated by available revetment borings, it was decided to drill four reconnaissance split-spoon holes (SPT-SE, SPT-SW, SPT-NE, and SPT-NW) in an 80 by 160 ft rectangular pattern as shown in Figure 8 just downstream of the existing failure scar on high ground relatively clear of large vegetation. The southwest corner boring (SPT-SW) was located on Lucy Revetment range D-50 (after Sinking Survey, October 1975, Record Map, Lucy, LA, Mile 135.5-R, 1962, NOD File No. H-13-27560, Sheet 5 of 7). The northwest cornet hole (SPT-NW) was thence riverward 80 ft and approximately 10 ft from the top of revetted bank. The SPT-NE and SPT-SE corner borings were 160 ft downstream near revetment range D-52. All four of these borings showed unstable conditions with respect to flow slides according to the empirical criteria with about 30 ft of overburden over about 70 ft of Zone A sands. Sands below a depth of about 100 ft exhibited a distinct change in color and gradations of Zone B sand. During the reconnaissance drilling, an open-riser piezometer was also installed with the tip set in the sands at a 65-ft depth as indicated in Figure 8. In addition to the detail site, it was realized that the area immediately landward of the central portion of the old failure scar warranted some investigation. This area was low-lying, subject to flooding, and was only about 15 ft wide between the top of bank and the old levee borrow pit. Drainage from the borrow pit into the river passed through this area. A location on revetment range D-45 (Figure 8) was selected to fill this need. Oblique and vertical aerial photographs of the Bonnet Carre Point area are shown in Figures 9 and 10.

24. The failure at Bonnet Carre Point was apparently the result of both "permanent" scour pool activity (see Part IV) and typical downstream end-of-revetment scour. However, this is one of the largest of such failures probably because it was a flow failure. In 1979 a downstream end-of-revetment

probable flow slide also occurred at Montz (see Figure 11 and Part V). A recommendation was made to River Engineering Branch of LMVD that the downstream limit of revetment placed along susceptible bank reaches be set to provide more batture, if possible, than would ordinarily be considered adequate. This practice might preclude levee stability problems should a large flow failure be triggered by the typical end-of-revetment scour.

Detailed Site Investigations

General

25. The investigational tools were selected specifically as applicable to the assessment of in situ density or relative density of sands. The intent was to compare the results yielded by the different approaches applied in close proximity to one another. Obviously, success was predicated upon sufficient consistency of the subsurface stratigraphy within the area of investigation to permit such comparisons. The methods selected were fixed-piston undisturbed sampling (U), SPT, electrical cone penetration tests (CPT), electrical resistivity cone penetration tests (RC), and electrical piezocone penetration tests (designated "W" for Wissa piezocone). The U and SPT's were performed by WES. The CPT holes were contracted to Fugro-Gulf Inc. The RC in situ testing was contracted through Fugro-Gulf to the Laboratorium voor Grond Mechanica of Delft, The Netherlands (Delft Soil Mechanics Laboratory). The W program was contracted to Ardaman and Associated, Orlando, FL, which is headed by Dr. Anwar Wissa. The undisturbed and SPT holes were drilled at the Montz site from December 1978 through January 1979 (except for SPT-6 taken in December 1979) and at Bonnet Carre Point site in November 1979. The RC testing using the Fugro-Gulf 20-ton cone penetrometer truck was performed at both sites in July 1980. The CPT holes were executed in early August 1980. Piezocone tests were performed by Ardaman and Associates using their 10-ton penetrometer rig during the latter part of August 1980.

26. During all phases of both detailed site investigations, ground-water levels were within the top strata so that all sampling and soundings in the substrata sands were below the water table. Ground-water levels indicated on the SPT logs of the reconnaissance holes (Appendixes B and C) at both sites were estimated using interpolated river stage data from July to September 1978 as shown in Appendix D, Exhibit D-1. During the detailed site explorations,

piezometer readings were used to monitor ground-water levels as shown in Appendix D, Exhibits D-2 through D-5. These exhibits also show river stage data and indicate that the use of such data for estimating ground-water levels in the reconnaissance holes did not result in significant error. Ground-water levels during detailed investigations at Montz were interpolated between the piezometer readings (385 ft from the top of the bank) and the river stage. The W data confirmed this procedure. At the Bonnet Carre Point site, river stage and piezometer readings were in close agreement, and ground-water levels during the detail site work were taken as indicated by the piezometer.

Montz site layout

27. For the detailed investigations, a grid pattern was laid out at a 20-ft spacing to mark the locations of the various borings/soundings as shown in Figure 12. The layout philosophy was to group SPT, CPT, RC, and W locations around each of two undisturbed sample borings (U1 and U2). Within the grid of overall dimensions of 40 by 160 ft were two undisturbed borings, five SPT holes, four CPT locations, five RC locations, and five W locations. In addition to these holes, four additional CPT's and one SPT were located at distances of 100 to 150 ft about the grid just to document peripheral conditions. The depth of exploration was selected to correspond to the approximate apparent depth at which the 1973 failure was initiated, i.e., between el -90 to -100 ft msl (ground surface at el 18 ft msl). One CPT (CPT 7) was pushed to the approximate elevation of the thalweg of the river of about el -125 ft msl.

Bonnet Carre Point site layout

28. A similar layout to that at Montz was used at Bonnet Carre Point but on a smaller scale as shown in Figure 13. A second undisturbed boring was taken only to ensure that adequate samples would be available for laboratory testing in association with the RC tests. As previously mentioned, additional SPT, CPT, RC, and W holes (see Figure 8) were taken in the confined working space immediately landward of the central area of the old failure scar. The depth of exploration was that to the Zone B sands of about 100 to 110 ft.

Undisturbed sampling

29. Undisturbed samples of the substrata sands from both sites were obtained using the osterberg fixed-piston sampler with 3.00-in. O.D. and 2.86-in. I.D. thinwalled, seamless Shelby tubes. The osterberg is a

self-contained sampler operated by hydraulic pressure applied through the drill string. The pressure drives a piston to which the Shelby tube is attached. The Shelby tube is thus pushed out of the sampler housing where it past a fixed O-ring sealed piston within the tube. In the fully "cocked" presampling position, the fixed piston is visible and flush with the Shelby tube cutting edge. The sampler is equipped with a locking mechanism which is engaged by rotating the sampler before lowering into the borehole. With the sampler resting on the bottom of the hole, a gentle reverse rotation of the drill rods unlocks the sampler in preparation for the application of hydraulic pressure and execution of the sampling stroke of 30 in. Completion of the sampling stroke is evidenced by the return to the surface of a flow of drilling fluid which is vented through the sampler from the pressurized drill string at the end of stroke. This automatic venting feature precludes overpushing a sample. Between sampling operations, the borehole was cleaned out an additional foot beyond the previous end-of-sampling-stroke depth using a 5-in. width baffled fishtail bit. The baffles on the fishtail discharge ports directed the flow of drilling fluid (bentonite slurry) up the borehole to minimize overdrilling and disturbance by erosion.

30. The rate of advance of the sampling tube cannot be precisely controlled using the WES model Osterberg sampler except by a hydraulic flow regulator on the drill rig. The WES rigs were not fitted with such a flow regulator. Therefore, the sampling stroke could not be controlled beyond the experience or "feel" of the driller in application of the push pressure. The driller was instructed and attempted with reasonable success to achieve the sampling stroke in a continuous manner at a rate within 0.5 to 1.0 ft per sec as recommended by Hvorslev (1949). Furthermore, in contrast to the Hvorslev fixed-piston sampler, the Osterberg does not provide the means to accurately measure sample compression or expansion. However, comparative study (unpublished) by WES has shown that the osterberg is comparable to the Hvorslev with respect to sample recovery and apparent quality of samples in sands. This study was performed at Kempe Bend in the Mississippi River point bar sands employing several type samplers. The SPT data obtained during the reconnaissance and detail site explorations ahead of the undisturbed sampling left little doubt that the sands in situ were from medium to dense. This observation lead to the decision that careful measurements of sample compression or expansion were not sufficiently important (i.e., the in situ densities were

not border line with respect to critical) to warrant the added costs and time associated with using the Hvorslev sampler.

31. After completion of a sampling stroke, the sampler with the Shelby tube fully extended from the housing was brought to the surface. With the sampler carefully maintained in a vertical position, a jar sample was trimmed from the end of the tube and a perforated O-ring packer installed. A piece of filter paper was placed between the packer and the sample. These operations were performed as quickly as practicable. After the bottom packer was secured, a 1/8-in. diam hole was drilled through the Shelby tube just below the fixed piston to relieve the vacuum properly developed between the piston and the sample to permit removal of the tube from the sampler. New models of the osterberg sampler provide a vacuum release mechanism. The counter-sunk allen-head bolts securing the tube to the hydraulic drive piston were removed and the tube was detached, carried in a vertical position to a rack, and hung to allow drainage of the sample through the perforated bottom packer. The filter paper between the bottom packer and the sample prevented material loss through the perforations during drainage. In general, drainage appeared to cease within about 2 hr, but no sample was left on the rack less than 6 hr. Drainage and field freezing of undisturbed samples are shown in Figure 14. Samples obtained late in the 10-hr workday were left to drain overnight, sheltered from rainfall by a plastic sheet. This practice obviously left more than half the total samples in risk of tampering. However, both detailed sites were in remote areas very rarely trafficked by citizens of the small local communities. Only one incident of intrusion occurred at the Montz site which was evidenced by missing gasoline and pilfering of a locked tool box affixed to the drill rig. Each morning, the area near the rack, the rack itself, and the samples were examined for any signs of tampering. None was ever seen. A photograph of the drainage rack is shown in Figure 14a.

32. After a sample had ceased to drain, a solid O-ring top packer was installed. The tube was then carefully removed from the rack and placed/secured in a vertical position in an upright freezer in operation onsite as shown in Figure 14b. After the sample had been in the upright freezer for at least 48 hr, it was transferred to a chest-type freezer also onsite, laid in a horizontal position, and padded with sawdust. At the end of each work day, both freezers were locked and additionally secured to the truck with heavy chain and padlocks. The frozen samples were transported to WES in the

chest-type freezer (the gasoline engine driven electric generator was also aboard the truck). At WES, the frozen tubes were stored upright in racks in an environmental room maintained at 20° F. Apparent quality of the samples is addressed in Part III.

Standard penetration tests

33. The SPT was performed using the DAMCO automatic trip hammer illustrated in Figure 15. A trip hammer is known to be more efficient in transmission of energy to the drill string as compared to the older conventional cathead-rope-donut hammer (C-R-DH) method. Therefore, trip hammer blow counts are lower than would be obtained by the C-R-DH method. Recent work associated with earthquake engineering (Seed et al. 1984) has established the average efficiency of the C-R-DH method as 60 percent of theoretical free-fall energy. This is now being taken as a standard by which blow counts obtained by other hammers are converted to equivalent C-R-DH blow counts. The conversion factor (C_{ER}) is determined as the ratio of the efficiency of the system used to that of the C-R-DH method, i.e., 60 percent (Tokimatsu and Seed 1987). Several years ago, Schmertmann (1978) measured the efficiency of one of the WES DAMCO trip hammers as 75 percent of theoretical free-fall energy. In 1986 Mr. Jeff Farrar of the US Bureau of Reclamation measured the efficiency of several of the WES trip hammers as averaging 70 percent of theoretical free-fall energy. Taking the lower efficiency for the DAMCO trip hammer of 70 percent, the blow counts at Montz and Bonnet Carre Point sites would be raised by a C_{ER} factor of 70/60 or 1.2 to correspond to C-R-DH values. This conversion of trip hammer blow counts, N, to equivalent C-R-DH values, N_{60}, has been applied to Montz and Bonnet Carre Point data. Further, the N_{60} blow counts have been "normalized" to an effective overburden pressure of 1 tsf, $(N_1)_{60}$, by multiplying N_{60} by the factor C_N. Thus

$$N_{60} = N \times C_{ER}$$

$$(N_1)_{60} = N_{60} \times C_N$$

where

N = observed blow count

N_{60} = observed blow count corrected to 60 percent of theoretical free-fall energy

C_{ER} = correction factor determined as the ratio of the efficiency of the hammer used to 60 percent efficiency

$(N_1)_{60}$ = N_{60} blow count corrected to 1 tsf effective overburden pressure

C_N = a correction factor depending on the effective overburden pressure at the depth of the SPT determination (see Figure 16).

Results of the SPT from both sites are given in Appendix E along with gradation data for the Montz site split-spoon/SPT samples. Gradation data for Bonnet Carre Point were shown with reconnaissance split-spoon/SPT holes in Appendix C since those borings were in very close proximity to that detail site.

Cone penetration tests

34. CPT data were obtained with the Fugro-Gulf electrical cone penetrometer which provided direct, downhole readings of tip resistance, q_c, and sleeve friction, f_s. The cone conformed to American Society for Testing and Materials (ASTM) D 3441-79 as indicated in Figure 17. Standard 1-m sections of Gouda push rods were prestrung with electrical signal cable from the cone tip and racked in order in the 20-ton cone rig (see Figure 18). The hydraulic pushing mechanism was also by Gouda, Inc. of The Netherlands. After each meter of rod was pushed into the ground, a delay of about 30 sec occurred in pushing for retraction of the push gripper mechanism and placement of the next threaded rod. Cone tip resistance and sleeve friction were plotted on a strip chart recorder during pushing. The cone rig was lifted off the vehicle suspension system during sounding by means of a hydraulic foot assembly (at the center of gravity of the vehicle) through which the cone and rods passed. The Fugro-Gulf CPT data are given in Appendix F.

Electrical resistivity cone penetration tests

35. Mr. H. L. Koning of the Delft Soil Mechanics Laboratory brought the electrical resistivity cone pictured in Figure 19 to the jobsite to be pushed by the Fugro-Gulf rig. A Delft expert technician accompanied Mr. Koning to operate the equipment and obtain the readings. From Figure 19, one can see that the device consists of an electrical cone penetrometer tip above which there is an insulator section containing two wider outermost electrode bands across which a known voltage is applied and three pairs of narrower electrode bands across which resistivity may be measured. In practice, the two

outermost resistivity electrodes are used for primary readings. Delft uses the innermost, closely spaced pair of resistivity electrodes to check consistency of readings but not for in situ density determinations because Delft contends that the readings reflect the zone of soil disturbance about the probe. In addition to readings of the specific resistivity of the soil/ground water combination, it is necessary to also obtain the specific resistivity of the ground water separately. This is achieved by use of a "water probe", as pictured in Figure 20, pushed separately within a foot or so of the resistivity cone hole. The water probe provides the capability of drawing ground water through a porous filter element into a cell where its specific resistivity is measured. After each depth increment measurement, the ground-water sample is expelled from the probe by application of a small pressure in preparation for advance of the probe for the next reading. The depths of readings of the soil-water resistivity cone and the water probe are carefully matched. For sands, the ratio of the specific resistivity of the soil-water to that of the water is a criterion of the porosity. The technical concepts upon which use of the ratio of specific resistivities for determining porosity of sands that is predicated are described in detail in the full Delft contract report given in Appendix G which also contains the results of soundings. It is noted that the method is not applicable to clays or clayey soils (electrically conductive constituents). With respect to the electrical cone tip, the friction sleeve did not conform to ASTM D 3441-79 because its area was 100 cm^2 instead of 150 cm^2. This results in depressed ratios of sleeve friction to tip resistance compared with the ASTM standard cone.

Piezocone penetration tests

36. Cone penetration tests providing dynamic pore pressure response data were performed using two probe configurations developed by Dr. Anwar Wissa. One device was the original Wissa piezometer probe with an 18-deg apex angle cone tip as shown schematically in Figure 21. This instrument yielded only dynamic and static pore pressure readings. The second piece of equipment was the Wissa piezocone (newly developed at that time) which provided readings of dynamic/static pore pressure, tip resistance, q_c, and sleeve friction, f_s. As a conventional cone penetrometer, it conformed to ASTM D 3441-79. A schematic of that probe is shown in Figure 22. At the Montz detailed site, holes W1 through W4 were sounded with the piezometer probe, and holes W5 and W6 were sounded with the piezocone. At the Bonnet Carre Point site, all W

holes were sounded with the piezocone. Ardaman and Associates contract report containing the field logs generated with the two probes is given as Appendix H. Because of the 10-ton weight of the Ardaman penetrometer truck, soundings could not be advanced more than about 80 ft at either site. To maintain saturations, water-filled plastic bottles were sealed over the porous tip elements of the two cones whenever the devices were out of the ground. If the tip element becomes even slightly partially saturated, dynamic pore pressure readings are severely adversely affected, if not completely lost. Several saturated replacement tip elements were brought to the jobsite just in case a sounding record indicated loss of saturation. Each sounding began by first pushing a pilot hole with a solid mandrel to a depth of about 3 ft below the ground-water table. The pilot hole was then filled with water to the ground surface. The piezometer probe or piezocone was then lowered until the bottle encased tip was below the water. The bottle was then removed and sounding proceeded beginning at the bottom of the pilot hole. This procedure was a fortuitous alternative at the two sites because the ground water was within a few feet of the ground surface, and the top stratum soils were sufficiently low in permeability to retain the water in the pilot holes. If this had not been the case, an oversized hole would have first been drilled to the saturation zone below the water table, and then the sounding would have been initiated at that depth with the plastic bottle left in place over the cone tip to be penetrated within the first few feet of the probe advance into the soil. At the time of this work, it was known that advance of a piezocone through even a few feet of partially saturated soil would likely unsaturate the tip element. Since that time, improvements in these devices and procedures have all but eliminated this problem.

Density measurements in fresh deposits

37. In-place density determinations were made using a nuclear gage (direct transmission mode) over the surface of fresh sand bars deposited at both Montz and Bonnet Carre Point. At Montz, the recent material partially filled the old failure scar. At the Bonnet Carre Point site, readings were taken in sand partially filling the old scar and just at the downstream end of the scar. Measurements were made in a rough grid pattern (not laid out by measurement) for both sites as shown in Figure 23. At each location, the surface measurements were taken by first removing 6 to 8 in. of drier "fluff", positioning the gage, and extending the probe 1 ft into the sand. At both

sites, the falling river had produced almost vertical faces in the deposits of 6 to 8 ft in height near water's edge. These faces were benched to a lateral depth of about 3 ft while taking readings in about 8-in. vertical increments. The locations of these bench tests are also shown in Figure 23. The density data obtained are given in Appendix I. A very interesting set of photographs was taken of the depositional fabrics in sands and silty sands exposed on the vertical face and along water's edge at Montz (see Appendix J). Such variations in fabrics over small increments of depth and area produced more than a little apprehension concerning what the undisturbed samples might reveal for the detail sites which would greatly complicate any comparisons of data from the exploration tools. This apprehension was unfounded.

Results of Geotechnical Field Investigations

General

38. This section will not attempt to treat each site in exhaustive detail relative to the implications of the various exploration tools used. Instead, each case will be addressed in overview summary of results obtained. In general, trends were very similar for both sites. Therefore, they will be discussed together except for occasional differences worthy of mention.

Split-spoon samples and associated SPT data

39. Grain size distribution curves obtained on split-spoon samples from SPT borings revealed the ranges in gradations of substratum sands as shown in Figure 24 for the Montz site and Figure 25 for the Bonnet Carre Point site. The sands tend to grade with depth from silty (SM) just below the top stratum contact to mostly (SP-SM) at a depth of 70 ft and below. Clean sands (SP) were infrequently encountered toward the maximum depths of exploration. At the Montz site, Zone A sands were still present at the maximum depth of exploration of about 120 ft and at Bonnet Carre Point, Zone B sands were encountered about 100 ft.

40. The SPT data obtained from both sites are presented in Appendix E. Blow counts, $(N_1)_{60}$, corrected to 60 percent of theoretical free-fall energy and to an effective overburden pressure of 1 tsf (see paragraph 33) ranged, in general, above 20 blows/ft and trended higher with depth as indicated in Figures 26 and 27. Occasional blow counts lower than 20 observed within the

substratum sands were attributable to lenses of very silty sand, clayey sand, or clay. SPT-5 located just landward of the old failure scar at Bonnet Carre Point exhibited somewhat lower blow counts than the SPT holes downstream at the detailed site. Figure 28 presents a comparison of blow count versus relative density correlations. The correlations are those of Gibbs and Holtz (1957), Bazaraa (1967), Bieganousky and Marcuson (1976), and ASCE (1977). The curves obtained by Bieganousky and Marcuson are based on tests of Ottawa and Reid Bedford Model Sand. The Reid Bedford Model Sand was selected years ago in the old potamology investigations to represent the traits of Mississippi River Reid Bedford revetment reach point bar sands in which many flow slides have occurred. As best as the author can determine, this was done to make available a nearby bulk source of comparable gradation and grain shapes for various studies. The model sand actually derives from a major deposit in the Campbell Swamp area of the floodplain of the Big Black River (a tributary of the Mississippi) and about 20 miles south of WES. This sand has been used in several other investigations over the years and, unfortunately, lost the "model" designation in the literature. With respect to the correlations of Figure 28, the Bazaraa curves are considered to underestimate relative density in situ while Gibbs and Holtz are believed to overestimate. The most recent correlation between blow count $(N_1)_{60}$ and relative density is offered by Tokimatsu and Seed (1987) and is shown in Figure 29. That relationship is based on field density tests and frozen samples. Tokimatsu and Seed pointed out that their curve is somewhat different from that provided by laboratory studies. They attribute the difference to the effect of aging on the SPT N-value of sands (Mitchell 1984). They consider their curve to be indicative of the relationship that might be expected from natural deposits. Also shown in Figure 29 is the laboratory curve obtained by Bieganousky and Marcuson (1976) for normally consolidated Reid Bedford Model Sand. Evidence that the sands at the Montz site are approximately normally consolidated is discussed subsequently in presentation of the cone penetration test data. However, such confirming evidence was not so clearly provided by cone penetration tests at the Bonnet Carre Point site. The author determined that a relatively small modification of the Bieganousky and Marcuson laboratory equation yielded a good approximation of the Tokimatsu and Seed "field" curve as indicated in the figure. The modified relationship is as follows and was employed to calculate

relative densities from the $(N_1)_{60}$ values obtained from the Montz and Bonnet Carre Point sites:

$$.0046D_r^2 = (N_1)_{60}$$

The summary plots of relative density thus calculated are given in Figures 30 and 31 for the Montz and Bonnet Carre Point sites. It is realized that silty sands (SM) are not usually characterized in terms of a relative density but, because the silt sizes of point bar sands are simply finer-grained quartz, the concept is not irrelevant. There is evidence from the older Potamology Investigations (to be presented later) that laboratory maximum/minimum density values and in situ densities trend consistently through the SP, SP-SM, and SM range in grain sizes. SPT data from both sites imply in situ relative densities of the substratum sands to range from a minimum of about 50 percent upward with an average calculated value of 85 percent for the Montz site and 90 percent for the Bonnet Carre Point site. In addition, using the correlation of DeMello (1971) among blow counts (N_{60} is taken here), effective vertical stress, and effective angle of internal friction, $\bar{\phi}$, as shown in Figure 32, it is estimated that $\bar{\phi}$ would be 35 deg or higher.

Undisturbed sample data

41. The data obtained from laboratory measurements and testing relative to the osterberg undisturbed samples are discussed in Part III.

Cone penetration tests

42. The results of the cone penetration tests are presented in Appendix F. The cone penetrometer is useful for estimating soil type in general and, for sands, estimating the in situ relative density and effective angle of internal friction. The most recent CPT classification chart based on the electrical cone is that by Douglas and Olsen (1981) and is shown in Figure 33. As shown in the chart, sands and silty sands are indicated by low values of friction ratio (sleeve friction/tip resistance, f_s/q_c, percent) and higher values of tip resistance as compared with clays which exhibit higher values of friction ratio and lower values of tip resistance. Summary plots of the CPT data obtained from both sites are shown in Figures 34 and 35. The cone records for both sites clearly show the overburden with generally low tip resistance and values of friction ratio of 2 percent and higher except for occurrence of some near-surface sand and overconsolidated (dessiccated) clays.

The point at which the probe enters the substratum sands is usually sharply evident by the immediate increase in tip resistance and a decrease in friction ratio to values usually less than about 1.5 percent. Occasional clay or silt lenses are encountered in the substratum as marked by a rapid decline in tip resistance accompanied by a spiked increase in friction ratio. However, it is noted, particularly for the Montz site, that there are occasional sharp declines in tip resistance to values less than 25 tsf, and the friction ratio remains at a value indicative of sand. At first glance, with no other information, this occurrence may be taken as reflecting a very loose lense/strata of sand. In reality, these are thin seams of clay or silt which points out one of the shortcomings of the cone penetrometer. While the tip resistance can respond to very thin layers, the approximately 5-in. long friction sleeve may not register changes (i.e., "see" the layer). In addition, Fugro-Gulf did not calculate the friction ratio data at very small depth increments. The additional information leading to the identification of the thin seams of clay or silt rather than loose sand is provided by the piezocone to be discussed below. The regularly occurring seams of clay soils, particularly at the Montz site, provide some insight concerning the consolidation history of the deposit. As shown in Figure 34, minimum tip resistances tend to lie along a straight line (dashed in the figure) with depth as drawn from the origin. It has been established that such a trend in a CPT record implies normal consolidation. In the case of the Bonnet Carre Point site, there are insufficient "marker" seams with depth to draw an inference.

43. Tip resistances in the substratum sands ranged from about 50 tsf near the top stratum contract to more than 300 tsf nearing the maximum depths of exploration. The records from the Bonnet Carre Point site reflect generally higher tip resistances with depth as compared with the Montz site except for CPT-3 immediately landward of the old failure scar which is in the same range as the Montz data. This difference in tip resistance trends between the two sites is consistent with relative density trends inferred from the SPT data and from densities of undisturbed samples as presented later herein. Taking a range in vertical effective stress for both sites of about 1.5 to about 3.5 tsf, tip resistances imply a range in relative densities by Schmertmann's (1978) chart in Figure 36 of 40 to 80 percent. Taking the same range in parameters and referring to Trofimenkov's (1974) chart in Figure 37,

it is seen by some extrapolation that estimated in situ values for effective angle of internal friction would exceed about 32 deg.

Delft resistivity cone penetration tests

44. The results obtained by resistivity cone are given in Appendix G. Noting that 1 MN/m^2 = 10.44 tsf and 1 m = 3.28 ft, the same trends and quantitative values of tip resistance are observed from the resistivity cone tests as compared with the CPT tests. The Dutch customary expression of friction ratio is the inverse of that of the CPT logs (i.e., q_c/f_{s_2}). In addition, the resistivity cone friction sleeve covered an area of 100 cm^2 as compared with 150 cm^2 for the ASTM standard cone. This results in lower values of friction ratio for the resistivity cone as compared with the standard cone.

45. Summary plots of the porosity data from the two sites are given in Figures 38 and 39. Examination of the porosity data in Appendix G from the Montz site indicated two distinct zones with depth. About 72 ft, porosities averaged about 47 percent. While below that depth they averaged about 43 percent. The open gaps in the porosity plots indicate sufficient clay to invalidate the method or the often correlative inability to extract water from the soil with the "water probe". Because of the regularity of these gaps, only the minimum values of the Montz records are considered useful readings and are those plotted in Figure 38. A decline in interpreted porosity toward a minimum reflected the continued influence of the clayey layer above, and the subsequent increase after the minimum reflected the clayey layer below. It is then possible that the minimum porosity values in the sands between clayey layers are also somewhat too high. In addition, if the silty sands from the Montz site were mixed with water, sustained discoloration of the water indicating colloids could be seen, and when oven-dried, a very thin crust of clay particles would form. This fraction could not be detected in routine mechanical grain-size tests being too small in weight as well as being mostly lost as dust during sieving. At the Bonnet Carre Point site, just as SPT blow counts and CPT tip resistances were generally higher than at Montz, the average porosities in hole BRC-1 were lower and averaged about 40 percent. The significant exception was a porosity value of 0.53 (void ratio of 1.13) in hole BRC-1 at a depth of 73.8 ft. When Mr. Koning of the Delft Laboratory delivered the contract report to WES, he specifically pointed out this anomaly. Consequently, the x-rays of samples from undisturbed hole U-1B some 20 ft away from BRC-1 were examined. As shown in Figure 40, precisely at a

depth of 22.5 m, a fractured zone (light tones) appears in the positive print of the undisturbed sample x-ray. Sand (SP) sample was opened in the frozen state and allowed to thaw. There was no exterior evidence of sample parture. However, probing along the sample with a pencil point indicated a very loose section of about 6 in. Taking a specific gravity of solids of 2.66 (a consistent value with depth at both sites), the range in porosities at Montz corresponds to a range in dry densities of 85 to 95 pcf and at Bonnet Carre Point corresponds to a range, excluding the anomaly, of 100 to 110 pcf. As shown later, these ranges are consistent with densities determined on undisturbed samples.

46. Porosity values inferred from the resistivity method are dependent on the laboratory correlations developed between the porosity and the ratio of the specific resistivities of the sandwater mixture and that of the water. Delft stated that these correlations surprisingly turned out to be a function of gradation so that several significantly different relationships were obtained from the several samples provided by WES (see Annex 3 through 11 of Appendix G). The authors speculate that this variation may have been more related to the small clay fractions than the gradations. This immediately casts doubt on the porosity data because laboratory correlation samples at close depth increments were not provided Delft. In addition, examination of groupings of samples for interpretation of the resistivity probe data, as shown on the Delft logs of Appendix G, revealed some cases of unlike gradations yielding almost identical correlations. WES has developed a resistivity probe of its own and has found it very difficult to obtain the laboratory correlations. It appears that the correlation can vary significantly with the method used to reconstitute the specimens to a given porosity. It is concluded that the technique is fraught with too many variables to place much confidence in the specific values of porosity inferred. Furthermore, laboratory maximum/minimum densities are also a function of gradation (documented in Part III). A value of porosity per se has no practical meaning until translated to some relative measure of the soils degree of compactness or behavior. An additional question is whether or not the probe's readings are predominantly within the zone of mechanical disturbance of the soil caused by insertion of the probe. Delft states that the electrical field generated by application of a voltage across the outermost electrodes extends about 6 ft around the probe. The resistivity readings taken between the lesser radius on

the order of the electrode spacing of about 10 in. It is possible, if not probable, that inferred porosities reflect the mechanical disturbance of the soil caused by insertion of the probe. As to whether the readings would be increased or decreased by such an effect, one could only speculate. In the Delft experience, it is true that porosities inferred from readings taken with the innermost, closely spaced electrodes are generally lower than those obtained at the wider electrode spacing. The Delft Laboratory is so confident of this pattern that it takes the closely spaced electrode readings too as a check on consistency of results. These readings were taken for both the Montz and Bonnet Carre Point sites and followed the expected pattern.

Piezometer probe and piezocone tests

47. The results of piezometer probe (piezoprobe) and piezocone penetration tests are given Appendix H. At the time of the fieldwork, there was hope that dynamic pore pressure responses yielded by a piezoprobe or cone might be useful for indicating whether a sand was contractive or dialatant in situ. Even though some in the profession still speak in these terms about piezocone response, there is little doubt left, based on additional work done by WES (Norton 1983) that the induced pore pressures are not useful as an indicator of in situ volume change characteristics of sands under stress changes of practical interest. The most obvious and often overlooked fact is that tip resistances in sands imply stress states about the probe under which even dense sands would contract (i.e., generate positive induced pore pressures). If dynamic pore pressure records are examined, negative induced pressure occur just before the probe tip passes from a pervious soil into a relatively impervious soil within which induced dynamic pore pressures may reach several tons per square foot, even to the extent that they exceed the vertical total stress. It is also known that position of the porous element on the probe affects response. The WES piezocone was also pushed at the Montz site at a location very close to the two Wissa piezocone holes W5 and W6. While the Wissa data exhibited regular occurrence of negative (with respect to hydrostatic) induced pore pressures, the WES data did not. The sole difference between the two probes was that the WES porous cylindrical tip element was about 1/8-in. shorter than the Wissa tip element. Davidson (1980) has documented the erratic patterns of volume change induced in sand around a penetrated probe.

48. The piezoprobe and piezocone have been found useful as pushed piezometers to obtain in situ hydrostatic pressures. Such usage does not require that the pressure measuring system be fully de-aired (saturated). If the measuring system is fully saturated, the devices can detect very thin seams of differing permeability by the dynamic pore pressure response. This capability can be very important in many geotechnical site investigations. Of the two Wissa probes pushed, the piezocone was more useful because its geometry produced more pronounced induced pore pressures compared with the more streamlined 18 deg apex angle piezoprobe and because of the CPT data also yielded.

49. As stated in previous discussion of CPT results, the piezocone data from Montz show that low tip resistance in the substratum sands corresponds to silt or clay and not loose sand. The Ardaman plots for piezocone holes W5 and W6 (see Appendix H) show that for each tip resistance of less than about 50 tsf there is also a spike in the dynamic induced pore pressure signifying a relatively impervious material. Furthermore, in contrast to the Fugro-Gulf CPT plots, the Ardaman friction ratio also shows corresponding increases indicative of silts or clays. Ardaman acquired its data on magnetic tape and processed by computer whereas, at that time (but no longer), Fugro-Gulf used hand calculation and plotting of friction ratio.

50. The piezocone revealed a distinct difference between the two sites. The usual push rate of 2 cm/sec produced excellent dynamic pore pressure responses at Montz but practically no response at Bonnet Carre Point. To obtain even somewhat muted responses at Bonnet Carre Point, the maximum push rate capability of the equipment was used (not measured but perhaps 5 cm/sec). The higher permeabilities of the Bonnet Carre Point sands were simply permitting almost instantaneous dissipation of the induced pressures. Of course, other factors also indicate that the Bonnet Carre substratum is the more permeable such as differences in piezometer lag relative to river stage, the coarser range in Bonnet Carre sand gradations, and the relative absence of clay or silt lenses at Bonnet Carre.

51. Very crude rising-head permeability tests were conducted in the piezometers at both sites. A miniature electronic pressure transducer (about 1/4 in. diam by 1/2-in. long) was first lowered about 35 ft below the water in the riser and checked for accuracy of its reading on the basis of an M-scope detection of the water level. Next, a plastic valve assembly was cemented to

the top of the plastic riser pipe. The cable for the transducer passed out of the valve assembly through a pressure grommet seal. After the cement afixing the valve assembly was fully set, air pressure controlled by a regulator was applied to the riser and the water pushed from the piezometer and down the riser to a level a couple of feet or so above the transducer. The water level was allowed to stabilize. The air pressure in the riser was isolated from the regulator by closure of a valve between the two. The strip chart recorder plotting the transducer readings was then turned on and the air pressure in the riser almost instantaneously vented to atmosphere by the rapid opening of the large (2-in.) valve in the top assembly. The return of the water up the riser was recorded with time in terms of pressure in pounds per square inches. The procedure was repeated several times at both sites with no significant differences among trials noted. Typical transducer readings converted to feet of water at the two sites are shown in Figure 41. These data coupled with an entrance condition shape factor based on the method of installation of the piezometer can be used to calculate a value of in situ permeability. It is beyond the scope of this report to include those calculations. The entrance conditions for the piezometers are not precisely known, but they were installed in exactly the same manner. In addition, there is no assurance that the permeability of the commercially manufactured, cemented coarse sand piezometer tip filter elements exceeded the in situ permeability by a ratio of at least 15 to 20 so that there was no retardation of return of water up the risers. However, the calculations indicated that in situ permeability (within the zone of influence of the tests) at the Bonnet Carre Point site was at least an order of magnitude (10 times) larger than that at the Montz site.

Density of fresh deposits

52. The readings of dry density by nuclear density gage (taken by a certified technician) obtained on the surface and in excavated benches of fresh sand bars at both sites are given in Appendix I. The gradations of these deposits were not examined in detail, but the gradation of single "grab samples" which appeared to be representative gradations are given in Figures 42 and 43. The Montz grab sample (Figure 42) is very similar to the Montz composite material used to perform critical void ratio tests (described in Part III). The Montz composite was derived by mixing portions of thawed undisturbed samples from top to bottom of the sand substratum. In comparison to the range of sand gradations encountered at Montz, the composite gradation

represents a fair average. However, the Bonnet Carre Point grab sample is not a Zone A sand and is finer than the substratum sands encountered in the detail site. In examining the nuclear dry densities obtained in sands (SP-SM) and silt sands (SM), the average dry density in the Montz fresh deposit was 90.2 pcf, and at Bonnet Carre Point, it was 86.6 pcf. Correlations obtained between grain-size and in situ density during early Potamology Investigations (presented in Part III) would imply lower densities for finer-grained sands. The Bonnet Carre Point fresh deposit is apparently finer than that at Montz and not representative of the older in situ sands. It is surprising that either deposit was similar to older in situ material because of the alteration in flow/velocity patterns caused by the old failure scars. In general, for both areas, dry densities between about 85 and 95 pcf were obtained in silty sands (SM). Dry densities of about 95 pcf indicated sands (SP) and below 80 pcf indicated sandy silt (ML).

53. Summary and conclusions relative to the field investigations are contained in Part IV which present laboratory and other data which bring the field results into focus.

PART III: GEOTECHNICAL LABORATORY INVESTIGATIONS

General

54. The laboratory testing program was somewhat limited, but it emphasized samples obtained from the Montz site. Testing included sieve analyses, triaxial consolidated undrained controlled stress (R) tests (with pore pressure measurements) on selected undisturbed specimens, maximum/minimum density determinations, and a critical void ratio triaxial test series on reconstituted specimens of Montz composite material.

Undisturbed Sample Data

Quality of the samples

55. All of the frozen osterberg samples were x-rayed in a vertical position in the Shelby tube from two orthogonal directions. The tubes were transported to the WES x-ray facility in a chest-type freezer. The x-ray operation exposed a tube to room temperature for about 5 min. There was no evidence of sample thaw. However, (just to be on the safe side), immediately after x-ray, the tubes were placed in a vertical position in an upright freezer which was being transported to the facility. The x-ray negatives were used to assess the quality of the samples and to select the sample portions from which to take triaxial test specimens. In general, the x-ray images indicated excellent sample recovery and infrequent evidence of disturbance such as cracks or voids. Wherever bedding patterns could be seen, there were no distortions suggesting disturbance. It was not uncommon that the x-ray image was of a uniform tone with no visible bedding pattern. There were limited occurrences of clay or silt lenses of a few inches thick within the Montz samples. The Bonnet Carre Point samples exhibited very rare presence of relatively impervious lenses or seams. Obviously, any sand above such lenses in the tubes could not possibly have drained, but there were no ice lenses noted in the x-rays or within any samples opened. Expansion (i.e., loosening of the sands due to freezing) would translate to a conservative effect in assessment of liquefaction susceptibility discounting sand fabric or structure (which may have been altered) as the major key to such susceptibility. After

all, every sample of a sand taken at depth rebounds to low effective stresses between sampling and testing.

Selection of test specimens

56. The tonal variations of the x-rays were used as an indicator to select tests specimens of sand with a bias toward the looser material (darker x-ray negative tone). Because of the expense and importance of the undisturbed samples, there was concern that an adequate laboratory testing program be performed while preserving (in the frozen state) a maximum number of samples for unforeseen future uses. Test specimens from each site are as follows:

a. Montz site. Boring U-2 at the Montz site was selected as the source of test specimens although one specimen was taken from boring U-1. Usually, two specimens were taken from each Montz tube for depths less than about 70 ft (the approximate depth of the 1973 failure). One specimen was selected from each tube from 70 ft to about 80 ft. Below 80 ft, one specimen from every other tube was tested.

b. Bonnet Carre Point site. Specimens from the Bonnet Carre site were taken from borings U-1B and U-3B. From boring U-1B within the main detailed site, specimens were selected at approximately 10-ft depth intervals. From boring U-3B immediately landward of the old failure scar, specimens were selected at about 5-ft depth intervals. Specimens were taken from U-3B because the various in situ tools had indicated a generally lower density of substratum sands at that location as compared with the trends seen at the downstream main detailed sites.

Specimen preparation and testing

57. Tubes containing the selected specimens were transported in the chest-type freezer to the WES machine shop. Each tube was cut longitudinally on a milling machine just through its wall thickness. The cut was made from just outside the packer at one end to just outside the packer on the other end. The uncut portions of the tube prevented it from springing open and perhaps damaging the sample. The cutting operation required less than 10 min. Before replacing the tube in the freezer, the cut was sealed with a vinyl caulk to minimize any sublimation of water from the sample during storage in the interim before specimen extraction. Initially, there was concern that the rapid cutting would generate heat sufficient to thaw partially the sample. This proved not to be the case, but, nonetheless, a CO_2 fire extinguisher was kept at hand to chill the tube if necessary. After the tubes were cut and

sealed, they were returned to the laboratory in the freezer and placed in the environmental room at 22° F.

58. To extract a test specimen, its location within the tube must be marked by measurements taken from the appropriate x-ray. Pairs of metal constriction bands were then placed and tightened on either side of each marked end of a specimen. The tube was then taken just outside the environmental room door, and the cross cuts of the tube were made using an automatic metal saw. The constriction bands again prevented the tube sections from springing open. The tube portions were immediately taken back into the environmental room. The constriction bands on each end of the specimen section were slowly loosened in a coordinated manner permitting the tube to open gradually. There were no instances of adherence of a specimen to the tube. It is also true that there was no observation of a film of clean ice about the periphery of any specimen. Once the constriction bands were removed, the specimen could slipped out of the tube intact. Specimens were handled with gloved hands. The ends were shaved square with a chilled stainless steel beveled straight edge in a chilled metal miter box. The length of the specimens varied between 6 and 7 in.

59. The triaxial chamber's top and bottom platens were prechilled in the environmental room. After trimming the specimen, the triaxial base and chamber were brought into the environmental room, and the chilled bottom platen was secured on the base. The specimen was then positioned on the bottom platen, the top platen placed, the specimen encased in a chilled latex membrane, and the chamber quickly assembled. The assembly was then carried straightforwardly to the loading station and a 5-psi confining pressure was imposed on the specimen. For a period of 24 hr, the specimen was allowed to thaw while axial deformation was monitored. Following thaw, a 5-psi vacuum was gradually applied to the specimen while the chamber pressure was reduced to zero. The triaxial chamber was then removed, and initial dimensions of the specimen were obtained. It was observed that a few specimens appeared to have increased in volume slightly during thaw while most exhibited very small decreases indicated by average height decreases of less than 0.05 in. and less or barely perceptible decrease in average diameter. Changes in dimensions during thaw also reflected the 5-psi confining pressure. Based on oedometer reloading curves for Carrollton Bend sand (Torrey 1981) which is similar in gradation to Montz composite sand, a 5-psi increase in vertical stress from

zero would translate to a height change of about 0.03 in. for specimens of the dimensions tested assuming no change in diameter. After specimen dimensions were obtained, the triaxial chamber was reassembled and filled with water except for a small air pocket which was maintained to prevent variation in confining pressure should the specimen liquefy and collapse during loading. The specimen was then brought to a maximum practical internal vacuum (-14.1 to -14.2 psi) using a differential vacuum procedure. This procedure entails raising the vacuum on the specimen while also increasing a vacuum on the triaxial chamber. This practice permits taking advantage of increased de-airing under full vacuum while avoiding overstressing the specimen. The vacuum on the top of the specimen was maintained about 5 psi higher than that on the chamber. The specimen was left to de-air for 24 hr. After this initial de-airing, highly de-aired water (produced in a Nold deaerator) was introduced at the base of the specimen under a controlled vacuum slightly less than the full value. In this manner, the water flow could be controlled very slowly to percolate up through the specimen (to avoid flushing of fines) and the differential vacuum across the specimen could be maintained such that about a 2-psi effective confining stress still acted at the base of the specimen. The de-aired water was percolated through the specimen until air bubbles in the exit line either ceased to exist or became minimal in number. The bottom drainage line was then closed and the differential vacuum procedure was reversed, reducing the specimen and chamber vacuums in concert until the chamber was at atmospheric pressure and the specimen was under a 5-psi internal vacuum. The chamber pressure was then raised as the specimen vacuum was decreased until the chamber pressure was 5 psi, and the specimen was at atmospheric pressure. From this point, conventional back-pressure saturation procedures were applied. The minimum acceptable "B" value before test was 0.95. In most cases B values of 0.98 or 0.99 were attained at back pressures less than 50 psi.

60. After saturation, the specimen was anisotropically consolidated under an effective principal stress ratio (σ_{1c}/σ_{3c}) of 2.0 to 2.3 using Jaky's approximation for $K_o = 1 - \sin \bar{\phi}$ and varied from 30 to 34 deg depending on depth. Initially, specimens were first taken to an effective vertical stress corresponding to the approximate in situ depth and a low water river stage of about 5 ft msl and then rebounded to an effective stress state corresponding to a high river stage of 20 ft msl. Later, it was decided that this

overconsolidation effective stress cycle of only about 6.5 psi was trivial, and subsequent specimens were consolidated directly to the high water conditions. The high water condition was chosen simply because flow slides have always been associated with high river stages. After consolidation, the drainage line was closed, and axial loading in 20 lb increments (under constant confining pressure $\sigma_3 = \sigma_{3c}$) was begun at 1 min intervals between load increments. Changes in pore pressure and deformation became negligible within a few seconds after application of a load increment.

61. Deviator stress and induced pore pressure versus axial strain data for all tested undisturbed specimens for both sites are given in Appendix K. In general, all specimens tended to dilate during undrained loading with peak positive induced pore pressures occurring within only 3 percent axial strain. The tests were terminated as induced pore pressure reached a negative 1 to 2 atmospheres. The one exception to the trend was for specimen 23.1 from Montz which did not begin to develop negative induced pore pressure until 10 percent axial strain. This specimen was a silty sand (SM) with a measured dry density of 84.9 pcf. A total of 26 specimens from the Montz site and 16 from the Bonnet Carre Point site were tested. The range in gradations and mean gradations of the specimens tested are given in Figures 44 and 45. The effective stress paths defined effective angles of internal friction from 33 to 36 deg.

62. For curiosity, one specimen from boring U-1 at Montz (specimen 20, see Appendix K) was consolidated to a high effective stress to see if it would liquefy upon loading. A vertical effective stress of 8 tsf and a lateral effective stress of 4 tsf were applied before undrained loading. That specimen also tended to dilate after about 2 percent axial strain. A high water vertical effective stress would correspond to a depth of about 300 ft. The maximum depth of the Montz failure was 70 to 80 ft, representing a vertical effective stress at high water of about 2 tsf.

63. The dry densities based on dry weights after testing corresponding to the as-thawed dimensions of the test specimens are given for Montz in Figure 46 and for Bonnet Carre Point in Figures 47 and 48. In Figure 46, Montz specimen dry densities ranged from 85 to 100 pcf. Specimen dry densities from boring U-1B in the Bonnet Carre Point main detailed site ranged from 94 to 107 pcf while (as expected) dry densities from boring U-3B just landward of the old failure scar were somewhat lower and ranged from 90 to 100 pcf.

64. The ovendry remains of each test specimen from Montz were used to perform laboratory maximum and minimum density tests after the old potamology procedures (Garber 1952) given in Appendix M, using the original hammer and mold. After comparative tests, the old potamology minimum density procedure was abandoned in favor of an alternative procedure which was simpler and yielded more consistent and slightly lower values. That procedure consisted of placing a 1.5-in. diam piece of plastic (PVC) pipe into the potamology mold which was sitting open-ended upon a glass plate and filling the PVC section with dry sand. The PVC pipe section was then raised steadily permitting the sand to flow out into the mold. The volume of the PVC section was sufficiently larger in volume than the mold so that excess material was struck off with a steel straight-edge. The mold was then tapped lightly to cause the sand to settle away from the mold rim. This prevented material loss as the spillage was brushed away from the mold's collar seat and off the plate glass. The mold, the sand within, and the plate glass were then weighed to obtain the weight of sand after subtraction of the tares. Figure 49 illustrates the differences in maximum and minimum void ratios obtained by current (CE) methods (Headquarters, Department of the Army 1971), by the old potamology methods, and by using the PVC sleeve method for maximum void ratio. From Figure 49 one can see that for both Reid Bedford and Montz sands the potamology methods and the alternative PVC sleeve method result in higher values of relative density for a given void ratio. However, the trend in differences are not consistent for the two sands. Using the potamology minimum void ratio method and the PVC sleeve maximum method, the lowest measured specimen relative density was 42 percent. That particular specimen's gradation was similar to that of Carrollton Bend sand. At the same void ratio, Carrollton Bend sand would be at a relative density of 35 percent by CE maximum/minimum methods.

65. Table 2 presents the dry densities of the Montz undisturbed triaxial specimens, their maximum/minimum void ratios, porosities, and relative densities. All values are for the as-thawed condition before application of consolidation stresses. Maximum densities were determined by the potamology method and minimum void ratios by the PVC sleeve method. Figure 40 presents the data of Table 2 in plotted form with depth. Table 2 and Figure 50 show that relative densities ranged from a low of 42 percent to a high of 87 percent. The porosities fell within a range similar to that indicated by the Delft resistivity probe method. In addition, the plots of porosity and

relative density with depth support the Delft contention that the trends of in situ density appeared to be different above a depth of about 72 ft as compared with density below that depth.

66. In addition to direct measurements of density from extracted specimens, the x-ray negatives of Bonnet Carre Point boring U-1B, samples 13 (depth = 36.0 to 38.3 ft), 21 (depth = 60.0 to 61.9 ft), and 26 (depth = 75.0 to 77.5) were scanned along their center lines using a film densiometer. The machine registers and continuously plots the variation of film density in terms of "counts". By placing substances of known density (aluminum, PVC, etc.) with the tube as it is x-rayed, the variations in counts can be roughly calibrated to infer variations in sample wet density. The scans indicated an increase in wet density with depth (i.e., from sample 13 to 26). Implied wet densities ranged from about 87 to 120 pcf while about two-thirds of each sample exceeded 110 pcf. Figure 51 presents a tracing of the record obtained for sample 21. Several water content determinations were made along the length of the sample to permit a calculation of dry density from the implied values wet density. Figure 51 shows that implied wet densities varied from about 90 to 123 pcf while dry densities appeared to vary from about 86 to 105.5 pcf. Figure 51 also shows that the scan records for the known substances exhibited some variation. This introduces an error in calibration of the method in addition to any flaws in the consistency of the chemical coating of the film. There is no way to judge the extent of error, but the numbers obtained correspond roughly to direct measurements of dry densities of Bonnet Carre Point triaxial specimens from boring U-1B in Figure 49.

Critical Void Ratio Test Series

67. Using the Montz composite material, a critical void ratio determination test series was performed after the method of Castro (1969). The stress-strain and induced pore pressure plots are given in Appendix N. Critical void ratio data are also available for two other Mississippi River point bar sands (i.e., Reid Bedford and Carrollton Bend). The Reid Bedford tests were performed by Durham (1971) and subsequently checked by the senior author. The Carrollton Bend testing was performed by Torrey (1981). The gradations of the three sands are shown in Figure 52. The Carrollton Bend sand was a composite Zone A material obtained by mixing similar samples from boring R-105.7-LU

located on the left descending bank and just downstream of the Huey P. Long Mississippi River Bridge. The critical void ratio curves for the three sands are compared in Figure 53. Striking differences among the critical void ratio curves are shown in Figure 53 with critical void ratios trending higher with increasing fineness of the sands. The curves also show that relative density at critical void ratio also increases as gradation becomes finer. From the laboratory behavior point of view, it must be remembered that sand will not completely liquefy unless the combination of density and confining stress are considerably above the critical void ratio curve. As the combination of density and confining stress are brought near the critical curve from above, the behavior of the material becomes that of partial liquefaction. A specimen tested from a position on the curve will tend to dilate during undrained shear. Likewise, specimens tested at densities and confining pressures corresponding to a position below the critical curve also tend to dilate more strongly with distance below the curve.

68. Another factor which is pertinent to flow slide development is the apparent stress path. Perhaps the more applicable loading path imposed on an element of sand behind the retrogressing face of the failure is that of decreasing lateral stress under constant vertical stress. Torrey (1981) applied this stress path in testing Carrollton Bend sand. He observed that loose specimens responded from the initiation of undrained loading with immediate negative induced pore pressure followed by positive induced pore pressure with increasing strain. Specimens tested at combinations of density and confining pressure positioned below the critical void ratio curve (i.e., dilatant under undrained shear) responded with only negative induced pore pressure from the outset of undrained loading. It appears that the stress path of constant vertical stress and decreasing lateral stress intensifies any dilatant tendency.

Pertinent Findings of Earlier Potamology Investigations

69. In studies leading to Report 12-2 (Garber 1952) of the old potamology report series, a large number of samples were taken using the Hvorslev fixed-piston sampler in point bar sands over a 500-mile reach from the vicinity of Memphis, TN, to Baton Rouge, LA. These sites were as follows from north to south:

a. Bauxippi - Wyanoke revetment.

b. Huntington Point revetment.

c. Goodrich revetment.

d. Reid Bedford revetment.

e. Kempe Bend revetment.

f. Morville Landing revetment.

g. Point Menior.

h. Wilkinson Point.

Sand samples (537 total) from these sites were examined for density, gradation, and maximum/minimum density. The multifaceted investigation of these parameters was perhaps one of the most thorough investigation ever conducted. It is not practical to address the many significant documented conclusions contained in Report 12-2. The reader is encouraged to review the report. It is interesting to note that at that time (1950-52) there was a simple confidence that liquefaction was the flow failure mechanism. The Reid Bedford standard penetration tests (US Army Engineer Waterways Experiment Station 1950b) had indicated (Report 12-2 so states) that the sands were dense in situ, but this was discredited in favor of the findings from testing of undisturbed samples. At that time, use of the SPT to interpret in situ relative density was an infant issue (Gibbs and Holtz 1957) and the WES investigators obviously had little confidence in the tool for that purpose. However, even the undisturbed sample data proved the sands to be relatively dense. Even though some feel for what densities were relatively loose or dense with respect to liquefaction was existent at the time, there was no clear focus on the question, especially since liquefaction of laboratory triaxial specimens was not achieved by anyone until the 1950 testing on the Reid Bedford undisturbed samples. The hypotheses of Geuze (1948) seemed to only confuse the situation. When the Reid Bedford tests were performed (US Army Engineer Waterways Experiment Station 1950a), back-pressure saturation techniques were not yet developed nor were there means to maintain an undrained condition while monitoring induced pore water pressures. Instead, induced pore pressures were indicated by the amount of pressure or vacuum required on a burette open to the specimen to prevent the specimen from changing volume during loading (i.e., prevent the meniscus in the burette from moving). The specimen saturation technique was by percolation of less than highly de-aired water, but it is probable that B values of at least 0.90 were actually achieved. It

is interesting to note that Reid Bedford sands could not be made to liquefy in those earlier tests unless specimens were reconstituted to negative relative densities. Allowing for the lack of saturation and maintenance of good undrained loading, Durham's (1971) findings which states that Reid Bedford sands would not liquefy above about 11 percent relative density for vertical consolidation stress up to 5 tsf with lateral stress of 2 tsf are supported. So, even the earlier data from the Reid Bedford tests were contraliquefaction as the failure mechanism.

70. The 537 3-in. Shelby tube undisturbed sample densities were obtained as follows:

a. After the sample was brought to the surface, the ends were trimmed. Expanding perforated packers were placed in both ends of the tube, and the sample was allowed to drain in a vertical position.

b. The sample was placed in a horizontal position and tapped with 50 blows of a rubber mallet to settle all loose strata.

c. The sample was shipped to WES laboratory in the horizontal position where it was cut into 3-in. long segments on a band saw.

d. The natural density of each segment was computed on the basis of its volume and dry weight.

Meticulous studies were conducted to assess the range of error in measured density including the amount of material lost during the sawing operation. In addition, a study was conducted to determine sample disturbance using the Hvorslev sampler in reconstituted large laboratory specimens (US Army Engineer Waterways Experiment Station 1952a).

71. It had been determined that peak grain diameter, D_p, (Bagnold 1943) was a parameter suitable as a descriptor of gradations of Mississippi River point bar sands. The peak grain diameter is that diameter representing the largest percentage by weight of the soil. It is obtained by converting the gradation curve which is nothing more than a cumulative frequency distribution to an equivalent frequency histogram. The gradation curve is first divided into small, equal increments (class intervals) by grain size, and the percent by weight of material represented by each interval is determined. These data are then plotted as a bar chart (frequency histogram) in percent of total sample in each interval versus the grain-size intervals. The grain size representing the center of the tallest bar (the model class mark) is taken as the peak grain diameter and corresponds to the steepest part of the gradation

curve. The smaller the class interval selected, the more accurate the value of peak grain diameter obtained. Correlations were developed among peak grain diameter, in situ density, and maximum/minimum density using the 537 data points for each parameter obtained from the undisturbed samples. Figure 54 shows the correlation between D_p and as-sampled dry density with the original data points. Figure 54 reveals that the minimum sample dry density measured was about 86 pcf and that the greatest majority of values fell above 95 pcf. Figure 55 shows the as-sample density correlation of Figure 54 along with the correlations developed between D_p and maximum and minimum densities, respectively. The results of corrections to as-sampled densities for sampling disturbance is also shown. Figure 56 presents the correlation between D_p and relative density as-sampled and corrected for sampling disturbance. There are three points to make concerning the correlations. First, the range in values of in situ dry densities in Figure 54 is commensurated with values from the Montz and Bonnet Carre Point undisturbed samples. Second, the trend in values of maximum/minimum did not break down as percent fines exceeded values corresponding to (SP-SM). Third, Figure 56 indicates no in situ relative density below about 50 percent including data scatter.

72. It has been previously stated that investigations at Montz and Bonnet Carre Point indicate consistently that relative densities in situ range from 40 to an excess of 80 percent, with the lower relative densities corresponding to higher silt content (some classified under the empirical criteria as overburden, i.e., greater than 20 percent fines). Taking a typical range in gradation, including borderline overburden and borderline Zone B, for the two detailed sites and obtaining D_p as shown in Figures 57 and 58, it is possible to check in situ density and relative density using the correlations of Figures 55 and 56, respectively. In situ densities predicted from the correlations using D_p values from Montz and Bonnet Carre Point sands correspond to the density measured from the osterberg samples very well. In addition, maximum/minimum values from the correlations predict those determined for Montz sands using essentially the same methods of determination given by Garber (1952). Furthermore, realizing that the borderline overburden/Zone A sands have a peak grain diameter of about 0.105, the correlations of Figure 56 yield a relative density of about 61 percent for this gradation. All gradations coarser than SM with more than 20 percent fines represent higher in situ relative densities because in situ dry density in the

correlations trends closer to maximum density and further from minimum density for higher values of D_p. For the borderline Zone A/Zone B sand encountered at the Bonnet Carre Point site (see Figure 58), the peak grain diameter is 0.360. From the correlations in Figure 56, D_p corresponds to a relative density of about 79 percent. The coarsest material encountered at Montz exhibits a D_p of 0.195 and corresponds to a relative density of about 70 percent. When such materials were reached with depth at the two sites, refusal sometimes occurred in the SPT tests for obvious reasons. Looking at the undisturbed triaxial specimen data in Table 2, the question arises as to what would be the correction for sampling disturbance. Taking the range in D_p for the Montz sands given in Figure 57 and then referring to Figure 56, the maximum reduction in as-sampled relative densities would be no greater than about 4 percent for the finer gradations and less than that for the coarser gradations. The authors are convinced that the correlations from Report 12-2 (Garber 1952) are excellent in representing the in situ densities of Mississippi River point bar sands.

73. It is particularly conclusive to compare the available critical void ratio data for point bar sands on the basis of peak grain diameter, D_p, for each gradation. These data have been acquired for Reid Bedford sand, composite Montz sand, and composite Carrollton Bend sand (see Figures 52 and 53). For those sands, the critical void ratio curves are plotted in terms of effective vertical stresses versus peak grain diameter in Figure 59. The Reid Bedford and Carrollton Bend sands were anisotropically consolidated, and the Montz sand was isotropically consolidated. There is no discrepancy in Figure 59 introduced by the mix of consolidation procedures because the critical void ratio curve is not a function of consolidation stress ratio (Poulos, Castro, and France 1985). The plotted points for each sand in Figure 59 were obtained from Figure 53 by selecting the values of critical void ratio for each of the values of effective confining pressure of 0.5, 1.0, and 4.0 tsf. The corresponding effective vertical stresses were taken as twice the effective confining pressures assuming a K_o in situ of 0.5. The values of effective vertical stresses thus obtained of 1.0, 2.0, and 8.0 tsf were then converted to an approximate equivalent depth assuming a bank-full high-water condition. Also shown in Figure 59 is the correlation of D_p to in situ density of Figure 55 (corrected for sampling disturbance) converted to void ratio by taking a specific gravity of solids of 2.66.

74. In interpreting Figure 59, it must be remembered that a sand will not liquefy if its in situ void ratio versus effective confining pressure (recall that effective confining stress is converted to effective vertical stress in the figure) coordinates are not above the critical void ratio curve. If the position falls on or below the curve, the sand will tend to dilate under undrained loading and more strongly so with increasing distance below the curve. Generally, higher values of D_p correspond to higher values of effective vertical stress because Mississippi River point bar deposits tend to trend coarser with depth. The largest flow failure of record occurred at Wilkinson Point, LA, and was about 100 ft deep. Therefore, the cross-hatched zone of Figure 59 implies how strongly dilatant Mississippi River point bar sands are on the average. The hypothesis of liquefaction as the failure mechanism is not sustained.

PART IV: GEOLOGIC AND HYDROGRAPHIC STUDIES OF THE MONTZ AND BONNET CARRE POINT SITES

Purpose and Scope

75. The purpose of this section is to treat the geologic and historical hydrographic aspects of the Montz and Bonnet Carre Point bank reaches and failures sites. The study will address this purpose by examining the recent historical development for the pertinent reach of river; defining and delineating the types, the distribution, and the soils comprising the various depositional environments encountered along the reach; defining total river migration through the study area during the past 80-year period; and examining some characteristics of failure development at each site during this same period.

76. The reach of the Mississippi River included in this study extends from Montz, LA, upstream to Reserve, LA, a distance of approximately 9 river miles (Figure 60). The area is located in south central Louisiana, approximately 35 miles upriver from New Orleans and within the St. John the Baptist and St. Charles Parishes. Pertinent USGS topographic maps are Mount Airy, Bonnet Carre, and Lac Des Allemands of the 15-min (1:62,500) series and the Reserve, LaPlace, Hanville, and Lac Des Allemands of the 7-1/2-min (1:24,000) series.

Geology and Historical Setting

77. In order to fully understand the geology of the study area, it is necessary to briefly review the historical development of the area. The reach of interest is located in the north central portion of the Mississippi River's deltaic plain and predominantly exhibits Holocene or Recent aged sediments. These sediments are a seaward thickening wedge of fluvial and fluvial-marine deposition overlying the Pleistocene Prairie Formation. The Prairie Formation is the youngest of four terraces in Louisiana, deposited during the interglacial periods of Pleistocene glaciation and formed by deltaic (Fisk 1944). The age of the Prairie Formation is recognized as being earlier than late Wisconsin and is estimated to have been deposited some 70,000 to 100,000 years ago. The burial of the Prairie Formation by recent sediments began sometime between

15,000 and 20,000 years ago with the advent of rising sea level as a result of the melting and final retreat of the Wisconsin aged ice sheets in the north.

78. Sea level prior to this period of time was approximately 270 ft below the present-day level due to the amassment of glacial ice in the north (Curray 1965). As a result of lowered sea level, the land surface extended far south of the present-day shoreline with the Pleistocene surface exposed and subject to erosion. The ancestral river was entrenched into the Pleistocene approximately 15 miles west of present-day Houma, LA, and was flowing southeasterly across the ancient coastal plain. The river valley at that time was about 10 to 25 miles in width with a drainage basin of branching tributaries from 60 to 100 miles in width.

79. As sea level began rising, the ancestral river and its tributaries began alluviating their valleys in response to the changing base level. Coarse fluvial sediments (sand and gravel) were deposited in the valley entrenchment while the finer fluvial sediments (fine sand, silt, and clay) were carried gulfward and deposited. Continued rising of sea level generated up-valley deposition of coarse fluvial sediments. At the same time, the advancing sea began reworking and redepositing the sediments in the distal end of the entrenchment in the new nearshore environment. Eventually, as sea level began stabilizing, the quantity and grain size of the sediments began to diminish as valley alluviation began decreasing.

80. Five to seven thousand years ago the rise in sea level ceased with the present-day base level established and a new shoreline located near Baton Rouge, LA, (Kolb and Van Lopik 1958). Numerous lobate deltas began displacing the open water with fine-grained alluvium, further covering the ancestral entrenchment and its tributaries. The lateral and gulfward movements of delta advancement have resulted from the up-valley shifting of the river's course for a shorter, more energy efficient route to the sea. Since the establishment of the modern sea level, seven major lobate deltas or complexes have been formed. From oldest to youngest, the delta complexes are Sale-Cydermor, Cocodrie, Teche, St. Bernard, LaFourche, Plaquemines, and the present-day Balize. These deltas are shown in Figure 61 (Kolb and Van Lopik 1958) with the study area located.

81. Recent deposition in the study area is probably first associated with the Cocodrie delta complex, established between 3,500 and 4,500 years ago. The next advance into the region was by the St. Bernard delta complex

some 1,800 to 2,500 years ago. This complex relatively corresponds to the current course of the river from Baton Rouge to New Orleans. With abandonment of the St. Bernard course, the river shifted westward and began forming the LaFourche course between 800 and 1,200 years ago; the river shifted eastward and built the Plaquemines delta and the present-day Balize delta.

Depositional Environments and Deposits

82. The geology of the study area was defined from aerial photography, boring data, and information obtained from previous geological studies of the region. Black and white aerial photographs flown in December 1940 and November 1980 at a scale of 1:62,500 and 1:40,000, respectively, were examined and a preliminary geologic map of the area was constructed. Boring data obtained from the New Orleans District, WES, Louisiana State Highway Department, and private engineering firms were plotted on USGS 7-1/2-min (1:24,000) topographic base maps of the area, and numerous detailed cross sections were constructed. A final geologic map was then constructed on a composite USGS 7-1/2-min topographic map after a detailed review and determination of the photographic, boring, and geologic data were completed.

83. Although former geological studies relating to the specific study area were lacking, those of southern Louisiana have contributed much towards the understanding and geological definition of the area (Fisk 1944, Kolb and Van Lopik, 1958, Kolb 1952, Saucier 1963, Fraiser 1967, and Coleman 1976). These works and others along with aerial photographs, topographic maps, and boring data define a complex geological setting along the reach of the river inclusive of the Montz and Bonnet Carre Point sites. Three major depositional environments and their related deposits that were detected are the fluvial environment composed of point bar, chute, natural levee, and crevasse deposits; the paludal environment composed of marsh deposits; and the fluvial-marine environment composed of interdistributary deposits. The horizontal limits of these various deposits are shown in Figure 62. Cross sections A through E given in Figures 63 through 67 show the vertical extent of these deposits. The deposits are discussed below.

Prairie formation

84. The Prairie Formation is a fluvial-marine, Pleistocene deltaic deposit underlying the study area at elevations ranging from -35 to

-45 ft msl. Where the Mississippi River has entrenched into the Pleistocene surface, the Prairie Formation is encountered at elevations ranging from -120 to -160 ft msl. Materials forming this deposit are composed of predominantly clay, silty clay, silt, and minor sand. The Prairie Formation was recognized in borings by such characteristics as stiff to very stiff consistency, dark grey to greenish grey or oxidized tan or yellow color, low water contents, and the presence of calcareous concretions. Borings reaching the Prairie surface throughout the study area encountered only the dark grey to greenish grey colors. The oxidized tan to yellow colors were absent and may have been removed by scour or perhaps these sediments were below the water table during times of lowered sea level thereby protected from oxidation. In either case, it should be noted that the Prairie Formation is a moderately erosion resistant surface. Its presence in the bed and bank of the river has had a significant effect in controlling river migration.

Interdistributary

85. The interdistributary deposit is a fluvial-marine deposit associated with the middle to late stage of deltaic advance. As the sediment-charged river water first enters the open water of the sea, coarse materials fall out of suspension because of the decrease in the river's velocity and consequent diminish ability to transport material. At the mouth of the river subaqueous bars are formed, and above-water natural levees are formed later. Numerous distributary channels are formed from the main channel with continuous seaward advancement of the river's mouth. Low regions develop between these distributary channels and the main channel into which is carried silt and clay burdened distributary overflows which build the interdistributary deposit. These overflows are especially frequent in the spring of the year when the natural levees flanking the distributaries are crested. The interdistributary deposit may later be reworked by tidal or wind driven currents since these low areas are often open to the sea or connected by small tidal channels.

86. The interdistributary deposit underlying the study area was probably deposited when the Cocodrie delta complex was active (Figure 61). This deposit is generally between 40 and 50 ft thick and overlies the Prairie Formation. The upper surface of the interdistributary unit ranges between 0 and 5 ft msl. The sediments comprising it are clay, silty clay, sandy clay, silt, and minor lenses of sand. The interdistributary unit was recognized in

borings by characteristics such as grey to dark grey color, moderate water content, soft to medium consistency, and the presence of a basal zone of shell fragments.

Point bar

87. The point bar deposit is the most distinct and easily recognized deposit of the fluvial environment. It is a lateral accretion deposit formed by the fluvial scouring of sediments from the outside bank (cut bank) of a river with subsequent deposition of those sediments on an inside bend at some point downstream, usually within the next two bends (Kolb 1962). The process of erosion and deposition causes a lateral and down-valley growth of sand bars along the inside bends of the river. The lateral growth of these bars can be clearly seen in aerial photographs as evidenced by a series of arcuate lineations reflecting ridges (former active bars) and swales (troughs between adjacent bars). The vertical thickness of point bar deposits is controlled by the depth of the river. The vertical distribution of sediments in point bar deposits is generally a progressive fining upward sequence from coarse-grained (sand) to fine-grained (silt and clay). The typical point bar deposit of the deltaic plain is approximately 70 percent well sorted (poorly graded) sand and silty sand, and 30 percent silt and clay according to Kolb (1962).

88. Three regions of point bar deposition were defined in the study area (Figure 62). The areal extent of these deposits varies from one-quarter to a half mile in width and several miles in length. The total area of point bar deposition is approximately 20 percent of the mapped area in Figure 62. The point bar deposits cut into the Pleistocene Prairie Formation and range from 80 to 160 ft in thickness as shown by the cross sections of Figures 63 through 67. The upper boundary of these deposits is at the base of the natural levee near elevation zero msl.

89. Point bar deposits varied in composition among the three locations. As noted earlier by Kolb (1962), the point bar deposited at LaPlace (opposite bank from Bonnet Carre Point site) is predominantly a thick fine-grained sequence of silt and clay over a smaller and less defined coarse-grained sequence of well-sorted (poorly graded) sand as seen in cross section B-B' of Figure 64. Although this sequence is unusual because it is mostly composed of fine-grained soils, aerial photographs and past hydrographic surveys confirm it as point bar. A similar sequence occurs near Killona as shown in cross section D-D' of Figure 66.

90. The point bar deposits at Bonnet Carre Point (cross section C-C', Figure 65) and Montz (cross sections A-A', B-B' and E-E', Figures 63, 64, and 67, respectively) are in total contrast to those described. The typical depositional pattern is exhibited with a thick basal sequence consisting of predominantly well-sorted sand and silty sand, overlain by a thin top stratum of mostly silt and clay. The division between the top stratum and the basal sequence (substratum) at both sites is indicated by the wavy dashed lines on the above sections. This division between the different soil types (i.e., fine-grained versus coarse-grained) indicated another fluvial deposit is present at Montz which is closely associated with the point bar deposit and tentatively identified as a chute.

Chute

91. The identification of a chute deposit at Montz is based on three factors: (a) the thick wedge of fine-grained soils (silt and clay) "intruding" or dividing otherwise uniform sandy substratum, (b) the sharp and distinct change in lithology passing laterally and the narrow channel-like appearance of the feature, and (c) the less defined but moderately thick downstream end of the chute as shown in cross section B-B' (Figure 64). The buried chute ranges from 1,000 to 1,500 ft in width. The depth of the chute extends to a minimum elevation of minus 130 ft msl at the upstream end and gradually pinches out at a minimum elevation of minus 35 ft msl at the downstream end. The chute is composed of silt and clay with minor lenses of sand.

92. Chute formation occurs during flood stage when the increased volume of water exceeds the capacity of the river channel. A portion of the flow is diverted across the point bar perhaps between adjacent ridges, scouring a temporary channel. This same process forms natural cutoffs of large meander loops, with the chute becoming the main channel and leaving the abandoned loop to become an oxbow lake. Chutes serving as temporary extreme high water flow channels may be eventually filled by cycles of overbank deposition during lesser high waters which do not keep the chute cleaned, and fine-grained materials settle out after each cycle of the river receding within its normal banks.

Natural levee and crevasse

93. Natural levee and crevasse deposits are mapped as a single unit in Figures 63 through 67 since it is not necessary for the purposes of this study to separate the two. The natural levee deposits are long, gently sloping, low

ridges or embankments flanking (paralleling) both sides of the main channel. Natural levees are formed by overbank deposition of materials onto the river's floodplain in times of high water. In general, the coarsest soils (sands and silts) are deposited near the river, and the fine-grained clays are carried some distance landward away from the river.

94. Crevasse deposits are formed by overbank deposition during high water when openings or cracks form in the natural levee and spill floodwaters onto the river's floodplain. Fine sands are deposited in a fan-shaped pattern away from the point of opening or breach of the natural levee, and the finer-grained soils (silts and clays) are carried to the distal portion of the fan. Evidence of crevassing is visible on aerial photographs and topographic maps of the eastern portion of the study are where numerous long, linear, easterly trending topographic highs are seen. Historically, the study area has been inundated by numerous crevasse flows spilling into Lake Pontchartrain to the east. The left descending bank in recent times has experienced several flows between river mile 131.0 to 133.3 AHP during 1849, 1857, 1867, 1871, 1874, and 1882. The right descending bank has experienced only one crevasse flow in recent times at river mile 130.5 AHP in 1912.

95. Natural levee deposits in the study region range from 1 to 3 miles in width and generally parallel the 5-ft msl topographic contour interval. Crevasse deposits are predominantly confined to the eastern portion of the study region and extend to Lake Pontchartrain several miles to the east. These deposits are from brown to grey in color and consist of sands, silty sands, silts, silty clays, and clays. Roots were generally present throughout the deposits which ranged in thickness from a few feet to 20 ft.

Marsh

96. Marsh deposits were found in the southwest corner of the study area (Figure 62). Boring MS-25 of Figure 63 contained a thin zone of organic material beneath the natural levee deposit. Marsh deposits are recognized by their high organic and water contents. The marsh region in the southwest corner of the study area was identified from aerial photographs and topographic maps. Materials forming this deposit are organic clays and silty clays.

River Migration and Failure Development

97. Past hydrographic surveys for the reach of the Mississippi River under study were obtained from the MRC files. The periods 1894 (earliest survey available), 1937, 1962, and the latest 1975 hydrographic surveys (scale of 1:20,000) were examined and the various periods compared to define the recent historical changes within the study area and the development of each failure site.

98. This investigation is divided into two parts: total development of the river reach under study and development at each site. Transparent overlays were prepared from the hydrographic surveys and bank lines established from low water reference plane (LWRP) or reach Mean Stage of Water (MSW) or average low water plane (ALWP) of the older surveys. The stages represented by these terms are taken as equivalent for the purposes of establishing bank lines since they fall within a 5-ft range in elevation. The overlays were compared and acreages of deposition or erosion determined with an electronic planimeter.

Bank lines and thalweg movement

99. Bank line movement is compared from the 1975 (latest hydrographic survey) to the 1962, 1937, and 1894 surveys. The reach of the river was expanded to allow for a greater accuracy in comparison of measured acreages of erosion/deposition between surveys. Bank line movement from 1962 to 1975 is shown in Figure 68 and reveals that erosion was the dominant process removing 181 acres, and deposition added only 13 acres. Figure 69 shows bank line movement from 1937 to 1975. Over this 38 year period deposition was the dominant process adding 492 acres, and erosion removed 392 acres. Figure 70 shows bank line movement from 1894 to 1975 which indicated deposition as the dominant process adding 1,107 acres, and erosion removed 1,026 acres. A ratio of erosion rate to deposition rate of 0.93 was calculated from 1894 to 1975, indicating a near-equilibrium state between the two. Figures 68 through 70 also reveal that bank line movement at the Bonnet Carre Point site has been continuously in a southerly direction, and the Montz site has been in a continuously southeasterly direction.

100. The position of the thalweg (deepest point of the stream at any given location) has remained constant with respect to each bank for the periods indicated. Figure 71 shows thalweg profiles for the years 1937, 1962, and

1975. Over the 38-year period covered by the three profiles, there has been no major change. In fact, overlaying the various thalweg profiles and calculating the erosion to deposition rates (as was done for the bank line movements) yield the conclusion of no major changes as evident in Figure 72. Examining the 1894 (thalweg profile not shown in Figure 71) to 1975 period shows that deposition was the dominant process with approximately 12.5 acres accreting and only 5.5 acres eroding. The 7.0 acre difference is roughly equivalent to a 550-ft square area over a total reach of river in excess of 10 miles.

Characteristics of Failure Site Development

Bonnet Carre Point failure

101. The characteristics of the Bonnet Carre Point failure site for the periods 1894, 1937, 1972, and 1975 are shown in Figure 73 where the scour pool is outlined on the basis of the minus 80 ft msl contour. The size, shape, depth, and position with respect to the top of the bank of the pool are relatively unchanged over the 81-year period of record, but it has moved in a southerly direction approximately 1,500 ft as the bank has been eroded.

102. Three hydrographic river profiles pertaining to the Bonnet Carre Point failure site are shown in Figures 74 and 75 for each of the periods 1894 and 1975, respectively. Profiles directly upstream of the failure, at the approximate center of the failure, and directly downstream are consistent between the two survey periods except for an approximate 17 percent decrease in channel width. The position of the thalweg with respect to each profile location has remained unchanged. Profiles for each period show a steep slope directly upstream of the failure location, a moderate slope at the failure location, and a steep slope (but less than that upstream) downstream. The 1975 set of profiles (Figure 75) reflects the same trend in bank slopes and a hummocky appearance to the profile through the failure which may be because of slumping associated with additional bank failure.

Montz failure

103. The characteristics of the Montz failure site for 1894, 1937, 1962, and 1975 are shown in Figure 76 where the scour pool outline is based on the minus 110 ft msl contour. The Montz scour pool has moved in a southeasterly direction some 3,500 ft over the 81-year period of record. Scour pool size

has steadily decreased through the years, but its shape (a wide and irregular crescent upstream tapering to a narrow crescent downstream) has been maintained. Variation in scour pool depth has been more irregular with a dramatic filling of the pool indicated between the 1963 and 1975 surveys.

104. Three hydrographic profiles of the river pertinent to the Montz failure site are shown in Figures 77 and 78 for the survey periods 1894 and 1975, respectively. The profiles were selected at a point slightly upstream of the failure location, within the failure location, and slightly downstream. The profiles are consistent over the period of record in that a narrow channel with steep sloping left bank is seen in the upstream profile, narrow channel and slightly less steep left bank slope in the downstream profile, and a wide channel and moderate left bank slope in the profile through the failure location. The overall position of the thalweg has remained unchanged with respect to each particular profile location over the 81-year period. The channel cross-sectional area has remained approximately the same between periods, indicating a balance between erosion and deposition.

Addendum note by Torrey

105. Interestingly, the Montz scour regime is exceptionally large as seen by the "bulge" in both top bank lines (see Figure 7). This anomaly is seen elsewhere below Baton Rouge, along the 48 Mile Point reach (below Angelina revetment). This may be attributed to the river passing from a scour resistant pleistocene bed into deep, more erodible point bar soils. At Montz, (see cross section D-D', Figure 66) a very steep "scarp" is implied in the Pleistocene surface at the transition. It is not known how the displacement occurred in the pleistocene elevation (i.e., whether it is an ancient scour hole or by faulting). The opposite bank from the Montz site has receded but probably not by flow sliding because the point bar deposits on that side do not consist of significant Zone A sands. In any case, the enlarged scour pattern brings to mind such pools formed off the downstream end of hydraulic structures' stilling basin slabs where the water flows from a highly scour resistant surface into erodible material.

PART V: HYDROGRAPHIC SURVEYS ALONG FOUR POINT BAR REACHES, 1979

106. In 1979, 16 hydrographic surveys were conducted along four point bar bank reaches below Baton Rouge, LA (two unrevetted and two revetted). The surveys were considered susceptible to flow failure by the empirical criteria and encompassed upstream inside of bendway locations subject to particularly severe river attack (Torrey and Strohm 1976). This work element was to begin some attempt to assess river attack on point bar deposits. The studies previously presented in Part IV have shown that attack is indeed intense over the last 81 years at the Montz and Bonnet Carre Point sites. The surveys were conducted by a contractor through the NOD. Four surveys were performed along each of the four reaches using the same layout of ranges for each reach for each survey. The original intent was to survey each reach on the rise of the river just before crest, just after crest, intermediate on the fall, and at low water. In actuality, because the river did not follow a usual seasonal pattern and because of other unavoidable difficulties, the first surveys occurred just after crest stage, and the three remaining surveys were performed during a protracted, slow falling stage. The final survey was ordered in November since the river had never reached typical low stages that are usually seen in August. The survey reaches shown in Figures 79 through 82 were as follows:

a. Eighty-One Mile Point, left descending bank, approximate river mile 180.0, levee baseline sta 2535+45 to 2610+00, unrevetted.

b. Forty-Eight Mile Point, left descending bank, approximate river mile 143.0, levee baseline sta 4473+00 to 4505+00, unrevetted.

c. Bonnet Carre Point, right descending bank, approximate river mile 134.5, levee baseline sta 2190+00 to 2220+00, Lucy revetment.

d. Montz, left descending bank, approximate river mile 134.5, levee baseline sta 180+00 to 205+00, Montz revetment.

The survey results are given in Appendix O in the form of contour maps.

107. It is proper to concede comprehensive assessment of the significance of the surveys to LMVD. However, some interesting observations are made in overview below:

a. All of the bank reaches suffered localized failures. For example, beginning with the June survey of 81 Mile Point, a failure can be seen centered on sta 2592+00. It continued to

enlarge through the final November survey and reached proportions of about 600 ft in maximum width parallel to the bank, about 400 ft into the bank, and a depth of about 60 ft. It has the appearance of a flow failure. In addition, between August and November surveys, a significant deposition of material developed at the upstream limit of the failure. This deposit, from above sta 2586+00 to sta 2588+00, is of interest because of the height and steepness of its riverward face as shown in Figure 83. It is hard to imagine a slope averaging 2V on 1H and 50 ft in height, but this is shown in the sections. Since the material was placed over a period of 3-1/2 months or less, it is reasonable to assume it to be sand. Was the face retrogressing after the mechanism to be described in Part VI? This is a provocative question without a documented answer.

b. Looking through the 48 Mile Point surveys, the encroachment of the "permanent" scour pool into the bank between sta 4475+00 and 4490+00 is seen. However, no major bank failure is shown.

c. At Bonnet Carre Point, very confined, trench-like bank loss is seen at about sta 2203+00 through the period of surveys. Encroachment of the scour pool is at best very subtle. Subsequent revetment surveys should be examined to see if the trench is run out of material from beneath the revetment mattress.

d. The interesting point about the Montz surveys is the development of the typical scour hole at the downstream end of the revetment mattress. The June survey shows the development of a very localized scour hole precisely at the end of mattress accompanied by the beginnings of bank loss. The November survey shows additional bank loss. As the authors remember, it was a year later during low water that a very large bank failure with the earmarks of a flow slide occurred at this location.

e. Along all survey reaches, the August surveys show the deepest scour pools.

f. The surveys do show bank slopes in sands between 1V on 1H and 1V on 2H. These slopes, if angles of repose, would correspond to effective angles of internal friction of from 32 to 36 deg obtained from the Montz and Bonnet Carre Point undisturbed triaxial specimens. The hydrographic sections in Part IV (Figures 74 through 78) also indicate such slopes.

PART VI: FLOW FAILURE MECHANISM

General

108. The field and laboratory investigations have shown that the substratum sands of both Montz and Bonnet Carre Point sites are, in general, medium to dense in situ. Only one apparent loose lense with a thickness less than a foot was detected by the Delft resistivity probe at Bonnet Carre Point. These findings are consistent with those of earlier investigations. Dr. Hvorslev (1956) summarized these studies in Report 12-5 as follows:

> Sand strata or lenses of subcritical density do exist, but the extent of such very loose deposits is small compared to the volume of displaced materials in major bank failures, and it is again emphasized that the average density of Zone A sands is between the upper and lower critical densities.

The reference to "upper" and "lower" critical densities pertains to results of drained triaxial tests after the method of Geuze (1948) illustrated in Figure 84. The lower critical density (upper critical void ratio) is represented by a limiting minimum density which is approached by very loose sands undergoing compaction (contraction) during and after failure. This value would roughly correspond to the "critical" void ratio as is currently determined by undrained triaxial tests. The upper critical density (lower critical void ratio) is represented by the density of a test specimen which does not undergo change in volume under relatively small shear strain. Therefore, the upper critical density would correspond to the density at which the initial response of a specimen under undrained loading would be neither dilation or contraction. However, even sands above 50 percent relative density will exhibit initial positive induced pore pressures followed by negative pore pressure as the Montz and Bonnet Carre Point undisturbed triaxial specimens did. The upper critical density would then be quite high indeed. Densities between the lower and upper critical values would correspond to a tendency to dilate under undrained loading.

109. The Reid Bedford bank reach, pictured in the aerial photograph (taken in 1977) in Figure 85, leaves little doubt that, whatever the mechanism of flow failures, it reflects general conditions rather than isolated pockets or lenses. This bank reach is perhaps that most thoroughly investigated point

bar deposit of record. The SPT data (US Army Engineer Waterways Experiment Station 1950b) from this reach do not reveal regular implications of loose sands. Furthermore, the failures have apparently encroached upon and taken the very locations of some of these SPT borings. Later sampling with the Hvorslev fixed-piston sampler (US Army Engineer Waterways Experiment Station 1948, 1950a) coupled with maximum/minimum laboratory tests placed the relative densities of the Reid Bedford sands as well as those of other sites above 50 percent (corrected for sampling disturbance). Undrained triaxial tests by Durham (1971), checked by the authors, revealed that a representative Reid Bedford gradation would not liquefy in the laboratory at relative density (CE procedures for maximum/minimum) at or above about 11 percent even under a confining pressure as high as 4 tsf. The depths of the many flow failures along the Reid Bedford reach have generally been less than 60 ft which corresponds to a maximum effective confining pressure at bank-full river stage of less than 1 tsf (taking K_o of 0.5). Such low confining pressure would dictate relative densities below about 5 percent to produce laboratory liquefaction of Reid Bedford sand. Even if it was contended that some special considerations of sand fabric in situ or severe sample disturbance, or laboratory specimen preparation techniques, etc., would force the in situ critical void ratio curve higher in relative densities, there seems to be no reason to expect that the large differences between liquefaction susceptibility and apparent in situ conditions relative to the Reid Bedford reach could ever be reconciled to support liquefaction as the likely failure mechanism.

110. If the liquefaction is not the mechanism, then what may it be? The answer may lie in the work of Padfield (1978). His final technical report (and PhD dissertation) submitted to the European Research Office, Corps of Engineers, specifically addresses the Mississippi Riverbank flow slide problem. He presents results of centrifuge model studies of overburden (top stratum) behavior and numerically analyzes the retrogression of a steep, subaqueous slope dilatant sand. The majority of the remainder of this part consists of portions of Padfield's work.

Behavior of the Overburden

Arching

111. Arching is the mechanism whereby load may be taken in a structure by compressive stresses alone without bending or tension (Figure 86). A masonry arch is a useful example. Consider the flat arch in Figure 86a. If the material is stiff with infinite compressive strength and the abutments remain fixed, there is no limit to the load which may be applied to the span because the line of thrust will always lie within the masonry. This is in contrast to the high arch of Figure 86b for which failure will occur when the only possible line of thrust touches the external surface of the arch at three or more points.

112. By extension of these concepts, a concave masonry arch such as that shown in Figure 86c can support the applied load if the line of thrust lies within the masonry. In this case, such a shallow line of thrust would require high abutment reactions and large compressive stresses in the upper portion of the arch at midspan.

113. Consider the deformation of a two-dimensional clay beam (Figure 87) since this is simpler than the deformation of a plate and also leads to conservative answers. Figure 87a shows half a span of a clay beam deformed into a shape similar to that shown in Figure 86c, in which the line of thrust touches the surface of the beam at the abutments and at midspan. The horizontal reaction can be calculated by taking moments about D to yield:

$$H = \frac{Wa}{2(h - \delta)} \tag{1}$$

which will produce a stress distribution in the beam at the abutments (similar at midspan) as shown in Figure 87b. If the material is regarded as elastic, the neutral axis of the beam is two-thirds of its thickness up from its base. By way of approximation to the behavior of the clay, the stress distribution (Figure 87c) may be substituted which gives the same moment about the neutral axis when:

$$\sigma_H = \frac{3Wa}{2h(h - \delta)} \tag{2}$$

where σ_H is a passive reaction stress. Padfield confirmed the feasibility of the above equation using centrifuge models in which support was removed from beneath clay layers upon sand by opening a trapdoor beneath the sand during flight of the models. At the end of the test, he could then measure δ/h and half-span, a . The centrifuging of models at different gravity (g) forces simulated different prototype thicknesses of clay.

114. Padfield also included in his report example computations of maximum clay top stratum arching spans (2a) in the field by substituting an assumed undrained strength, c_u , for σ_H in the above equation. However, σ_H would appear to be more properly taken as the passive pressure required to mobilize c_u . To do this, the following expedient and simplifying assumptions are made:

a. The top stratum is entirely of clay which is normally consolidated with a strength to depth profile equivalent to $c_u/P = 0.24$ ($c = 0$, $\phi = 13.5$ deg). The assumption of normal consolidation is expedient since an overconsolidated and stronger surface layer is not uncommon.

b. In the submerged case, i.e., buoyant unit weight used to calculate top stratum weight, the undrained strength profile remains as in a. above.

From Figure 88, the approximate value of σ_H (realizing difference between Mohr circle point of tangency and peak shear stress, i.e., Q strength, which is negligible for small ϕ) required to mobilize c_u at depth 1/3 h would be 1,610 psf and at the base of the top stratum, 4,824 psf. An average value of $\sigma_H = 3{,}217$ psf is adopted. Taking this value for σ_H , the plots of δ/h versus maximum stable span, 2a, of Figure 89 can be generated. Assuming that the river falls to a level below the top stratum, the maximum stable span decreases simply because the weight of the span increases from its buoyant value to its saturated weight. Therefore, if one were observing failure, it might appear to be by classical drawdown when in actuality there existed a cavity under the submerged or partially submerged top stratum, and it collapsed into the cavity upon loss of ability to arch as its effective self-weight increased.

115. If (as seems likely) the underlying sand supports the majority of the weight of the top stratum as it deforms intact, larger total spans are plausible up to δ/h of 0.7. If, however, deformation resulting from loss of

underlying sand proceeds so far, there is no further possibility of arching, and the top stratum will break away around the edges of the depression.

Interpretation of field events

116. Figure 90 shows the correlation of behavior which led to the WES empirical criteria for determining riverbank stability with respect to flow failure. If the thickness of Zone A sand is assumed to represent the maximum top stratum deformation, δ, then the empirical evidence is consistent with the above discussion and indicates that stratigraphies which are stable have δ/h, (A/O), less than 0.7. Cases designated unstable would correspond to δ/h, (A/O), of 1.2 or greater for which the clay (Figure 91) will break away and be borne away as shown in Figure 91a. There is no possibility of arching in this range. Between these two definite extremes, there is a transition region where the nature of the failure would depend on site conditions.

117. It seems likely that in stable cases the clay will indeed collapse, following and being largely supported by the sand but will inhibit the flow of sand (Figure 91b). The clay will remain in place folded down into the crater and attached at the edges when the crater has developed to its full width. Less sand will flow away in this case than if the clay were not present. The failure may be interpreted as a shear failure.

118. Very little is known from field observations concerning how an overburden layer might restrict the flow of an underlying liquefied sand layer. However, the mechanisms proposed in this section help to answer one further question concerning Mississippi River flow slides. It becomes possible to understand why a flow slide, one initiated, is brought to a halt. Consider the initiation of a slide where $O/A = 0.2$. The slide will expand with blocks of overburden breaking off and riding away upon the sand. As the slide retrogresses, the base of the failure climbs up through the sand layer progressively reducing the depth of sand involved in the failure and thereby increasing the effective ratio O/A or decreasing the equivalent δ/h. The flow slide will stabilize when O/A becomes greater than about 0.85 at the active face.

Liquefaction and Flow of Sand

Introduction

119. Two aspects of this phenomenon are discussed: the initiation of liquefaction in a previously stable deposit and how the flowing sand suspension maintains itself in motion. The first part of this discussion argues that the sand can come into motion and leave a scar similar to the flow slide scars observed along the lower Mississippi even if it is densely packed in the deposit. The second part of the argument develops an analysis which, within the limitations of the assumptions made, accounts for the transportation away from the failure of any sand that starts to flow.

120. The discussion below deals in detail with the process of liquefied flow and flow initiation. The moderating influence of the clay overburden layer is not included in the analyses, although the results obtained are expected to be modified if an overburden is present.

Spontaneous liquefaction.

121. As previously mentioned, a sand layer may be induced to liquefy as a result of the deformation involved in failure or, conversely, a slope may fail as a result of spontaneous propagation of liquefaction within the stratum. In either case, it is possible to achieve an understanding (in terms of soil mechanics) of the process involved up to the point where the sand becomes liquefied and viscous deformations begin.

122. For a horizontal sand layer, consider the initial disturbance of equilibrium to be caused by an oversteepening or removal of support from the toe of the slope. Consider a mass of soil behind a retaining wall as shown in Figure 92. If support to the soil from the wall is steadily reduced, the horizontal stress on an element of soil close to the wall decreases. This change of stress state rotates the planes of maximum shear and increases the deviator stress, q. The same process occurs when a sand layer is steepened because of erosion of a scour hole. The soil is loaded in shear, possible to failure.

123. Examine the stress-strain properties of sands under this loading. The plots shown in Figure 93 are experimental results obtained by Castro (1969) from undrained stress-controlled triaxial tests on two sand specimens. Specimen a was loose, and specimen b was dense at the start of the test. Specimen b behaved stably with deviator stress increasing with axial strain. The induced pore pressures were initially positive but became negative with

increasing axial strain. The loose specimen, a, behaved unstably exhibiting increasing positive pore pressure with strain up to a peak deviator stress followed by rapid collapse of the specimen and further increase in pore water pressure. Castro described this phenomenon as liquefaction.

124. By this mechanism of structural collapse, loose sand layers are postulated to have liquefied along the Dutch coast, (Koppejan and VanWamelan 1948) and on the continental slope (Morgenstern 1967), but it is not self-evident that the failures on the Mississippi are of this type. It is by no means proven that the susceptible sand layers of the Mississippi River banks are to be found in a very loose condition. Very few failures have been observed during the flow failure process itself. The top of the bank is submerged at the time and it is only as the water recedes that a failure becomes evident. In fact, available evidence suggests that mid to higher range relative densities are to be expected. The evidence from the Montz and Wilkinson Point failures implies a process of retrogression of the failure over perhaps 12 hr. This relatively extended mechanism indicates that the process may be one of failure before liquefaction which is discussed in the following section. It is not a spontaneous liquefaction at all.

Retrogressive liquefaction

125. Denner and James (1977) performed a series of small scale tests on the retrogression of an unsupported subaqueous face of dense, fine sand. They found that an artificially induced steep face is able to retrogress stably in dense sand, maintaining the steepness of the face itself. In most cases the height of the face diminished steadily (Figure 94) because of the fact that the base of the face climbed up at an angle to the horizontal (because of deposition of sand at its base) and eventually intersected the top surface. They also found that the phenomenon of retrogression did not occur at all for a loose sand deposit. The unsupported face of loose sand slumps to an angle of repose, and no retrogression ensues.

126. Meijer and Van Os (1976) report larger scale experiments and theoretical work on the same topic (Figure 95). In this case a suction dredge (Figure 95a) moves steadily along the x' axis, removing the material which flows off a steep subaqueous face of dense, fine sand. They studied the magnitudes of the negative pore pressures that are developed within the sand and serve to sustain the face. They showed that the dominant feature is the dilation induced by shear of the dense sand. As the base of the steep slope

advances on an element of soil, P , (see Figure 95b) the shear stress on the element increases. The element develops negative pore pressures which are sufficient to hold up the slope.

127. The first part of the analysis that follows is derived from that presented by Meijer and Van Os (1976). Thereafter, a suggestion from Denner and James (1977) is worked into the calculation to derive a new analysis of the retrogression of a steep unsupported face in dense sand. In later paragraphs this analysis is combined with equations which describe the flow of the liquefied sand away from the face to develop a comprehensive new explanation of the phenomenon of the Mississippi River flow slides.

128. Consider the two coordinate systems of Figure 95b which describe the steady state retrogression of the face at velocity Z. Diffusion of pore water into the sand body in terms of stationary (x', y) frame of reference is described by:

$$\frac{\partial^2 u}{\partial x'^2} = -\frac{\gamma_w m_{vc}}{k}\left(\frac{\partial u}{\partial t}\right) = -\frac{-\gamma_w}{(1 + e_c)k}\left(\frac{\partial e}{\partial t}\right) = \frac{-\gamma_w}{k}\left(\frac{\partial v'}{\partial t}\right) \qquad (3)$$

where

u = pore water pressure

m_{vc} = coefficient of volume compressibility

k = coefficient of permeability

γ_w = density of water

e = void ratio

$v' = v/v_o$, volumetric strain

A transformation from the stationary (x', y) frame to the moving (x, y) frame of reference requires that derivatives with respect to x' be replaced by those with respect to x ; derivatives with respect to y remain unchanged and the differential quotient for (x' y = constant) becomes

$$\frac{\partial}{\partial t}(x', y = \text{constant}) = \frac{\partial}{\partial t}(x, y = \text{constant}) - Z\left(\frac{\partial}{\partial x}\right) \qquad (4)$$

where

$$x = x' - Zt \qquad (5)$$

Diffusion of pore water into the dilating sand body for any element P moving with the reference frame is now described by

$$\frac{\partial^2 u}{\partial x^2} = -\frac{\gamma_w}{k}\left(\frac{\partial v'}{\partial t} - \frac{Z\partial v'}{\partial x}\right) \tag{6}$$

Under steady state conditions when element P moves at velocity Z with the retrogressive face, $\partial v'/\partial t = 0$ and

$$\frac{\partial^2 u}{\partial x^2} = \frac{\gamma_w Z}{k}\left(\frac{\partial v'}{\partial x}\right) \tag{7}$$

Equation 7 no longer describes a time dependent diffusion problem. The transformation has resulted in a steady state boundary value problem which for the purposes of the present analysis can be integrated to give

$$\frac{\partial u}{\partial x} = \frac{\gamma_w Z}{k}(v') \tag{8}$$

where

$$Z = \frac{ki}{v'} \tag{9}$$

where $i = du/dx$ is the hydraulic gradient horizontally into the face.

129. The analysis may be further simplified by using an equation derived by Bernatzik (1947) who points out that a simple triangle of forces as shown in Figure 96 yields the following relation for seepage into a slope for the condition of limiting equilibrium

$$\frac{\gamma_w i}{\sin(\beta - \phi)} = \frac{\gamma'}{\sin \phi} \tag{10}$$

$$i = \frac{\gamma'}{w}\left[\frac{\sin(\beta - \phi)}{\sin \phi}\right] \tag{11}$$

where ϕ is the angle of internal friction. The experimental validity of this relationship has been demonstrated by Bernatizik. We can observe the stable angle β from experiments and require only a value for v' for a determination of Z in Equation 9. If we estimate like values for e in the undisturbed bed and at the free face to be 0.67 and 0.75, respectively, the volumetric strain becomes $v' = 0.048$ and hence the velocity of retrogression of the face may be calculated from Equations 9 and 11 to give

$$Z = \frac{k\gamma'}{0.048\gamma_w}\left[\frac{\sin(\beta - \phi)}{\sin\phi}\right] \tag{12}$$

Z depends chiefly on the particle size distribution and packing, not on the height of the slope.

130. It is possible to check this by doing a back analysis on the data given by Meijer and Van Os. Using their experimental values for $\beta \approx 80$ deg, $\gamma'/\gamma_w = 0.6$, $k = 0.15$ mm/sec, and $\phi = 30$ deg, Equation 3 yields $Z = 0.29$ cm/sec. The actual value of Z in the experiments was 0.5 cm/sec. The two values are in fairly close agreement, but this agreement depends entirely on the values chosen for e and hence the value of v'.

Prediction of flow properties

131. In the previous section an expression was developed which predicts the rate of regression of a steep face in dense sand. The material which falls off the face in the experiments is expected to flow for a short way before coming to rest. In this section the flow away from the face will be quantified, and the two analyses will be related to each other in Paragraph 148.

132. Numerous studies (Bagnold 1943, Happel and Brenner 1965, Clarke 1967, and Davidson and Harrison 1963) have shown that a dispersion of solid particles in water may be treated as a viscous liquid. At low rates of shear, there is little evidence of viscous dilatancy, although at higher shear rates, the viscosity is found to increase, and eventually at high Reynolds numbers the process must be treated as turbulent flow. A fully liquefied sand bed is a concentrated dispersion which resediments from the bottom upwards, but the portion of the bed which is mobile is able to flow for a limited time as a viscous fluid under the action of gravity. If the bed is only partially liquefied, a component of frictional resistance modifies the viscous behavior.

133. An analysis presented by Allen and Banks address the shear deformations induced in liquefied layers of sand by surficial current drag. In the analysis presented in this section, the loading in shear is gravitational. Several assumptions are made in the analysis. The gravitational loading has been lumped for simplicity into a concentrated load on the surface of the layer. Furthermore, the simplifying assumptions have been made that the flow is laminar and displays a linear velocity gradient with depth. The latter assumption leads to an overestimate of the distance traveled by the uppermost grains.

134. Figure 97 shows the liquefied bed incline at an angle α to the horizontal. The total initial depth of the bed perpendicular to the slope is H_o, and h is the instantaneous depth from the top surface of the bed to the upward moving surface of resedimentation. The thickness of the bed is steadily decreasing: the upper surface is moving downwards with a velocity W_d, the fall velocity of the grain aggregate takes with it the coordinate axis x,y. The particle volume concentration in the dispersion and the deposit (Figure 97) are C_o and C_1, respectively
where

$$C = \frac{1}{1 + e} \tag{13}$$

135. The surface resedimentation is moving upwards with respect to stationary axes (x,y) (Figure 98) at velocity V. The resedimentation of a fine sand dispersion obeys the equation of Richardson and Zaki (1954):

$$W_d = W_\infty (1 - C_o)^n \tag{14}$$

where

W_d = the fall velocity of the grain at concentration C_o
W_∞ = the fall velocity at infinite dilution
n = 4 for the present purposes

Relative to the coordinate axes (x,y) that are descending with the upper most grains, the surface of redeposition is moving upwards with velocity $(V + W_d)$. Therefore, in 1 sec $(V + W_d)C_o$ grains land on the surface. The velocity of

accretion of the surface of redeposition is then, with respect to the fixed coordinate axes (x,y)

$$V = \frac{(V + W_d)C_o}{C_1} \tag{15}$$

and hence

$$V = \frac{C_o W_d}{(C_1 - C_o)} = \frac{C_o W_d}{\Delta C} = \frac{C_o W_\infty (1 - C_o)^n}{\Delta C} \tag{16}$$

The length of time taken for the layer to resediment completely is then given in Equations 14 and 16 as

$$T = \frac{H_o}{V} = \frac{\Delta C H_o}{W_\infty C_1 (1 - C_o)^n} \tag{17}$$

Experimental values of T/H_o are given in the tabulation below. These values were obtained by Lowe (1976) for the resedimentation of liquefied beds of uniform glass spheres in salt water for which $C_o = 0.54$ and $C_1 = 0.60$.

Grain Diameter $\times 10^{-3}$ mm	$\frac{\text{Resedimentation Time}}{\text{Bed Thickness}} = \frac{T}{H}$ $\frac{\text{sec}}{\text{mm}}$
0.062	1.19
0.125	0.27
0.25	0.071
0.50	0.026
1.0	0.011
2.0	0.006

136. The use of these sedimentation equations represents a slight departure from normal soil mechanics practice which often uses the initial value diffusion equations. The sedimentation is a steady state process involving a linear pressure gradient and constant fluid velocity through the depth of the suspension. The diffusion equations are not involved.

137. In order to calculate the distance traveled by the flowing sand layer before it resediments, it is necessary to write the equations of equilibrium and continuity for the layer. The two coordinate systems will again be used, the moving coordinate reference frame (x,y) on the descending upper surface of the layer and (x,y) on the fixed lower boundary (Figures 97 and 98). The assumption of linear velocity gradient is shown in

$$a \text{ (at depth Y)} = a\ (Y) = A \left(1 - \frac{Y}{h}\right) \tag{18}$$

where h is the current thickness of the flowing layer.

138. The shear stress within the flowing layer is assumed to be constant over the full depth. This derives from the simplifying assumption discussed above which states that gravitational stress is lumped on the surface of the layer. The shear stress is

$$\tau = h\ \gamma' g \sin \alpha \tag{19}$$

where h is f(time). For viscous flow of the liquefied layer

$$\tau = -\mu \frac{da}{dY} \tag{20}$$

where μ is the viscosity. From Equations 18 and 20

$$a(Y) = \frac{\tau}{\mu} (h - Y) \tag{21}$$

139. Consider the motion of a particle P_o at initial height y_o above the base of the bed in Figure 98. After resedimentation P_o moves to P_1 and the y coordinate of P_1 becomes $y_1 = y_o\ C_o/C_1$, the final depth of the deposit will be $H_1 = H_o\ C_o/C_1$. Equation 21 may be transformed into (x,y) coordinates to obtain

$$a(y_o) = \frac{\tau}{\mu} (h - H_o + y_o) = \frac{h\gamma' g \sin \alpha}{\mu} (h - H_o + y_o) \tag{22}$$

It is possible to relate the value of h to time as follows:

$$h = H_o - t\ (V + W_d) \tag{23}$$

which, substituting Equation 16 becomes

$$h = H_o - t\ W_d \left(\frac{C_o}{\Delta C} + 1\right) \tag{24}$$

where $t = t_o$ at $H = H_o$ and hence Equation 22 becomes

$$a(y_o,t) = \frac{\gamma' g \sin \alpha}{\mu} \left[y_o - t\ W_d \left(\frac{C_o}{\Delta C} + 1\right)\right] \left[H_o - t\ W_d \left(\frac{C_o}{\Delta C} + 1\right)\right] \tag{25}$$

The particle P will come to rest when $d = H_o - y_o$, that is when

$$t = t_1 = \frac{y_o}{W_d \left(\frac{C_o}{\Delta C} + 1\right)} \tag{26}$$

from Equation 24. At this time $t = t_1$, $y = y_1$, and $x = x_o + X$ where

$$X = \int_{t_o}^{t_1} a(y_o, t)\ dt \tag{27}$$

$$= \frac{\gamma' g\ y_o^{\,2} \sin \alpha}{6\mu W_d \left(\frac{C_o}{\Delta C} + 1\right)} (3H_o - y_o) \tag{28}$$

Equation 28 is a general expression for distance traveled by a particle at any depth y_o. The distance traveled by the uppermost layer of grains for $y_o = H_o$ is

$$X = \frac{\gamma' g H_o^3 \sin \alpha}{3\mu W_\infty \left(\frac{C_o}{\Delta C} + 1\right) \left(1 - C_o\right)^n} = \frac{\gamma' g \sin \alpha \, \Delta C}{3\mu C_1 W_\infty \left(1 - C_o\right)^n} H_o^3 \qquad (29)$$

and the average speed of travel of the uppermost grains is

$$\bar{A} = \frac{X}{T} = \frac{\gamma' g H_o^2 \sin \alpha}{3\mu} \qquad (30)$$

The choice of values for these parameters is discussed in Paragraph 149. The values given below are quoted to a high degree of accuracy only for the purposes of that section. The values listed below are intended to be reasonable ones:

$C_1 = 0.590$ ($e_1 = 0.69$)
$C_o = 0.577$ ($e_o = 0.732$)
$\Delta C = 0.013$
$\gamma = 0.58\gamma$
$\alpha = 20$ deg $\sin \alpha = 0.342$
$\mu = 200$ poise (Bagnold 1954, Lowe 1976, Allen and Banks 1972)
$g = 9.81$ m/s^2
$W_\infty = 4 \times 10^{-4}$ m/s for sand of grain diameter 125 μm

where $x = 5{,}470\ H_o^3$ and $\bar{A} = 3.24\ H_o^2$.

140. The flow begins to become turbulent for a Reynolds number greater than 500 or H_o greater than 0.16 m and values of thickness less than $H_o = 0.16$ m . The following flow distances and velocities are obtained:

H_o	X	$\bar{A}$
10 mm	5 mm	0.32 mm/sec
0.1 m	5.47 m	0.0324 m/sec
0.16 m	22 m	0.082 m/sec

141. The sand travels a long way if the layer which starts to flow is thicker than about 100 mm. Velocities of several meters/second have been suggested for turbidity currents much greater than the values derived. The flow

of a liquefied layer can evolve into a turbidity current. If it is accelerated on a steep subaqueous slope, it becomes turbulent and dilates.

142. The development of the flow from rest requires a period of acceleration. Schlichting (1960) found that this steady state condition was developed for all practical purposes once the dimensionless quantity

$$\frac{1}{H}\sqrt{\frac{\mu t}{\gamma}} = 1 \tag{31}$$

where the symbols are previously defined

or

$$t \cong \frac{H^2 \gamma}{\mu} \tag{32}$$

The time may be compared with the time for which the layer remains mobile (Equation 7). The period of acceleration is short for the purposes of this analysis if:

$$\frac{H_o^2 \gamma}{\mu} << \frac{\Delta C H_o}{W_\infty C_1 (1 - C_o)} n \tag{33}$$

143. The inequality in Equation 33 is considered to determine whether the time taken to accelerate the flow is indeed small in comparison with the lifetime of the layer:

If H_o = 10 mm

0.001 sec << 17 A factor of 1,700

If H_o = 1 mm

100 sec << 1,700 A factor of 17

With increasing thickness, the inertial acceleration of the layer becomes more important.

144. It must be stressed that the analysis presented herein is largely speculative and requires substantiation. The analysis can be strengthened by experimental verification of the assumptions which concern viscous deformation and the void ratios involved in the flows. However, the phenomenon may be observed in the laboratory at small scale, and the observations of Allen and Banks (1972) of flow structures in sandstones support the physical possibility of the mechanism hypothesized.

Scaling of flow
behavior in the centrifuge

145. From this analysis, two important points emerge. First, the distance traveled by a liquefied sand layer increases with the cube of the initial layer thickness (Equation 29). The flow process is heavily scale dependent. Thus, a thick layer of Zone A sand will flow further and faster than a thinner layer. Second, the speed of movement of the unsupported face during retrogressive failure in dense sand depends on the permeability and dilatational properties of the deposit. The mass flow rate of material falling off the face varies linearly with the height. Only the flow of material from the base of the face is governed by the cube rule.

146. It should be noted that the analyses presented above are very sensitive to the assumptions made about slope angle and void ratios. In fact, any assumption about void ratio is the governing assumption which is discussed in the following section. The slope angle may be calculated once values have been assumed for the void ratios.

147. From the equation for distance traveled by the uppermost grains in the flowing sand layer (Equation 29), it may be seen that very thin sand layers sediment so rapidly that they are only able to flow a short distance. Even if full liquefaction is achieved in a small scale model, the sand will not flow far, and the effects of the liquefaction may not even be noticed.

148. This point is of fundamental importance in modeling. In Equation 9 for X, the free fall velocity of a particle at infinite dilution, W_∞, varies linearly with $n \times g$. For a sphere falling at terminal velocity under gravity in a viscous fluid, Stokes' law is

$$W_\infty = \frac{1}{12}\left(\frac{D^2 \gamma' g}{\mu}\right) \tag{34}$$

X is in effect independent of g but is extremely dependent on the scale. The centrifuge may be of some use in modeling the flow behavior of reduced scale granular materials, although it may only be useful in the qualitative sense of visualization of failure mechanisms. However, certain aspects of material transport may be scaled by altering the grain size distribution of the granular material. Inspection of the equation shows that the distance X scales linearly if both the layer thickness H_o and the particle diameter D are scaled by the same factor. X is independent of the value of gravitational acceleration, g . However, for other types of processes not dominated by sedimentation, a different scaling factor may be appropriate for D . For example, where diffusion of water pressure and permeability govern the behavior, D may have to be scaled by $1/\sqrt{n}$ if H_o is scaled by $1/n$. The proper scaling factor depends on the process involved by Pokrovski and Fyoderov (1968). The centrifuge may also, in certain circumstances, be required to initiate a flow. It has been suggested that the time scale of a small scale model be extended by increasing the viscosity μ of the fluid phase, but Equation 29 shows that X is also independent of μ since W_∞ varies inversely with μ . It seems that flow phenomena can only be fully reproduced at full scale.

Prediction of failure geometry

149. Using the analyses developed above, it is possible to make a prediction of the final shape of a flow slide scar. The results depend strongly on the assumptions made, but the necessary assumptions do not seem unreasonable, and until experimental evidence is presented to verify or reject the assumptions, the prediction does describe the phenomenon to a great extent.

150. Imagine that some activity has scoured away the face of a point bar sand deposit to leave a steep retrogressing face as shown in Figure 99. The sand layer is horizontal and uniform, and the sand which flows into the scour hole is immediately removed.

151. In front of the moving retrogressing face, a continuous process of sedimentation is taking place. The sand which falls off the face collects in a smoothly flowing viscous carpet of grains. The base of the moving layer is traveling upwards at a speed

$$V = \frac{C_o W_d}{\Delta C} \tag{35}$$

This means that the toe of the retrogressing face is being continuously choked up by sediment grains which result in a steady decrease in the height of the face. Figure 100 shows the steep face (drawn in the figure as vertical) moving through the layer and becoming progressively shorter. The angle of the wedge of undisturbed material, α, is given by the relation between V and the velocity of retrogression, Z, of the face. Hence, Equations 14 and 16 are used:

$$\tan \alpha = \frac{V}{Z} = \frac{C_o W_\infty (1 - C_o)^n}{Z \Delta C} \tag{36}$$

This angle depends strongly on the assumptions made for C_o and C_1. The grains which sediment out are rolled over one another and will achieve a medium dense packing, $e = 0.7$. The packing of the grains in the suspension must remain a guess in the absence of experimental evidence. The values $e = 0.732$ and $Z = 0.5$ cm/sec give a wedge angle of 6.5 deg which agrees well with results of flow failures along the Mississippi and are used in the following computations. The variation of α with C_o is considerable, however, for $C_1 = 0.59$, $e_1 = 0.69$, and $Z = 0.5$ cm/sec, the following is calculated:

C_o	0.54	0.55	0.56	0.57	0.5775	0.58	0.585
e_o	0.85	0.82	0.79	0.75	0.73	0.72	0.71
$\alpha°$	2.21	2.58	3.20	4.46	6.5	8.21	30.3

152. In Figure 100, the datum height of the face is D_o at an arbitrary origin along the x axis. Consider a point, P, through which the base of the face has passed. The coordinates of P are x_p, Vx_p/Z. After the face has passed, sand grains will flow over P steadily building up a layer of newly deposited grains. The flowing layer will thin slowly as the face moves further away, but the rate of deposition is constant until some instant T_p seconds after the scarp passed through P, when the "last grain" will settle above P. X is given by:

$$X = \frac{\gamma' g \sin \alpha \ \Delta C}{3 \mu W_\infty C_1 (1 - C_o)} n H_o^3 = b H_o^3 \tag{37}$$

where H_o was the thickness of the flowing layer when the last grain set off. The time taken for the particle to get to P from the moment it set off is:

$$t_F = \frac{\Delta C\ H_o}{W_\infty\ C_1(1 - C_o)}\ n \tag{38}$$

The time taken by the vertical retrogressing face to get from P to the point where the last grain started its journey is:

$$t_R = \frac{X}{Z} = \frac{bH_o^3}{Z} \tag{39}$$

Between the time the face passed through P and the time the last grain landed above P, the elapsed time is:

$$T_p = t_F + t_R = \frac{bH_o^3}{Z} + \frac{\Delta C\ H_o}{W_\infty\ C_1(1 - C_o)}\ n \tag{40}$$

At the time the last particle sets off, the height of the face was:

$$d = D_o - \frac{xV}{Z} - \frac{bVH_o^3}{Z} \tag{41}$$

and the flow velocity of the last grain away from the face on the top of its layer was:

$$A = \frac{\tau H_o}{\mu} = \frac{H_o^2\ \gamma' g \sin\alpha}{\mu} \tag{42}$$

153. A value for H_o may be obtained by equating the flow rates of material leaving the face and that flowing away on the carpet of grains to give:

$$dZC_1 = \frac{AH_oC_o}{2}$$

$$\therefore \left(D_o - \frac{xV}{Z} - \frac{bVH_o^3}{Z} \right) ZC_1 = \frac{H_o^3 \gamma' g \sin \alpha}{2\mu} C_o \tag{43}$$

where

$$H_o = \sqrt[3]{\frac{2\mu C_1 (ZD_o - xV)}{\gamma' g \sin \alpha \; C_o + 2\mu bVC_1}} \tag{44}$$

In time T_p the sedimenting sand has built up a layer T_pV thick on top of P , and the new coordinate of the upper surface above P and the equation of the final surface are:

$$y = \frac{xV}{Z} + T_pV \tag{45}$$

$$= \frac{xV}{Z} + V \left[\frac{bH_o^3}{Z} + \frac{\Delta CH_o}{W_\infty C_1 (1 - C_o)} n \right] \tag{46}$$

$$= \frac{2D_o}{5} + \frac{3W_\infty C_o (1 - C_o)^n x}{5Z \Delta C} + \frac{C_o}{C_1} \sqrt{\frac{6\mu C_1 (ZD_o \Delta C - xW_\infty C_o (1 - C_o)^n}{5\gamma' g \sin \alpha \; C_o \Delta C}} \tag{47}$$

Substituting the values used previously,

$W_\infty = 4.10^{-4}$ m/sec
$C_o = 0.577$ ($e_o = 0.73$)
$C_1 = 0.59$ ($e_1 = 0.69$)
$\Delta C = 0.013$
$Z = 5 \times 10^{-3}$ m/sec
$\mu = 200$ poise
$\gamma' = 0.58\gamma_W$
$g = 9.81$ m/sec^2

$$\sin \alpha = 0.115$$

$$\alpha = 6.5 \text{ deg}$$

$$n = 4$$

Equation 35 simplifies to

$$y = 0.07x + 0.4D_o \tag{48}$$

This may be further simplified by taking a typical value for D_o = Zone A thickness = 20 m to give $y = 0.07x + 8.0$ (y and x in meters) which generates the after failure profile shown in Figure 101. In this diagram, the vertical scale is exaggerated. A wedge of redeposited material is left behind at a slope of approximately 4 deg. The steep face has eaten its way 172 m into the deposit in 9-1/2 hr at an angle of 6.6 deg. The shape of the final surface is slightly curved and the material removed (1,030 m^3 per m run) has been transported by the river.

154. Although this mechanism is not proven, it accounts well for the observations relative to the 1973 Stanton flow failure shown in Figure 102.

155. It is more likely that this stable process of retrogression is the cause of the spectacular flow failures along the Mississippi than that of spontaneous liquefaction. The calculation presented above is not a complete answer to the problem since several anomalies remain to be cleared up, and further research is required.

156. Manipulation of the equations yields for the distance traveled by the upper most grain which has fallen off a retrogressing face of height D

$$X = \frac{2DZ\ \Delta C}{3W_\infty\ C_o(1 - C_o)}\ n \tag{49}$$

The numerical values used above is $X = 5.74D$. In this case X varies linearly with D but implicit in this equation is the liquefied flow behavior which may not be scaled. Simple small scale tests with fine sand show that the angle is closer to 30 deg rather than 6 deg, which reiterates that small scale tests are inappropriate to model flow behavior. Very probably, the assumption of pure viscous flow and the assumptions about void ratios will not be valid for all scales. At small scale and at large scale, the analysis may

be inadequate, but at intermediate scale it agrees well with the process observed both in experiment and in the field. It should be stressed that this quantitative agreement depends heavily on the numerical values chosen for all the parameters.

Relation of the analysis to prototype sand flow

157. The analysis has shown that:

a. The distance traveled by the uppermost grain of a liquefied layer increases with the cube of the initial thickness of the layer.

b. The distance traveled by the uppermost grain of the liquefied layer which flows away from a steep retrogressing face in a dense sand layer increases linearly with the depth of the dense layer.

158. If the process involved in a liquefied flow slide on the Mississippi is spontaneous liquefaction involving the whole depth of the layer, then the distance traveled by the debris varies with the cube of the layer thickness. The results of such a mechanism in the thick deposits would be very deep failures which develop extremely rapidly. This is contrary to the empirical evidence. If the process is on a retrogression in a dense layer, then the material transport is directly proportional to the depth of the sand layer. The time predicted for the development of such a failure agrees well with the available field information. The WES empirical criterion is a simple linear relation which describes the facts.

159. The analysis presented herein was developed only after it was realized that alternative explanations had to be sought for Mississippi River flow slides. At the outset of the project, Padfield (1978) accepted the premise that loose sand strata were responsible for the failures. The first approach to the subject was an experimental investigation to model a flow slide on the centrifuge. It was the failure of this investigation in its attempt to demonstrate flow sliding in small scale which led to the analytical description of the phenomenon presented above.

160. The sequential drawings of Figure 103 are presented to further clarify the development and retrogression of failure in the dilatant point bar sand deposits of the Mississippi River after the process described by Padfield.

PART VII: SUMMARY

161. It is necessary to draw conclusions based on the considerable field and laboratory data presented herein and that from earlier studies. These data sets (i.e., old and new) are consistent and mutually supportive. With regard to failure mechanism, the choice seems to be between that which would represent very minor supportive evidence or that which conforms to the major indicators. The record shows that the apparent presences of loose sands in Mississippi River point bar deposits are sporadic if not meager. In these instances, the word strata does not appear appropriate, but instead lenses or pockets. Wherever the river has severely attacked point bar deposits of sands, flow failures have occurred. Padfield (1978) makes it clear that even many of the failures identified as "shear type" in the old "Verification of Empirical Method for Determining Riverbank Stability" studies were probably the result of the same flow mechanism except that the overburden successfully halted the process by deforming intact. It cannot be said that loose sand lenses have been characteristic of failure locations. Instead, particularly for failure locations below Baton Rouge, the specific point of river attack is the key and not the presence of loose lenses. This is even more evident for downstream end of revetment flow failures at Montz and elsewhere.

162. The failures in Mississippi Riverbanks which have been denoted as flow failures are not instantaneous. They are retrogressive and orderly. The author was shown evidence in a visit to the Delft Laboratory of a flow slide set in motion by dredging operations. In that event, the docks of a yacht club more than 800 ft from the dredge were taken by the slide. A line of instruments in the sand between the dredge and the dock facilities showed the entire mass of material to be in motion virtually simultaneously. This was a true case of "spontaneous liquefaction" triggered by the spot removal of sand which propagated catastrophically and immediately far beyond the point of that removal. Is this behavior consistent with all that is known about Mississippi River flow failures? Have gigantic masses of sand and overburden over large areas simply disintegrated into the river? The answer is no. If spontaneous liquefaction which is known to propagate freely was the case, why would so many levee sections below Baton Rouge where batture is relatively narrow and old flow failure scars exist still be intact? Mississippi Riverbank flow failures are not spontaneous mass outrushing of sand but rather a development

or progress over a time period that is found in older Potamology Investigations Reports. In Report 11-6 (US Army Engineer Waterways Experiment Station 1951a), eyewitness accounts by Messrs. Senour and Latimer of LMVD are cited. In that case, a small failure was observed to progress over about a 45-min period based on what could be seen above water. In the December issue of the Mississippi River Commission (US Army Engineer Mississippi River Commission 1950), the investigation of the Wilkinson Point failure of March 1949, it is stated that the bank receded 800 ft in 12 hr or less. Hvorslev (1956) also took the failures to be progressive in nature reflecting the evidence available to him probably by word of mouth and his own observations at that time rather than formally recorded. The following paragraphs are taken directly from Hvorslev's review of the potamology soils studies (1956) wherein he first addresses Koppejan's (1948) failure hypothesis and then presents his own modified hypothesis as to failure propagation.

General Dutch Hypothesis

163. A hypothesis for the development of progress flow failures, subsequent to their initiation by simple shear or other causes, has been proposed by Koppejan, et al., in connection with the study of numerous flow slides in the Dutch province of Zeeland. This hypothesis is illustrated in Figure 104 and briefly discussed in the following paragraphs. It is assumed that the sands below the overburden are very loose with a density equal to or less than the lower critical density.

164. The successive slices or sections of the progressive failure are shown in Figure 104A. The failure and removal of section A reduces the external forces on section B, but the corresponding tendency of this section to expand produces temporary negative pore water pressures and inward seepage which delays lateral displacement and a reduction in effective lateral stresses, so that the stability of section B is not initially affected by the removal of section A. In the course of time, inward seepage equalizes the negative pore water pressures with the result that expansion and lateral displacements or shearing strains occur (Figure 104B). The shearing strains produce excess pore water pressures in the very loose sand, and these pressures increase with increasing strains, but they do not affect the effective shearing stresses, whereas the effective normal stresses and shearing resistance

decrease until failure occurs and section B moves down (Figure 104C). The ensuing disturbance of the soil may further increase the excess pore water pressure or degree of liquefaction which, together with the momentum of the original failure movement, carries the soil in section B out over the flat lower slopes and the neck of the failure area to a point where the soil can be removed by the river current.

165. Application of this hypothesis to the major bank failures along the Lower Mississippi River encounters the difficulty that the density of large parts of Zone A sands is between the upper and lower critical densities. All laboratory tests indicate that an initial tendency of such sands to decrease in volume under shearing strains changes to a tendency to increase in volume at and immediately after failure. Therefore, the initial small excess pore water pressures, caused by the small lateral strains shown in Figure 104B, should later change to negative pore water pressures which may arrest further immediate development of the failure.

Hvorslev's Modified Hypothesis

166. Zone A sands of the Lower Mississippi River point bar deposits generally contain some strata of subcritical density, and the initial tendency of such sands to decrease in volume under lateral strain would not change to expansion under large strains. The corresponding excess pore water pressures in the very loose strata will spread to parts of the neighboring strata (Figure 105A), and failure of the bank section may occur before excess pressures can be dissipated. The general disturbance caused by failure, combined with load changes or vibrations and entrapment of water, may cause excess pore water pressures in or partial liquefaction of other parts of Zone A sands and enable these sands and the overburden soils to flow out through the neck of the failure area. The possibility that excess pore water pressures in singular, very loose strata, rather than in the entire Zone A sands, may be sufficient to cause progressive failure and is enhanced by the probability that the factor of safety of a slope is smaller against arcuate forms of failure than against strip or two-dimensional failure (Prof. Donald Taylor took exception to this statement in a later meeting of consultants). The difference between the original (Koppejan) and the modified hypothesis may be summarized as follows: according to the original hypothesis, large excess pore water pressures

are developed in the entire Zone A sands immediately before actual failure, whereas according to the modified hypothesis, such excess pore water pressures are developed before failure only in singular strata of subcritical density, and excess pore water pressures in some other parts of Zone A sands are caused by and occur after the initial failure. The thickness and position of very loose strata within Zone A sands will have considerable influence on the type and full development of the failure, as discussed in the following paragraphs.

Undermining and Tipping

167. It is possible that a relatively thin stratum of subcritical density may become partially liquefied and flow out before general failure of the bank develops as indicated in Figure 105B. The undermining of the upper bank causes a block of overburden soil to tip riverward when it fails (Figure 105C), but the surface of a section which fails by sliding (Figure 105A), tips backward. Whether the failure occurs by sliding or undermining depends not only on the character of the soils but also on the position of the very loose sand stratum with respect to the overburden. The impact and momentum of the tipping block of overburden materials may cause failure of the underlying Zone A sands (Figure 105C), and the general disturbance combined with entrapment of water may result in partial liquefaction of these sands so that the entire failed section moves out through the neck of the failure area, setting the stage for failure of the next section. Complete removal of the failed material and further progress of the failure depend on the relative thickness of the overburden materials and Zone A sands, and also on the already existing length of the failure area.

168. Failure by undermining and riverward tipping was observed and first suggested to the writers by Mr. W. J. Turnbull and has since been verified by others. These observations indicate the probable presence and initial failure of very loose sand strata, and they furnish partial corroboration of the modified hypothesis of progressive failure.

Blocked Failures

169. If the overburden materials have considerable cohesion and in addition a relatively great thickness compared to that of Zone A sands, then

the sliding or tipping block of overburden soils (Figure 105), may come to rest in front of Zone A or strata of very loose sands. Such a blocking by cohesive overburden soils not only prevents further immediate progress of the failure but may also, according to verbal information furnished by Mr. Key Woods (Chief of the Navigation Branch, Operations Division, Vicksburg District, CE), protect the bank from normal scour and attrition for several years. For a lesser thickness of overburden materials or a greater thickness of Zone A sands, the failing block of overburden soils may come to rest in the bowl of the failure area, thereby interfering with movement of successively failing sections and limiting further development of the failure, but the protection of the bank obtained in this manner is usually less than provided by direct blocking. The blocking of flow failures and the ultimate length of the failure area depend on the character and relative thickness of overburden materials and Zone A sands.

170. Hvorslev dismisses Koppejan's hypothesis on the basis of development of negative pore water pressures in the most dense Zone A sands but, in his own "modified" hypothesis neglects any moderating influences of negative pore pressures in the mass of sands surrounding a "very loose" strata. In effect, he submits that positive pore pressures can develop, be sustained, and even propagate with significant strains while negative pore pressures due to similar strains and in the same global field are somehow totally neutral and do not propagate their influence. Following the modified hypothesis and remembering Hvorslev's own statement to the effect, one must reason the relative thickness and depths of very loose strata to permit full development of a failure. The reference to very loose strata as opposed to lense or pocket is also significant because a very small areal extent of loose sand would also, according to the hypothesis, limit the process. Any dilatant sands above the loose strata would have to disintegrate en masse (which is improbable) rather than remain intact just long enough to seal off the loose strata (i.e., block the failure). If spontaneous liquefaction begins in a very loose strata, why would such a violently unstable energy release mechanism not propagate instantaneously throughout that strata but instead remain in perfectly balanced control to permit "orderly" retrogression? All of the special condition "ifs" of Hvorslev's hypothesis become improbable in light of the hundreds of failures of record (a much larger record than available to Hvorslev in 1956) which did fully develop and in "orderly" fashion, one by one, especially

with the apparent scarcity of anything approaching very loose point bar sands. It is interesting to note in Figure 105 that Hvorslev refers to the greater proportion of Zone A sand as medium loose. It seems clear that Geuze (1948) concepts of and "upper" and "lower" critical density had introduced ambiguities about the behavior of sands at a density between the two values when, in fact, such densities are dilatant under undrained shear (i.e., are not liquefaction susceptible). For Mississippi River point bar sands, the evidence suggests the better term to be "medium dense," if not dense. It is recalled that a total loading stress patch of essentially constant vertical stress and decreasing lateral stress intensifies any tendency toward development of negative pore water pressures because throughout the loading the mean normal stress is decreasing. Neither Koppejan or Hvorslev speaks on the fact that sand grains at the retrogressing face are under no appreciable effective stresses and will not remain in place of slopes exceed angle of repose or if there is minor disturbance by river currents. This material could readily build up at the base of the slope and "seal off" any thin loose layer. Final failure profiles show throat slopes of from less than 5 deg to up to 15 deg depending on scour modification. Padfield calculated an angle, α , or about 7 deg as representing the Zone A sands actually involved in the failure process. Furthermore, final failure profiles are relatively smooth in transition of slopes with no apparent alteration in mechanism throughout the process. The obvious question then arises. How far into the bank would such a consistent mechanism have to retrogress, assuming it is initiated as Hvorslev suggests at the depth of a "very loose" strata, before the failure activity is above that strata entirely? Taking an average final slope just for the sake of argument of 10 deg, it is seen that for a failure length into the bank of only 200 ft, a thickness of 35 ft of sand has been involved. If the looser strata is only 5 or 10 ft thick (the sort of thicknesses seen for the rare cases of loose material), then how has the overlying 30 ft of dilatant sand continued to yield the same after-failure profile? In considering the very large, deep failures such as Montz, much less Wilkinson Point (US Army Engineer Mississippi River Commission 1950), the logic of the modified failure hypothesis breaks down totally simply because there is absolutely no evidence of loose sands of the required strata thickness or areal extent. There appears to be no way to avoid accepting the hypothesis that the failure mechanism is within the dilatant sands and that the behavior of any loose lenses,

if present, complements (or at least does not stop) the retrogression rather than drives it.

171. Retrogression in dilatant sand has been observed in even small-scale physical models and, after Padfield's work, numerically treated as well. The hypothesized mechanism fits in every way, without specious arguments and special conditions, the observations of the traits of Mississippi Riverbank flow slides and the materials in which they occur. Where Hvorslev makes a special point of discussing "undermining and tipping" of blocks of overburden, the new hypothesis suggests it is the expectable occurrence. Indeed, failure profiles generally show very steep or near-vertical slopes in overburden soils which implies deep tension cracking and "break aways." This process virtually assures efficient removal of the blocks as they fall freely through the water to land upon the flowing carpet of sand grains which conveys them out into the main river current. Any evidence of top stratum blocks remaining within failure scars or even about the riverward mouth of the failure "neck" has been a real rarity.

172. Unfortunately, a new concept for failure mechanism is of little value in stopping the problem although it may offer a means to predict potential batture loss and judge threat to the mainline levee. In any case, the problem of "liquefied" or "fluidized" sand flowing from the bank in large quantity remains. Any top stratum thicknesses and characteristics which cannot survive the loss of underlying support can be expected to lead to serious and sustained bank retrogression. The only differences may lie in the nature of scour in the sands (i.e., whether less severe and trench-like or very severe and highly localized) and the time lapse before the inevitable consequences are seen. Thin top strata over Zone A sands and localized flood stage scour will translate to "flow slides" of a few hours duration while thicker top strata over "deep" sands and trench scour will result in seasonal, but relentless "bank caving." As Mr. Weaver of LMVD has often said, any Mississippi River point bar sand subjected to sufficient river attack will suffer the "flow slide" mechanism, and in like manner the investigations reported herein have strongly tied that mechanism to the apparent general character of those deposits rather than to anomalies within them.

PART VIII: CONCLUSIONS AND RECOMMENDATIONS

Conclusions

173. The following conclusions are drawn from the work performed under the current study title and from past Potamology Investigations:

a. The articulated concrete revetment mattress currently used for bank protection will not prevent "flow slides" if placed in a single layer as is typical. It appears that the mattress is rendered ineffectual by any combination of three processes. First, the failure may be initiated at the or riverward of the mattress toe. It is not uncommon that the mattress does not extend across the scour pool or trench. It may then be breached by exposure to turbulence because it cannot conform to and seal off a cavity developing beneath it. Second, the process may begin upslope of the mattress toe if sufficient sand is "sucked" through the mattress by intense verticity. Loss of sand through the open-work mattress was documented in earlier Potamology Investigations. The apparently successful use of plastic filter cloth to prevent such loss was reported in 1970 in Potamology Investigations Report 21-4. The "liquefied" or fluidized" and resuspended sand must either breach the mattress itself or continue out through it until a sufficient cavity leading to breaching develops. A large percentage of documented flow slides in the Vicksburg District have occurred within the limits of the mattress. Third, the mattress may be breached by the first blocks of failing overburden.

b. The sands and silty sands deposited by the Mississippi River at Montz and Bonnet Carre Point, LA, are medium to dense in situ. The methods of exploration and associated laboratory tests were consistent in the indication of relative densities in excess of 50 percent.

c. Correlations among sample density, maximum density, minimum density, relative density, and peak grain diameter developed under past Potamology Investigations are accurate. Those correlations substantiate conclusion b above.

d. Using correlations referred to in c above and critical void ratio data for three point bar Zone A sands representing a range in gradation, it is concluded that in situ densities of Reid Bedford, Montz, and Carrollton Bend Zone A sands are well above their critical densities (below their critical void ratios). If the trends among critical void ratio, confining pressure, and peak grain diameter are accepted as valid, then the same is true for Bonnet Carre Point sands and Mississippi River point bar Zone A sands in general.

e. In light of these observations the range in typical maximum failure depths is maximum in situ effective confining

stresses. Typical failures retrogress to conclusion from 20 to more than 50 ft above the apparent elevation of initiation. The presence of lenses or strata below 50 percent in relative density is considered rare. The thickness of any rare loose lense or strata is on the order of a few feet, and the frequency of failures along extensive bank reaches such as Reid Bedford implies retrogression in the prevailing denser sands rather than as dictated by any sporadic looser sands. The hypothesis of liquefaction in loose sand lenses or strata as the dominant flow failure mechanism is improbable.

f. On the basis of e above and Padfield's analysis, the hypothesis of failure by retrogression in sands which are dilatant under prevailing conditions of density, effective confining stresses, and probable total stress path is considered the most plausible explanation of Mississippi Riverbank flow failures. Full development of a failure remains predicated on the unimpeded flow of liquefied or fluidized sand away from the retrogressing face.

g. The empirical criteria for predicting susceptibility to flow failure have been shown by Padfield to be rationally explained on the basis of arching in the top stratum.

h. Historical geological/hydrographical studies of the Montz and Bonnet Carre Point reaches confirm the severity of river attack and the presence of "permanent" scour pools which are now, as in the past, steadily migrating into the bank. Severe localized scour is clearly indicated as the flow failure trigger. Such studies extended to the entire reach of river below Baton Rouge offer promise in narrowing the scope of the problem to specific sites. On the basis of a above and results of the studies of the Montz and Bonnet Carre Point reaches, flow slides will continue to occur below Baton Rouge during severe floods until preventative measures are devised and placed.

i. With respect to the investigational tools employed at Montz and Bonnet Carre Point, the following conclusions are drawn:

(1) The osterberg fixed-piston sampler performed even in dense sand at a depth of 120 ft. Sample recovery was excellent. Sample disturbance appeared to be minimal.

(2) The piezoprobe or piezocone is not a useful tool at this time to indicate in situ dilatancy/contraction by dynamic pore pressure response. As long as the probe remains saturated, the device is most useful in detecting very thin seams of soils of differing permeability.

(3) The cone penetrometer (CPT) is a valuable and inexpensive means for determining stratigraphy and estimating in situ relative density of sands. It is not as accurate in detecting very thin seams as is the piezocone. It is an inexpensive method since 300 to 400 ft can be pushed in a work day at a cost of about $5/ft including data interpretation.

(4) The SPT/split-spoon advantages are well known. The use of the split-spoon for disturbed samples in conjunction with CPT for relatively cheap areal and depth coverage is a powerful site investigation approach.

(5) The Delft resistivity probe for obtaining in situ porosity yielded questionable results for the two sites investigated. While the values the method produced roughly corresponded to measurements made on undisturbed samples (allowing for sampling disturbance), the laboratory correlations by which in situ readings were translated to values of porosity proved to be very dependent on gradation of the sands and other unidentified factors. This introduced considerable ambivalence in judging which correlate to use for any given reading in the very variable alluvial deposits. It cannot be said, however, that the method (coupled with laboratory max/min data) was any less accurate than estimation of in situ relative density from SPT or CPT data.

Recommendations

174. Recommendations for the tasks to be performed under the new study entitled, "Evaluation of Potentially Unstable Riverbank Sites Below Baton Rouge, LA, and Selection of Measures to Prevent Failure," are briefly discussed below.

a. The need for historical geological/potamological studies is as the basis of getting down to specifics in identifying the sites below Baton Rouge which are most critically in need of preventative measures. A prioritization is required for planning purposes. At the very least these efforts should establish the direction and relative rates of "permanent" scour pools' migrations.

b. It is recommended that additional efforts be directed at verifying that retrogression in dilatant sands is the failure mechanism. It is important, if possible, to quantify the process, particularly with respect to the "runout" angle which is the key to confident assessment of foreshore (batture) adequacy. There are two elements to this task. First, available empirical data should be reviewed to determine if it supports the concept of "runout" angle. Second, the numerical approach of Padfield should be examined with the objective of improvement or refinement supported by any necessary testing or studies to determine best values for the various input parameters.

c. The time has come to decide what configurations of bank/scour pool protection may be effective and then construct and monitor test sections. The protection scheme(s) should probably have components as follows:

(1) Above the toe of the riverbank slope, the system should be designed to retain fine sands while providing free drainage. Hydraulic models may be required to design the filtration/drainage component. Filter cloth under conventional mattress may be found to meet the needs.

(2) From just above the riverbank toe riverward and completely across the scour pool/trench, the system should be heavy, yet flexible, and preferably extra-weighted along its riverward edge. Multiple layers of conventional mattress may serve adequately.

(3) Both of the above aspects of a total system are problematical with respect to placement/construction. In light of the implications of the Marchand levee failure discussed below, the necessity of developing a deep-water, "beefed up" revetment system may be inevitable anyway as an alternative to setbacks below Baton Rouge. Trial and error is anticipated in developing a satisfactory system. Given shortfalls in ability to really "see" the performance of a test section and the fact that very variable and highly localized scour attack are the only conditions under which valid evaluation can be achieved, the risk that test sections will not prove conclusive is high. At the very least, there should be no delusions that quality evaluation will come easily or over short periods of time. The writers believe that the installation and monitoring of test sections must be approached with dogged determination that each case will be treated as nonroutine in every way and deserving of the best in accuracy and frequency of measurements for as long as necessary. If test sections studies are conformed to the current routine of bank protection activities, there is a likelihood that monitoring data will be inadequate and insufficient to draw conclusions concerning relative performance. Obviously, the locations of test sections are a critical issue. The siting of test sections then demands treatment as a separate and major study which draws from geotechnical, geological, potamological, and hydraulic disciplines to the maximum degree including the obtaining of any needed field data.

d. In late March 1984, WES submitted a draft proposal to LMVD for the final phase of the flow slide studies. However, WES was asked to attend a meeting to review technical data relative to the Marchand levee failure. The meeting was predicated on Mr. Weaver's concern that the development of the failure was attributable to the possible retrogressive loss of deep sands beneath the very thick (about 60 ft) cohesive top stratum. After review of the site conditions and chronology of bank losses, it was the consensus that Mr. Weaver's concerns were well founded. The specifics of the Marchand case clearly imply severe localized river attack and undercutting of the mostly clay overburden leading to progressive shear failure which culminated in perhaps a large wedge-type failure with a

section of the levee driving the active wedge. Logically it appears that the flow slides of past concern represent the short-term results of retrogression in dilatant sands beneath thin overburden strata which shear immediately permitting the failure to proceed to conclusion. The Marchand case may then represent the same process occurring much deeper but delayed intermittently by the time required for the thick top stratum to fail and expose the underlying sands to reinitiation of the process. It may also be true that the two problems differ by the flow regimes producing failure. It is known that the flow slides in point bars with thin top strata are associated with severe flood conditions. The deep-seated Marchand type problem may be associated with more ordinary seasonal conditions and not necessarily high water. This should be investigated. It is recommended that the scope of the flow slide studies be expanded to include consideration of the several sites already designated by NOD as potential Marchand type situations. This increases the work to be done but does not alter the basic approach since the problem remains essentially the same. The historical geological/potamological studies would include the added sites. Progress toward identifying preventative measures is not affected because the obstacle of deep water construction is common to both cases.

e. The NOD has raised the question as to whether or not there is a flow slide threat to levees above Baton Rouge. The NOD has the capability of addressing that question. If a sufficient threat is identified, that reach can be brought into the studies.

REFERENCES

Allen, J. R. L. and Banks, N. L. 1972. "An Interpretation and Analysis of Recumbent Folded Deformed Cross Bedding," Sedimentology, Vol 19.

Bagnold, R. A. 1943. The Physics of Blown Sand and Desert Dunes, Morrow and Co., NY.

Banks, D. C. and Strohm, W. E. 1965. "Methods of Preventing Flow Slides," Potamology Investigations Report No. 12-16, US Army Engineer Waterways Experiment Station, Vicksburg, MS.

Bazaraa, A. R. S. S. 1967. Use of the Standard Penetration Test for Estimating Settlements of Shallow Foundations on Sand, PhD dissertation, University of Illinois, Urbana, IL.

Bernatzik, W. 1947. Baugrund and Physik.

Bieganousky, W. A. and Marcuson, W. F. 1976. "Liquefaction Potential of Dams and Foundations, Report 1, Laboratory Standard Penetration Tests on Reid Bedford Model and Ottawa Sands," Research Report S-72-2, US Army Engineer Waterways Experiment Station, Vicksburg, MS.

Castro, G. 1969. Liquefaction of Sands, Harvard Soil Mechanics Series No. 81, Cambridge, MA.

Clarke, B. 1967. "Rheology of Coarse Settling Suspension," Transaction, Institute of Chemical Engineering, Vol 45.

Coleman, J. M. 1976. "Deltas: Process of Deposition and Models for Exploration," Continuing Education Publication Co., Inc., Champaign, IL.

Curray, J. R. 1965. The Quaternary of the United States, Princeton University Press, Princeton, NJ, pp 723-735.

Davidson, J. F. and Harrison, D. 1963. "Fluidized Particles," University Press, Cambridge, England.

Davidson, J. L. 1980. "A Study of Deformations in Sand Around a Penetrated Probe Using Stereo Photography," University of Florida, Gainesville, FL.

DeMello, V. 1971. "The Standard Penetration Test: A State-of-the-Art Report," 4th Pan American Conference on Soil Mechanics and Foundation Engineering, American Society of Civil Engineers, San Juan, Puerto Rico.

Denner, and James, R. L. 1977. "The Propagation of Flow Slides in Submerged Slopes," Undergraduate Project Report, Cambridge University Engineering Department, Cambridge, England.

Douglas, B. J. and Olsen, R. S. 1981. "Soil Classification Using Electric Cone Penetrometer," Cone Penetration Testing and Experience, American Society of Civil Engineers, NY, pp 209-227.

Durham, G. N. 1971. "A Study of the Liquefaction Phenomena of a Fine Sand Utilizing the Consolidated-Undrained Triaxial Compression Test Under Controlled Stress Loading," masters thesis, Mississippi State University, Mississippi State, MS.

Fisk, H. N. 1944. "Geological Investigations of the Alluvial Valley of the Lower Mississippi," US Army Corps of Engineers, Mississippi River Commission, Vicksburg, MS.

Fraiser, D. E. 1967. "Recent Deltaic Deposits of the Mississippi River: Their Development and Chronology," Gulf Coast Association of Geologic Societies, Vol XVII.

Gann, A. R. 1981. "Verification of Empirical Method for Determining Riverbank Stability, Report 12-24, 1974 through 1977 Data," Miscellaneous Paper S-78-5, US Army Engineer Waterways Experiment Station, Vicksburg, MS.

Garber, P. K. 1952. "Summary Report of Soils Studies," Potamology Investigations Report 12-2, US Army Engineer Waterways Experiment Station, Vicksburg, MS.

Geuze, E. C. W. A. 1948. "Critical Density of Some Dutch Sands," Proceedings of the Second International Conference on Soil Mechanics and Foundation Engineering, Vol 3, Rotterdam, The Netherlands.

Gibbs, H. J. and Holtz, W. G. 1957. "Research on Determining the Density of Sands by Spoon Penetration Testing," Proceedings of the Fourth International Conference on Soil Mechanics and Foundation Engineering, Vol 1, London, England.

Happel, J. and Brenner, H. 1965. Low Reynolds Number Hydrodynamics, Prentice Hall, Englewood Cliffs, NJ.

Headquarters, Department of the Army, Office of the Chief of Engineers. 1971. "Laboratory Soils Testing," Engineer Manual EM 1110-2-1906, Washington, DC.

Hvorslev, M. J. 1949. "Subsurface Exploration and Sampling of Soils for Civil Engineering Purposes," US Army Engineer Waterways Experiment Station, Vicksburg, MS.

_____. 1956. "A Review of the Soils Studies," Potamology Investigations Report 12-5, US Army Engineer Waterways Experiment Station, Vicksburg, MS.

Kolb, C. R. and Van Lopik, J. R. 1958. "Geology of the Mississippi River Deltaic Plain, Southeastern Louisiana," Technical Report 3-483, Vols 1 and 2, US Army Engineer Waterways Experiment Station, Vicksburg, MS.

Kolb, C. R. 1962. "Distribution of Soils Bordering the Mississippi River from Donaldsville to Head of Passes," Technical Report 3-601, US Army Engineer Waterways Experiment Station, Vicksburg, MS.

Koppejan, A. W. and Van Wamelan, B. M. 1948. "Coastal Flow Slides in the Dutch Province of Zeeland," Proceedings of the Second International Conference on Soil Mechanics and Foundation Engineering, Rotterdam, The Netherlands.

Krinitzsky, E. L. 1965. "Geological Influences on Bank Erosion Along Meanders of the Lower Mississippi River," Potamology Investigations Report 12-15, US Army Engineer Waterways Experiment Station, Vicksburg, MS.

Lowe, D. R. 1976. "Subaqueous Liquefied and Fluidized Sediment Flows and Their Deposits," Sedimentology, Vol 23.

Marcuson, W. F. and Bieganousky, W. A. 1977. "Laboratory Standard Penetration Tests on Fine Sands," Journal of the Geotechnical Engineering Division, Vol 103, No. GT6, ASCE.

Meijer, K. L. and Van Os, A. G. 1976. "Pore Pressures Near Moving Underwater Slope," Journal of the Geotechnical Engineering Division, GT4, American Society of Civil Engineers.

Mitchell, J. K. 1984. "Practical Problems From Surprising Soil Behavior," Terzaghi Lecture, presented at ASCE Conference held in San Francisco, CA.

Morgenstern, N. R. 1967. "Submarine Slumping and the Initiation of Turbidity Currents," Marine Geotechnique.

Norton, W. E. 1983. "In Situ Determination of Liquefaction Potential Using the PQS Probe," Technical Report GL-83-15, US Army Engineer Waterways Experiment Station, Vicksburg, MS.

Padfield, C. J. 1978. "The Stability of River Banks and Flood Embankments," Final Technical Report, US Army European Research Office, London, England.

Pokrovski, G. I. and Fyoderov, I. S. 1968. "Centrifugal Model Testing in the Construction Industry," Translation from the Russian.

Poulos, S. J., Castro, G., and France, J. W. 1985. "Liquefaction Evaluation Procedure," Journal of Geotechnical Engineering, Vol III, No. 6, American Society of Civil Engineers.

Richardson, J. F. and Zaki, W. N. 1954. "Sedimentation and Fluidization," Transactions of the Institute of Chemical Engineers, Part I, Vol 32.

Saucier, R. T. 1963. "Recent Geomorphic History of the Pontchartrain Basin," Coastal Studies Series No. 9, Louisiana State University, Baton Rouge, LA.

Schlichting, H. 1960. Boundary Layer Theory, McGraw Hill, 4th ed.

Schmertmann, J. H. 1978. "Guidelines for Cone Penetration Test Performance and Design," Report FHWA-TS-78-209, US Department of Transportation, Federal Highway Administration, Washington, DC.

Seed, H. B., Idriss, I. M., and Arango, I. 1983. "Evaluation of Liquefaction Potential Using Field Performance Data," Journal of Geotechnical Engineering, Vol 109, No. 3, American Society of Civil Engineers.

Seed, H. B., Tokimatsu, K., Harder, L. F., and Chung, R. M. 1984. "The Influence of SPT Procedures in Soil Liquefaction Resistance Evaluation," Report No. UCB/EERC-84/15, Earthquake Engineering Research Center, University of California, Berkeley, CA.

Tokimatsu, K. and Seed, H. B. 1987. "Evaluation of Settlements in Sands Due to Earthquake Shaking," Journal of Geotechnical Engineering, Vol 113, No. 8, American Society of Civil Engineers.

Torrey, V. H. and Strohm, W. E. 1976. "Investigation of Liquefaction and Methods of Preventing Flow Slides in Mississippi Riverbanks," US Army Engineer Waterways Experiment Station, Vicksburg, MS. (report to the sponsor, unpublished).

Torrey, V. H. 1981. "Some Effects of Rate of Loading and Applied Total Stress Path on the Critical Void Ratio of a Fine Uniform Sand," PhD dissertation, Texas A&M University, College Station, TX.

Trofimenkov, J. G. 1974. "Penetration Testing in the USSR," Proceedings of the European Symposium on Penetration Testing, Vol 1, National Swedish Building Research, Stockholm.

US Army Engineer, Mississippi River Commission. 1950. "Investigation of Free Nigger Point Crevasse, Mississippi River," Vicksburg, MS.

US Army Engineer Waterways Experiment Station. 1948. "Field Investigation of Reid Bedford Bend Revetment, Mississippi River," Potamology Investigations Report 5-2, Vicksburg, MS.

US Army Engineer Waterways Experiment Station. 1950a. "Triaxial Tests on Sands, Reid Bedford Bend Revetment, Mississippi River," Potamology Investigations Report 5-3, Vicksburg, MS.

US Army Engineer Waterways Experiment Station. 1950b. "Standard Penetration Tests, Reid Bedford Bend Revetment, Mississippi River," Potamology Investigations Report 5-5, Vicksburg, MS.

US Army Engineer Waterways Experiment Station. 1951a. "Report of Conference on Potamology Investigations," Potamology Investigations Report 11-6, Vicksburg, MS.

US Army Engineer Waterways Experiment Station. 1951b. "Undisturbed Sand Sampling and Cone Sounding Tests, Reid Bedford Bend Revetment, Mississippi River," Potamology Investigations Report 5-6, Vicksburg, MS.

US Army Engineer Waterways Experiment Station. 1952a. "Density Changes of Sand Caused by Sampling and Testing," Potamology Investigations Report 12-1, Vicksburg, MS.

US Army Engineer Waterways Experiment Station. 1952b. "Study of the Variability of Sand Deposits," Miscellaneous Paper 3-12, Vicksburg, MS.

Table 1

Comparison of Original and Modified Classification Criteria

Material	Original Criteria*	Modified Criteria**
Overburden soils	More than 10 percent passing No. 200 sieve	More than 20 percent passing No. 200 sieve
Upper sands	50 percent or more passing No. 40 sieve	50 percent or more passing No. 40 sieve
Zone A	50 percent or more passing No. 60 sieve	25 percent or more passing No. 60 sieve
Zone B	Less than 50 percent passing No. 60 sieve	Less than 25 percent passing No. 60 sieve
Lower sands	Less than 50 percent passing No. 40 sieve	Less than 50 percent passing No. 40 sieve

* These classification criteria were used prior to 1959.

** These criteria are presently used in the classification of individual soil samples. However, in establishing thicknesses of overburden and Zone A materials, strata of other soils may be included in these zones as described in the text.

Table 2

Undisturbed Specimen Data, Montz Site, Boring U2

Specimen No.	Depth ft	e_{max}	e_{min}	Maximum Dry Density pcf	Minimum Dry Density pcf	Specimen Dry Density pcf	Void Ratio	Relative Density %	Porosity n
14.1	40.5	1.145	0.712	97.0	77.4	92.5	0.794	81	0.442
14.2	41.8	1.152	0.716	96.7	77.1	89.9	0.848	70	0.459
16.1	46.5	1.035	0.603	103.6	81.6	96.4	0.722	72	0.419
16.2	47.1	0.955	0.625	102.1	84.9	96.3	0.724	70	0.420
18.1	52.3	1.167	0.730	96.0	76.6	90.9	0.826	78	0.452
18.2	53.1	1.116	0.703	97.5	78.4	92.6	0.792	78	0.442
20.1	58.7	1.080	0.716	96.7	79.8	93.5	0.775	84	0.437
20.2	59.3	1.038	0.652	100.5	81.4	97.1	0.709	85	0.415
21.1	61.3	1.229	0.745	95.1	74.5	91.9	0.806	87	0.446
21.2	62.4	1.095	0.714	96.9	79.2	92.4	0.796	78	0.443
22.2	65.2	1.047	0.646	100.8	81.1	97.2	0.708	84	0.414
23.1	67.4	1.323	0.751	94.8	71.4	84.9	0.955	64	0.488
23.2	68.2	1.040	0.654	100.3	81.4	88.4	0.878	42	0.468
24.1	70.5	1.051	0.658	100.1	80.9	94.3	0.760	74	0.432
24.2	71.0	1.060	0.653	100.4	80.6	94.1	0.764	73	0.433
25.1	73.6	1.248	0.675	99.1	73.8	89.6	0.852	69	0.460
26.2	76.5	0.975	0.637	101.4	84.0	94.2	0.762	63	0.432
29.3	86.3	0.975	0.639	101.3	84.0	93.2	0.781	58	0.438
31.1	92.1	0.923	0.609	103.1	86.3	97.7	0.700	71	0.412
34.4	100.5	0.944	0.604	103.5	85.4	97.2	0.708	69	0.414
34.3	101.0	0.026	0.625	102.2	81.9	90.2	0.840	46	0.456
34.1	101.6	0.927	0.548	107.2	86.1	96.1	0.727	53	0.421
38.2	112.7	0.948	0.600	103.8	85.2	100.1	0.658	83	0.397

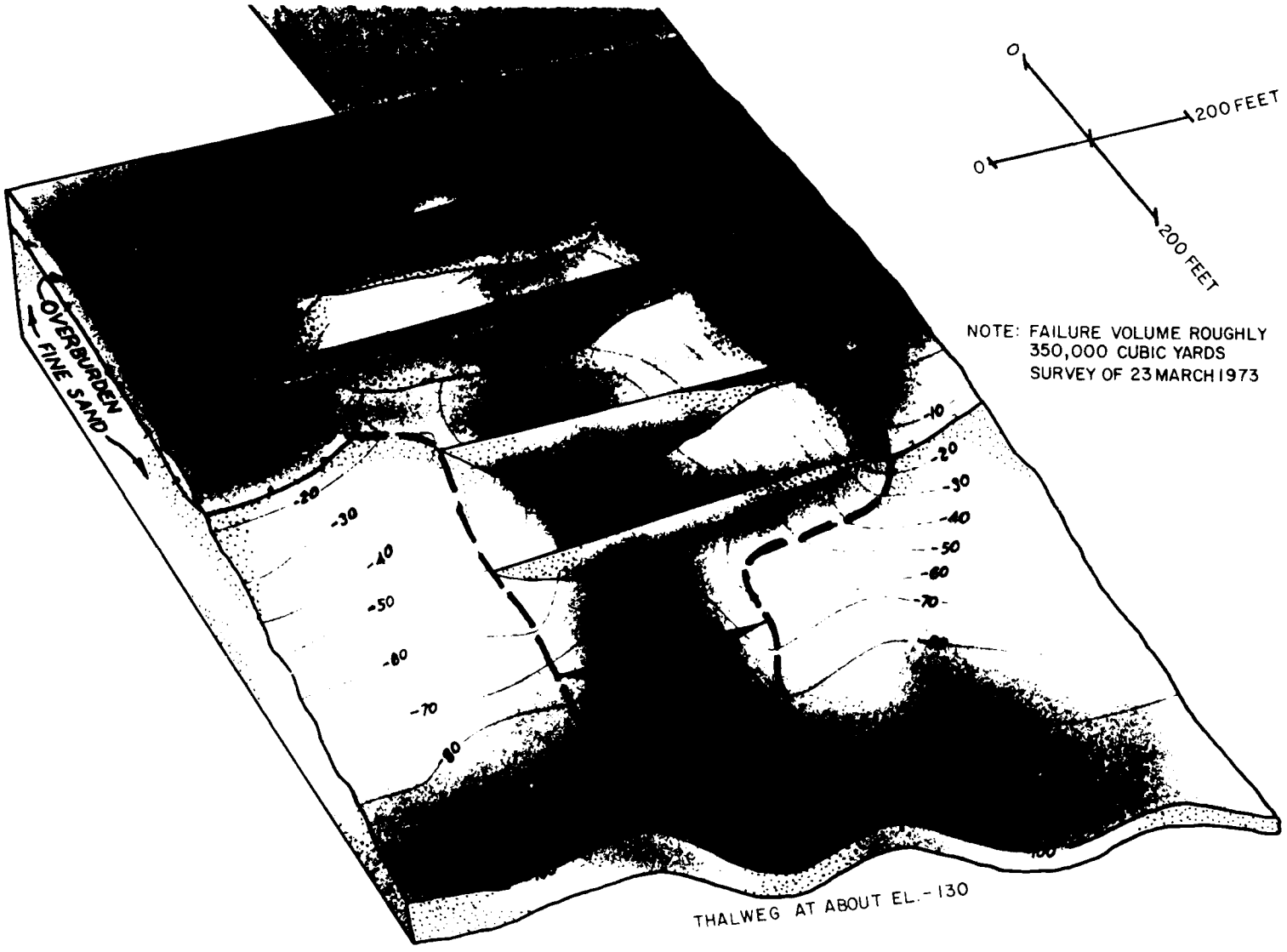


Figure 1. Isometric drawing of the Montz flow failure of 1973

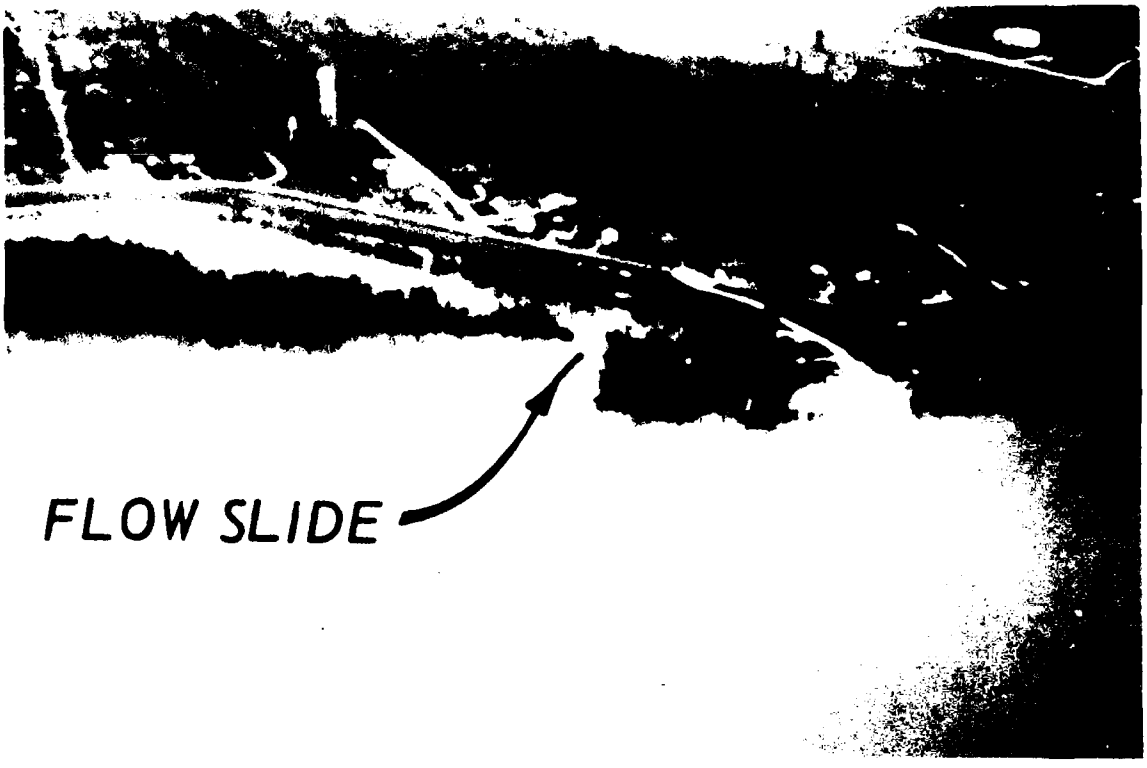


Figure 2. Aerial view of the Montz flow failure shortly after occurrence

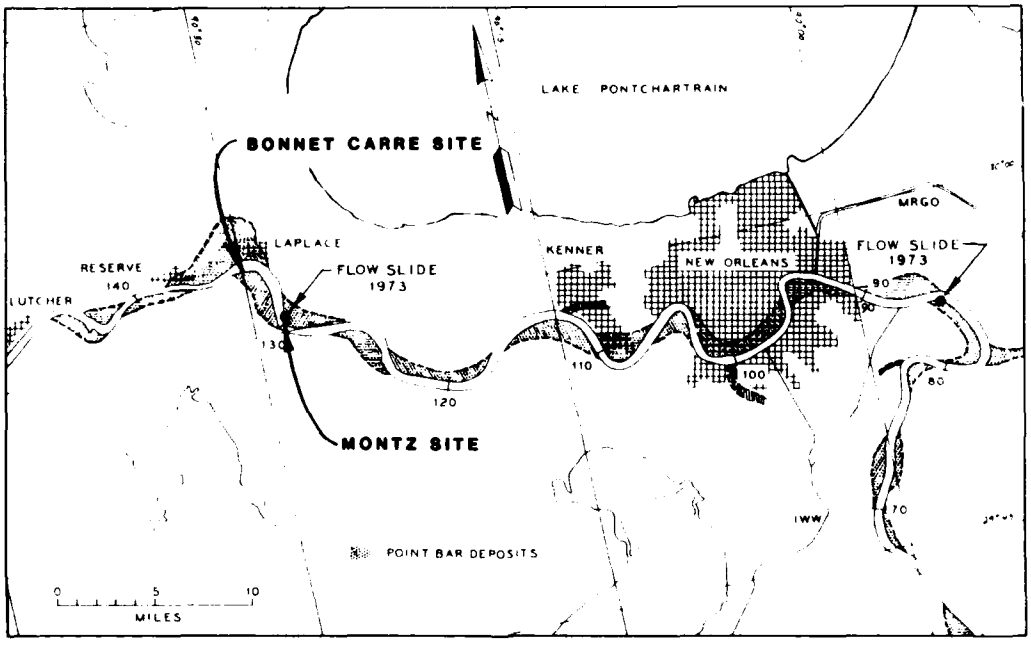


Figure 3. Location of the Montz and Bonnet Carre Point sites

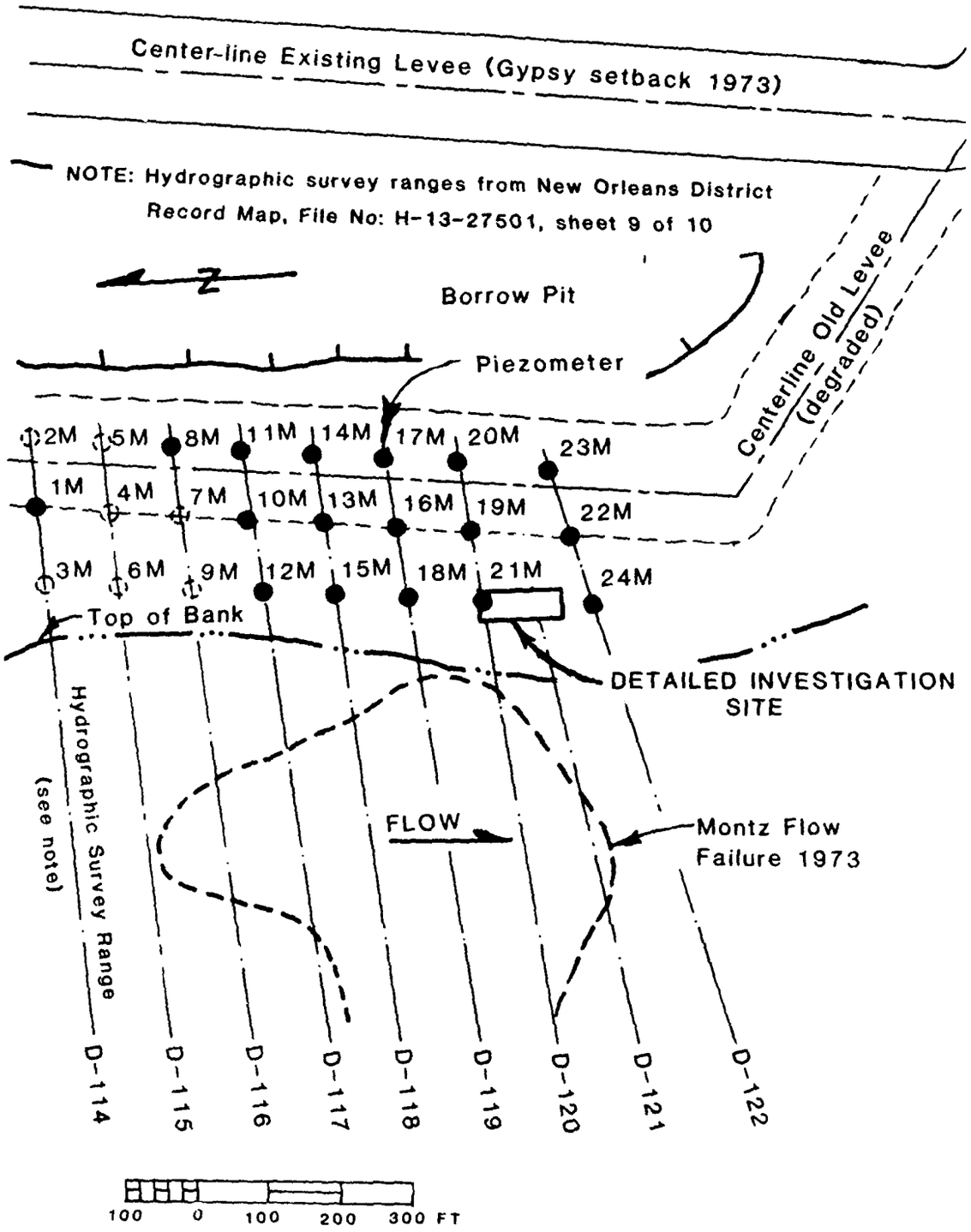


Figure 4. Montz reconnaissance exploration plan

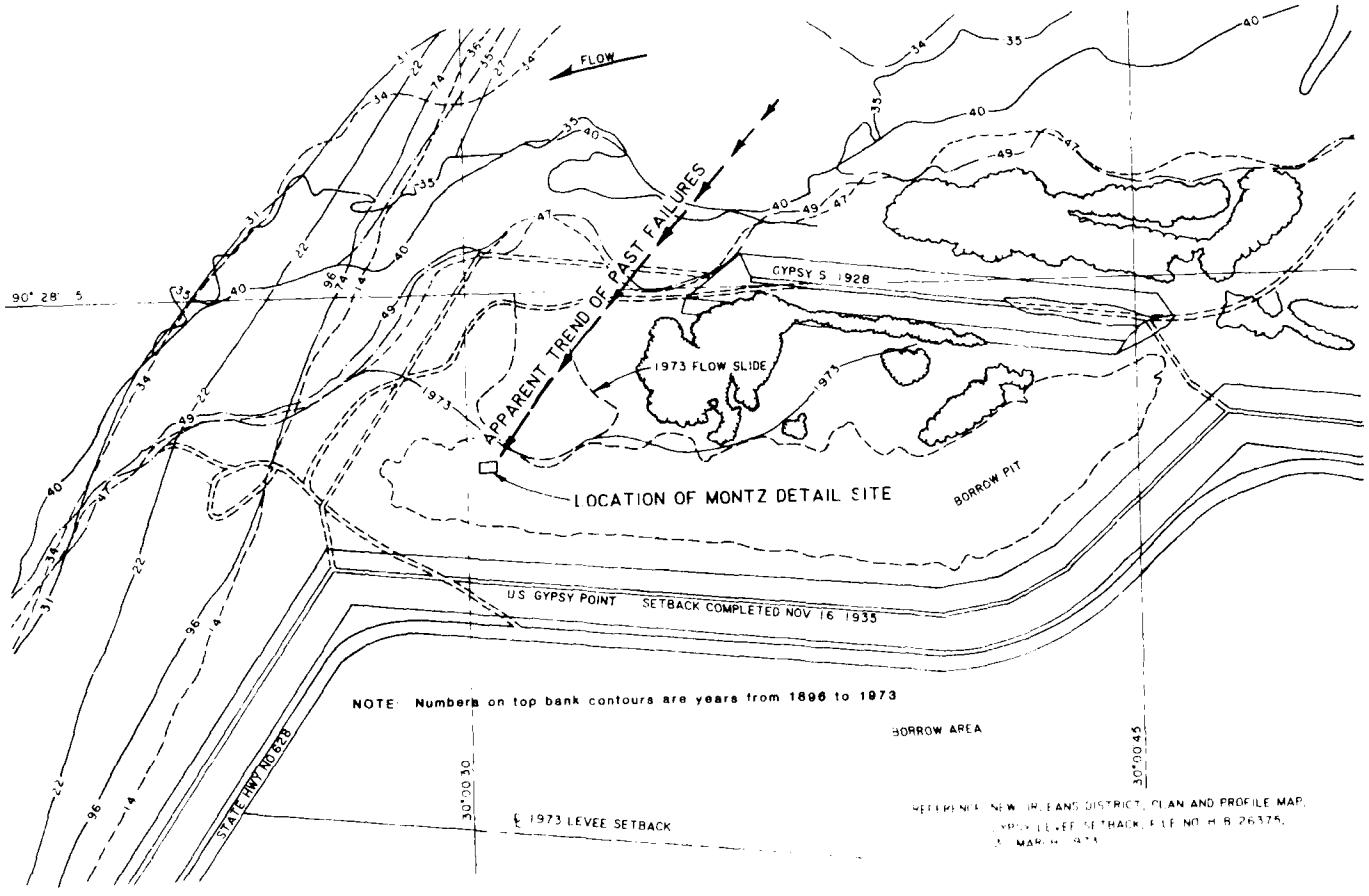


Figure 5. Use of past failure trends to locate Montz detailed site



Figure 6. Oblique aerial view of the Montz area and detailed site

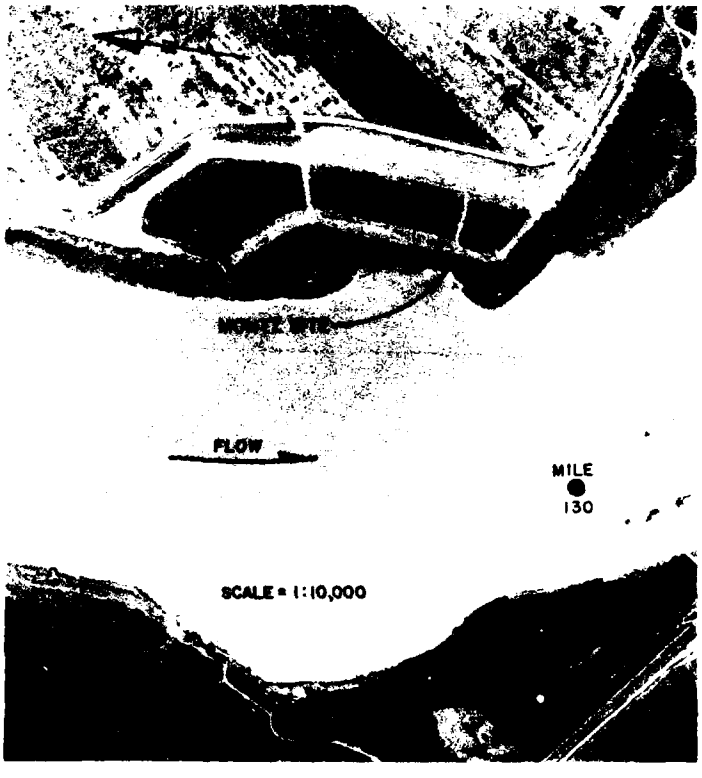


Figure 7. Montz flow failure scar and location of the detailed investigation site

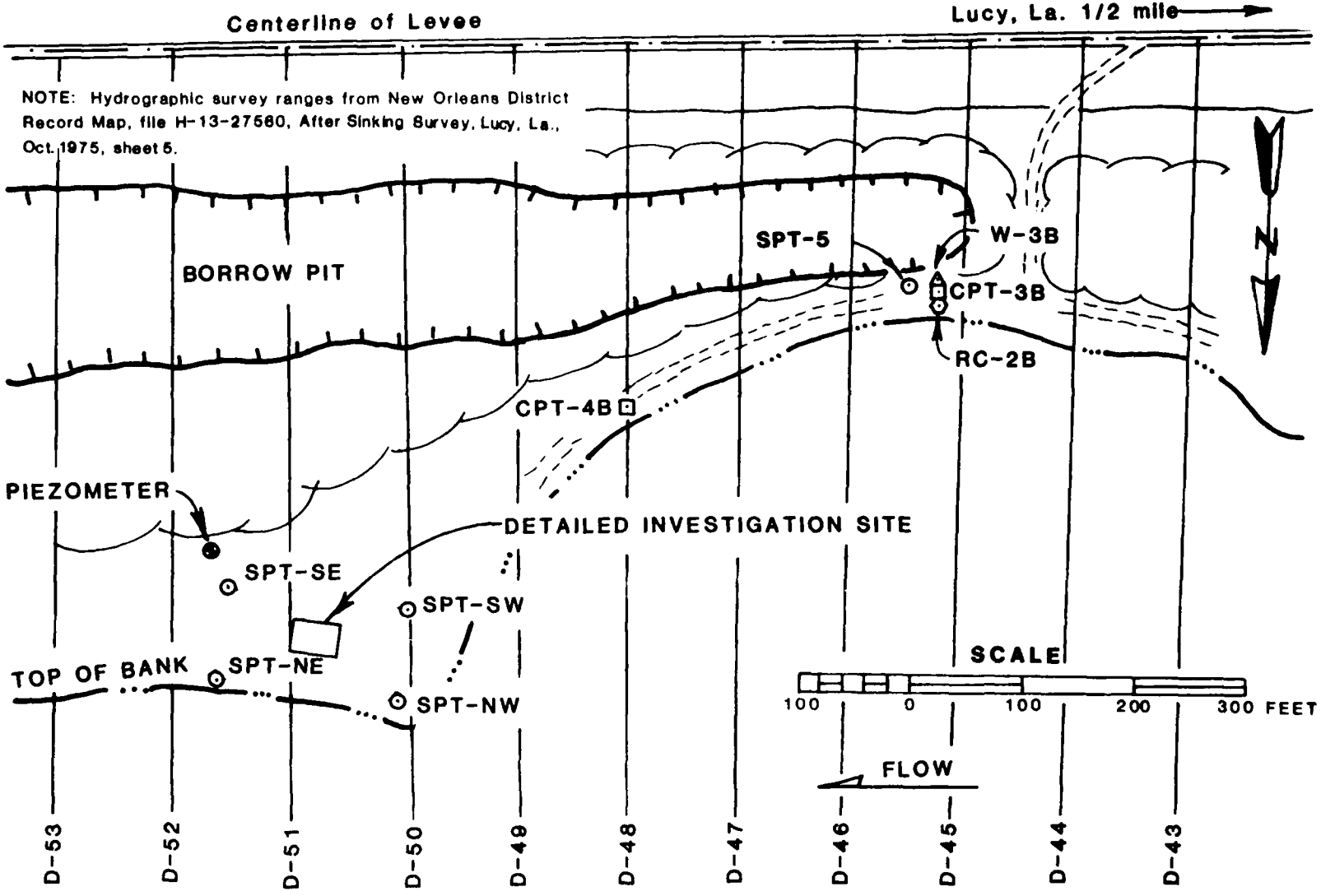


Figure 8. Bonnet Carre Point, locations of reconnaissance borings, detailed site and supplemental borings



Figure 9. Oblique aerial view of the Bonnet Carre Point area and detailed site

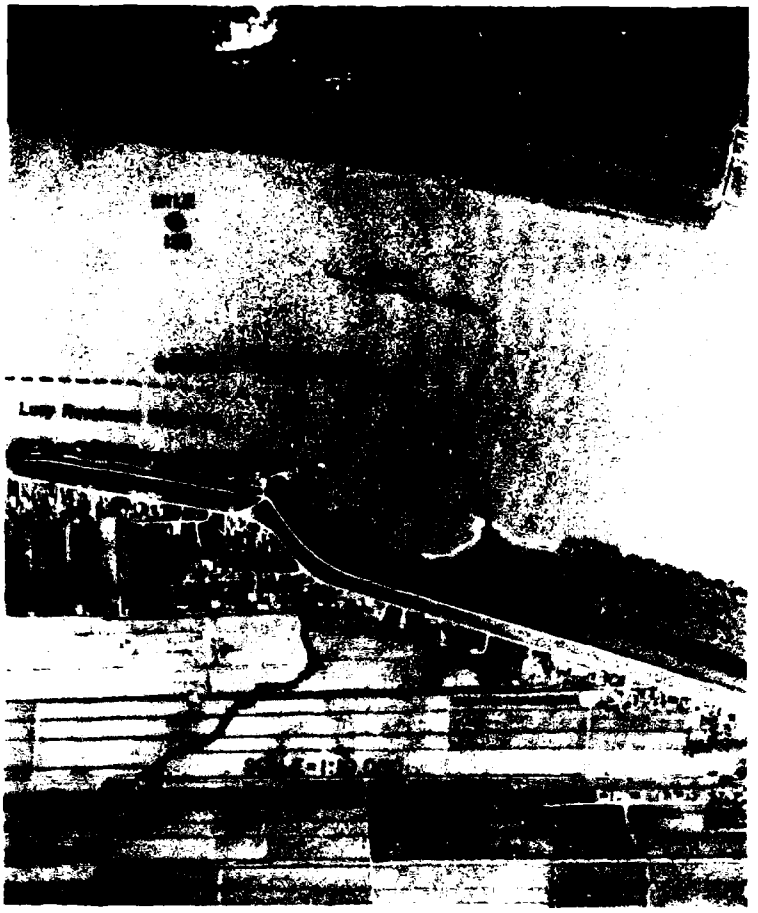


Figure 10. Bonnet Carre Point failure scar and location of the detailed investigation site

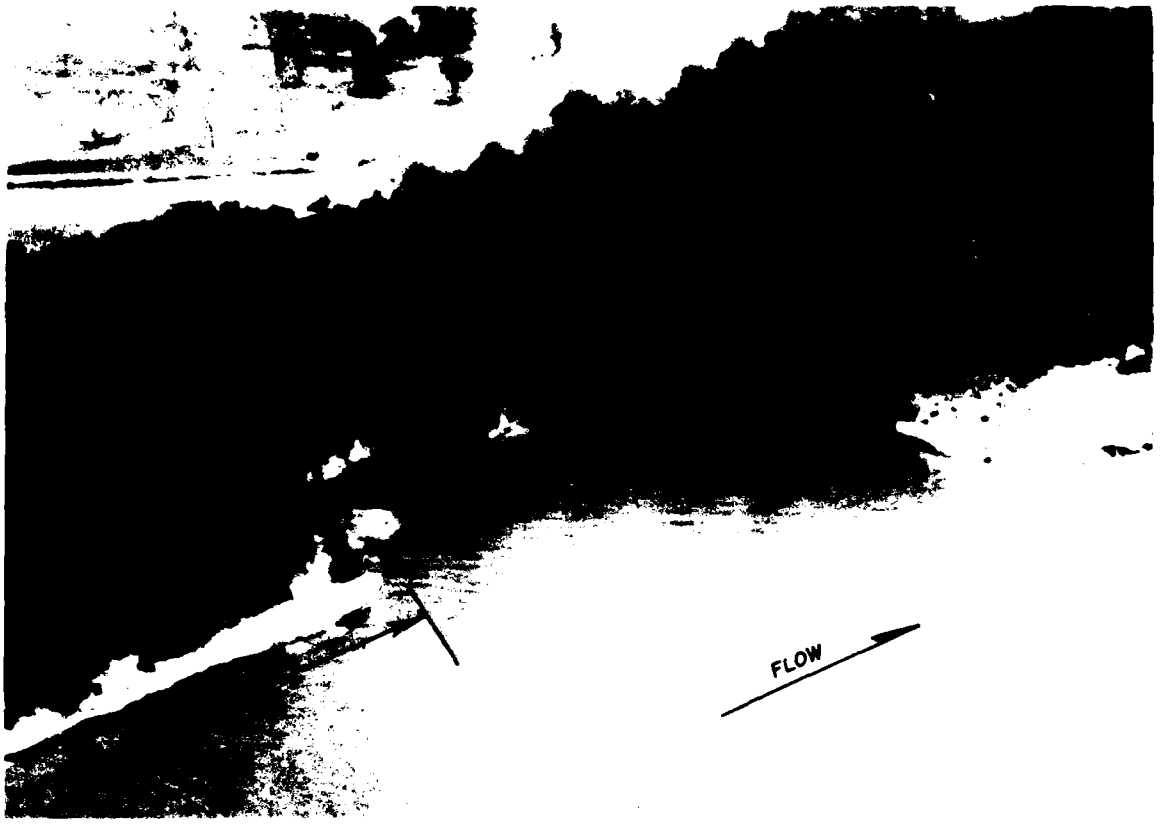


Figure 11. Downstream end-of-revetment failure, Montz, La

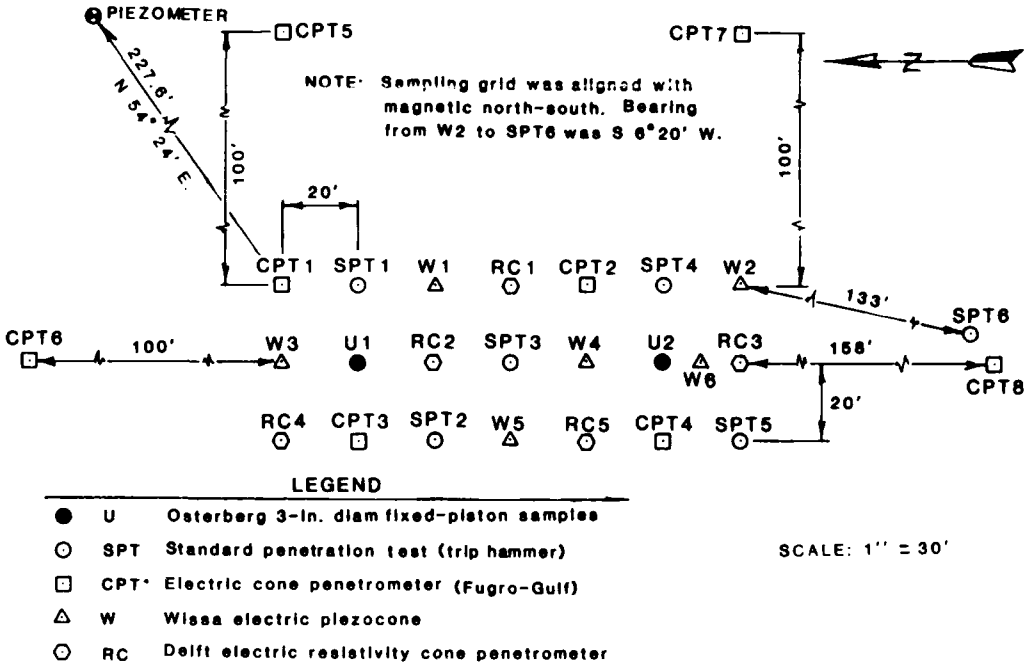


Figure 12. Layout of the sampling and sounding program, Montz detailed site

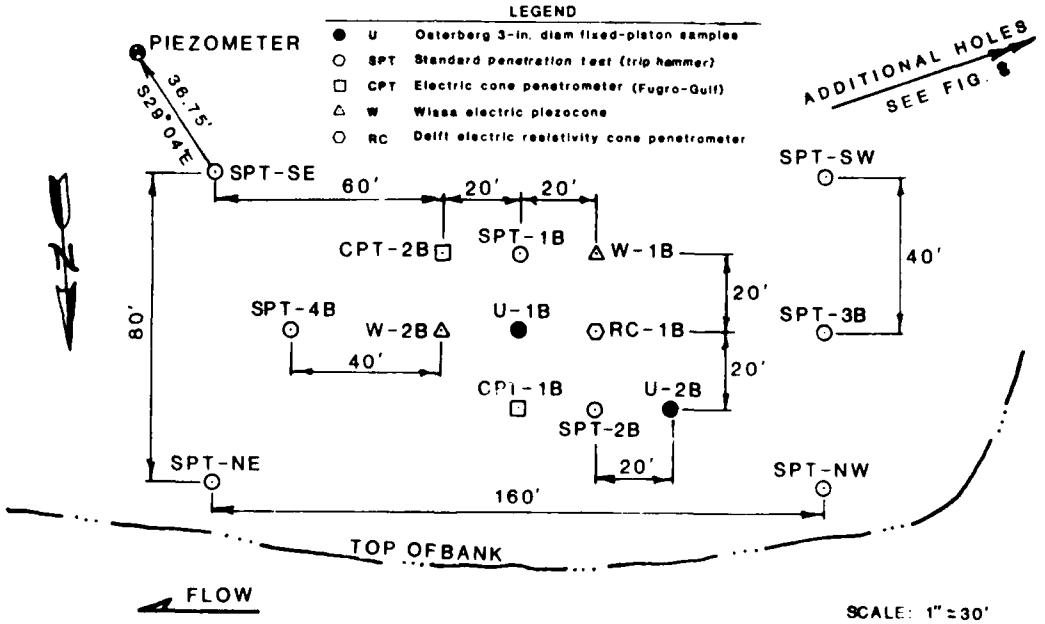


Figure 13. Layout of the sampling and sounding program, Bonnet Carre Point site



a. Samples hung to drain



b. Onsite freezing equipment

Figure 14. Drainage and field freezing of undisturbed samples

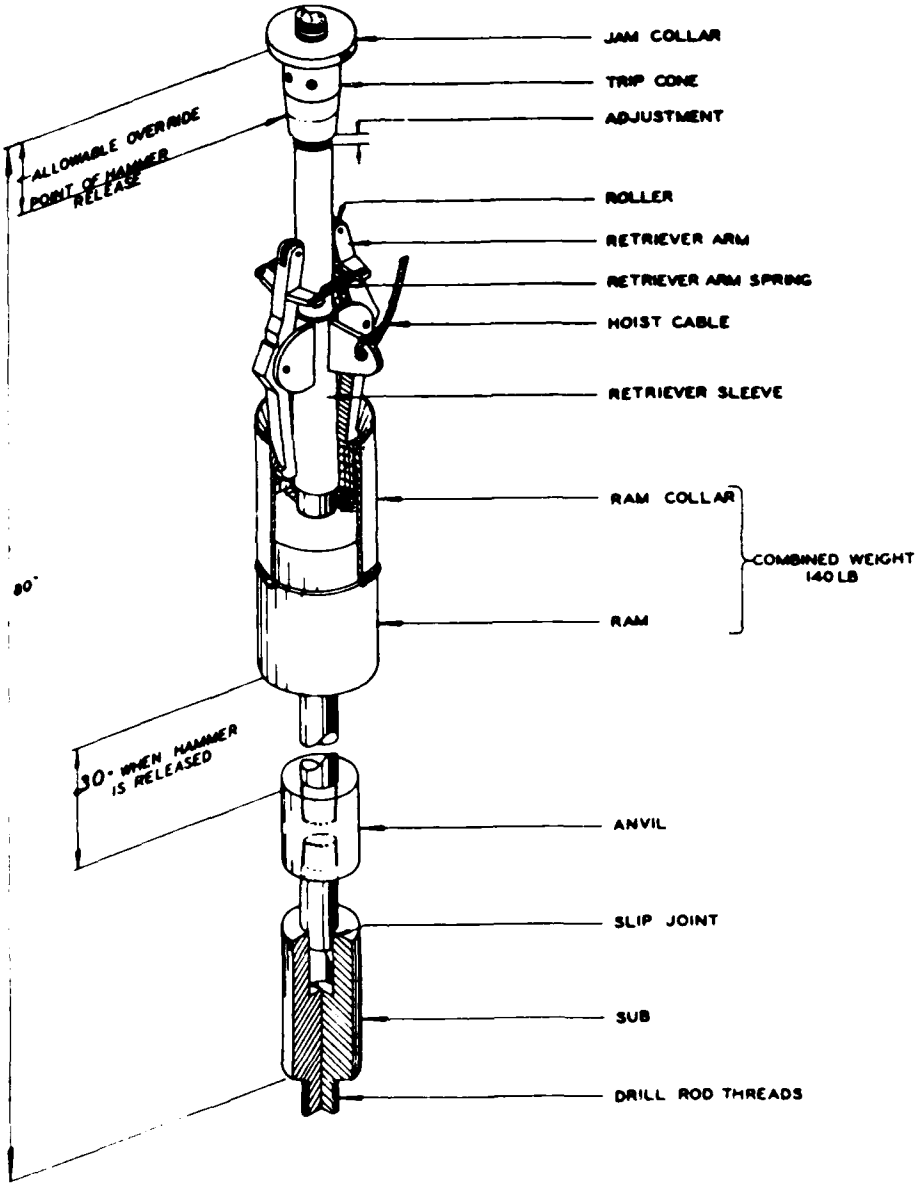


Figure 15. SPT automatic trip hammer, DAMCO

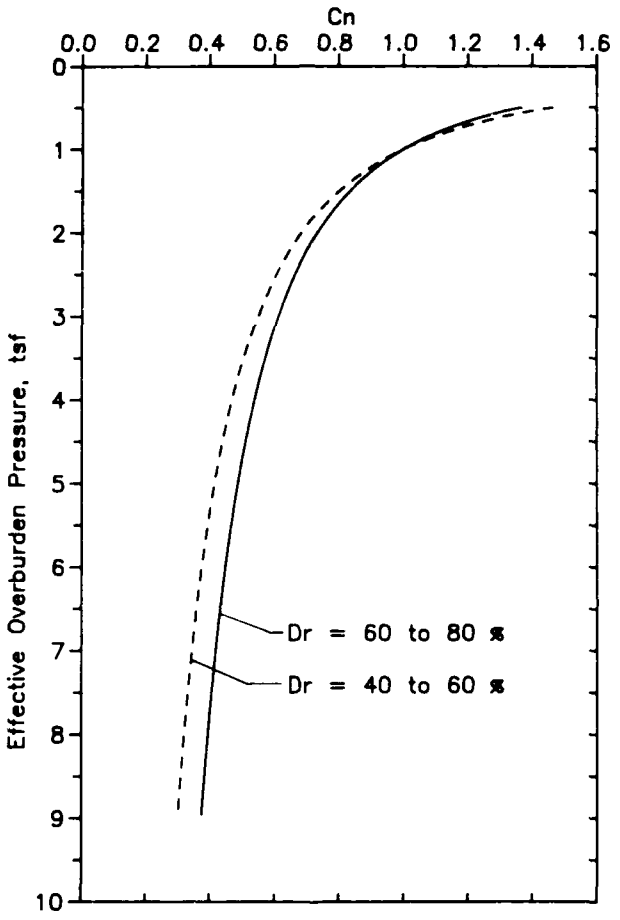
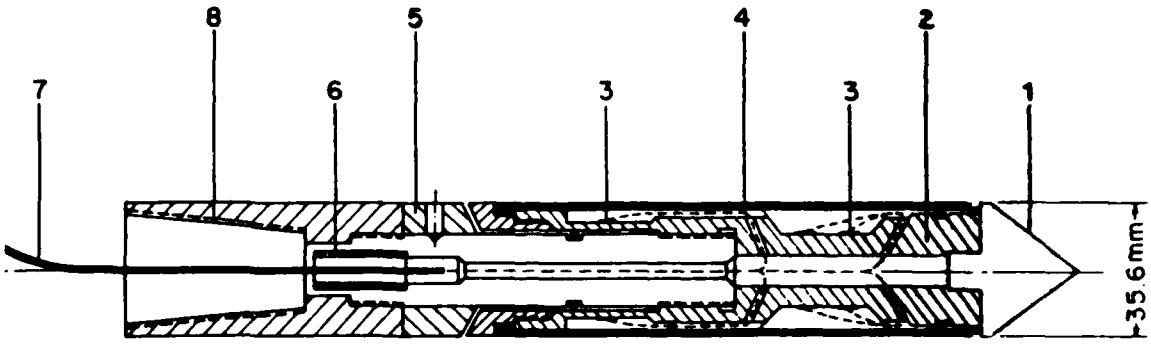


Figure 16. C_N versus effective overburden pressure (after Seed, Idriss, and Arango 1983)



1 Conical point (10 cm²)
2 Load cell
3 Strain gages
4 Friction sleeve (150 cm²)
5 Adjustment ring
6 Waterproof bushing
7 Cable
8 Connection with rods

Figure 17. Electric cone penetrometer



Figure 18. Fugro-Gulf, Inc., 20-ton cone penetrometer rig

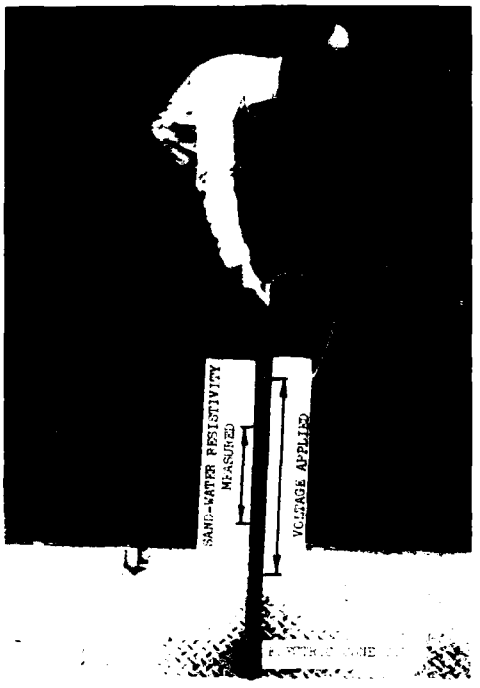


Figure 19. Delft resistivity cone penetrometer



Figure 20. Delft water probe

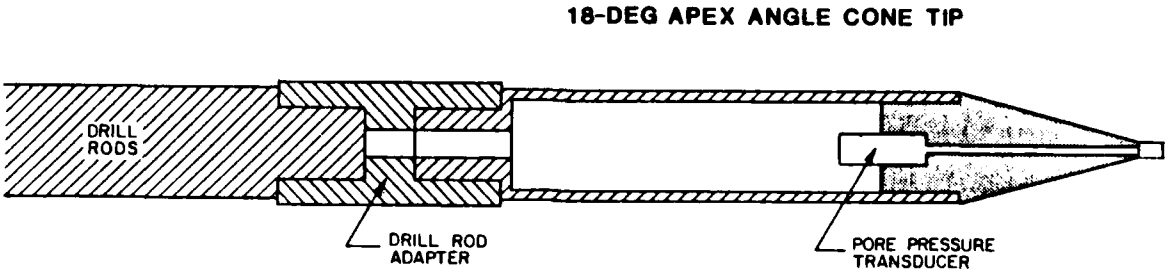


Figure 21. Wissa piezometer probe

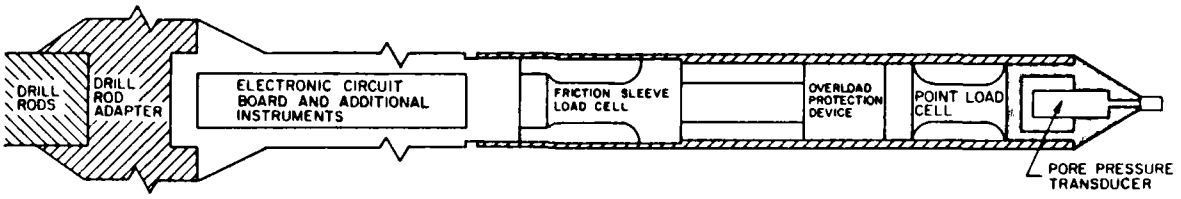
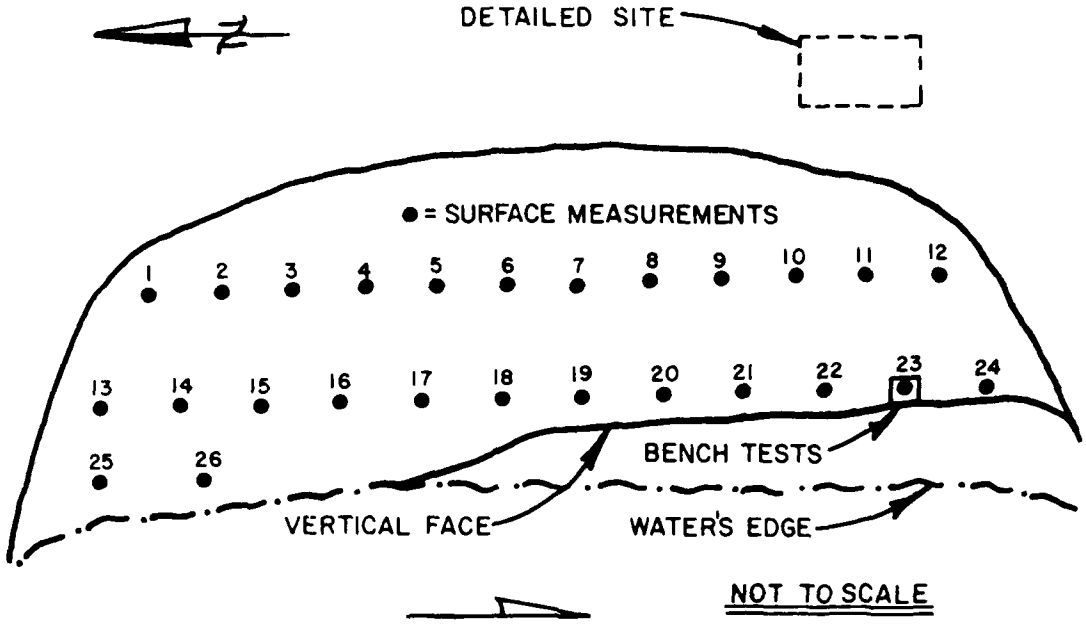
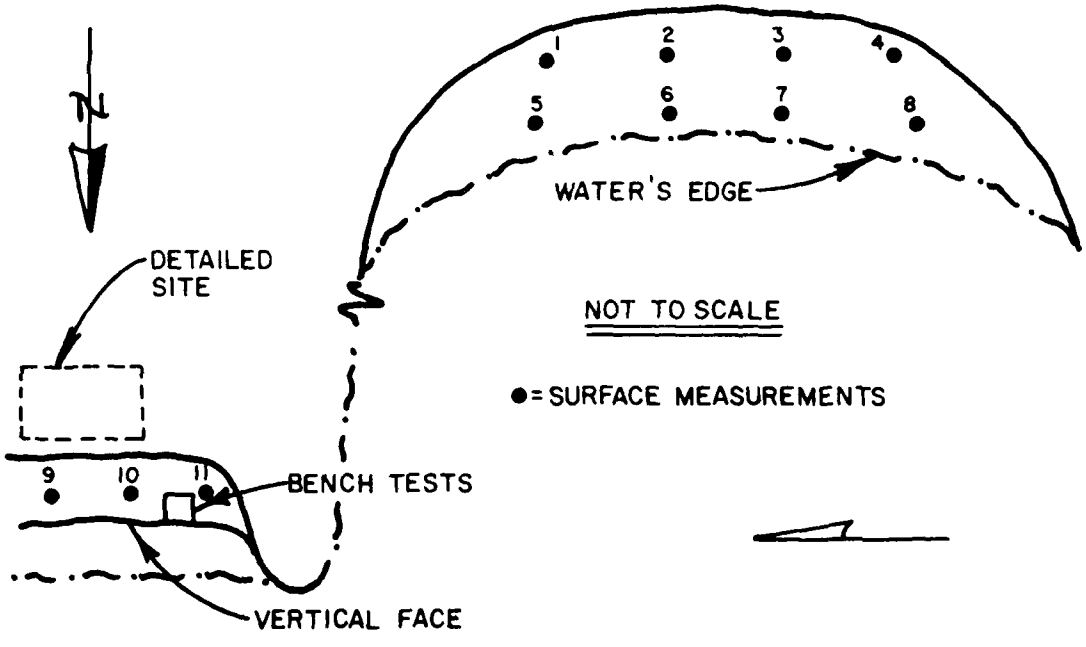


Figure 22. Wissa piezocone



a. Montz fresh deposit



b. Bonnet Carre Point fresh deposits

Figure 23. Nuclear gage density measurements

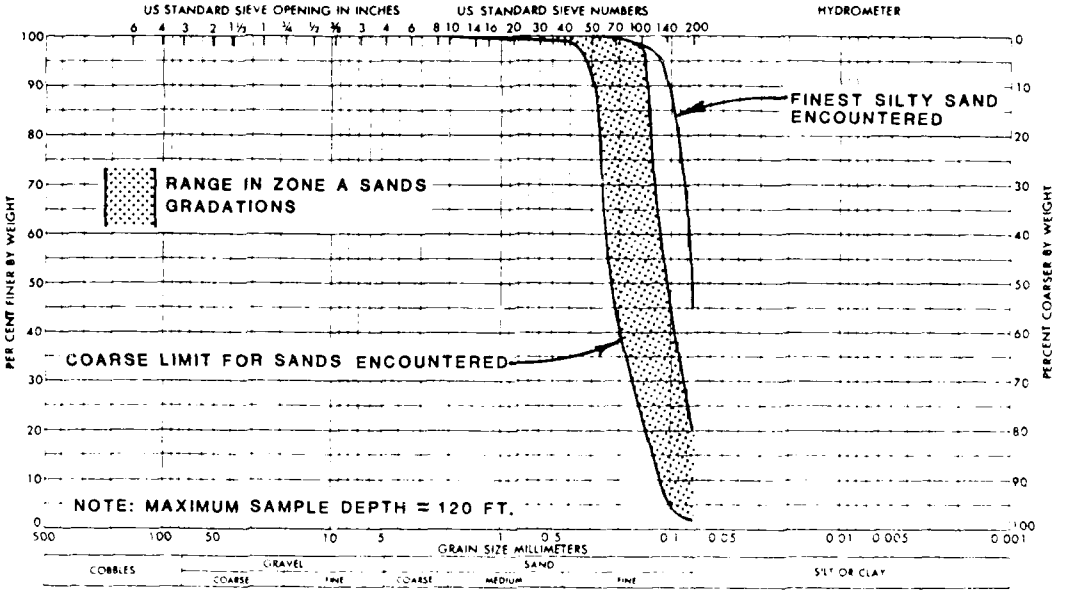


Figure 24. Range in gradations of substratum sands, Montz site

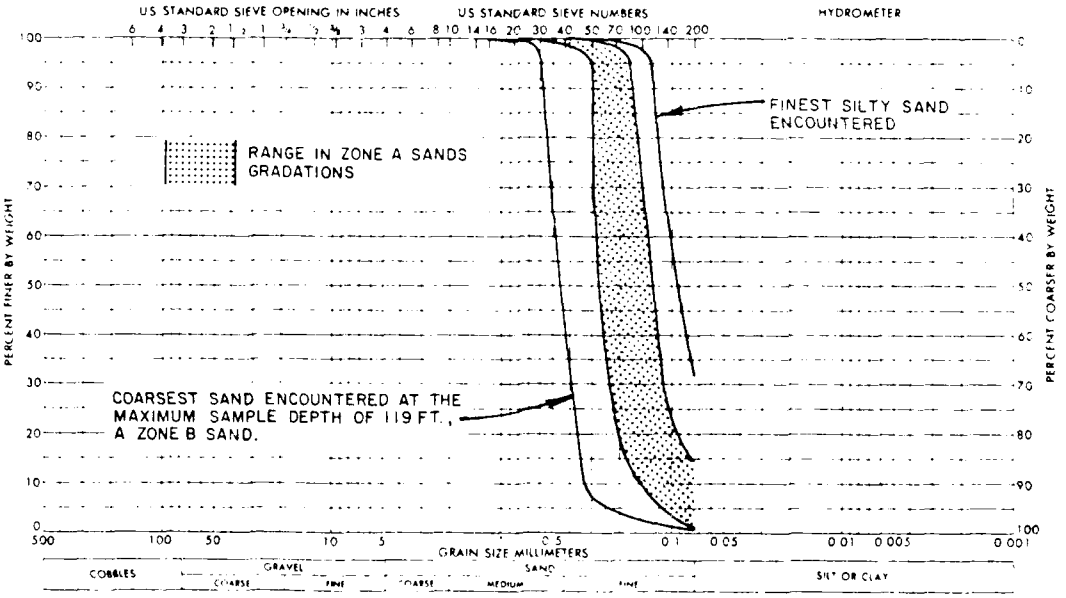


Figure 25. Range in gradations of substratum sands, Bonnet Carre Point site

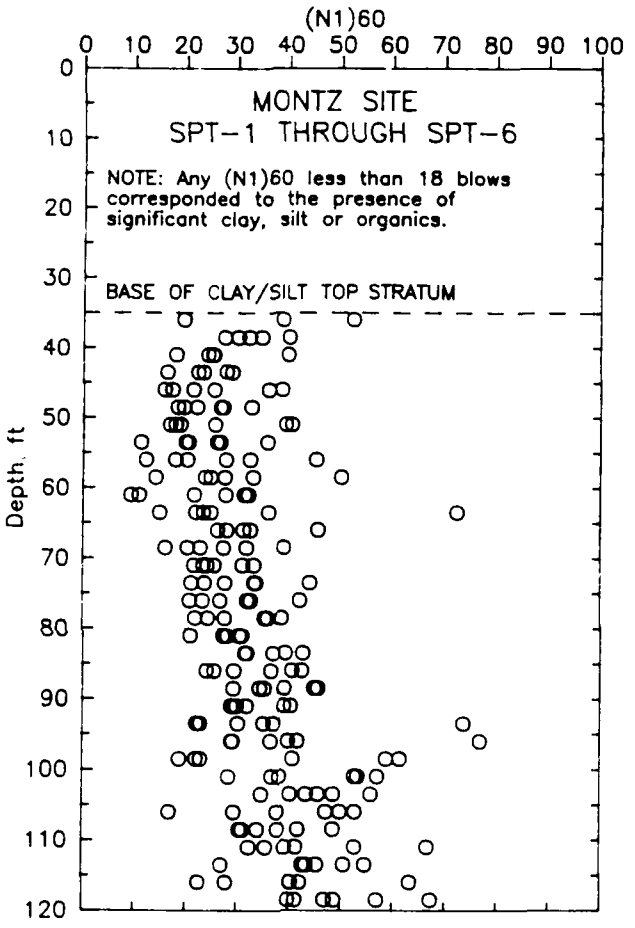


Figure 26. Summary plot of corrected SPT data, Montz site

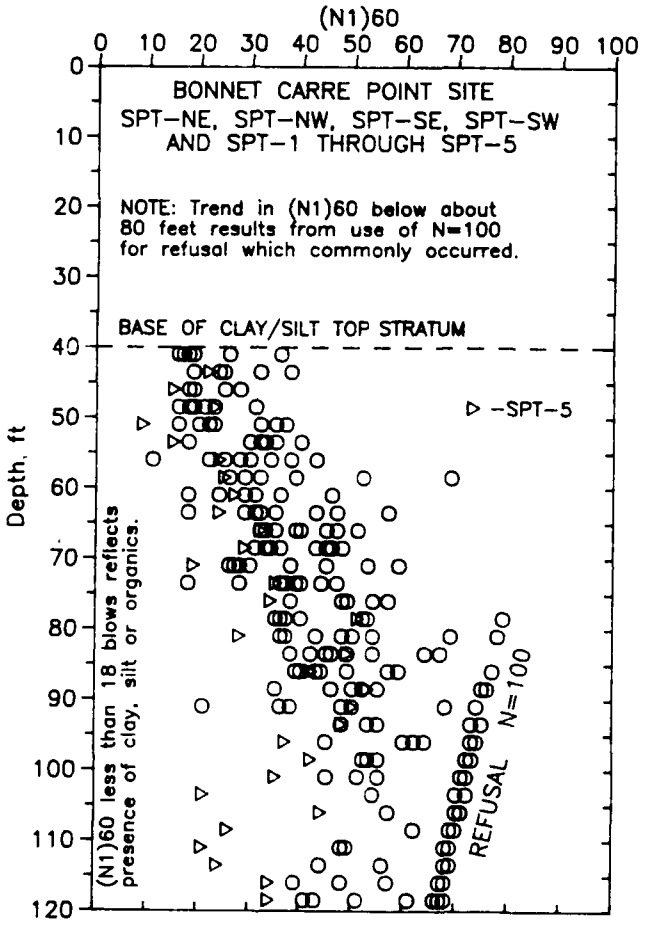


Figure 27. Summary plot of corrected SPT data Bonnet Carre Point site

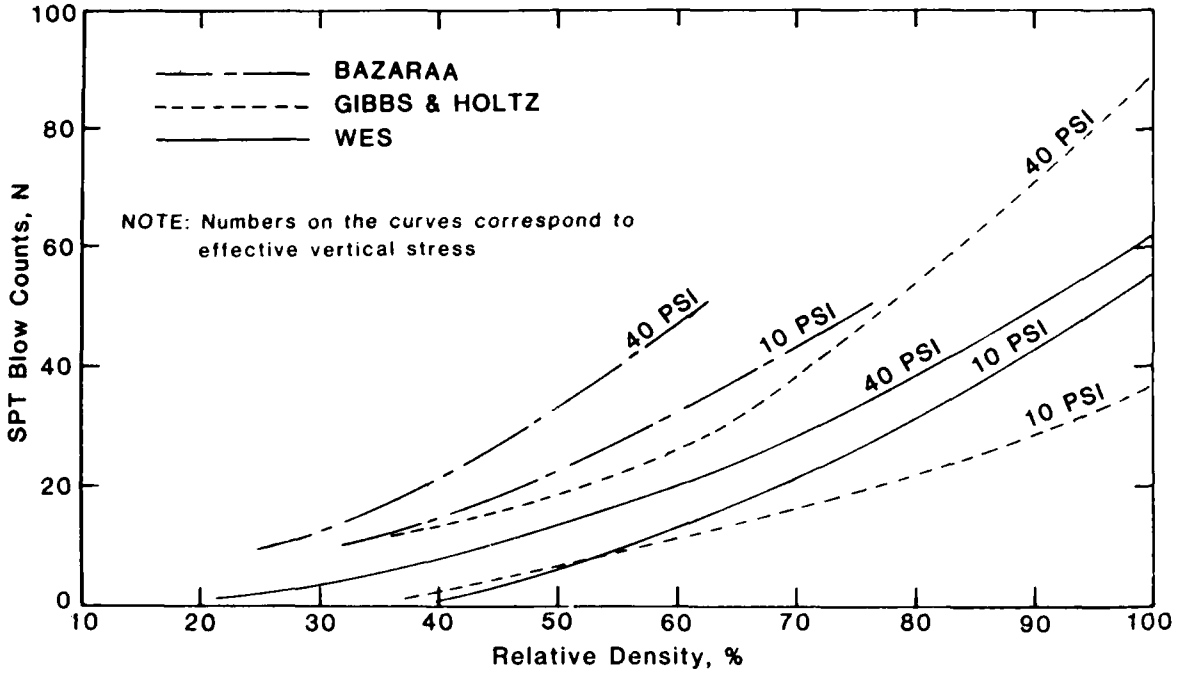


Figure 28. Laboratory correlations between SPT blow count and relative density

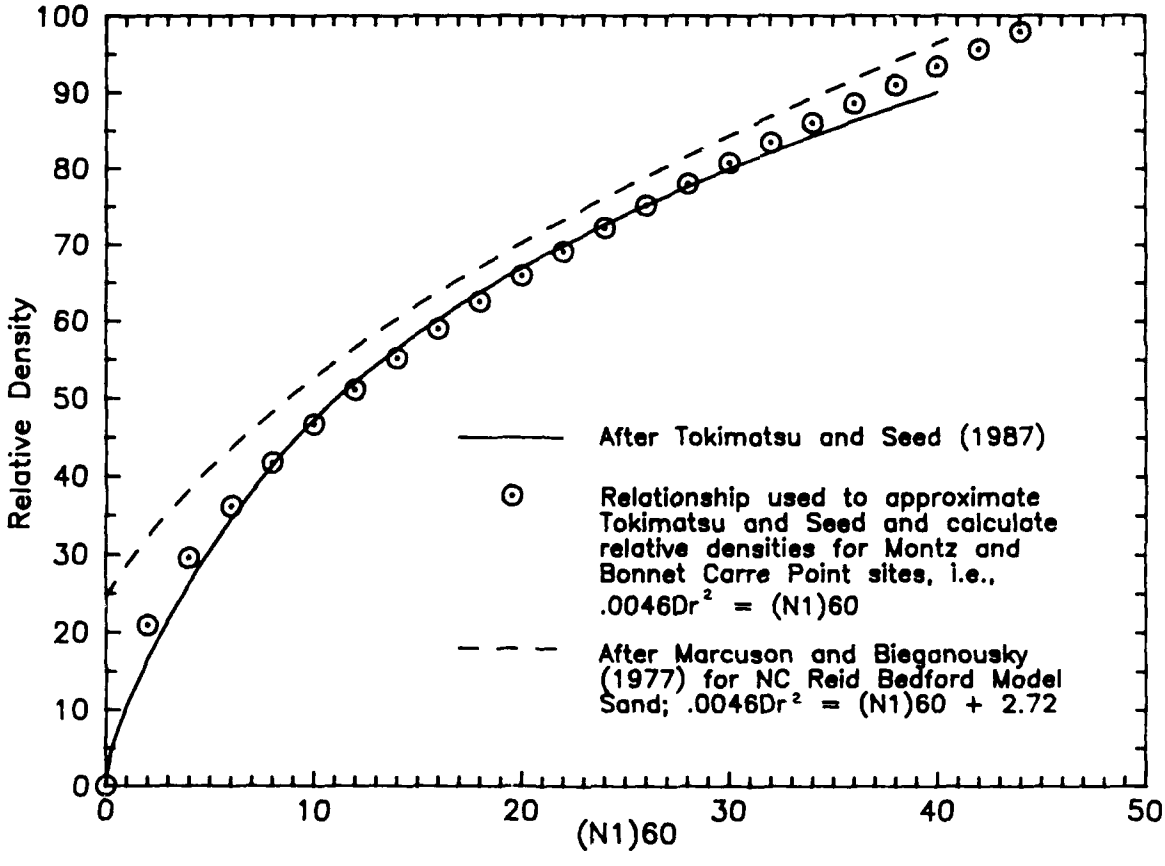


Figure 29. Relationship between relative density and $(N_1)_{60}$

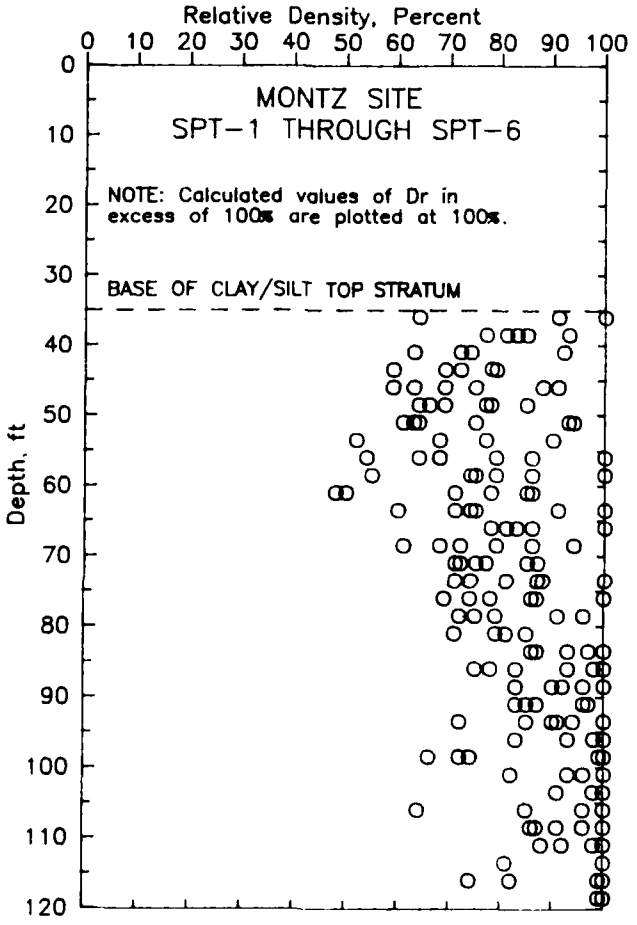


Figure 30. Summary plot of calculated relative densities, Montz site

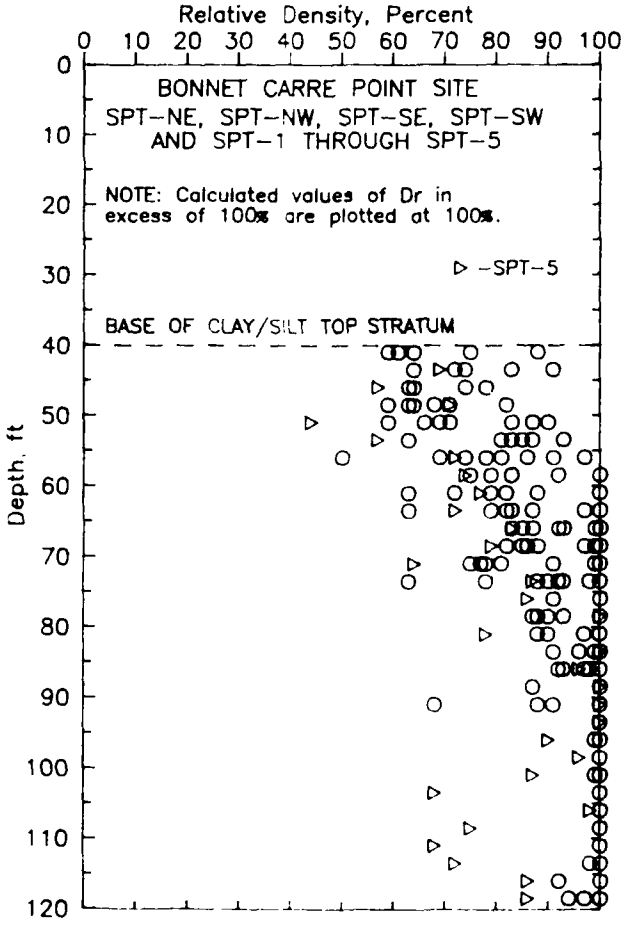


Figure 31. Summary plot of calculated relative densities, Bonnet Carre Point site

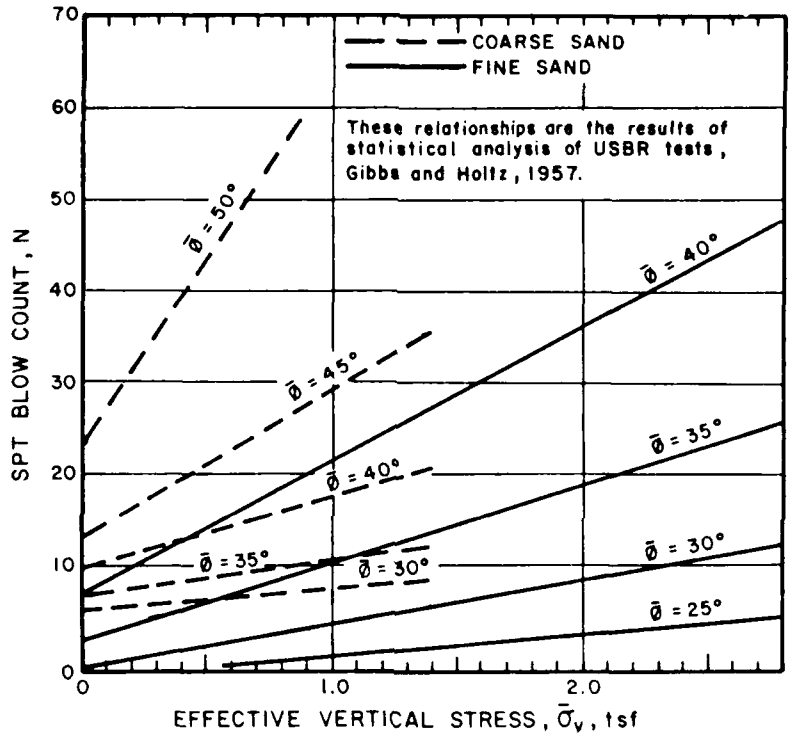


Figure 32. SPT blow count versus effective vertical stress and effective angle of internal friction (after DeMello 1971)

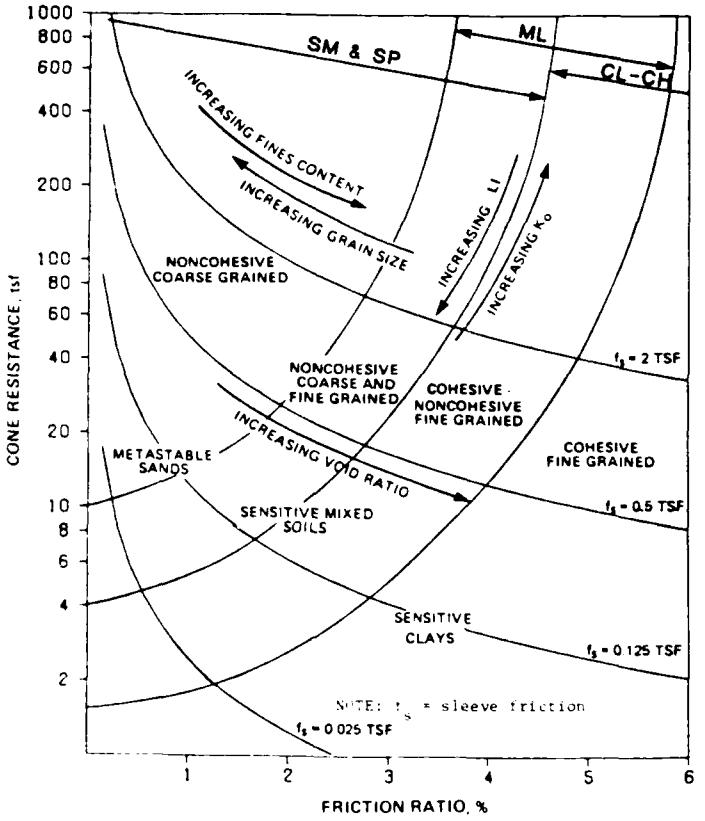


Figure 33. CPT soil classification chart (after Douglas and Olsen 1981)

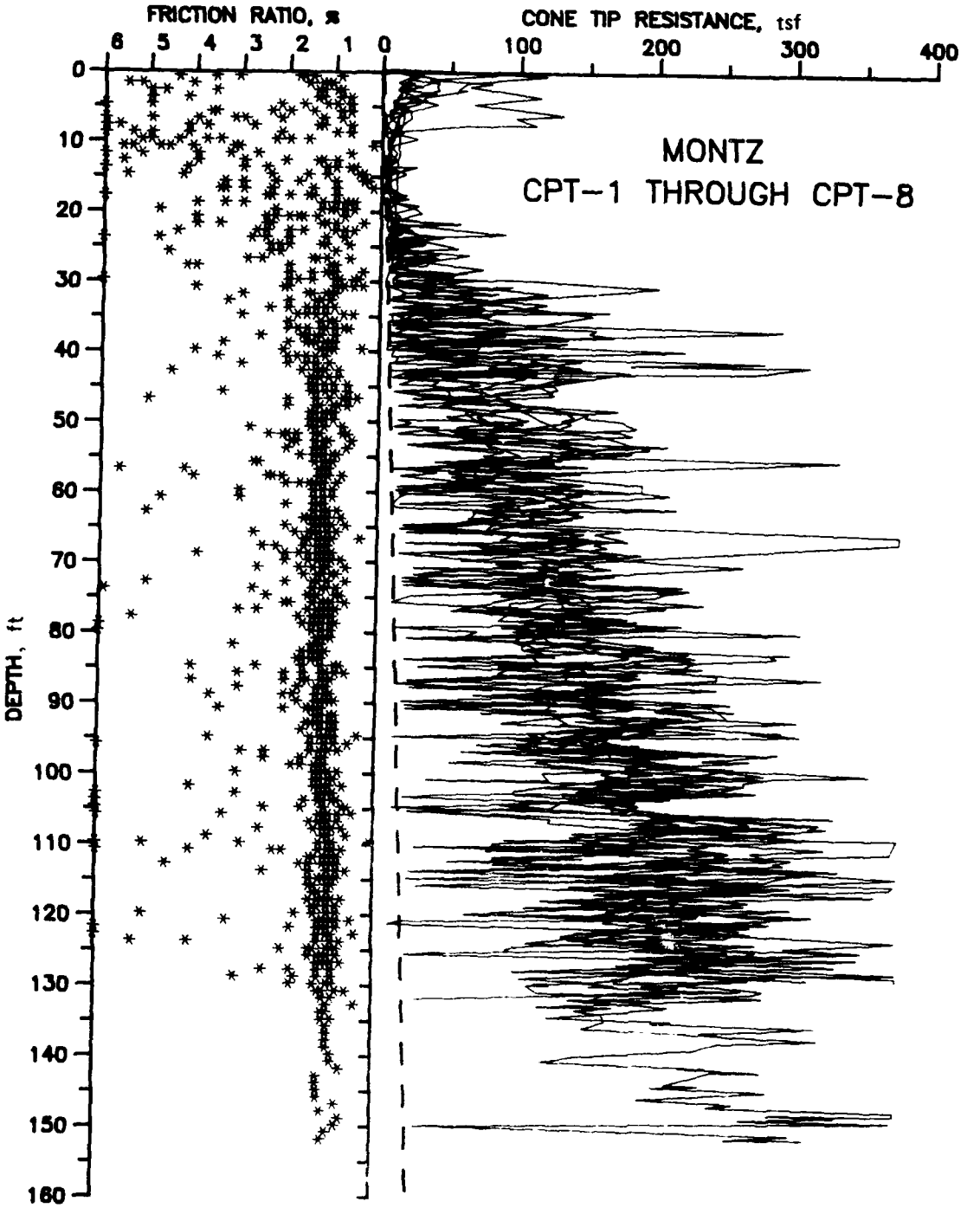


Figure 34. Summary plot of CPT results, Montz site

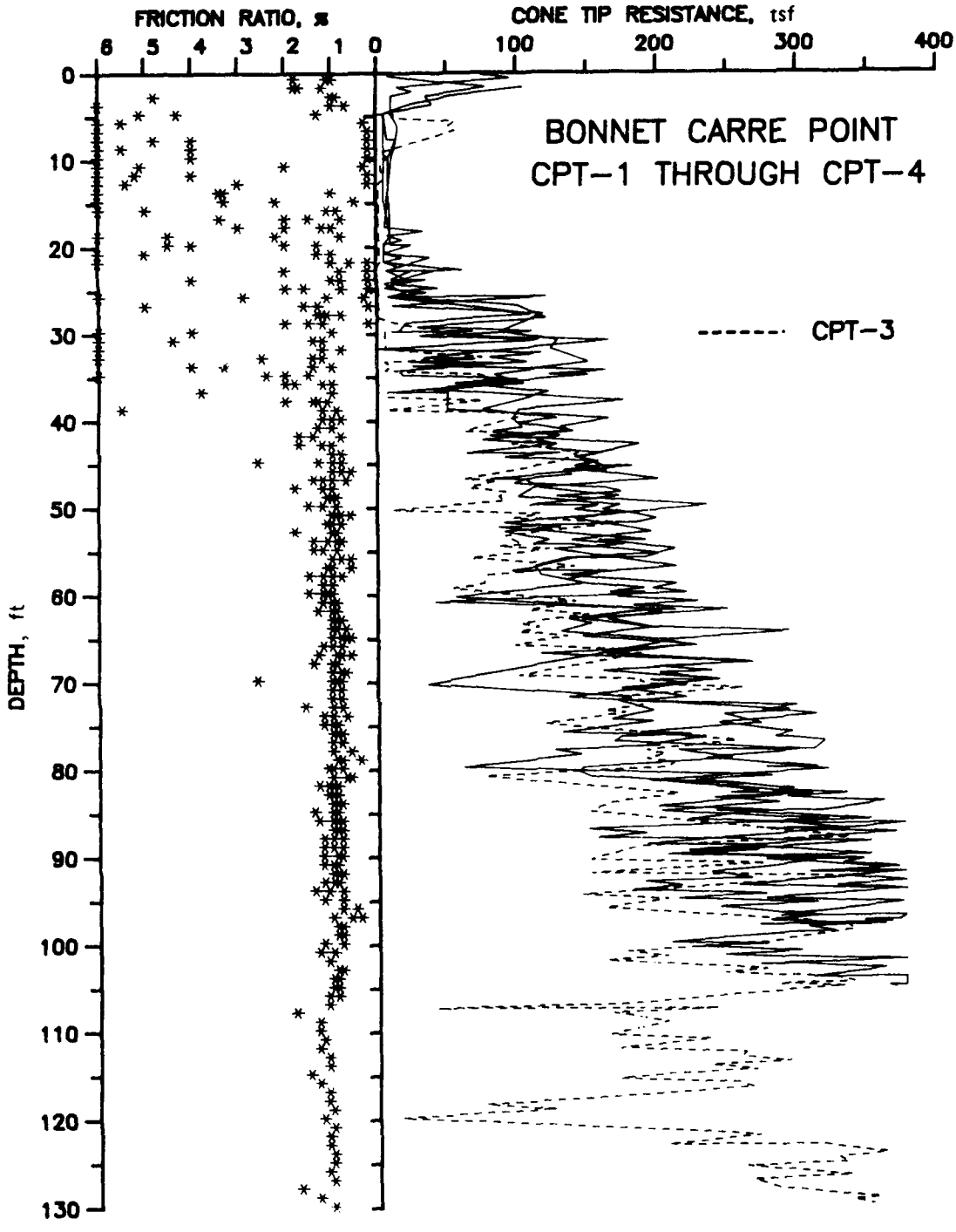


Figure 35. Summary plot of CPT results, Bonnet Carre Point site

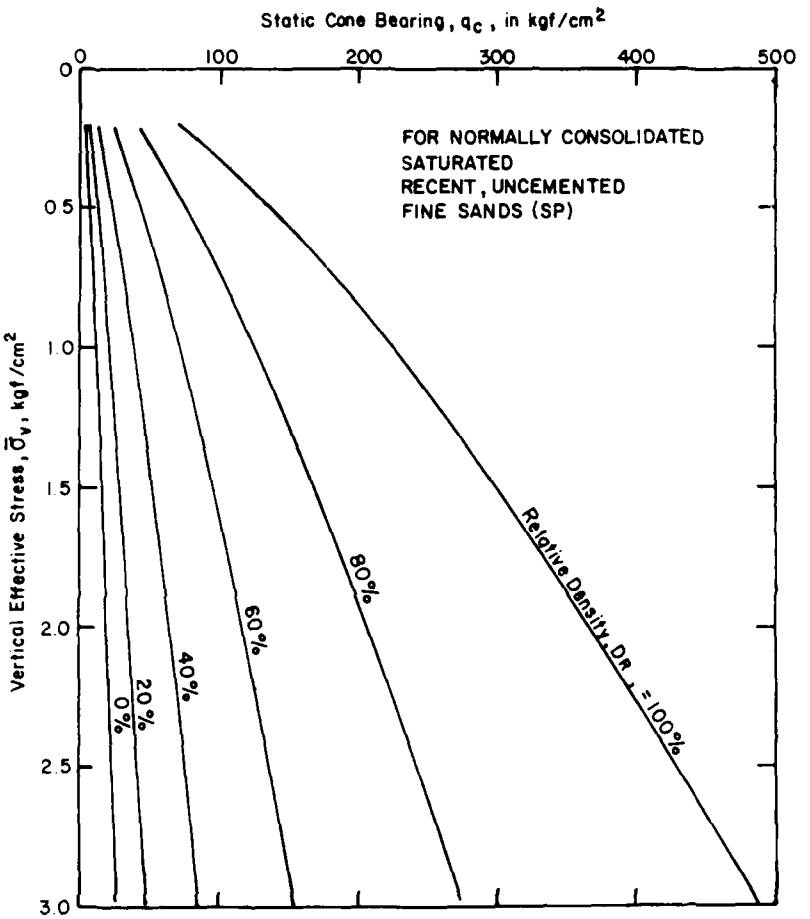


Figure 36. CPT relative density chart
(after Schmertmann 1978)

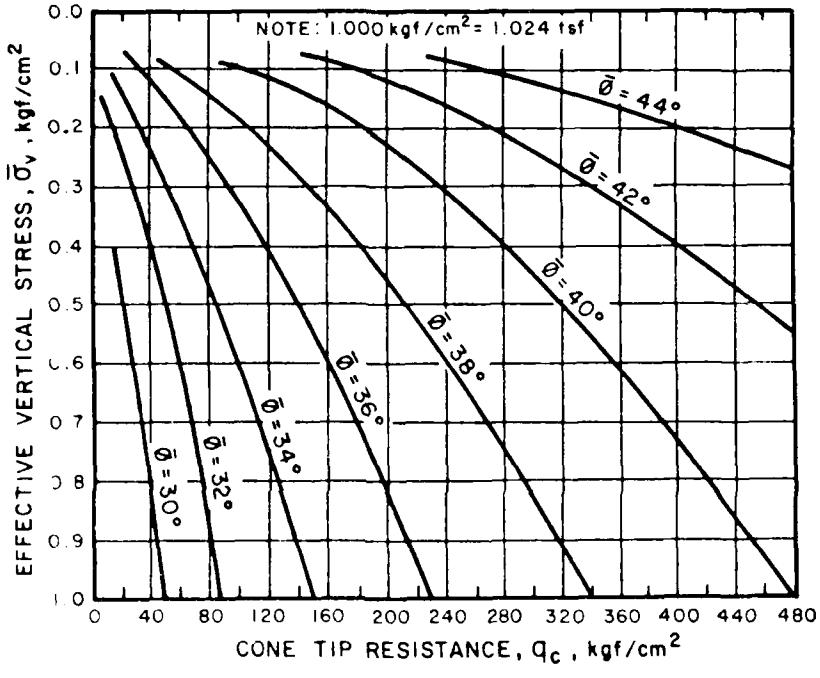


Figure 37. CPT chart for estimating in situ effective angle of internal friction (after Trofimenkov 1974)

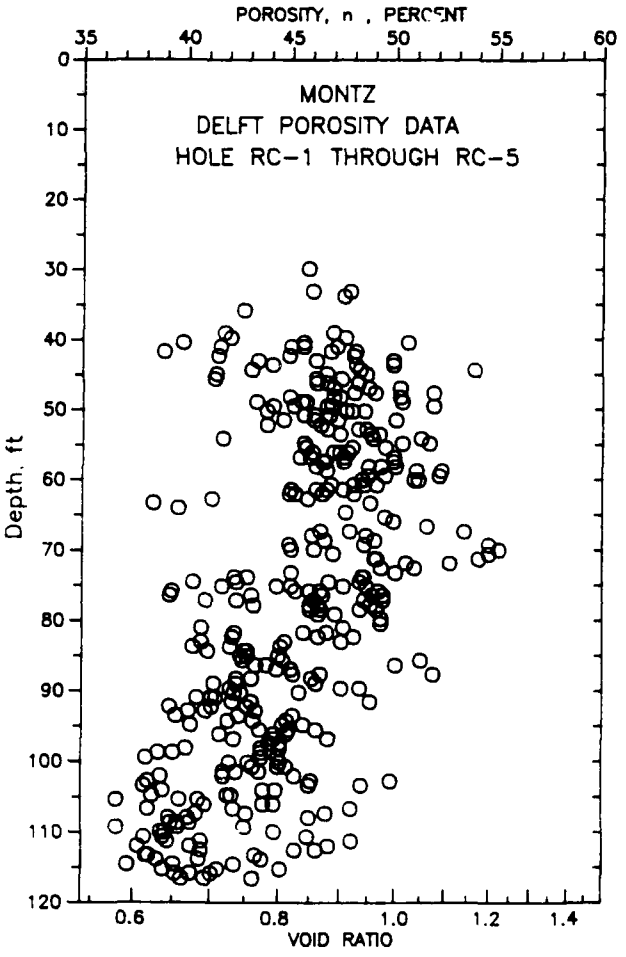


Figure 38. Summary plot of DELFT porosity data, Montz site

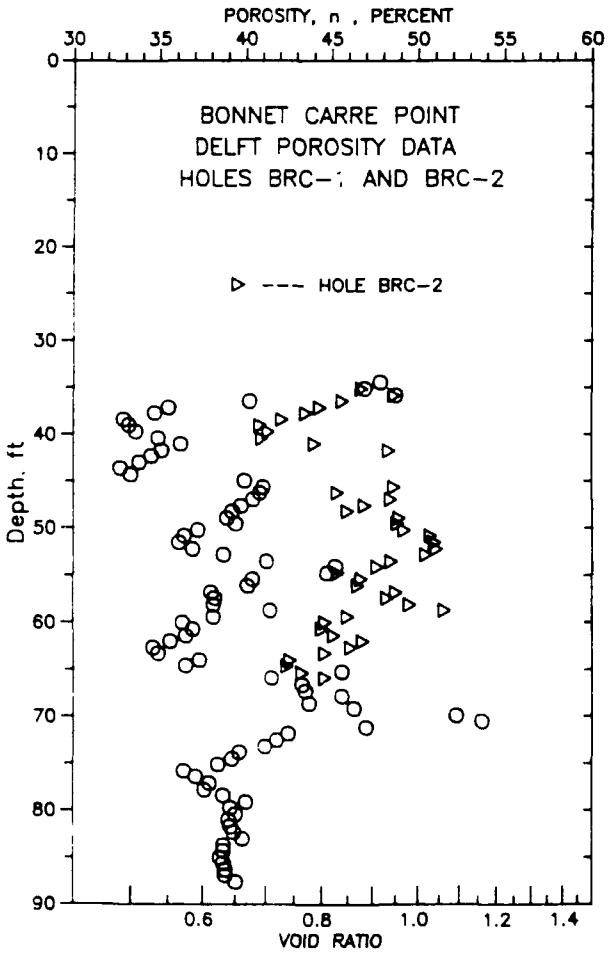


Figure 39. Summary plot of DELFT porosity data, Bonnet Carre Point site

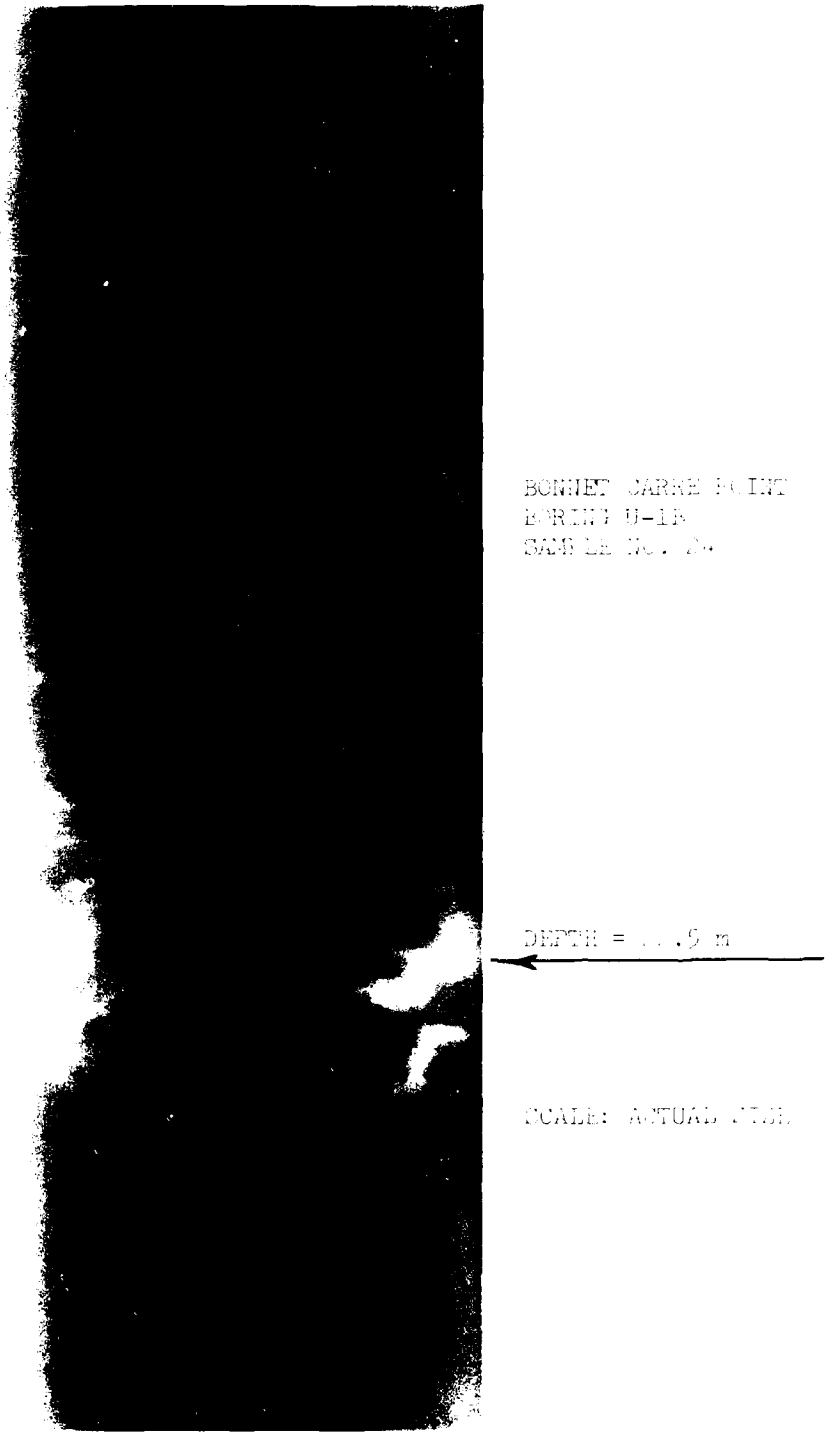


Figure 40. Loose lense anomaly detected by DELFT resistivity probe, Bonnet Carre Point site

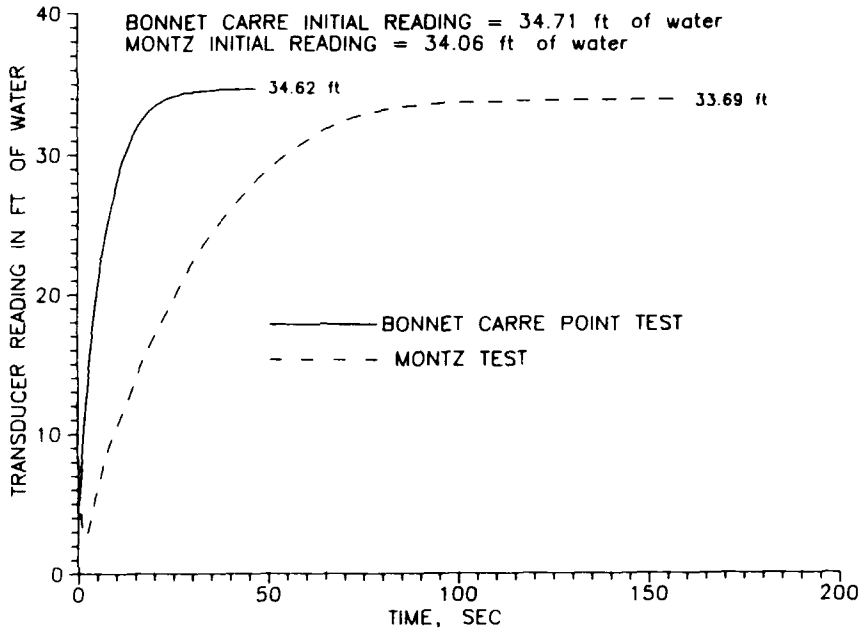
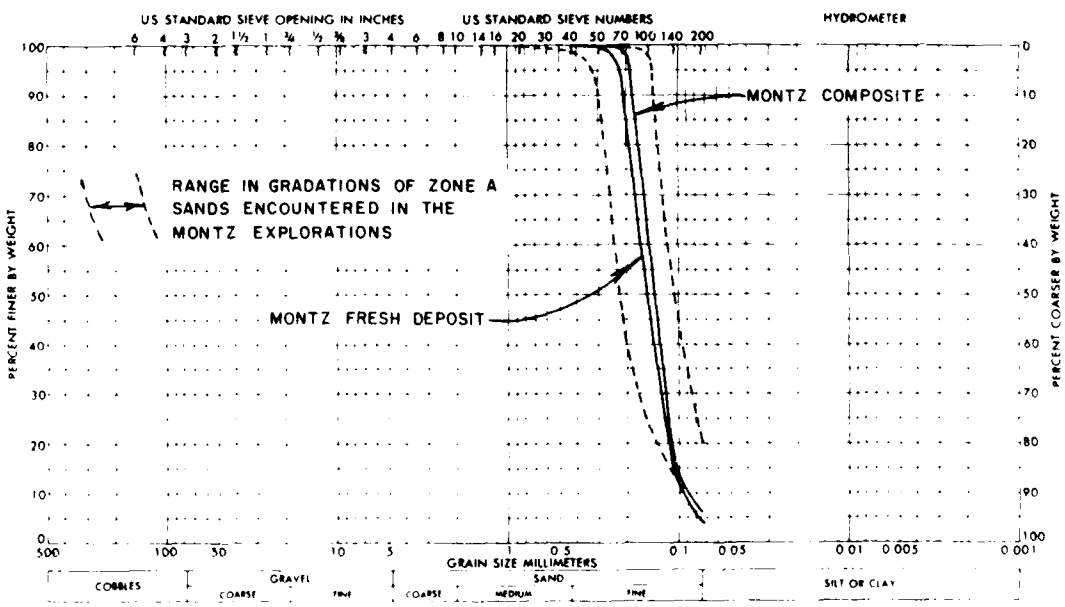


Figure 41. Rising-head tests in piezometers at the Montz and Bonnet Carre Point sites



42. Montz fresh deposit, grab sample gradation

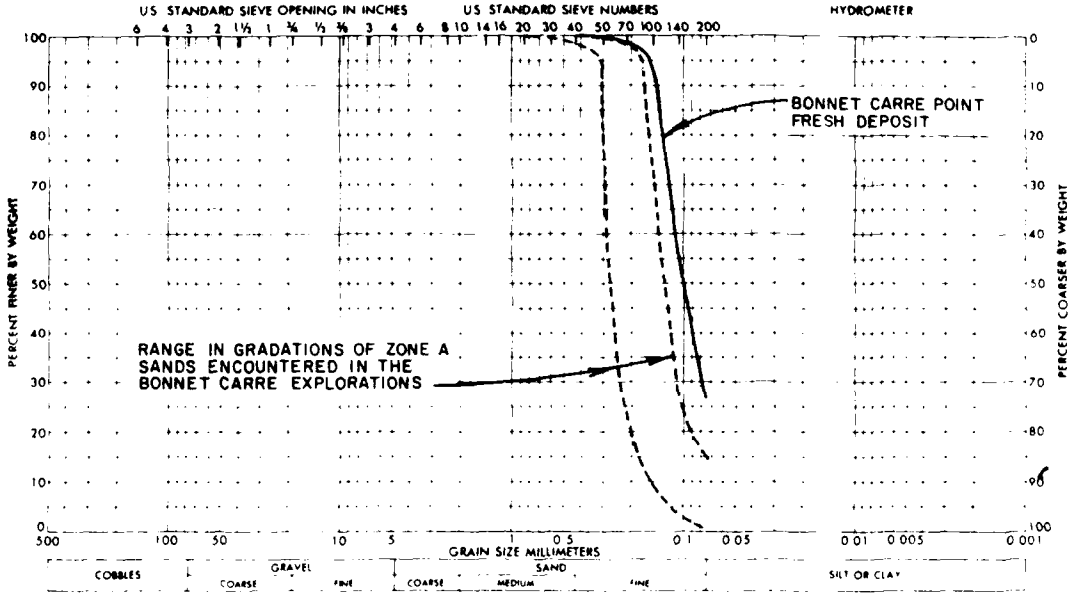


Figure 43. Bonnet Carre Point, fresh deposit grab sample gradation

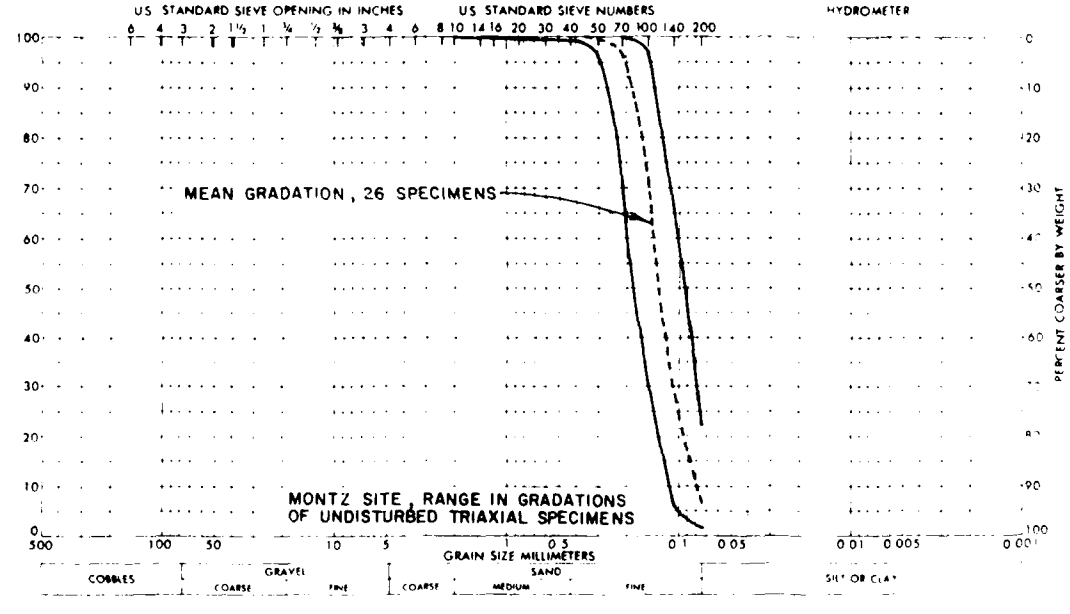


Figure 44. Range in gradations of undisturbed triaxial specimens, Montz site

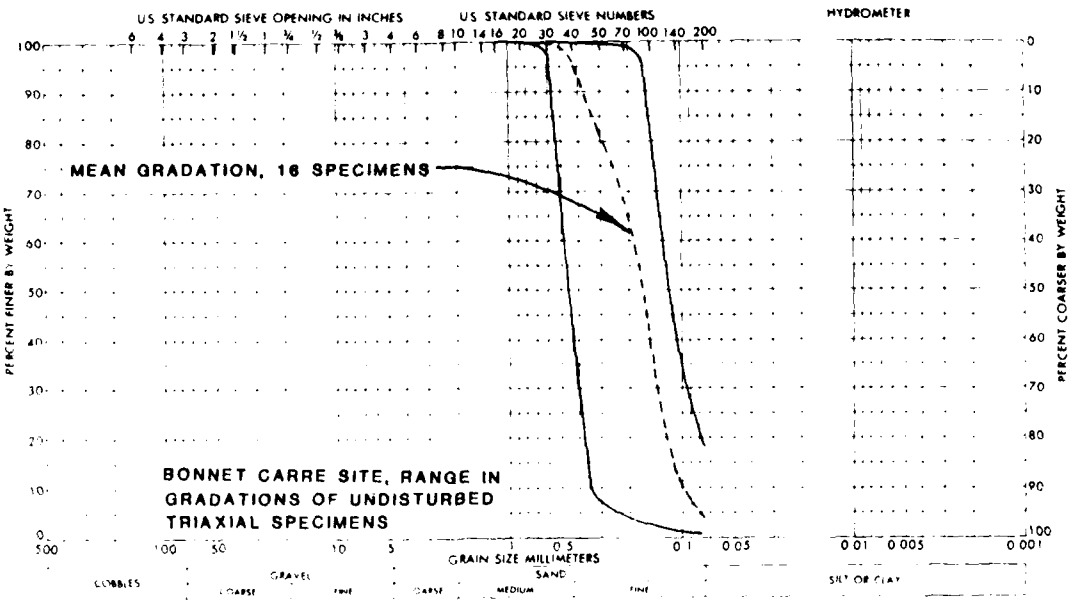


Figure 45. Range in gradations of undisturbed triaxial specimens, Bonnet Carre Point site

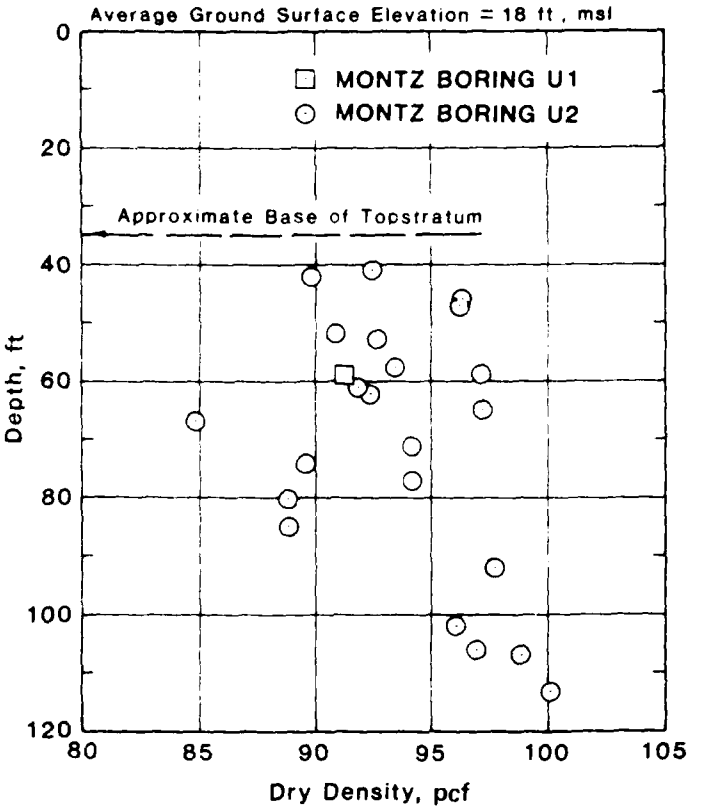


Figure 46. Dry densities of Montz undisturbed specimens

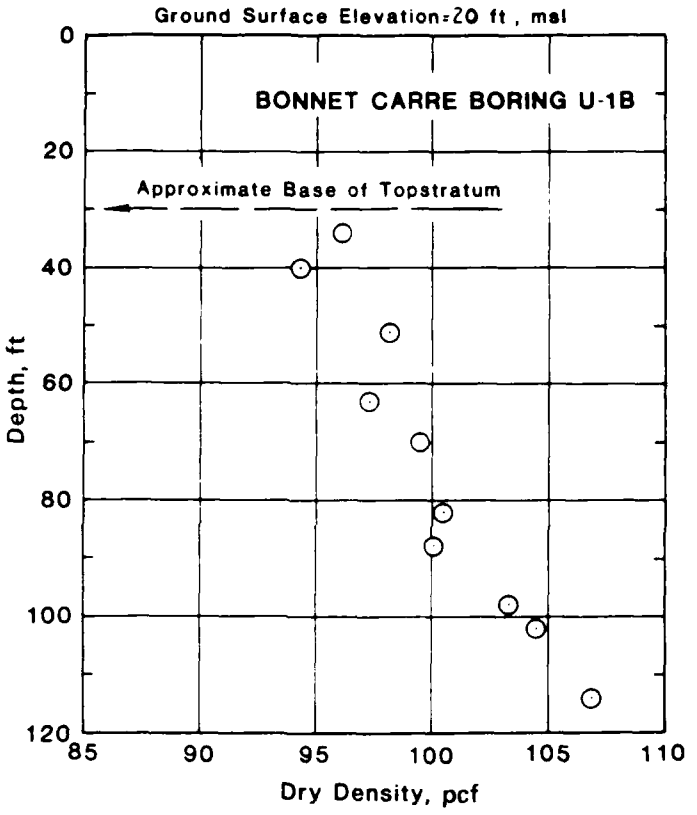


Figure 47. Dry densities of Bonnet Carre Point undisturbed triaxial specimens from boring U-1B

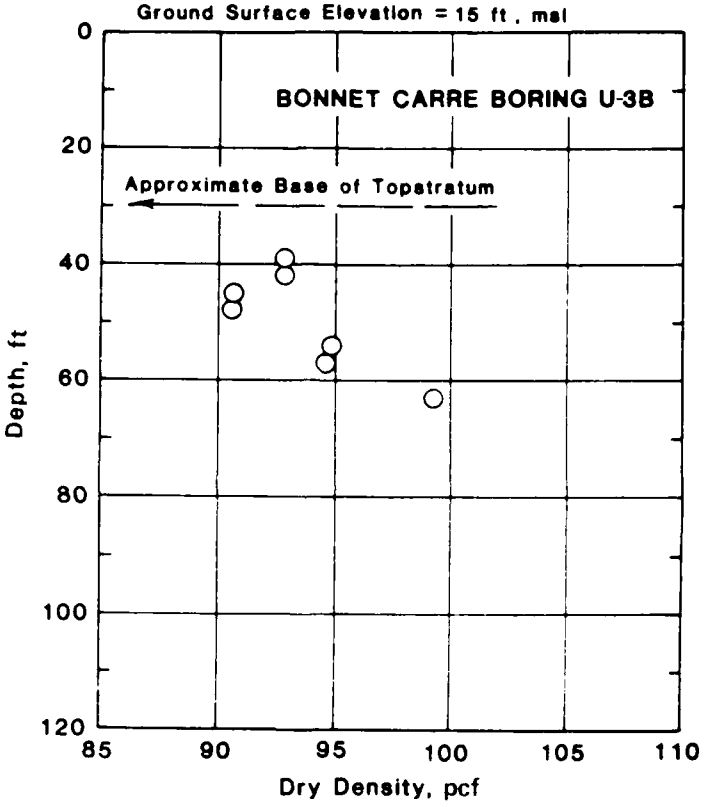


Figure 48. Dry densities of Bonnet Carre Point undisturbed triaxial specimens from boring U-3B

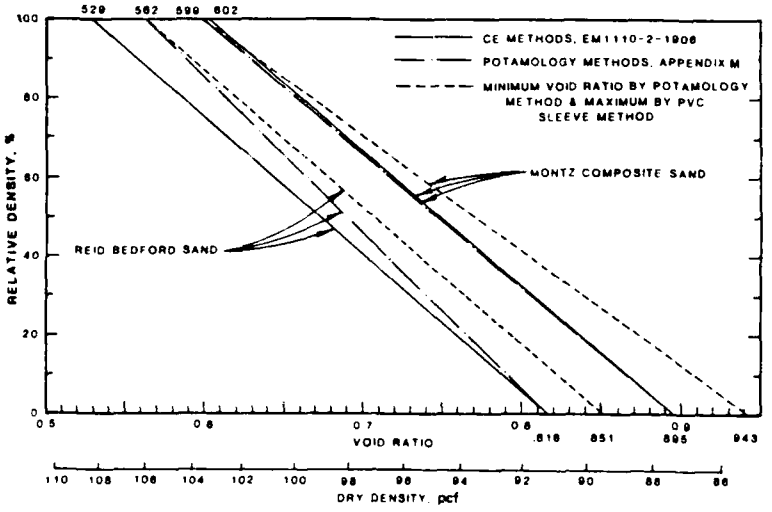


Figure 49. Comparison of maximum and minimum void ratios obtained by CE and potomalogy methods

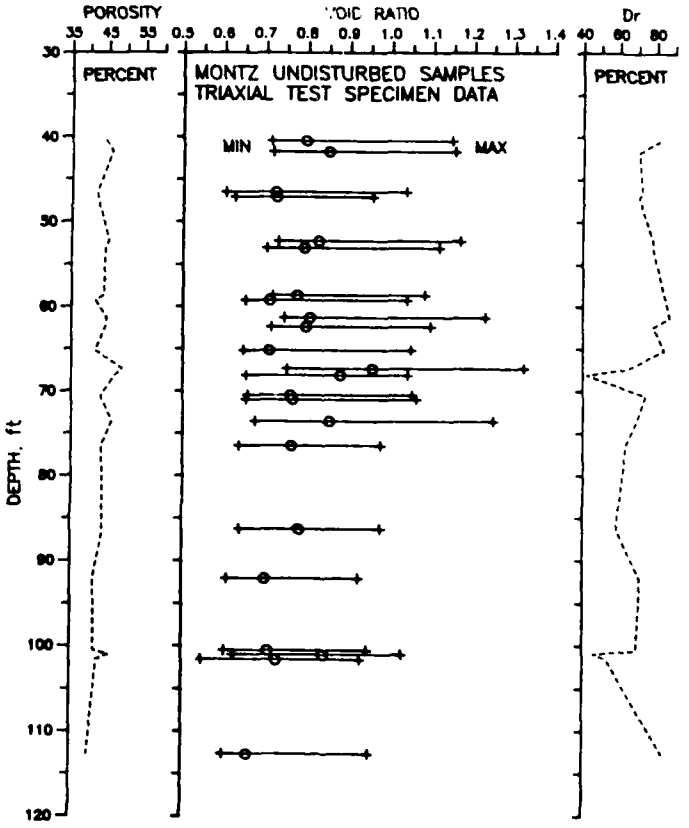
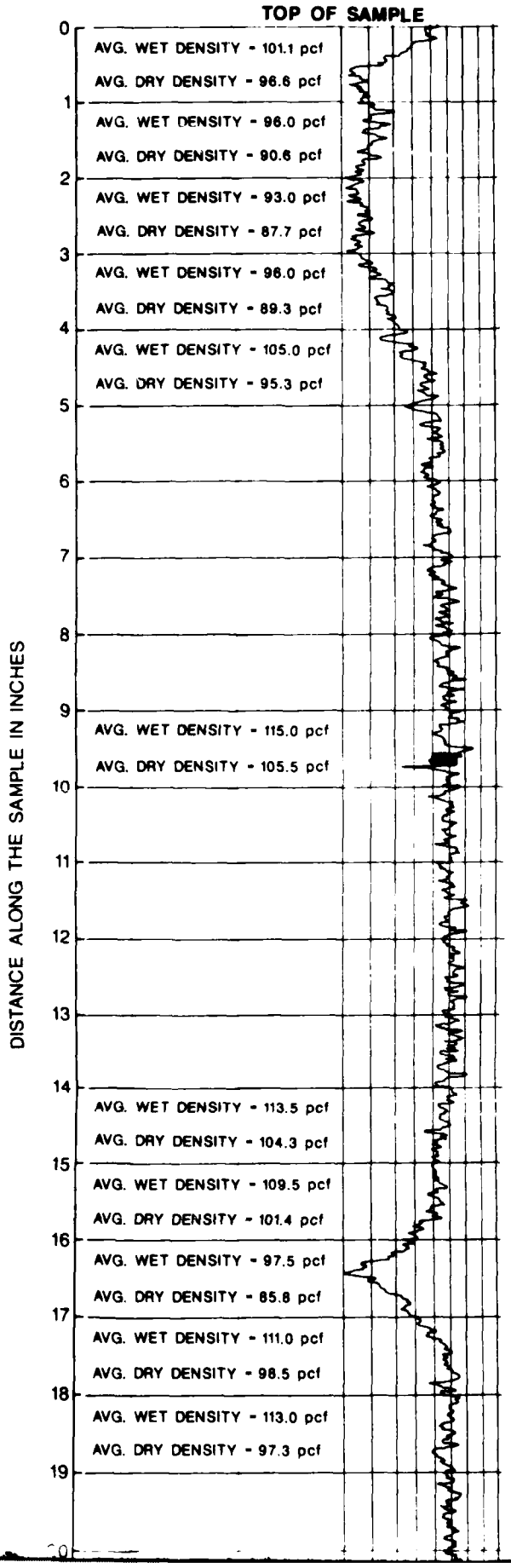


Figure 50. Relative densities and porosities of Montz undisturbed triaxial specimens, dry densities


TOP OF SAMPLE
DISTANCE ALONG THE SAMPLE IN INCHES
0
1
2
3
4
5
6
7
8
9
10
11
12
13
14
15
16
17
18
19
AVG. WET DENSITY - 101.1 pcf
AVG. DRY DENSITY - 96.6 pcf
AVG. WET DENSITY - 96.0 pcf
AVG. DRY DENSITY - 90.6 pcf
AVG. WET DENSITY - 93.0 pcf
AVG. DRY DENSITY - 87.7 pcf
AVG. WET DENSITY - 96.0 pcf
AVG. DRY DENSITY - 89.3 pcf
AVG. WET DENSITY - 105.0 pcf
AVG. DRY DENSITY - 95.3 pcf
AVG. WET DENSITY - 115.0 pcf
AVG. DRY DENSITY - 105.5 pcf
AVG. WET DENSITY - 113.5 pcf
AVG. DRY DENSITY - 104.3 pcf
AVG. WET DENSITY - 109.5 pcf
AVG. DRY DENSITY - 101.4 pcf
AVG. WET DENSITY - 97.5 pcf
AVG. DRY DENSITY - 85.8 pcf
AVG. WET DENSITY - 111.0 pcf
AVG. DRY DENSITY - 98.5 pcf
AVG. WET DENSITY - 113.0 pcf
AVG. DRY DENSITY - 97.3 pcf

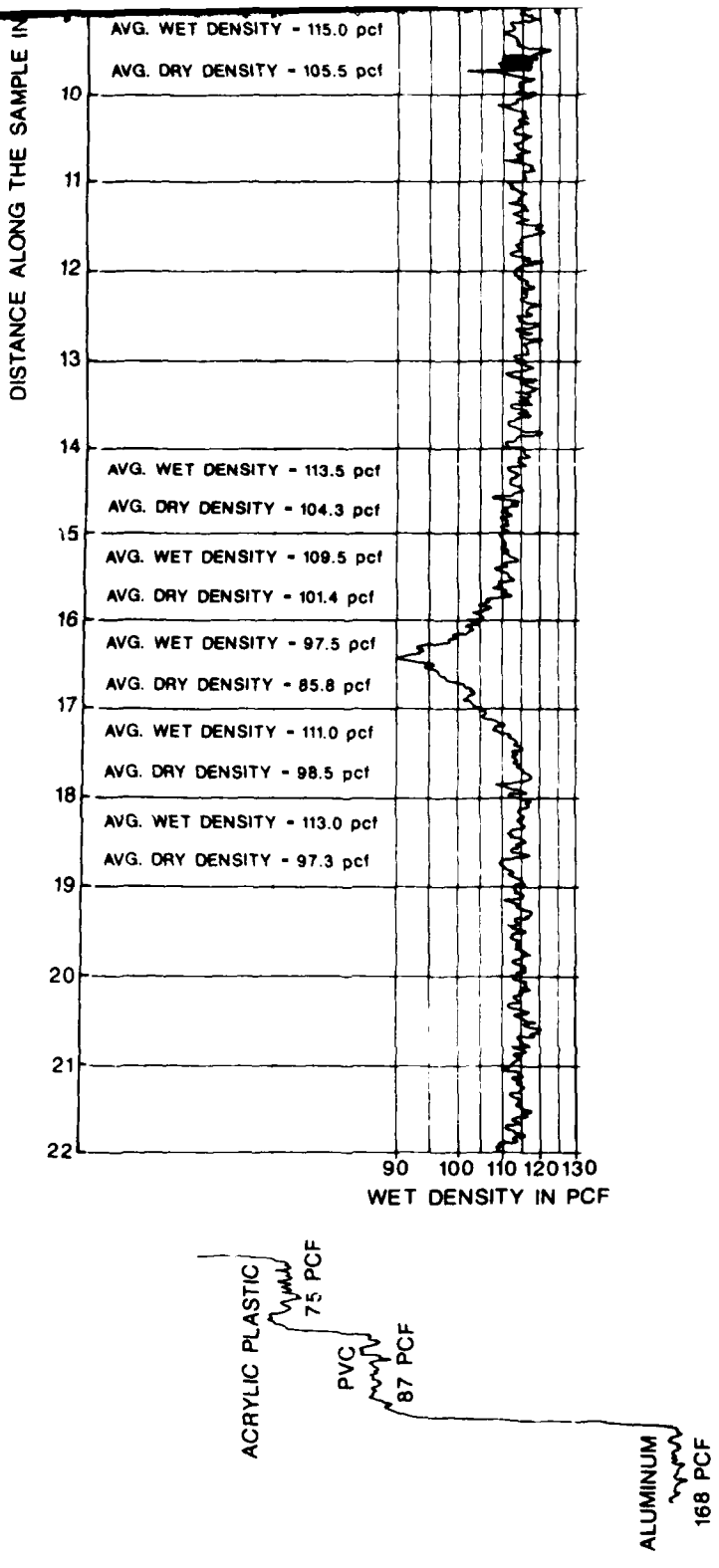


Figure 51. Film densiometer scan of X-ray negative of Bonnet Carre Point sample 21 from boring U-1B

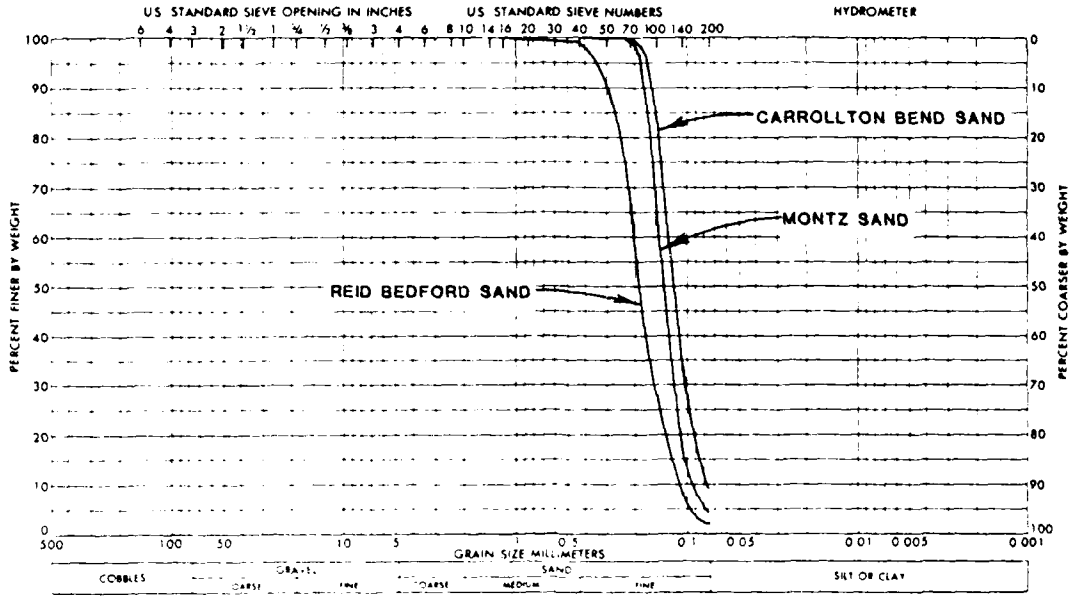


Figure 52. Gradation curve for Reid Bedford, composite Montz, and composite Carrollton Bend sands

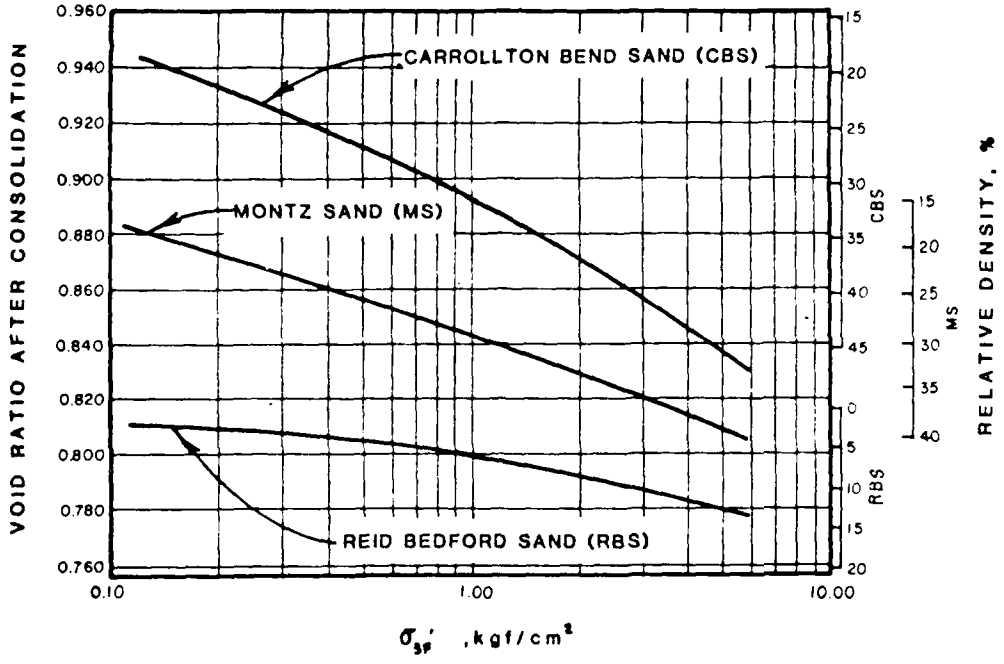


Figure 53. Critical void ratio curves for composite Carrollton Bend, composite Montz, and Reid Bedford Sands

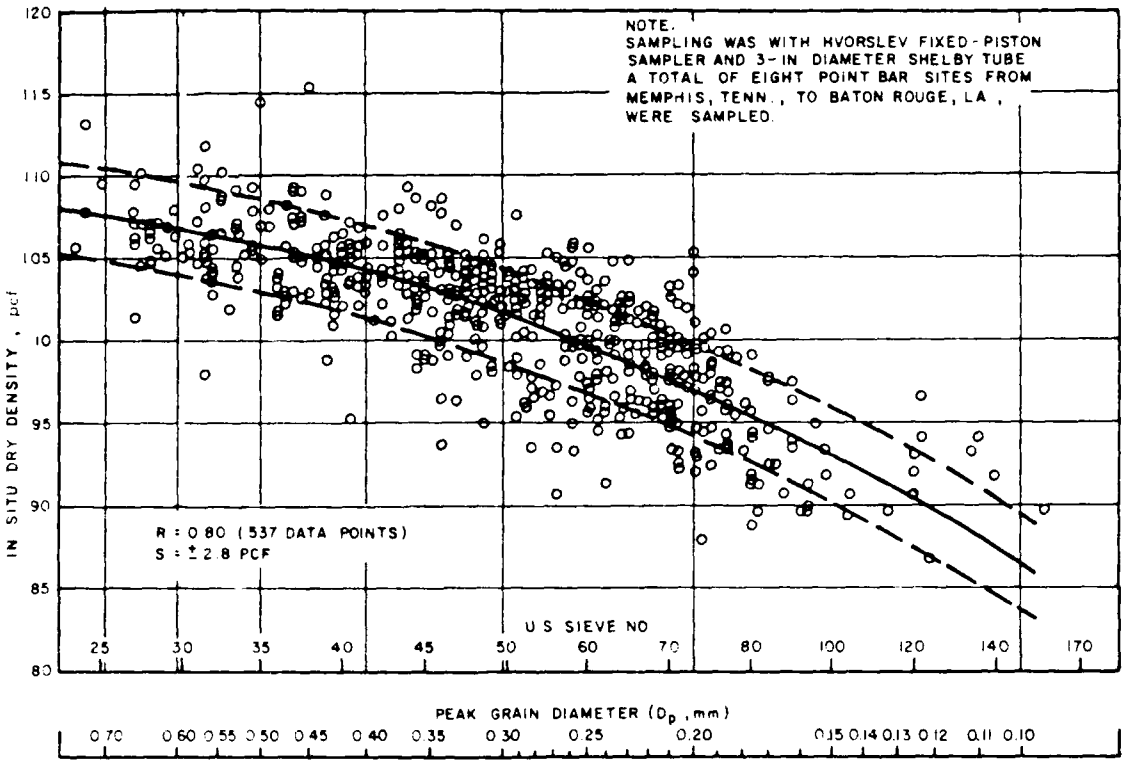


Figure 54. Correlation of in situ dry density with peak grain diameter (from Garber 1952)

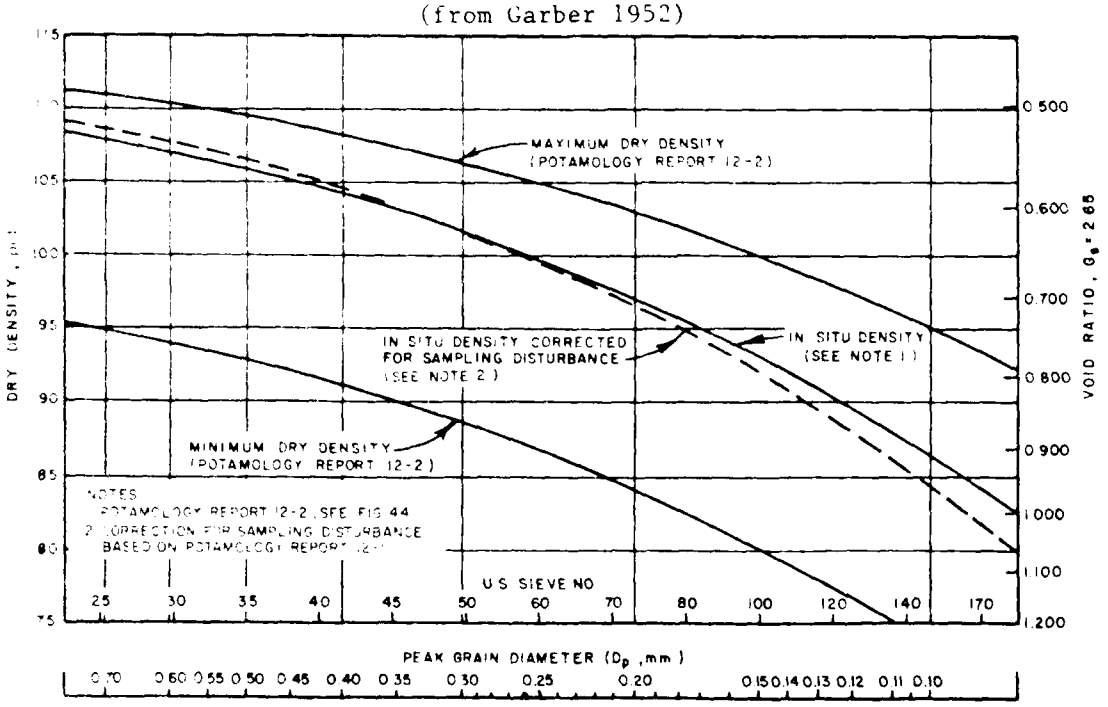


Figure 55. Correlations among as-sampled dry density, peak grain diameter, and maximum/minimum density (from Garber 1952)

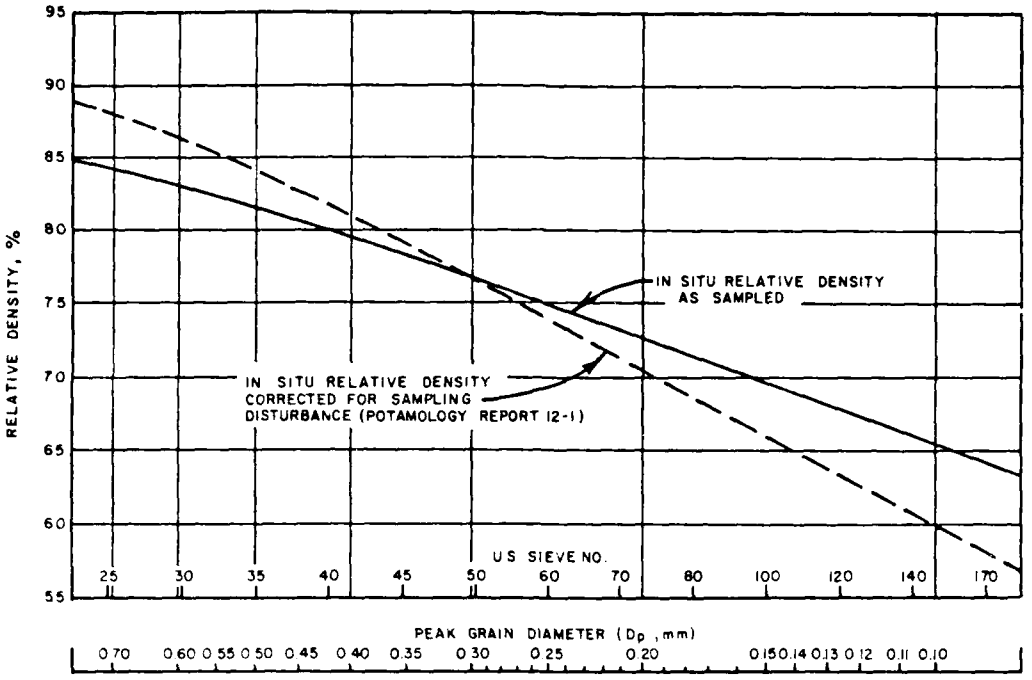


Figure 56. Correlation between in situ relative density and peak grain diameter (from Garber 1952)

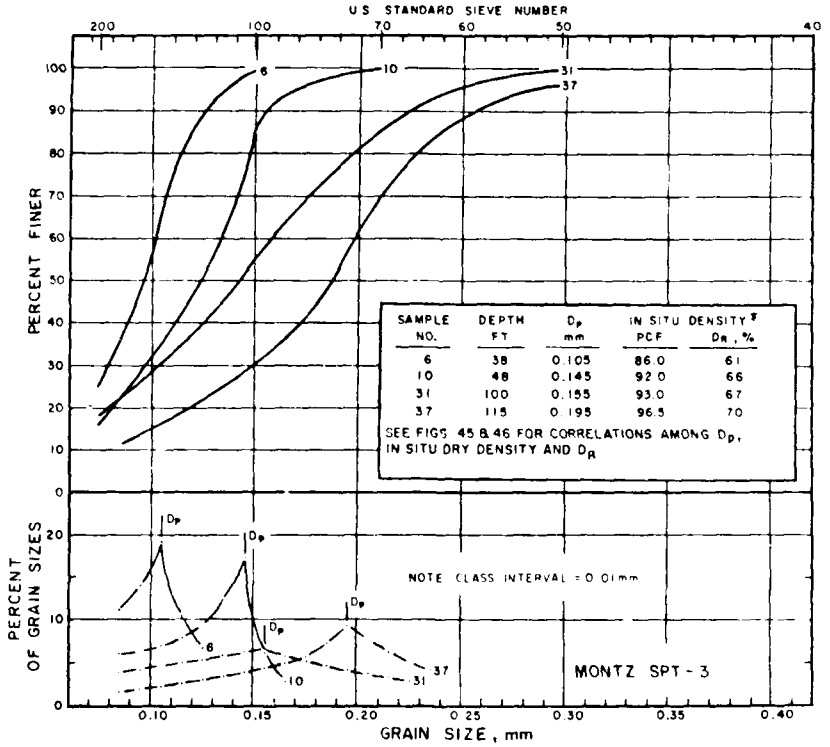


Figure 57. Peak grain diameters for range in sand gradations encountered at Montz site

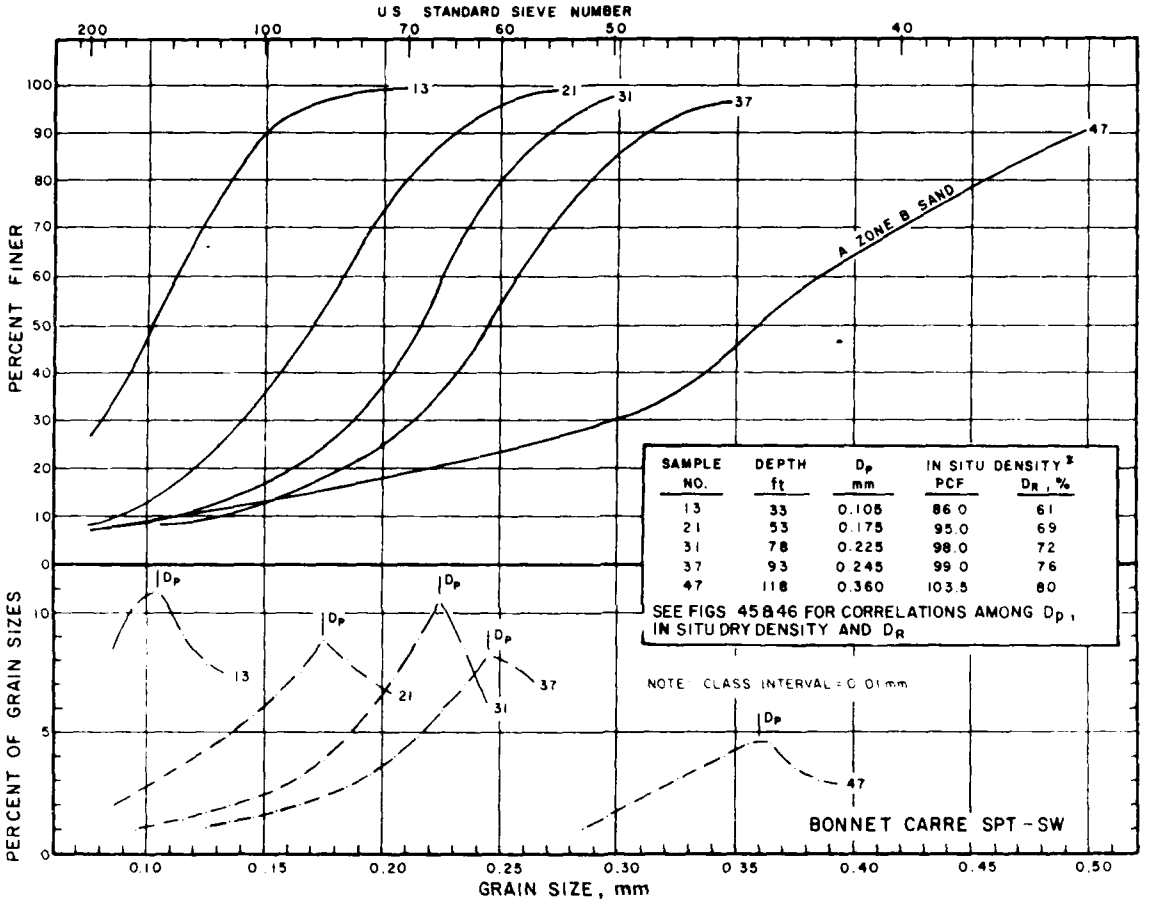


Figure 58. Peak grain diameters for range in sand gradations encountered at Bonnet Carre Point site

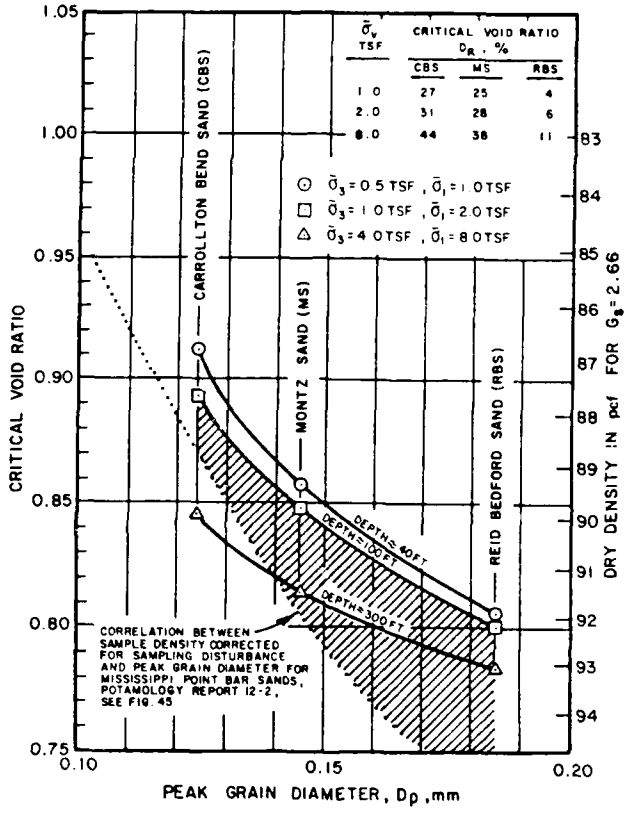


Figure 59. Critical void ratio versus peak grain diameter and effective vertical stress

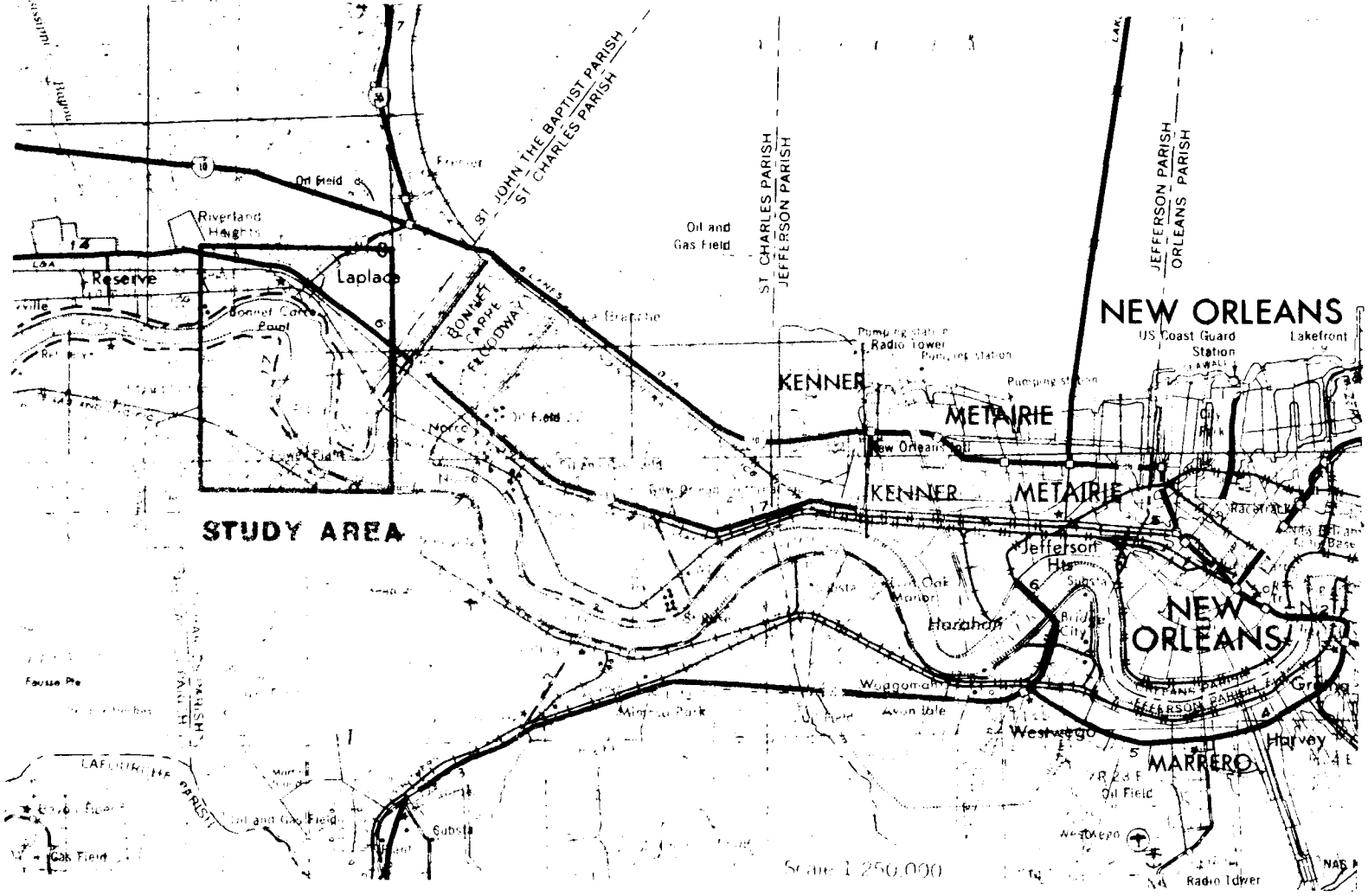


Figure 10. Location of the study area

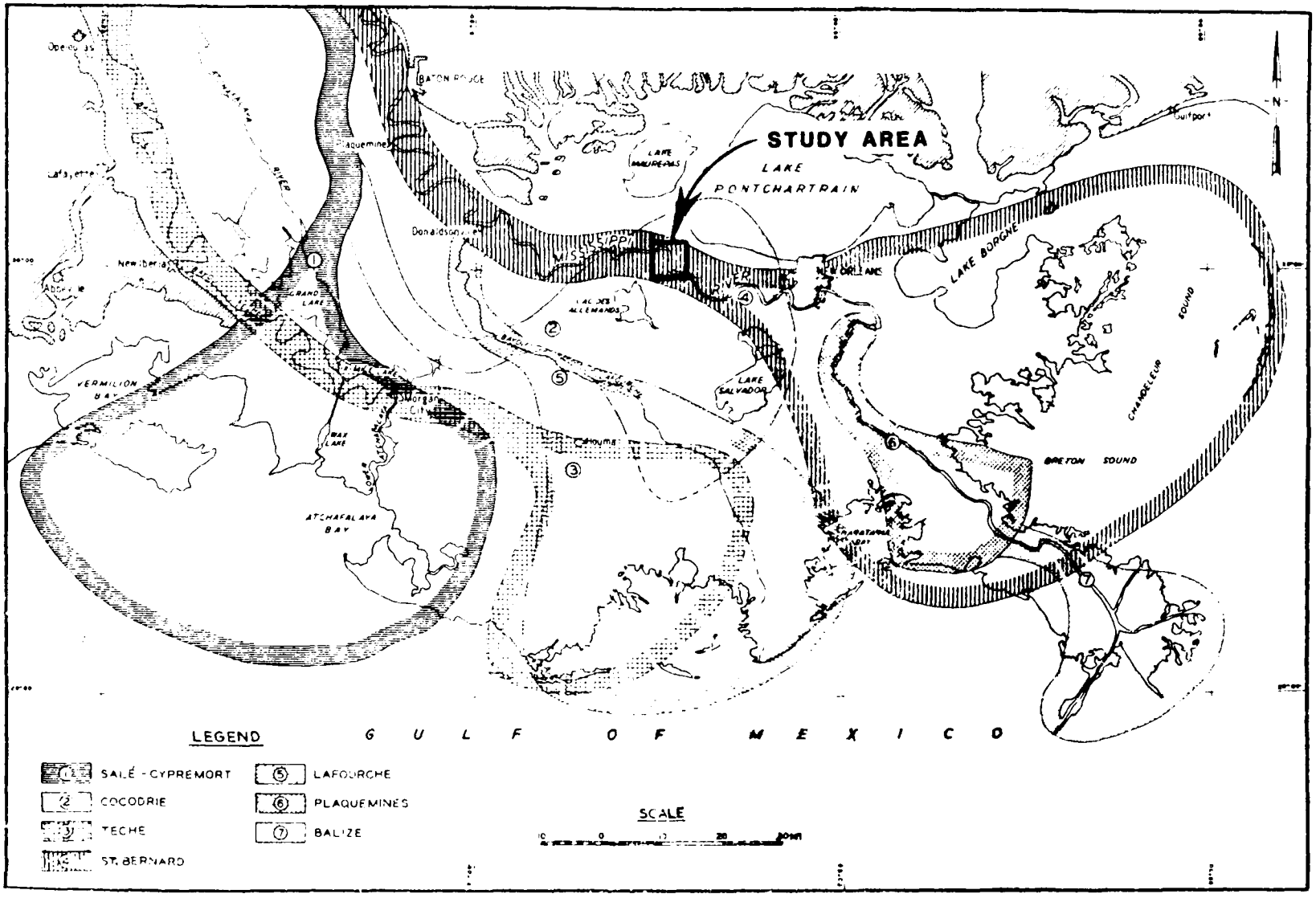


Figure 61. Mississippi River deltas and study area location (after Kolb and Van Lopik 1958)

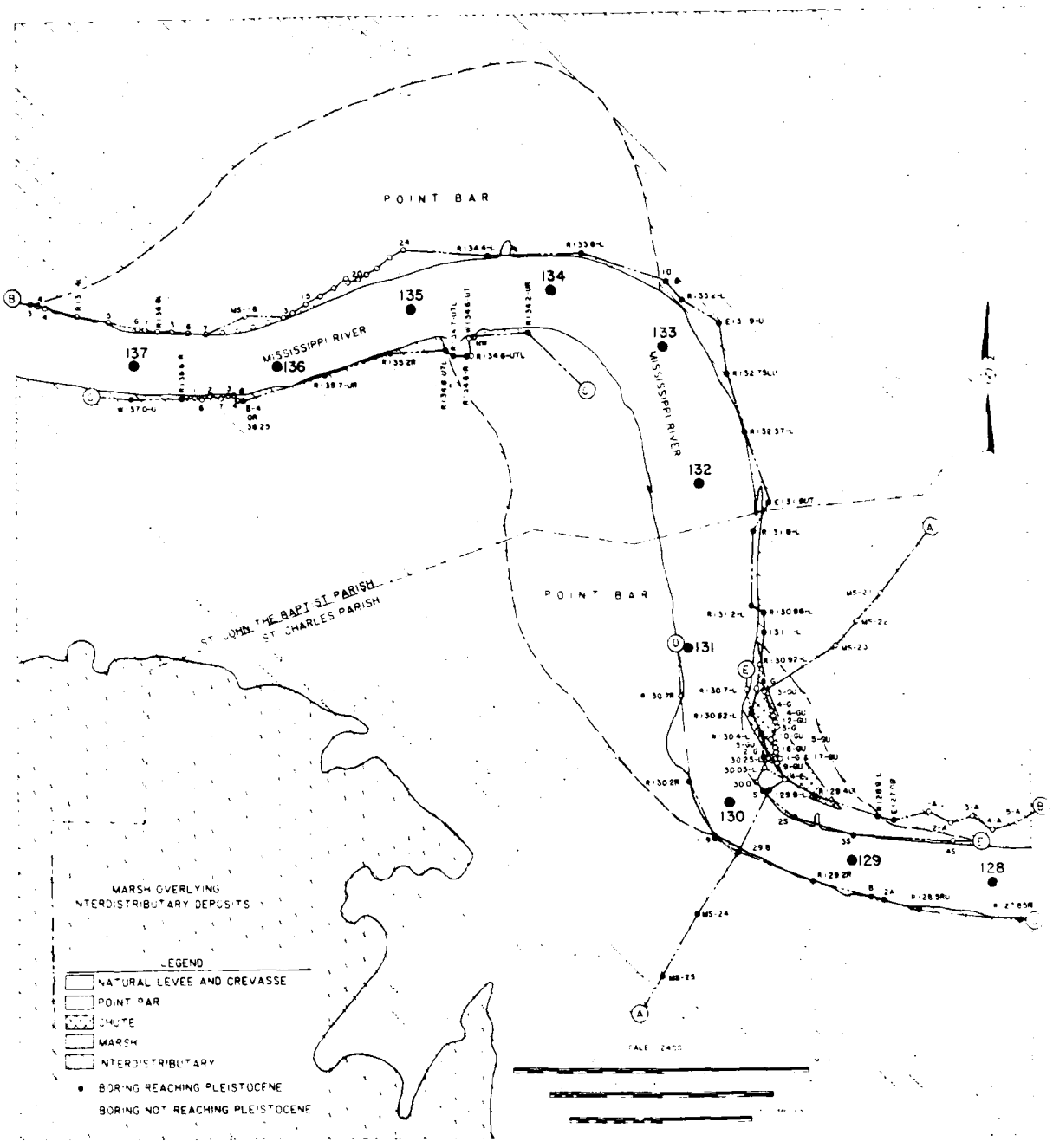


Figure 62. Depositional environments of the study area and cross section locations

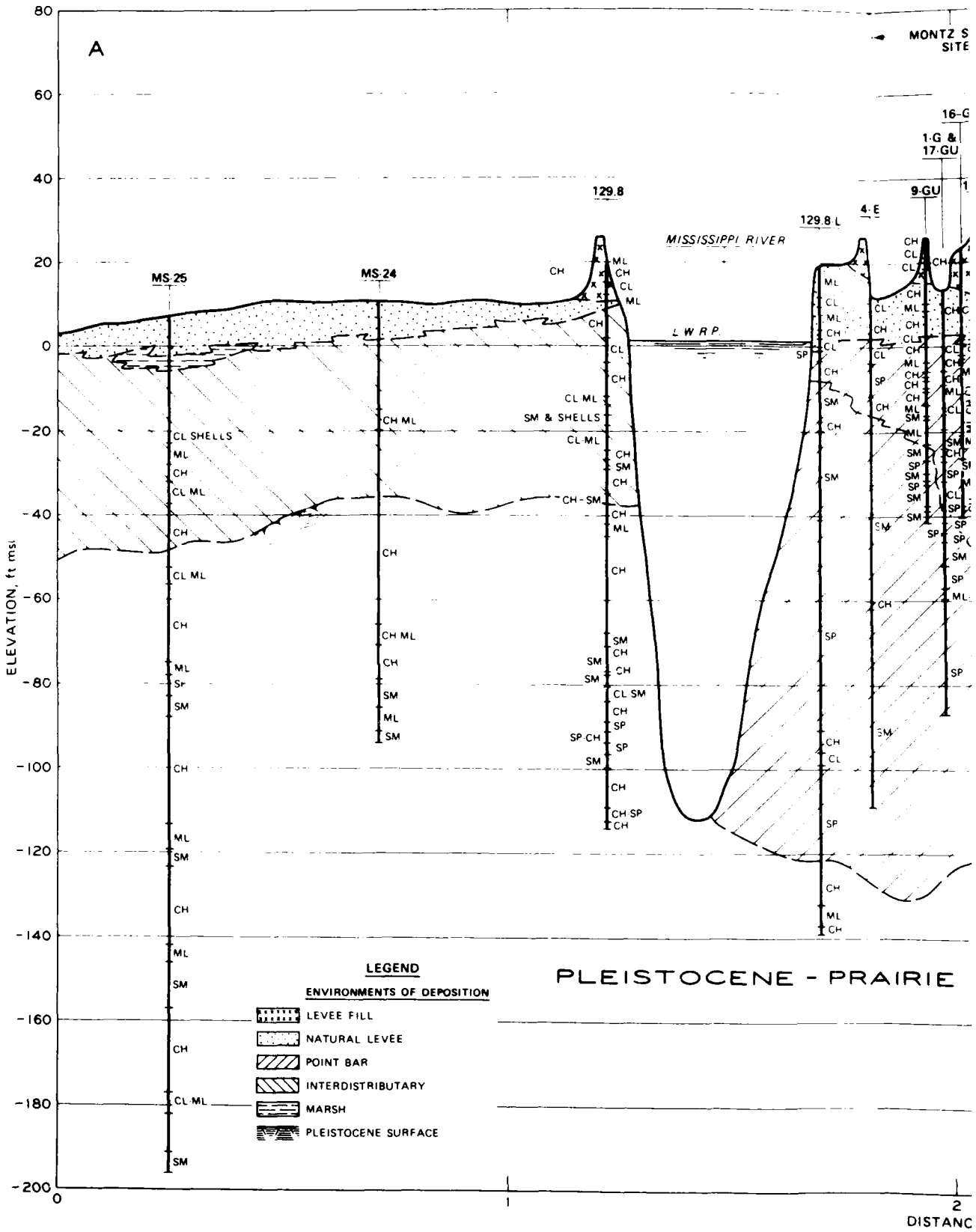
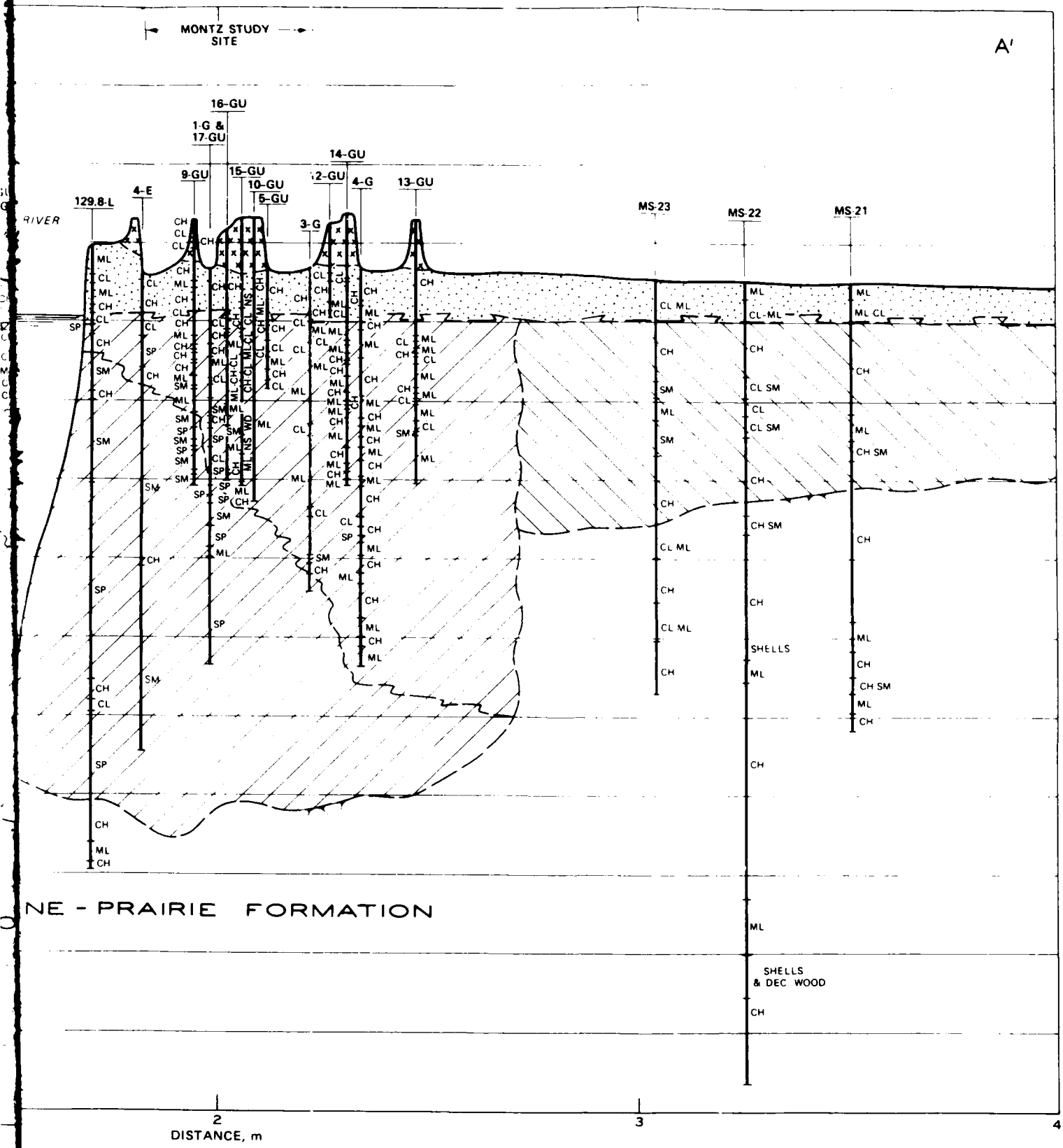


Figure 63. Cross section A



63. Cross section A-A'

2

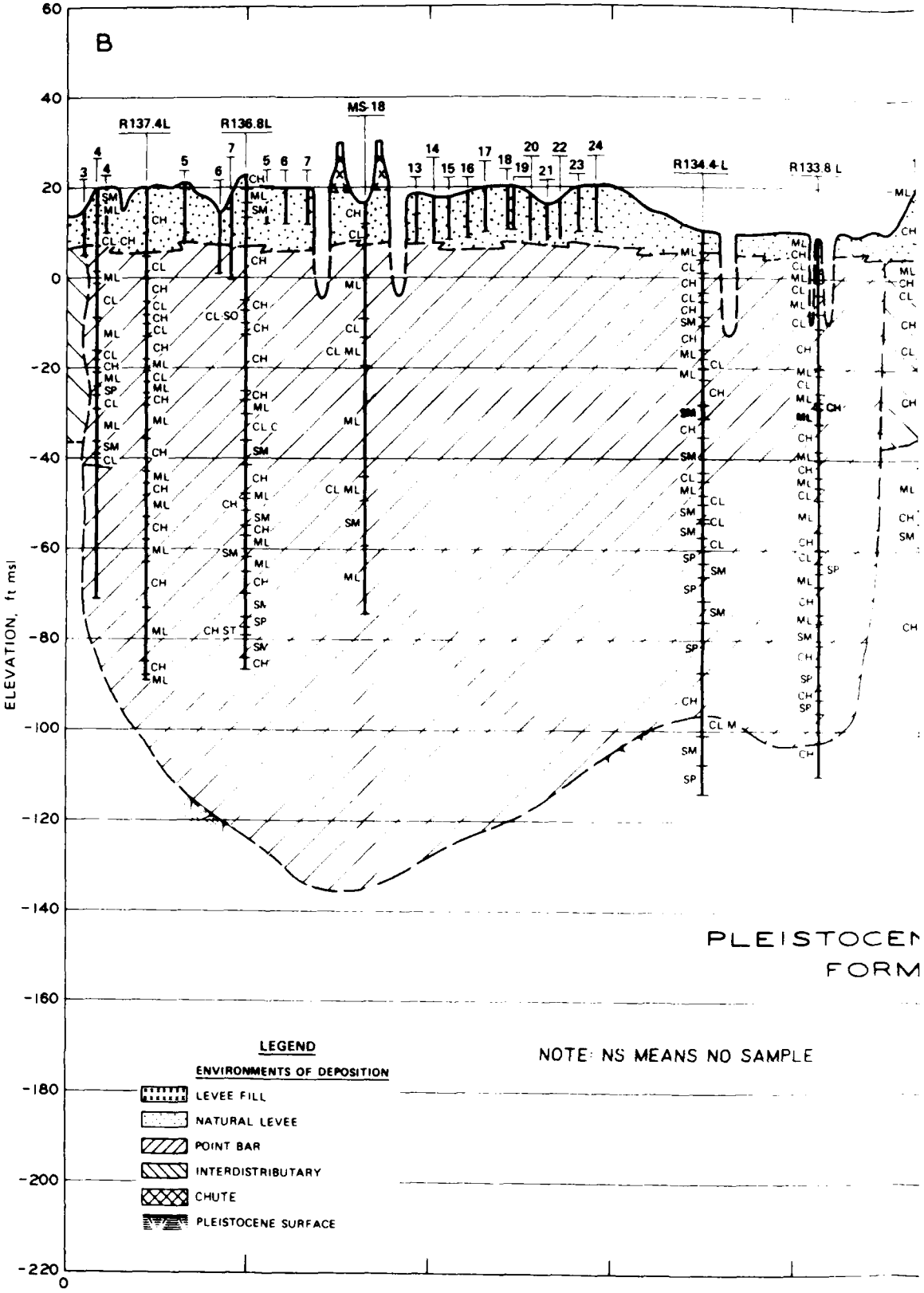
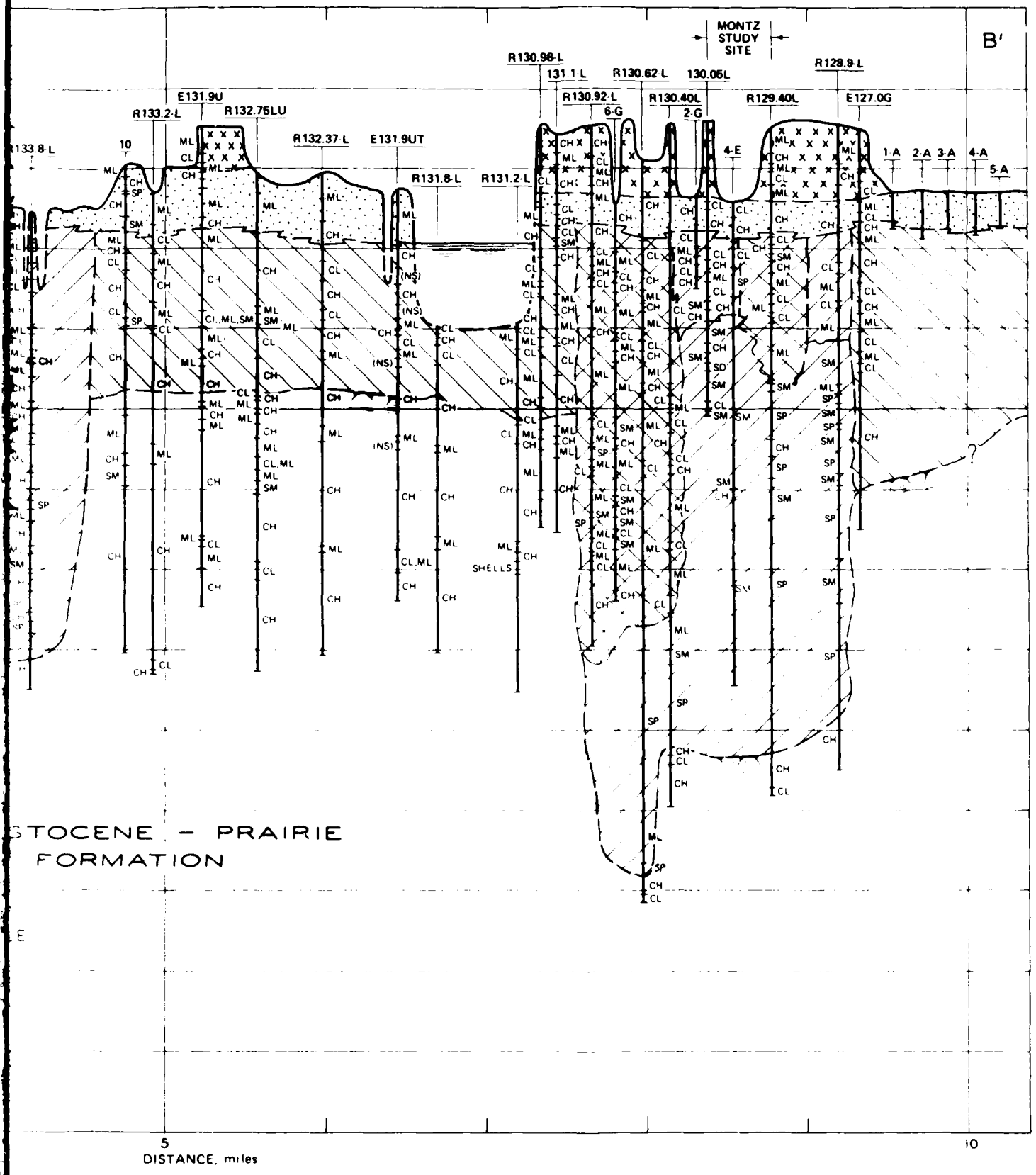


Figure 64. Cross sectio



STOCENE – PRAIRIE
FORMATION

E

oss section B-B'

1

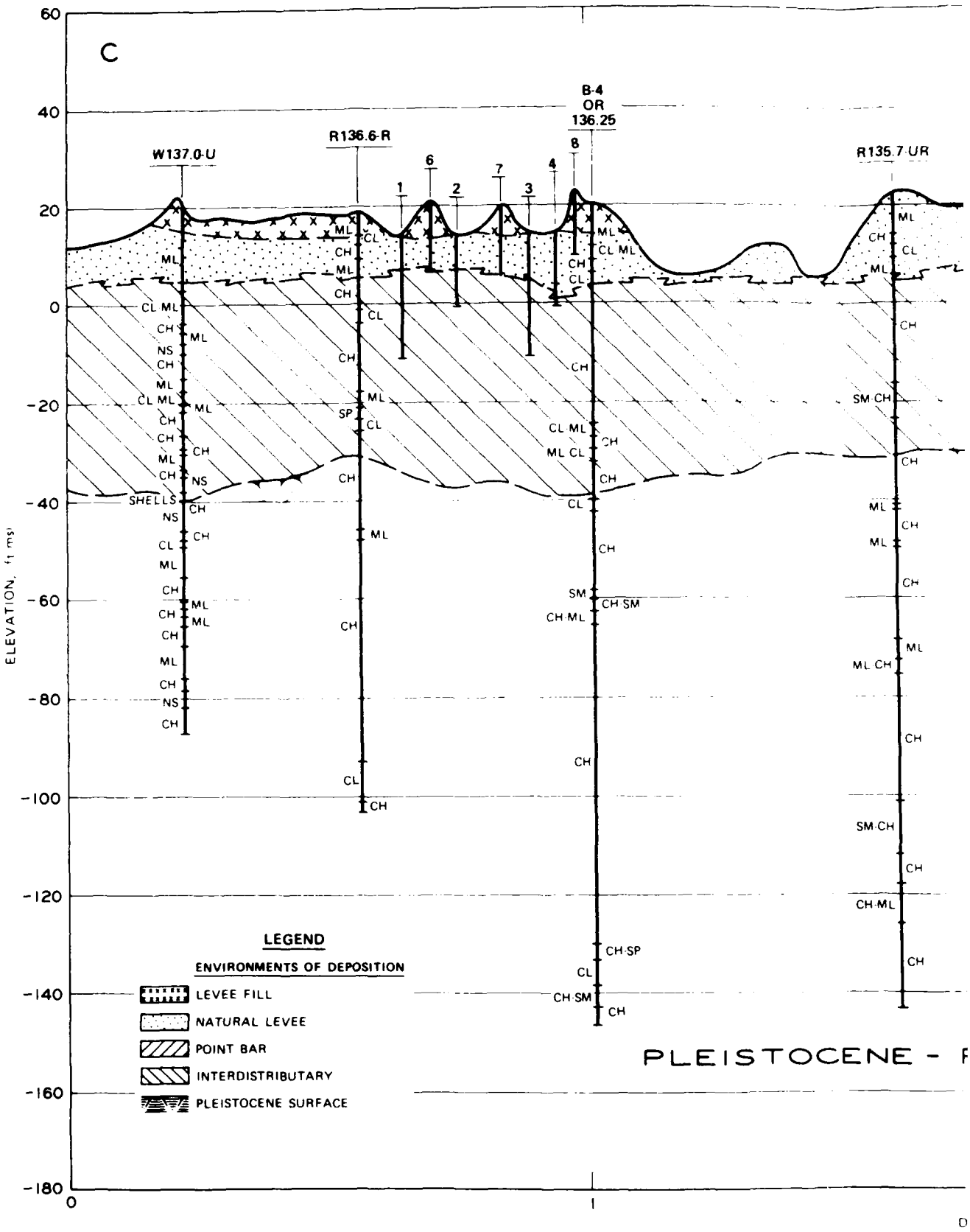
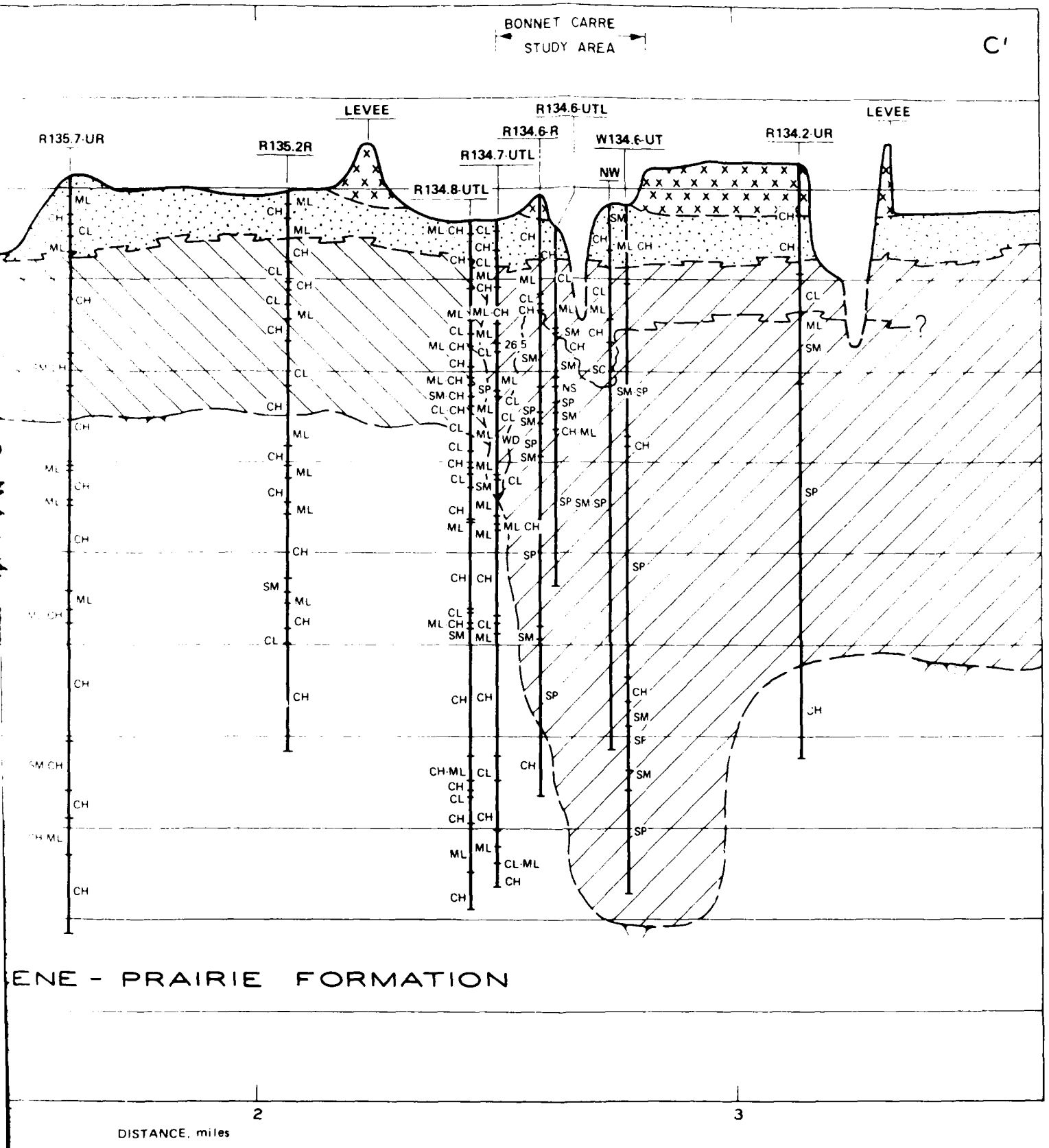


Figure 65. Cross section C-C'


BONNET CARRE
STUDY AREA
C'
LEVEE
R135.7-UR
R135.2R
R134.8-UTL
R134.7-UTL
R134.6-UTL
R134.6-R
W134.6-UT
NW
R134.2-UR
LEVEE
?
ENE - PRAIRIE FORMATION
2
3
DISTANCE, miles

tion C-C'

2

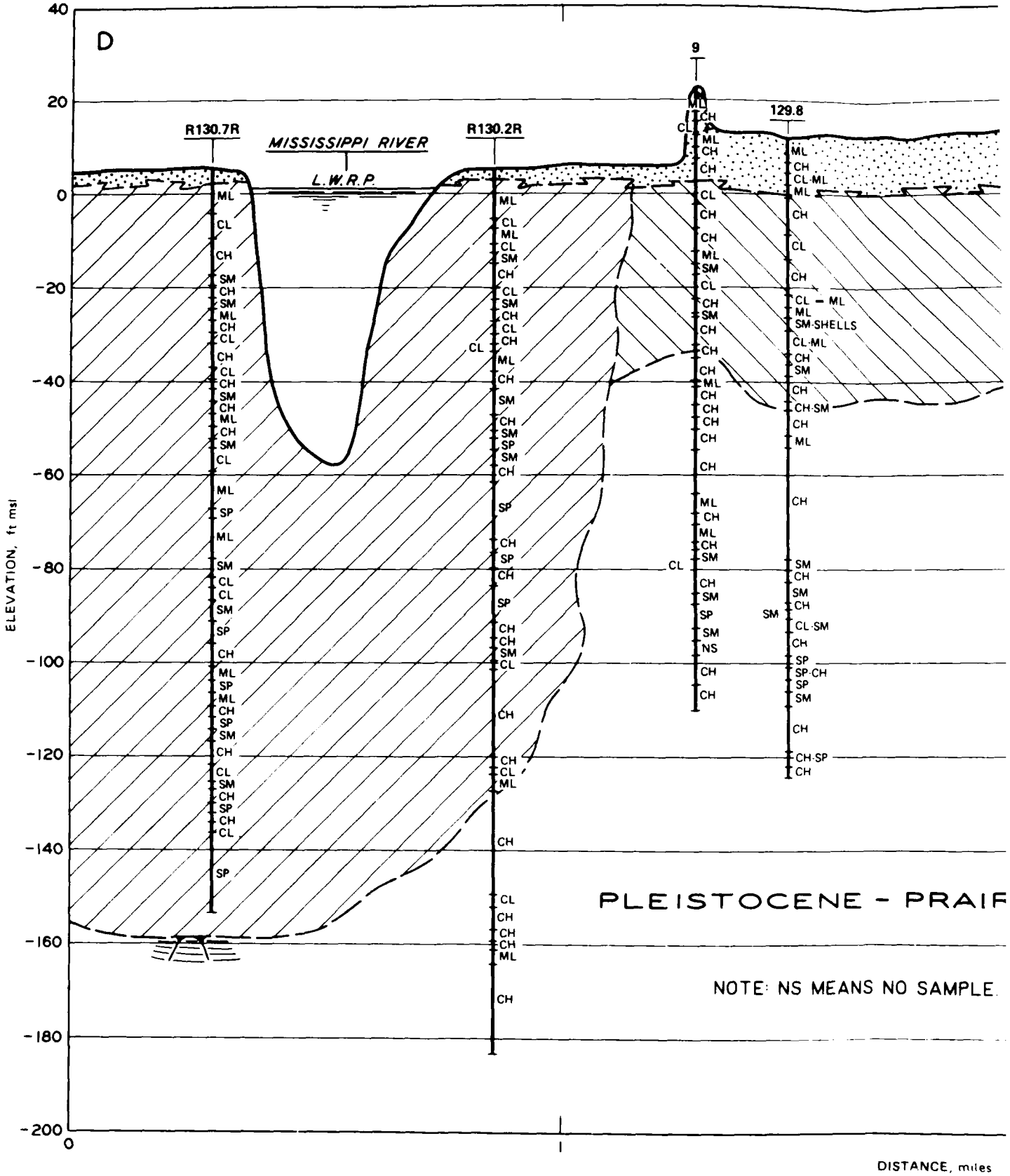
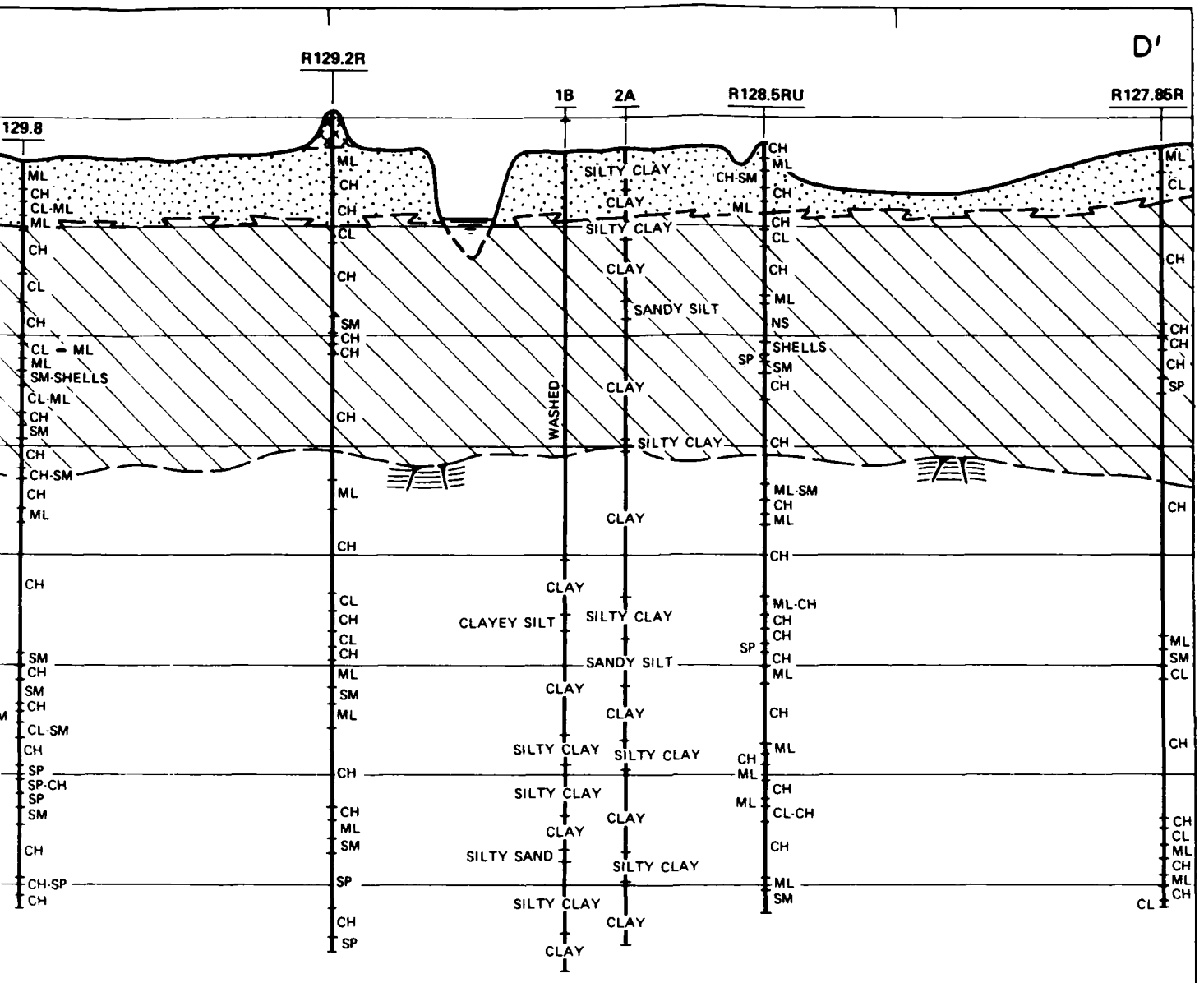


Figure 66. Cross section D-D'



CENE - PRAIRIE FORMATION

NS MEANS NO SAMPLE.

LEGEND

ENVIRONMENTS OF DEPOSITION

- LEVEE FILL
- NATURAL LEVEE
- POINT BAR
- INTERDISTRIBUTARY
- PLEISTOCENE SURFACE

2 3

DISTANCE, miles

ction D-D'

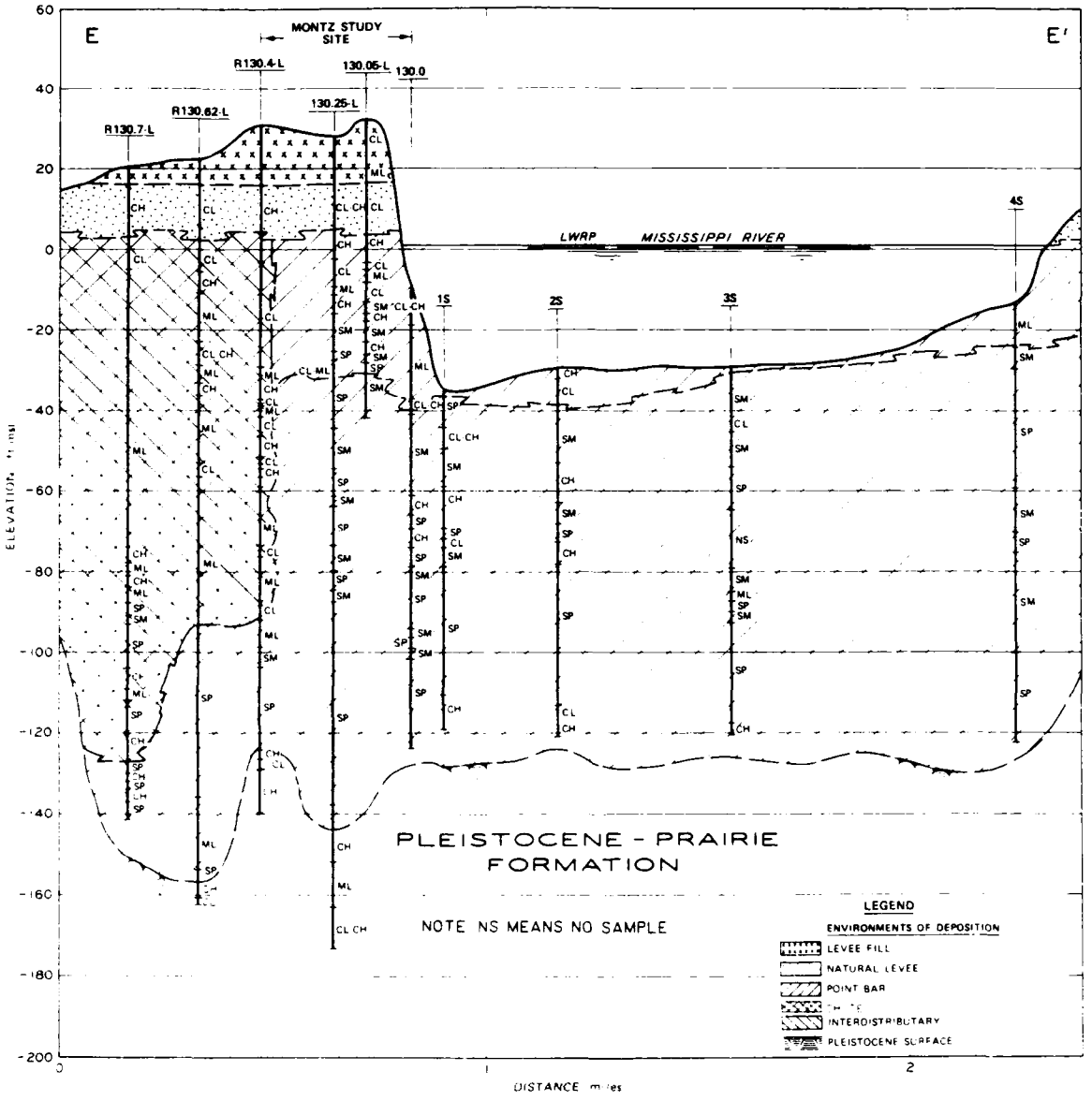


Figure 67. Cross section E-E'

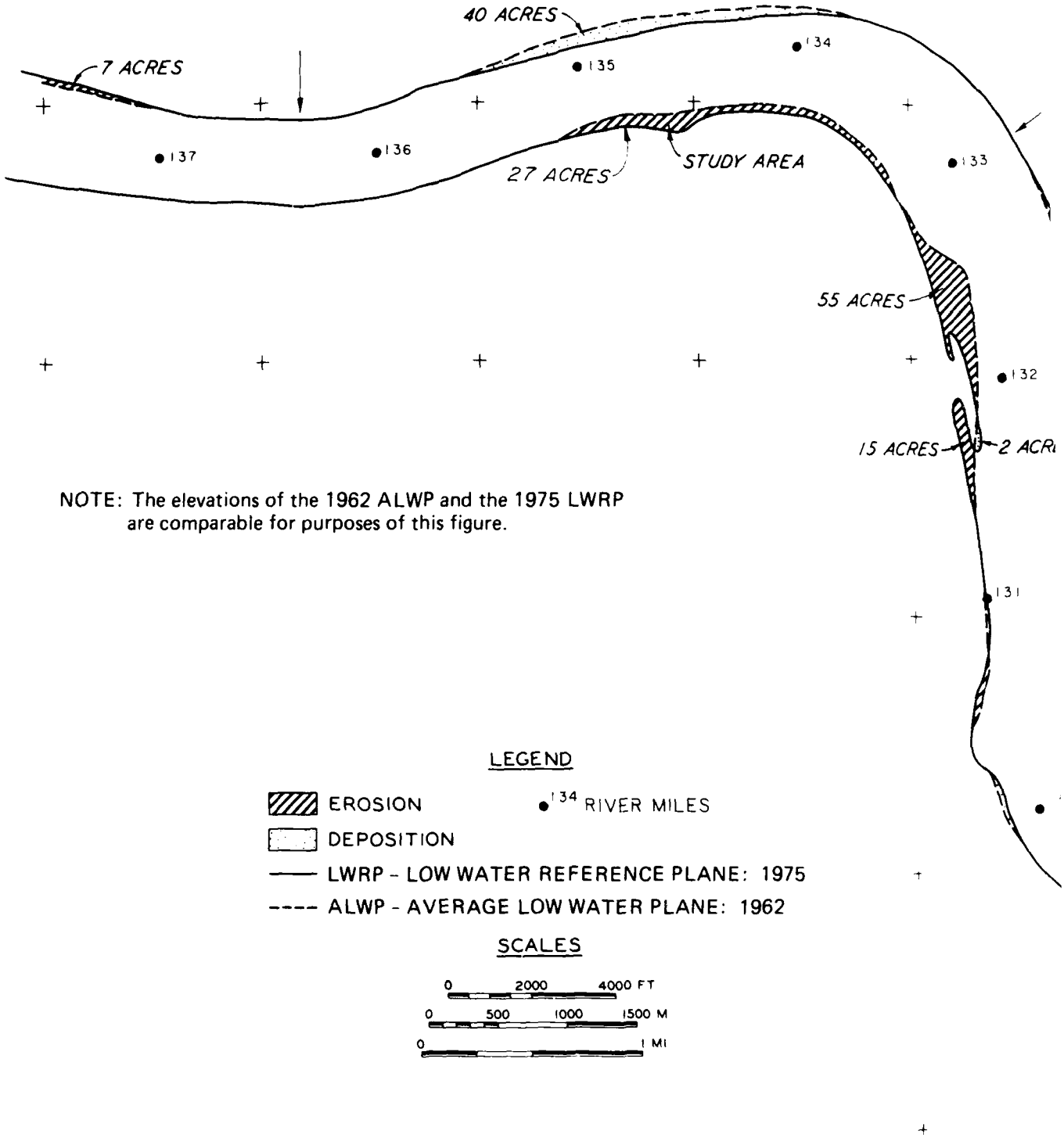
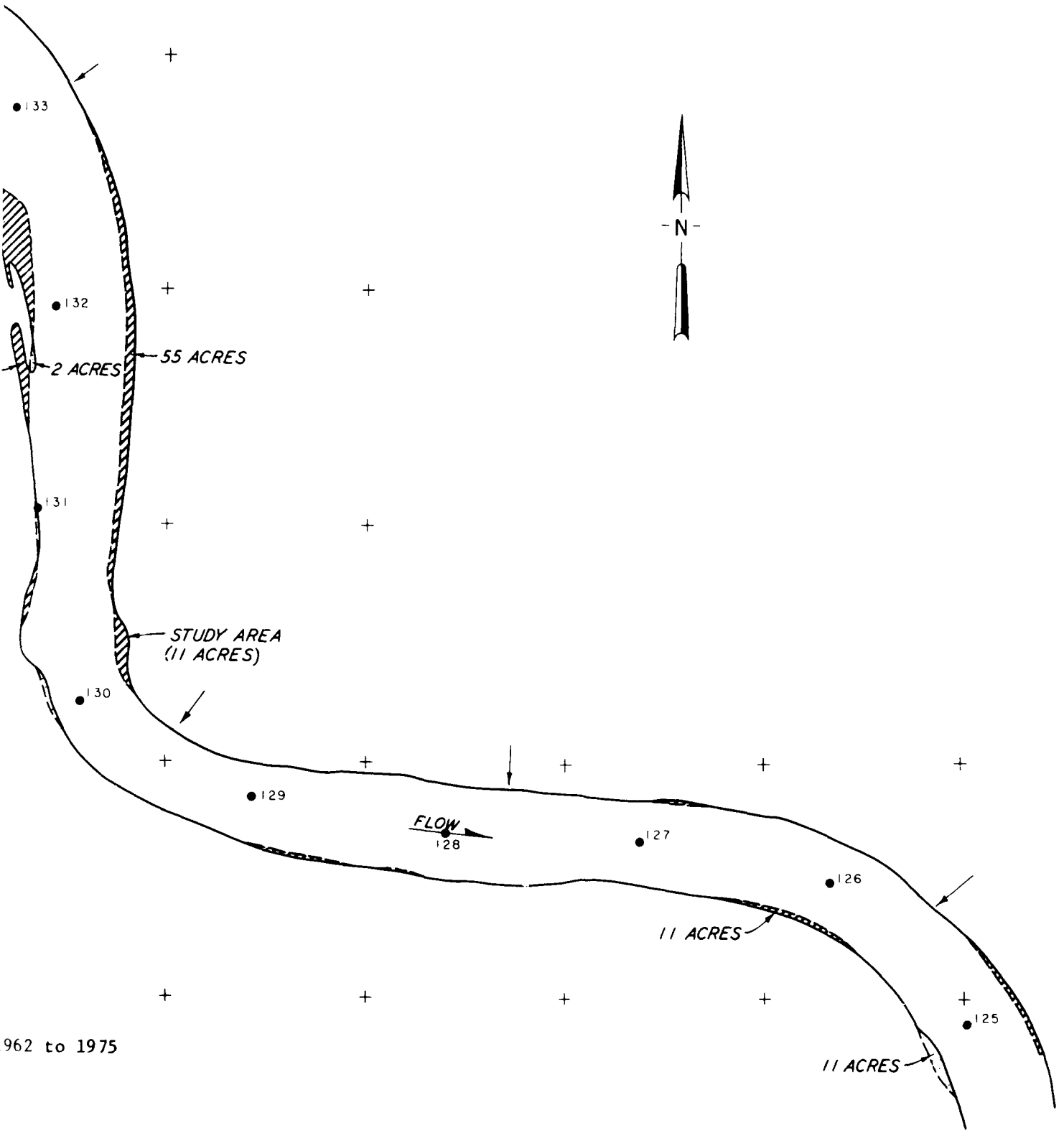


Figure 68. Bank line movement during 1962 to 19



962 to 1975

1

2

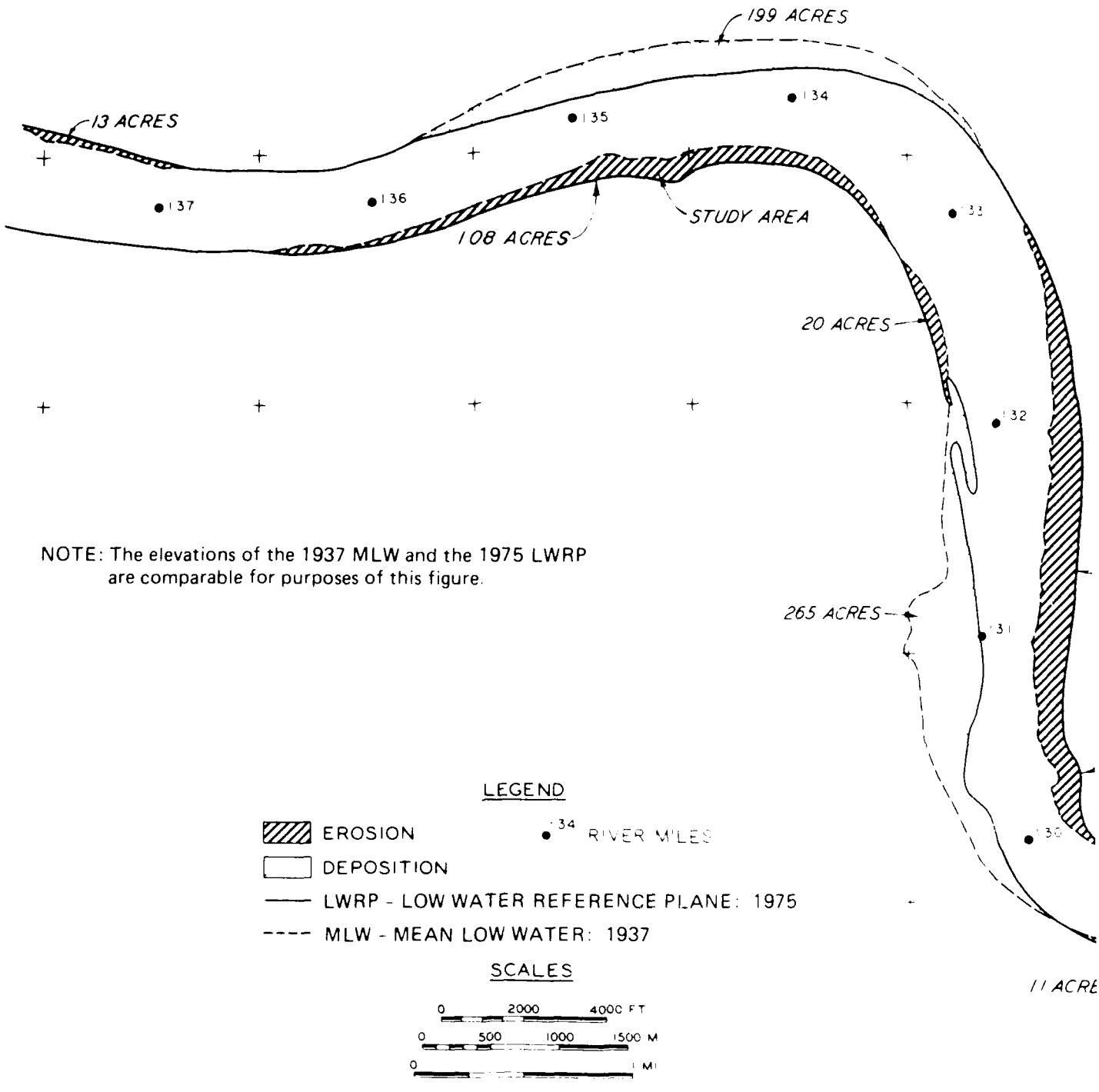
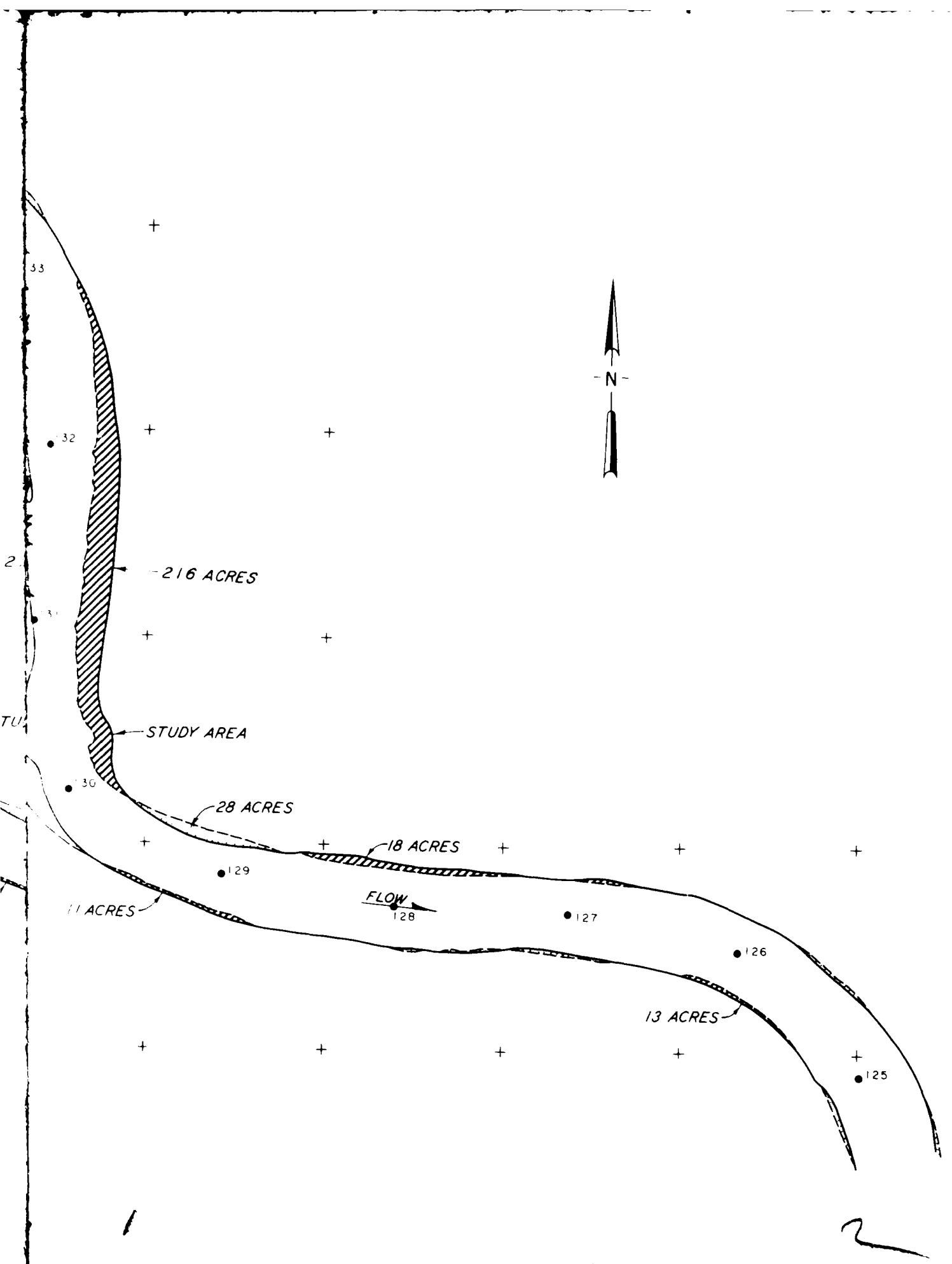
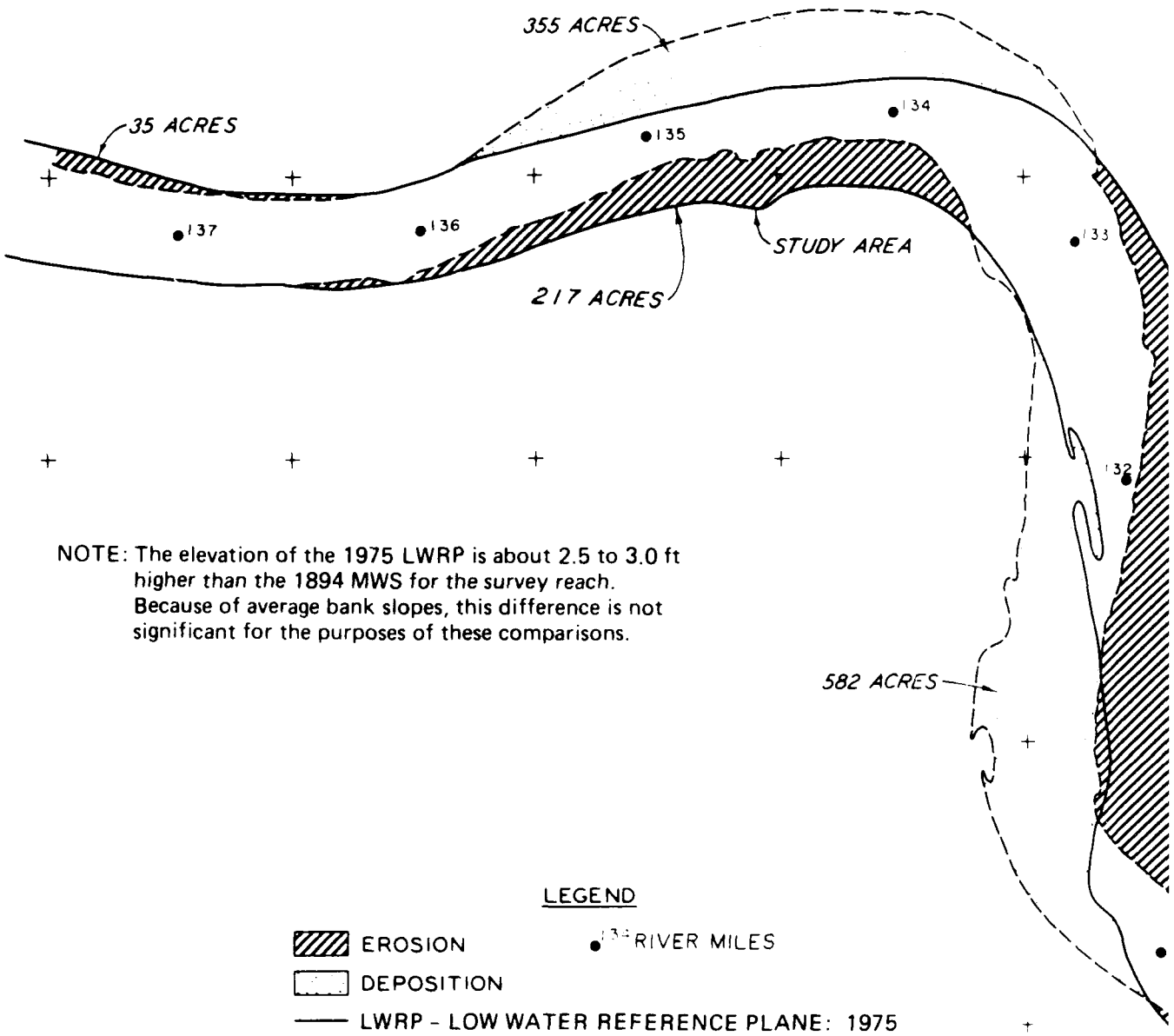


Figure 69. Bank line movement during 1937 to 1975


33
32
216 ACRES
STUDY AREA
30
28 ACRES
18 ACRES
129
FLOW
128
127
126
13 ACRES
125
N



NOTE: The elevation of the 1975 LWRP is about 2.5 to 3.0 ft higher than the 1894 MWS for the survey reach. Because of average bank slopes, this difference is not significant for the purposes of these comparisons.

LEGEND

EROSION

DEPOSITION

RIVER MILES

LWRP - LOW WATER REFERENCE PLANE: 1975

MWS - MEAN WATER SURFACE: 1894

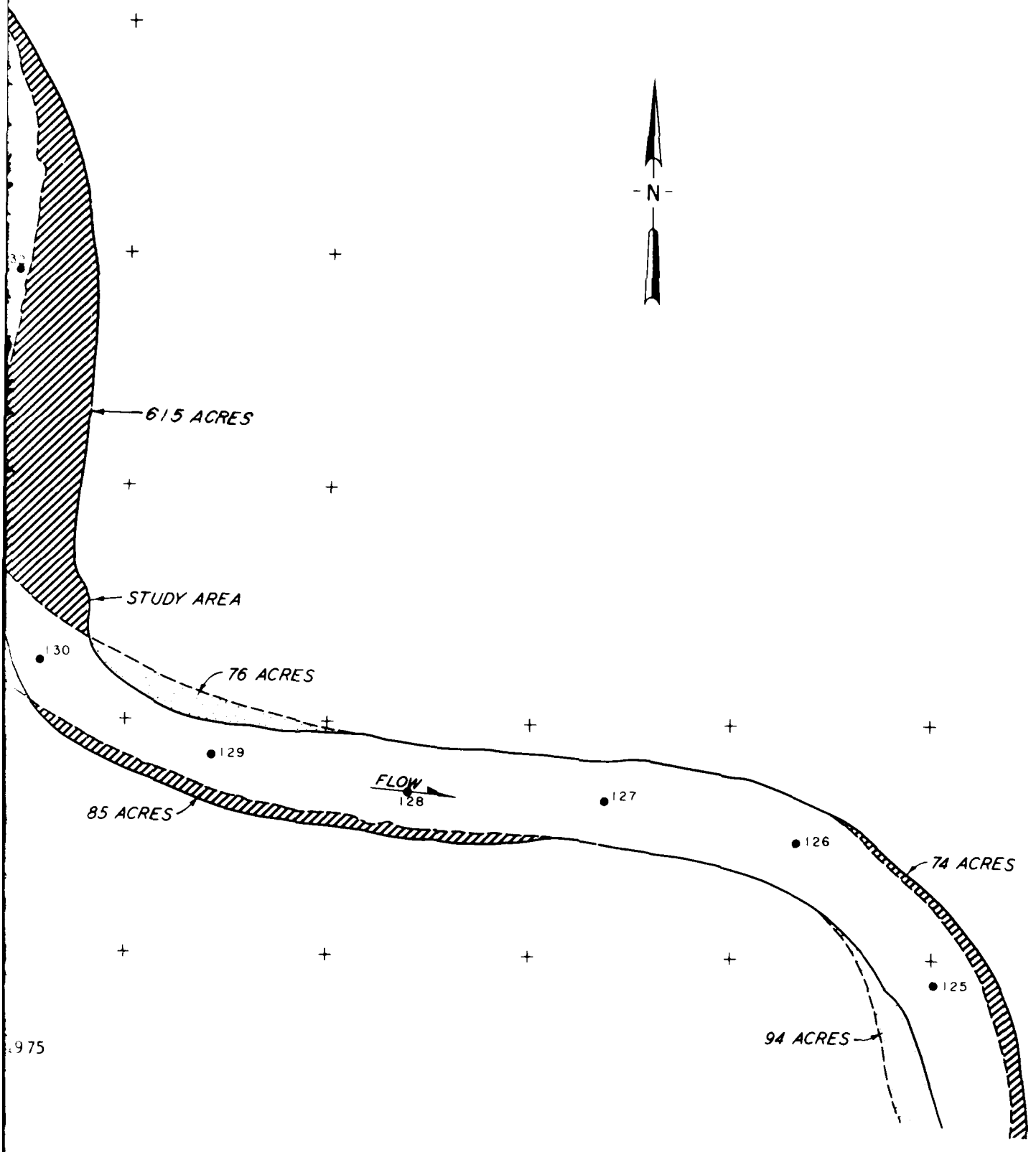
SCALES

0 2000 4000 FT

0 500 1000 1500 M

0 1 MI

Figure 70. Bank line movement during 1894 to 197


N
615 ACRES
STUDY AREA
130
76 ACRES
129
FLOW
128
127
85 ACRES
126
74 ACRES
125
94 ACRES
975

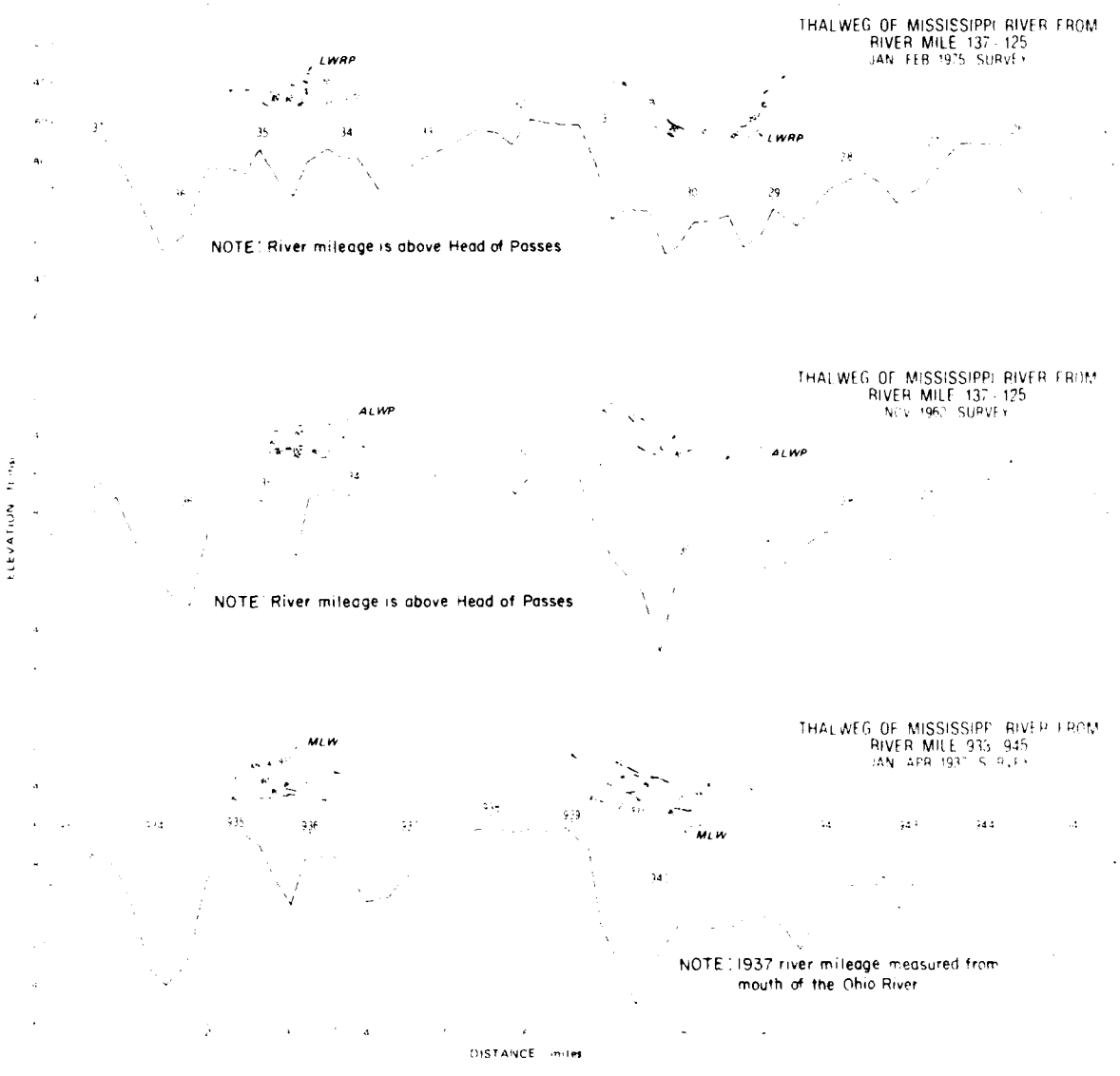


Figure 71. Thalweg profiles for 1937, 1962, and 1975

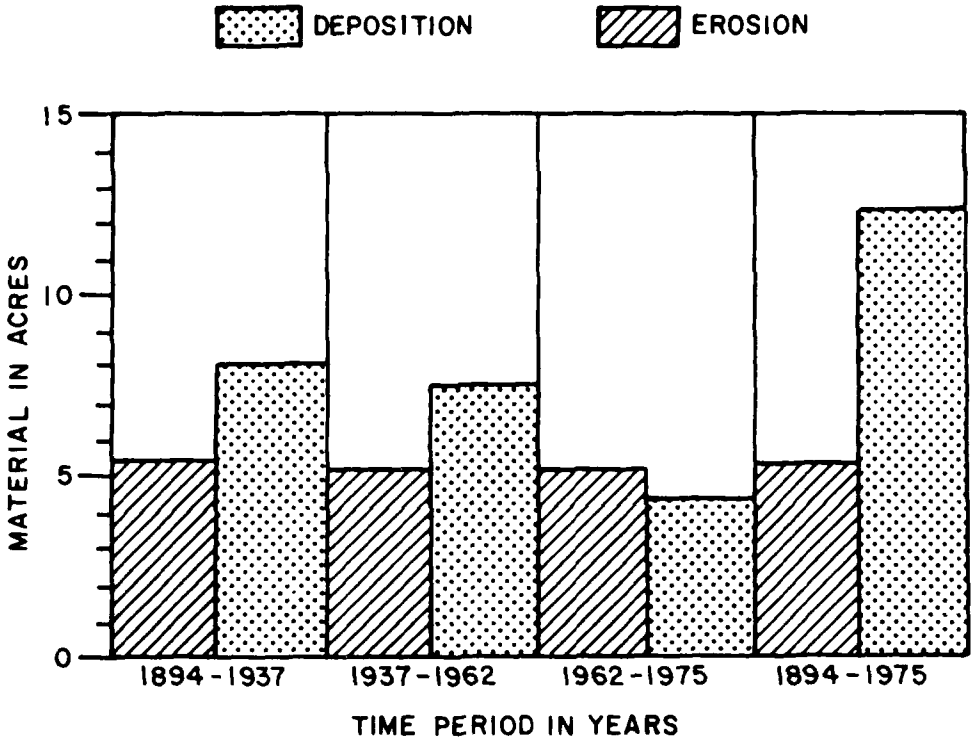


Figure 72. Areas of erosion and deposition of Mississippi River thalweg from river mile 125 to 137 within selected time intervals

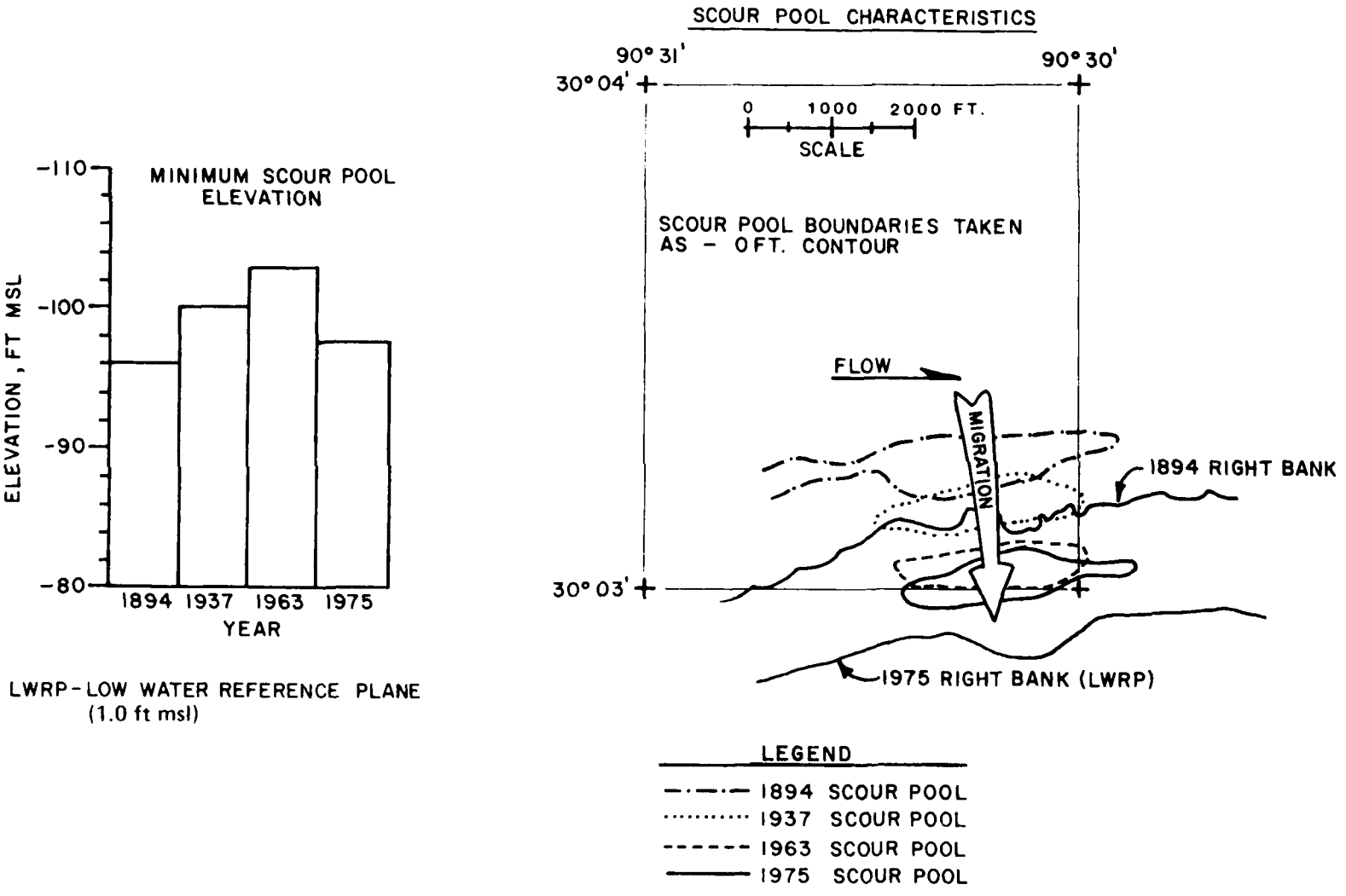


Figure 73. Bonnet Carre Point scour pool characteristics

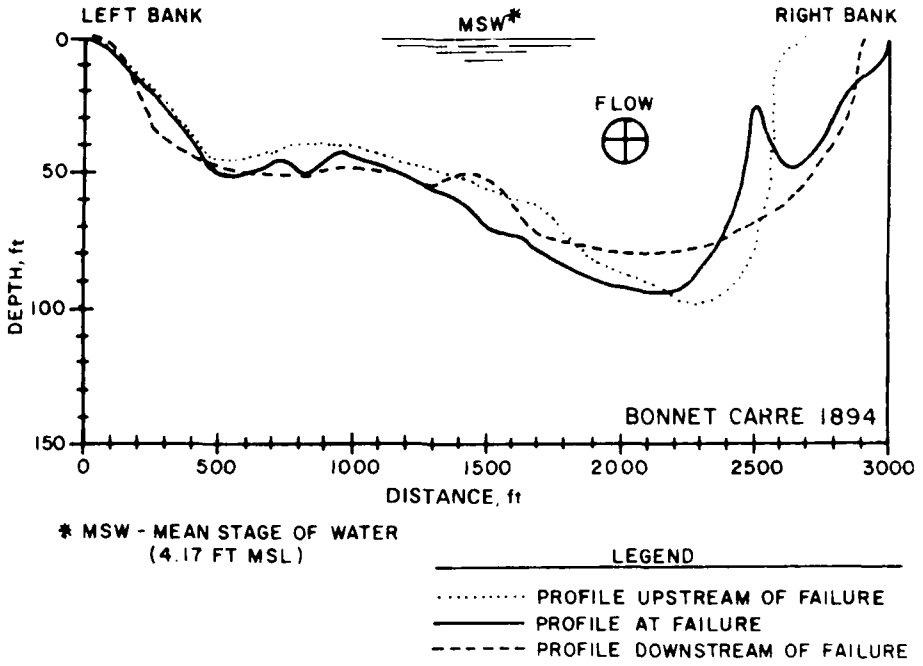


Figure 74. Hydrographic profiles of Mississippi River at Bonnet Carre Point failure, 1894

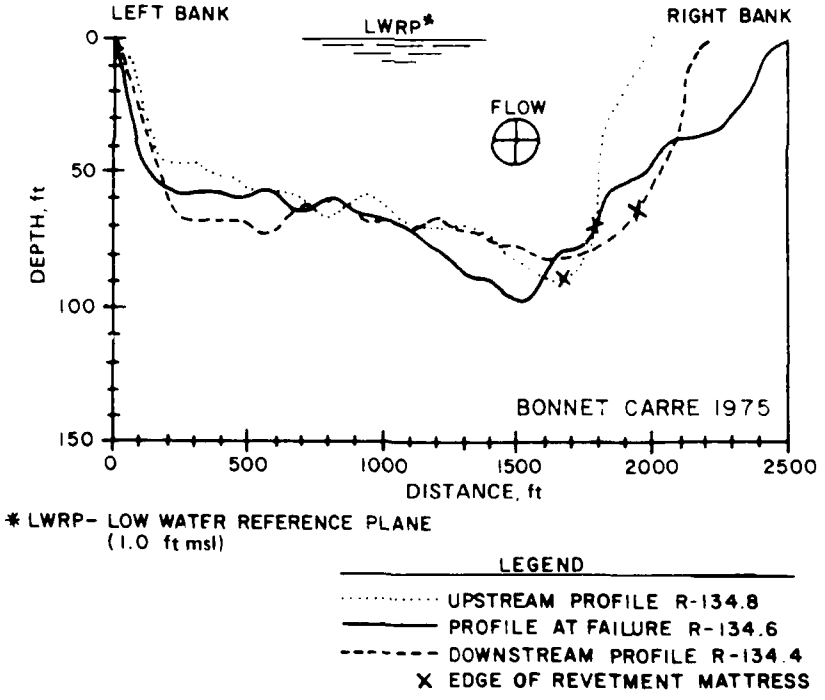


Figure 75. Hydrographic profiles of the Mississippi River at the Bonnet Carre Point failure, 1975

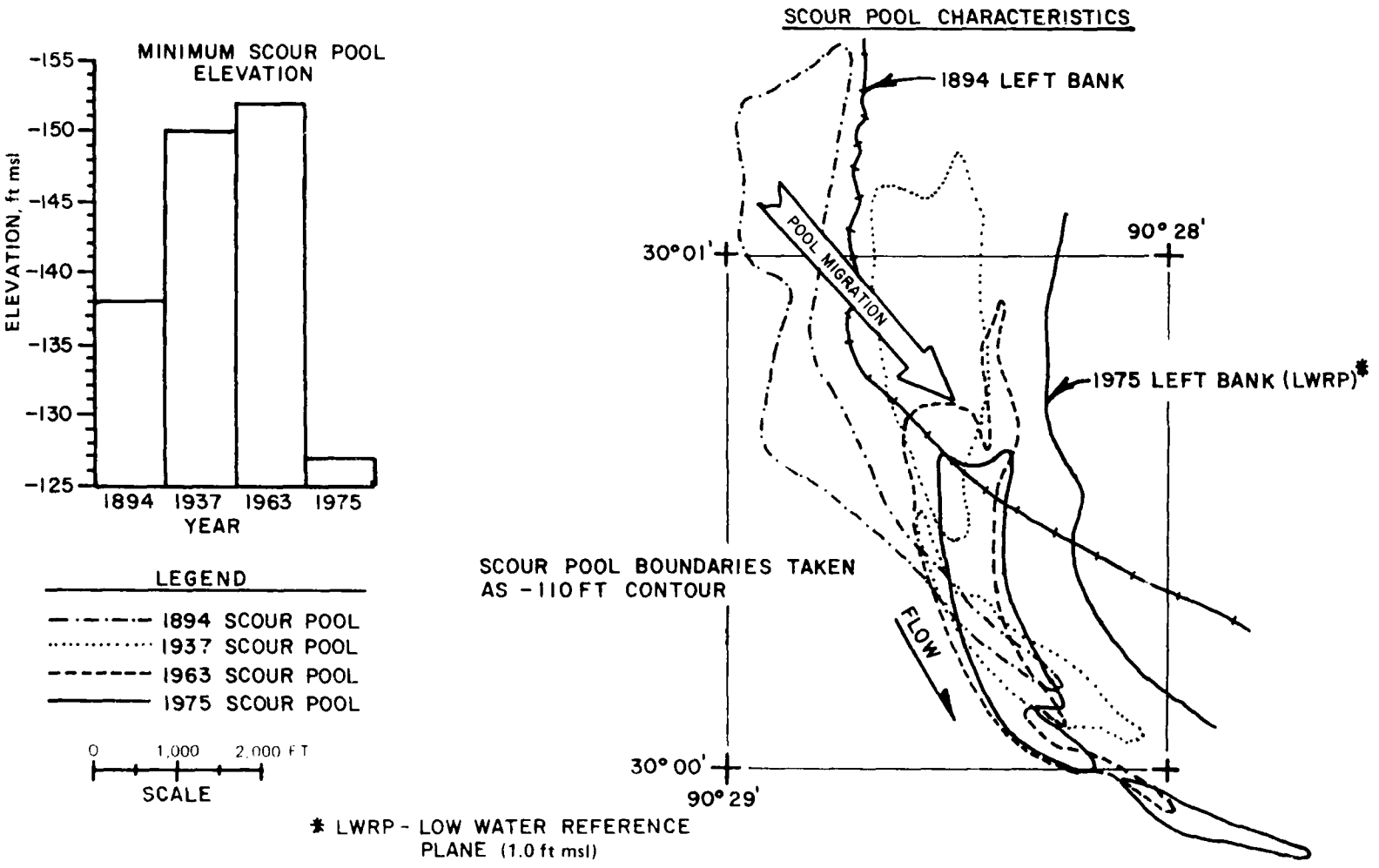


Figure 76. Montz scour pool characteristics

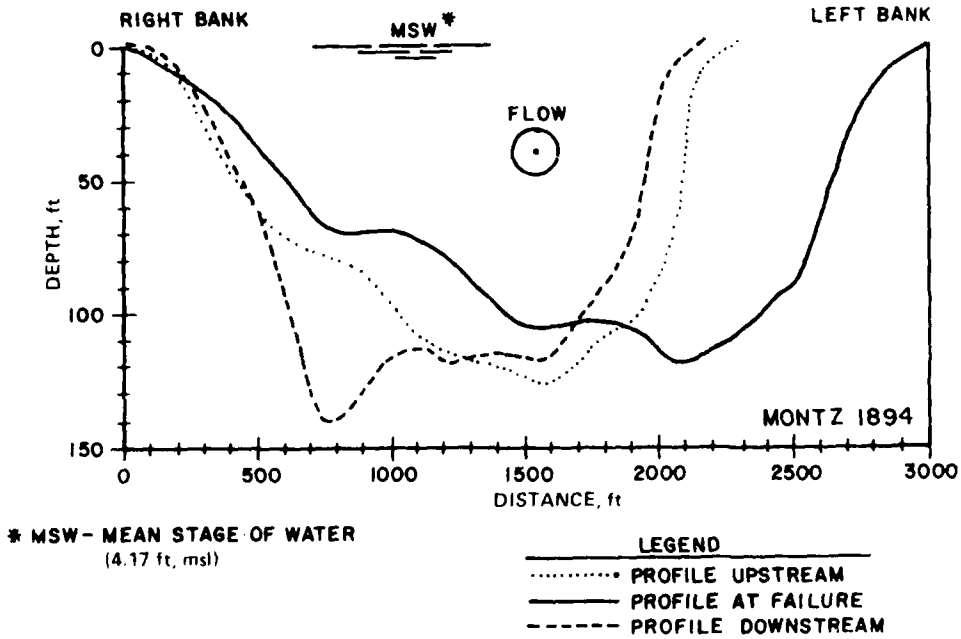


Figure 77. Hydrographic profiles of the Mississippi River at the Montz failure, 1894

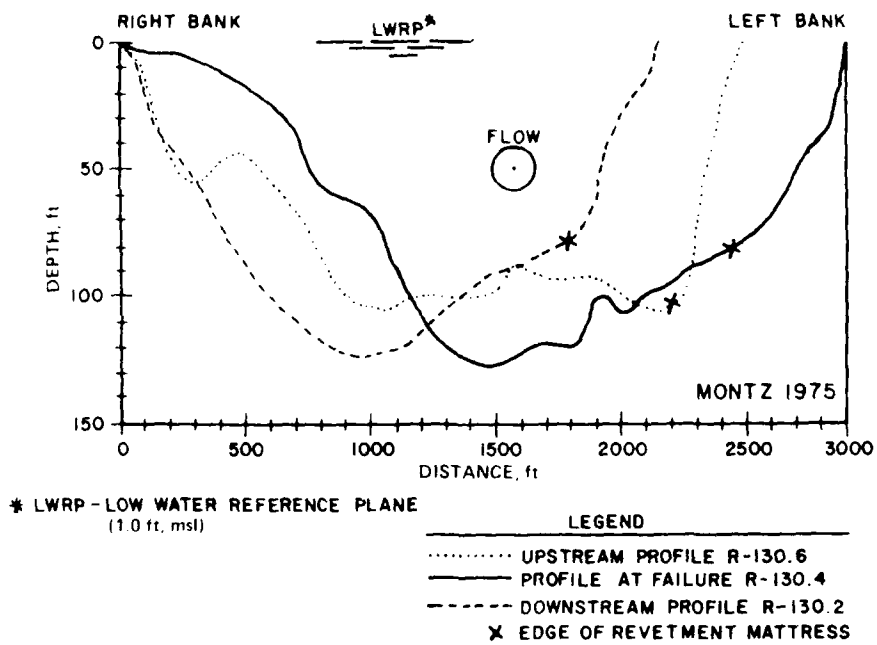
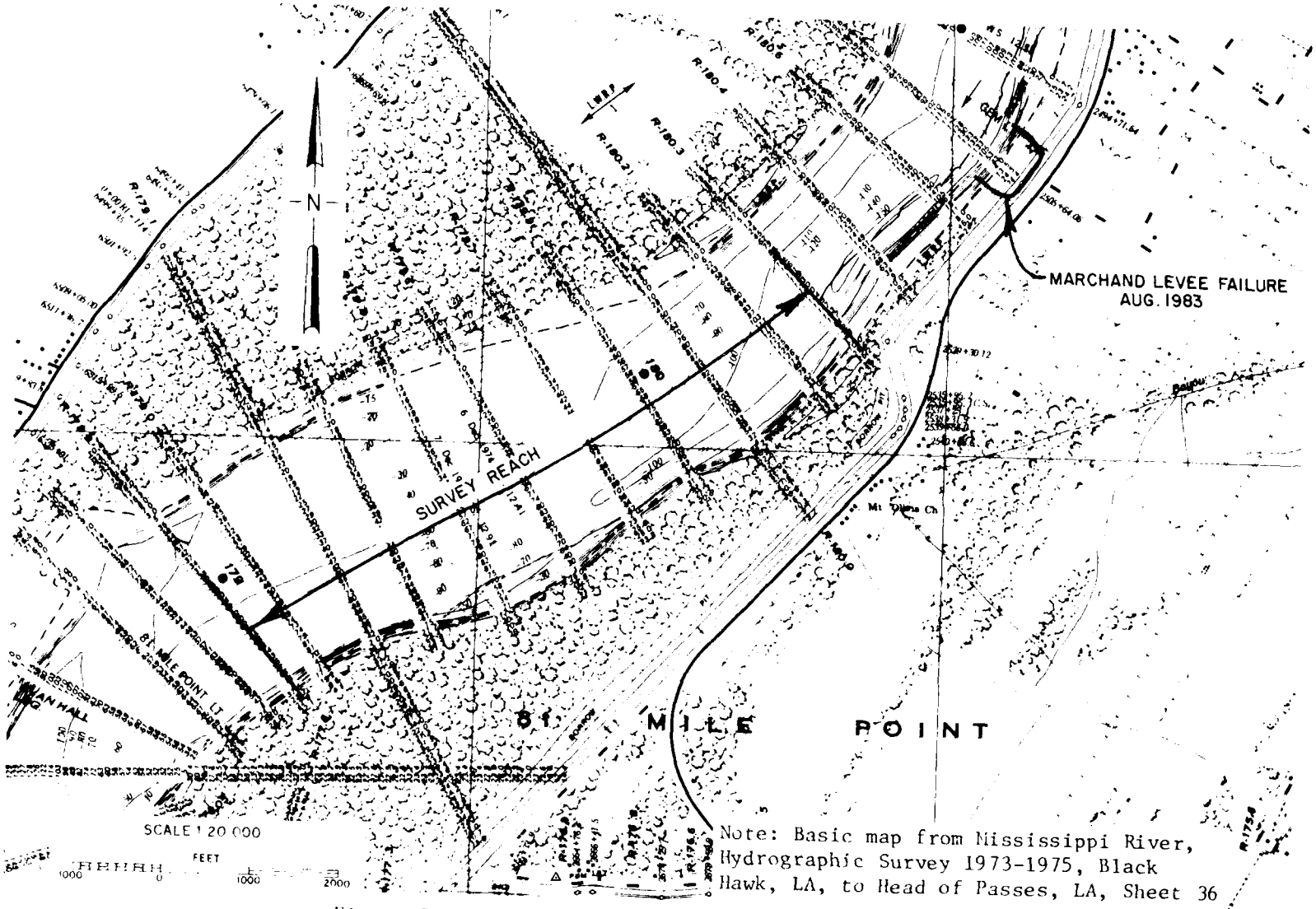


Figure 78. Hydrographic profiles of the Mississippi River at the Montz failure, 1975



Note: Basic map from Mississippi River, Hydrographic Survey 1973-1975, Black Hawk, LA, to Head of Passes, LA, Sheet 36

Figure 79. Location of 81-Mile Point survey reach

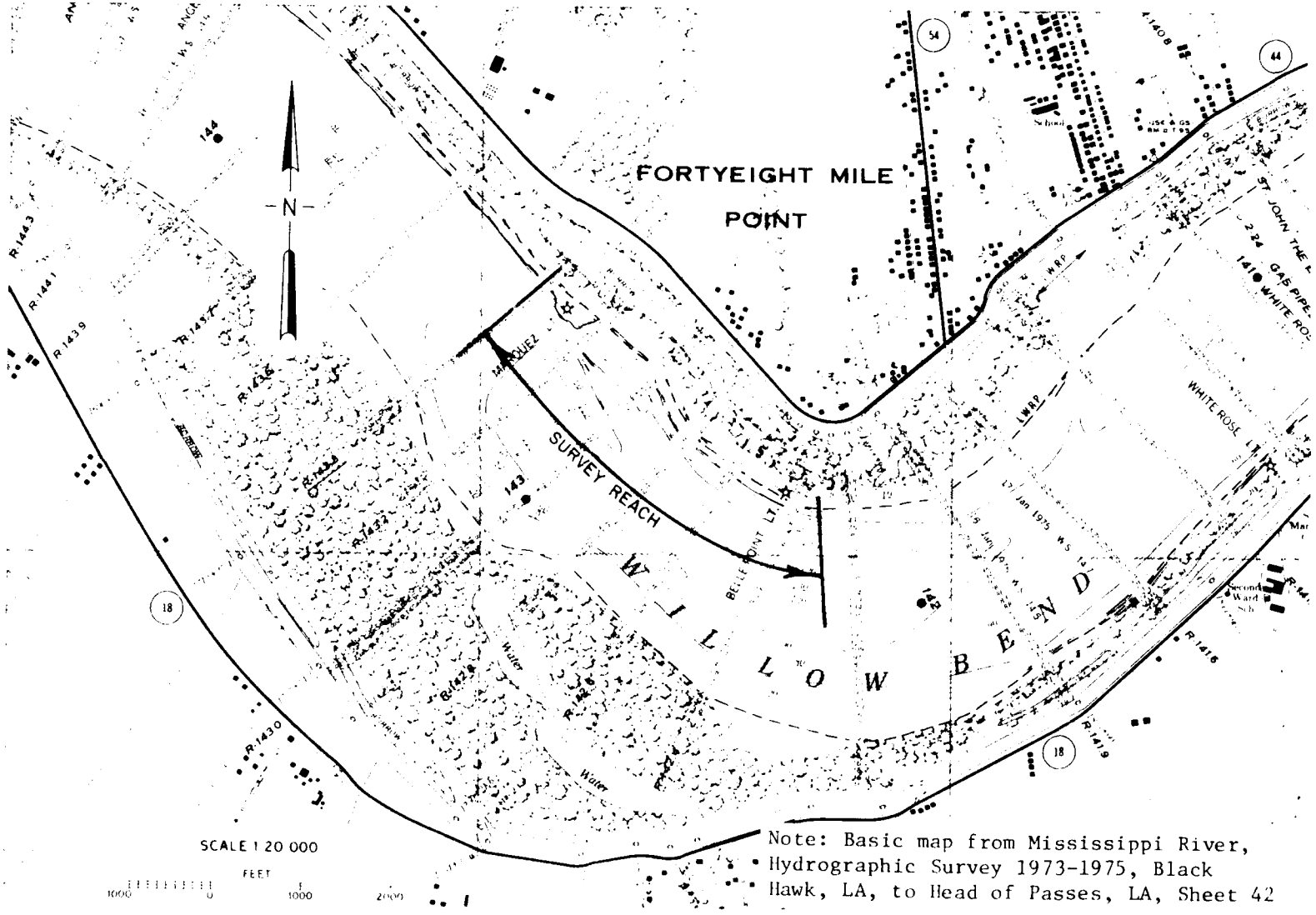
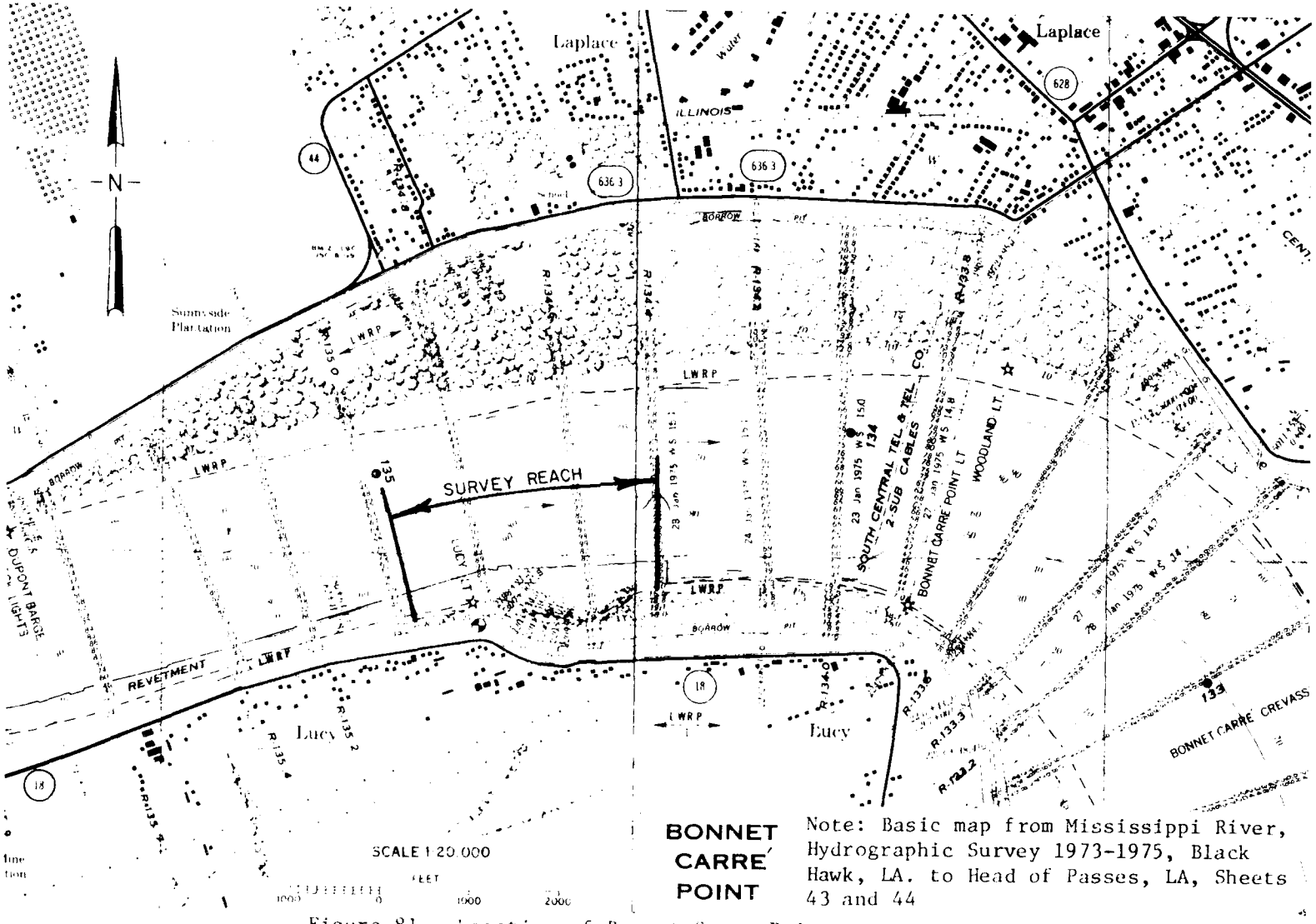
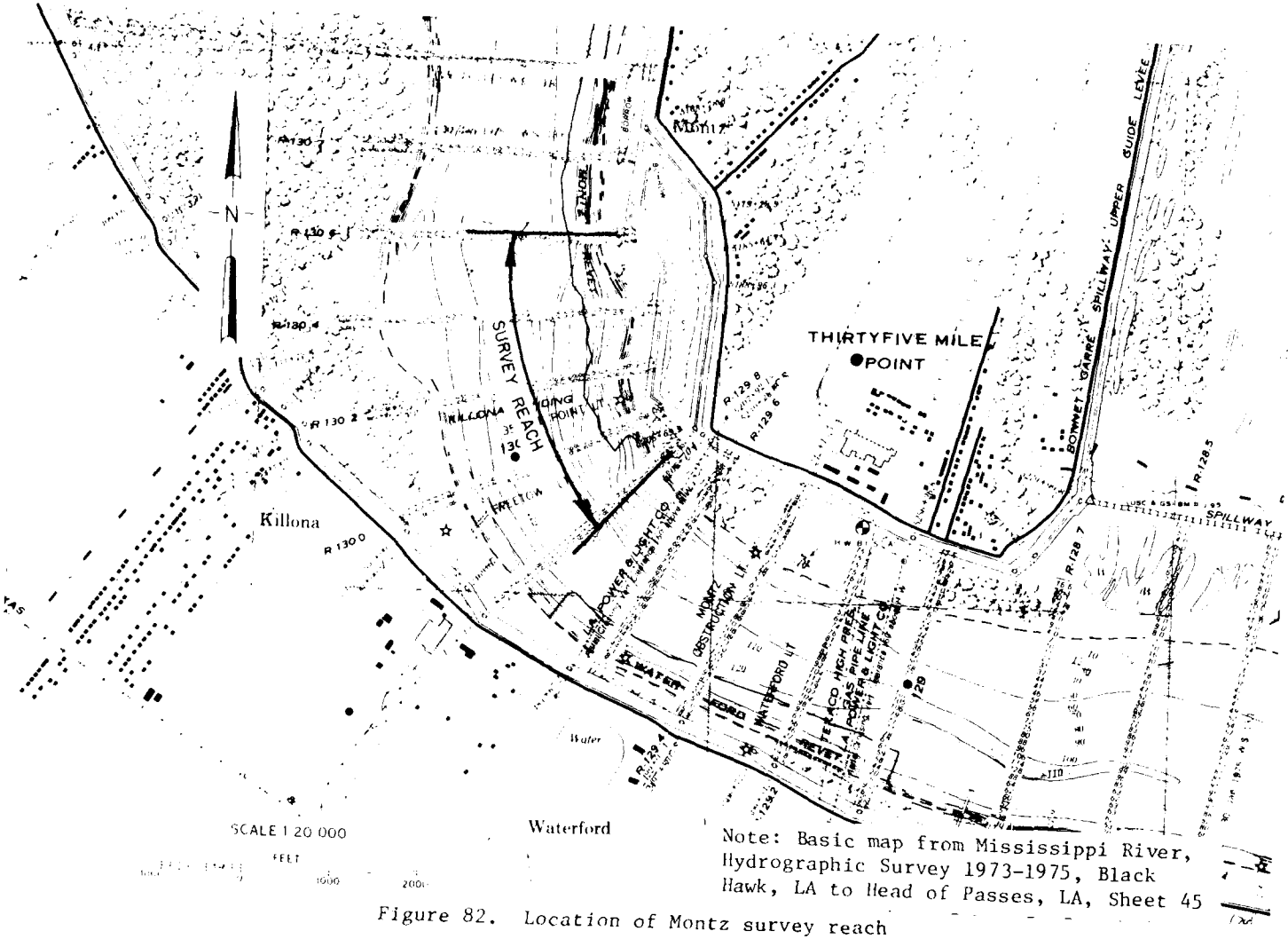


Figure 80. Location of 48-Mile Point survey reach



Note: Basic map from Mississippi River, Hydrographic Survey 1973-1975, Black Hawk, LA. to Head of Passes, LA, Sheets 43 and 44

Figure 81. Location of Bonnet Carre Point survey reach



Note: Basic map from Mississippi River, Hydrographic Survey 1973-1975, Black Hawk, LA to Head of Passes, LA, Sheet 45

Figure 82. Location of Montz survey reach

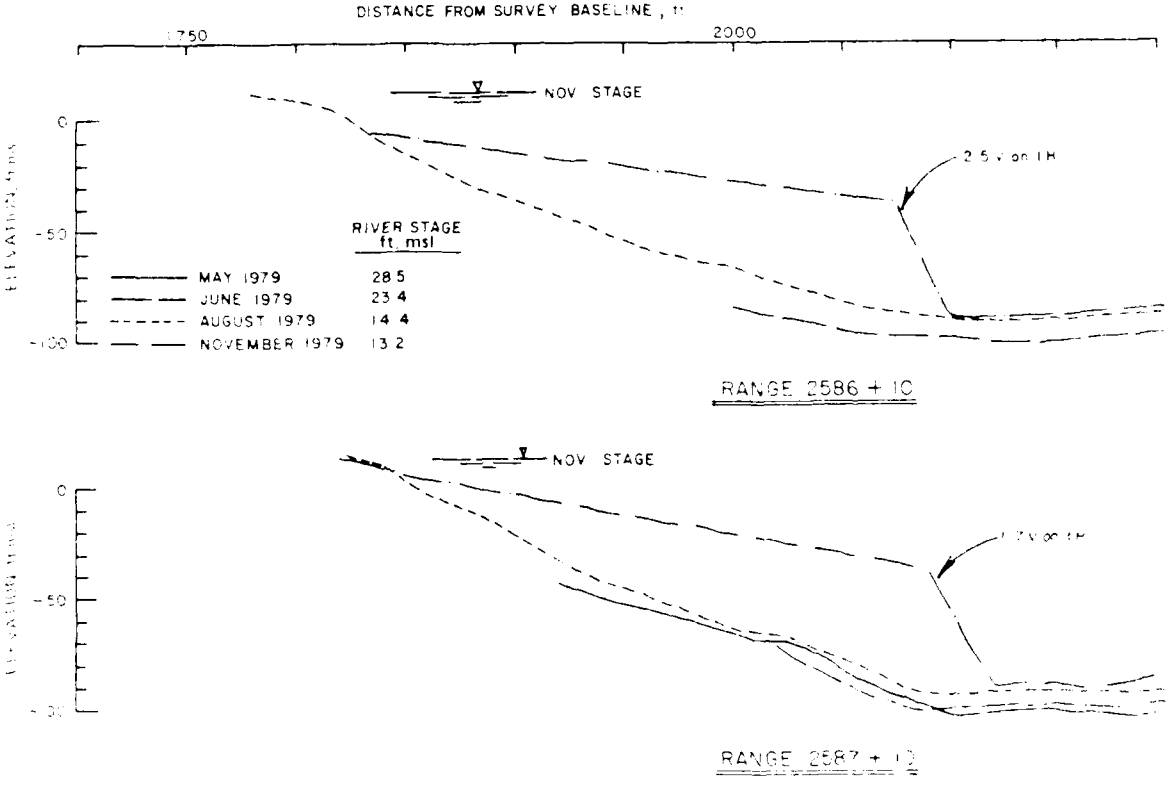
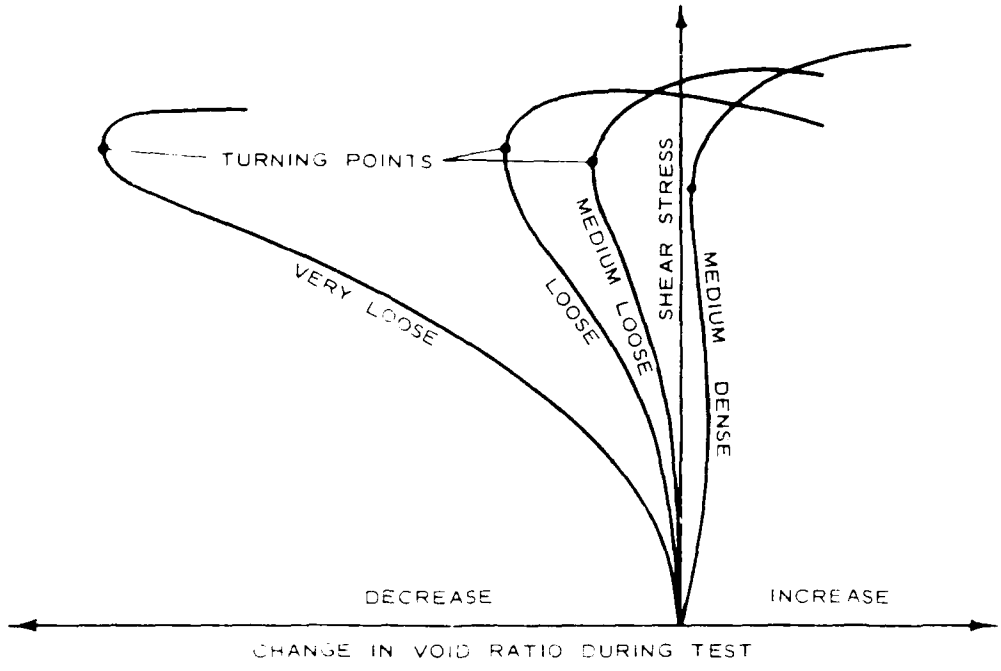
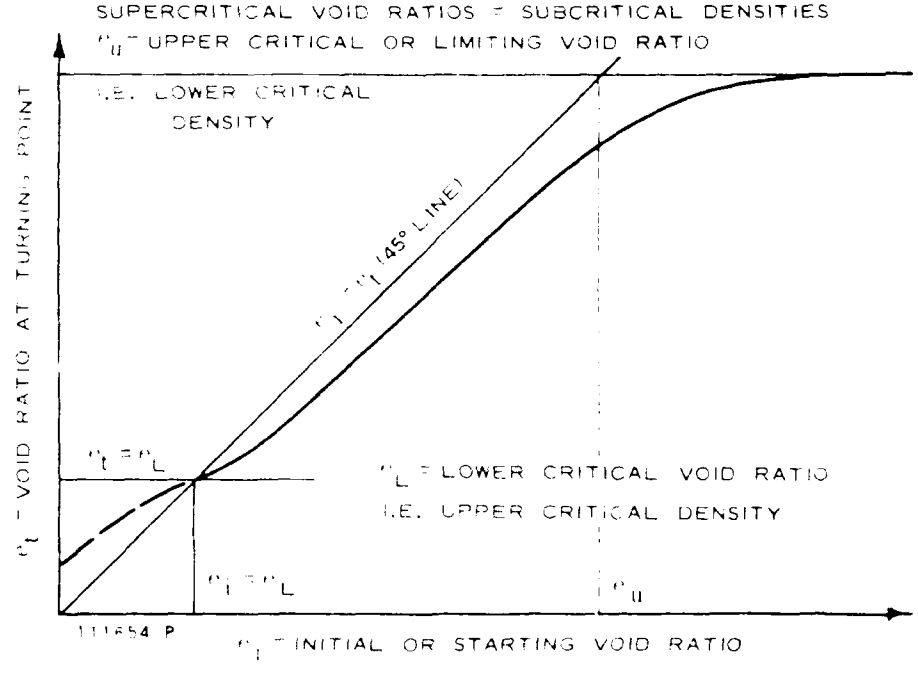


Figure 83. Eighty-One Mile Point hydrographic sections



A



B

Figure 84. Upper and lower critical void ratios (after Geuze 1948)

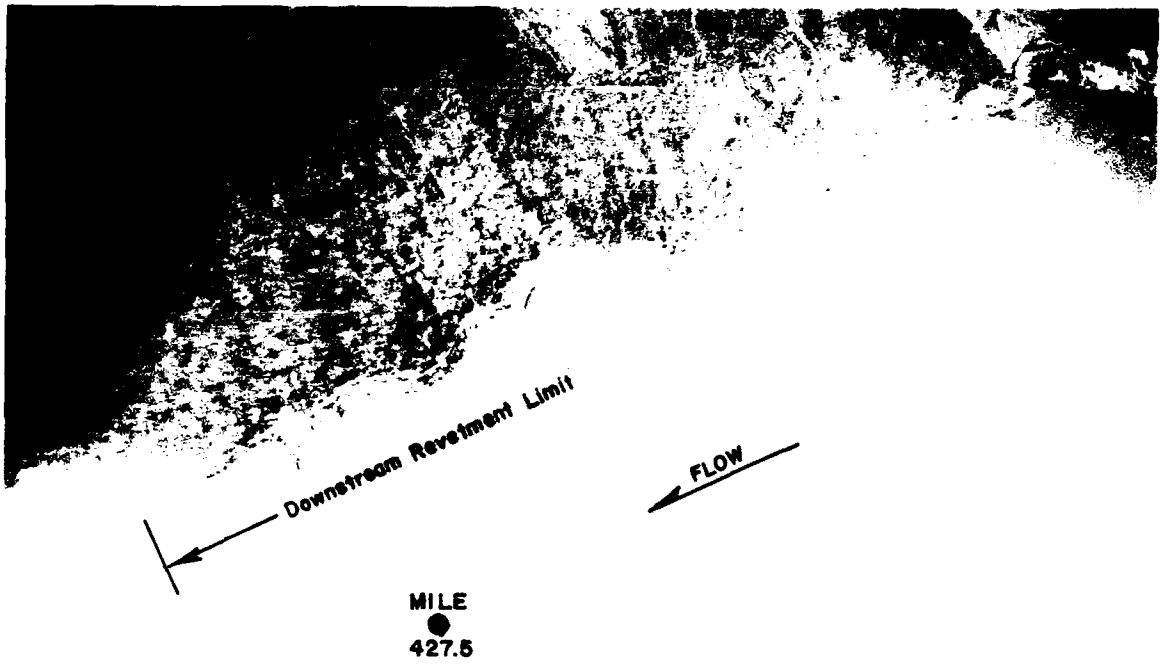
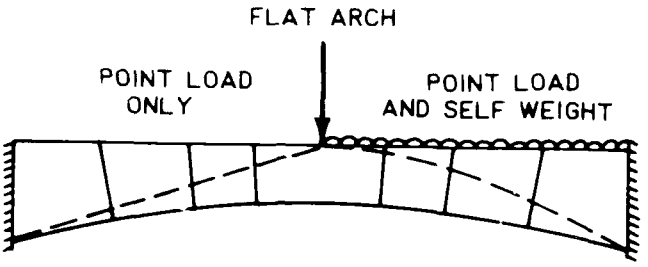
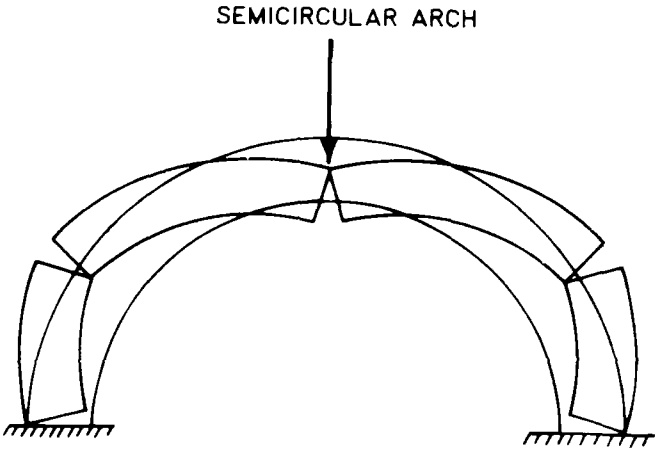


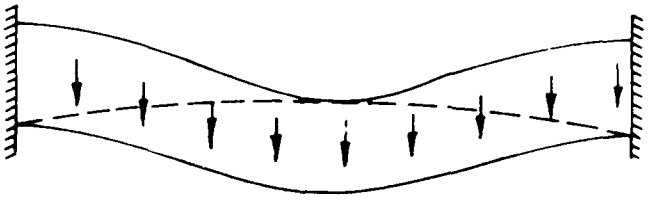
Figure 85. Aerial view of the Reid Bedford bank reach, Mississippi River



a. NO COLLAPSE MECHANISM POSSIBLE

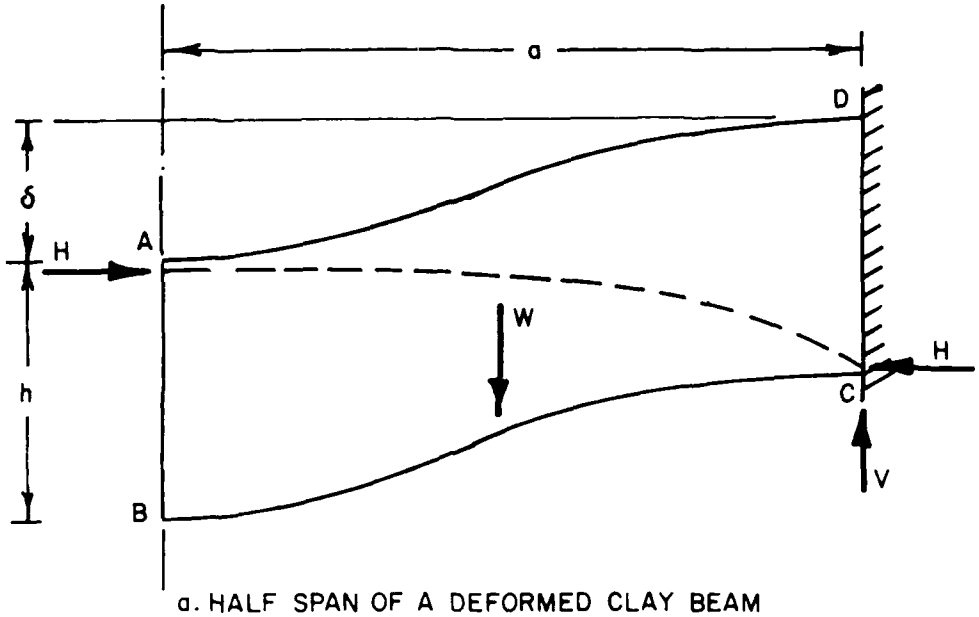


b. MECHANISM OF COLLAPSE

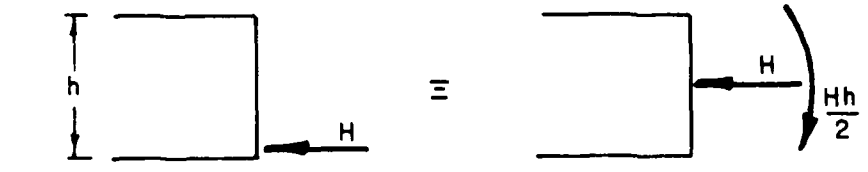


c. CONCAVE MASONRY OR CLAY ARCH

Figure 86. Illustration of arching behavior (after Padfield 1978)

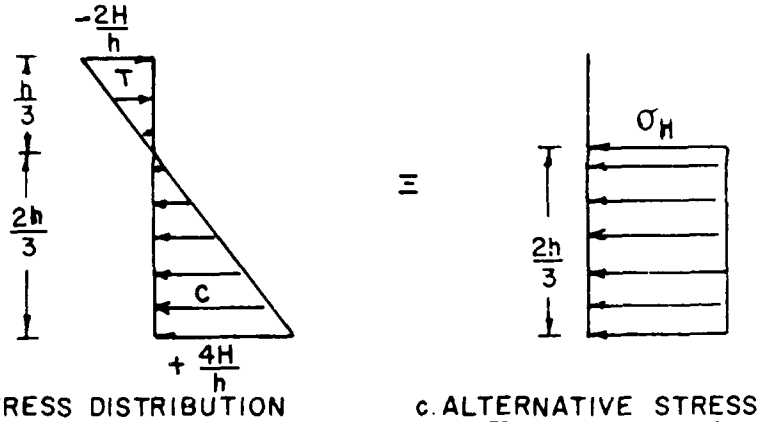


a. HALF SPAN OF A DEFORMED CLAY BEAM



HORIZONTAL REACTION AT CD

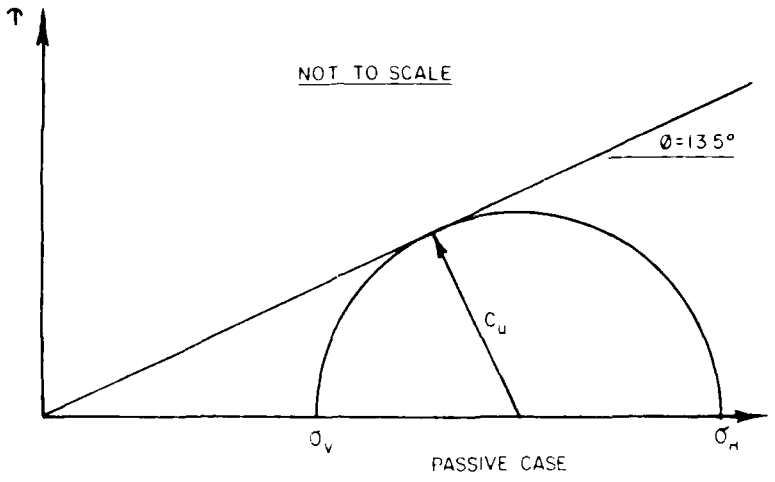
EQUIVALENT REACTIONS



b. STRESS DISTRIBUTION

c. ALTERNATIVE STRESS DISTRIBUTION FOR A PLASTIC MATERIAL

Figure 87. Stress distribution in a two-dimensional clay beam (after Padfield 1978)



$$\text{SIN } \emptyset = 0.233 = \frac{\sigma_H - \sigma_V}{\sigma_H + \sigma_V}$$

$$\sigma_H = 1.61\,\sigma_V$$

Figure 88. Passive stress required to mobilize c_u

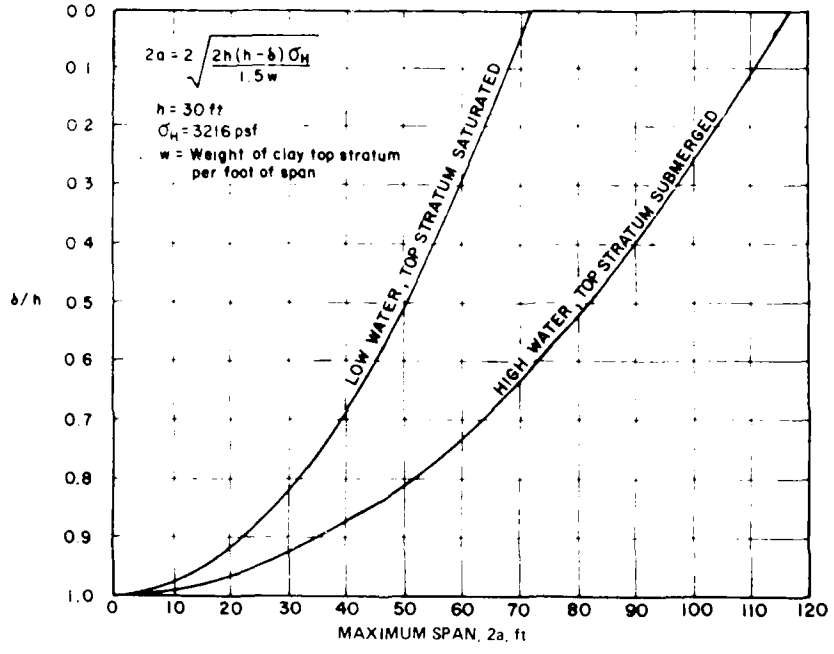


Figure 89. Example computations of δ/h versus maximum arching span, 2a

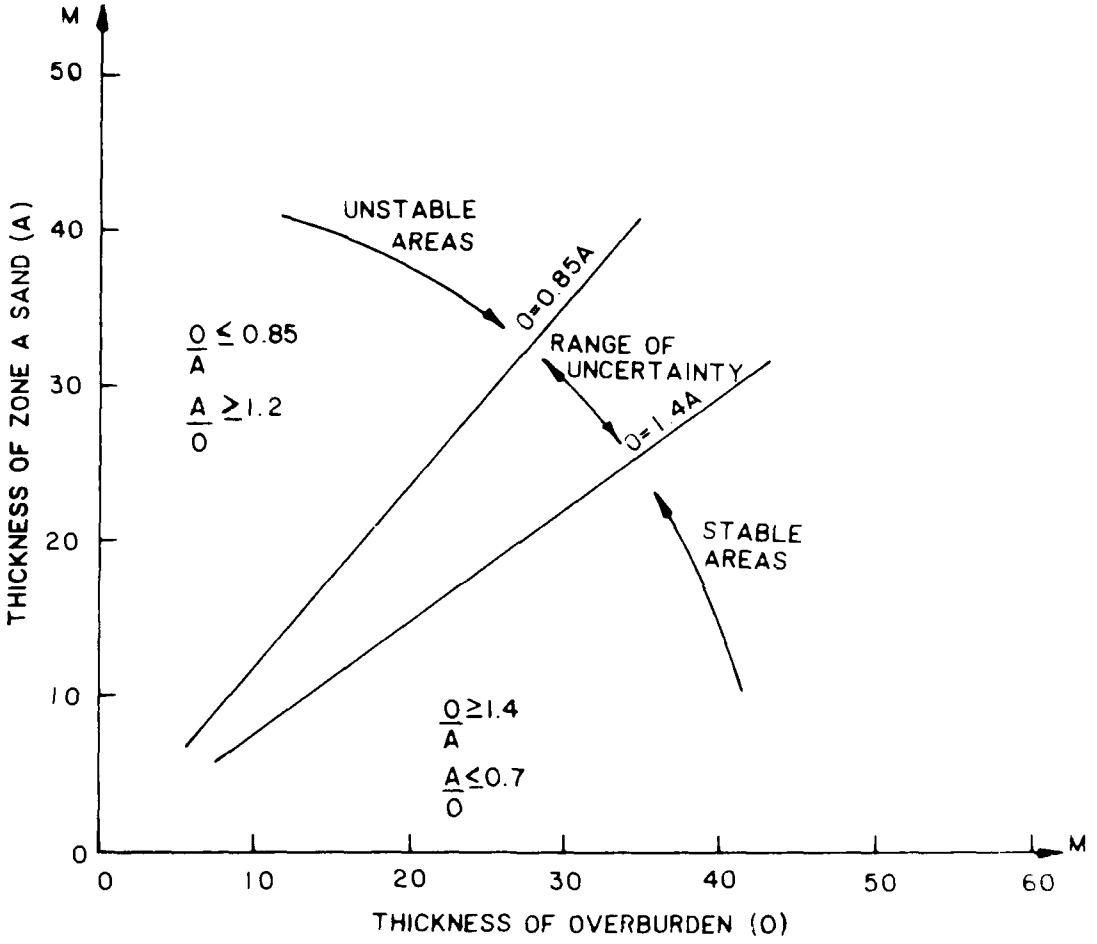
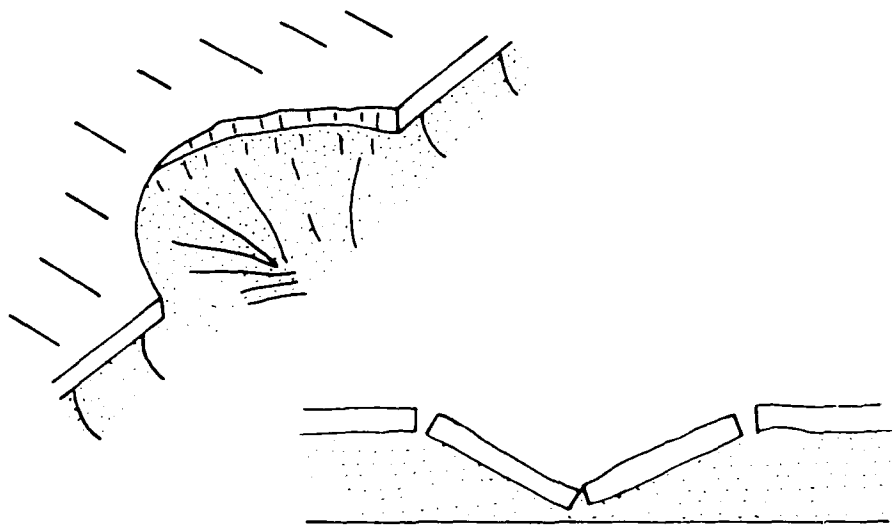
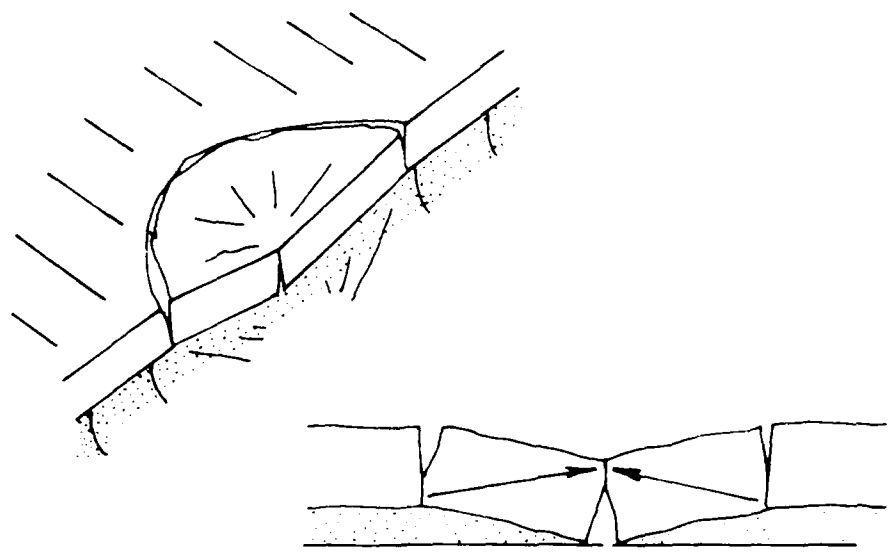


Figure 90. WES empirical criteria for determining riverbank stability with respect to flow failure



a. $0 < A$, arching impossible, clay cracks away, "flow type" failure



b. $0 > A$, arching possible, clay remains in place, "shear type" failure

Figure 91. Clay top stratum behavior

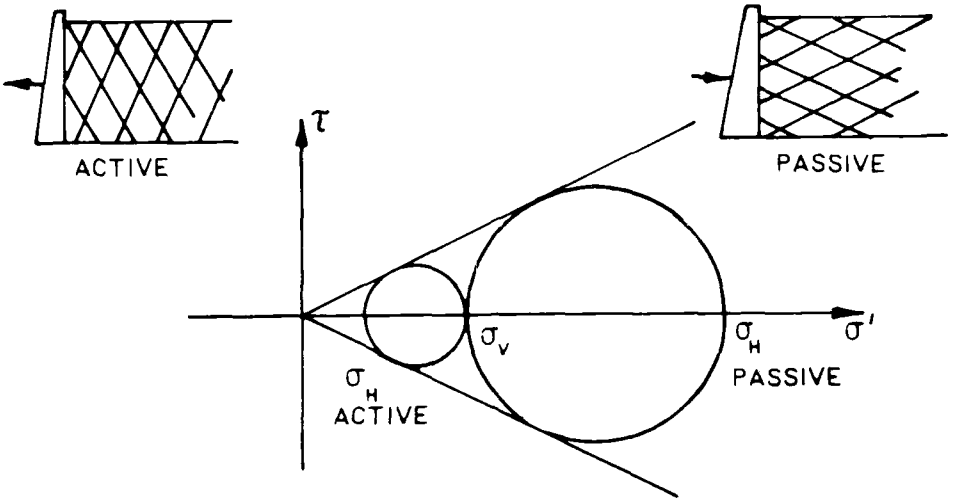


Figure 92. Active and passive earth pressures

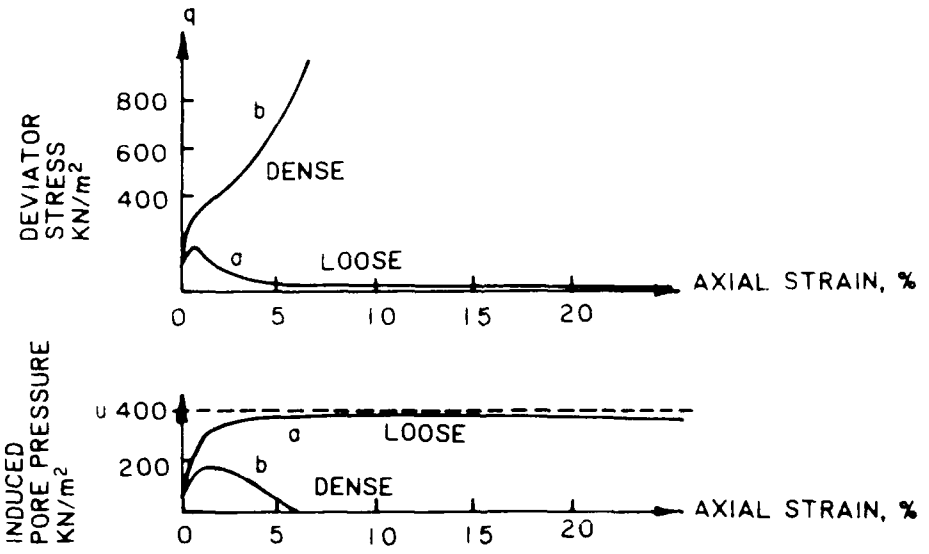


Figure 93. Test results for undrained stress controlled triaxial tests on loose and dense sand specimens (after Castro 1969)

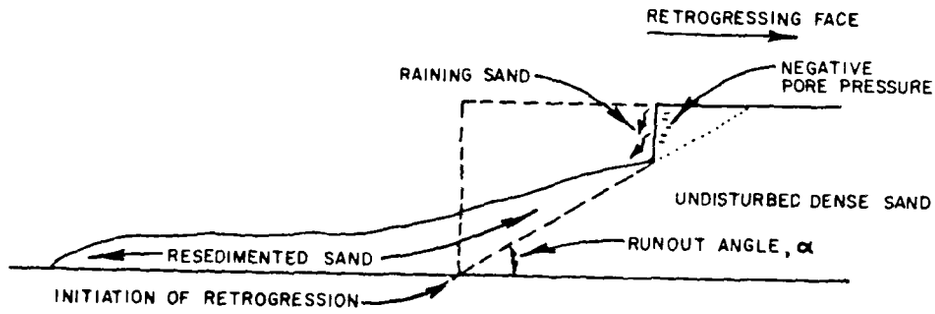
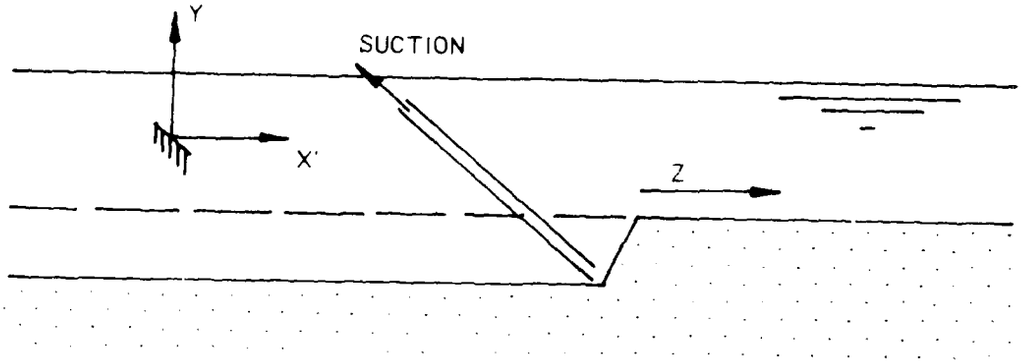
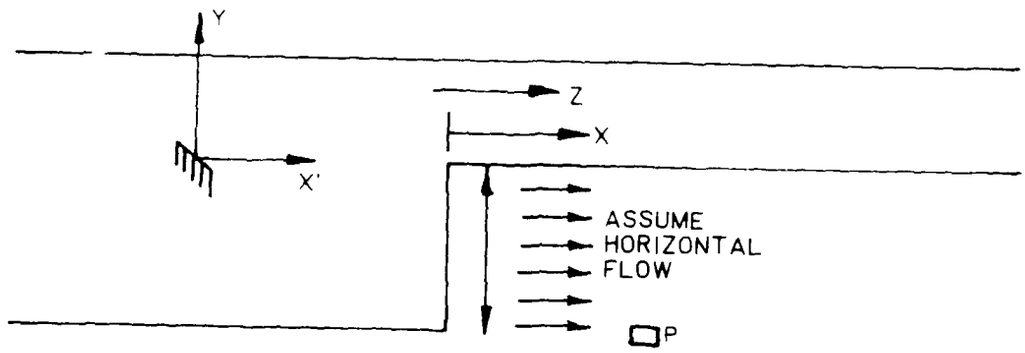


Figure 94. Retrogressing face in dense sand decreasing in height



a. Suction dredge moves at speed Z removing sand which falls off dense sand face



b. Moving and stationary reference frame

Figure 95. Suction dredging of dense sand (after Meijer and Van Os 1976)

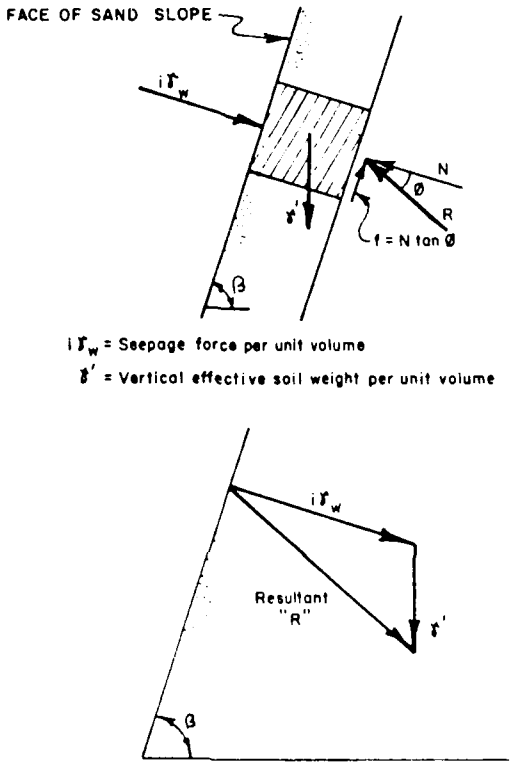


Figure 96. Triangle of forces for steep slope in dense sand maintained in limiting equilibrium by inward seepage

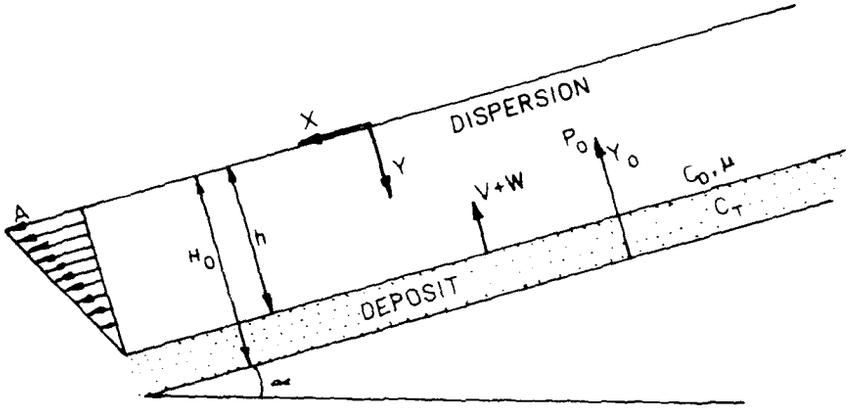


Figure 97. Viscous flow downhill of liquified sand layer moving coordinate axes

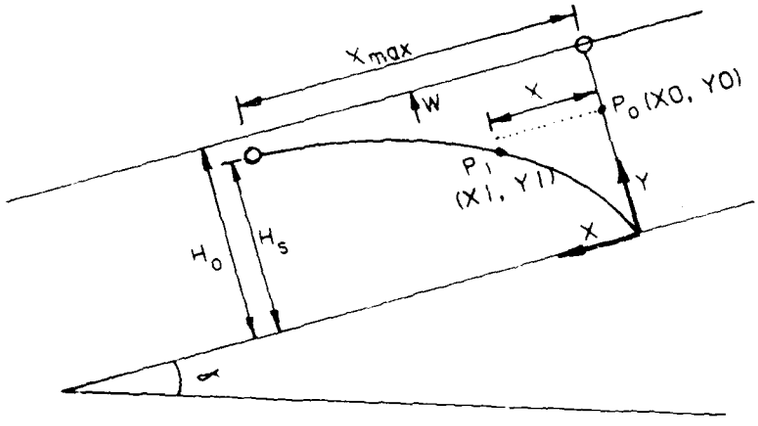


Figure 98. Stationary coordinate axes

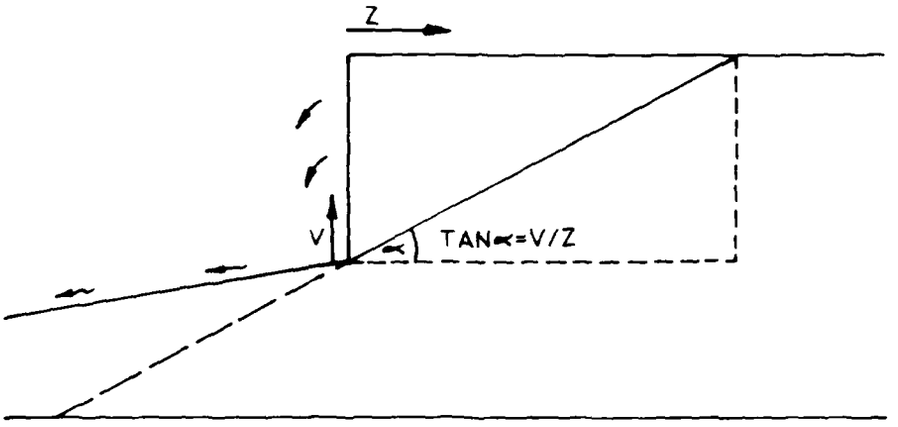


Figure 99. Steep retrogressing face in dense sand, rate of decrease in height

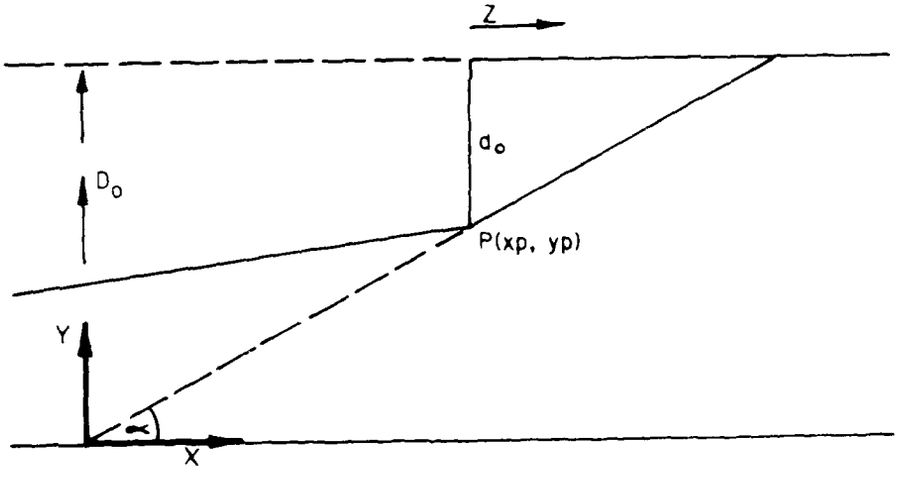


Figure 100. Coordinate axes

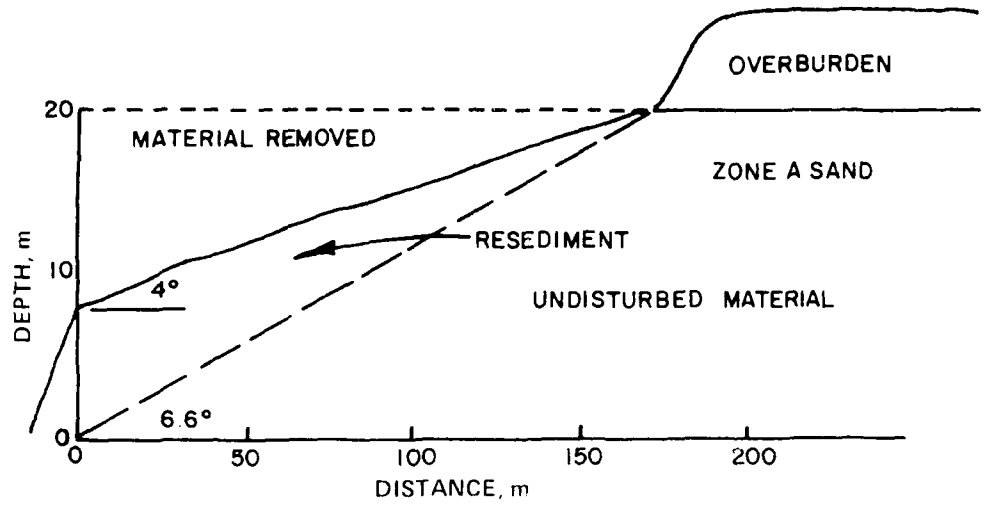


Figure 101. Theoretical after failure profile for initial scarp of 20 m in Zone A sand

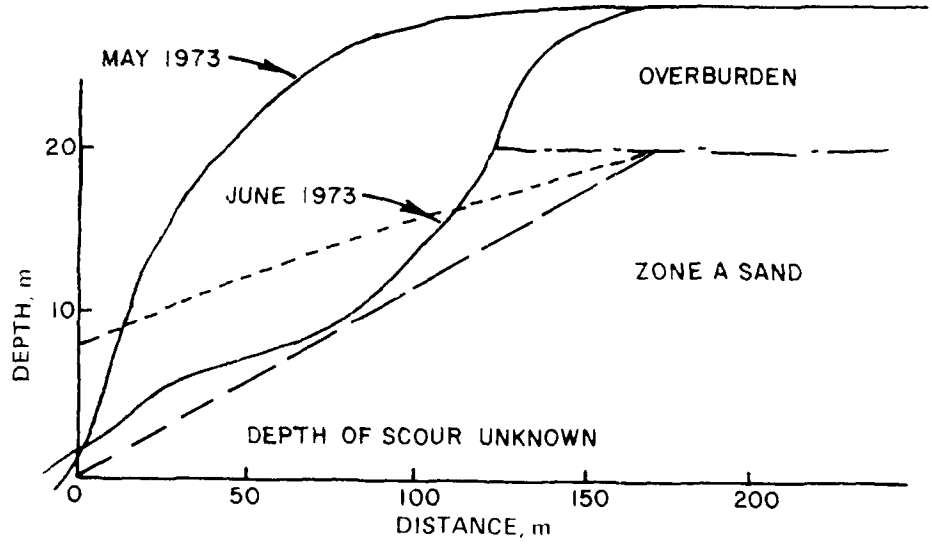


Figure 102. Profiles before and after flow, Stanton flowslide of 1973

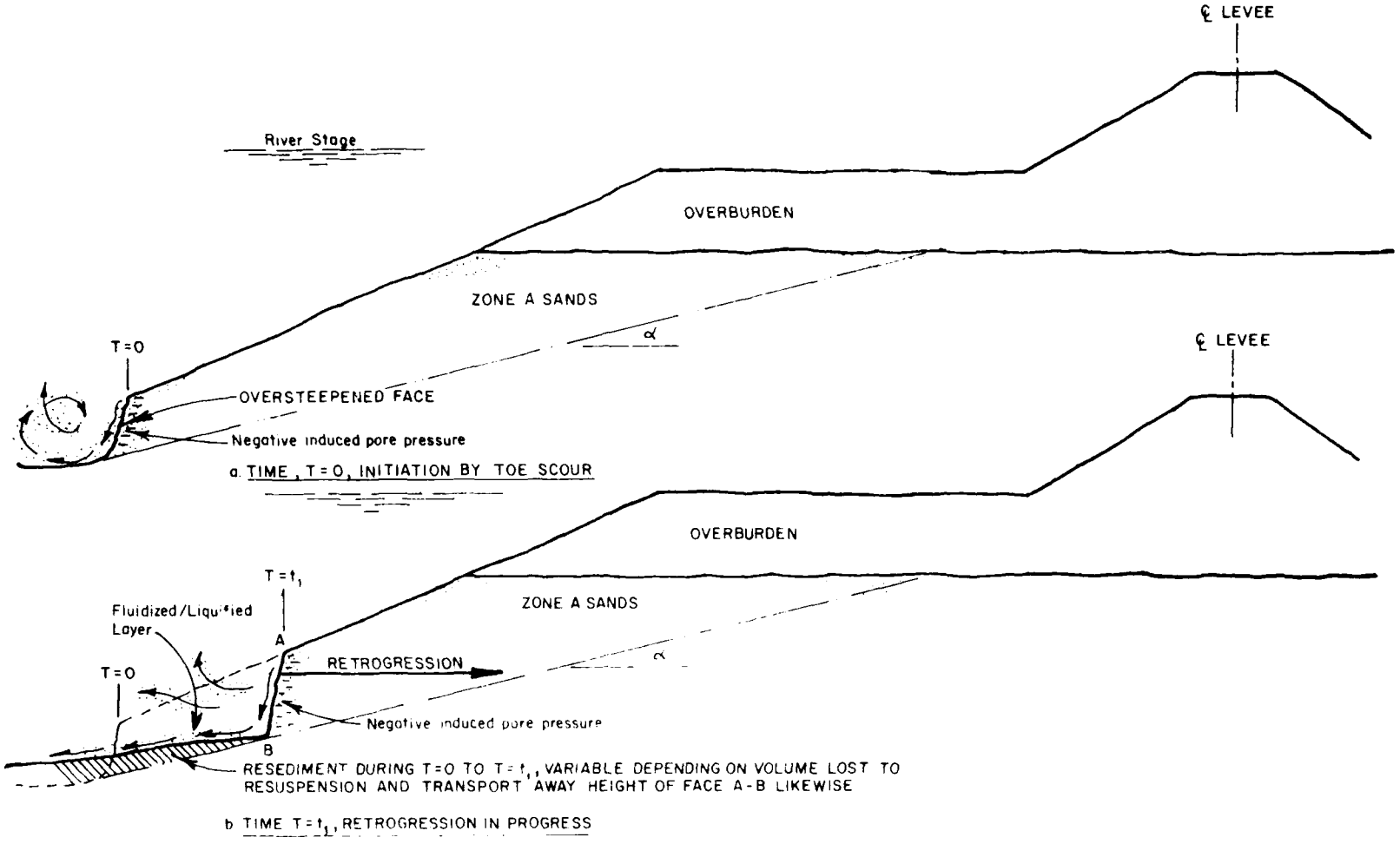


Figure 103. Sequential stages of a retrogressive failure in dilatant sands of Mississippi River point bars (Sheet 1 of 3)

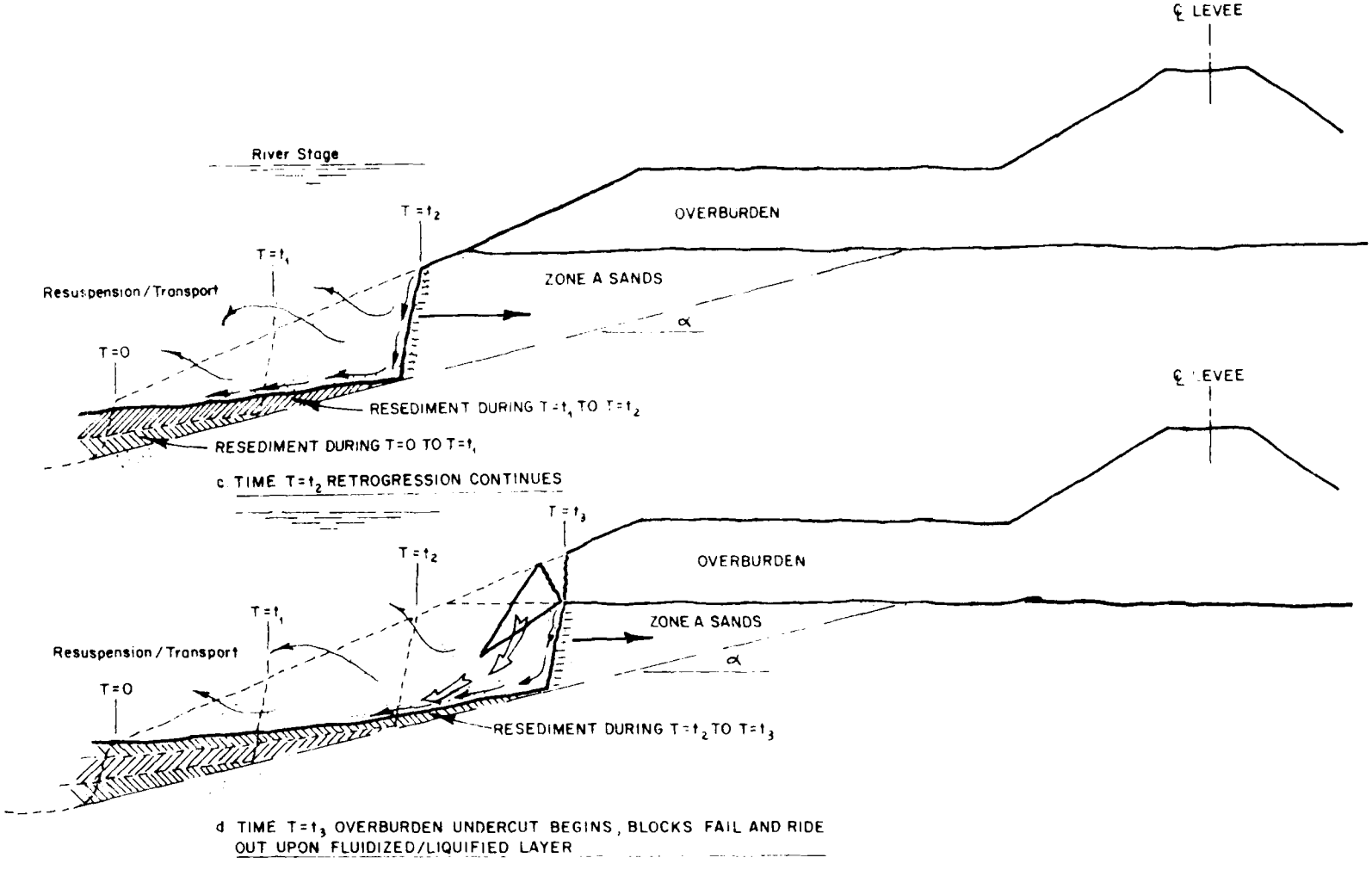


Figure 103. (Sheet 2 of 3)

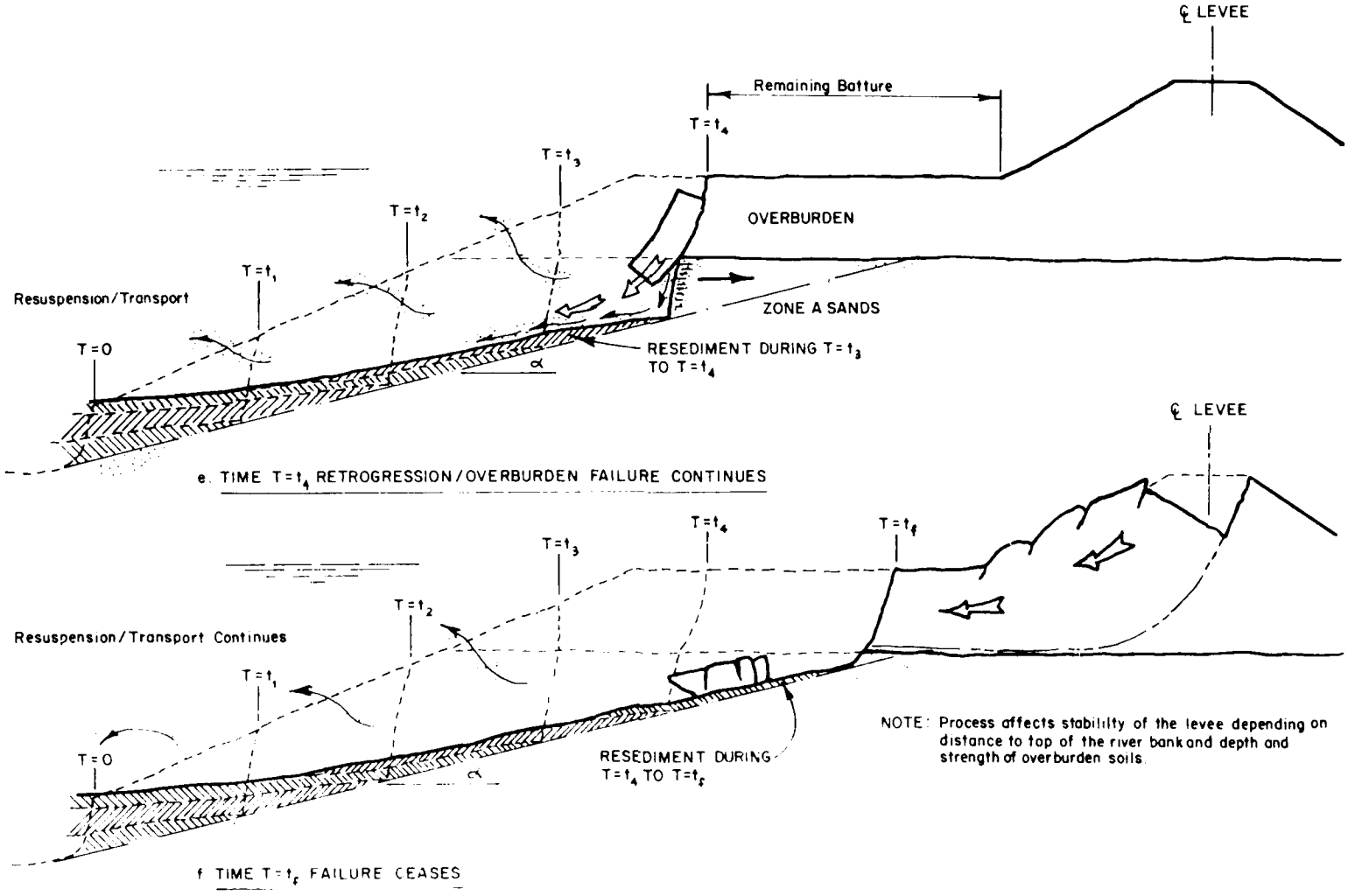


Figure 103. (Sheet 3 of 3)

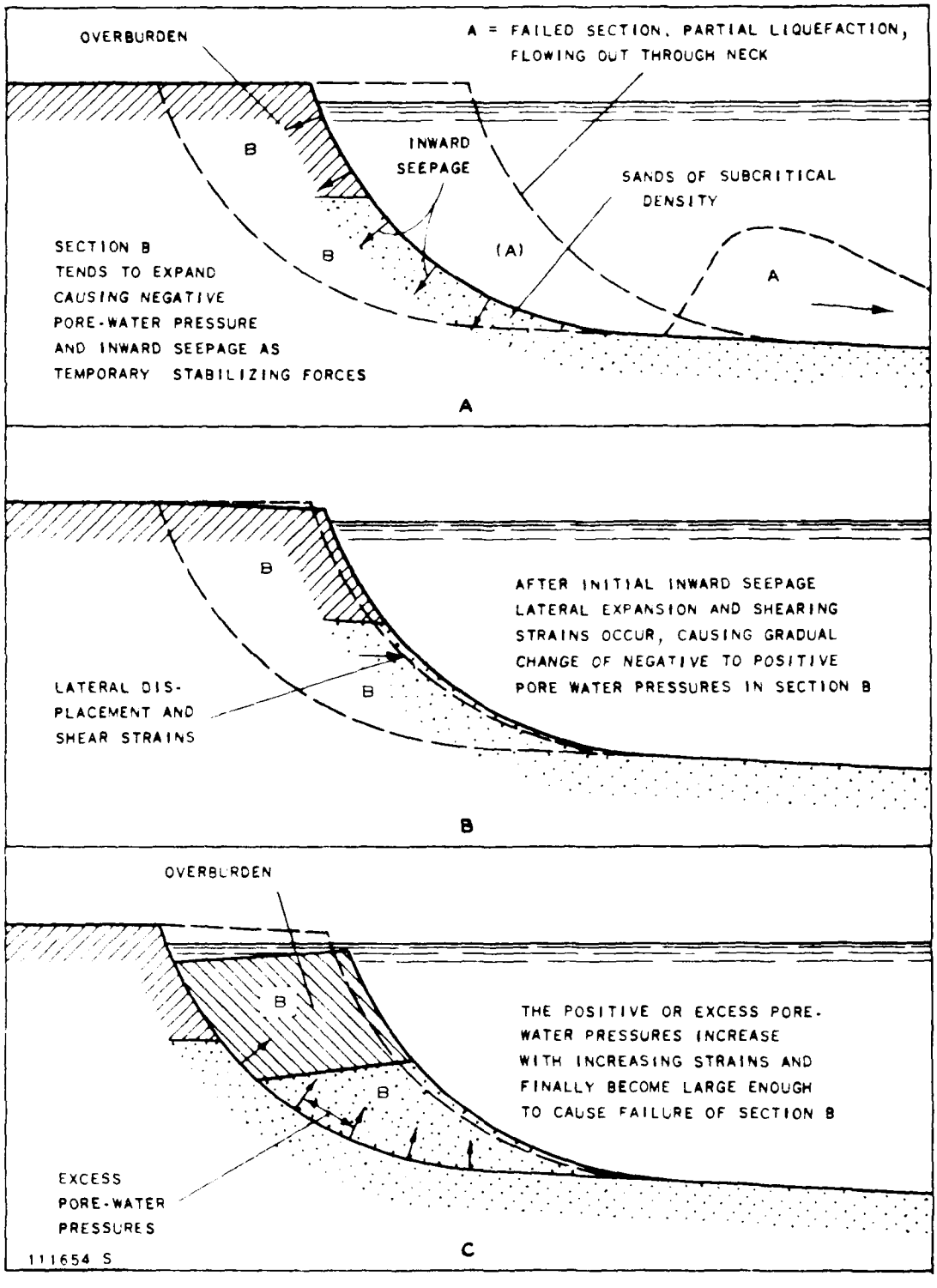


Figure 104. Dutch hypothesis for progressive flow failure (after Koppejan 1948)

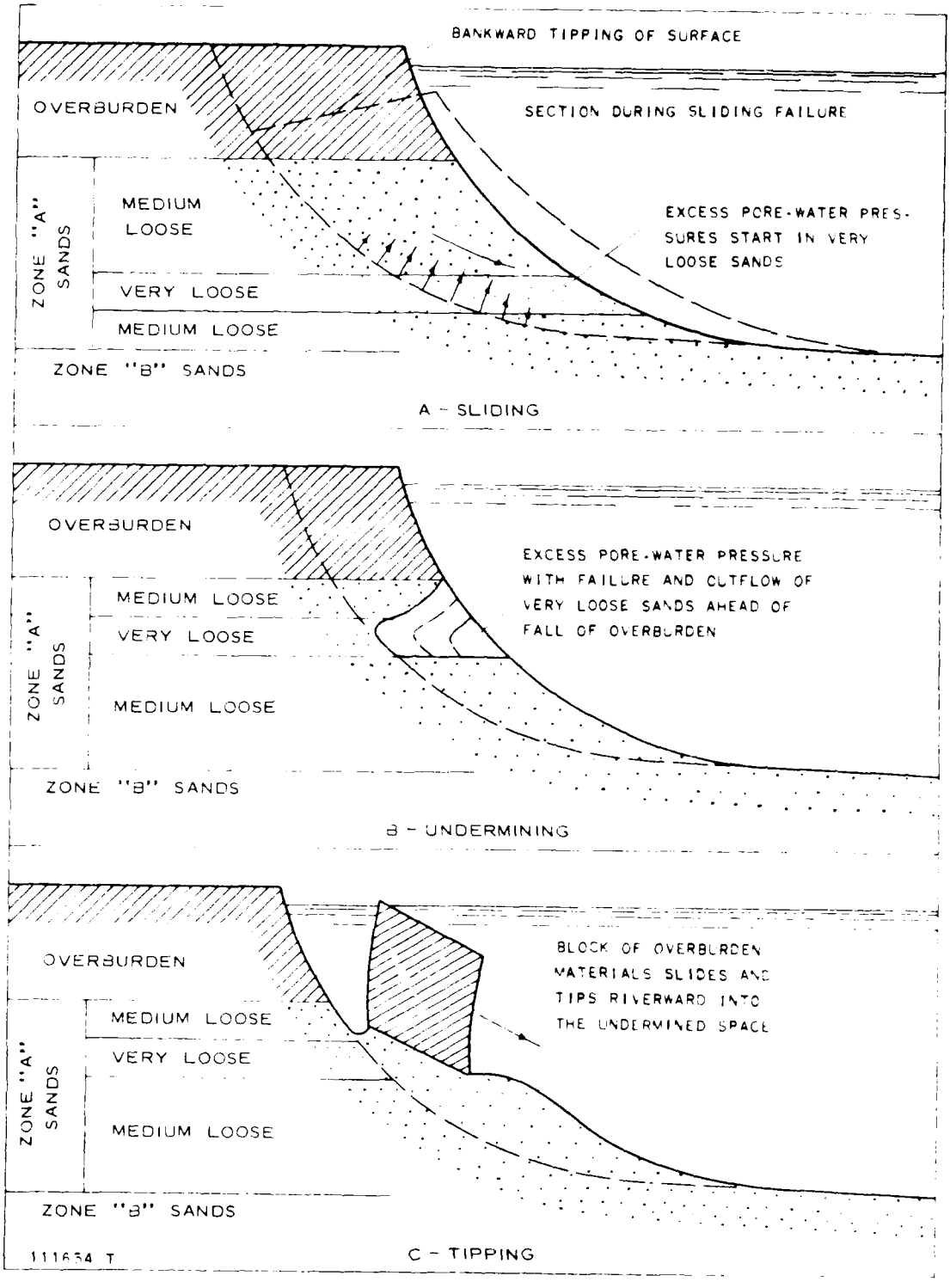


Figure 105. Failure by singular strata of subcritical density (after Hvorslev 1956)

APPENDIX A

LIST OF POTAMOLOGY INVESTIGATIONS REPORTS AND ASSOCIATED REPORTS

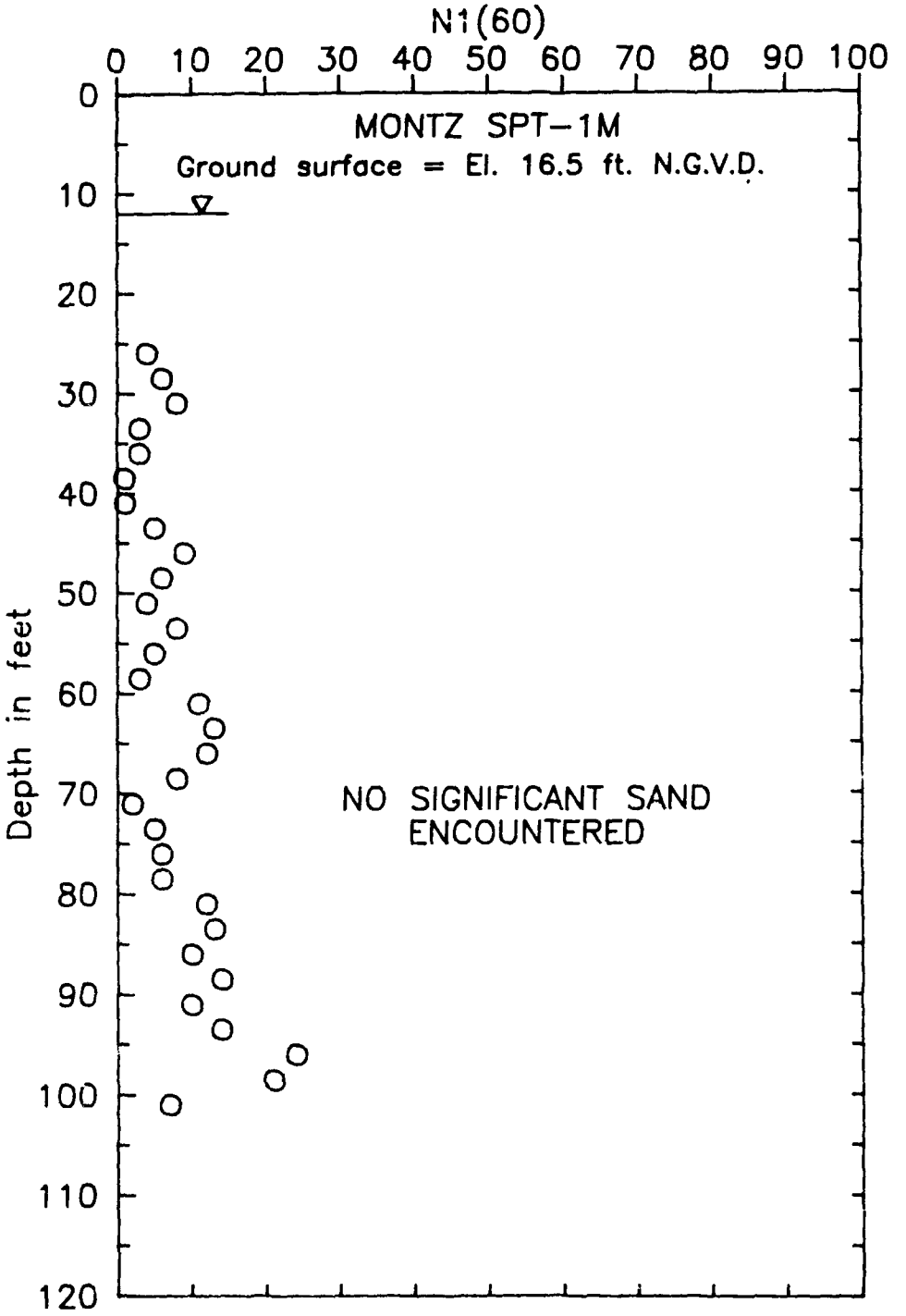
ASSOCIATED REPORTS*

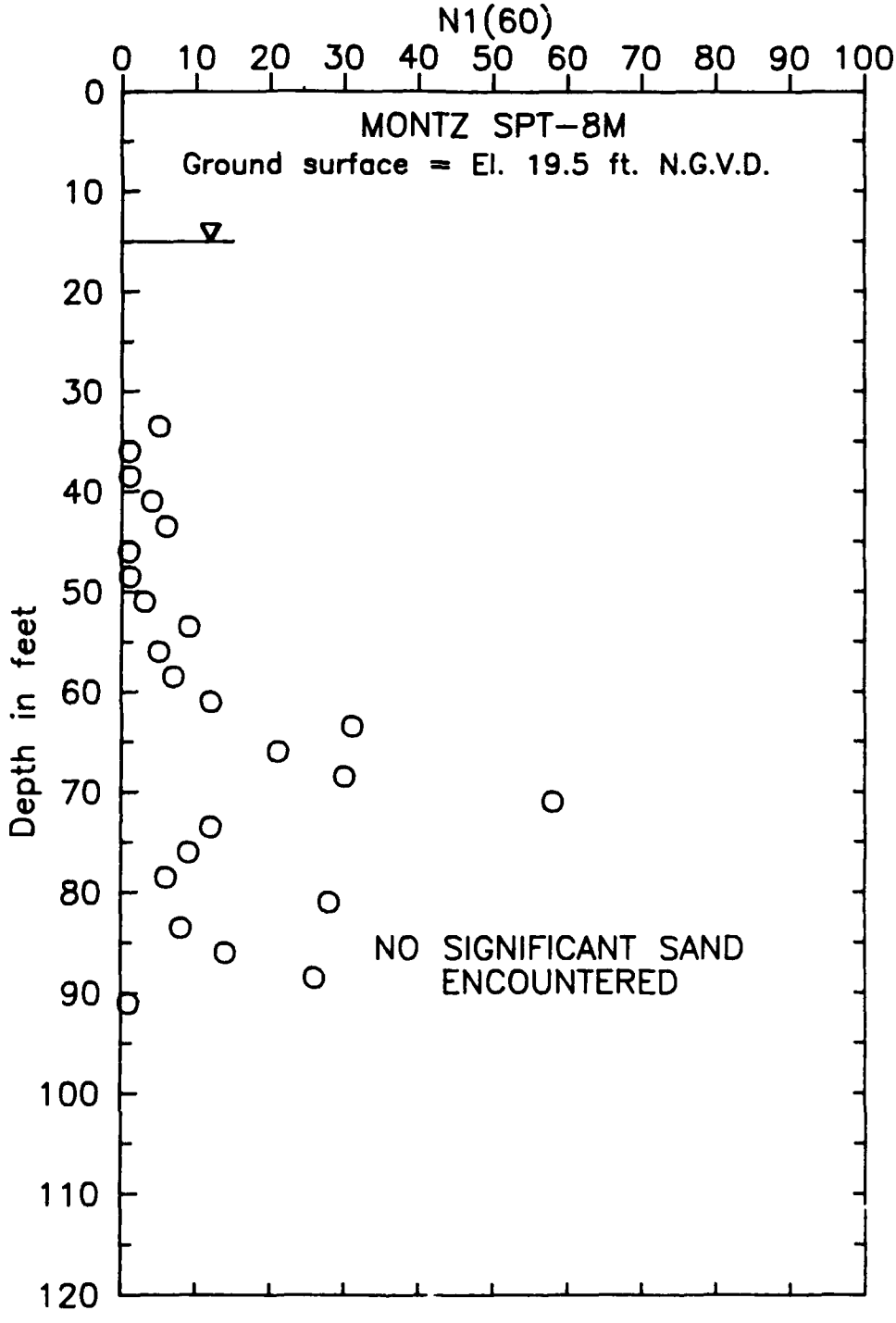
Study of Materials in Suspension, Mississippi River; T.M. No. 122-1	February 1939
Study of Materials in Transport, Passes of the Mississippi River; T.M. No. 138-1	September 1939
Geological Investigation of the Alluvial Valley of the Lower Mississippi River; Mississippi River Commission	December 1944
A Laboratory Study of the Meandering of Alluvial Rivers	May 1949
Fine-Grained Alluvial Deposits and Their Effects on Mississippi River Activity	July 1949
Report of Conference on Sand-Asphalt Revetment, 12 August 1948	August 1949
Geological Investigation of Mississippi River Activity, Memphis, Tenn., to Mouth of Arkansas River; T.M. No. 3-288	June 1950
Bank Caving Investigations, Morville Revetment, Mississippi River; T.M. No. 3-318	September 1950
Investigation of Free Nigger Point Crevasse, Mississippi River; Mississippi River Commission	December 1950
Mississippi River Revetment Studies; St. Anthony Falls Hydraulic Laboratory Project Report No. 21	June 1951
Investigation of Mass Placement of Sand Asphalt for Underwater Protection of River Banks; T.M. No. 3-329	August 1951
Mississippi River Revetment Studies - Tests on a Double Layer Articulated Concrete Mattress; St. Anthony Falls Hydraulic Laboratory Project Report No. 28	May 1952
Petamelgav Barrel Samples; Miscellaneous Paper No. 3-4	August 1952
Torsion Shear Study; Miscellaneous Paper No. 3-13	[illegible] 1952
Study of Variability of Sand Deposits; Miscellaneous Paper No. 3-1	August 1952
Flume Investigation of Prototype Revetment; Miscellaneous Paper No. 3-[illegible]	[illegible] 1952
Investigation of Bituminous Cold Mixes for the Protection of Inner River Banks; T.M. No. 3-367	[illegible] 1953
Feasibility Study of Improved Methods for Revetment Stabilization; Interim Report No. 3-[illegible] by Waterways Experiment [illegible]	[illegible] 1953

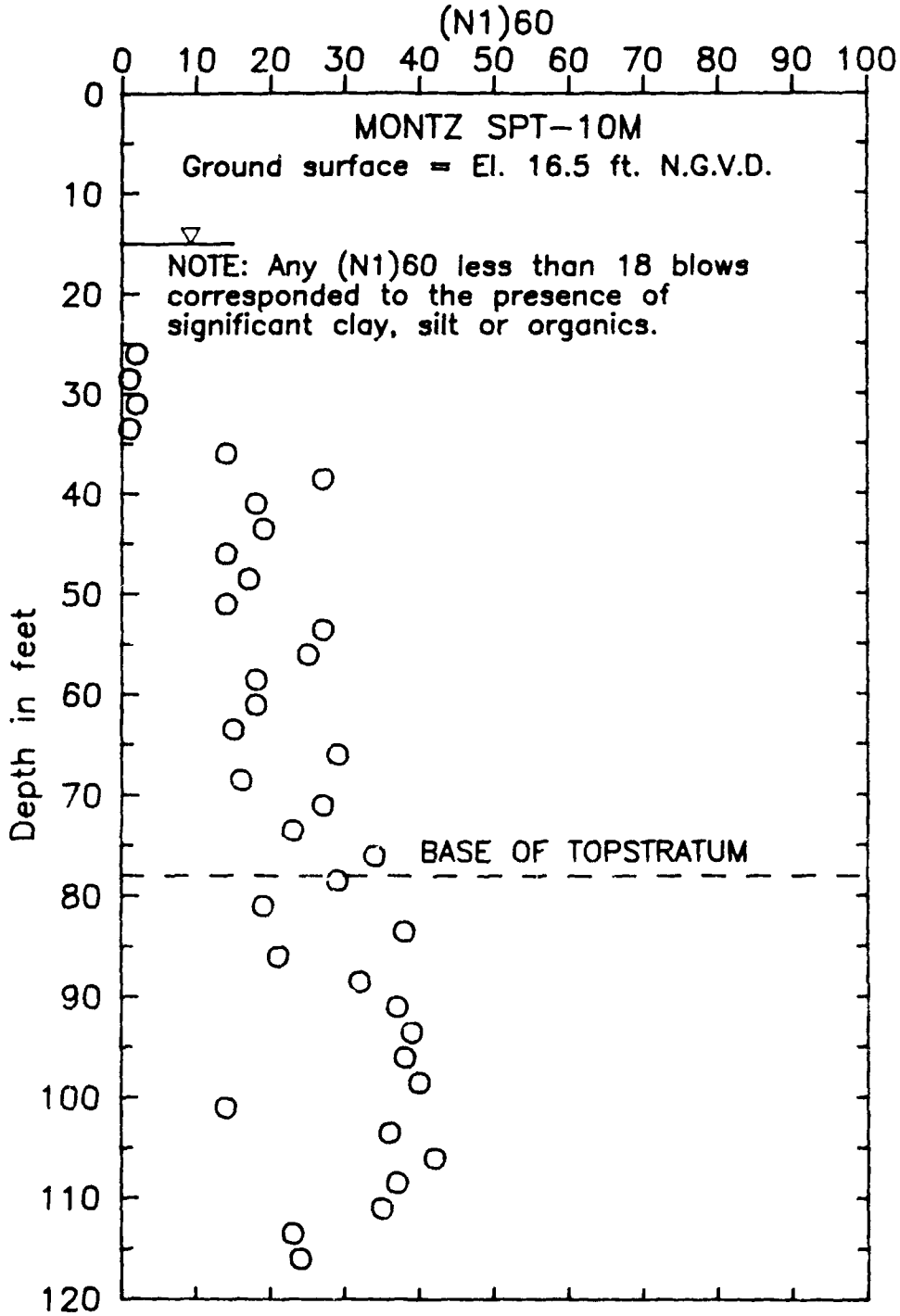
* Unless otherwise noted, all reports listed are publications of the Waterways Experiment [illegible]

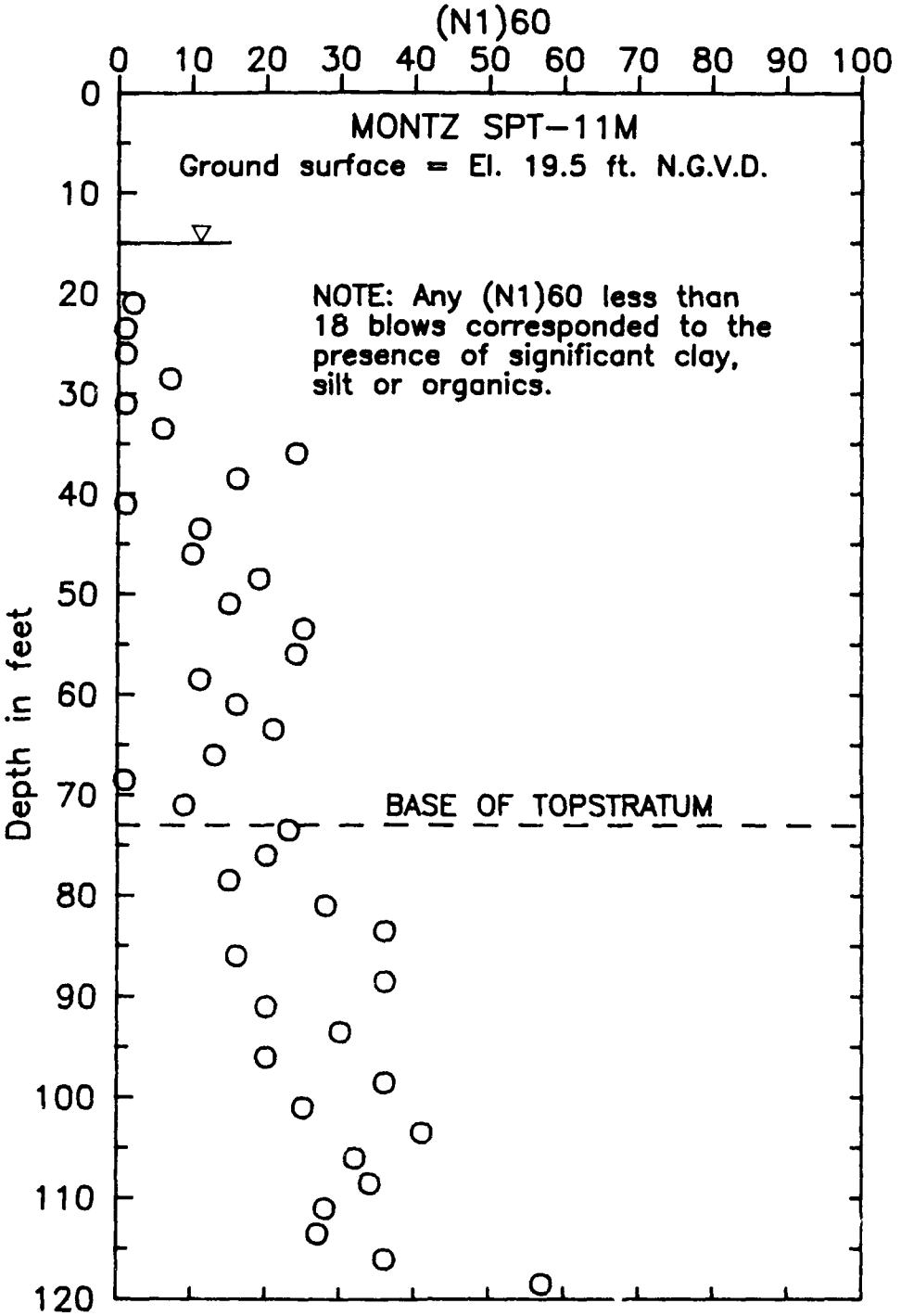
APPENDIX B

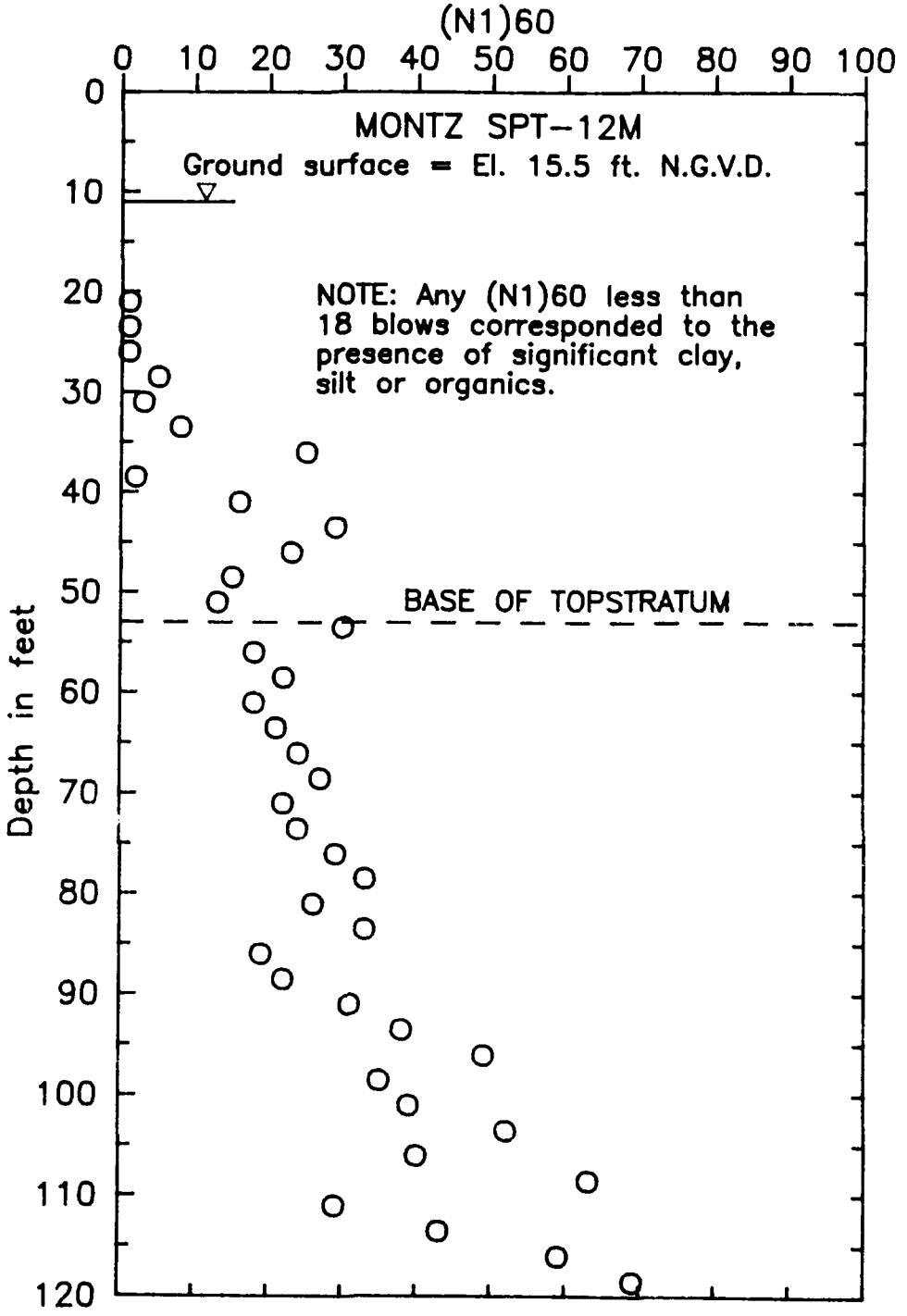
SPT AND GRADATION DATA, MONTZ RECONNAISSANCE BORINGS

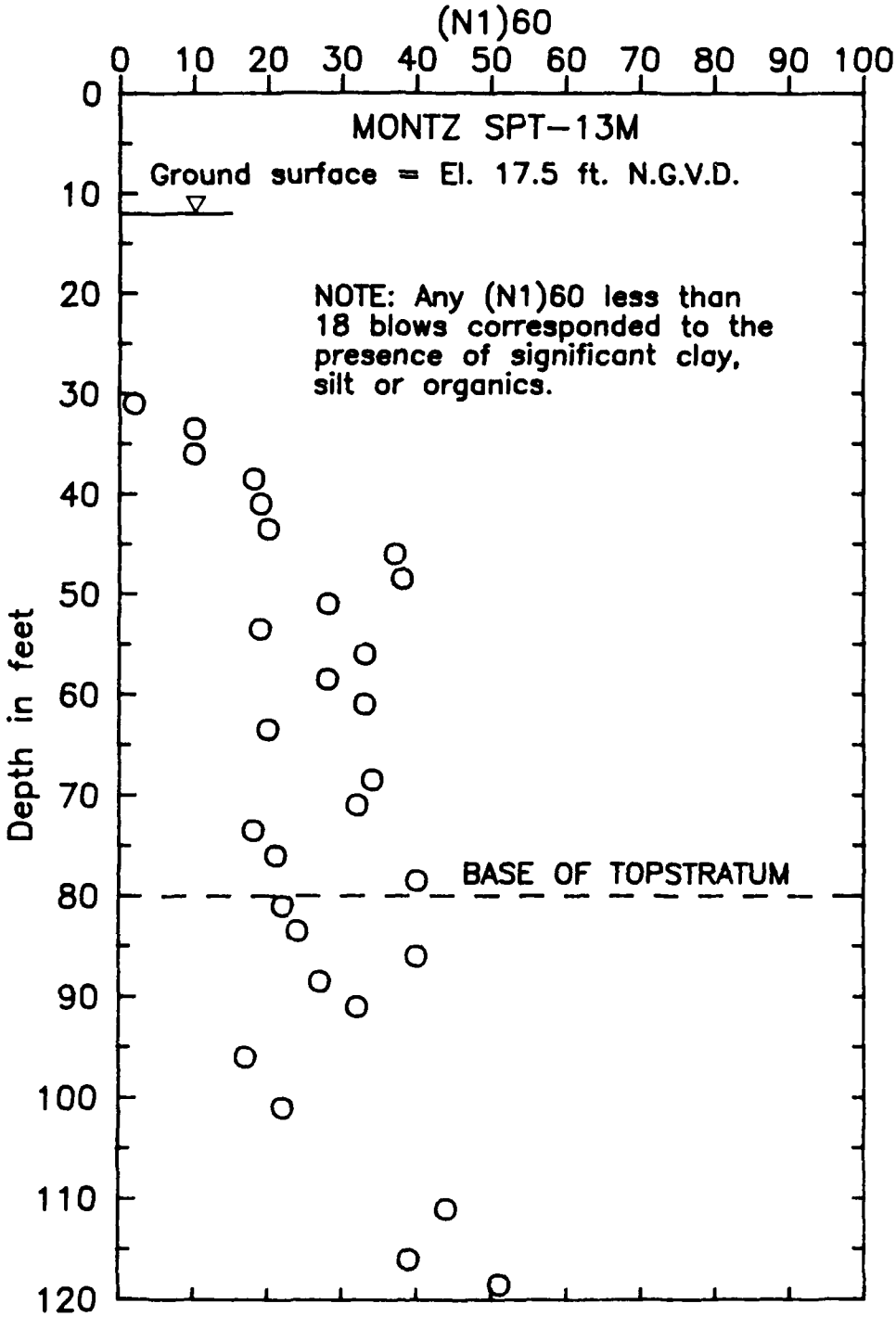

N1(60)
0 10 20 30 40 50 60 70 80 90 100
MONTZ SPT-1M
Ground surface = El. 16.5 ft. N.G.V.D.
Depth in feet
0 10 20 30 40 50 60 70 80 90 100 110 120
NO SIGNIFICANT SAND
ENCOUNTERED

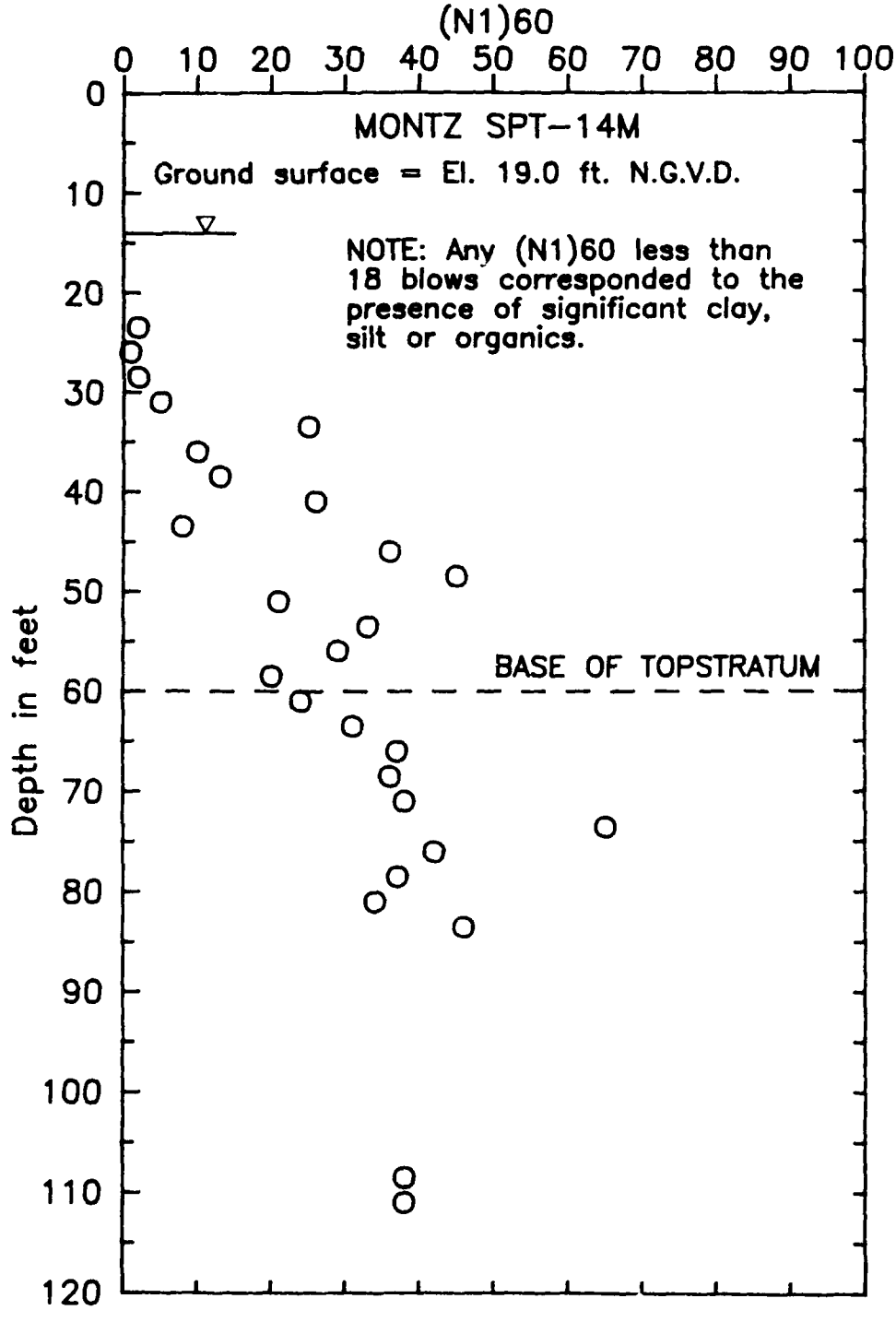

N1(60)
0 10 20 30 40 50 60 70 80 90 100
MONTZ SPT-8M
Ground surface = El. 19.5 ft. N.G.V.D.
Depth in feet
0 10 20 30 40 50 60 70 80 90 100 110 120
NO SIGNIFICANT SAND
ENCOUNTERED

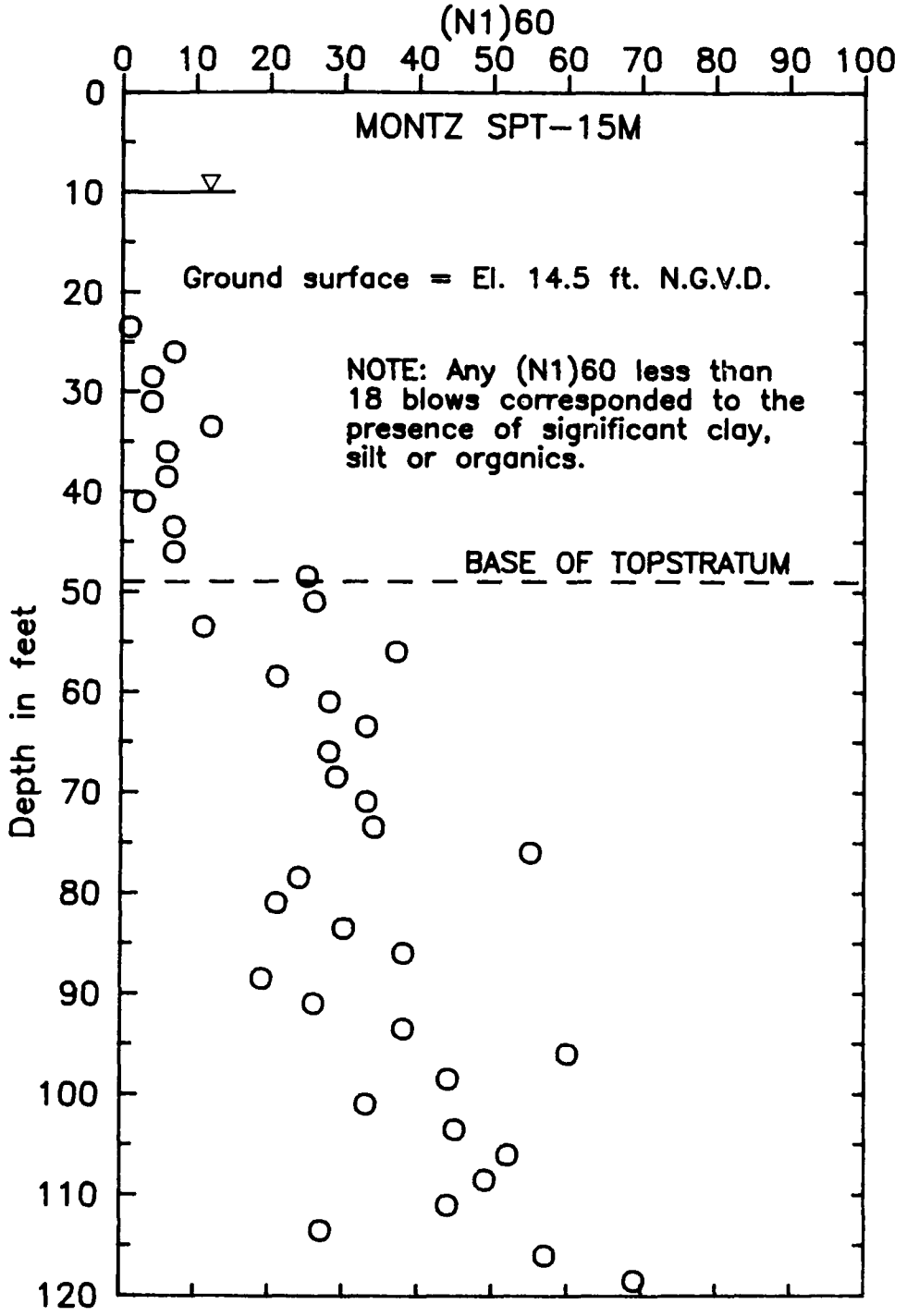

(N1)60
0 10 20 30 40 50 60 70 80 90 100
MONTZ SPT-10M
Ground surface = El. 16.5 ft. N.G.V.D.
NOTE: Any (N1)60 less than 18 blows corresponded to the presence of significant clay, silt or organics.
Depth in feet
0 10 20 30 40 50 60 70 80 90 100 110 120
BASE OF TOPSTRATUM

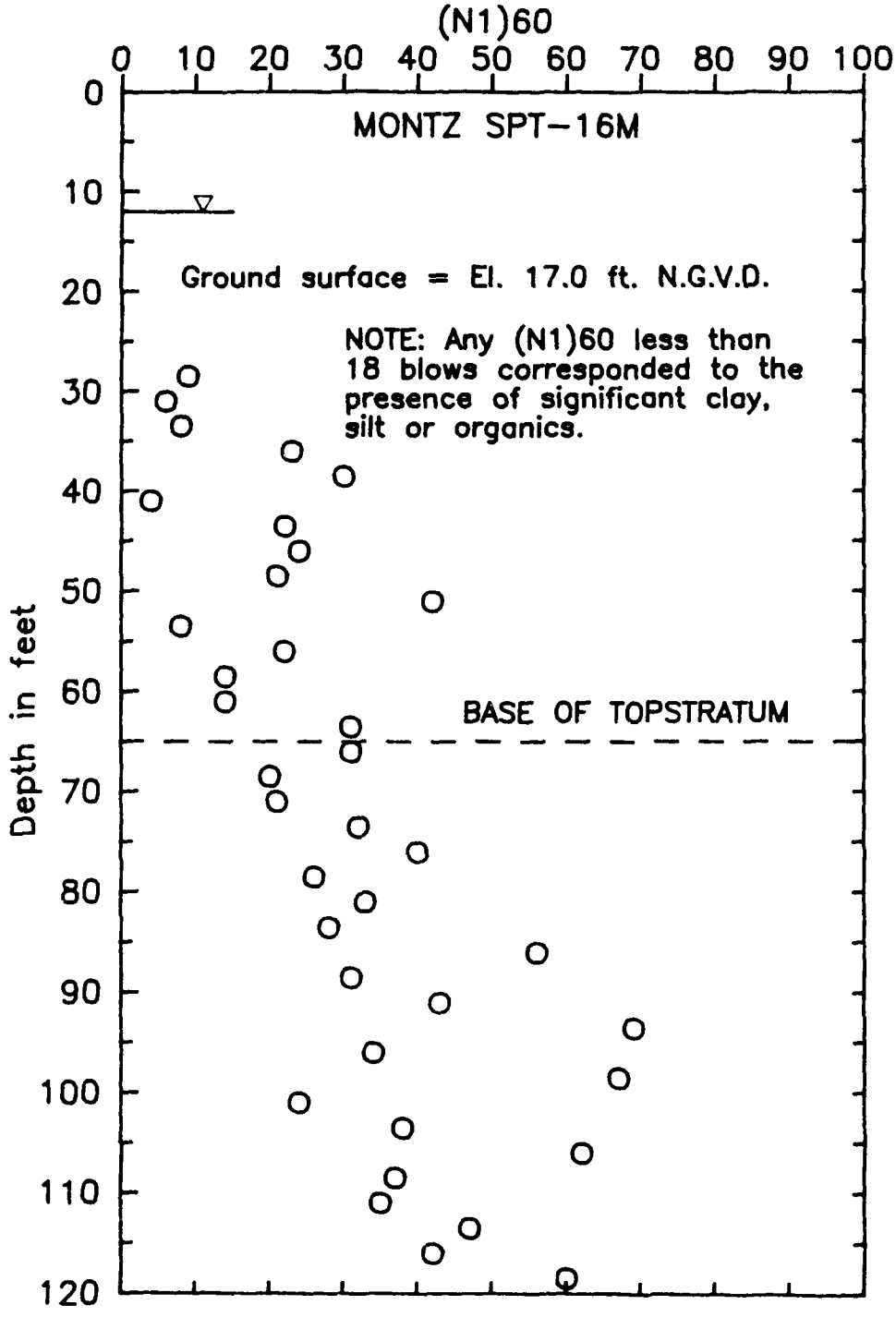

(N1)60
0 10 20 30 40 50 60 70 80 90 100
MONTZ SPT-11M
Ground surface = El. 19.5 ft. N.G.V.D.
NOTE: Any (N1)60 less than 18 blows corresponded to the presence of significant clay, silt or organics.
BASE OF TOPSTRATUM
Depth in feet
0 10 20 30 40 50 60 70 80 90 100 110 120

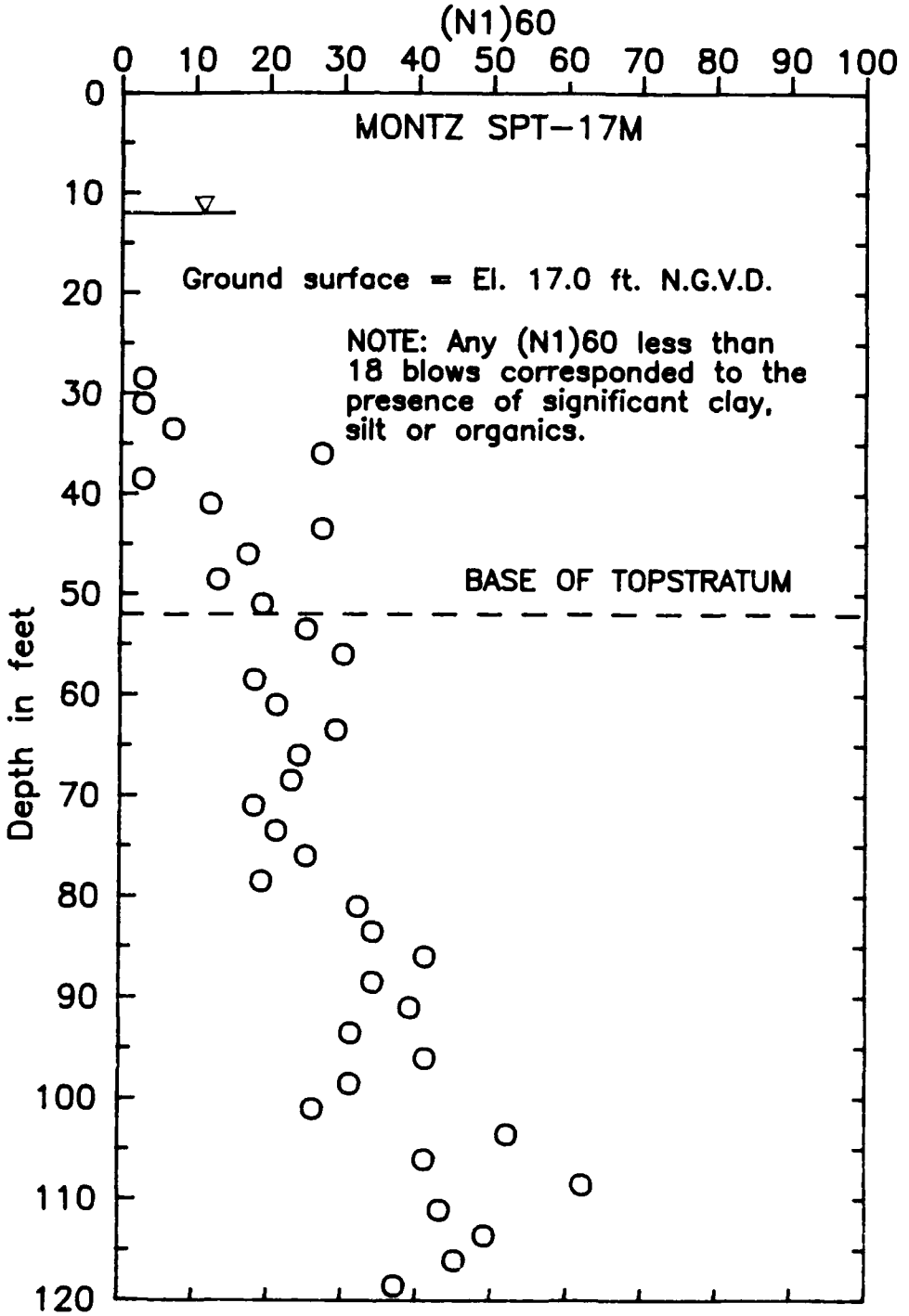

(N1)60
0 10 20 30 40 50 60 70 80 90 100
MONTZ SPT-12M
Ground surface = El. 15.5 ft. N.G.V.D.
NOTE: Any (N1)60 less than 18 blows corresponded to the presence of significant clay, silt or organics.
BASE OF TOPSTRATUM
Depth in feet
0 10 20 30 40 50 60 70 80 90 100 110 120

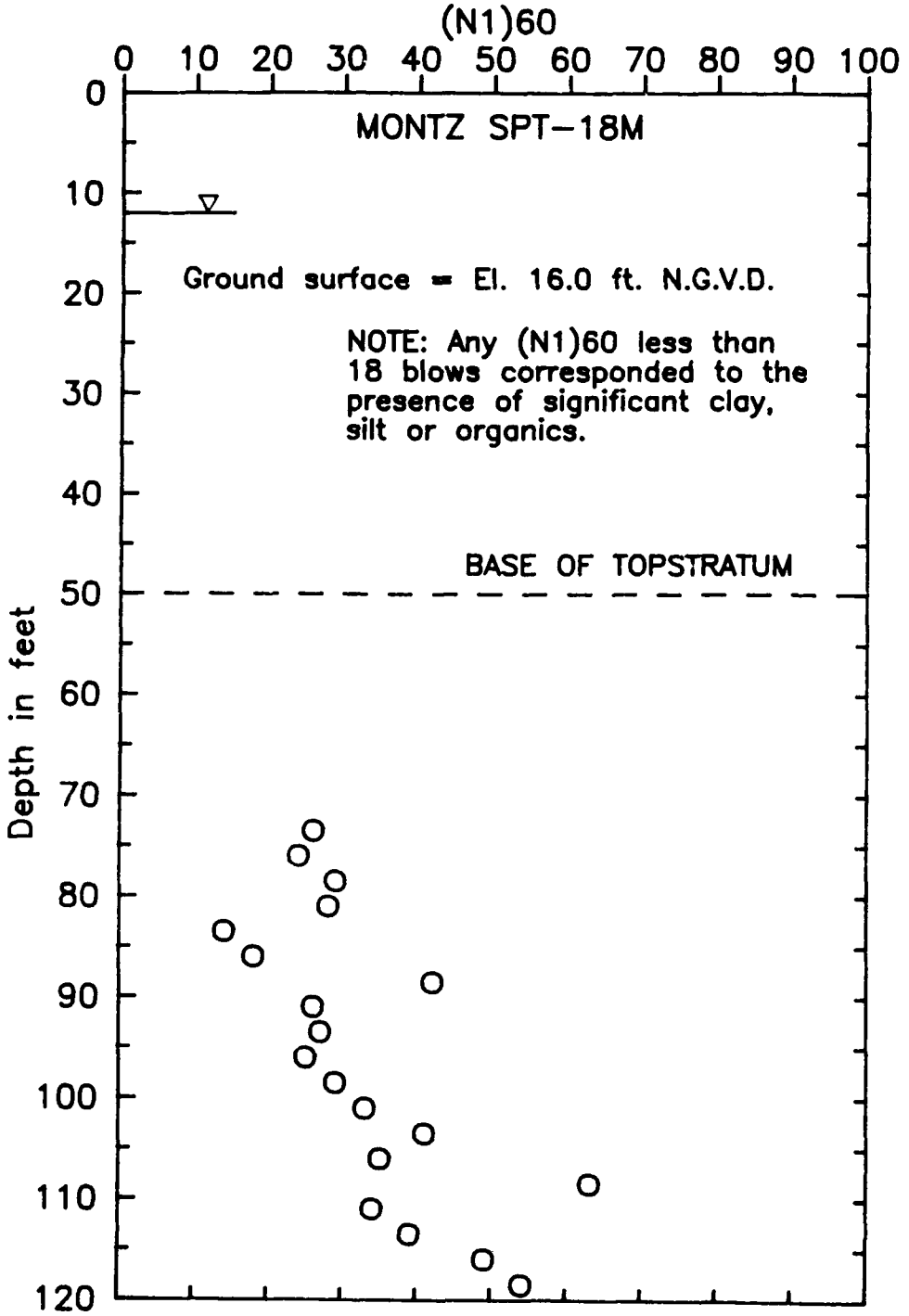

(N1)60
0 10 20 30 40 50 60 70 80 90 100
MONTZ SPT–13M
Ground surface = El. 17.5 ft. N.G.V.D.
NOTE: Any (N1)60 less than 18 blows corresponded to the presence of significant clay, silt or organics.
Depth in feet
0 10 20 30 40 50 60 70 80 90 100 110 120
BASE OF TOPSTRATUM

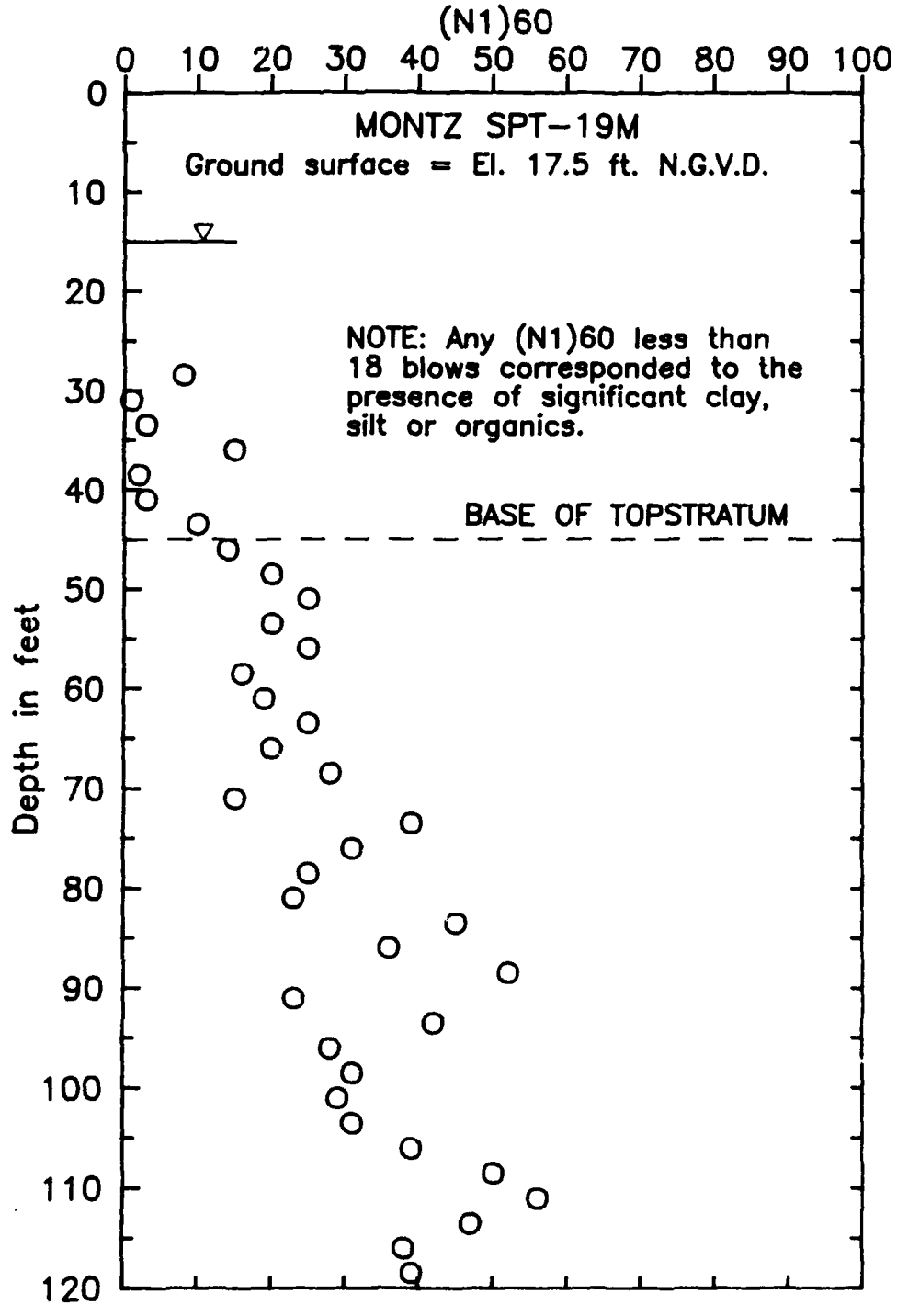

(N1)60
0 10 20 30 40 50 60 70 80 90 100
MONTZ SPT-14M
Ground surface = El. 19.0 ft. N.G.V.D.
NOTE: Any (N1)60 less than 18 blows corresponded to the presence of significant clay, silt or organics.
BASE OF TOPSTRATUM
Depth in feet
0 10 20 30 40 50 60 70 80 90 100 110 120

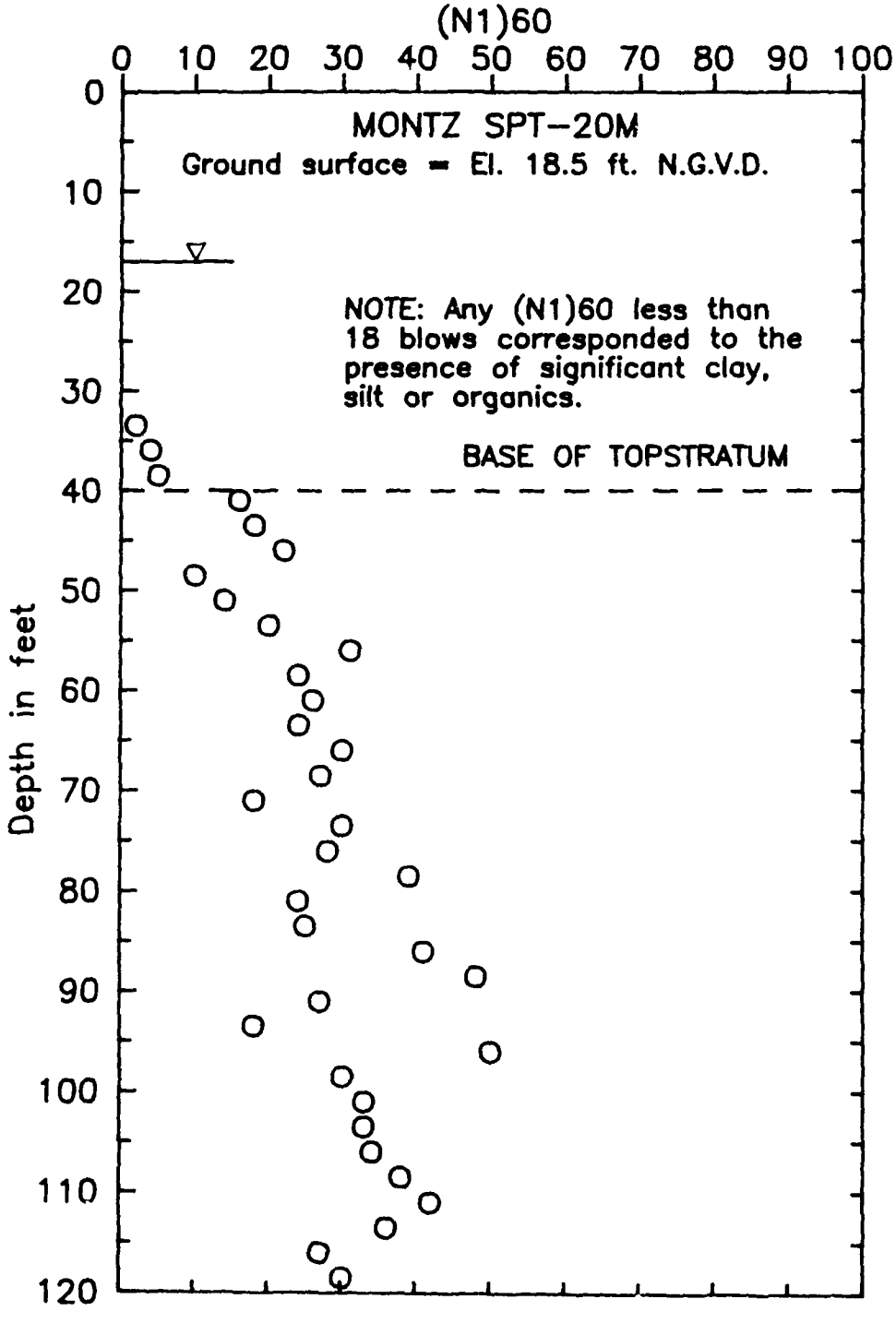

(N1)60
0 10 20 30 40 50 60 70 80 90 100
MONTZ SPT-15M
Ground surface = El. 14.5 ft. N.G.V.D.
NOTE: Any (N1)60 less than 18 blows corresponded to the presence of significant clay, silt or organics.
BASE OF TOPSTRATUM
Depth in feet
0 10 20 30 40 50 60 70 80 90 100 110 120

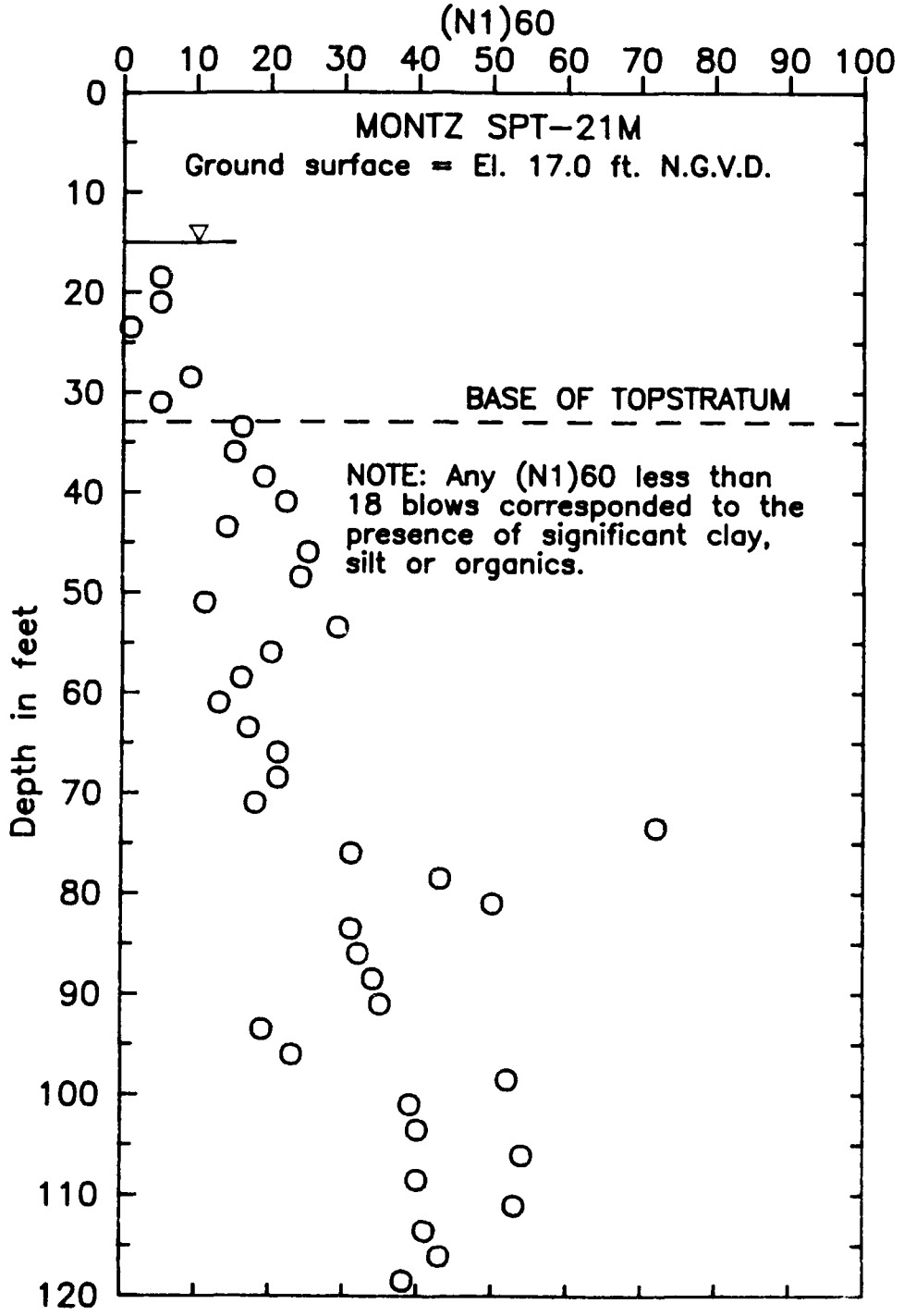

(N1)60
0 10 20 30 40 50 60 70 80 90 100
MONTZ SPT-16M
Ground surface = El. 17.0 ft. N.G.V.D.
NOTE: Any (N1)60 less than 18 blows corresponded to the presence of significant clay, silt or organics.
BASE OF TOPSTRATUM
Depth in feet
0 10 20 30 40 50 60 70 80 90 100 110 120

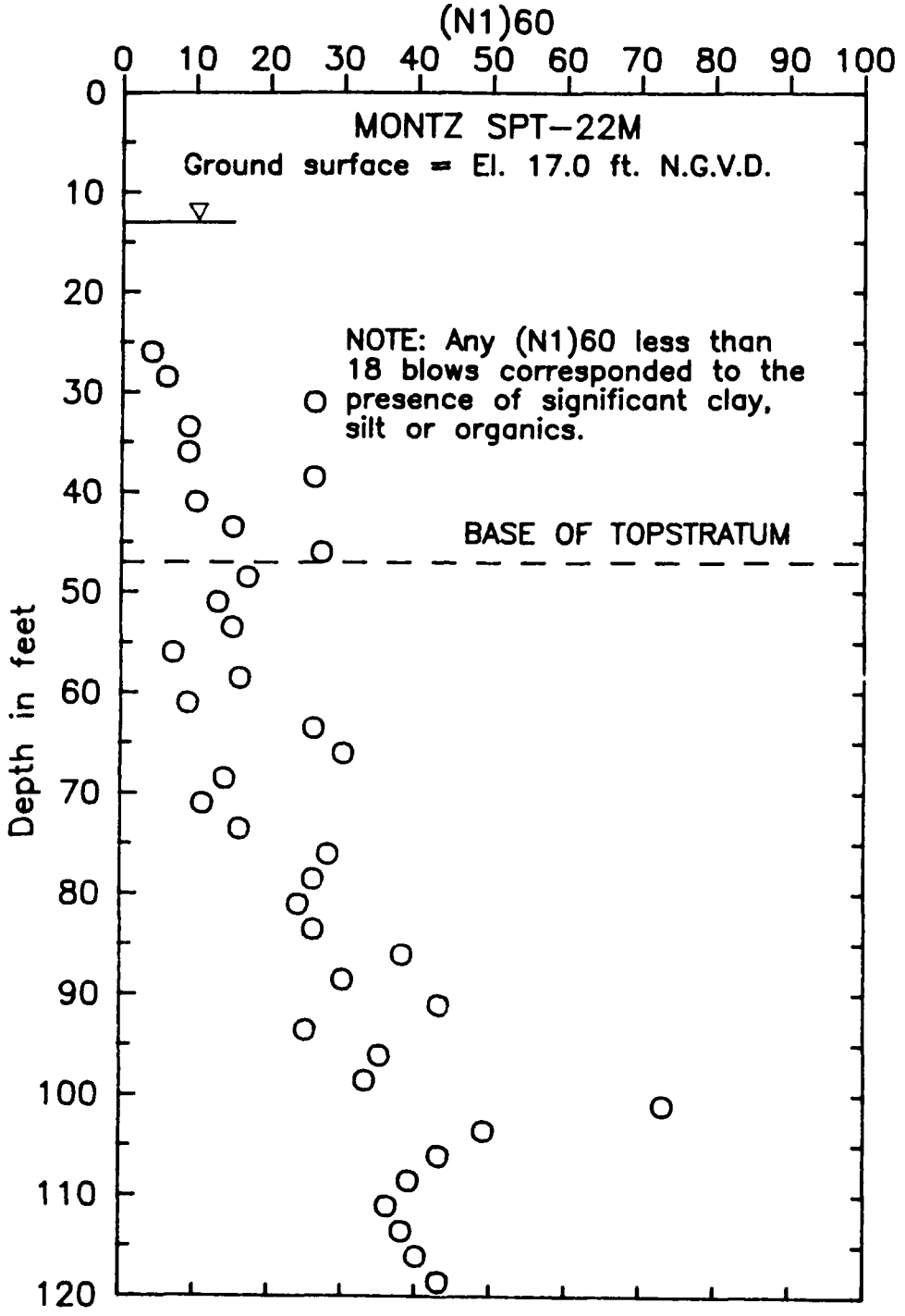

(N1)60
0 10 20 30 40 50 60 70 80 90 100
MONTZ SPT-17M
Ground surface = El. 17.0 ft. N.G.V.D.
NOTE: Any (N1)60 less than 18 blows corresponded to the presence of significant clay, silt or organics.
BASE OF TOPSTRATUM
Depth in feet
0 10 20 30 40 50 60 70 80 90 100 110 120

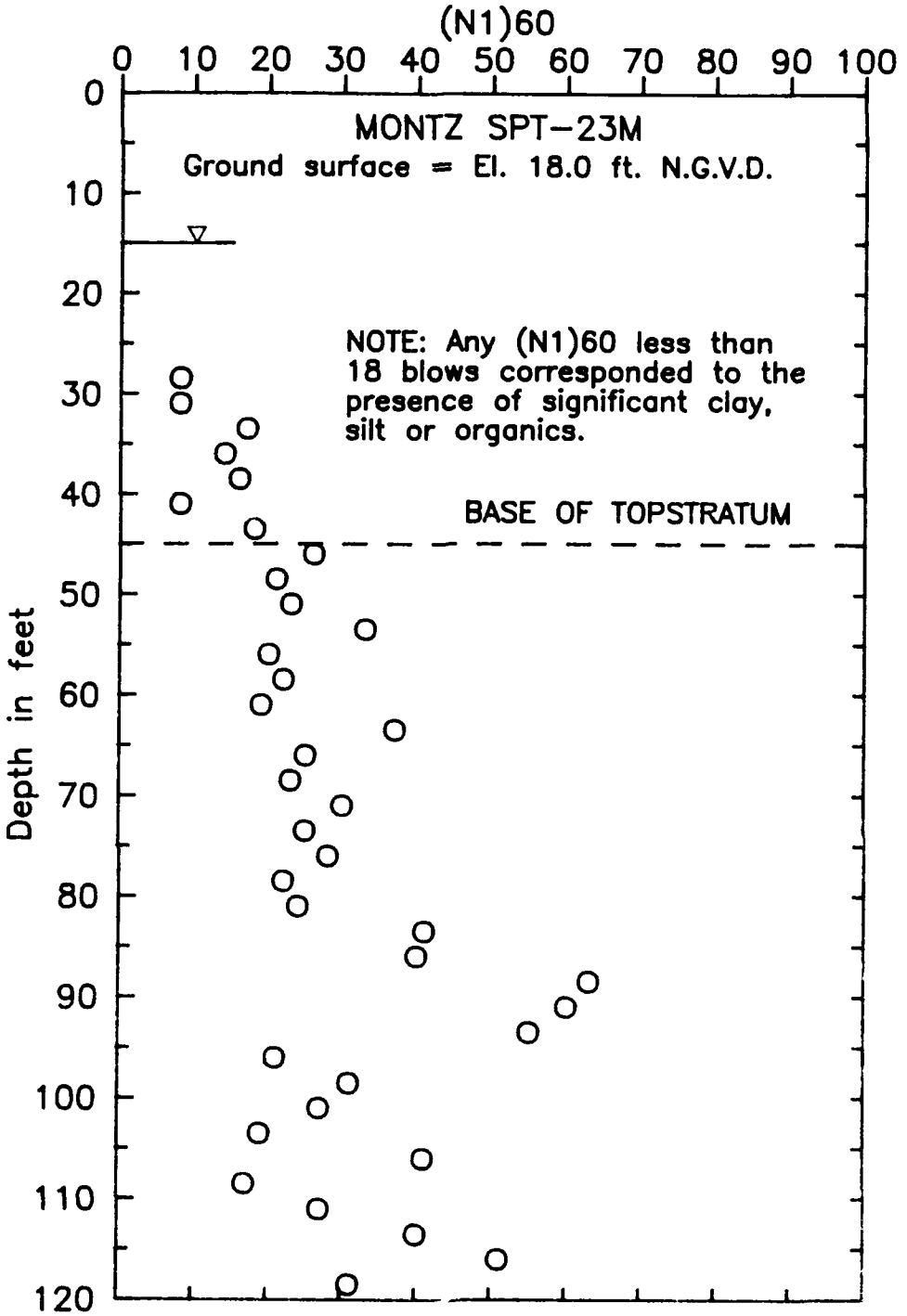

(N1)60
0 10 20 30 40 50 60 70 80 90 100
MONTZ SPT–18M
Ground surface = El. 16.0 ft. N.G.V.D.
NOTE: Any (N1)60 less than 18 blows corresponded to the presence of significant clay, silt or organics.
BASE OF TOPSTRATUM
Depth in feet
0 10 20 30 40 50 60 70 80 90 100 110 120

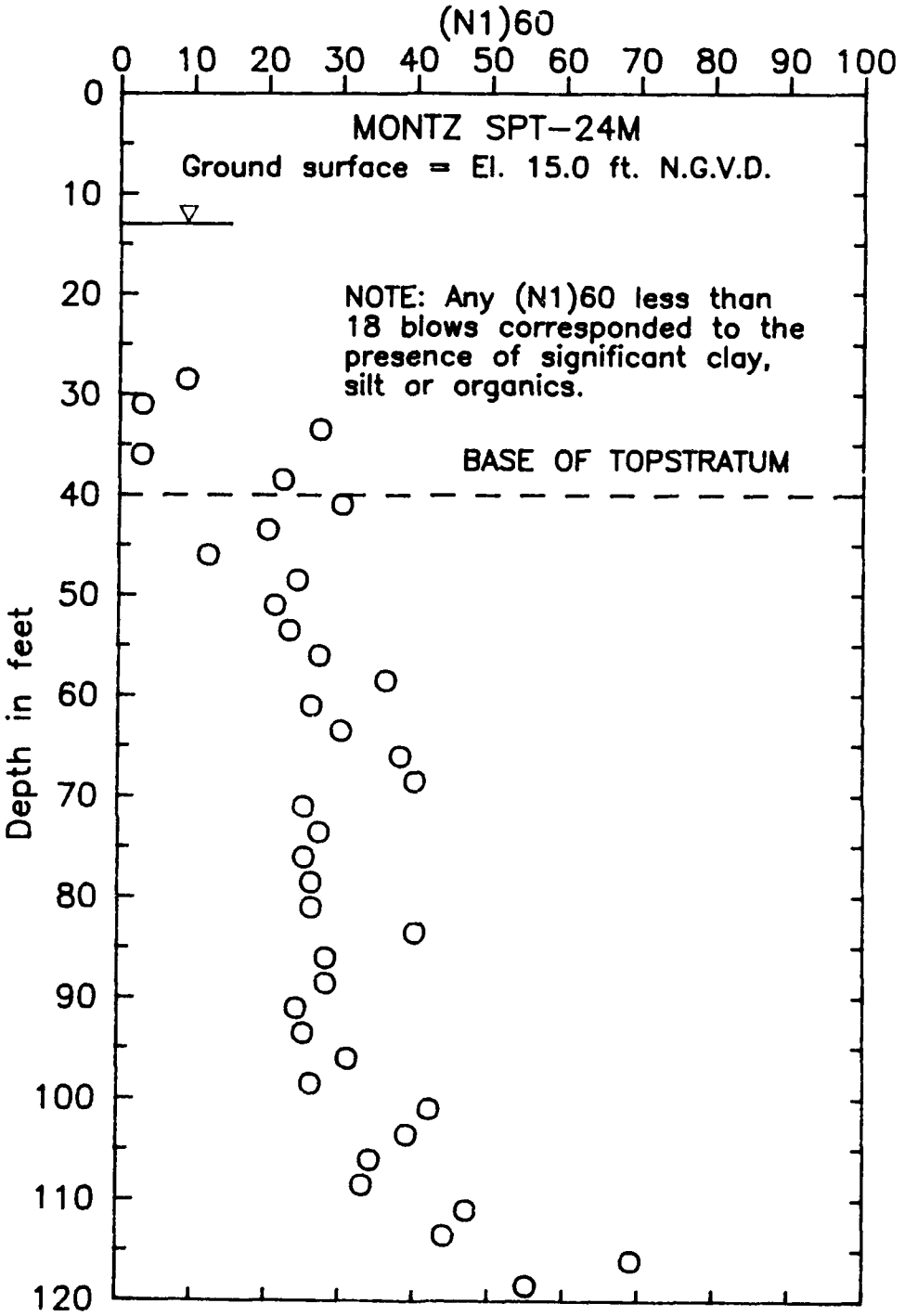

(N1)60
0 10 20 30 40 50 60 70 80 90 100
MONTZ SPT-19M
Ground surface = El. 17.5 ft. N.G.V.D.
NOTE: Any (N1)60 less than 18 blows corresponded to the presence of significant clay, silt or organics.
BASE OF TOPSTRATUM
Depth in feet
0 10 20 30 40 50 60 70 80 90 100 110 120

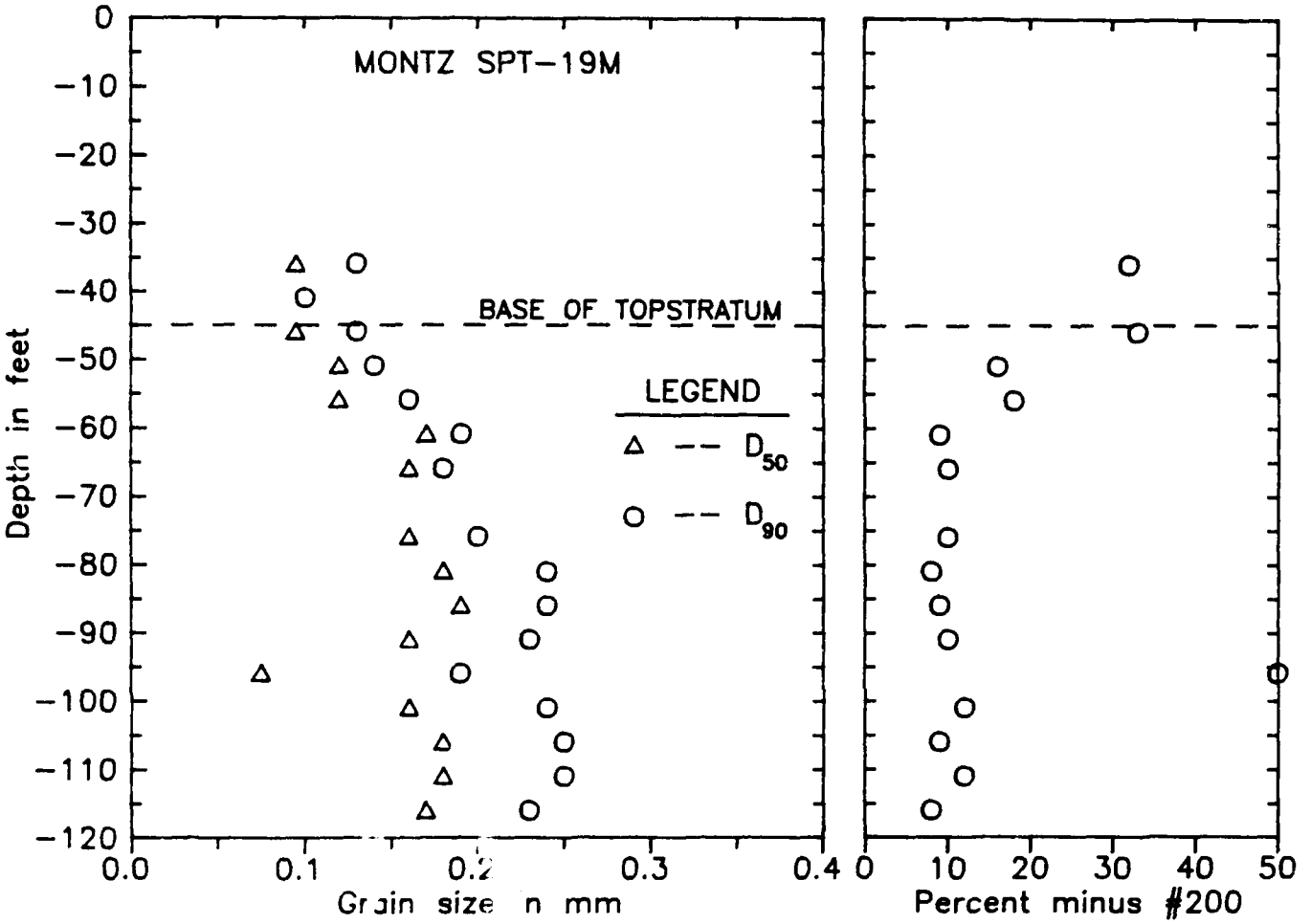

(N1)60
0 10 20 30 40 50 60 70 80 90 100
MONTZ SPT–20M
Ground surface = El. 18.5 ft. N.G.V.D.
NOTE: Any (N1)60 less than 18 blows corresponded to the presence of significant clay, silt or organics.
BASE OF TOPSTRATUM
Depth in feet
0 10 20 30 40 50 60 70 80 90 100 110 120

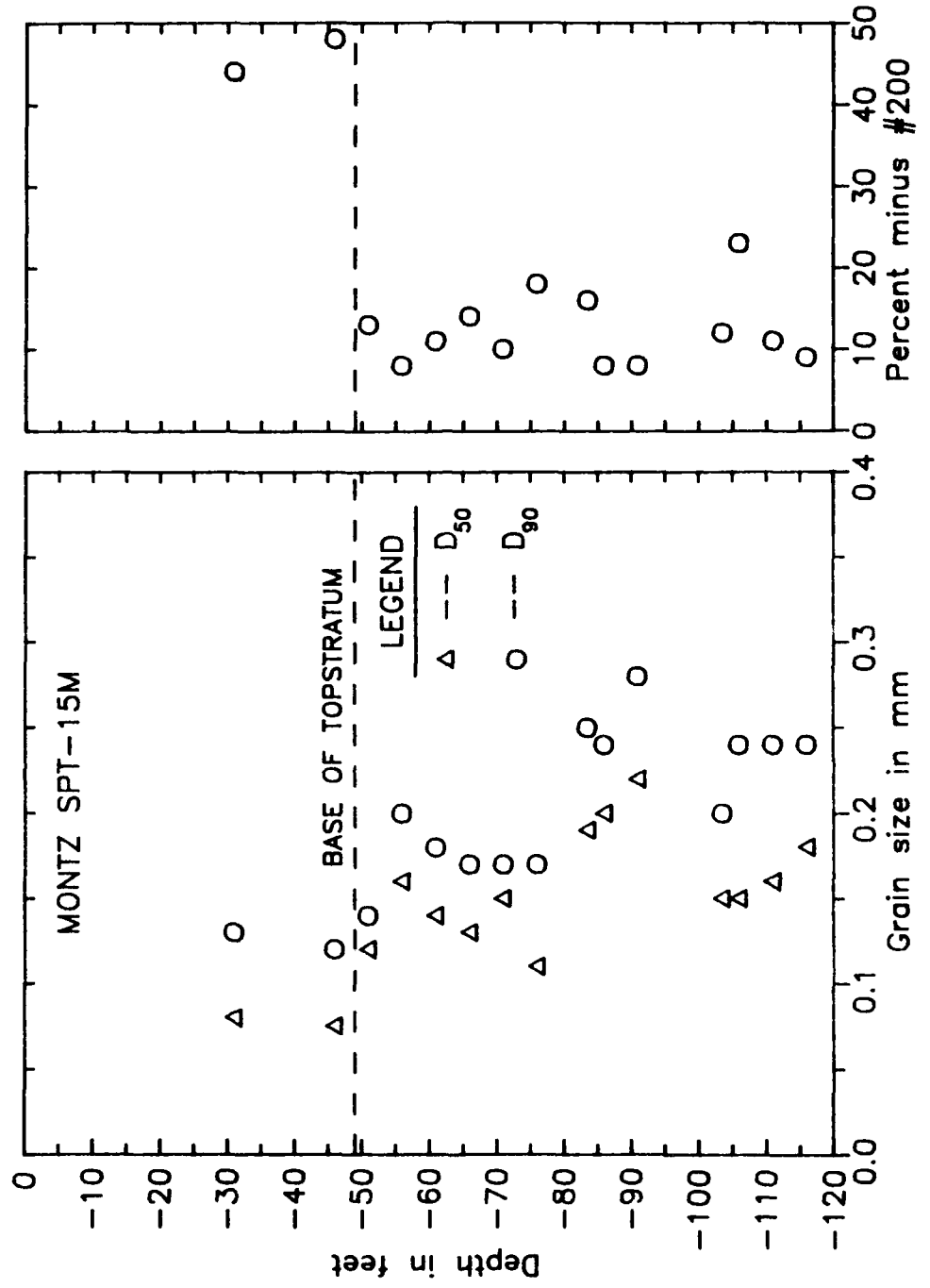

(N1)60
0 10 20 30 40 50 60 70 80 90 100
MONTZ SPT-21M
Ground surface = El. 17.0 ft. N.G.V.D.
BASE OF TOPSTRATUM
NOTE: Any (N1)60 less than 18 blows corresponded to the presence of significant clay, silt or organics.
Depth in feet
0 10 20 30 40 50 60 70 80 90 100 110 120

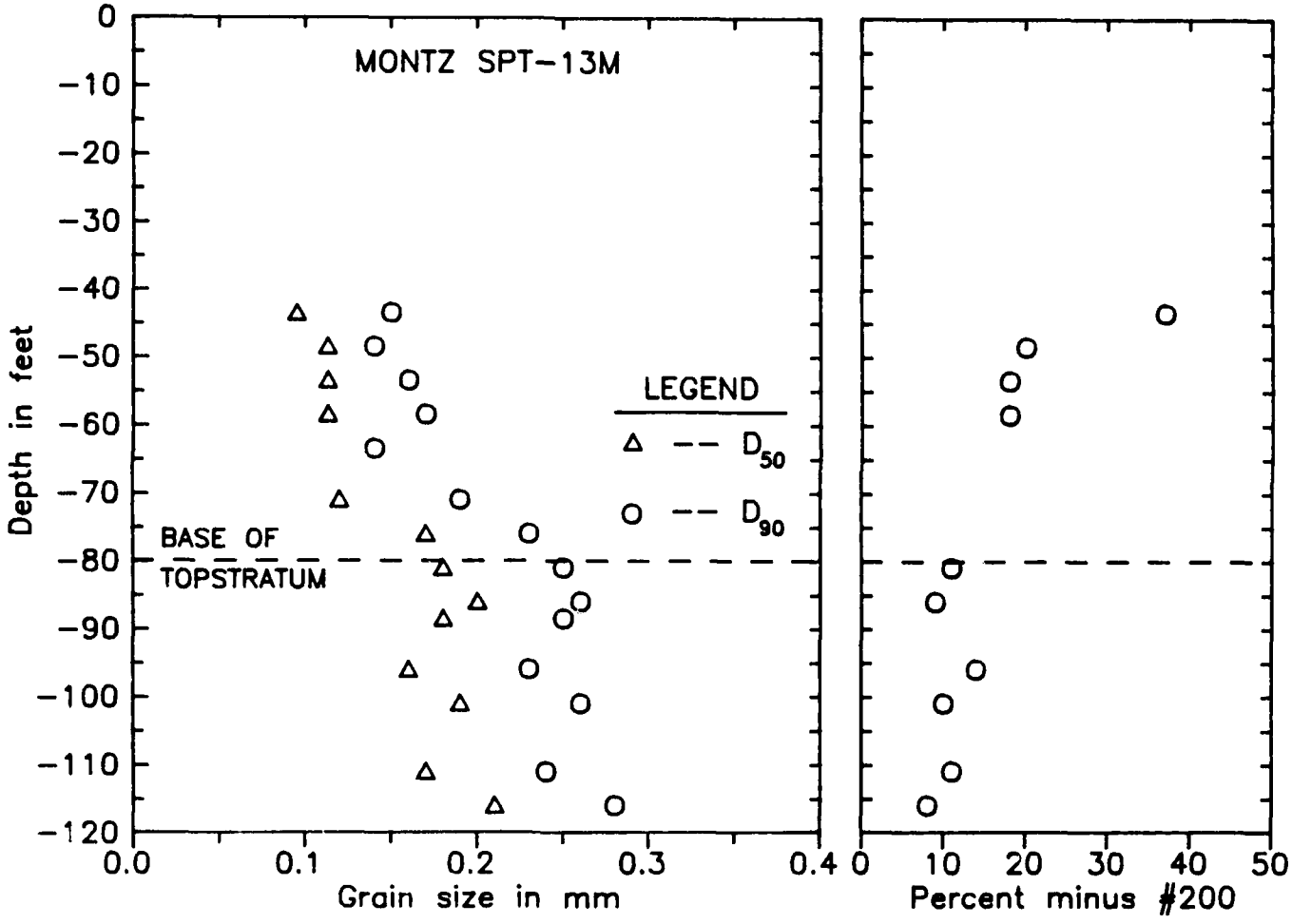

(N1)60
0 10 20 30 40 50 60 70 80 90 100
MONTZ SPT–22M
Ground surface = El. 17.0 ft. N.G.V.D.
NOTE: Any (N1)60 less than 18 blows corresponded to the presence of significant clay, silt or organics.
BASE OF TOPSTRATUM
Depth in feet
0 10 20 30 40 50 60 70 80 90 100 110 120

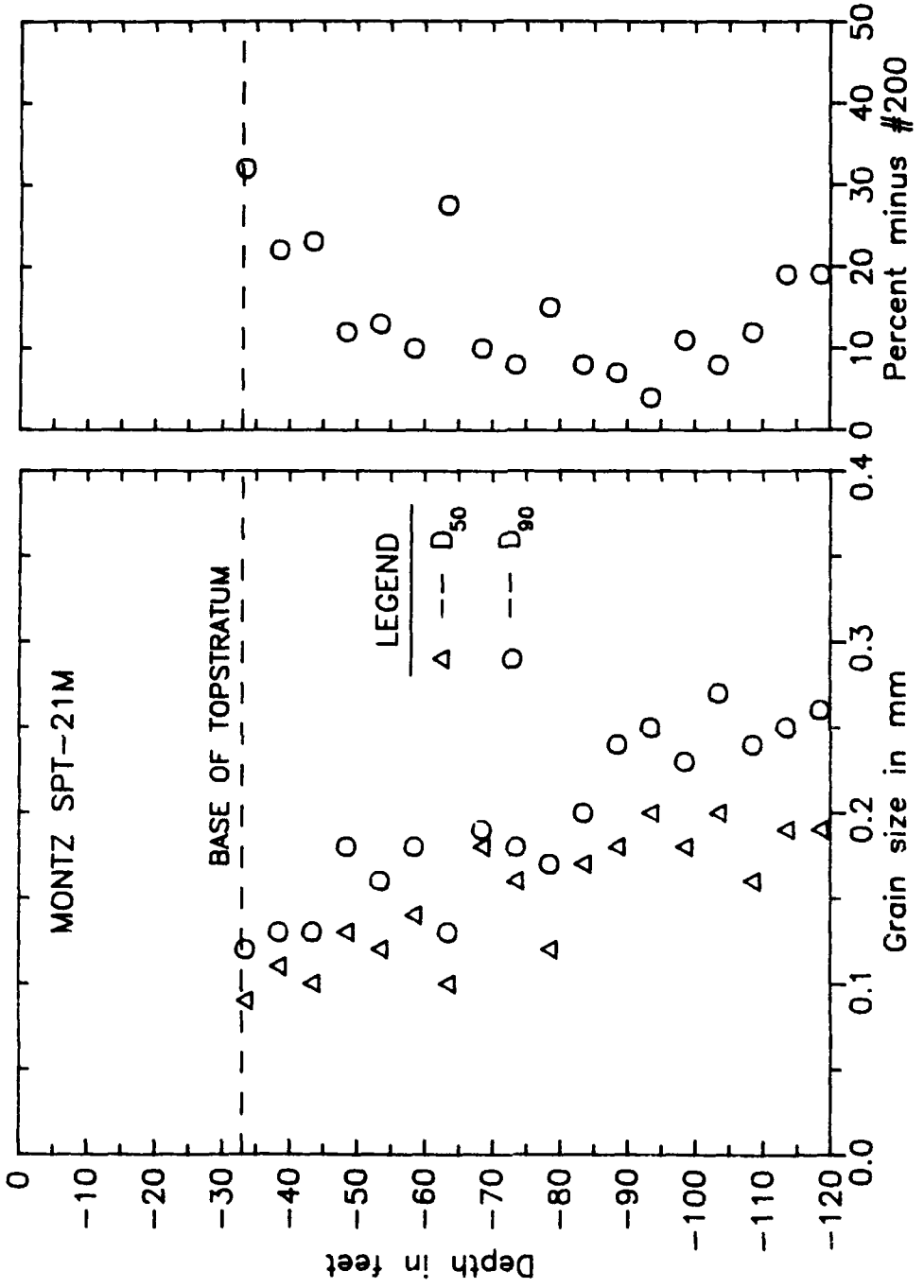

(N1)60
0 10 20 30 40 50 60 70 80 90 100
MONTZ SPT-23M
Ground surface = El. 18.0 ft. N.G.V.D.
NOTE: Any (N1)60 less than 18 blows corresponded to the presence of significant clay, silt or organics.
BASE OF TOPSTRATUM
Depth in feet
0 10 20 30 40 50 60 70 80 90 100 110 120

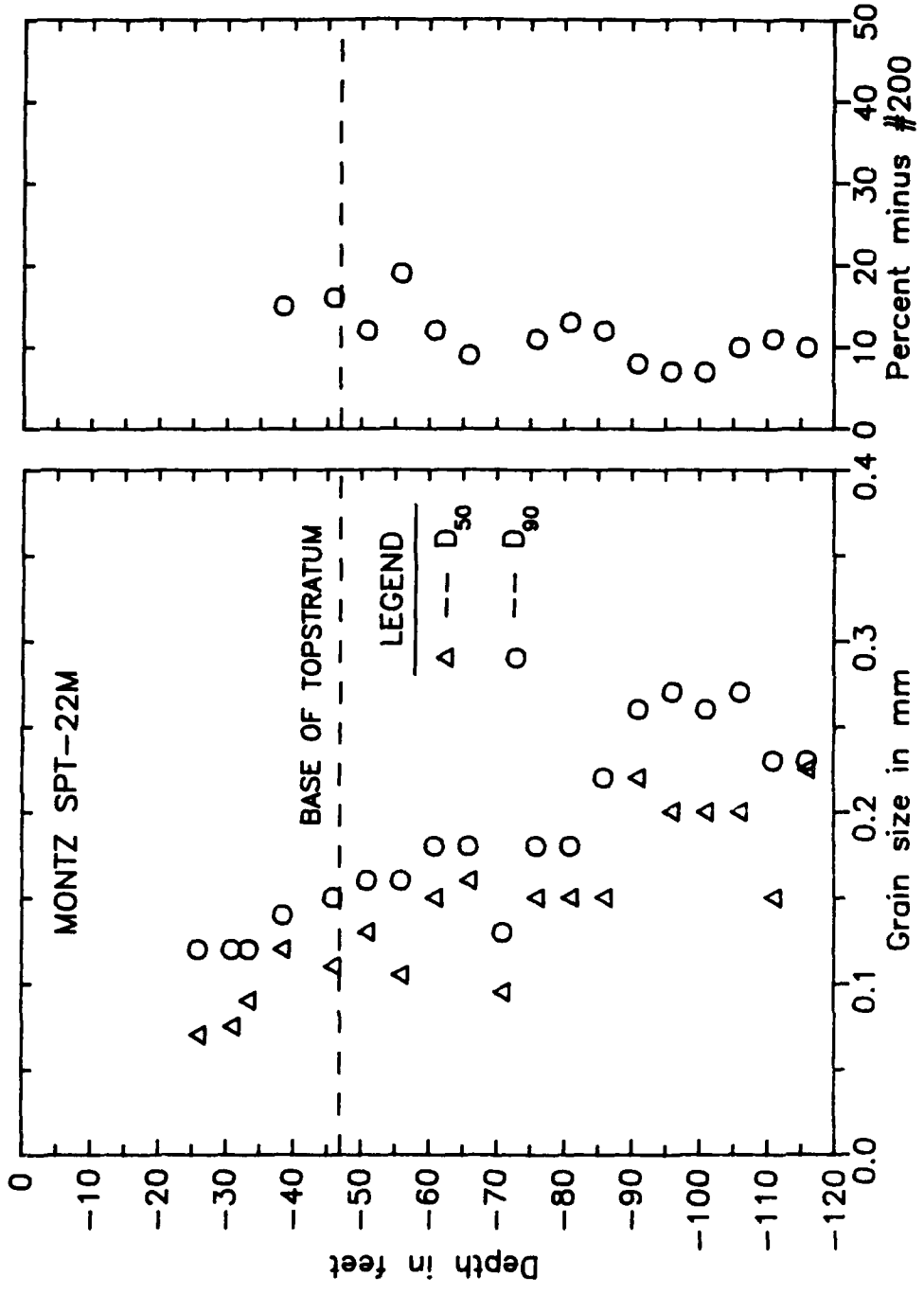

(N1)60
0 10 20 30 40 50 60 70 80 90 100
MONTZ SPT-24M
Ground surface = El. 15.0 ft. N.G.V.D.
NOTE: Any (N1)60 less than 18 blows corresponded to the presence of significant clay, silt or organics.
BASE OF TOPSTRATUM
Depth in feet
0 10 20 30 40 50 60 70 80 90 100 110 120


MONTZ SPT-19M
BASE OF TOPSTRATUM
LEGEND
Δ -- D50
O -- D90
Depth in feet
0
-10
-20
-30
-40
-50
-60
-70
-80
-90
-100
-110
-120
0.0
0.1
0.2
0.3
0.4
Grain size in mm
0
10
20
30
40
50
Percent minus #200


MONTZ SPT-15M
BASE OF TOPSTRATUM
LEGEND
D_{50}
D_{90}
Depth in feet
Grain size in mm
Percent minus #200
0
-10
-20
-30
-40
-50
-60
-70
-80
-90
-100
-110
-120
0.0
0.1
0.2
0.3
0.4
0
10
20
30
40
50

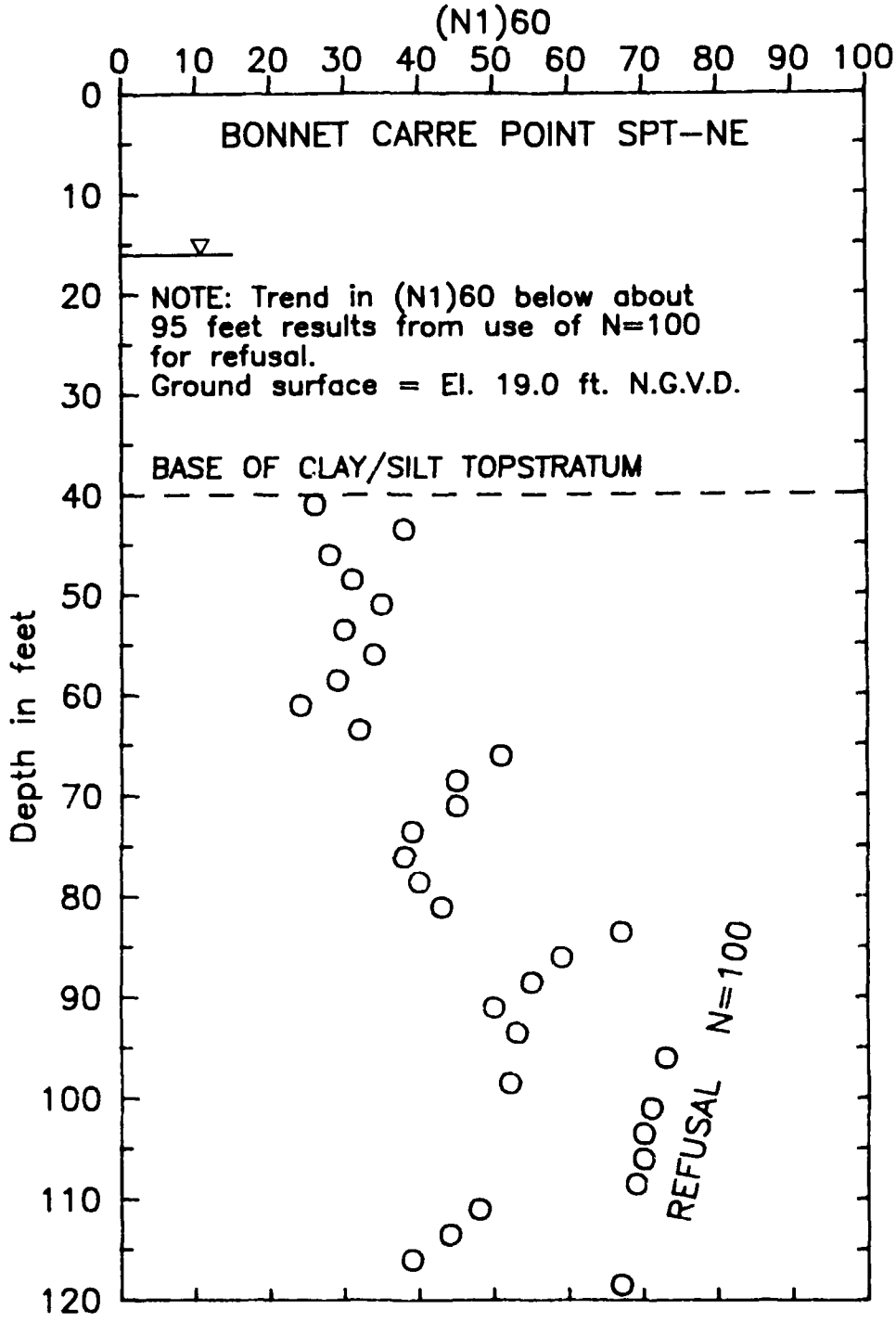

MONTZ SPT-13M
LEGEND
D_{50}
D_{90}
BASE OF TOPSTRATUM
Depth in feet
0
-10
-20
-30
-40
-50
-60
-70
-80
-90
-100
-110
-120
0.0
0.1
0.2
0.3
0.4
Grain size in mm
0
10
20
30
40
50
Percent minus #200

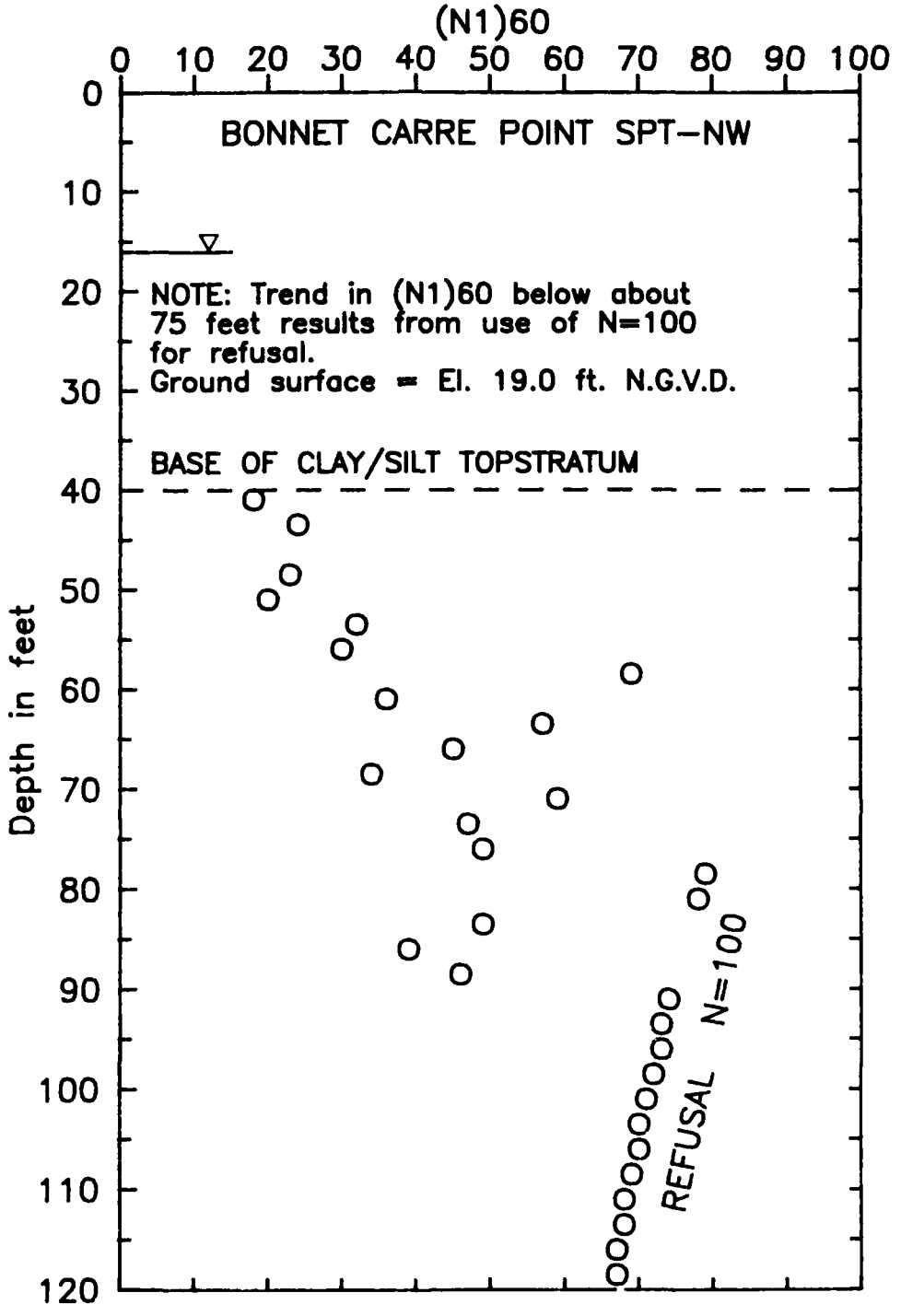

MONTZ SPT-21M
BASE OF TOPSTRATUM
LEGEND
D_{50}
D_{90}
Depth in feet
0
-10
-20
-30
-40
-50
-60
-70
-80
-90
-100
-110
-120
0.0
0.1
0.2
0.3
0.4
Grain size in mm
0
10
20
30
40
50
Percent minus #200

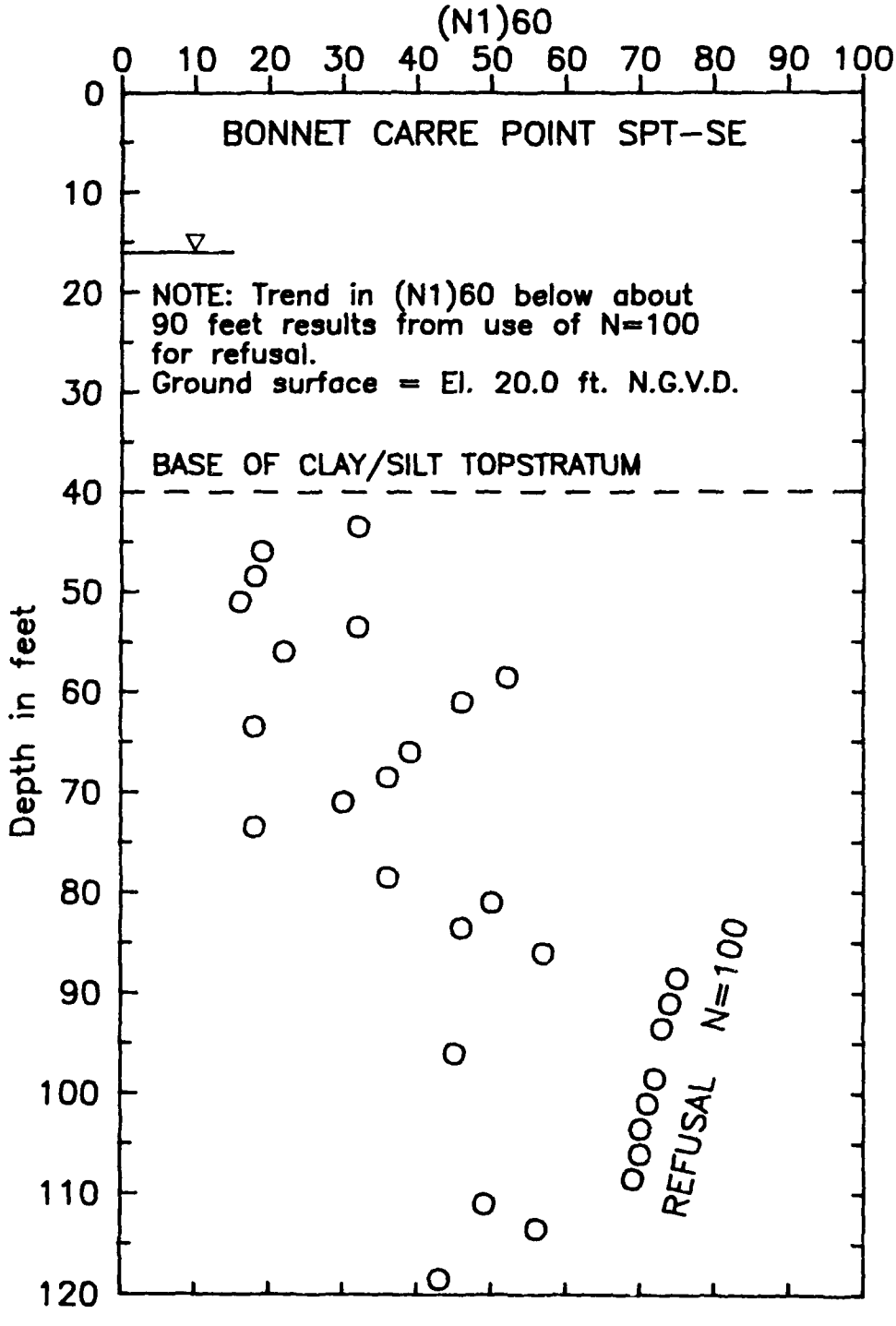

MONTZ SPT-22M
BASE OF TOPSTRATUM
LEGEND
D_{50}
D_{90}
Depth in feet
0
-10
-20
-30
-40
-50
-60
-70
-80
-90
-100
-110
-120
0.0
0.1
0.2
0.3
0.4
Grain size in mm
0
10
20
30
40
50
Percent minus #200

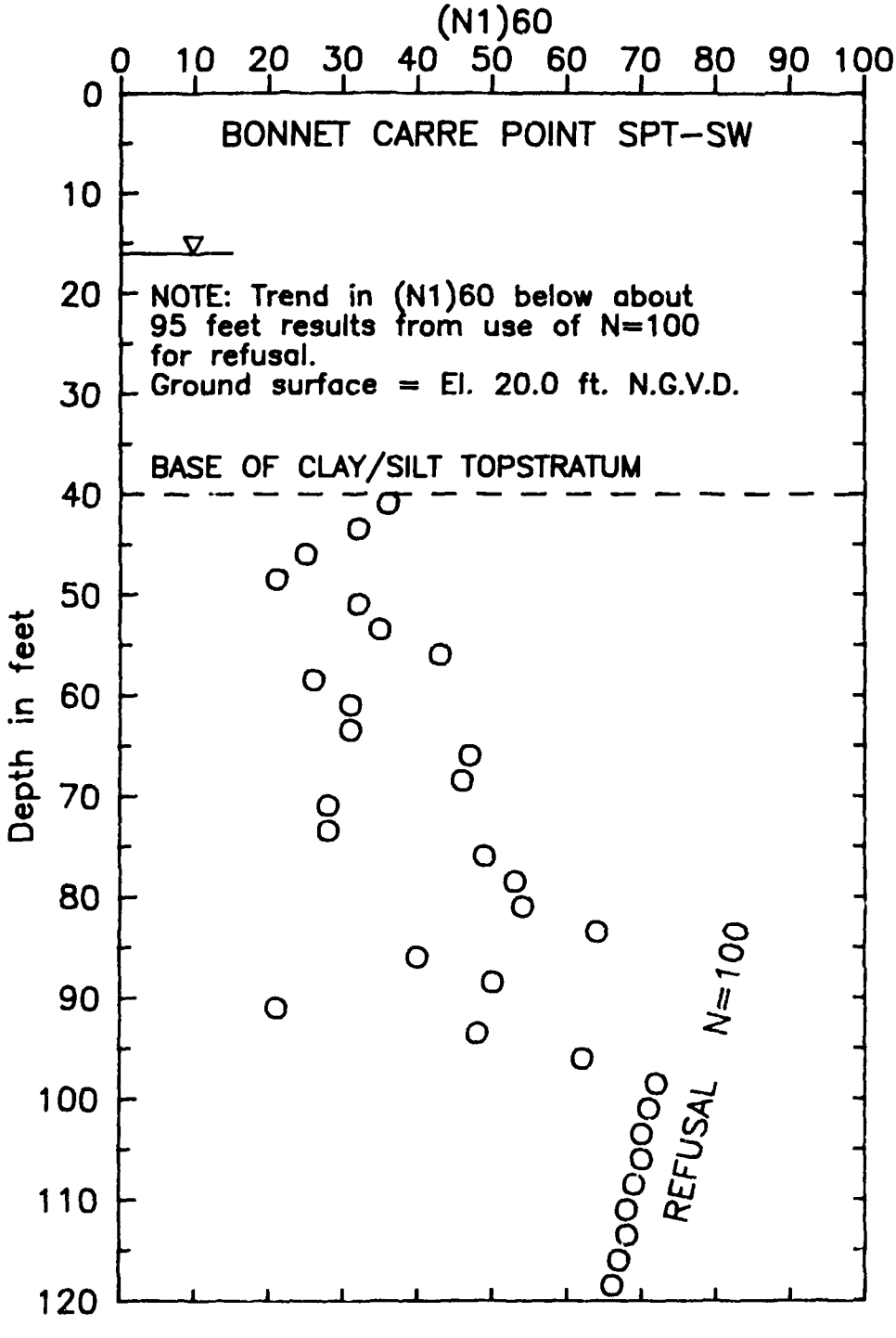
APPENDIX C

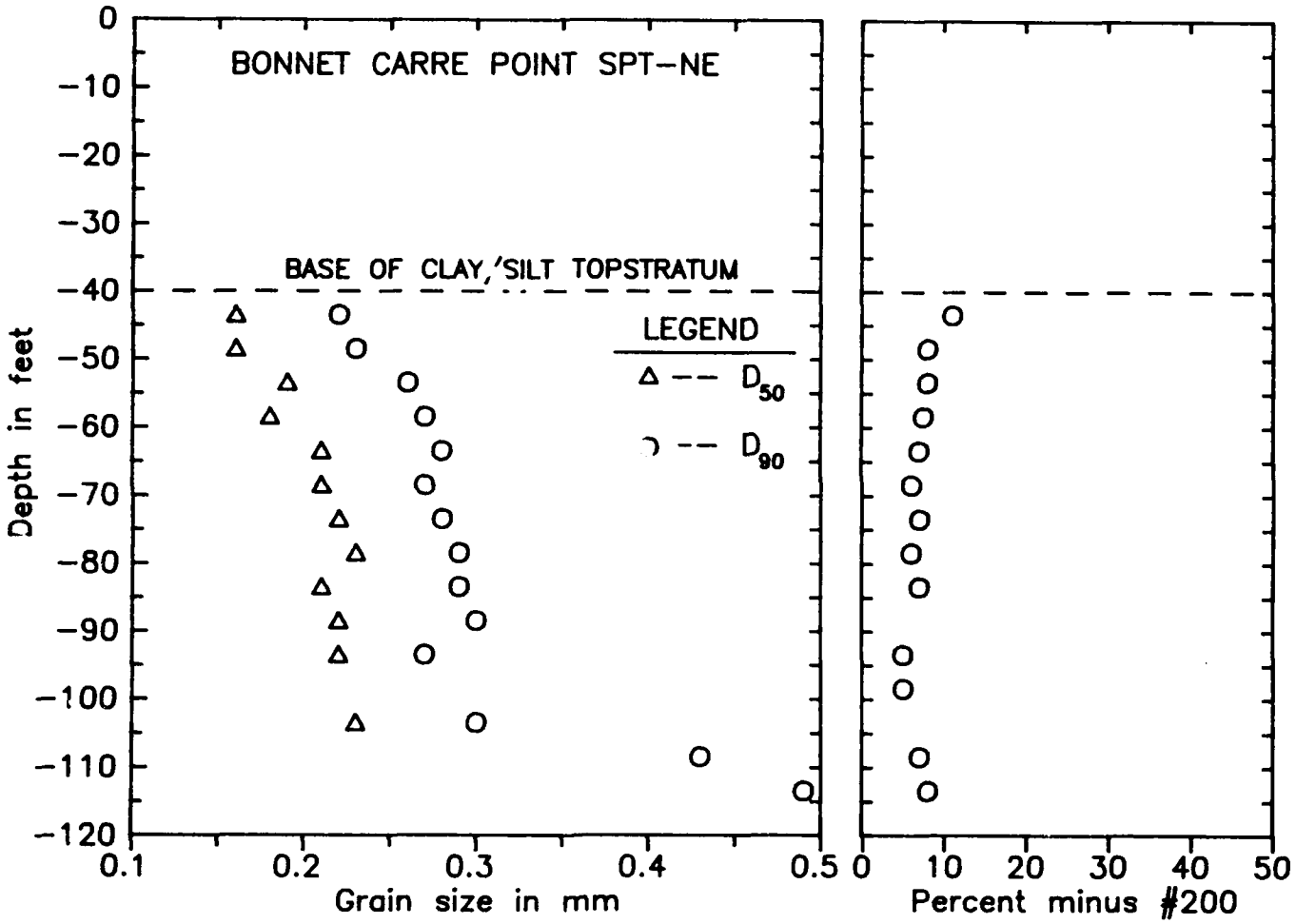
SPT AND GRADATION DATA, BONNETT CARRE POINT RECONNAISSANCE BORINGS

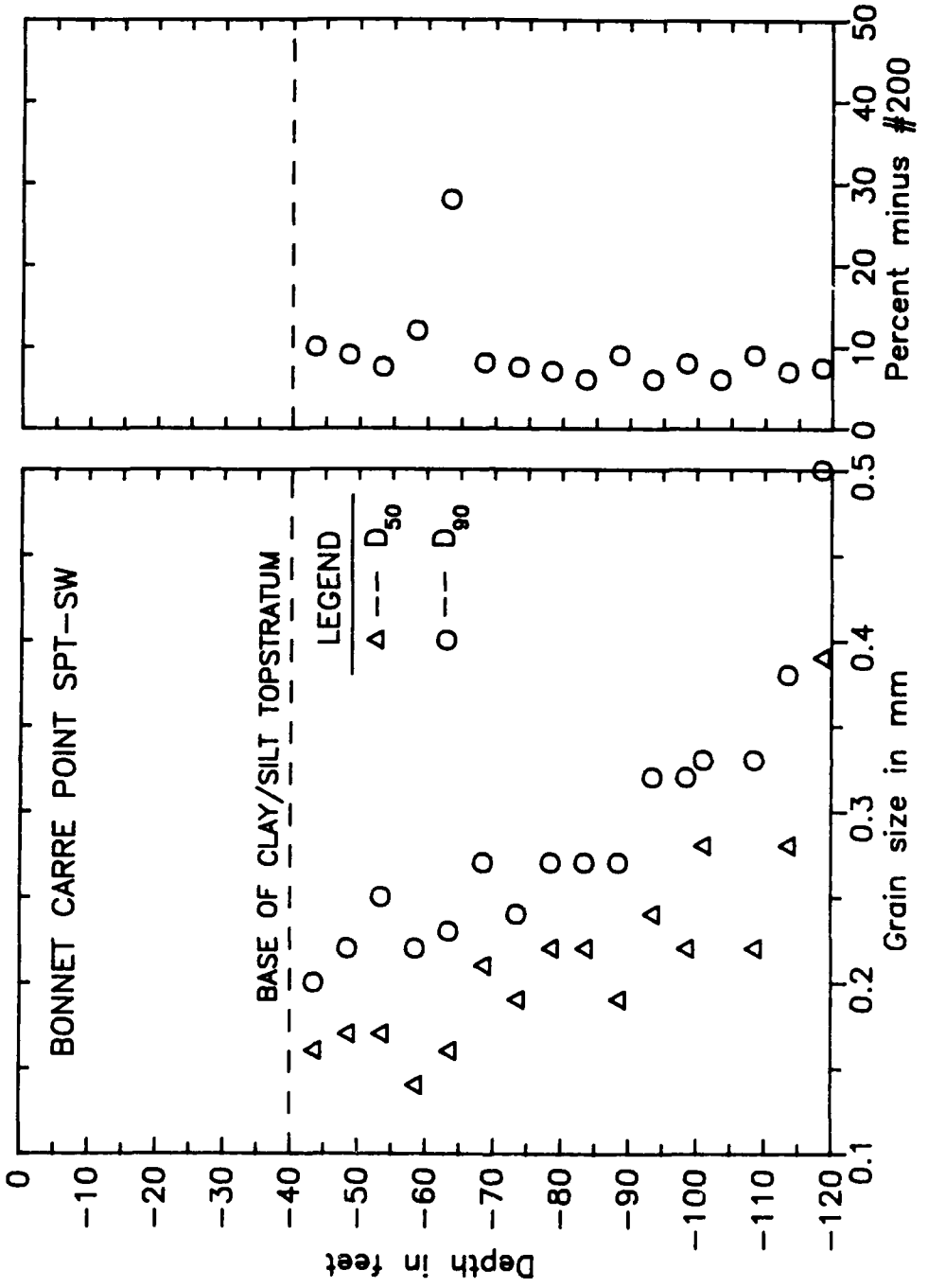

(N1)60
0 10 20 30 40 50 60 70 80 90 100
BONNET CARRE POINT SPT-NE
NOTE: Trend in (N1)60 below about 95 feet results from use of N=100 for refusal.
Ground surface = El. 19.0 ft. N.G.V.D.
BASE OF CLAY/SILT TOPSTRATUM
Depth in feet
0 10 20 30 40 50 60 70 80 90 100 110 120
REFUSAL N=100


(N1)60
0 10 20 30 40 50 60 70 80 90 100
BONNET CARRE POINT SPT-NW
NOTE: Trend in (N1)60 below about 75 feet results from use of N=100 for refusal.
Ground surface = El. 19.0 ft. N.G.V.D.
BASE OF CLAY/SILT TOPSTRATUM
Depth in feet
0 10 20 30 40 50 60 70 80 90 100 110 120
REFUSAL N=100


(N1)60
0 10 20 30 40 50 60 70 80 90 100
BONNET CARRE POINT SPT-SE
NOTE: Trend in (N1)60 below about 90 feet results from use of N=100 for refusal.
Ground surface = El. 20.0 ft. N.G.V.D.
BASE OF CLAY/SILT TOPSTRATUM
Depth in feet
0 10 20 30 40 50 60 70 80 90 100 110 120
REFUSAL N=100


(N1)60
0 10 20 30 40 50 60 70 80 90 100
BONNET CARRE POINT SPT-SW
NOTE: Trend in (N1)60 below about 95 feet results from use of N=100 for refusal.
Ground surface = El. 20.0 ft. N.G.V.D.
BASE OF CLAY/SILT TOPSTRATUM
Depth in feet
0 10 20 30 40 50 60 70 80 90 100 110 120
N=100
REFUSAL


BONNET CARRE POINT SPT-NE
BASE OF CLAY,'SILT TOPSTRATUM
LEGEND
Δ -- D50
○ -- D90
Depth in feet
0
-10
-20
-30
-40
-50
-60
-70
-80
-90
-100
-110
-120
0.1
0.2
0.3
0.4
0.5
Grain size in mm
0
10
20
30
40
50
Percent minus #200


BONNET CARRE POINT SPT-SW
BASE OF CLAY/SILT TOPSTRATUM
LEGEND
D_{50}
D_{90}
Depth in feet
0
-10
-20
-30
-40
-50
-60
-70
-80
-90
-100
-110
-120
0.1
0.2
0.3
0.4
0.5
Grain size in mm
0
10
20
30
40
50
Percent minus #200

APPENDIX D

RIVER STAGE AND PIEZOMETER DATA

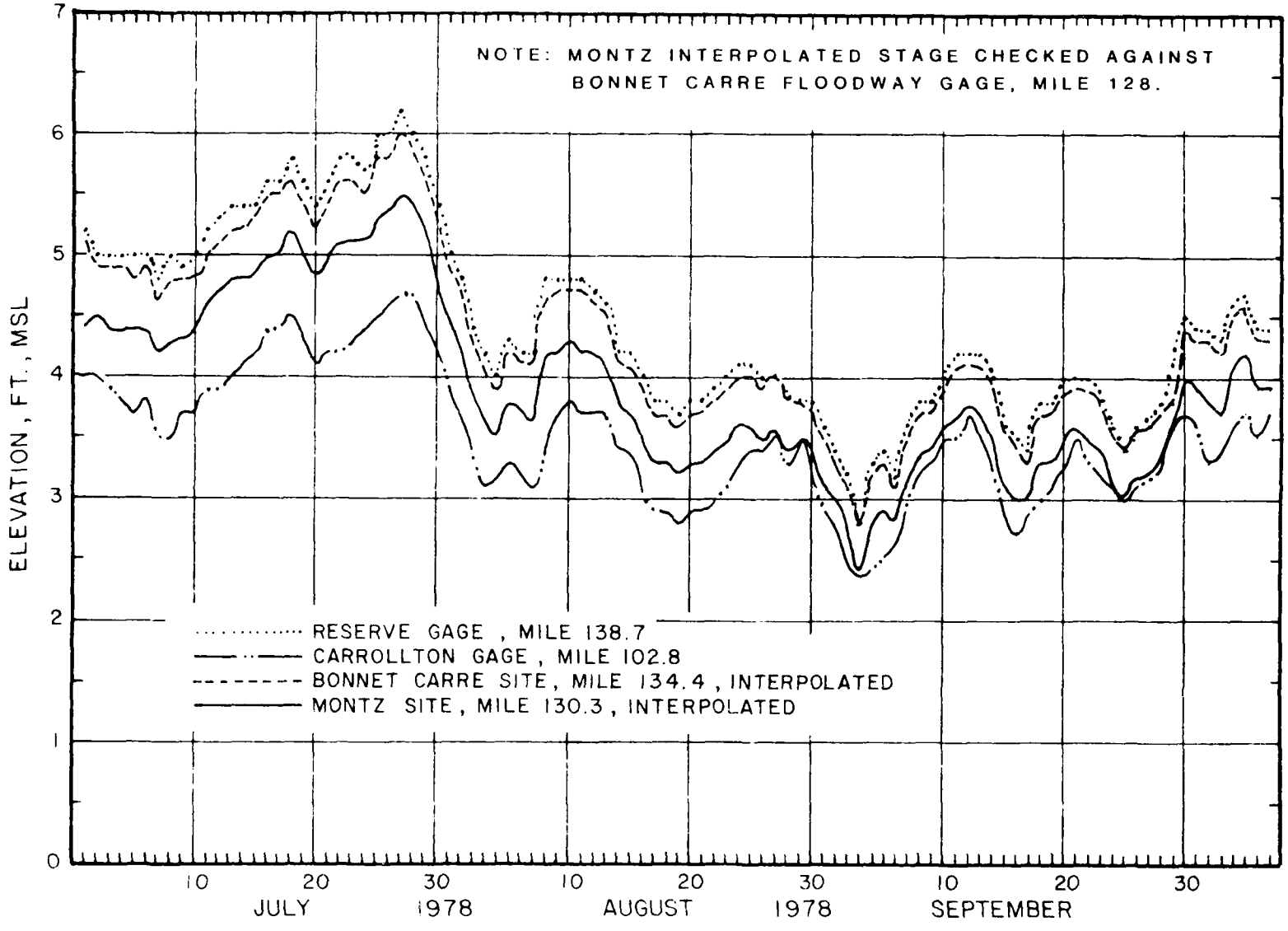


Figure D1. Interpolated river stages for Montz and Bonnet Carre Point sites

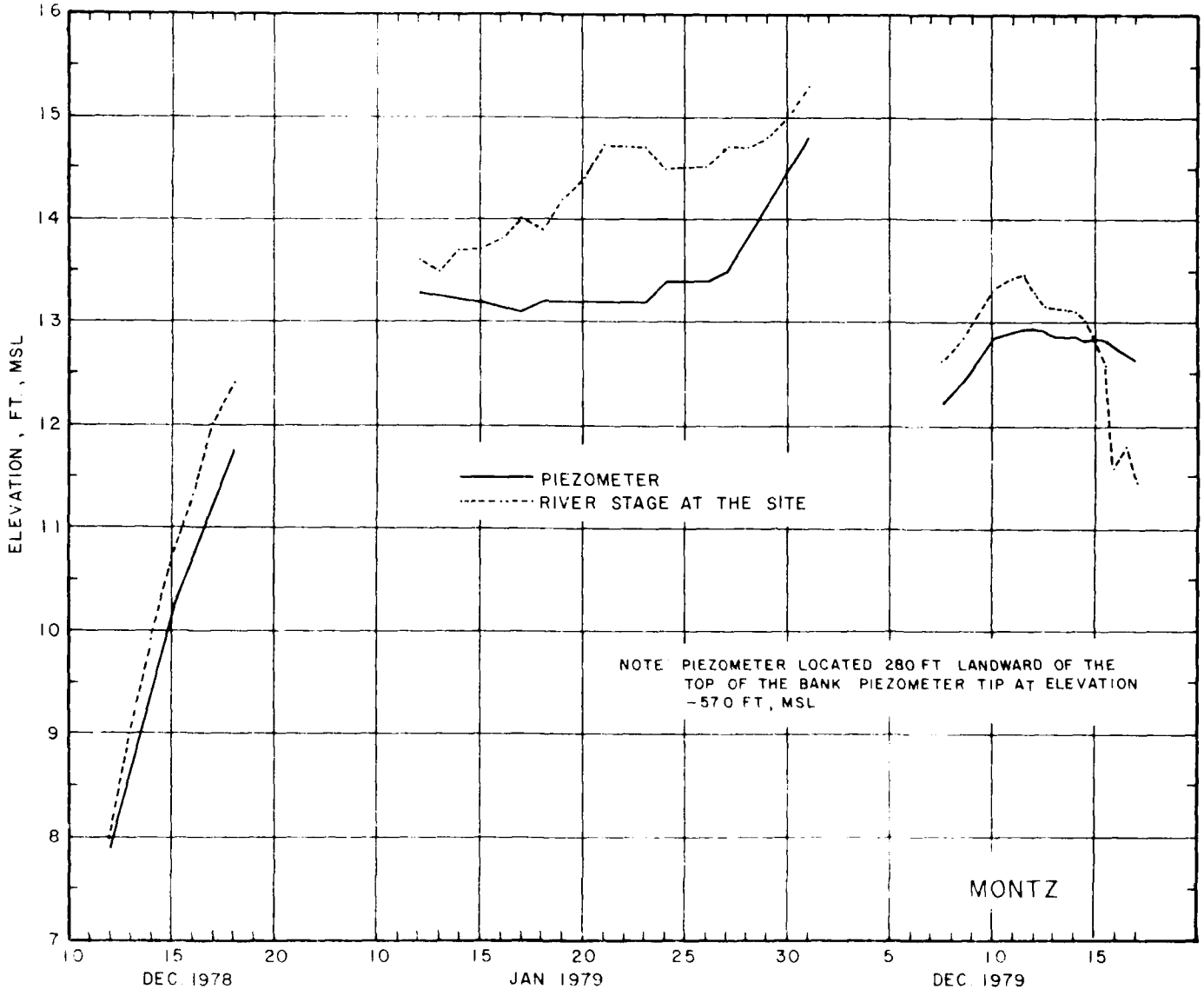


Figure D2. Piezometer and river stage data during undisturbed sampling and SPT borings, Montz detailed site

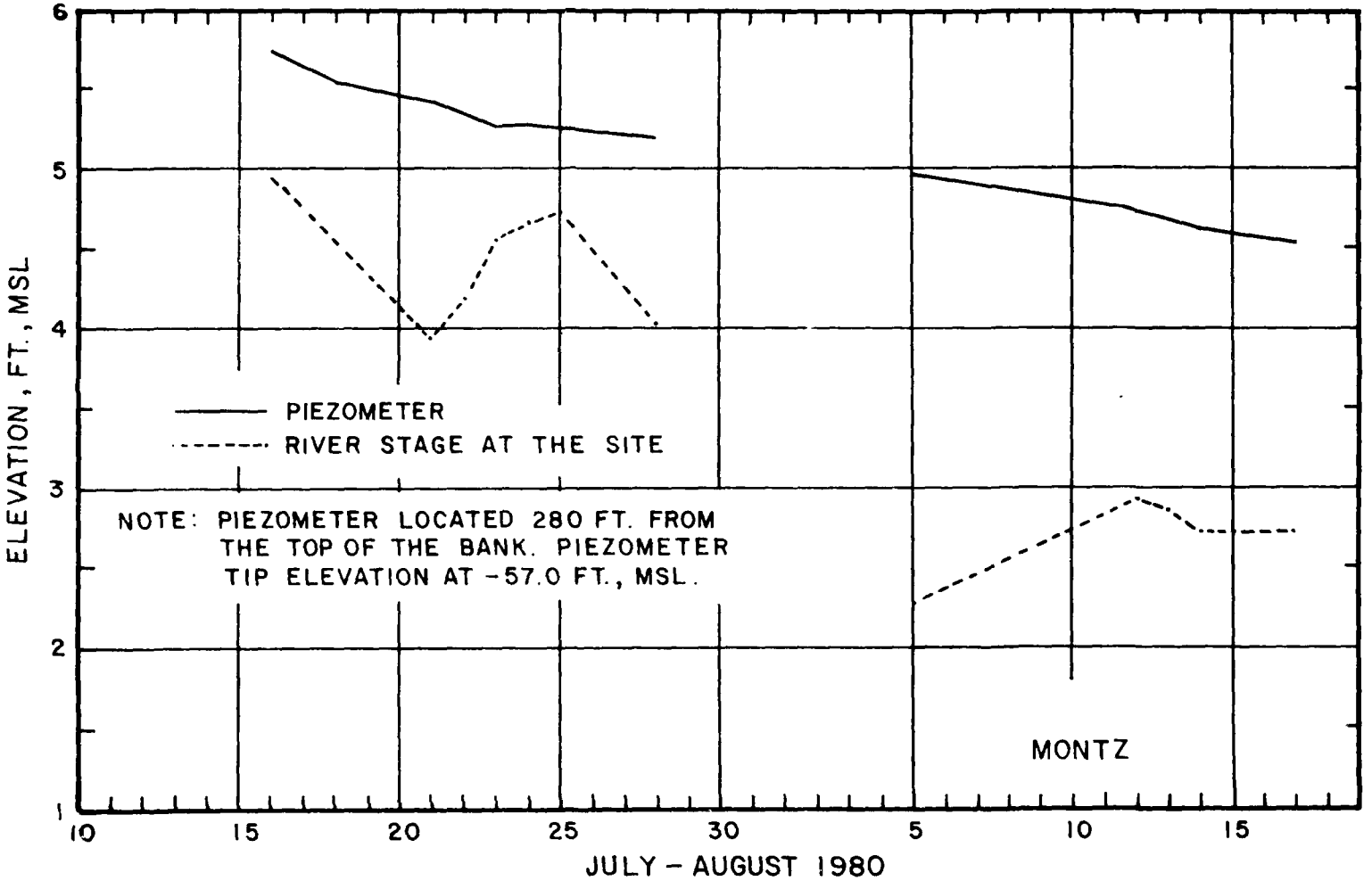


Figure D3. *Piezometer and river state data during RC, CPT, and Piezocone soundings, Montz detailed site*

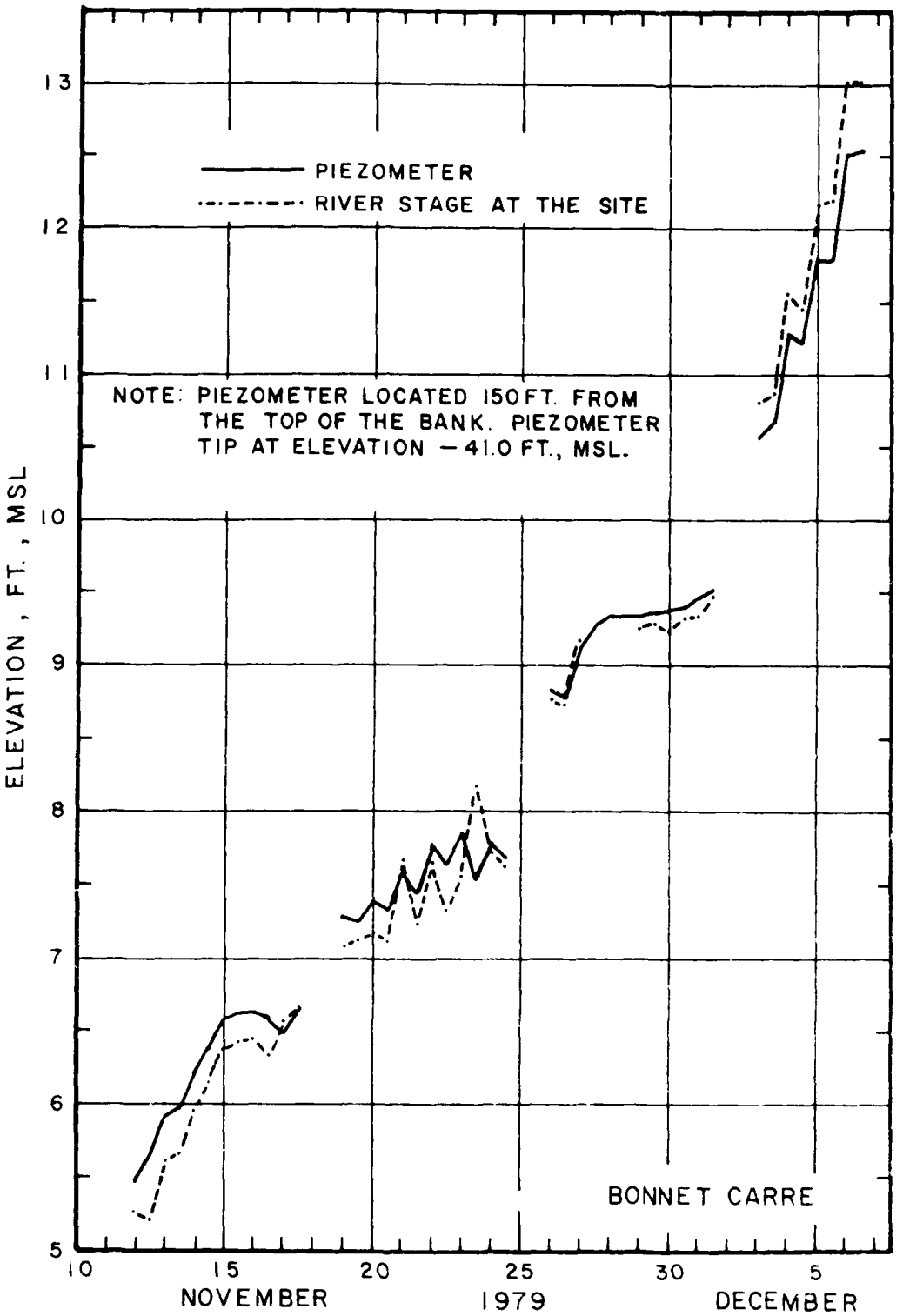


Figure D4. Piezometer and river stage data during undisturbed sampling and SPT soundings, Bonnet Carre Point detailed site

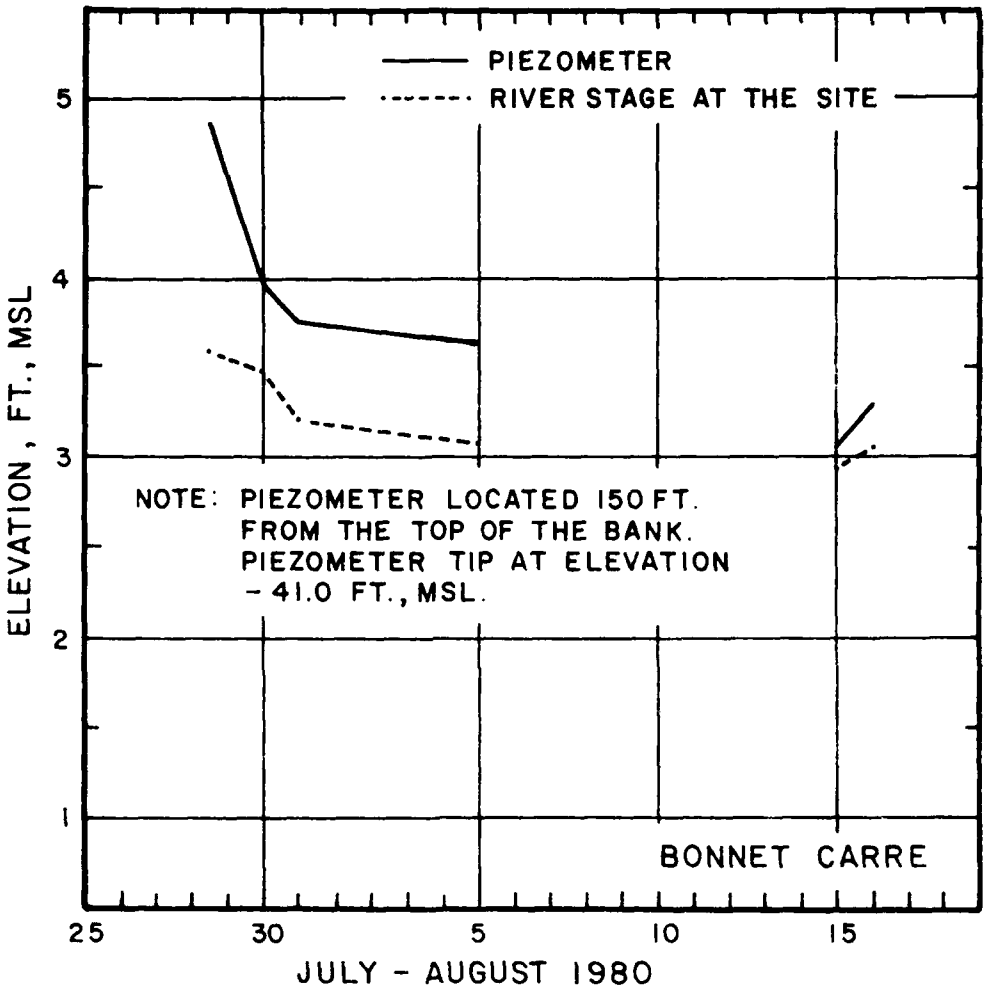
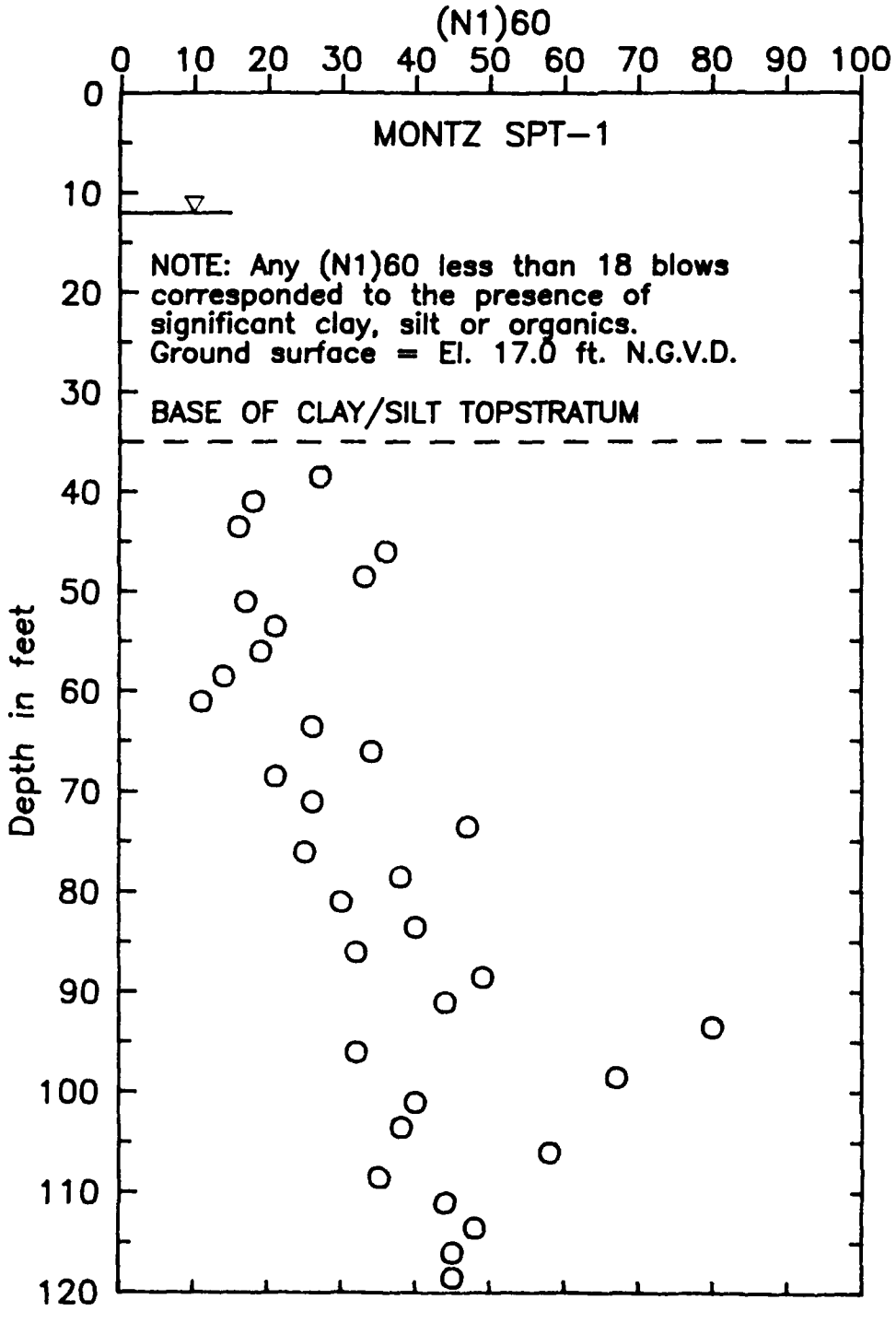
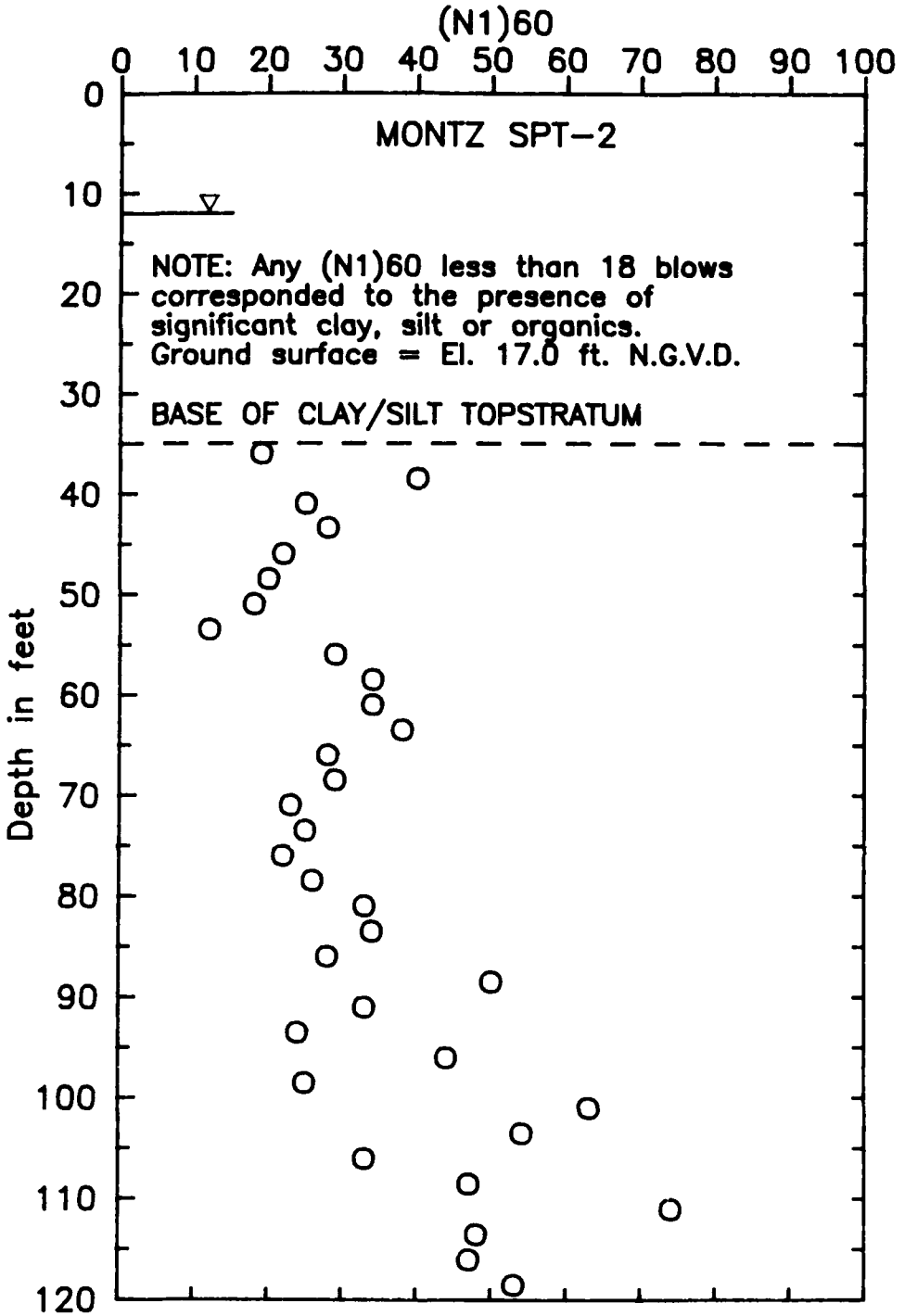


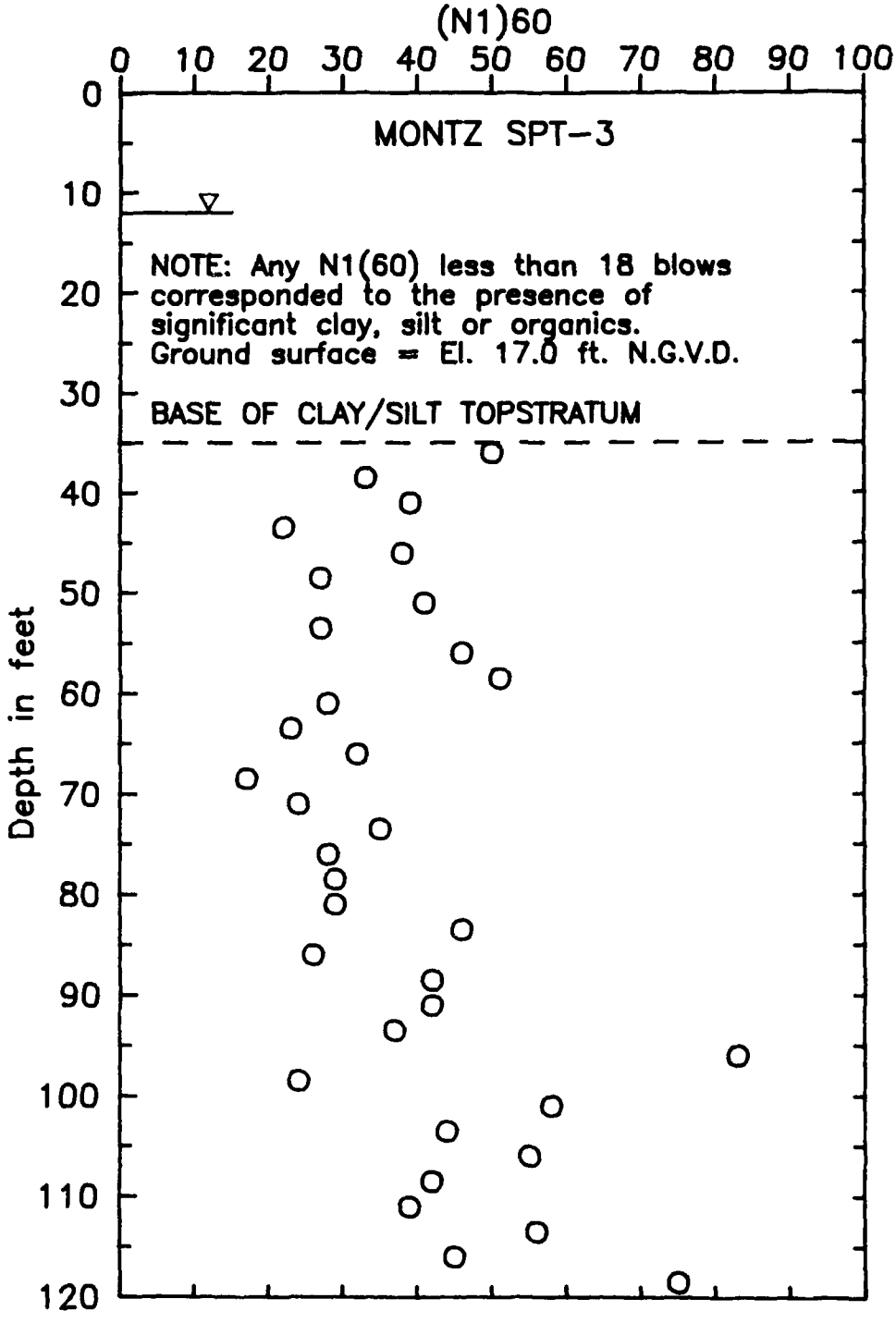
Figure D5. Piezometer and river stage data during RC, CPT, and Piezocone soundings, Bonnet Carre Point detailed site

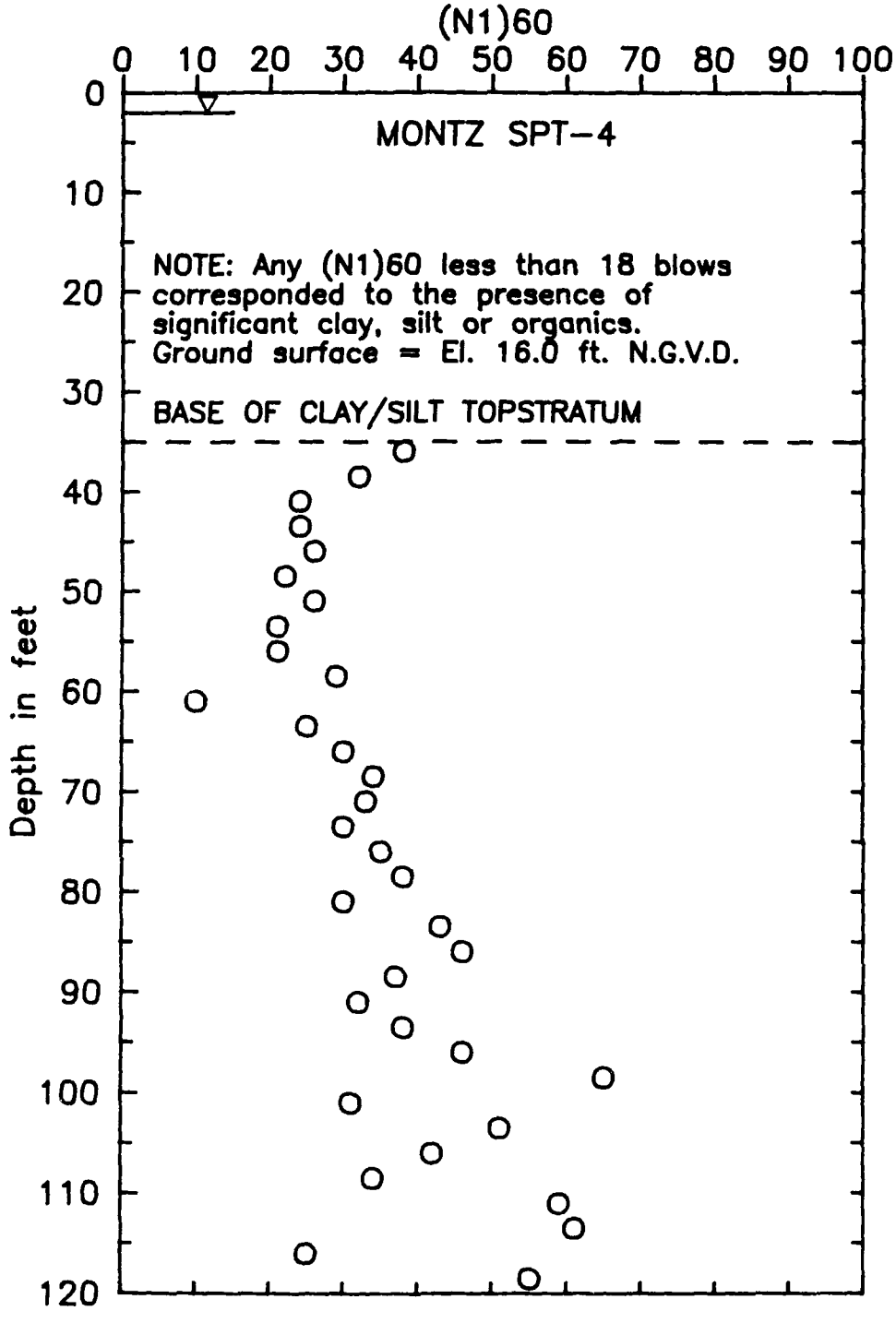
APPENDIX E

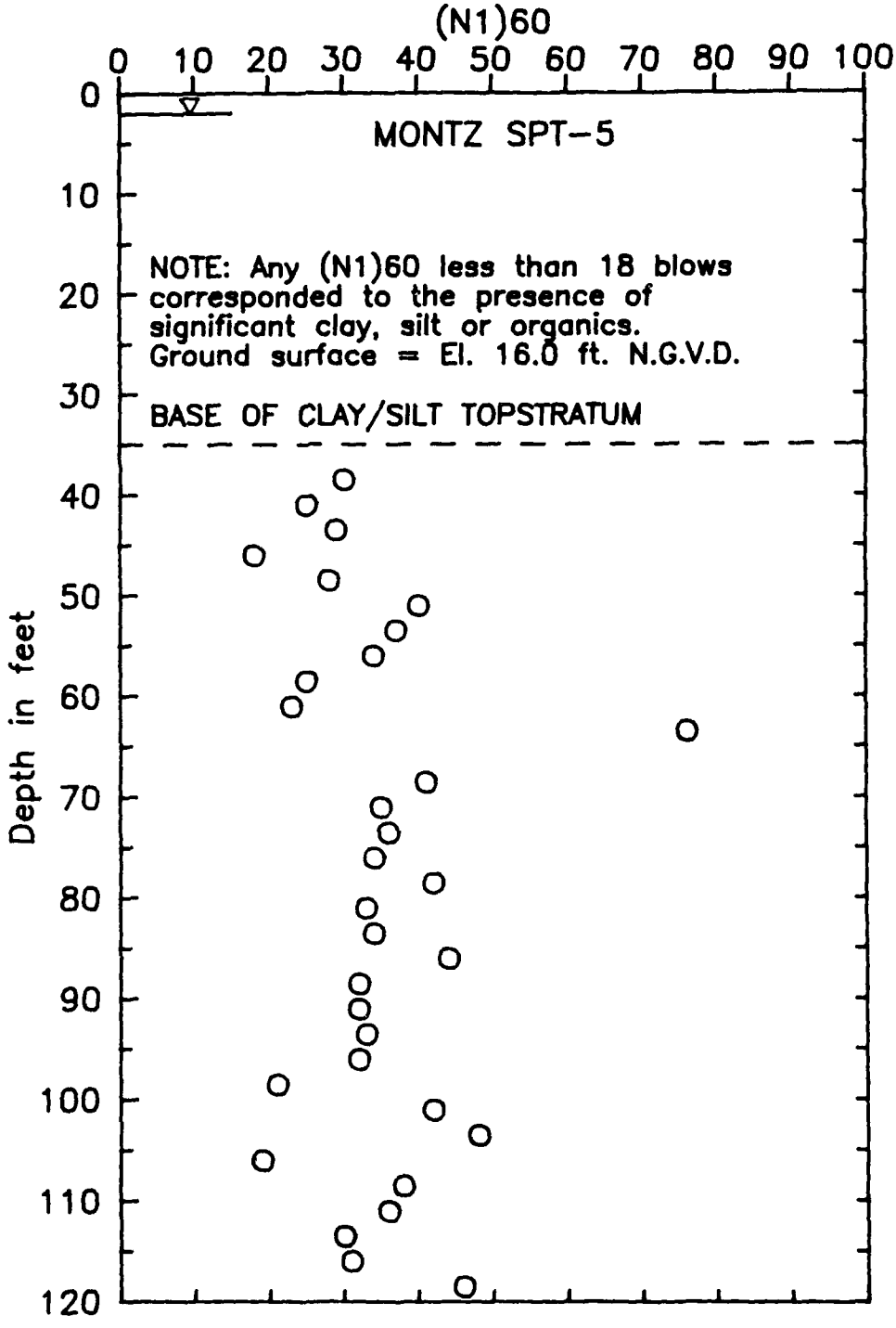
SPT DATA, MONTZ AND BONNET CARRE POINT DETAILED SITES

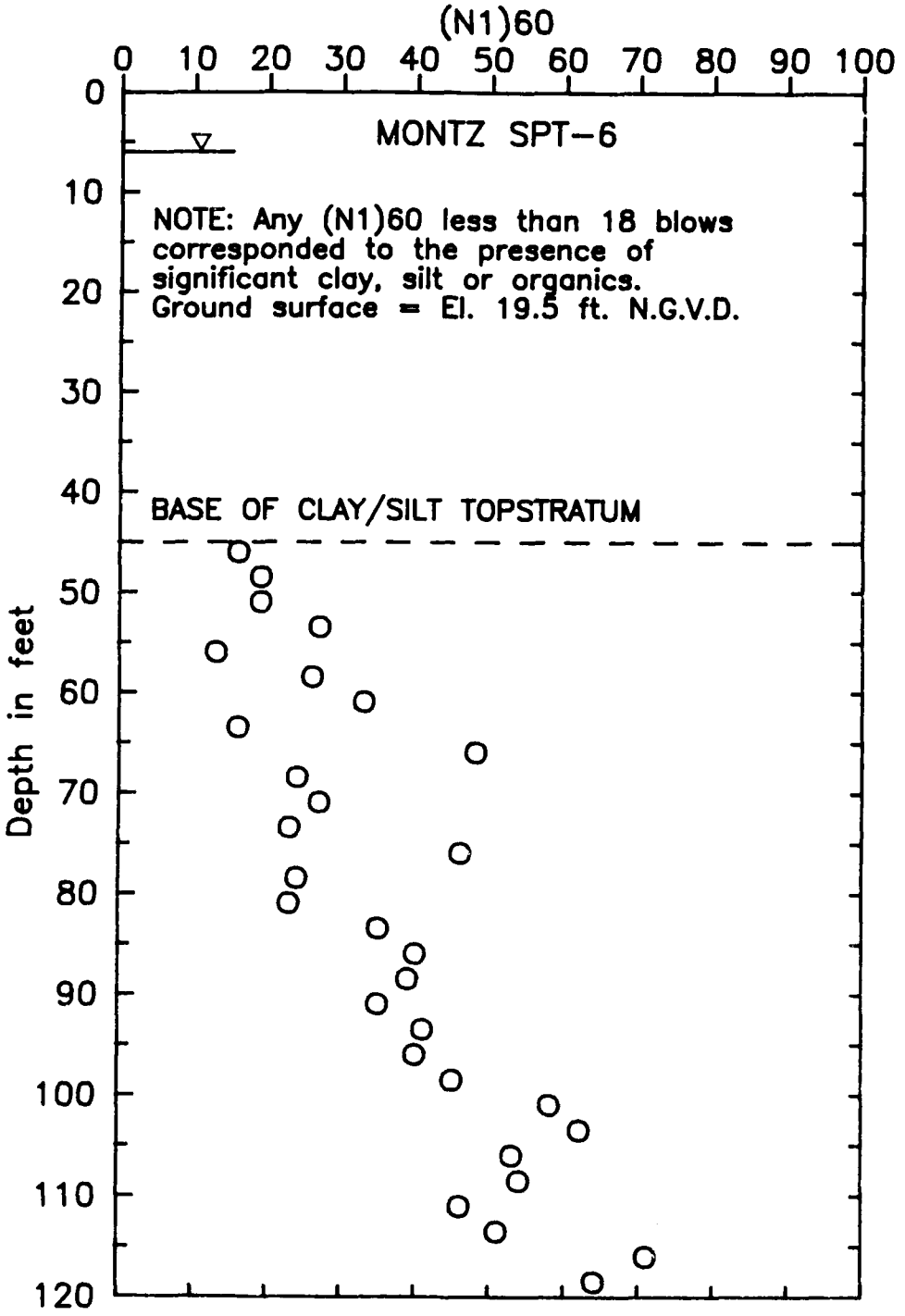

(N1)60
0 10 20 30 40 50 60 70 80 90 100
MONTZ SPT-1
NOTE: Any (N1)60 less than 18 blows corresponded to the presence of significant clay, silt or organics.
Ground surface = El. 17.0 ft. N.G.V.D.
BASE OF CLAY/SILT TOPSTRATUM
Depth in feet
0 10 20 30 40 50 60 70 80 90 100 110 120

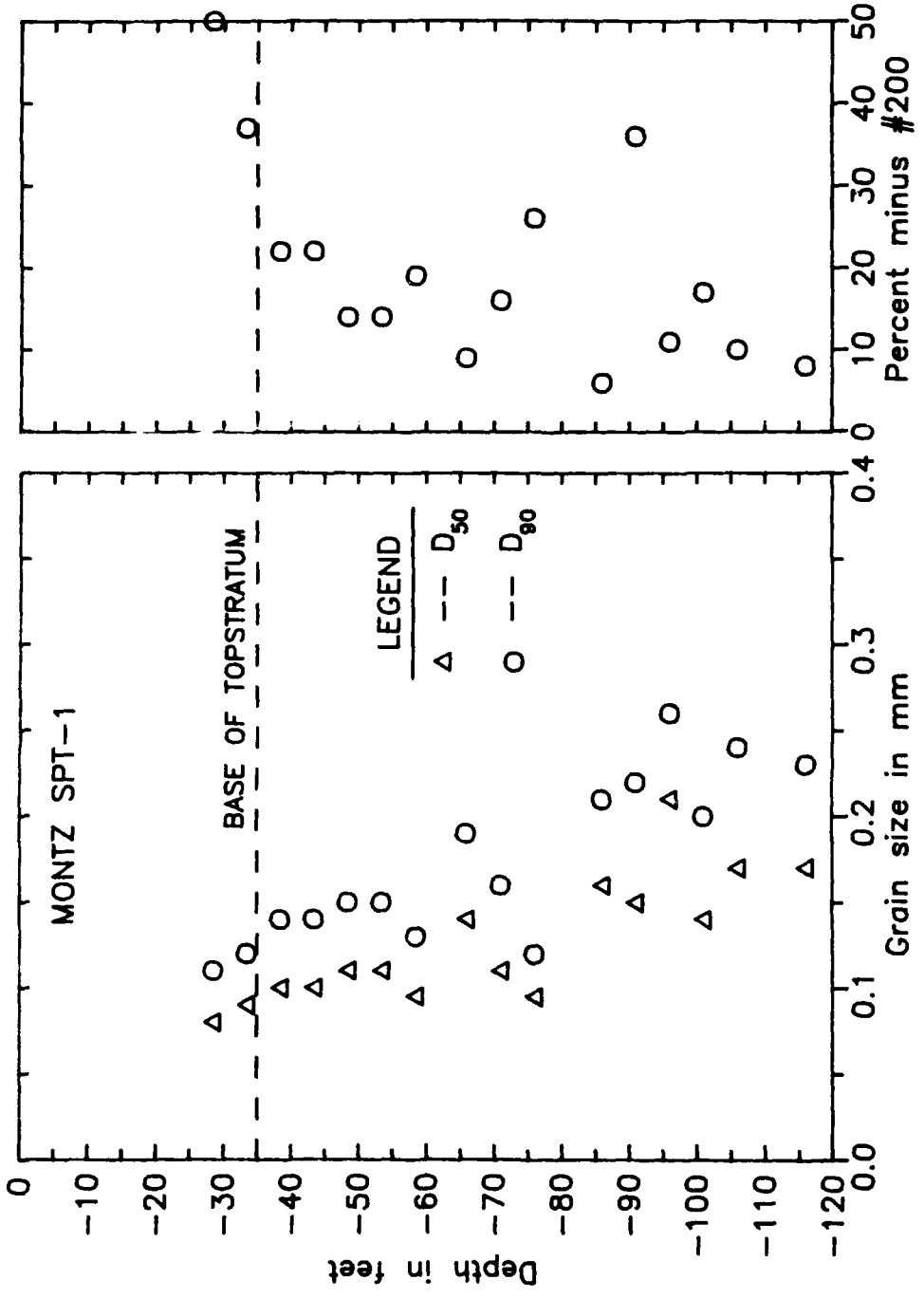

(N1)60
0 10 20 30 40 50 60 70 80 90 100
MONTZ SPT-2
NOTE: Any (N1)60 less than 18 blows corresponded to the presence of significant clay, silt or organics.
Ground surface = El. 17.0 ft. N.G.V.D.
BASE OF CLAY/SILT TOPSTRATUM
Depth in feet
0 10 20 30 40 50 60 70 80 90 100 110 120

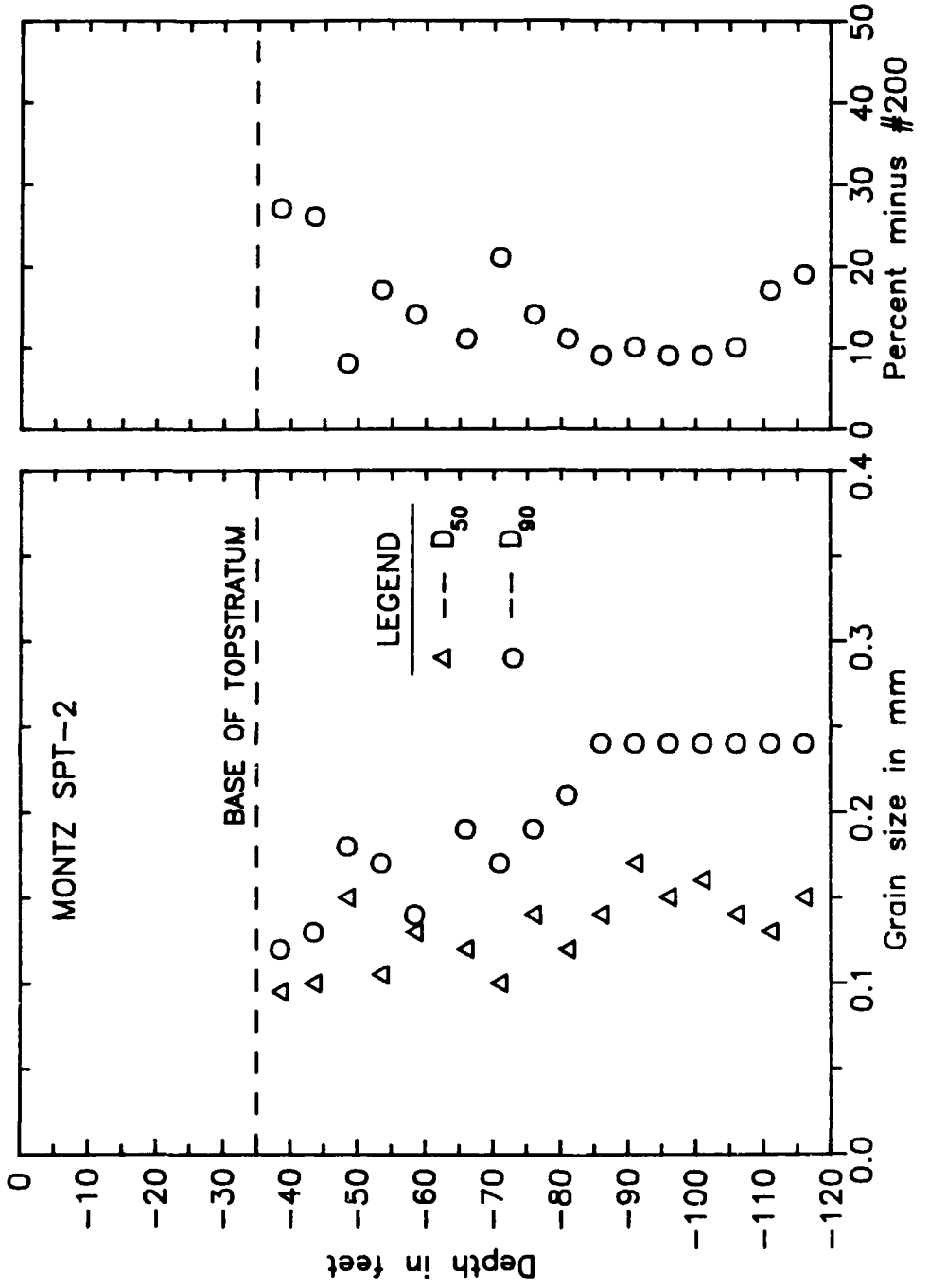

(N1)60
0 10 20 30 40 50 60 70 80 90 100
MONTZ SPT-3
NOTE: Any N1(60) less than 18 blows corresponded to the presence of significant clay, silt or organics.
Ground surface = El. 17.0 ft. N.G.V.D.
BASE OF CLAY/SILT TOPSTRATUM
Depth in feet
0 10 20 30 40 50 60 70 80 90 100 110 120

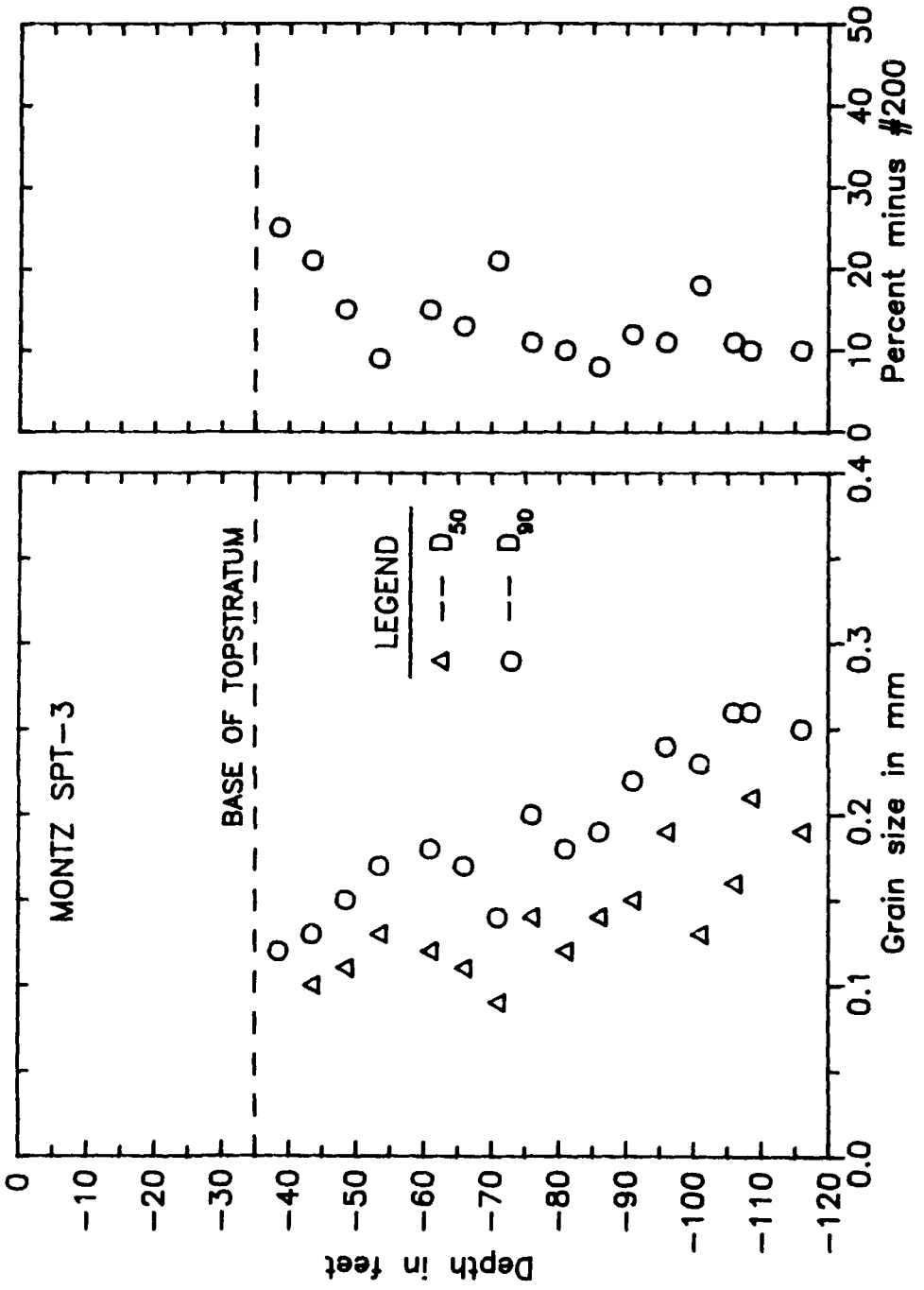

(N1)60
0 10 20 30 40 50 60 70 80 90 100
0
10
20
30
40
50
60
70
80
90
100
110
120
Depth in feet
MONTZ SPT-4
NOTE: Any (N1)60 less than 18 blows corresponded to the presence of significant clay, silt or organics.
Ground surface = El. 16.0 ft. N.G.V.D.
BASE OF CLAY/SILT TOPSTRATUM

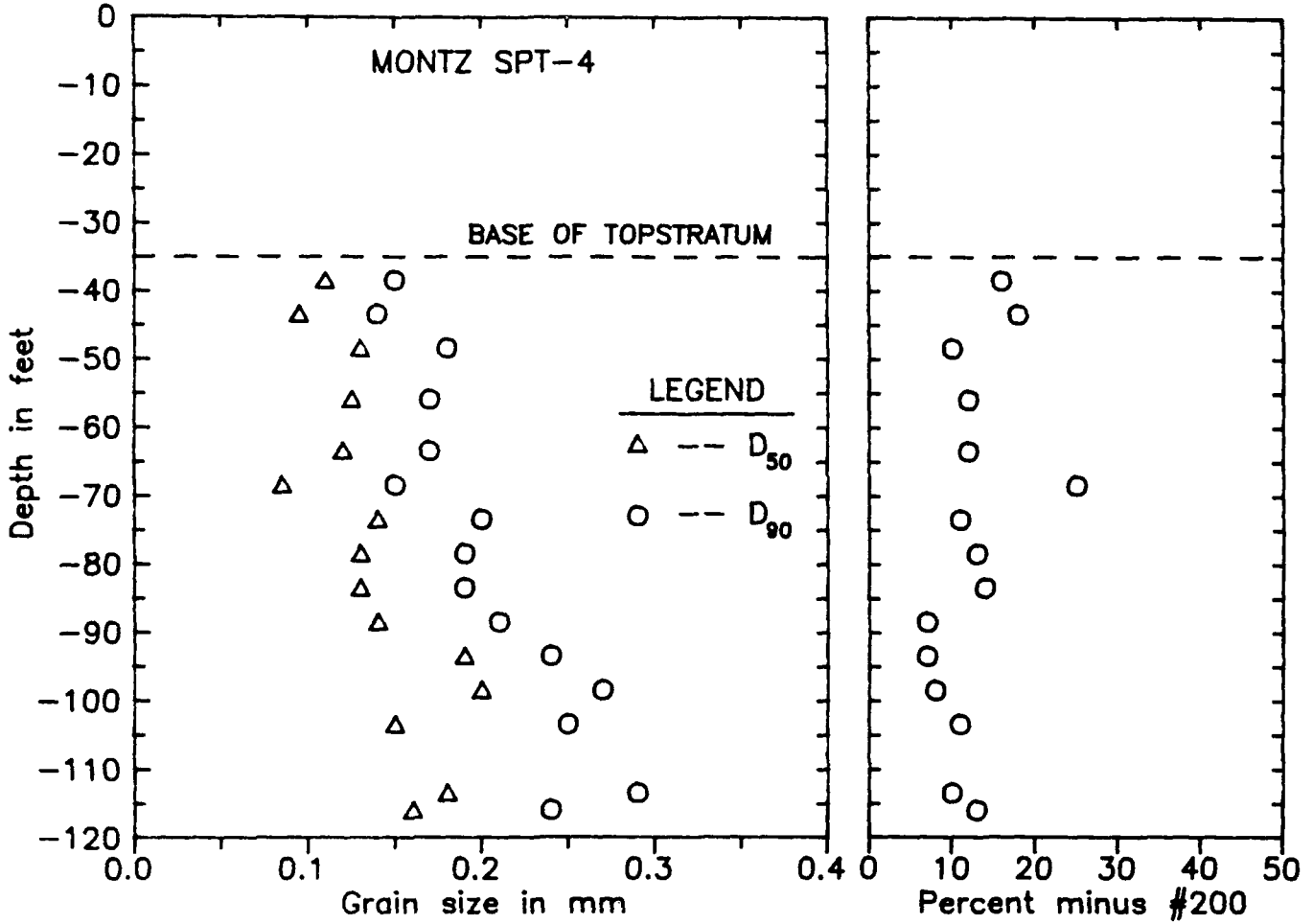

(N1)60
0 10 20 30 40 50 60 70 80 90 100
MONTZ SPT-5
NOTE: Any (N1)60 less than 18 blows corresponded to the presence of significant clay, silt or organics.
Ground surface = El. 16.0 ft. N.G.V.D.
BASE OF CLAY/SILT TOPSTRATUM
Depth in feet
0 10 20 30 40 50 60 70 80 90 100 110 120

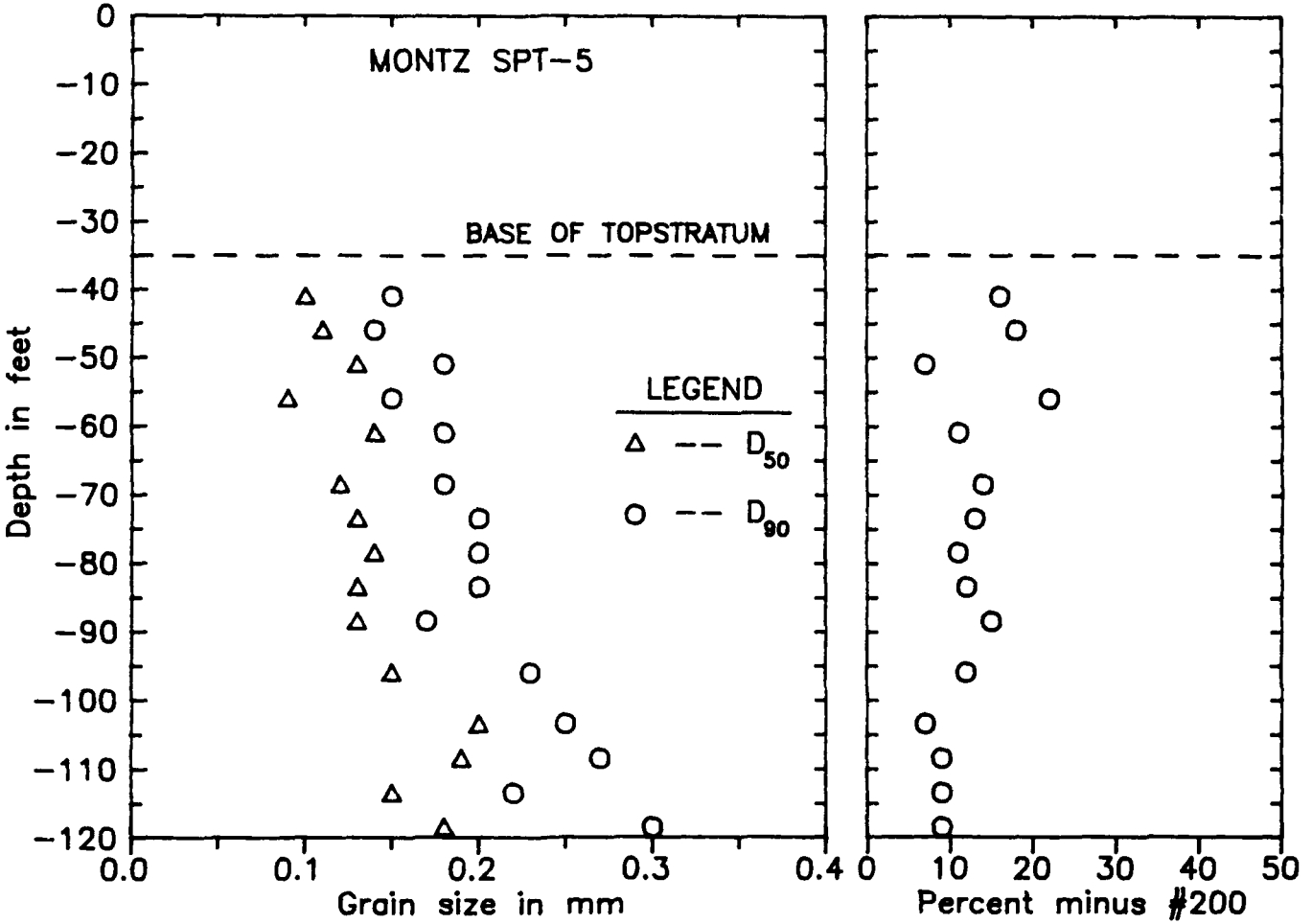

(N1)60
0 10 20 30 40 50 60 70 80 90 100
MONTZ SPT-6
NOTE: Any (N1)60 less than 18 blows corresponded to the presence of significant clay, silt or organics.
Ground surface = El. 19.5 ft. N.G.V.D.
BASE OF CLAY/SILT TOPSTRATUM
Depth in feet
0 10 20 30 40 50 60 70 80 90 100 110 120

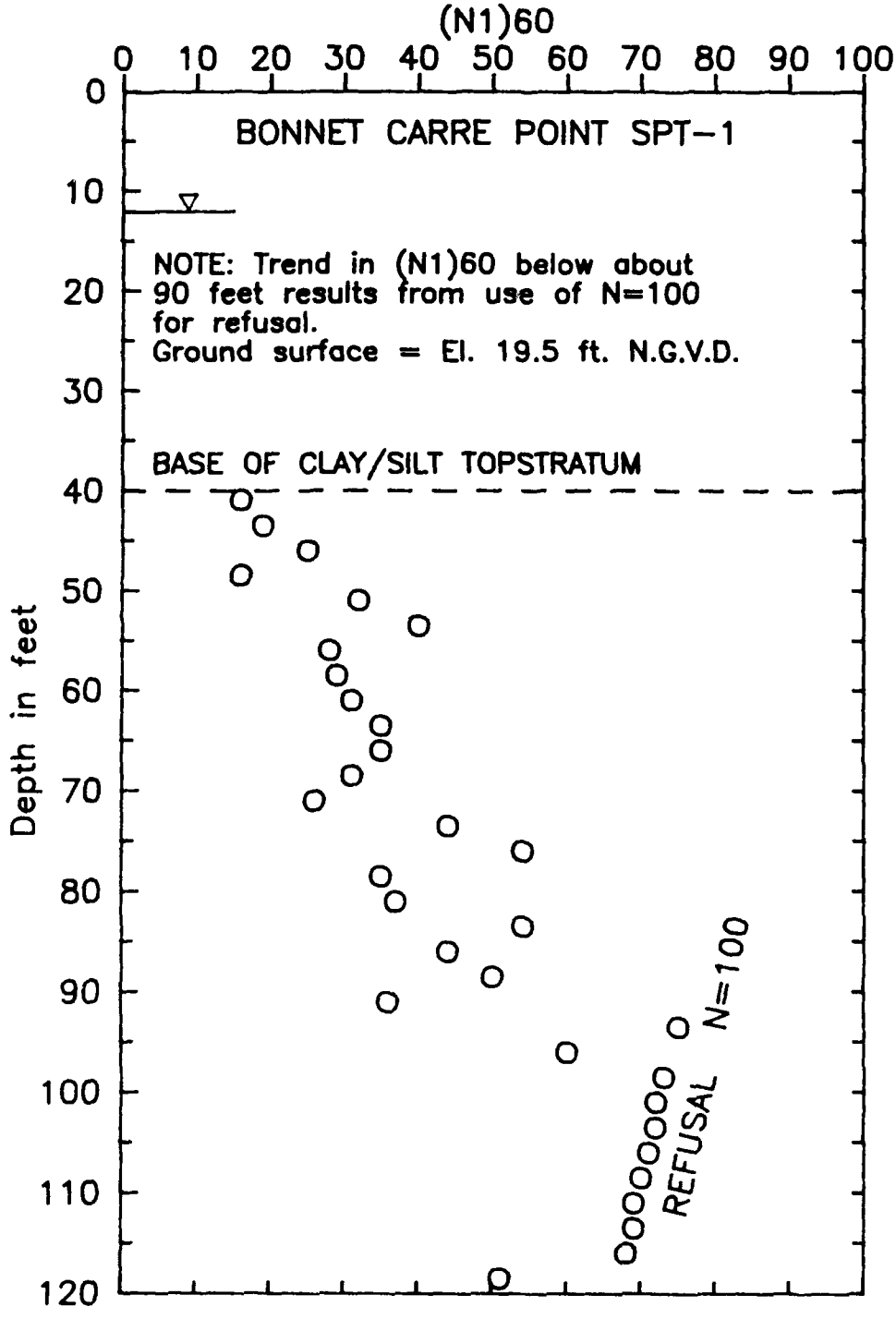

MONTZ SPT-1
BASE OF TOPSTRATUM
LEGEND
D_{50}
D_{90}
Depth in feet
0
-10
-20
-30
-40
-50
-60
-70
-80
-90
-100
-110
-120
0.0
0.1
0.2
0.3
0.4
Grain size in mm
0
10
20
30
40
50
Percent minus #200

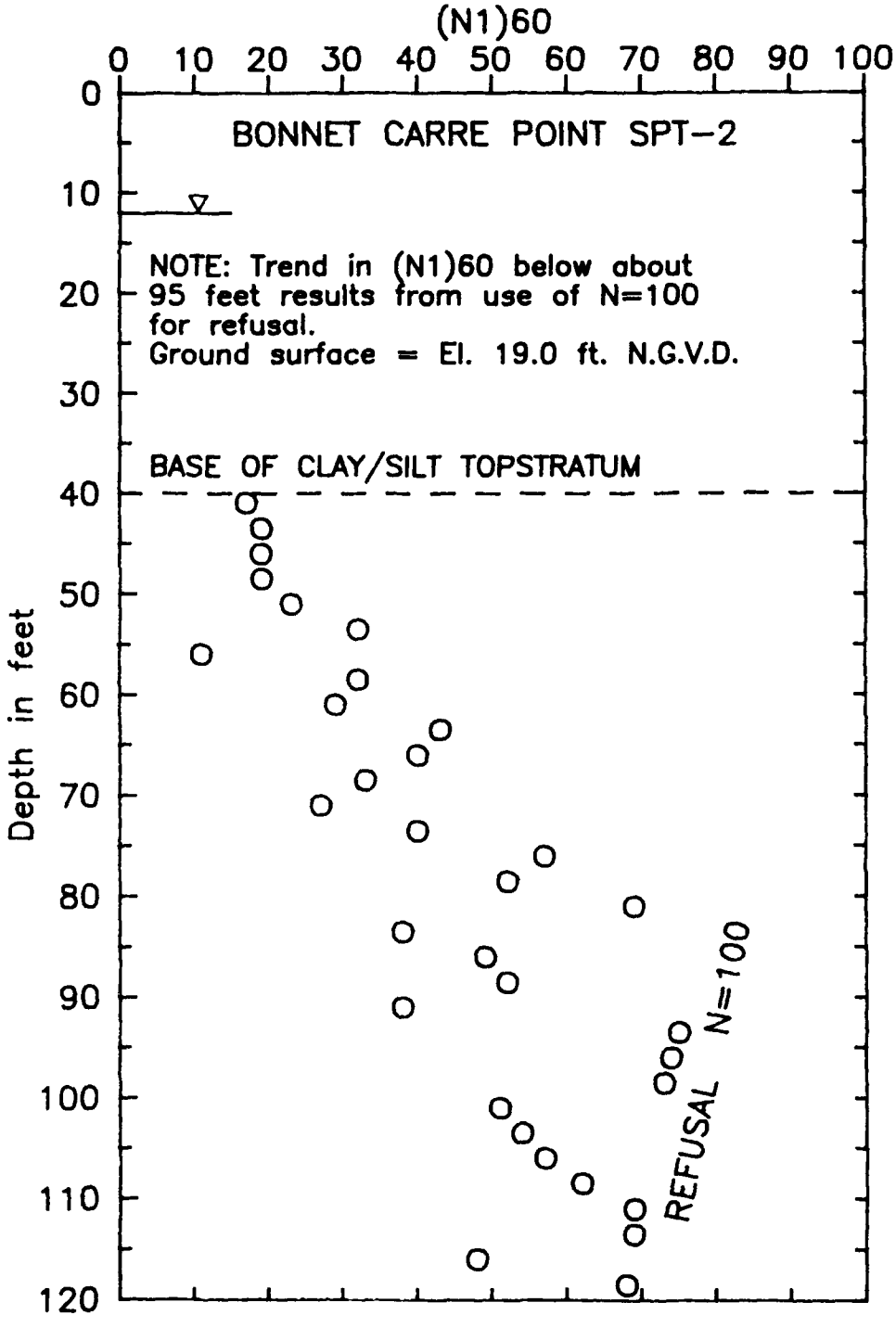

MONTZ SPT-2
BASE OF TOPSTRATUM
LEGEND
D_{50}
D_{90}
Depth in feet
0
-10
-20
-30
-40
-50
-60
-70
-80
-90
-100
-110
-120
0.0
0.1
0.2
0.3
0.4
Grain size in mm
0
10
20
30
40
50
Percent minus #200

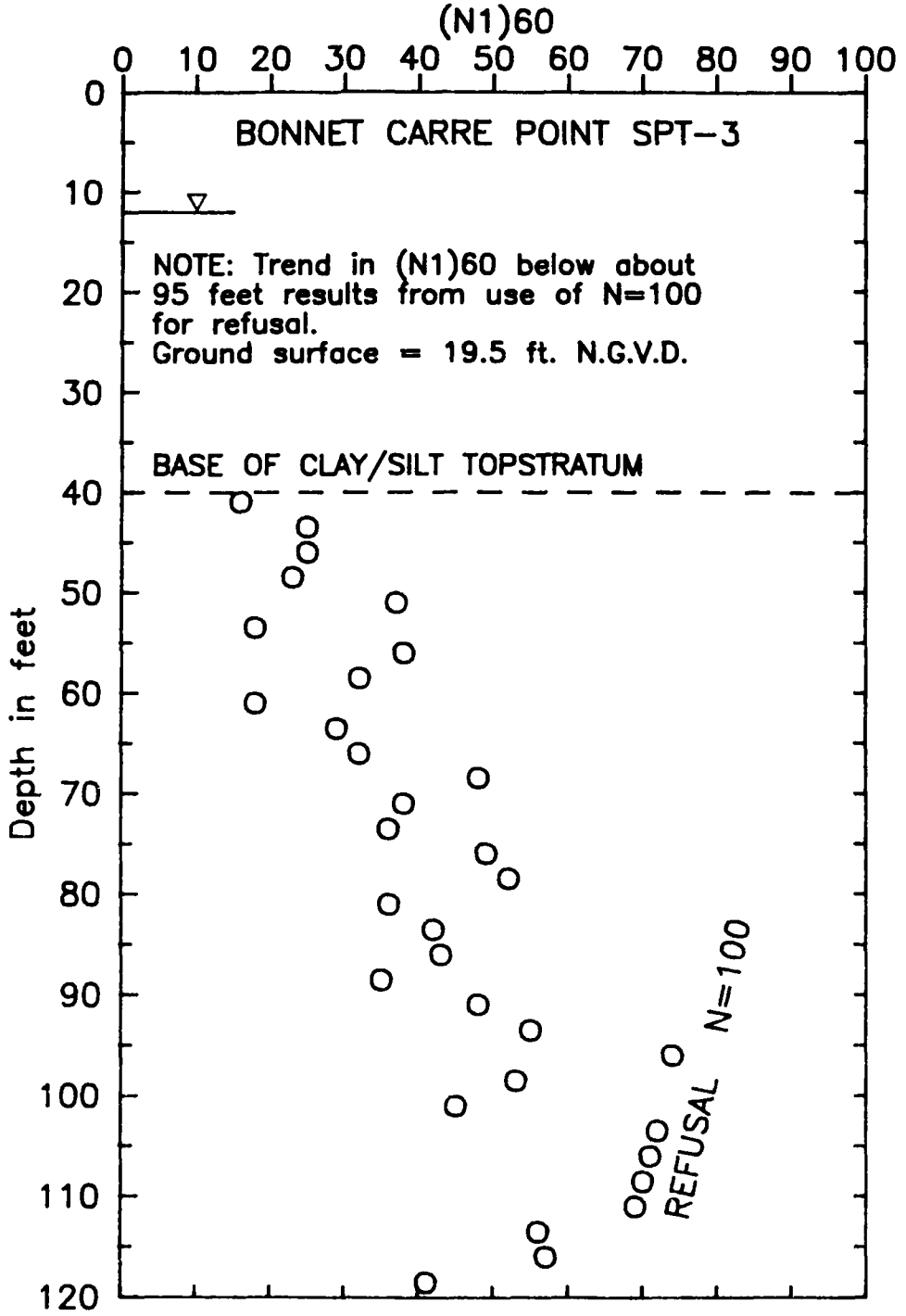

MONTZ SPT-3
BASE OF TOPSTRATUM
LEGEND
D_{50}
D_{90}
Depth in feet
0
-10
-20
-30
-40
-50
-60
-70
-80
-90
-100
-110
-120
0.0
0.1
0.2
0.3
0.4
Grain size in mm
0
10
20
30
40
50
Percent minus #200

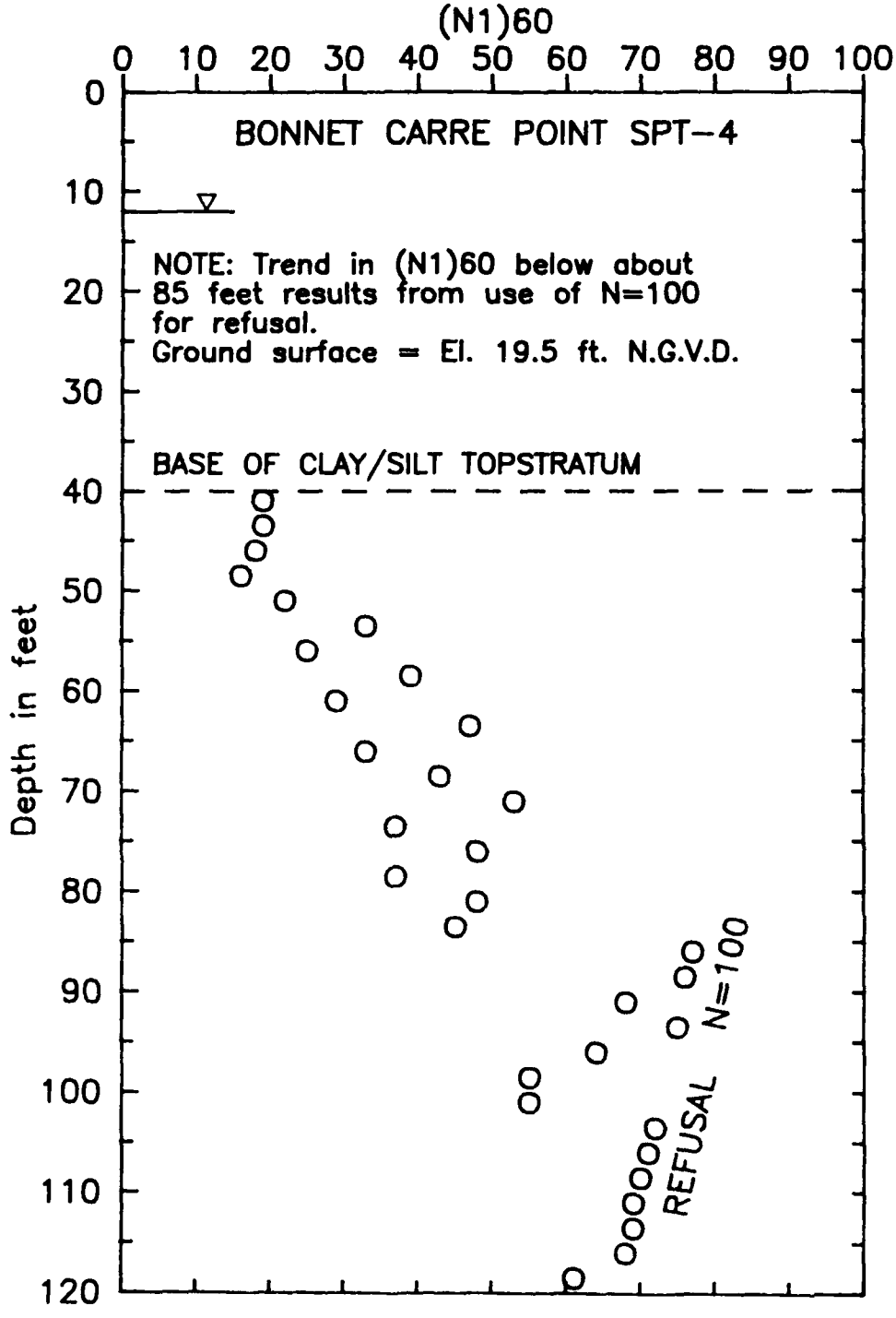

MONTZ SPT-4
BASE OF TOPSTRATUM
LEGEND
D_{50}
D_{90}
Depth in feet
0
-10
-20
-30
-40
-50
-60
-70
-80
-90
-100
-110
-120
0.0
0.1
0.2
0.3
0.4
Grain size in mm
0
10
20
30
40
50
Percent minus #200

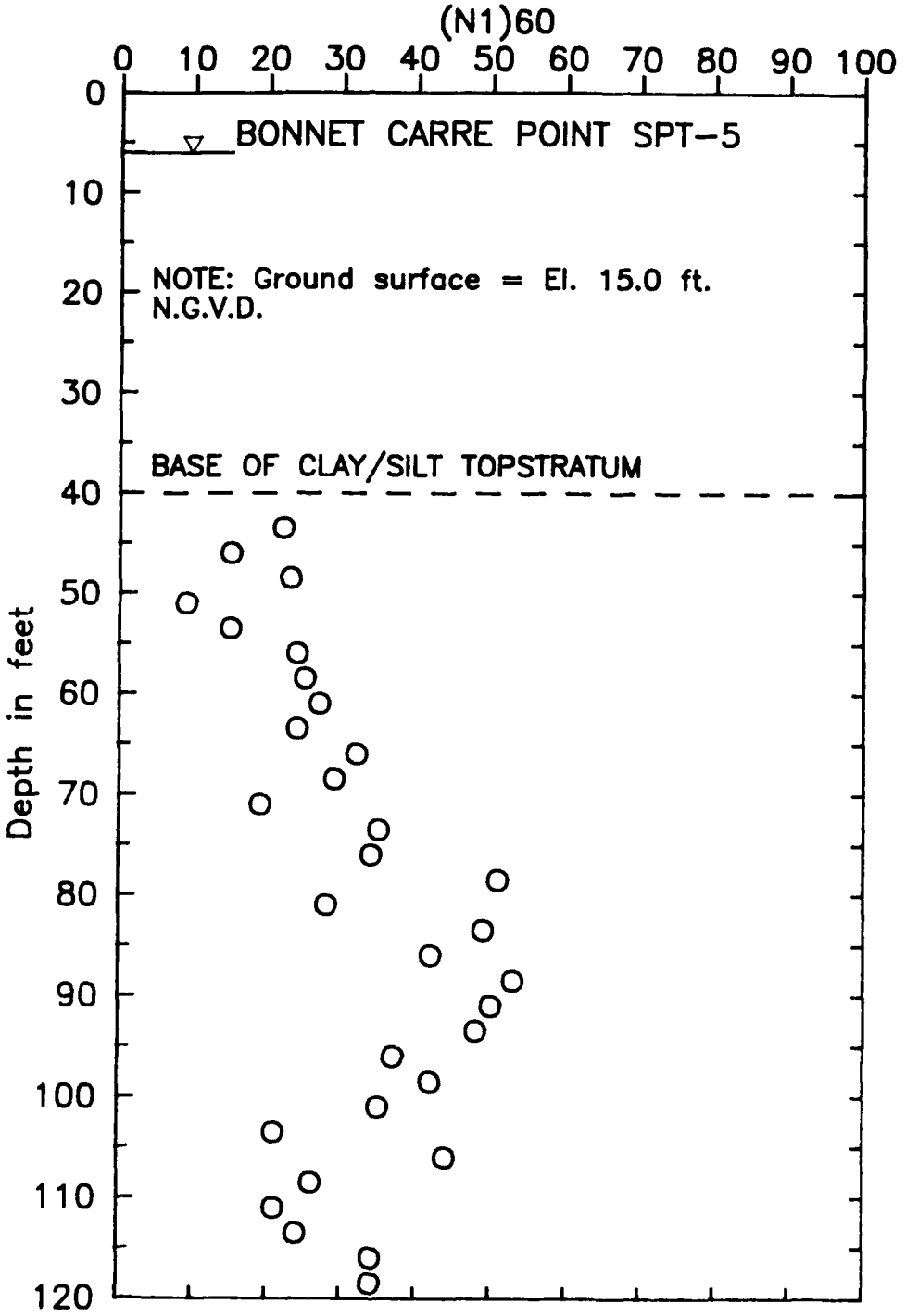

MONTZ SPT-5
BASE OF TOPSTRATUM
LEGEND
Δ -- D50
O -- D90
Depth in feet
0
-10
-20
-30
-40
-50
-60
-70
-80
-90
-100
-110
-120
0.0
0.1
0.2
0.3
0.4
Grain size in mm
0
10
20
30
40
50
Percent minus #200


(N1)60
0 10 20 30 40 50 60 70 80 90 100
BONNET CARRE POINT SPT-1
NOTE: Trend in (N1)60 below about 90 feet results from use of N=100 for refusal.
Ground surface = El. 19.5 ft. N.G.V.D.
BASE OF CLAY/SILT TOPSTRATUM
Depth in feet
0 10 20 30 40 50 60 70 80 90 100 110 120
N=100
REFUSAL


(N1)60
0 10 20 30 40 50 60 70 80 90 100
BONNET CARRE POINT SPT-2
NOTE: Trend in (N1)60 below about 95 feet results from use of N=100 for refusal.
Ground surface = El. 19.0 ft. N.G.V.D.
BASE OF CLAY/SILT TOPSTRATUM
Depth in feet
0 10 20 30 40 50 60 70 80 90 100 110 120
REFUSAL N=100


(N1)60
0 10 20 30 40 50 60 70 80 90 100
BONNET CARRE POINT SPT-3
NOTE: Trend in (N1)60 below about 95 feet results from use of N=100 for refusal.
Ground surface = 19.5 ft. N.G.V.D.
BASE OF CLAY/SILT TOPSTRATUM
Depth in feet
0 10 20 30 40 50 60 70 80 90 100 110 120
N=100
REFUSAL


(N1)60
0 10 20 30 40 50 60 70 80 90 100
BONNET CARRE POINT SPT-4
NOTE: Trend in (N1)60 below about 85 feet results from use of N=100 for refusal.
Ground surface = El. 19.5 ft. N.G.V.D.
BASE OF CLAY/SILT TOPSTRATUM
Depth in feet
0 10 20 30 40 50 60 70 80 90 100 110 120
N=100
REFUSAL


(N1)60
0 10 20 30 40 50 60 70 80 90 100
BONNET CARRE POINT SPT-5
NOTE: Ground surface = El. 15.0 ft. N.G.V.D.
BASE OF CLAY/SILT TOPSTRATUM
Depth in feet
0 10 20 30 40 50 60 70 80 90 100 110 120

APPENDIX F

ELECTRICAL CONE PENETRATION TESTS, FUGRO-GULF CONTRACT REPORT

Fugro Gulf, Inc./Consulting Engineers and Geologists

5[illegible] West Drive, Houston, Texas 77036
[illegible] 772-2041 Telex 775494

Report No. 80-085
January 5, 1981

U. S. Army Engineer Waterways Experiment Station
Corps of Engineers
P. O. Box 631
Vicksburg, Mississippi 39180

Attention: Mr. V. Torrey

RESISTIVITY PROBE AND CONE PENETROMETER STUDY
BONNET CARRE POINT, LOUISIANA

Gentlemen:

Presented herein are the cone penetrometer logs from our investigations at two sites near the Mississippi River at Bonnet Carre Louisiana. The locations for the Montz site are shown on Plate Lucy site is shown on Plate 2. The cone penetrometer testing (C was performed in conjunction with resistivity probe work. Resistivity probe results will be presented by the Delft Laboratory, Holland, at a later date.

Cone penetrometer testing was performed using a Fugro electric cone penetrometer. The penetrometer has a conical tip with a base area of 10 square centimeters and an apex angle of 60°. The cylindrical friction sleeve located immediately above the tip has a total surface area of 150 square centimeters. Two independently operating strain gage load cells are housed in the penetrometer body with output recorded in real time by a two-channel strip-chart recorder. Full-scale span of the recorder can be varied to provide maximum sensitivity of the recorded data.

The CPT soundings were performed with the previously described instrument and Fugro's truck-mounted cone penetrometer unit. This unit has a self-contained hydraulic system which pushes the penetrometer, and an electric system to record the data. The truck weight, approximately 20 tons, provides the reaction force as the cone rods are pushed into the soil.

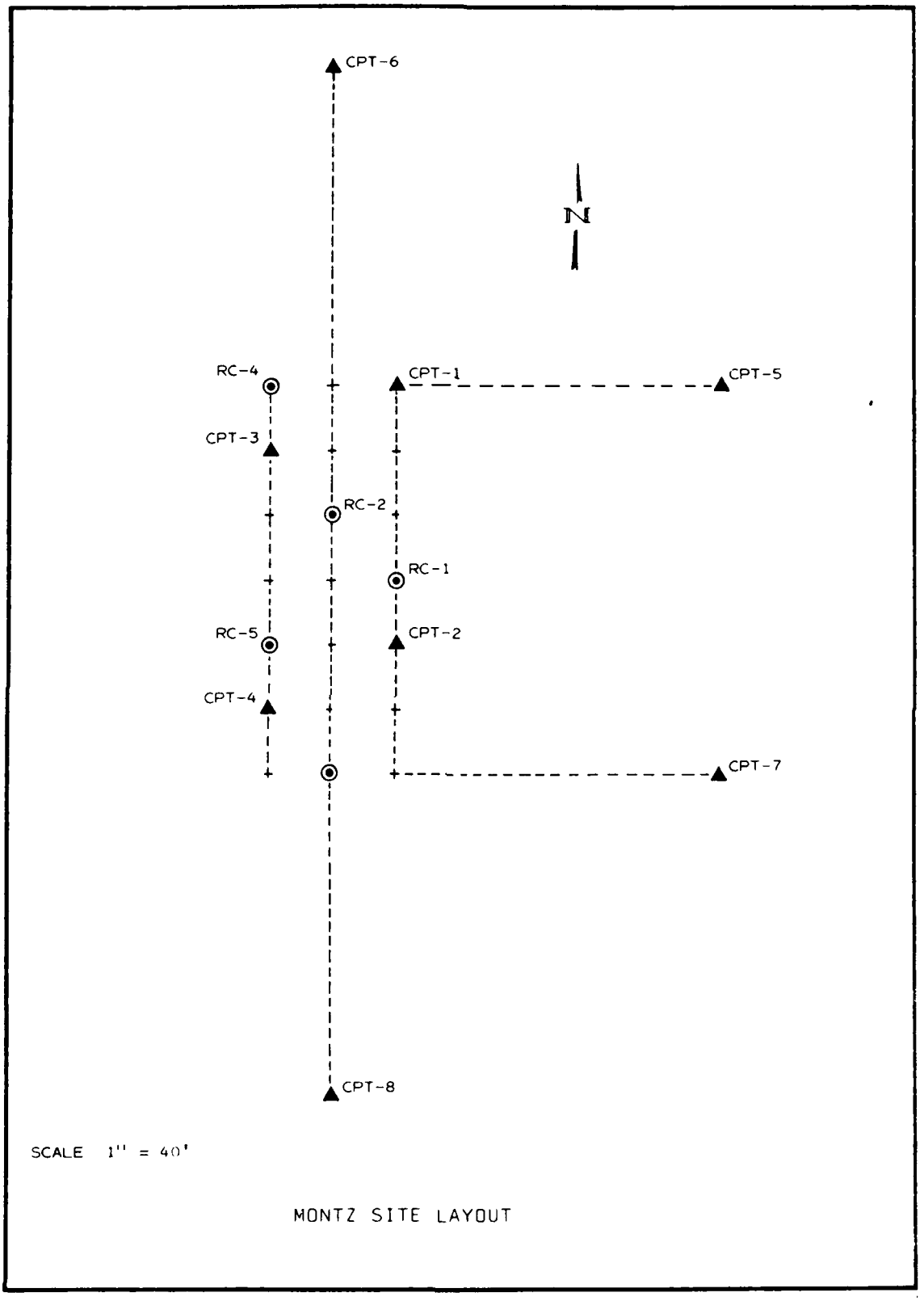
Results of the CPT program are shown on Plates 3 through 14. The solid lines represent cone tip resistance, qc; the dashed lines show the unit resistance on the friction sleeve, fs. Also shown, on the left side of the logs, are calculated "friction ratios". The friction ratio is defined as fs/qc expressed as a percentage.

We have appreciated the opportunity to work with you on this project. If you have any questions concerning the logs, please contact us.

Very truly yours,

Charles D. Oliver
Manager of Onshore Projects

Enclosures
CDO/dj

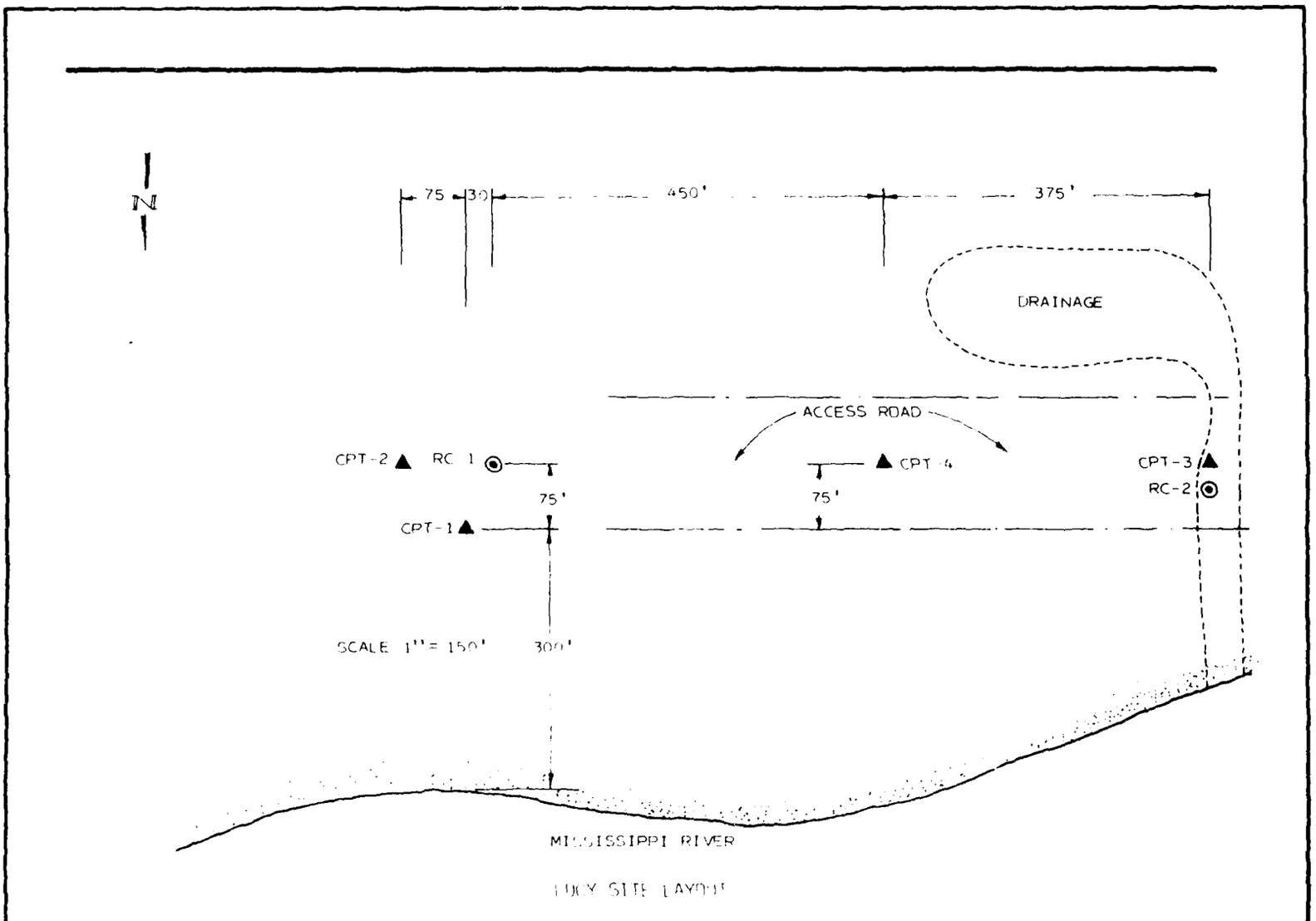


SCALE 1" = 40'

MONTZ SITE LAYOUT

PLATE 1

PLATE 2



BUOY SITE LAYOUT

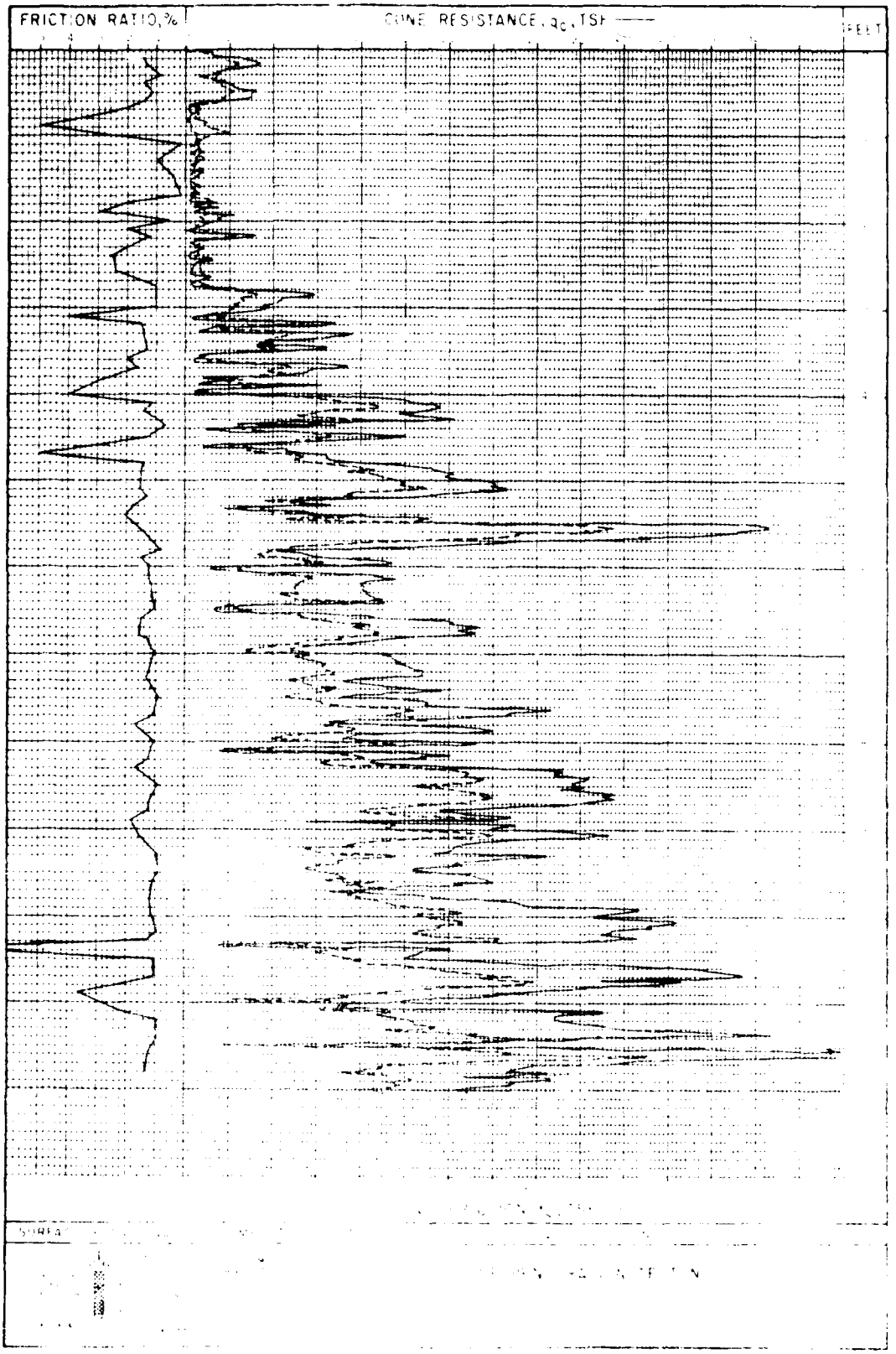
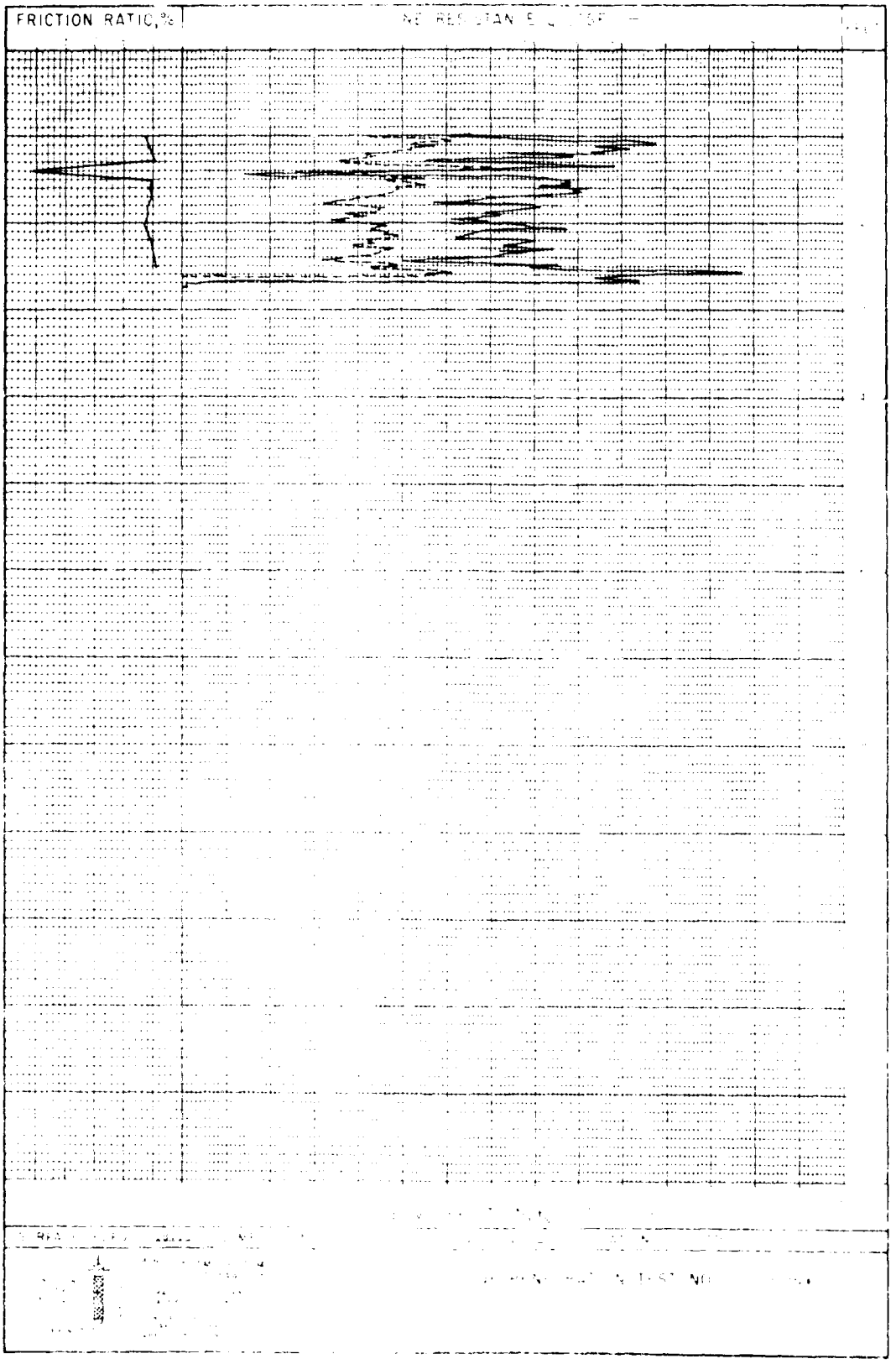
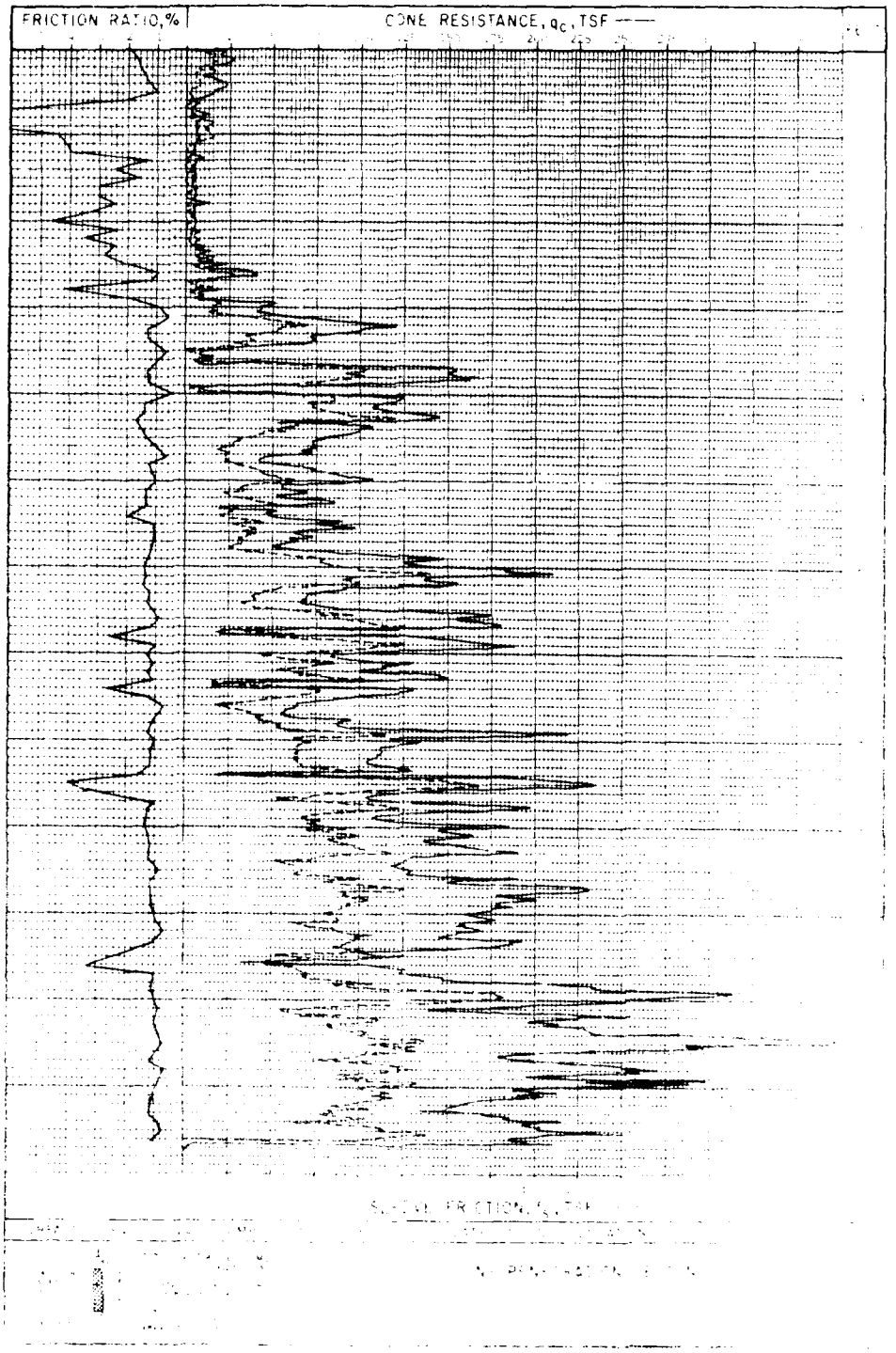
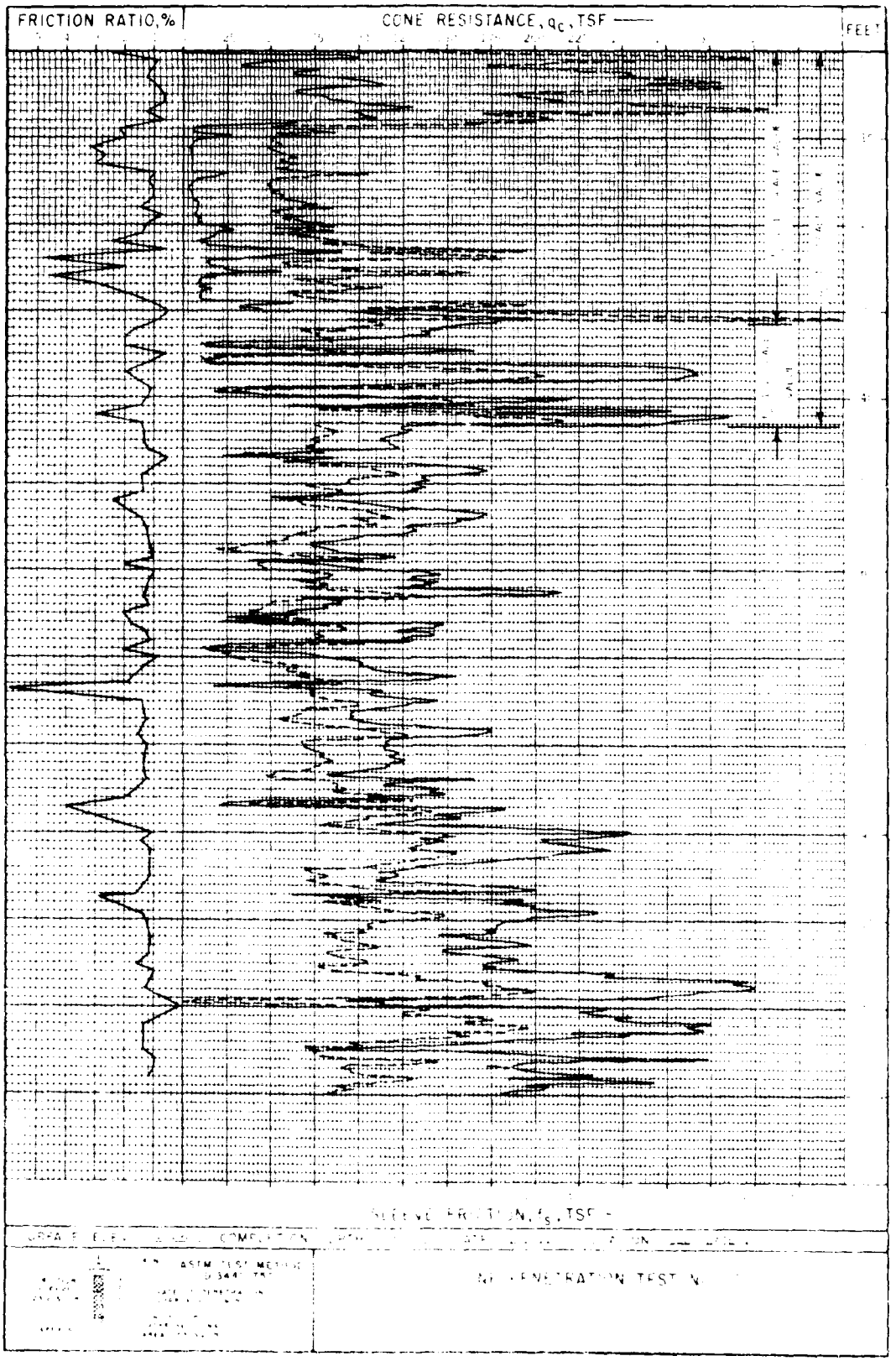
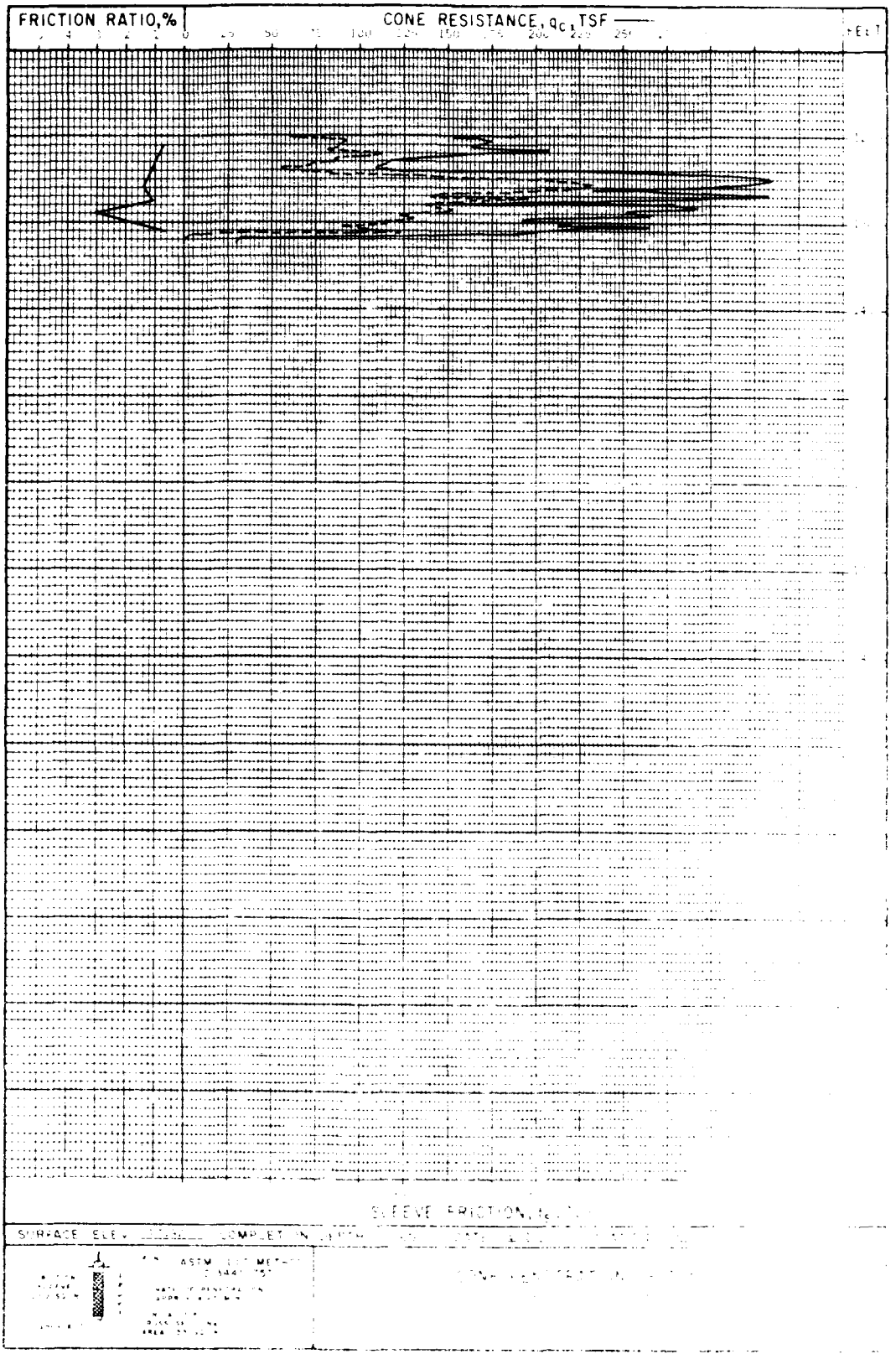


PLATE 3


FRICTION RATIO, %


FRICTION RATIO, %
CONE RESISTANCE, q_c, TSF


FRICTION RATIO, %
CONE RESISTANCE, q_c, TSF
FEET
SLEEVE FRICTION, f_s, TSF


FRICTION RATIO, %
CONE RESISTANCE, q_c, TSF
FEET
SLEEVE FRICTION, f_s, TSF

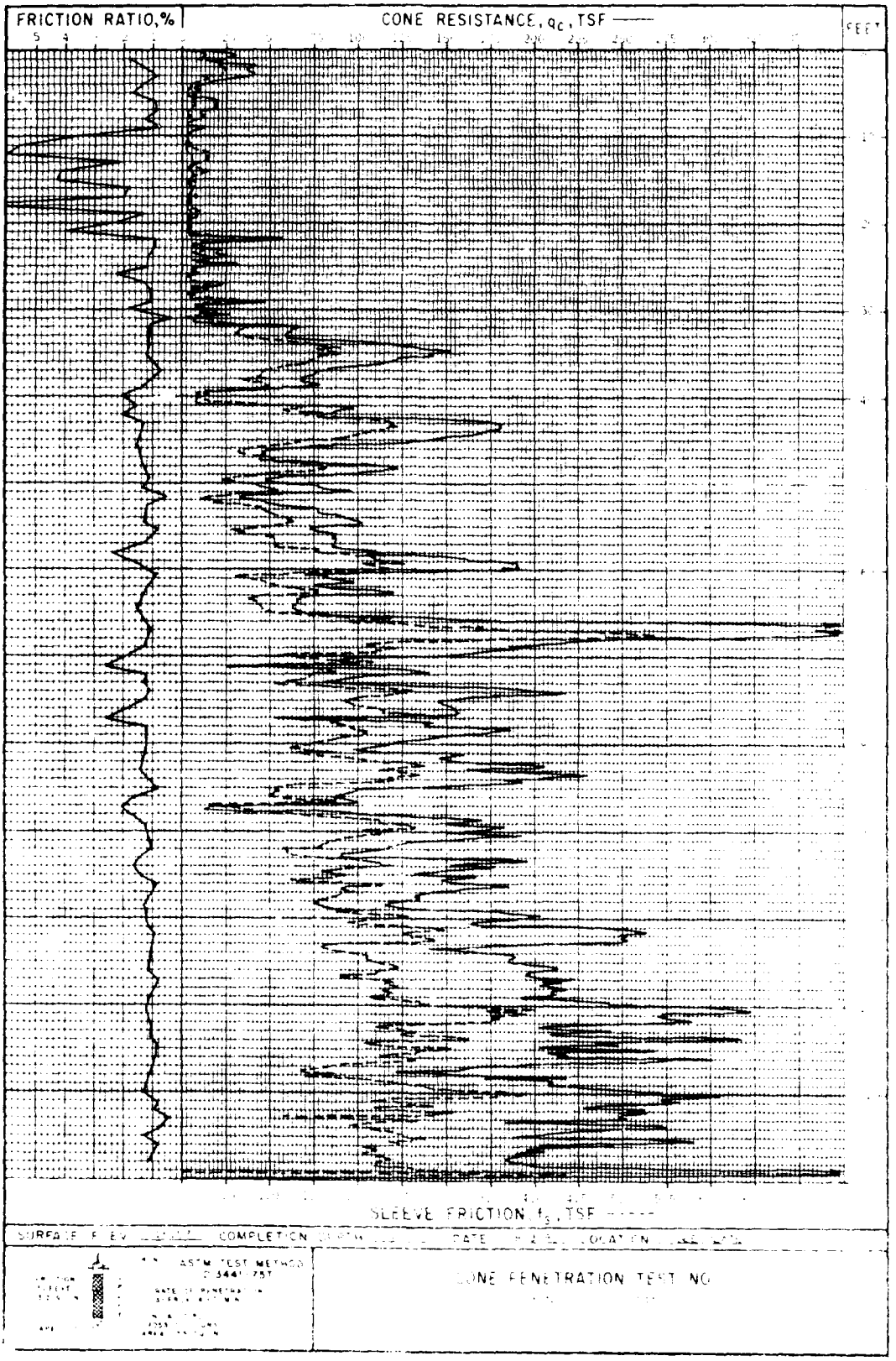
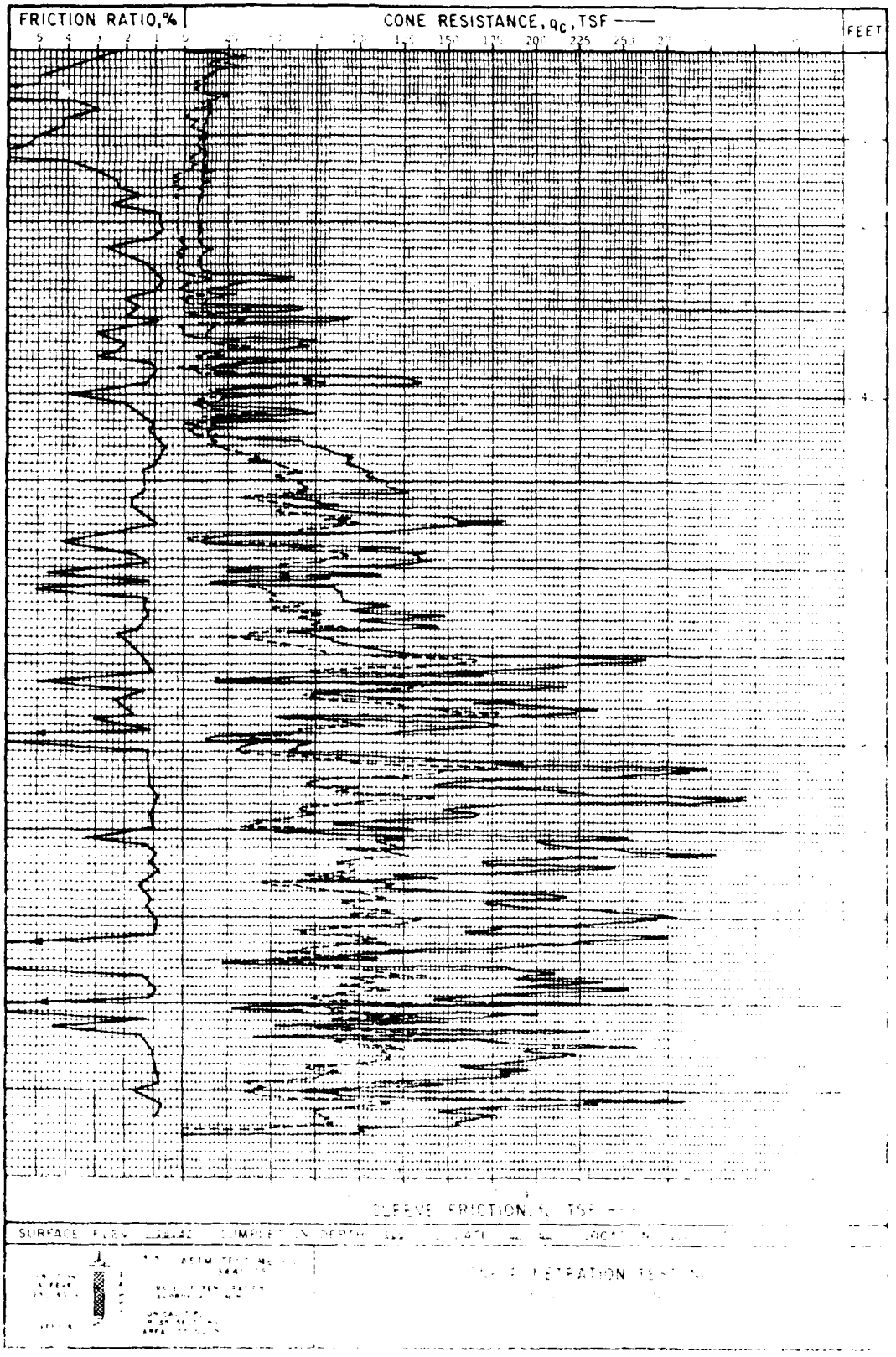

FRICTION RATIO,%
CONE RESISTANCE, q_c, TSF
FEET
SLEEVE FRICTION, f_s, TSF
ASTM TEST METHOD
D 3441-75T
CONE PENETRATION TEST NO.

PLATE 4


FRICTION RATIO, %
CONE RESISTANCE, q_c, TSF
FEET
SLEEVE FRICTION, f_s, TSF

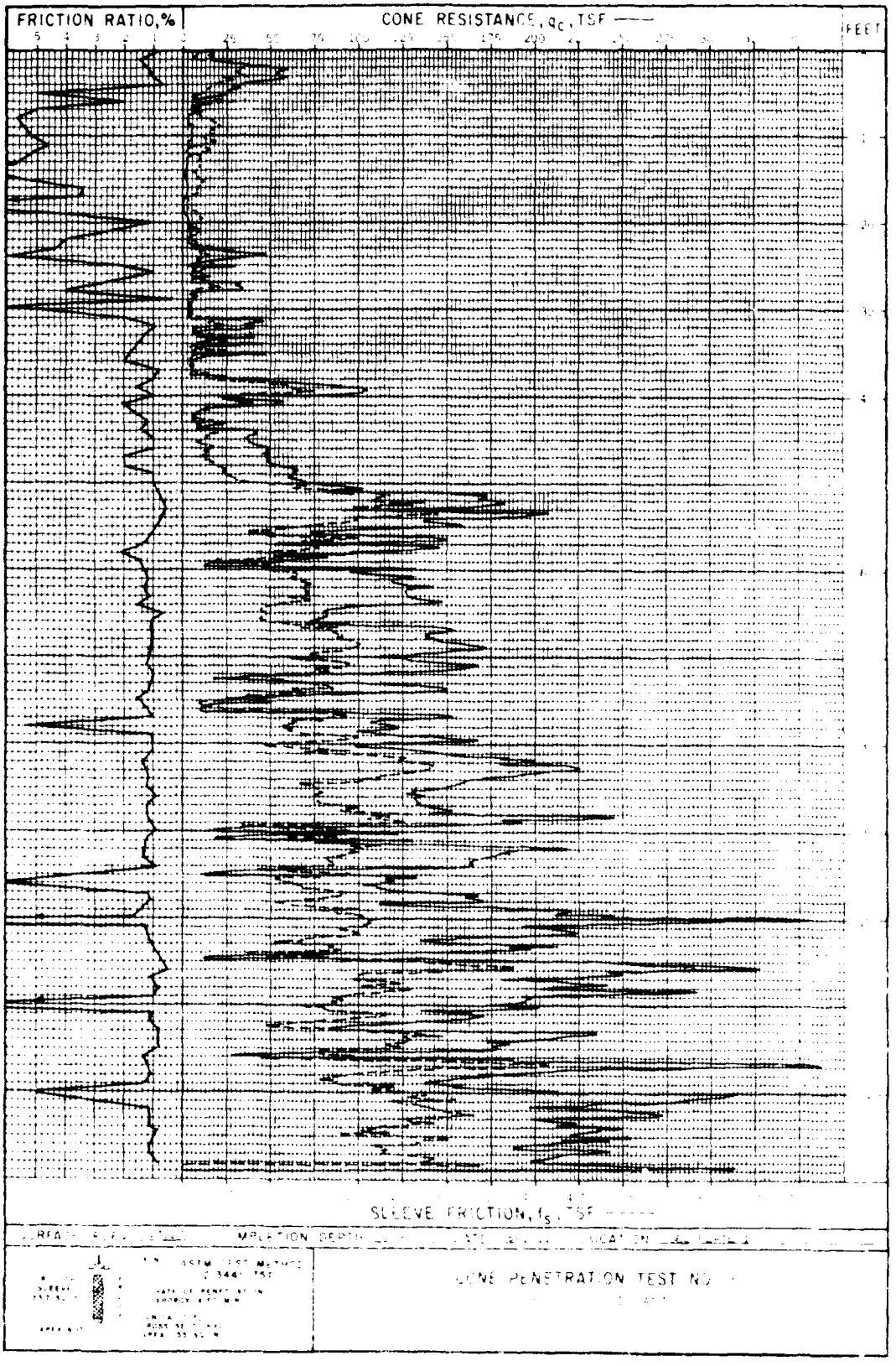
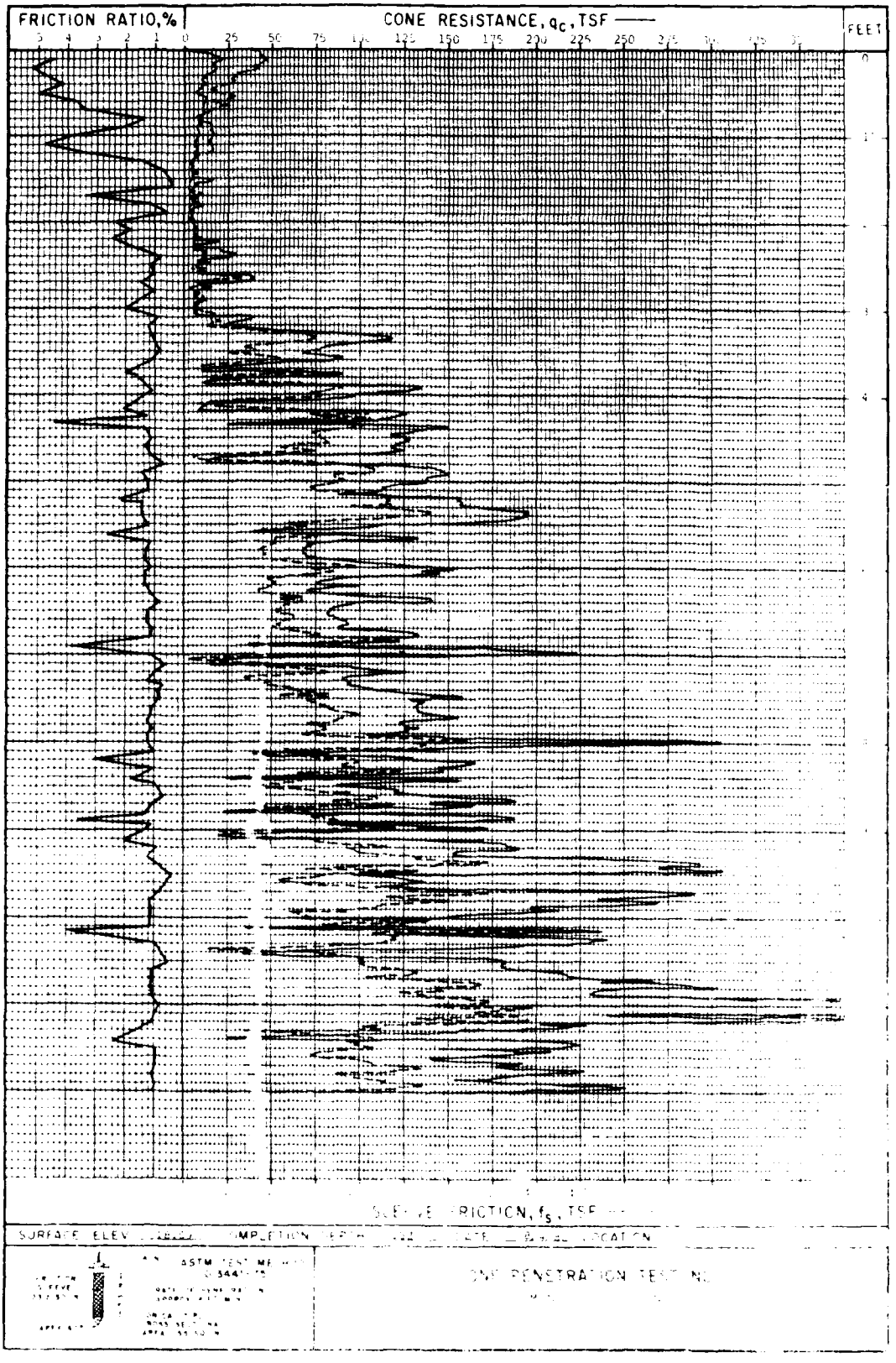

FRICTION RATIO, %
CONE RESISTANCE, q_c, TSF
FEET
SLEEVE FRICTION, f_s, TSF
CONE PENETRATION TEST NO.

PLATE 1


FRICTION RATIO,%
CONE RESISTANCE, q_c, TSF
FEET
SLEEVE FRICTION, f_s, TSF
SURFACE ELEV.
COMPLETION
LOCATION
ASTM TEST METHOD D 3441-75
CONE PENETRATION TEST NO.

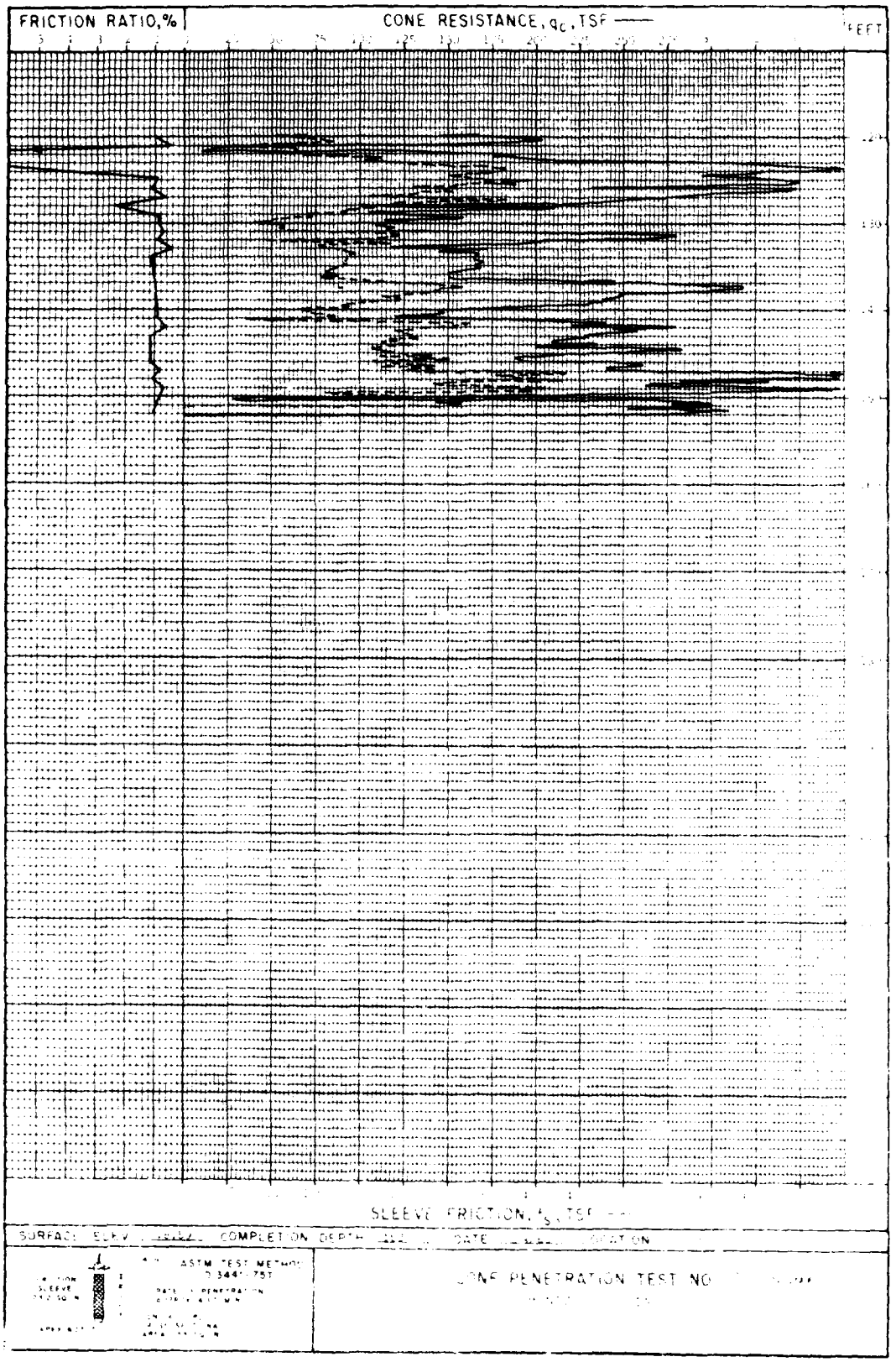
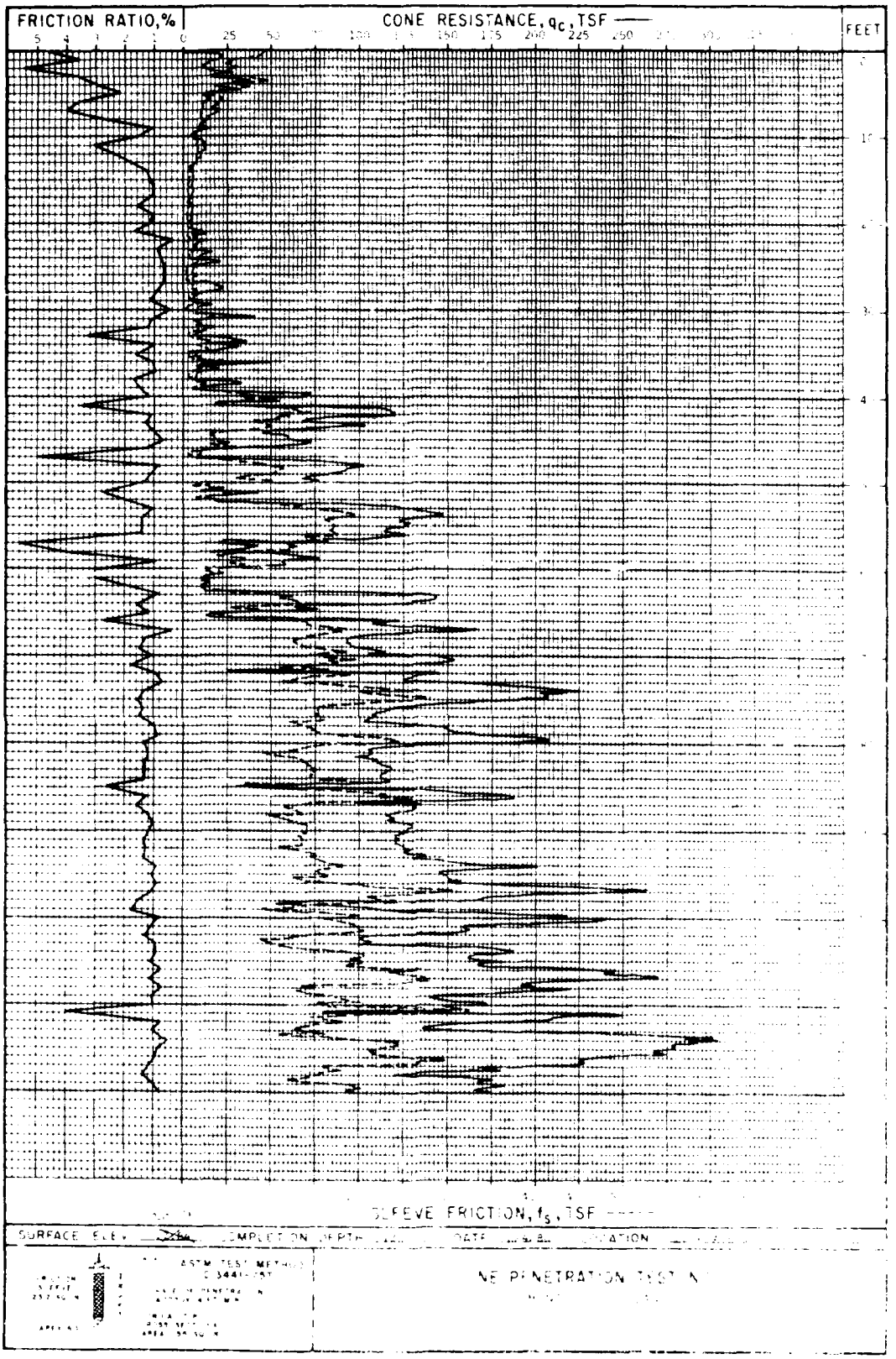

FRICTION RATIO,%
CONE RESISTANCE, q_c, TSF
FEET
SLEEVE FRICTION, f_s, TSF
SURFACE ELEV.
COMPLETION DEPTH
DATE
LOCATION
ASTM TEST METHOD
D 3441-75T
CONE PENETRATION TEST NO.

PLATE 12


FRICTION RATIO,%
CONE RESISTANCE, q_c, TSF
FEET
SLEEVE FRICTION, f_s, TSF
SURFACE ELEV.
COMPLETION DEPTH
DATE
LOCATION
ASTM TEST METHOD
D 3441-75T
NE PENETRATION TEST N

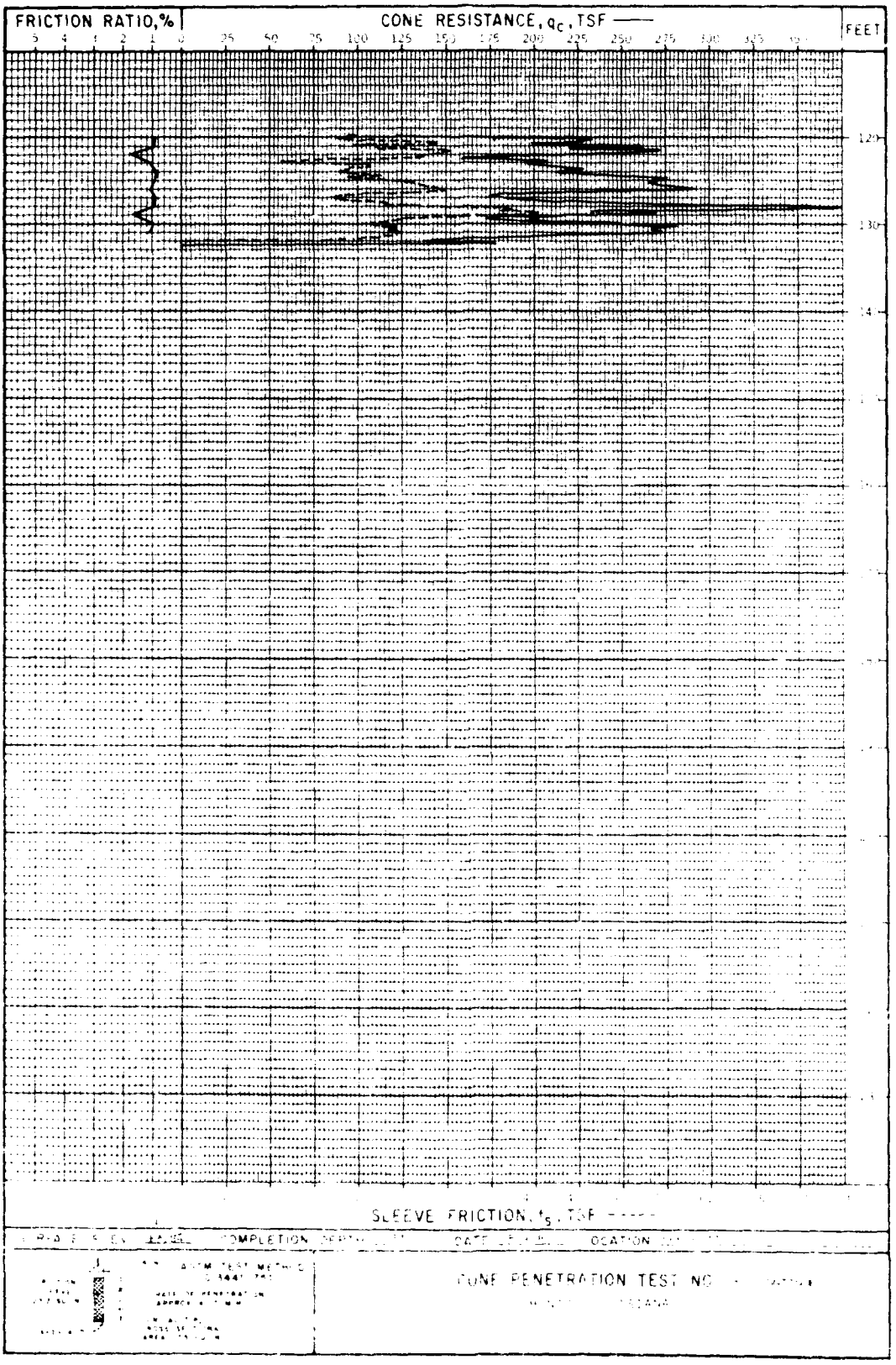
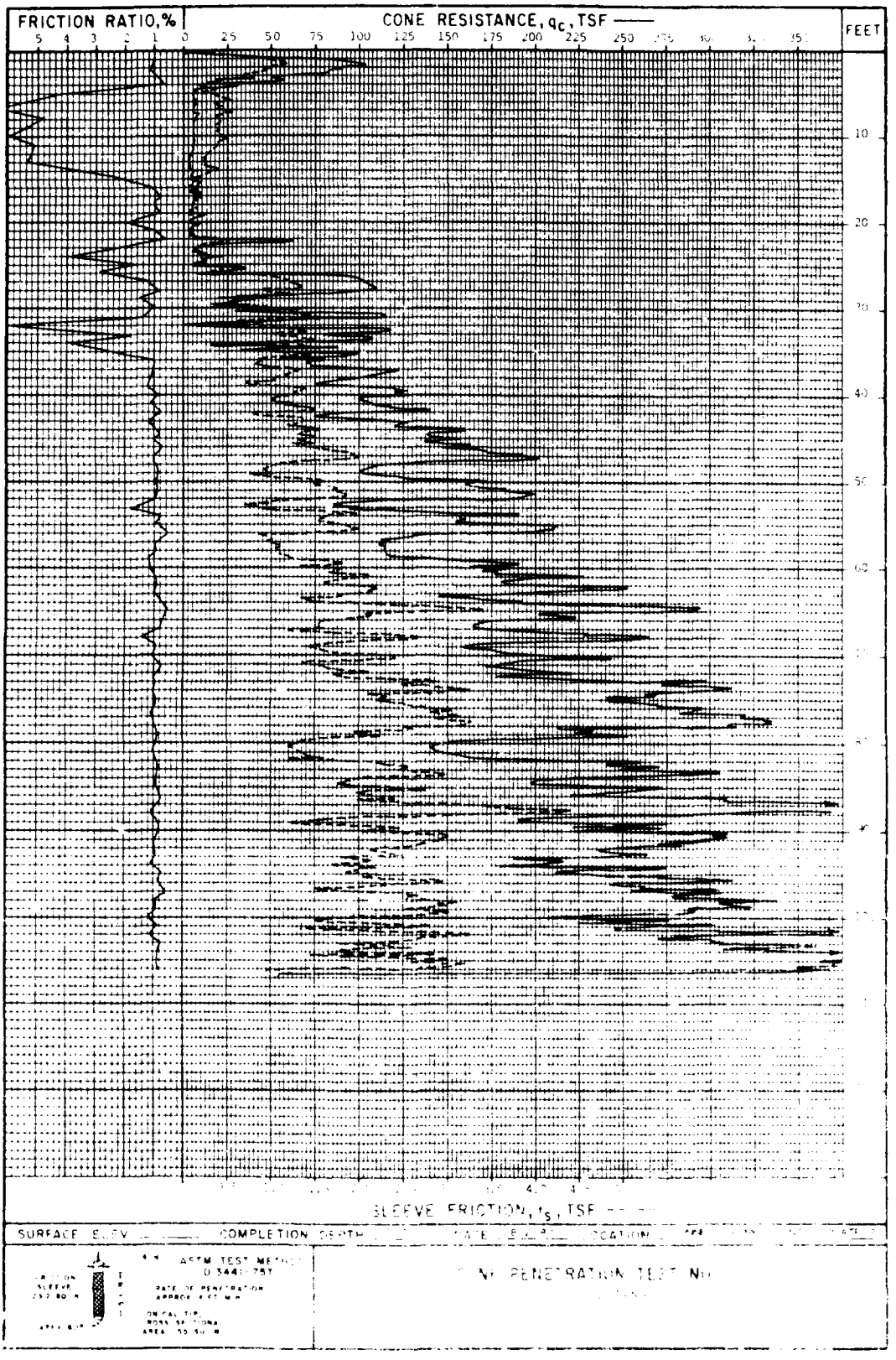

FRICTION RATIO, %
CONE RESISTANCE, q_c, TSF
FEET
SLEEVE FRICTION, f_s, TSF
CONE PENETRATION TEST NO.

PLATE 11


FRICTION RATIO,%
5 4 3 2 1 0
CONE RESISTANCE, q_c, TSF
0 25 50 75 100 125 150 175 200 225 250
FEET
10
20
40
50
60
SLEEVE FRICTION, f_s, TSF
SURFACE ELEV.
COMPLETION DEPTH
DATE
LOCATION
ASTM TEST METHOD
D 3441-75T
RATE OF PENETRATION
APPROX. 4 CM/SEC
PENETRATION TEST NO.

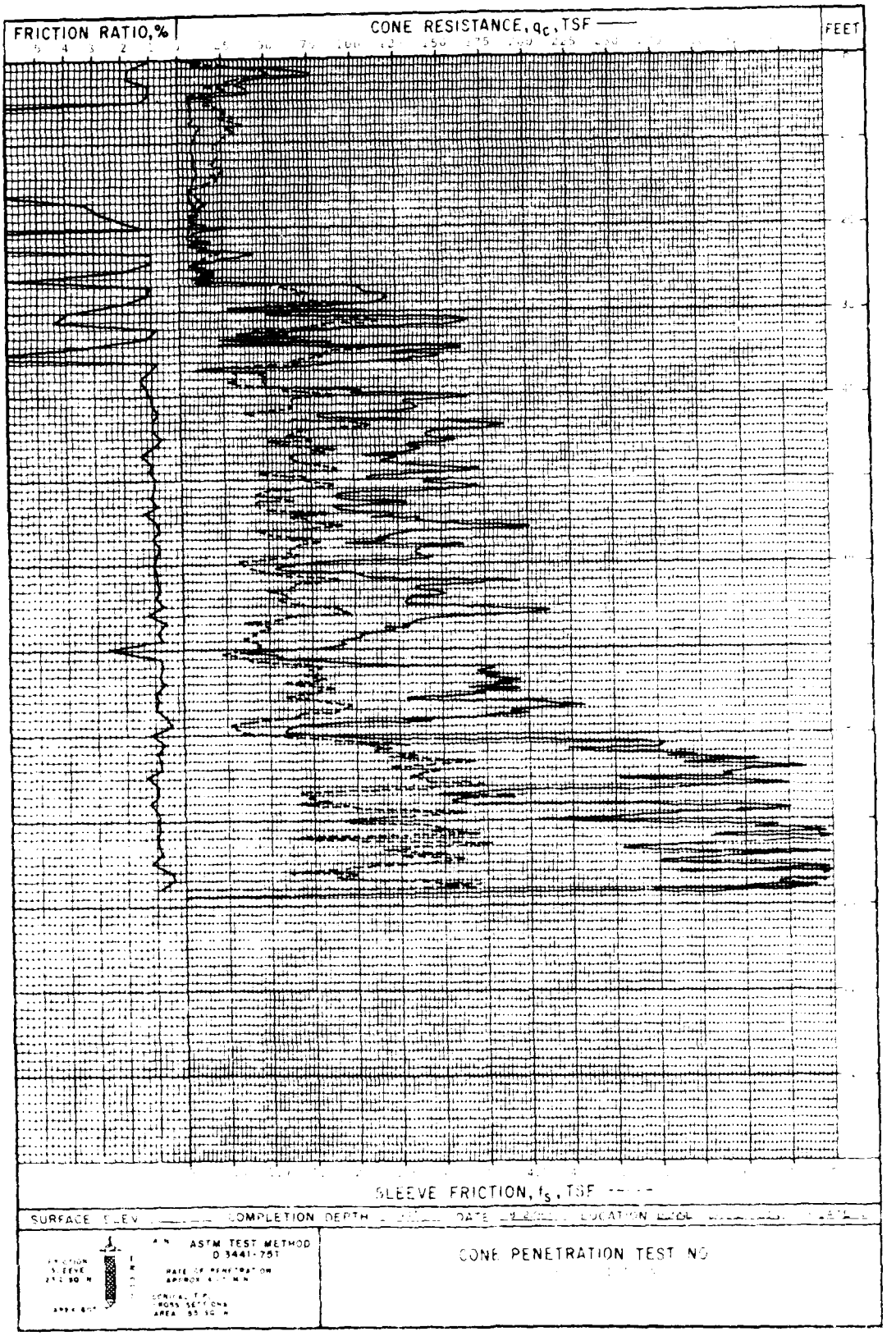
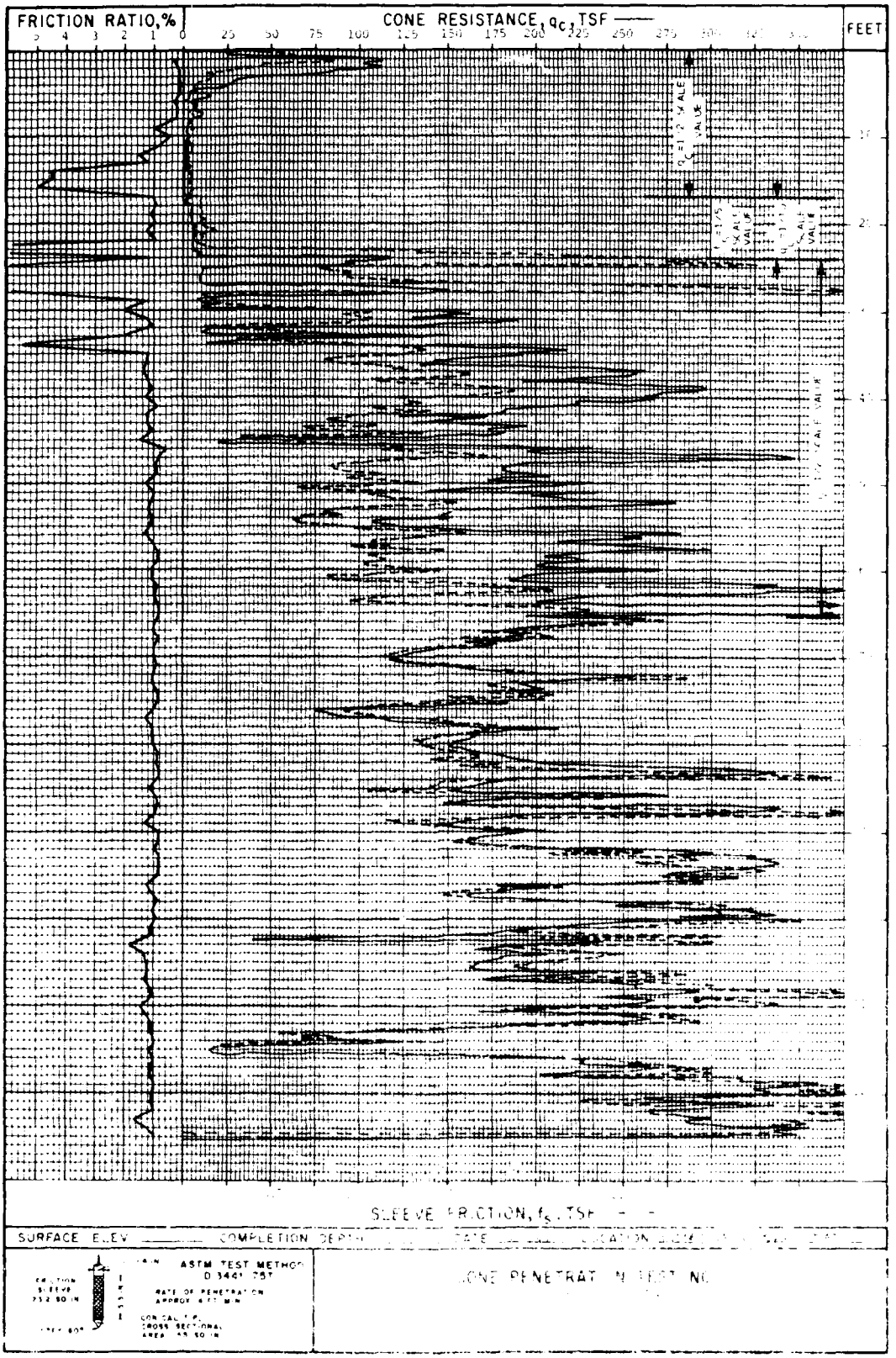

FRICTION RATIO, %
CONE RESISTANCE, q_c, TSF
FEET
SLEEVE FRICTION, f_s, TSF
SURFACE ELEV.
COMPLETION DEPTH
DATE
LOCATION
ASTM TEST METHOD
D 3441-75T
CONE PENETRATION TEST NO.

PLATE 16


FRICTION RATIO, %
CONE RESISTANCE, q_c, TSF
FEET
SLEEVE FRICTION, f_s, TSF
SURFACE ELEV.
COMPLETION DEPTH
DATE
LOCATION
ASTM TEST METHOD
D 3441-75T
RATE OF PENETRATION
APPROX. 4 FT./MIN.
CONE PENETRATION TEST NO.

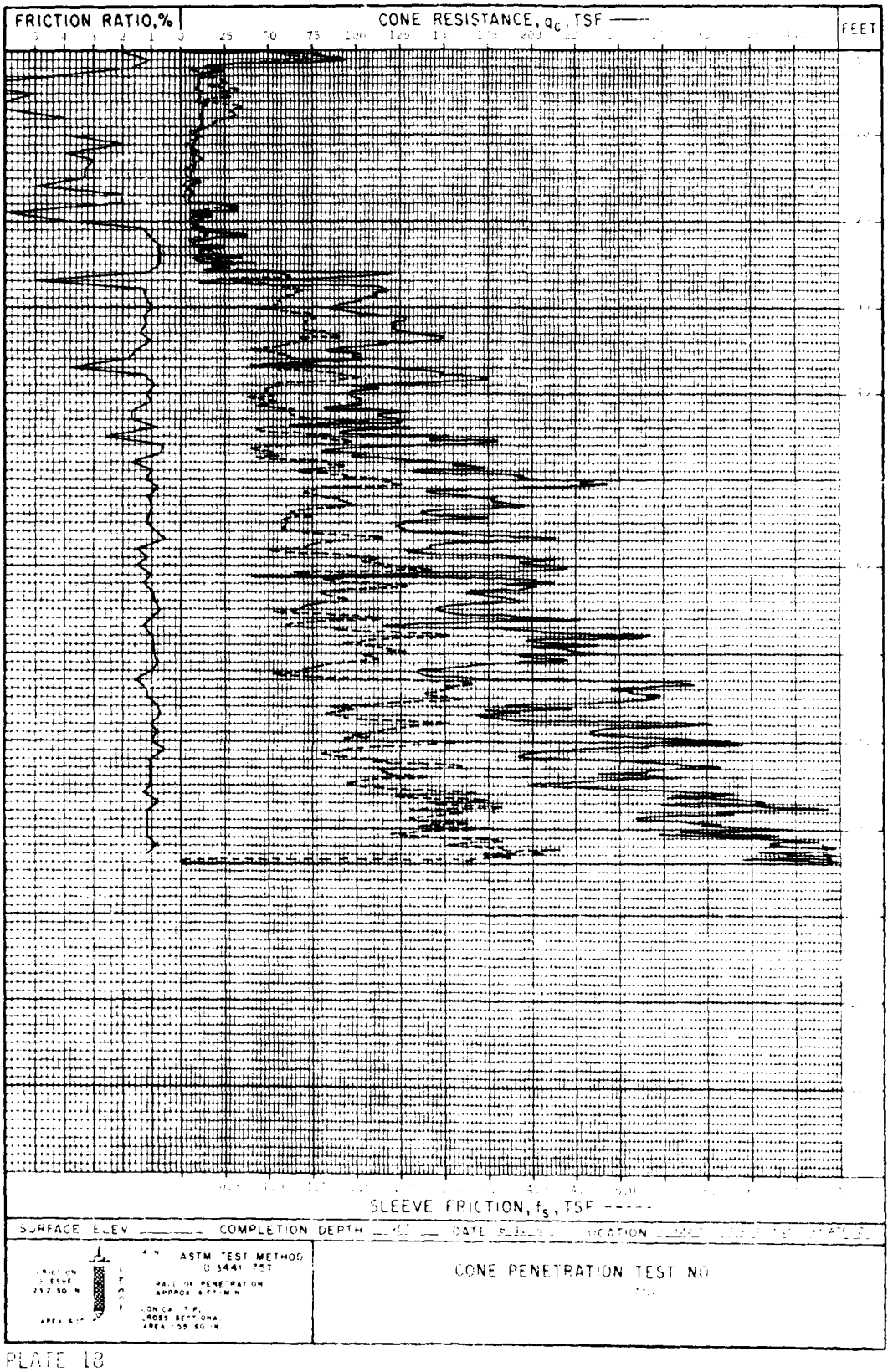

FRICTION RATIO,%
CONE RESISTANCE, q_c, TSF
FEET
SLEEVE FRICTION, f_s, TSF
SURFACE ELEV
COMPLETION DEPTH
DATE
LOCATION
ASTM TEST METHOD
D 3441 75T
CONE PENETRATION TEST NO

PLATE 18

APPENDIX G

ELECTRICAL RESISTIVITY CONE PENETRATION TESTS, DELFT SOIL MECHANICS LABORATORY, CONTRACT REPORT

laboratorium voor grondmechanica delft
delft soil mechanics laboratory

stichting waterbouwkundig laboratorium

p.o. box 69 2600 AB delft
2 stieltjesweg delft
the netherlands
telephone 31 (0)15 569223
telex 38234 soilab nl
postal account 234342
bank mees en hope nv delft
25 92 35 311

RESULTS OF DENSITY MEASUREMENTS ALONG THE MISSISSIPPI RIVER AT THE MONTZ AND BONNET CARRE SITES, LOUISIANA

REPORT BO-253500/63

JANUARY 1981

In this report, compiled by ir. H.L. Koning of the Delft Soil Mechanics Laboratory, the results and conclusions of the density investigations at the Montz and Bonnet Carré sites, Louisiana, are presented to the U.S. Army Corps of Engineers, Waterways Experiment Station, Vicksburg, Miss.

January, 1981

CONTENTS

1. Introduction

2. Description of the density measurement in situ

3. Results of the laboratory testing

4. Results of site investigation Montz site, Louisiana

5. Results of site investigation Bonnet Carré site, Louisiana

6. Summary and conclusions

***

LIST OF ANNEXES

1	Montz site, Louisiana. Plan of site investigations			
2	Bonnet Carrè site, Louisiana. Plan of site investigations			
3	Montz site. Sand calibration test samples			1 + 2
4	"	"	"	3
5	"	"	"	4 + 5
6	"	"	"	6 + 7
7	"	"	"	12 + 13
8	"	"	"	14 + 15
9	"	"	"	16 + 17
10	"	"	"	18
11	"	Summary of sand calibration tests		
12	"	Visual examination of samples		
13	Bonnet Carrè site. Sand calibration test samples			8 + 10
14	"	"	"	9 + 11
15	"	Summary of sand calibration tests		
16	"	Visual examination of samples		
17a,b	Montz site. Density measurement			RC-1
18a,b	"	"		RC-2
19a,b	"	"		RC-3
20a.b	"	"		RC-4
21a.b	"	"		RC-5
22a,b	Bonnet Carrè site	"		BRC-1
23a,b	"	"		BRC-2

1. Introduction

Many flow slides have been observed on the banks of the Mississippi river. The occurrence of these flow slides is attributed to the existence of loosely packed sandlayers. Consequently it is important to determine the porosity of the sandlayers in situ and to compare this porosity with the critical density, determined in the laboratory. For that reason the U.S. Army Corps of Engineers, Waterways Experiment Station, Vicksburg, Miss. decided to determine the porosity in situ with the aid of the method developed by the Delft Soil Mechanics Laboratory (DSML), the Netherlands.

These field investigations were planned at two sites in the New Orleans, Louisiana area. At site number one, the Montz site, the execution of five soundings to a depth of 120 feet was demanded. At site number two, the Bonnet Carré site, it was judged sufficient to make two soundings to a depth of 90 feet. At either site no testing was required in the surface clay layers to a depth of 30 feet.

In these investigations DSML worked as a subcontractor to Fugro Gulf, Inc., Houston, Texas. Fugro Gulf made a 20-tons gmf truck mounted cone penetration apparatus available with a two-men crew. DSML supplied the probes and the necessary electronic equipment with a field engineer to operate the device. The field measurements were carried out during the period July 14 to August 1, 1980.

In this report a short description of the density measurement in situ will be given. Then the results obtained at both sites will be discussed.

2. Description of the density measurement in situ

The density measurement of sand in situ is based on the fact that the sand grains consist of minerals which do not conduct an electric current. On the other hand the pore water is electrically conducting, especially if it contains dissolved salts. The more pores are present in a mass of sand, the lower is the electrical resistance of the total mass of soil However, this resistance is determined not only by the amount of water, but also by the electrical properties of the water itself. In can be shown now that the ratio of the specific electrical resistivity of the pore water to the specific electrical resistivity of the total mass of soil is a criterion of the porosity. So the field investigation consists of two measurements: viz. the specific electrical resistivities of the pore water and of the total mass of soil.

The specific electrical resistivity of the soil is determined by means of a "soil probe". This probe consists of a sounding tube supplied with four insulated electrodes. The probe is pushed into the ground by means of a sounding apparatus and at every 20 cm a reading is made. For this purpose a voltage difference is applied to the two outer electrodes and the resistivity of the soil is under non-load conditions determined with the aid of the two inner electrodes. The probe is supplied also with an electrical cone and a friction sleeve, so these quantities are obtained simultaneously. The depth which can be attained depends on the met cone and friction resistances and is practically equal to the depth attained in a normal static cone penetration test.

The specific electrical resistivity of the pore water is measured with the aid of a "water probe". This probe too consists of a sounding tube, now supplied with a filter and a measuring cell inside. The probe is pushed into the ground by means of a sounding apparatus and at regular intervals, normally 20 cm, a reading is made. Then some water is sucked through the filter into the measuring cell and its resistivity can be measured.

As stated above the ratio of these two resistivities is a criterion of the porosity. The theoretical determination of the connection between this ratio and the porosity is unfeasible, so a calibration curve is established in the laboratory. For this purpose a water-saturated sample with a known porosity is built up in a cylinder and the specific electrical resistivities of the saturated sand as well as of the porewater are measured. This test is executed at various porosities of the sample.

From the starting-points it follows that in principle this method of density measurement is not applicable in peat and clay layers, due to the electrical properties of these soils. Moreover, it follows that the sand deposit must be saturated. Some further information is given in the enclosed brochure "density measurement in situ and critical density".

3. Results of the laboratory testing

As mentioned in the preceding chapter calibration curves, relating the field measurements to the porosity, have to be established in the laboratory. For that purpose 18 samples were sent to DSML; 14 of these samples came from the undisturbed borings U-1 and U-2 at the Montz site and the remaining 4 samples were taken in the undisturbed boring U-1B at the Bonnet Carré site. The location of these borings is given in the plans of the site investigations on the annexes 1 and 2.

To determine the calibration curve a known weight of dry sand is poured into a cylinder such that a high porosity is obtained. After replacing the air by carbondioxide, the sample is saturated with water which has a specific electrical resistivity of - in this investigation - about 10 Ωm, corresponding to the in situ value of the pore water. Now the volume of the sample is measured and the porosity can be calculated. Then the specific electrical resistivities of the sample and of the porewater are determined. After that the sample is compacted somewhat and all measurements are done again. This procedure is repeated until four points of the calibration curve are determined.

The samples 1 through 11 were received on September 23, 1980. The calibrations of these samples gave unexpected results, so it was deemed necessary to determine the specific mass of the grains. The results of these determinations were such that it did not seem necessary to ascertain these specific masses of the samples 12 through 18, which arrived at DSML on October 8, 1980.

The results of the calibration tests on the samples 1 through 7 and 12 through 18, borrowed from the borings U-2 and U-1 respectively at the Montz site, are shown on the annexes 3 through 10. Annex 11 contains a summary of these calibration tests. When a number of samples, coming from a restricted area is calibrated, it usually is found that all calibration points lie within a narrow band in such a way that one calibration curve suffices. However, these sands unexpectedly showed much dispersion in the calibration results. As a rule the porosity is calculated from the volume and the weight of the sample by introducing a specific mass of the grain of 26,5 kN/m^3. From experience it is known that differences can be caused by a deviating specific mass, so it was deemed necessary to determine these masses. Nevertheless it was not possible to explain the above-mentioned deviations by the obtained results, which are shown on annex 12. So it remained to establish five calibration curves as shown on annex 11, the correct specific masses have been taken into account herein.

The results of the calibration tests on the samples 8 through 11, borrowed from boring U-1B at the Bonnet Carré site, are shown on annexes 13 and 14; the summary is shown on annex 15. After determination of the specific masses of the grains, the results of which are given on annex 16, the two calibration curves on annex 15 have been established.

As will be explained in the next chapter the grainsizes of the calibration samples have been determined visually. From the obtained data in general it follows that the calibration curve shifts to the right as the samples contain more fines. Why nevertheless in the graph on annex 11 calibration curve c of sample 15 deviates from

line b of samples 2, 3, 4, 14 and 16, while these samples have comparable grainsizes, is not known. It is possible that the shapes of the grains are different as it is known that the shape has a certain influence. The same remark can be made in relation to the calibration lines d and e.

4. Results of site investigation Montz site, Louisiana

At Montz site five density measurements were executed; their locations are shown on annex 1. In the measurements RC-1, RC-2 and RC-3 the required depth of 36 m-soil surface was attained; while executing the site investigations this depth was changed by the principal to 24,5 m - soil surface at the locations RC-4 and RC-5. As already mentioned in chapter 2 the cone resistance and the local skin friction are measured in the density measurement as well. The results of these measurements and their ratio are shown on annexes 17a through 21a. Except in location RC-2 these quantities have been read with intervals of 1 m in the surface claylayers also. Annexes 17b through 21b show the obtained values of the specific electrical resistivities of the total soil mass and of the porewater, just as the from these values derived porosities, the latter so far as the measurements were done in sandlayers.

Apart from the surface clay layers to a depth of about 10 m - soil surface two distinct layers can be distinguished in the results of the static cone penetration tests, viz. between about 10 en 25 m - soil surface and beneath 25 m - soil surface. The following numbers, obtained by eye-fitting, give a rough approximation of the tendencies of the measured quantities.

In the layer between 10 en 25 m - soil surface the overall mean of the cone resistance increases more or less gradually from 7 MN/m^2 at a depth of 10 m - soil surface to 13 MN/m^2 at a depth of 25 m - soil surface. However, values as low as 2 MN/m^2 are measured fairly frequently, whereas values higher than 20 MN/m^2 are scarce. The local skinfriction shows a similar course, to wit a gradual increase of the overall mean from 0,05 to 0,11 MN/m^2, with fairly frequently occurring low values of 0,02 MN/m^2 and scarce values higher than 0,16 MN/m^2.

The overall mean of the ratio of static cone resistance to local skin friction has a moderately constant value of about 140. Only a limited number of values higher than 250 has been obtained, but numerous values are got lower than from 80 to 100. According to Dutch experience these low values indicate the presence of clay or clayey layers.

In the layer beneath 25 m - soil surface the overall mean of the static cone resistance increases gradually from 15 MN/m^2 at a depth of 25 m - soil surface to 20 MN/m^2 at a depth of 36 m - soil surface. Most values are bounded by 10 and 25 MN/m^2. On the other hand the local skin friction in general shows a somewhat decreasing tendency in this layer. The overall mean value decreases from 0,12 to 0,10 MN/m^2 at depths of 25 and 34 m - soil surface respectively and then increases to 0,12 MN/m^2 at a depth of 36 m - soil surface. The bordering values of the local skin friction in this layer are 0,06 and 0,16 MN/m^2.

In consequence of these tendencies the ratio of the static cone resistance to the local skin friction shows some increase between 25 and 34 m - soil surface, viz. from about 140 to about 180 and then a slight decrease to 170 at a depth of 36 m - soil surface. In this layer the ratio is bounded by values of about 100 and 260.

As already mentioned in chapter 3 five calibration curves had to be established to determine the porosity of the sandlayers at Montz site. Consequently the determination of the porosities from the field measurements produced many difficulties. It goes without saying that the main problem was to ascertain which calibration curve had to be used in a specific layer. It turned out that at Montz site a number of standard penetration tests was executed and that the grainsize distributions from the SPT-samples were determined. This data, comprising D90, D50 and the percentage passing the no. 200 sieve was made available to DSML. However, to use these results it was necessary

to investigate the grainsize distributions of the calibration samples. For simplicity this was done visually with the aid of a magnifying-glass by comparing with standard fractions of known grainsizes. In this way the range and the mean value of the grainsizes present in the calibration samples were assessed; the results of these determinations are shown on annex 12.

It soon became clear that the comparison of the grainsizes of the SPT-samples and of the calibration samples was a minor help only. Probably this was due to the differences in estimating the grainsize distributions and to the small number of calibration samples. So the selection of the calibration curves was made by judgement of the results of the static cone penetration test and of the measured specific electrical resistivities. The determined porosities are shown on annexes 17b through 21b; beside the graphs the calibration curves that are used are pointed out.

In the graphs of the porosity versus depth the same two layers as described above can be distinguished, viz. between about 10 and 25 m - soil surface and beneath 25 m - soil surface. A rough indication of the tendencies of the porosities, obtained by eye-fitting again, is given below.

In the sand layers between 10 and 25 m - soil surface the overall mean of the porosity increases from about 47% at a depth of 10 m - soil surface to about 50% at a depth of 22 m - soil surface and then decreases to about 46% at a depth of 25 m - soil surface. In the layer beneath 25 m - soil surface the overall mean of the porosity decreases from about 44% to about 41% at depths of 25 and 35 m - soil surface respectively.

As mentioned before the ratio of the cone resistance to the local skin friction indicates that there are numerous clay or clayey layers between 10 and 25 m - soil surface. This is confirmed by the results of the density measurement. In these clay or clayey layers very high porosities are determined. But as it is explained in chapter 2, the applied method of density measurement in principle does not work in

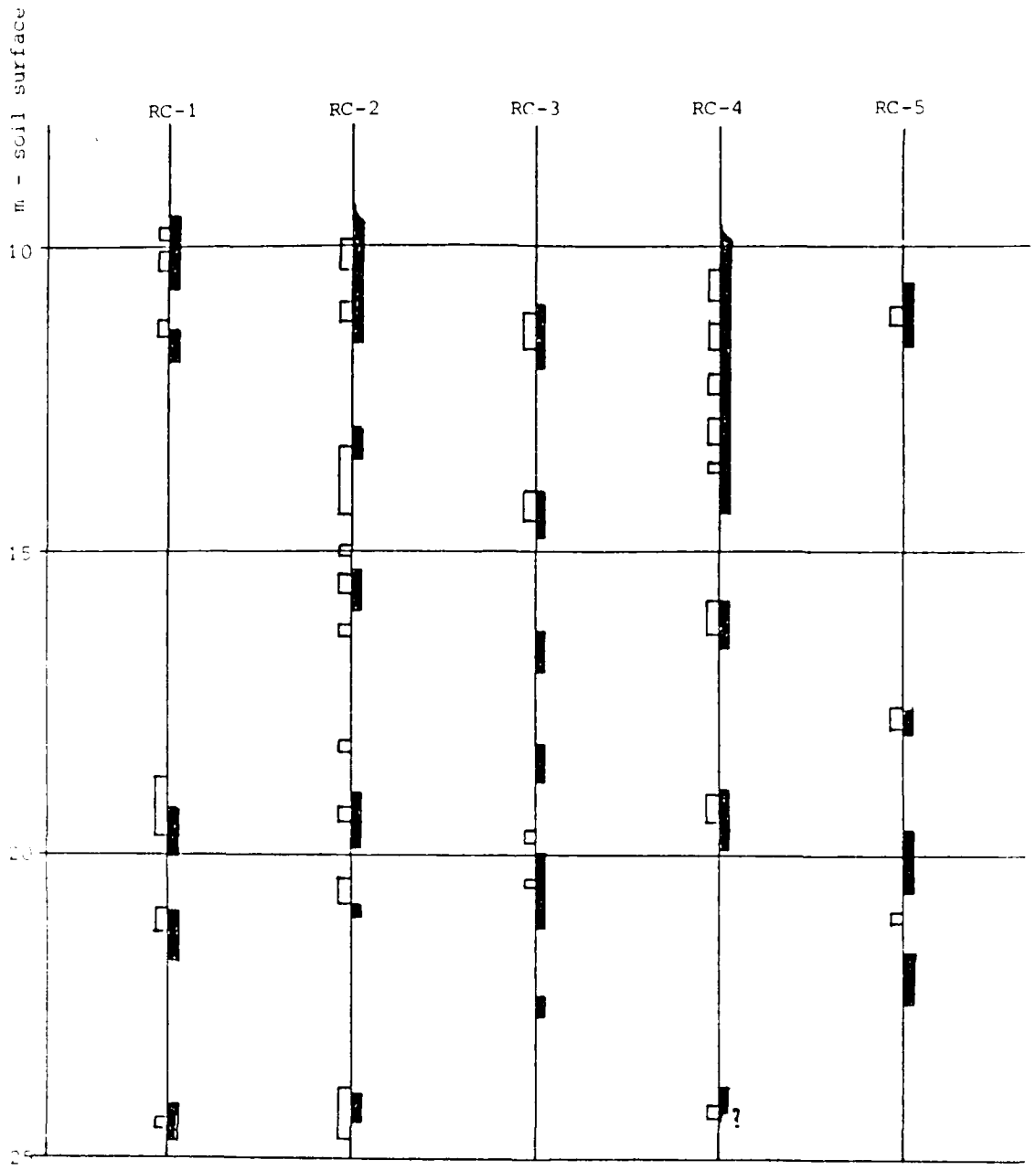
clay layers and therefore the calculated values are not included in the graphs. In general due to the extent of the influenced zone around the probe the thickness of claylayers is exaggerated somewhat. Apart from that the correspondence between the depths of the clay layers determined with the aid of both methods, is very good. In some cases (RC-3 and RC-5) the density measurement seems more sensitive to the presence of clay layers than the mentioned ratio, a property that has been met before in several other investigations.

In the figure on the following page the several clay layers determined with the aid of the ratio of the cone resistance to the local skinfriction (according to Dutch experience) and of the density measurement are predicted schematically. It seems that to a depth of about 12 m - soil surface, claylayers extend over the whole site. Likewise there seems to be a continuous claylayer at a depth from 19 to 21 m - soil surface, which layer dips somewhat from RC-2 and RC-4 to RC-5 and RC-3. Between these two claylayers and between 21 and 25 m - soil surface claylayers of restricted extent are present locally.

In general the porosities in the sandlayers between 10 and 25 m - soil surface fluctuate between 46 and 51%. However, in some locations lower porosities have been found:

- in RC-3 and RC-5 between 12 and 14 m - soil surface porosities from 40 to 44%,
- in RC-4 and RC-5 between 15 and 16 m - soil surface a porosity of about 44%,
- in RC-1, RC-2 and RC-3 between 22,5 and 23,5 m - soil surface porosities from 40 to 43%.

Beneath 25 m - soil surface the determined porosities show a decreasing tendency. The ascertained values in general are less than in the sandlayers above. This is in correspondence with the fact that in the layer referred to coarser sand is present as



Claylayers corresponding to

ratio $\frac{\text{cone resistance}}{\text{local skinfriction}}$ (Dutch experience)

density measurement

follows from the visual examination of the samples (annex 12). The upper boundary of the porosities amounts to about 48%; the lower boundary between 25 and 30 m - soil surface amounts to about 40% and between 30 and 35 m - soil surface to about 38%. At some depths rather high porosities (about 50%) have been determined. It is not clear whether these high values are caused by the presence of clay, the results of the static cone penetration tests do not indicate that.

The background of the execution of these density measurements is to investigate whether the sandlayers are susceptible to liquefaction due to some triggering mechanism. When the circumstances are unfavourable a flow slide can occur then. In a quasi-static case the porosity in situ has to be compared with the critical density, determined in the laboratory. Apart from that the presence of the clay or clayey layers in the deposit between 10 and 25 m - soil surface seems to be a favourable factor. When such a layer has a sufficient extent and thickness it is deemed that a potential flow slide will be stopped by bending down of the clay layer and in this way blockading the flowing sand.

5. Results of site investigation Bonnet Carré site, Louisiana

At Bonnet Carré site, Louisiana two density measurements have been executed as shown in the plan of site investigations on annex 2. Measurement BRC-1 has been performed to the required depth of 27 m - soil surface and BRC-2 to a depth of 20 m - soil surface according to a replacement by the principal during the execution of the field measurements. The cone resistances and local skin friction and their ratio are depicted on annexes 22a and 23a. The obtained values of the specific electrical resistivities of the soil and of the porewater, just as the in the sandlayers derived porosities, are shown on annexes 22b and 23b. The results are diverging in such a way that a combined treatment is not well possible.

In location BRC-1 two layers can be specified beneath the surface clay layers to a depth of about 10 m - soil surface. In the layer between 10 and 17,5 m - soil surface the mean value of the cone resistance gradually increases from 7 to 14 MN/m^2; these resistances are bounded by 7 and 15 MN/m^2. The local skinfriction also snows an increase, on the average from 0,06 to 0,07 MN/m^2, with extreme values of about 0,05 and 0,09 MN/m^2. The ratio of these two quantities fluctuates between 90 and 300, with the mean value increasing from 130 to 200.

Beneath 17,5 m - soil surface to the attained depth of 27 m - soil surface higher values of these quantities have been measured. The cone resistances fluctuate between 16 and 35 MN/m^2; the average values increase from 22 to 26 MN/m^2. The value of the local skinfriction increases from 0,10 to 0,11 MN/m^2 on an average with boundaries of 0,07 and 0,16 MN/m^2. The mean value of the ratio of the cone resistance to the local skinfriction increases from 210 to 240; this ratio is bounded by 160 and 310.

In the static cone penetration test in location BRC-2 lower values have been attained than in location BRC-1. In the layer between 10 and 13,5 m - soil surface the mean value of the cone resistances decreases from 10 to 5 MN/m^2; the boundary values in this layer are 4 and 10 MN/m^2. The local skinfriction also decreases, viz. from 0,055 to 0,035 MN/m^2 on the average; these friction values fluctuate between 0,03 and 0,06 MN/m^2. The ratio of the cone resistance to the local skin friction fluctuates between 120 and 220, with the mean value decreasing from 170 to 150.

In the layer beneath 13,5 m - soil surface to the reached depth of 20,5 m - soil surface the cone resistances show an increase, on the average from 11 to 17 MN/m^2, with extreme values of 10 and 20 MN/m^2. The local skinfriction fluctuates between 0,05 and 0,10 MN/m^2; the average value increases from 0,05 to 0,09 MN/m^2. The mean of the ratio of these two quantities shows a decrease from 210 to 190; the boundaring values of this ratio are 140 and 300.

The porosities had to be determined with the aid of the two calibration lines shown on annex 15. Also from these samples the specific masses of the grains were determined and the grainsizes were examined visually; the results are shown on annex 16. Apart from that the remarks made in chapter 4 on the determination of the layering also hold good for the Bonnet Carré site.

In the results got at location BRC-1 two layers have been distinguished. Between 11 and 17,5 m - soil surface the mean porosity increases from 35 to 41% with extreme values of about 33 and 41%. In the layer beneath 17,5 m - soil surface the porosity fluctuates between 35% and about 46%, apart from some porosities of over 50% at a depth of 21,5 m - soil surface. Possibly this is caused by the presence of clay, though this is not confirmed by the results

of the static cone penetration test. The mean value of the porosity is about 37% between 18 and 20 m - soil surface and about 39% beneath 24 m - soil surface to the reached depth; in between higher porosities of about 44% have been determined.

Location BRC-2 was at a distance of 146 m from location BRC-1. So the question aroses whether the calibration curves determined upon the samples 8 through 11 also are representative for location BRC-2. Comparison of the calibration lines on annexes 11 and 15 show that these lines fit nicely, so it was decided to answer the above question affirmative. A second question was related to the layering of the soil in location BRC-2. Based on the results of the static cone penetration test two layers were discriminated with the boundary at 13,5 m - soil surface. In the upper layer calibration curve f was supposed to be representative, in the lower layer calibration line g. Between 10 and 13 m - soil surface the porosity fluctuates between 50 and 41%. At a depth of 13,5 m - soil surface very high porosities were measured in a claylayer as indicated by the ratio of cone resistance and local skinfriction also. In the layer between 14 m - soil surface and the reached depth of 20 m - soil surface the porosity fluctuates between 43 and 51% with a mean value of about 47%. From this data it follows that the porosity in location BRC-2 is much higher than in location BRC-1.

The course of the specific electrical resistivities indicates the possibility that calibration curve f also can be representative in the layer beneath 13,5 m - soil surface. In that case the porosities in this layer are about 2% lower than is depicted on annex 23b. The above given comparison with the results at location BRC-1 still holds good, however.

A quantitative statement on the susceptibility to liquefaction cannot be made without the results of critical density tests. However, on the assumption that the properties of he sand-layers at both sites are comparable it seems that the layers between 10 and 20 m - soil surface at location BRC-1 are less susceptible to liquefaction than the corresponding layers at location BRC-2. At location BRC-1 the porosities obtained at depths of 16,5 and between 20 and 22 m - soil surface are relatively high, so a comparison with the results of critical density tests seems inevitable.

6. Summary and conclusions

In studying the occurrence of the flow slides on the banks of the Mississippi river the U.S. Army Corps of Engineers, Waterways Experiment Station, Vicksburg, Miss. decided to determine the porosity in situ of the existing sandlayers. The Delft Soil Mechanics Laboratory, the Netherlands, acting as a subcontractor to Fugro Gulf, Inc., Houston, Texas, executed the necessary investigations at two sites, viz. the Montz site and the Bonnet Carré site, Louisiana.

In a density investigation the specific electrical resistivities of the total soil mass and of the porewater are measured. From the ratio of these two values the porosity can be ascertained as is described in chapter 2. In this test the static cone resistance and the local skinfriction are measured simultaneously. The laboratory testing necessary to determine the porosity from the field measurements, is dealt with in chapter 3.

At Montz site, Louisiana five density measurements were executed. The location is shown on annex 1, the results of the necessary laboratory testing on annexes 3 through 12 and the results of the field investigations on annexes 17a,b through 21a,b.

Apart from the surface claylayers to a depth of about 10 m - soil surface two layers could be distinguished. In the upper layer between 10 and 25 m - soil surface the cone resistance fluctuates between 2 and 20 MN/m^2 and the local skinfriction between 0,02 and 0,16 MN/m^2. The ratio of these two quantities is less than 250, but numerous values lower than from 80 to 100 are obtained. According to Dutch experience these low values indicate the presence of claylayers. This is confirmed by the high porosities that are measured at corresponding depths locally. In general the porosities in the sandlayers vary between 46 and 51%, though lower values have been obtained.

In the layer beneath 25 m - soil surface to the reached depth of 36 m - soil surface the cone resistance fluctuates between 10 and 25 MN/m^2 and the local skin friction between 0,06 and 0,16 MN/m^2; their ratio is bounded by about 100 and 260. There is no indication that claylayers occur between these depths. The porosities obtained in this layer vary between 38 and 48%. This is in accordance with the fact that the sand in this layer is coarser than the sand in the upper layer.

In the lower layer higher values of cone resistance and local skin friction have been measured than in the upper layer whereas the porosities are lower. However, as there are at least differences in grainsizes it cannot be concluded that the lower layer is less susceptible to liquefaction than the upper layer. This susceptibility only can be judged by a comparison with the critical density, determined in the laboratory. The presence of the claylayers in the deposit between 10 and 25 m - soil surface seems to be a favourable factor. It is deemed that such a layer having sufficient extent and thickness, can stop a flowslide by bending down and blockading the flowing sand.

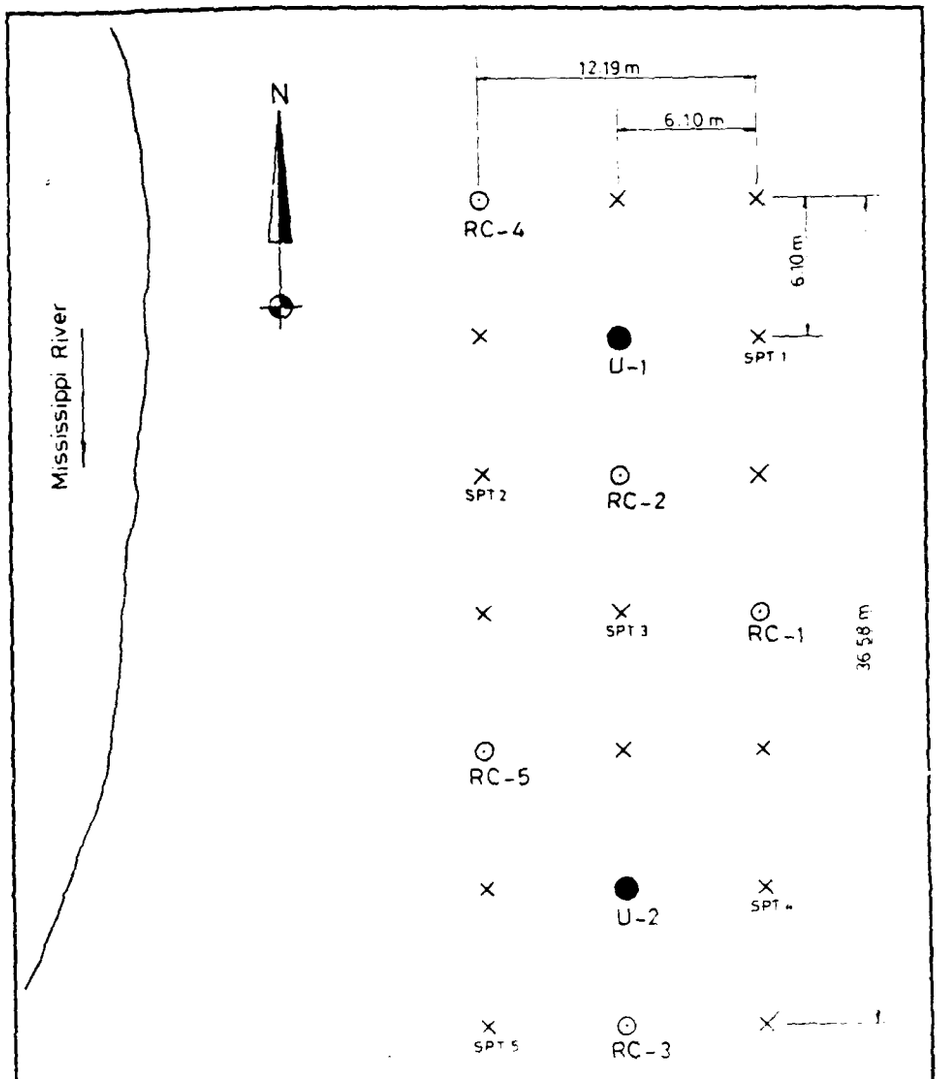
At Bonnet Carré site, Louisiana two density measurements were executed. Their location is shown on annex 2, the results of the laboratory testing on annexes 13 through 16 and the results of the field investigations on annexes 22a,b and 23a,b. The diverging results exclude a combined treatment.

In location BRC-1 two layers can be specified in the stretch of the measurements. In the upper layer between 10 and 17,5 m - soil surface the cone resistance fluctuates between 7 and 15 MN/m^2 and the local skinfriction between 0,05 and 0,09 MN/m^2. The ratio of these two quantities varies between 90 and 300. The extreme values of the porosity are about 33 and 41%. In the layer beneath 17,5 m -

soil surface to the reached depth of 27 m - soil surface the cone resistances vary between 16 and 35 MN/m^2 and the local skinfriction between 0,07 and 0,16 MN/m^2; their ratio is bounded by about 160 and 310. The porosities in this layer fluctuate between 35 and 46%.

At location BRC-2 in the layer between 10 and 13,5 m - soil surface the cone resistance is bounded by about 4 and 10 MN/m^2 and the local skinfriction by about 0,03 and 0,06 MN/m^2; the ratio of these two quantities varies between 120 and 220. The porosity in this layer fluctuates between 41 and 50%. At a depth of 13,5 m - soil surface a claylayer is present. In the layer beneath 13,5 m - soil surface to the attained depth of 20,5 m - soil surface the cone resistance fluctuates between 10 and 20 MN/m^2 and the local skinfriction between 0,05 and 0,10 MN/m^2; their ratio varies between 140 and 300. The porosities obtained in this layer vary between 43 and 51%.

Once again a quantitative statement on the susceptibility to liquefaction cannot be made without the results of critical density tests. On the assumption that the properties of the sandlayers at both sites are comparable it seems that the layers between 10 and 20 m - soil surface at location BRC-1 are less susceptible to liquefaction than at location BRC-2. The relative high porosities at location BRC-1 obtained at depths of 16,5 and between 20 and 22 m - soil surface have to be compared with the results of critical density tests.



U-1 AND U-2 -UNDISTURBED BORINGS
RC-1 TO RC-5 -DENSITY MEASUREMENTS
X -LOCATIONS WHERE OTHER TYPES OF INSITU DEVICES WERE USED

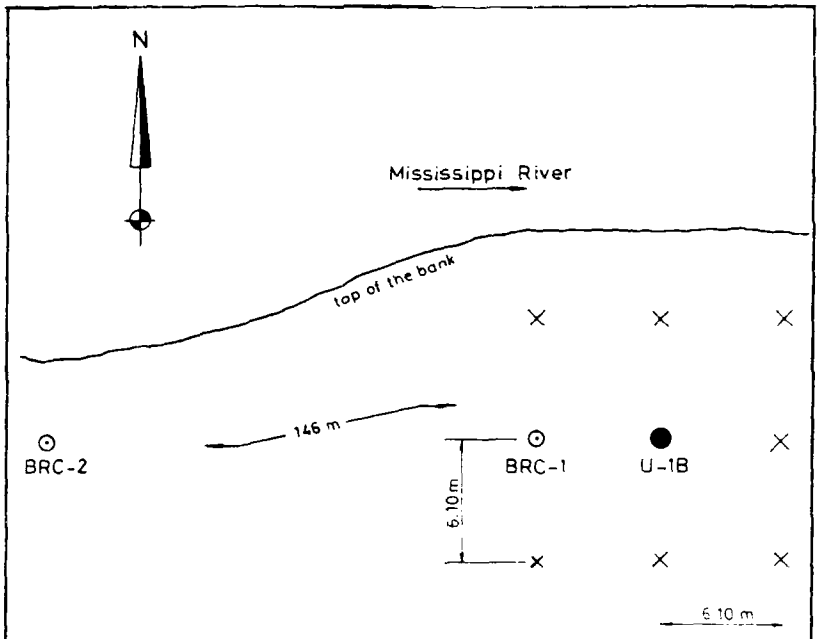
delft soil mechanics laboratory
telephone (015) - 56 92 23 holland telex 33326 soilb nl

date

INVESTIGATION FLOW SLIDES MISSISSIPPI RIVER
MONTZ SITE, LOUISIANA
PLAN OF SITE INVESTIGATIONS

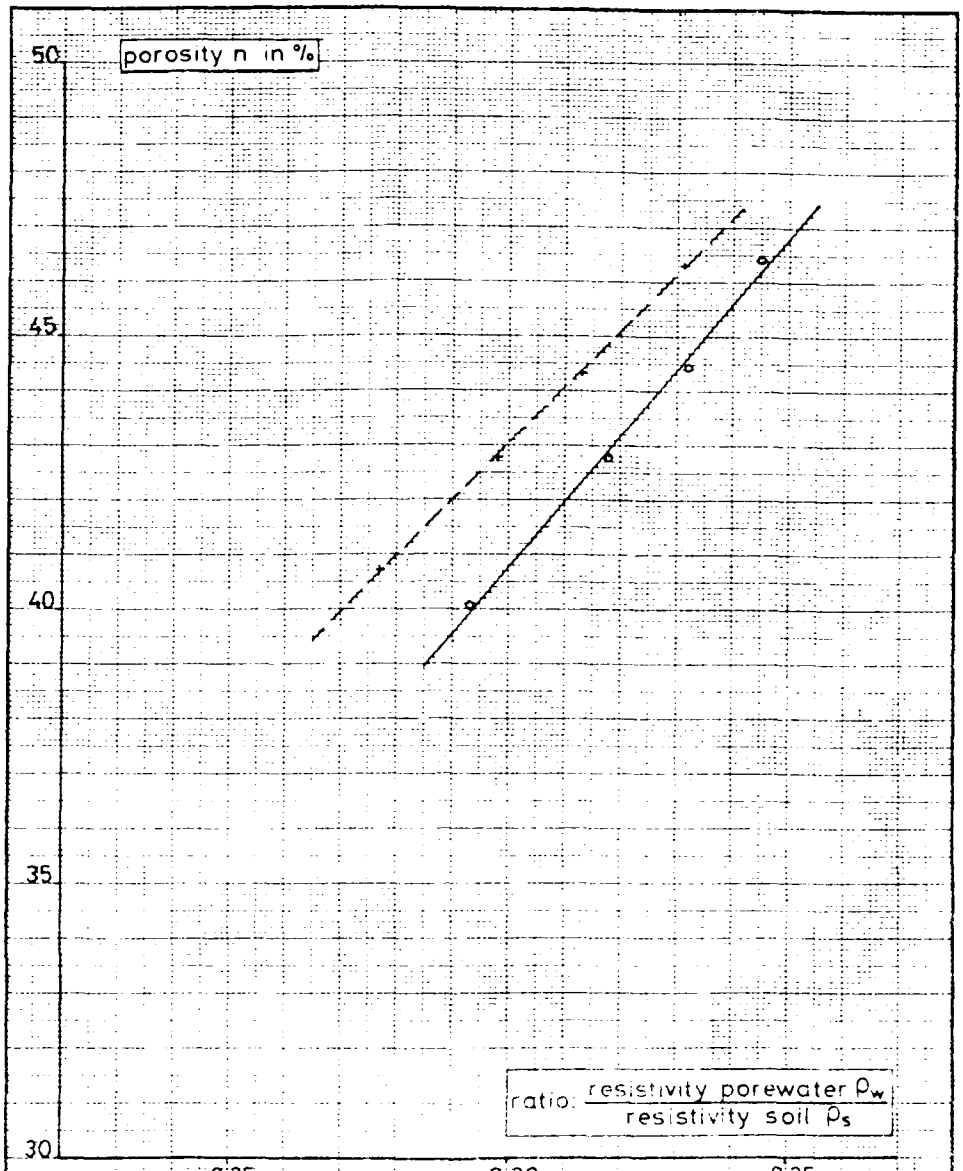
BO-253500

ANNEX 1 A4



U-1B - UNDISTURBED BORING
BRC-1 AND BRC-2 - DENSITY MEASUREMENTS
X - LOCATIONS WHERE OTHER TYPES OF INSITU DEVICES WERE USED

delft soil mechanics laboratory telephone (015)-56 92 23 holland telex 38326 solab nl	date	
INVESTIGATION FLOW SLIDES MISSISSIPPI RIVER BONNET CARRE SITE, LOUISIANA	BO-253500	
PLAN OF SITE INVESTIGATIONS	ANNEX 2	A_4



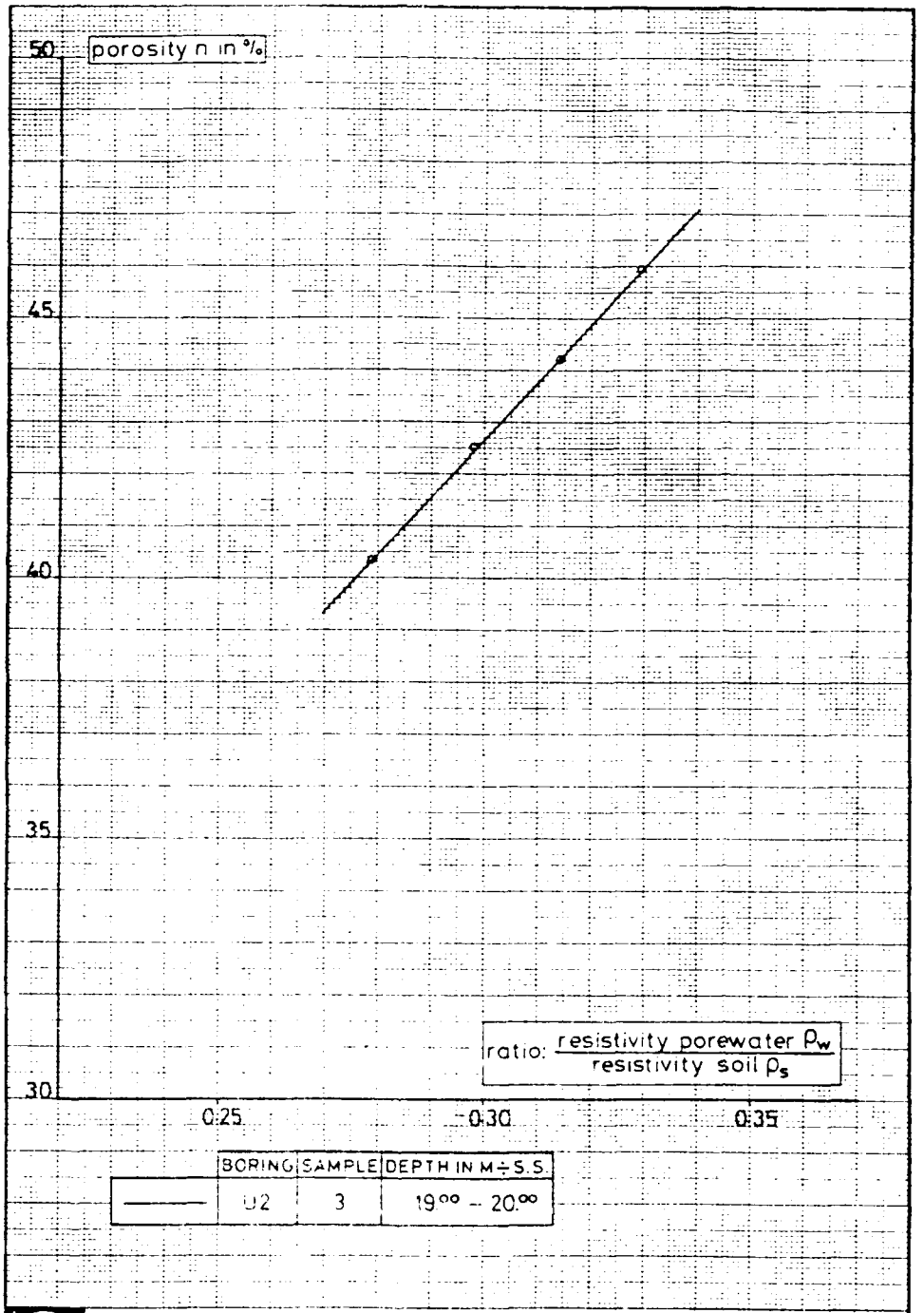
	BORING	SAMPLE	DEPTH IN M - S.S.
———	U2	1	$12^{00} - 13^{00}$
- - - - -	U2	2	$14^{00} - 16^{00}$

delft soil mechanics laboratory

INVESTIGATION FLOW SLIDES MISSISSIPPI RIVER BC 253-00

MONTZ SITE

SAND CALIBRATION TEST SAMPLES 1 + 2 ANNEX 3 A_4



delft soil mechanics laboratory

telephone 015-56 92 23 telex 33326 solab nl

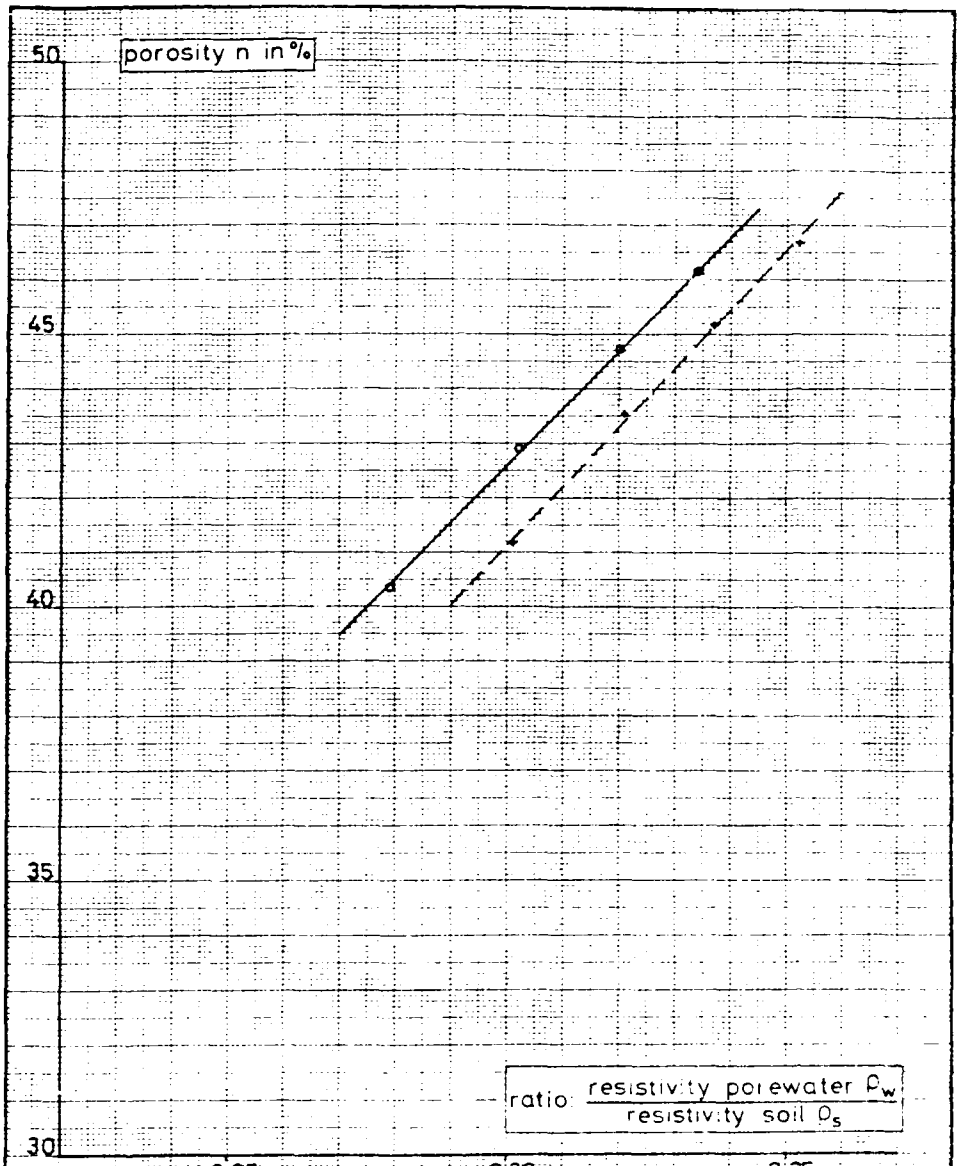
date

INVESTIGATION FLOW SLIDES MISSISSIPPI RIVER MONTZ SITE

BO - 253500

SAND CALIBRATION TEST SAMPLE 3

ANNEX 4 A_4

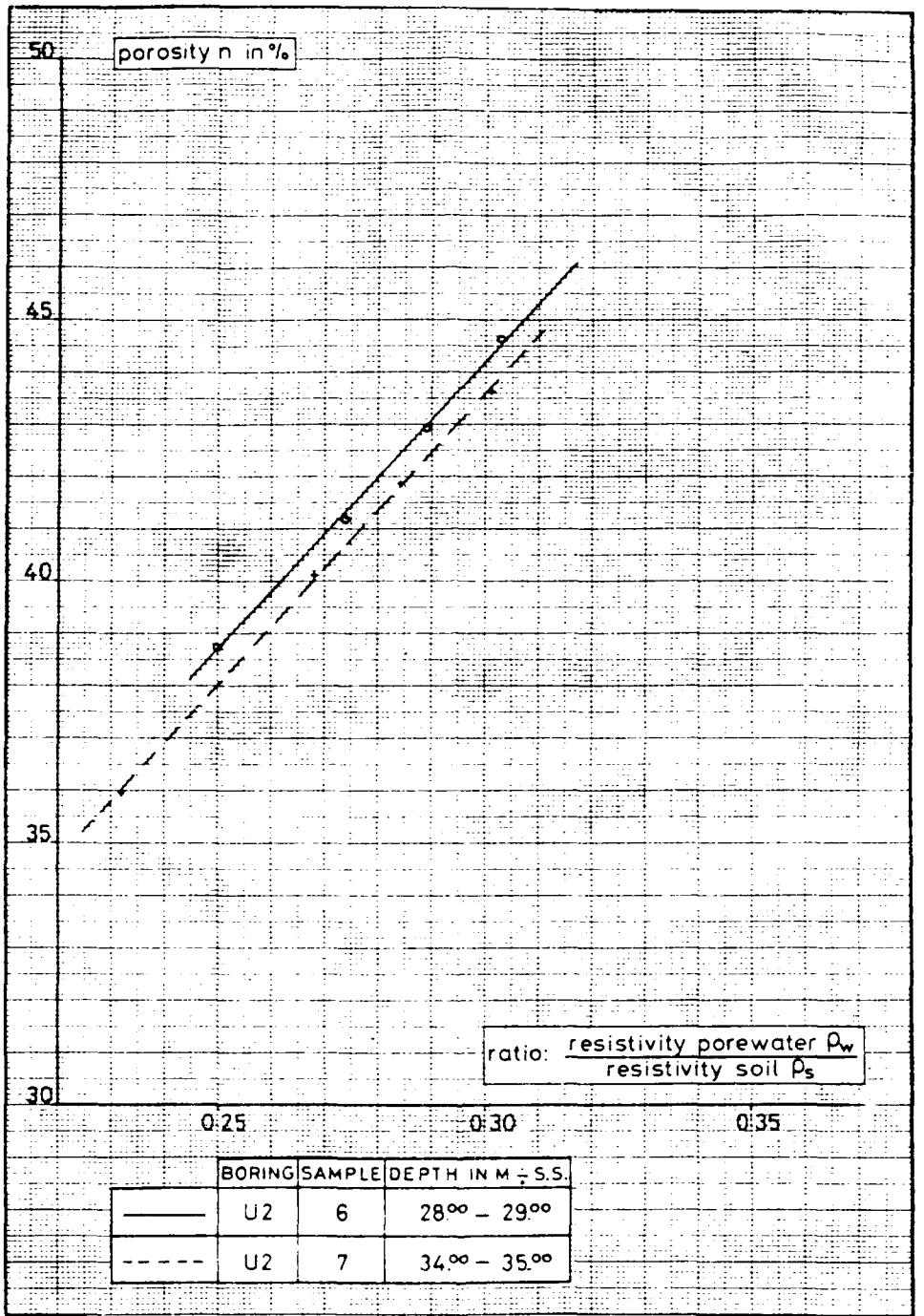


	BORING	SAMPLE	DEPTH IN M ÷ S.S.
———	U2	4	22.00 – 23.00
– – – –	U2	5	24.00 – 25.00

delft soil mechanics laboratory

INVESTIGATION FLOW SLIDES MISSISSIPPI RIVER BC - 253500
MONTZ SITE

SAND CALIBRATION TEST SAMPLES 4 + 5 ANNEX 5 A..



delft soil mechanics laboratory

telephone (015) - 56 92 23 holland telex 33326 solab nl

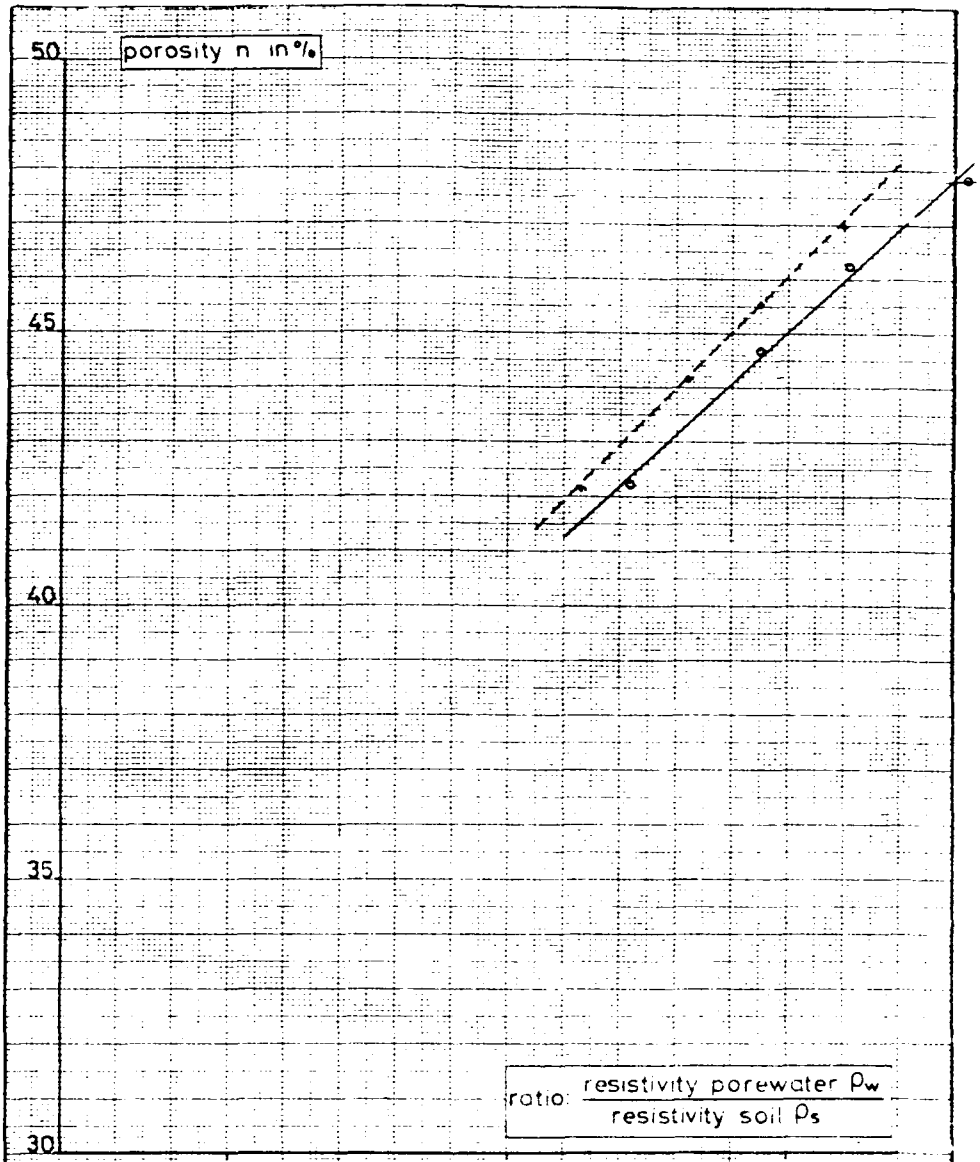
date

INVESTIGATION FLOW SLIDES MISSISSIPPI RIVER MONTZ SITE

BO - 253500

SAND CALIBRATION TEST SAMPLES 6 + 7

ANNEX 6 A4



	BORING	SAMPLE	DEPTH IN M – S.S
———	U1	12	$12^{00} - 13^{00}$
- - - - - -	U1	13	$14^{00} - 16^{00}$

delft soil mechanics laboratory

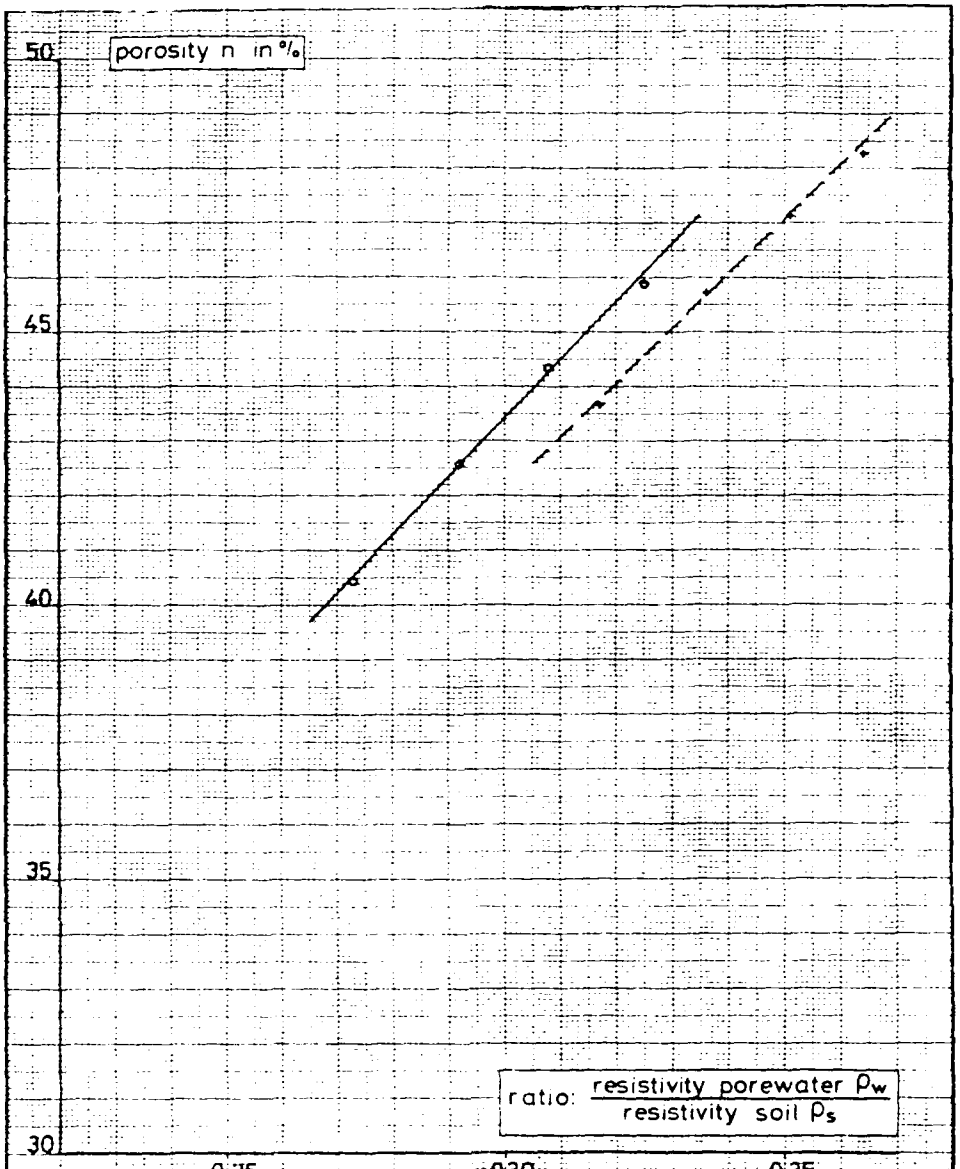
telephone (015) - 56 92 23 holland

INVESTIGATION FLOW SLIDES MISSISSIPPI RIVER
MONTZ SITE

BC - 253500

SAND CALIBRATION TEST SAMPLES 12 + 13

ANNEX 7 A.



	BORING	SAMPLE	DEPTH IN M - S.S.
———	U1	14	19.00 - 20.00
- - - - - -	U1	15	22.00 - 23.00

delft soil mechanics laboratory

telephone (015) 56 92 21 holland telex 33326 solab n

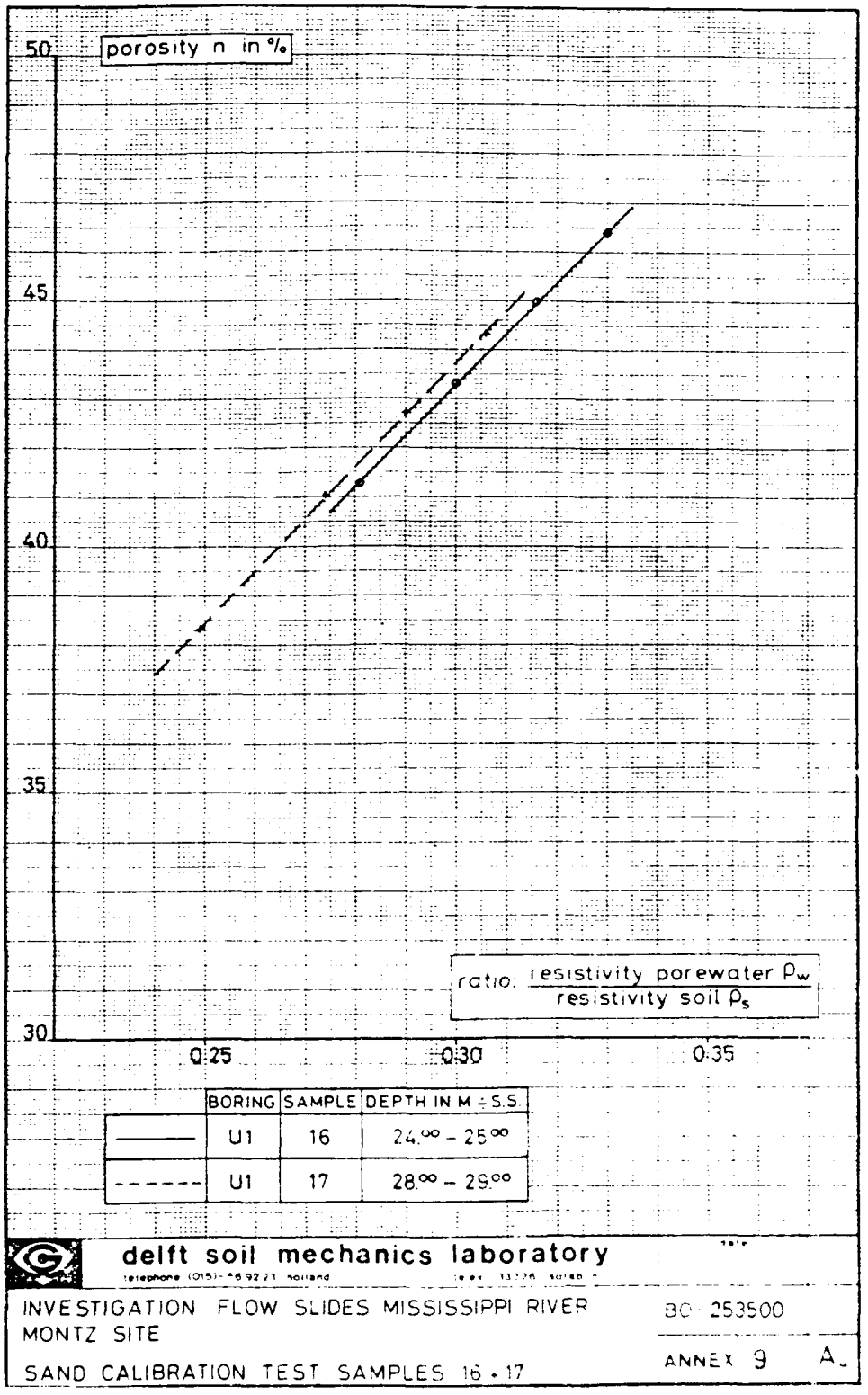
date

INVESTIGATION FLOW SLIDES MISSISSIPPI RIVER
MONTZ SITE

BO - 253500

SAND CALIBRATION TEST SAMPLES 14 + 15

ANNEX 8 A_4



delft soil mechanics laboratory

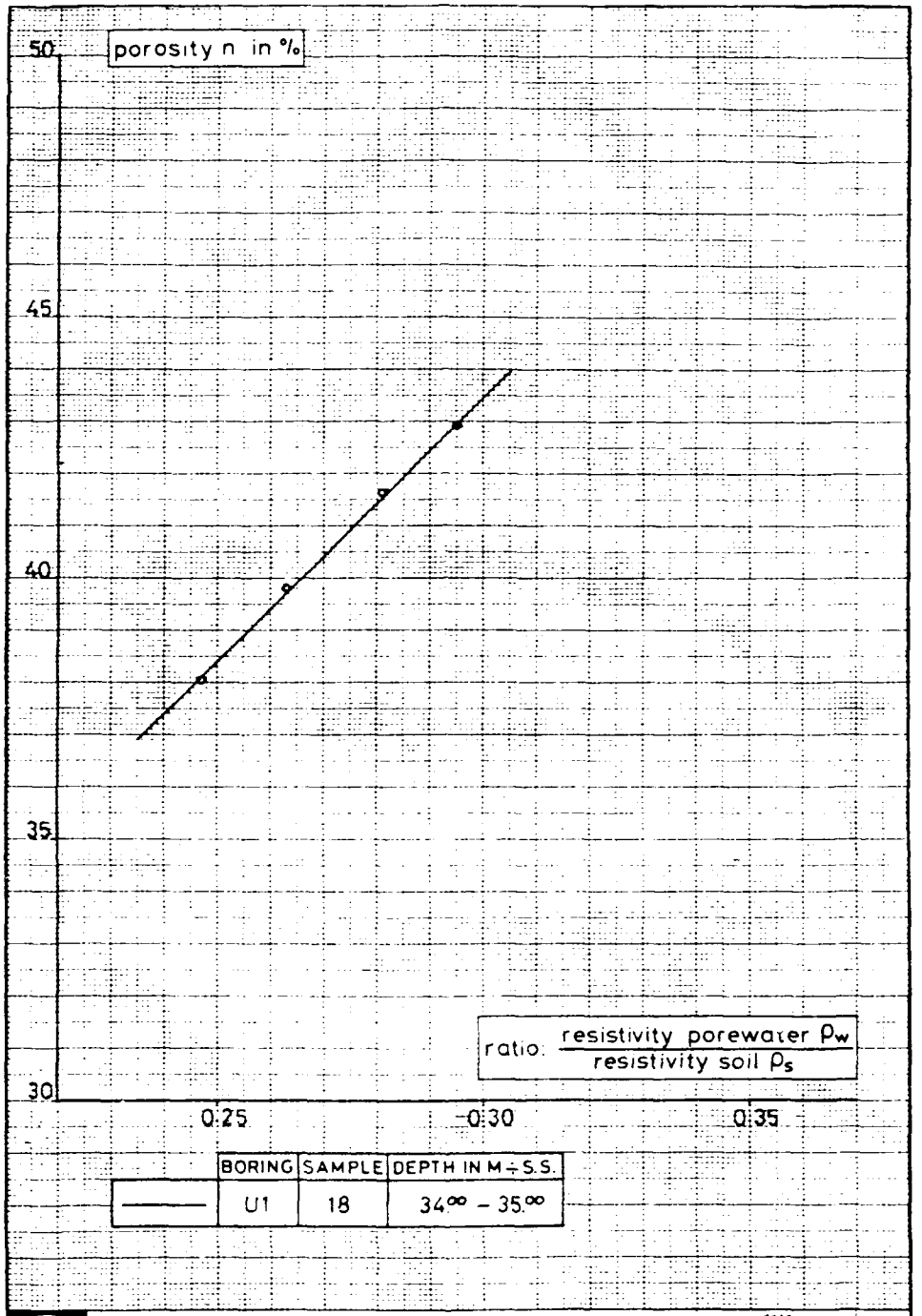
telephone (015) - 56 92 21 holland

INVESTIGATION FLOW SLIDES MISSISSIPPI RIVER
MONTZ SITE

SAND CALIBRATION TEST SAMPLES 16 + 17

BO - 253500

ANNEX 9 A.



	BORING	SAMPLE	DEPTH IN M ÷ S.S.
———	U1	18	$34.^{00} - 35.^{00}$

delft soil mechanics laboratory

telephone (015) 56 92 23 holland telex 33326 solab -

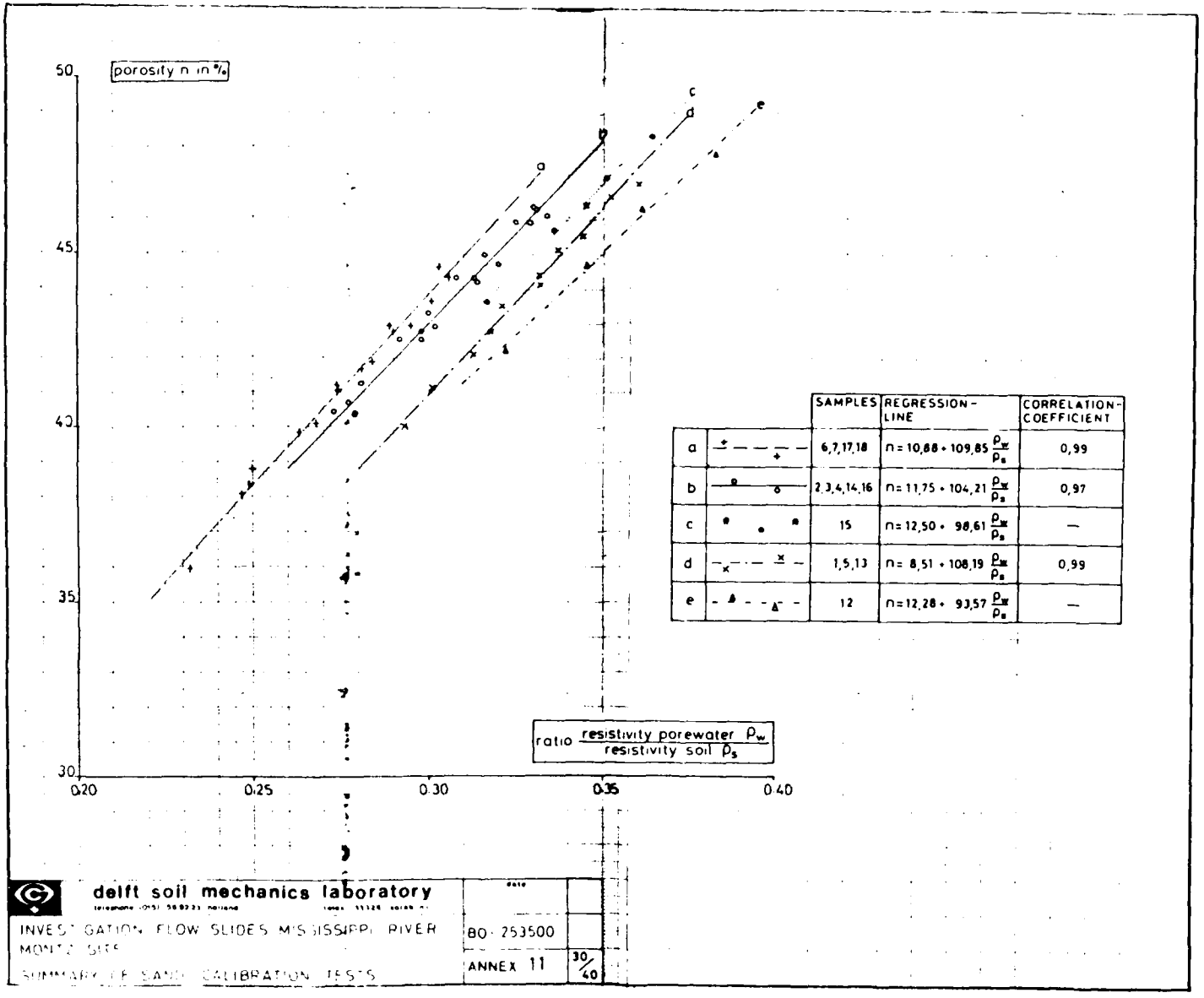
date

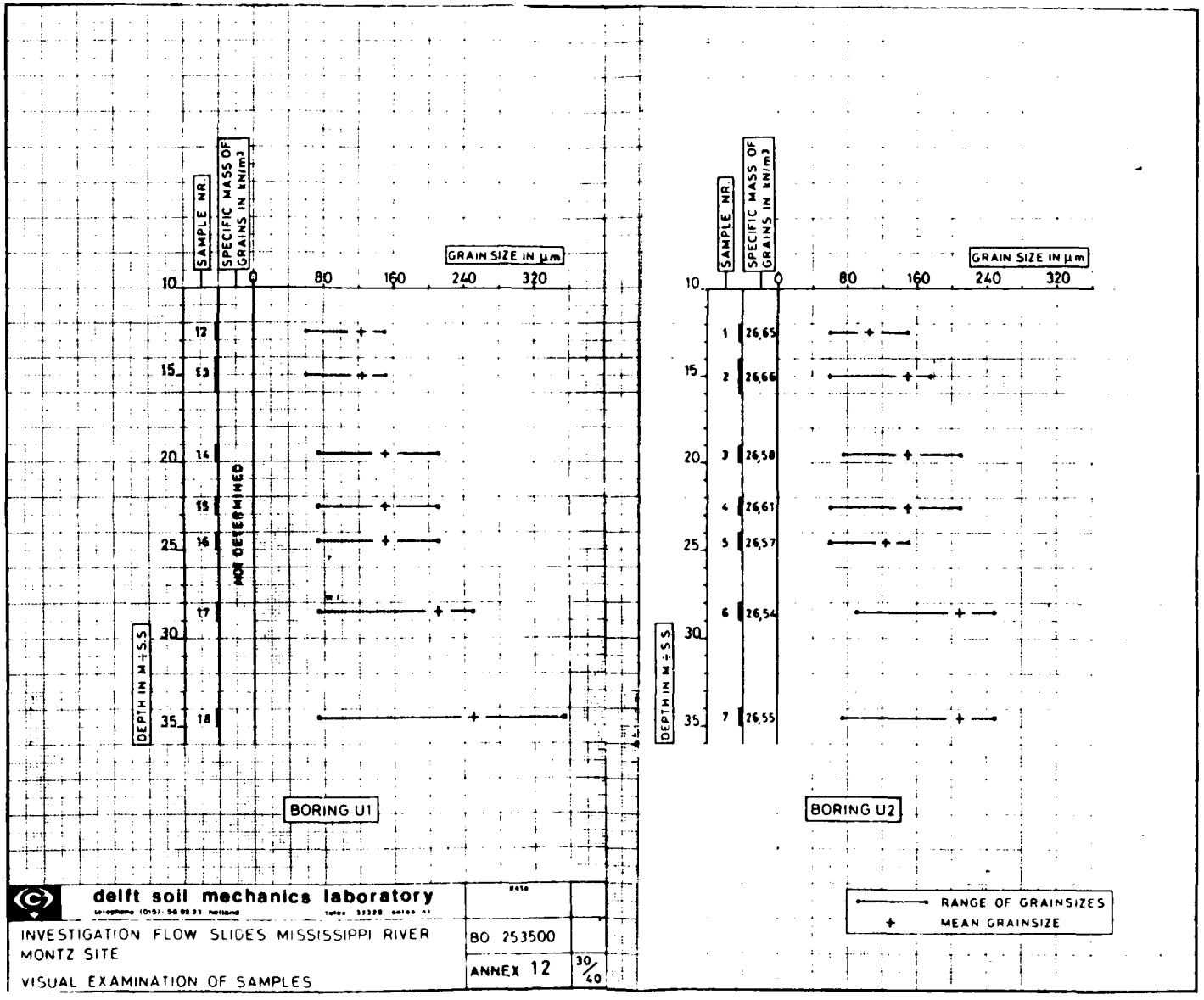
INVESTIGATION FLOW SLIDES MISSISSIPPI RIVER
MONTZ SITE

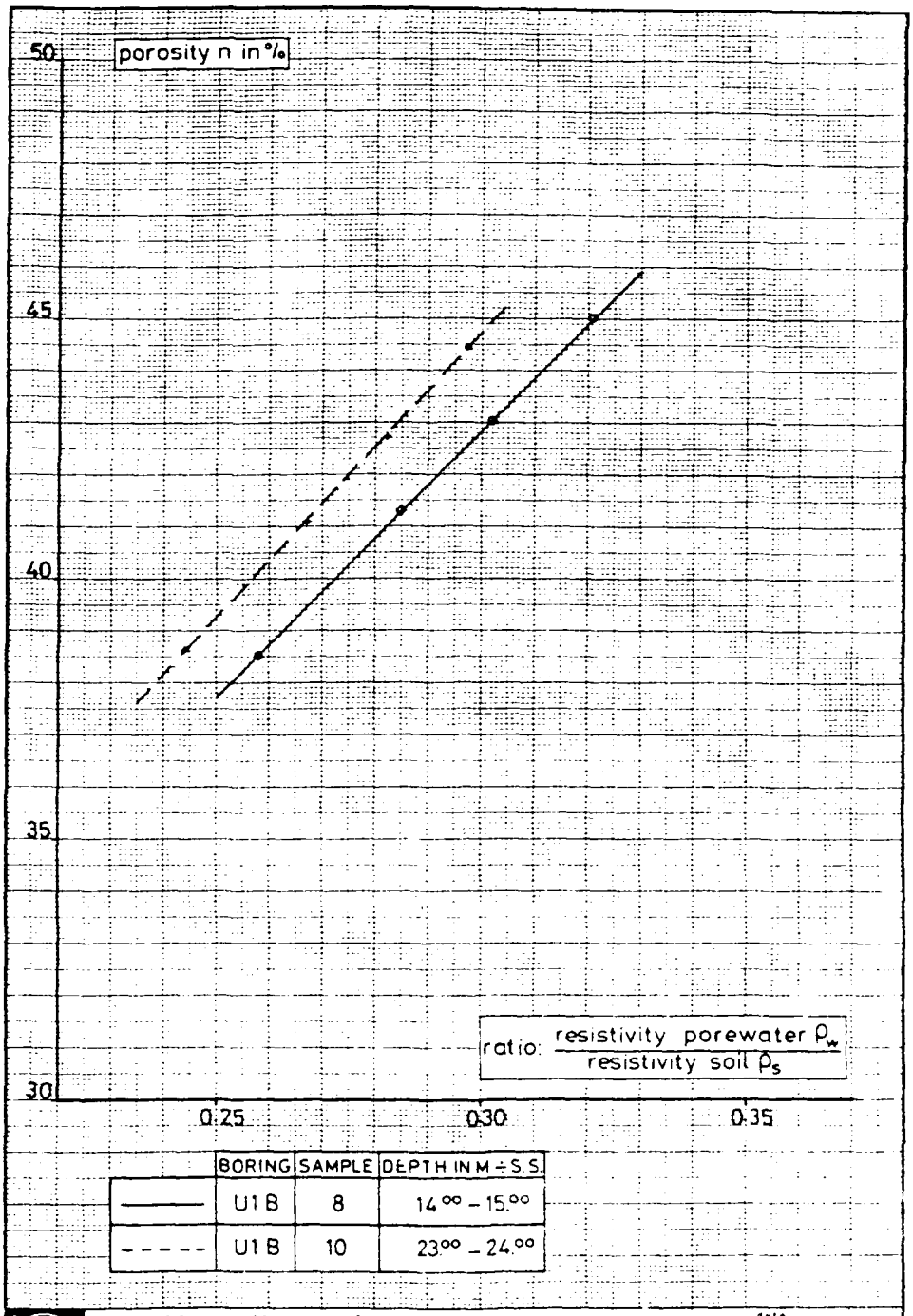
BO - 253500

SAND CALIBRATION TEST SAMPLE 18

ANNEX 10 A_4


porosity n in %
50
45
40
35
30
0.20
0.25
0.30
0.35
0.40
ratio resistivity porewater ρ_w / resistivity soil ρ_s
a
b
c
d
e
SAMPLES
REGRESSION-LINE
CORRELATION-COEFFICIENT
a 6,7,17,18 $n = 10{,}88 + 109{,}85 \frac{\rho_w}{\rho_s}$ 0,99
b 2,3,4,14,16 $n = 11{,}75 + 104{,}21 \frac{\rho_w}{\rho_s}$ 0,97
c 15 $n = 12{,}50 + 98{,}61 \frac{\rho_w}{\rho_s}$ —
d 1,5,13 $n = 8{,}51 + 108{,}19 \frac{\rho_w}{\rho_s}$ 0,99
e 12 $n = 12{,}28 + 93{,}57 \frac{\rho_w}{\rho_s}$ —
delft soil mechanics laboratory
INVESTIGATION FLOW SLIDES MISSISSIPPI RIVER
MONTZ SITE
SUMMARY OF SAND CALIBRATION TESTS
BO - 253500
ANNEX 11
30/40


SAMPLE NR.
SPECIFIC MASS OF GRAINS IN kN/m3
GRAIN SIZE IN µm
0
80
160
240
320
DEPTH IN M+S.S.
10
15
20
25
30
35
12
13
14
15
16
17
18
NOT DETERMINED
BORING U1
1
2
3
4
5
6
7
26,65
26,66
26,58
26,61
26,57
26,54
26,55
BORING U2
RANGE OF GRAINSIZES
MEAN GRAINSIZE
delft soil mechanics laboratory
INVESTIGATION FLOW SLIDES MISSISSIPPI RIVER
MONTZ SITE
VISUAL EXAMINATION OF SAMPLES
BO 253500
ANNEX 12
30/40



	BORING	SAMPLE	DEPTH IN M ÷ S.S.
———	U1 B	8	$14^{00} - 15^{00}$
- - - - -	U1 B	10	$23^{00} - 24^{00}$

delft soil mechanics laboratory

telephone (015) - 56 92 23 holland telex 33326 solab nl

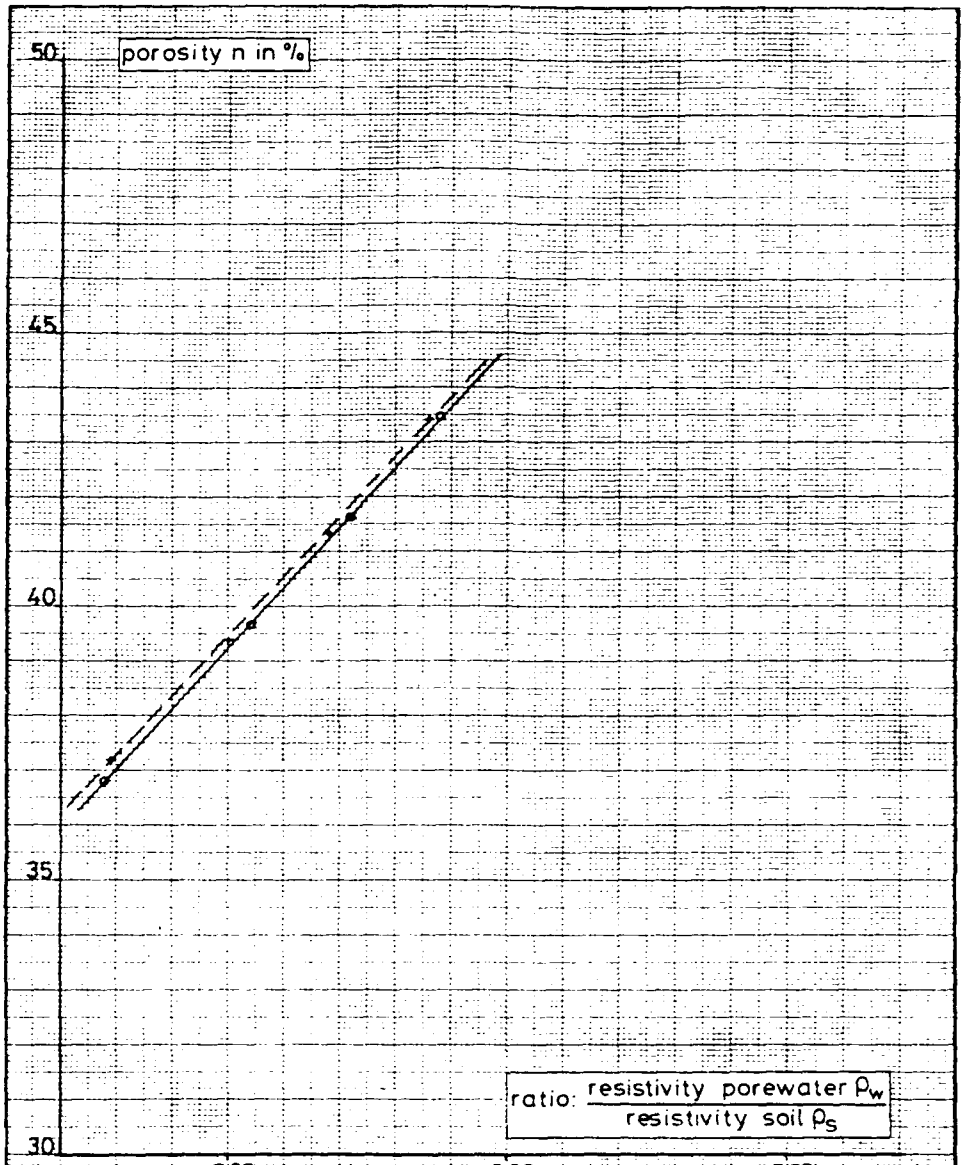
date

INVESTIGATION FLOW SLIDES MISSISSIPPI RIVER
BONNET CARRE SITE

BO - 253500

SAND CALIBRATION TEST SAMPLES 8 + 10

ANNEX 13 A.



	BORING	SAMPLE	DEPTH IN M÷S.S.
———	U1 B	9	20.00 – 21.00
– – – –	U1 B	11	26.00 – 27.00

delft soil mechanics laboratory

telephone (015) - 56 92 23 holland telex 33326 solab nl

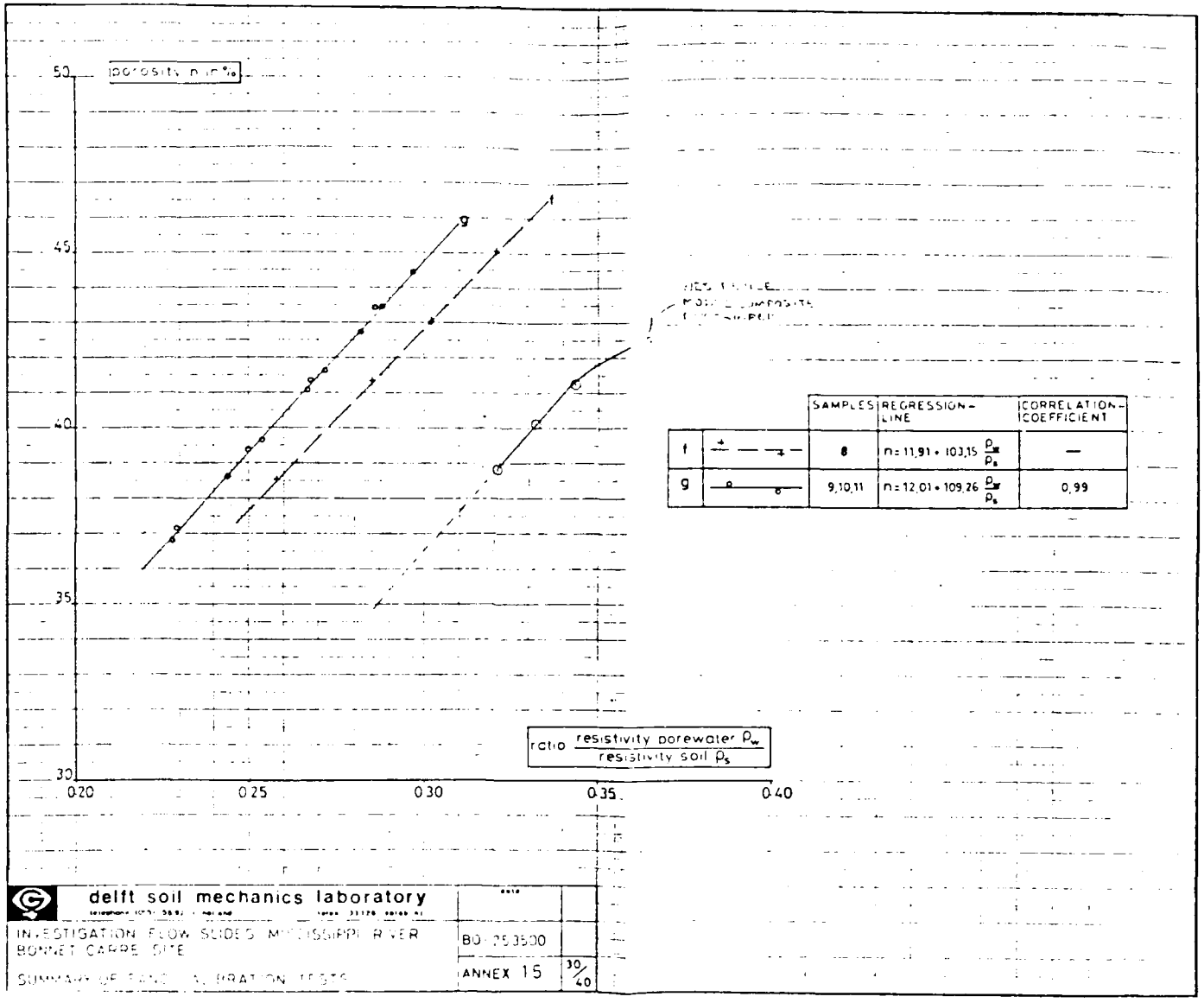
date

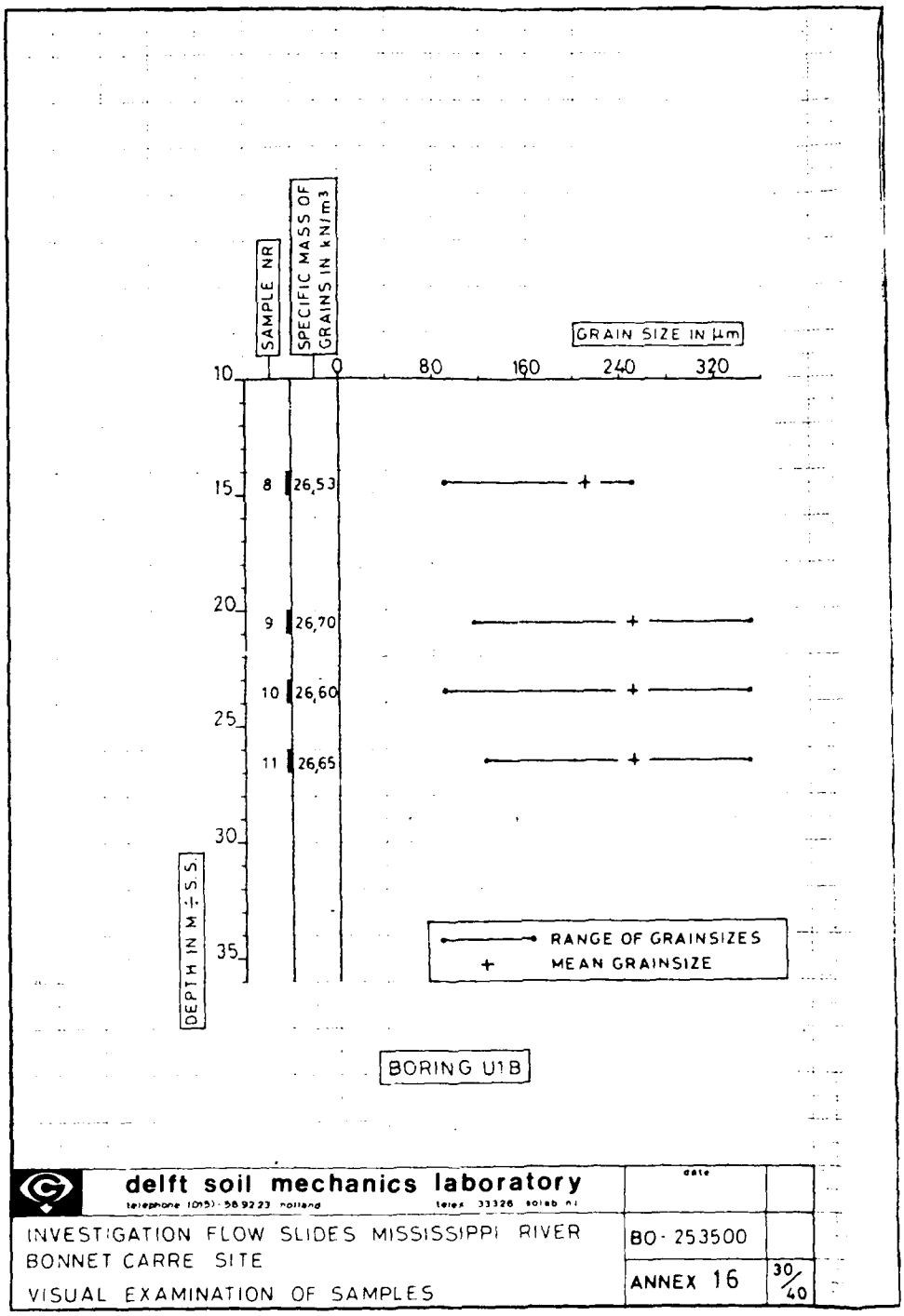
INVESTIGATION FLOW SLIDES MISSISSIPPI RIVER
BONNET CARRE SITE

BO - 253500

SAND CALIBRATION TEST SAMPLES 9 + 11

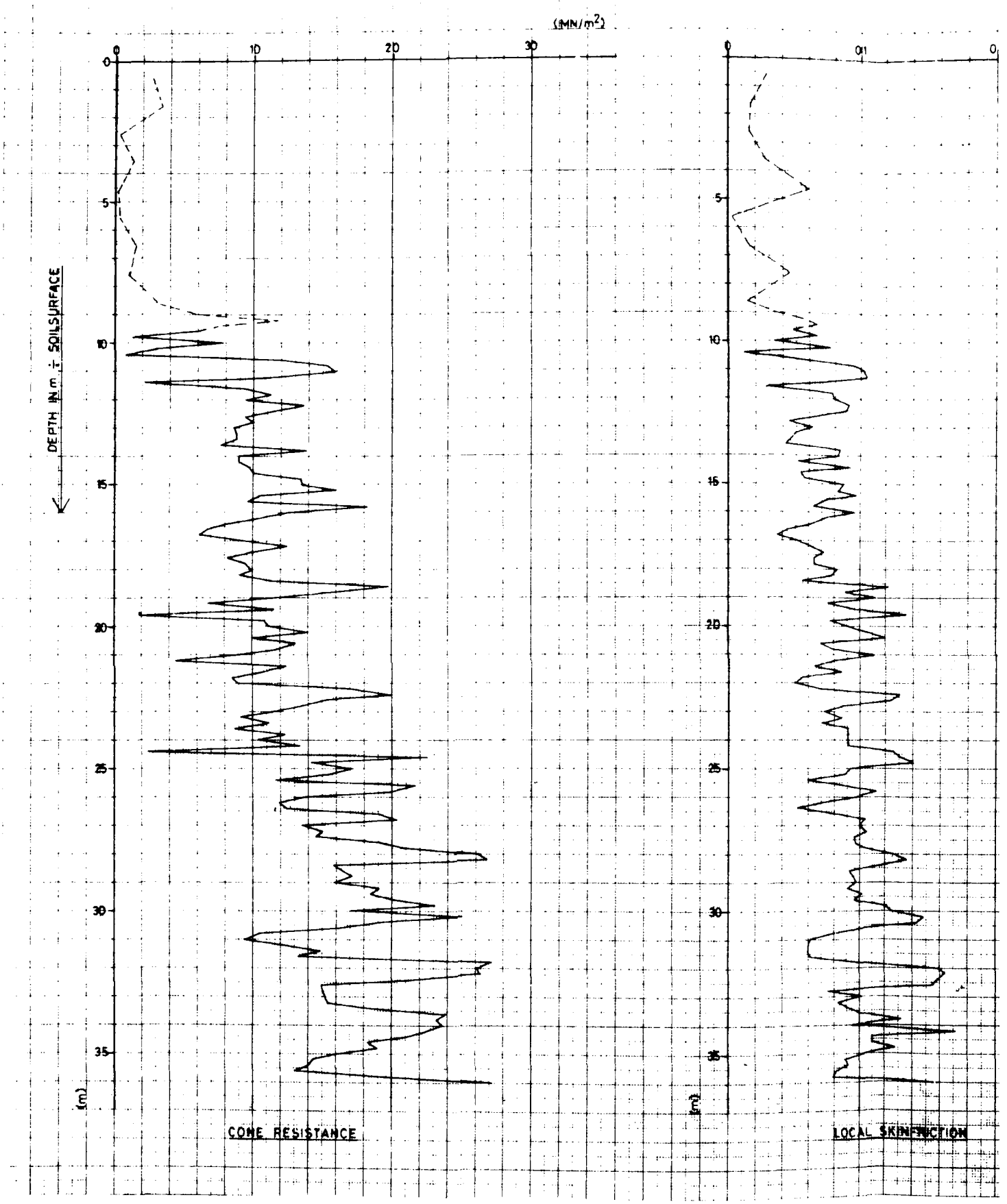
ANNEX 14 A_4

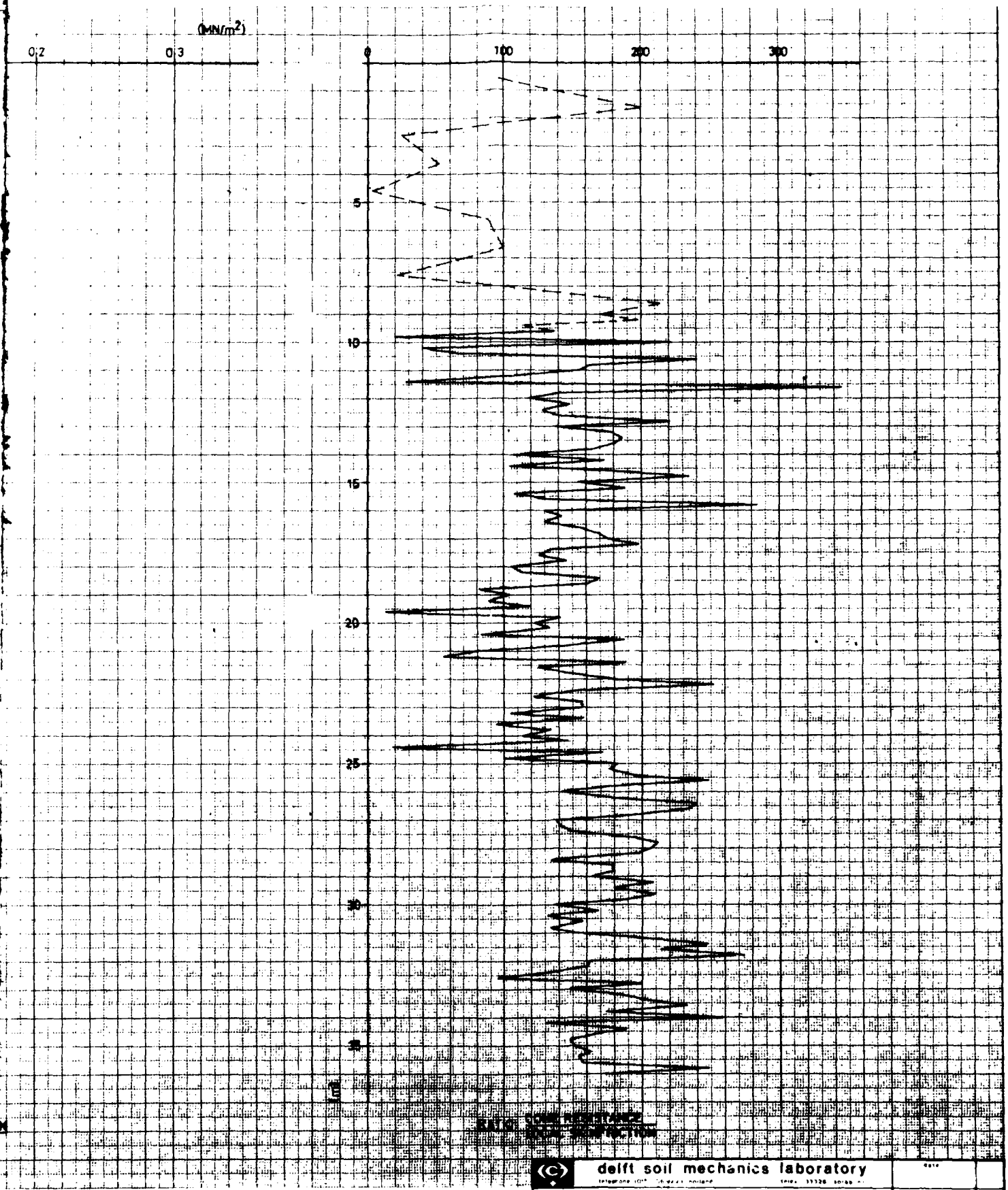

50
45
40
35
30
0.20
0.25
0.30
0.35
0.40
ratio resistivity porewater ρ_w / resistivity soil ρ_s
SAMPLES
REGRESSION-LINE
CORRELATION-COEFFICIENT
f
8
n = 11,91 + 103,15 $\frac{\rho_w}{\rho_s}$
—
g
9,10,11
n = 12,01 + 109,26 $\frac{\rho_w}{\rho_s}$
0,99
delft soil mechanics laboratory
INVESTIGATION FLOW SLIDES MISSISSIPPI RIVER
BONNET CARRE SITE
BO-253500
ANNEX 15
30/40



delft soil mechanics laboratory
telephone (015)-56 92 23 holland telex 33326 solab nl

INVESTIGATION FLOW SLIDES MISSISSIPPI RIVER	date	
BONNET CARRE SITE	BO-253500	
VISUAL EXAMINATION OF SAMPLES	ANNEX 16	30/40


(MN/m²)
0
10
20
30
DEPTH IN m ↓ SOILSURFACE
5
10
15
20
25
30
35
(m)
CONE RESISTANCE
0
01
0
5
10
15
20
25
30
35
(m)
LOCAL SKINFRICTION



delft soil mechanics laboratory

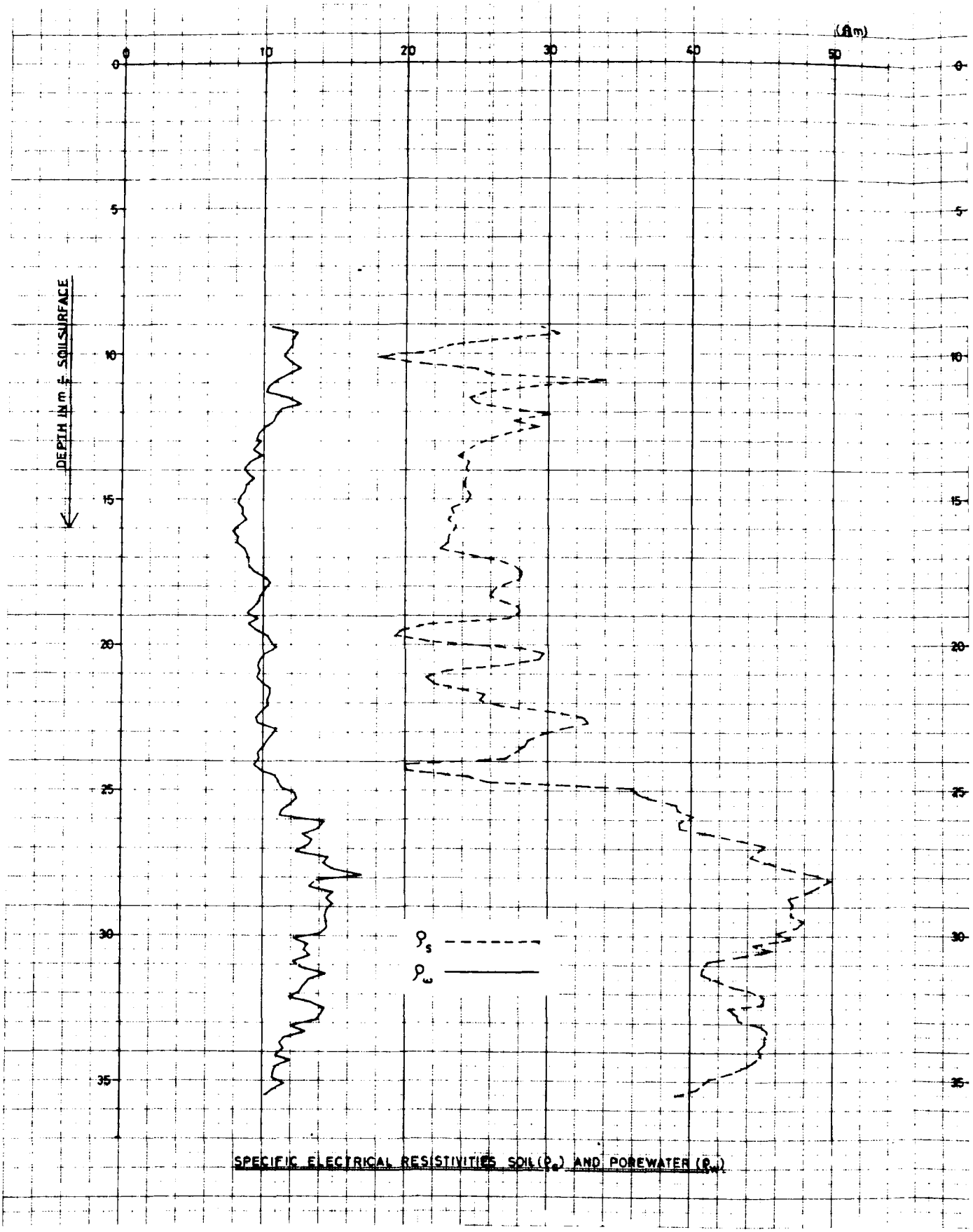
INVESTIGATION FLOW SLIDES MISSISSIPPI RIVER
MONTZ SITE

DENSITY MEASUREMENT RC-1

B0-253500

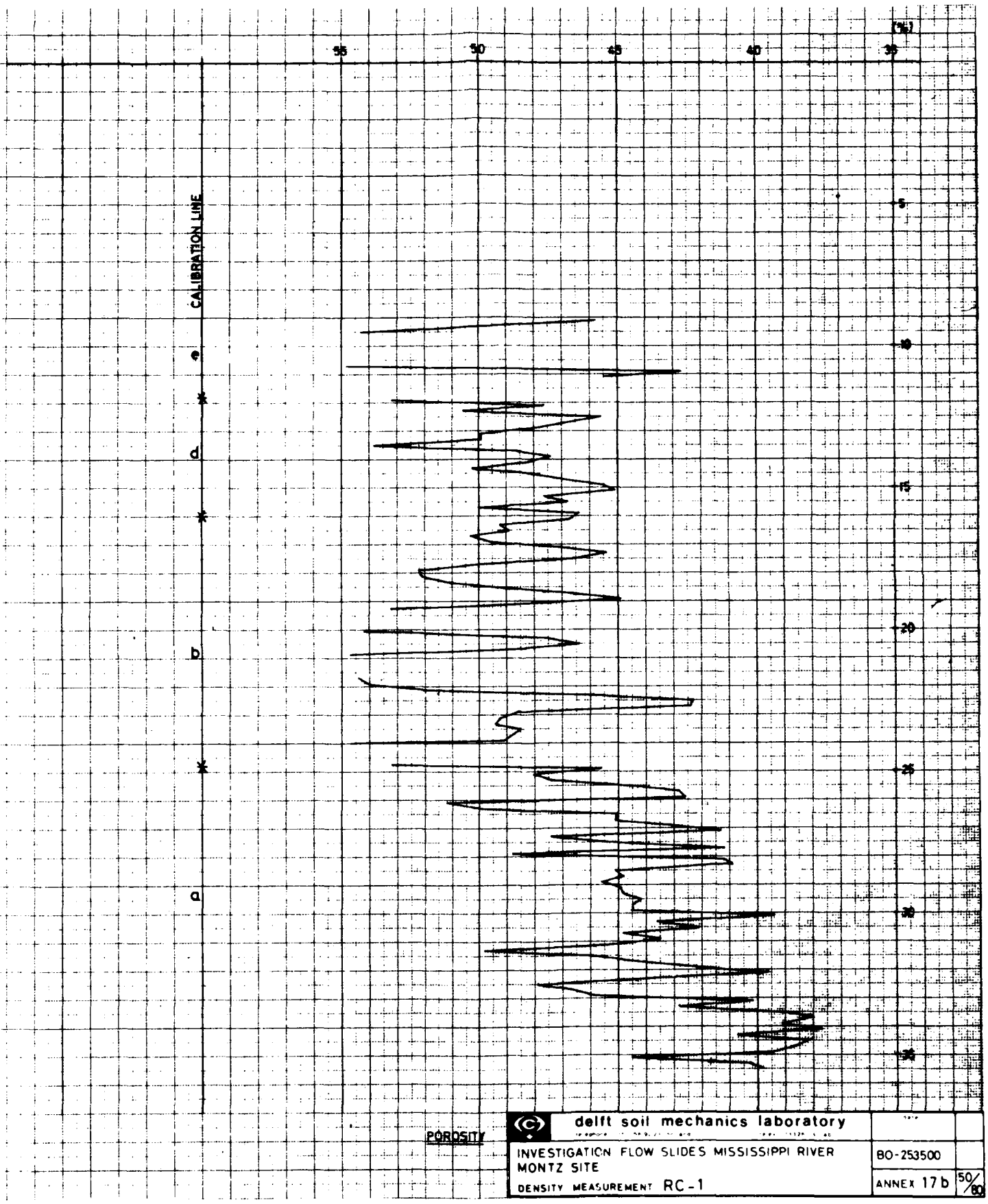
ANNEX 17a

50/80



SPECIFIC ELECTRICAL RESISTIVITIES SOIL (ρ_s) AND POREWATER (ρ_w)

1



delft soil mechanics laboratory

INVESTIGATION FLOW SLIDES MISSISSIPPI RIVER
MONTZ SITE

DENSITY MEASUREMENT RC-1

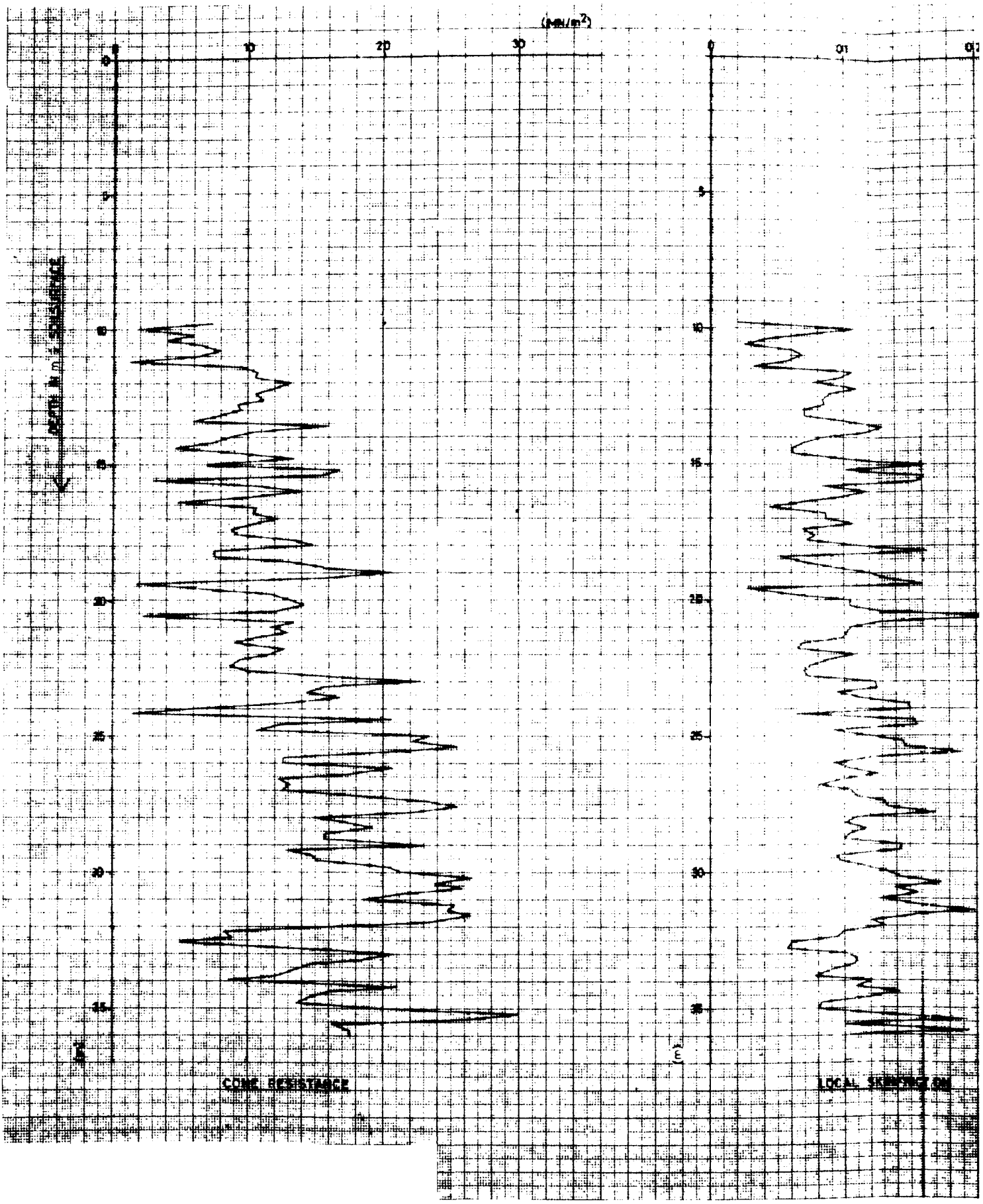
BO-253500

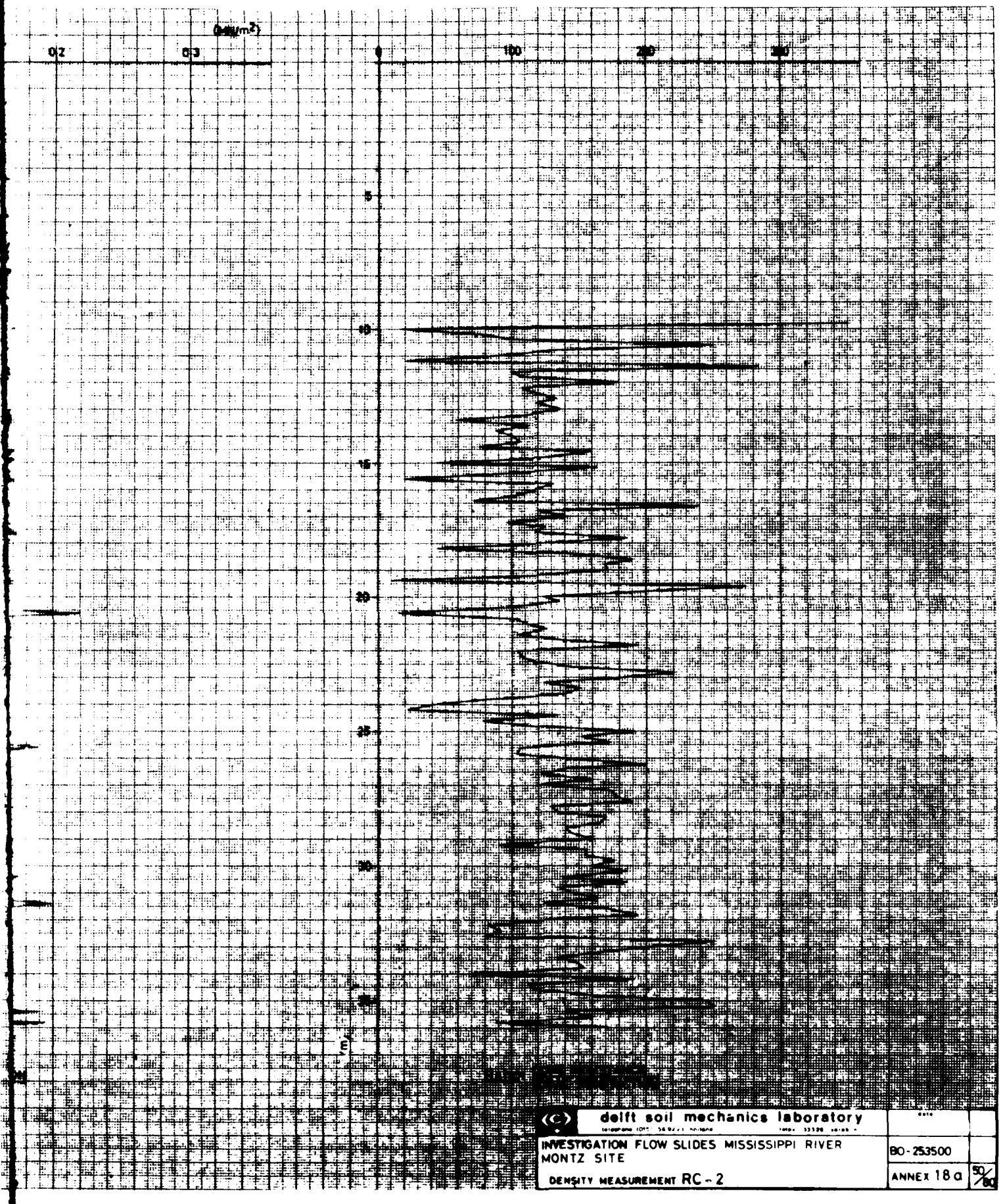
ANNEX 17 b

50/80

1

2


(MN/m²)
0
10
20
30
0
0.1
0.2
5
10
15
20
25
30
35
DEPTH IN METRES
CONE RESISTANCE
LOCAL SKIN FRICTION



(c) delft soil mechanics laboratory

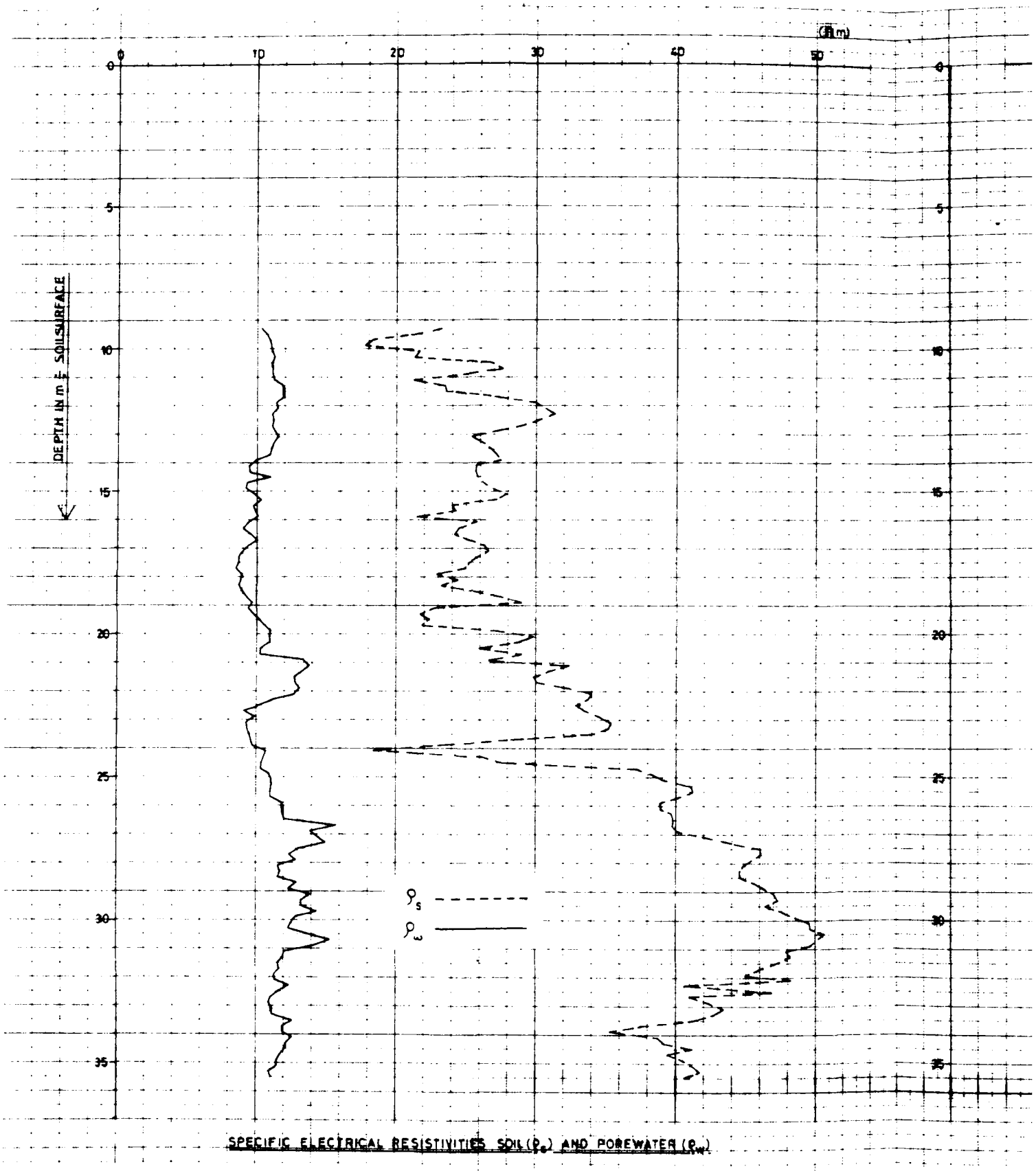
INVESTIGATION FLOW SLIDES MISSISSIPPI RIVER
MONTZ SITE

DENSITY MEASUREMENT RC - 2

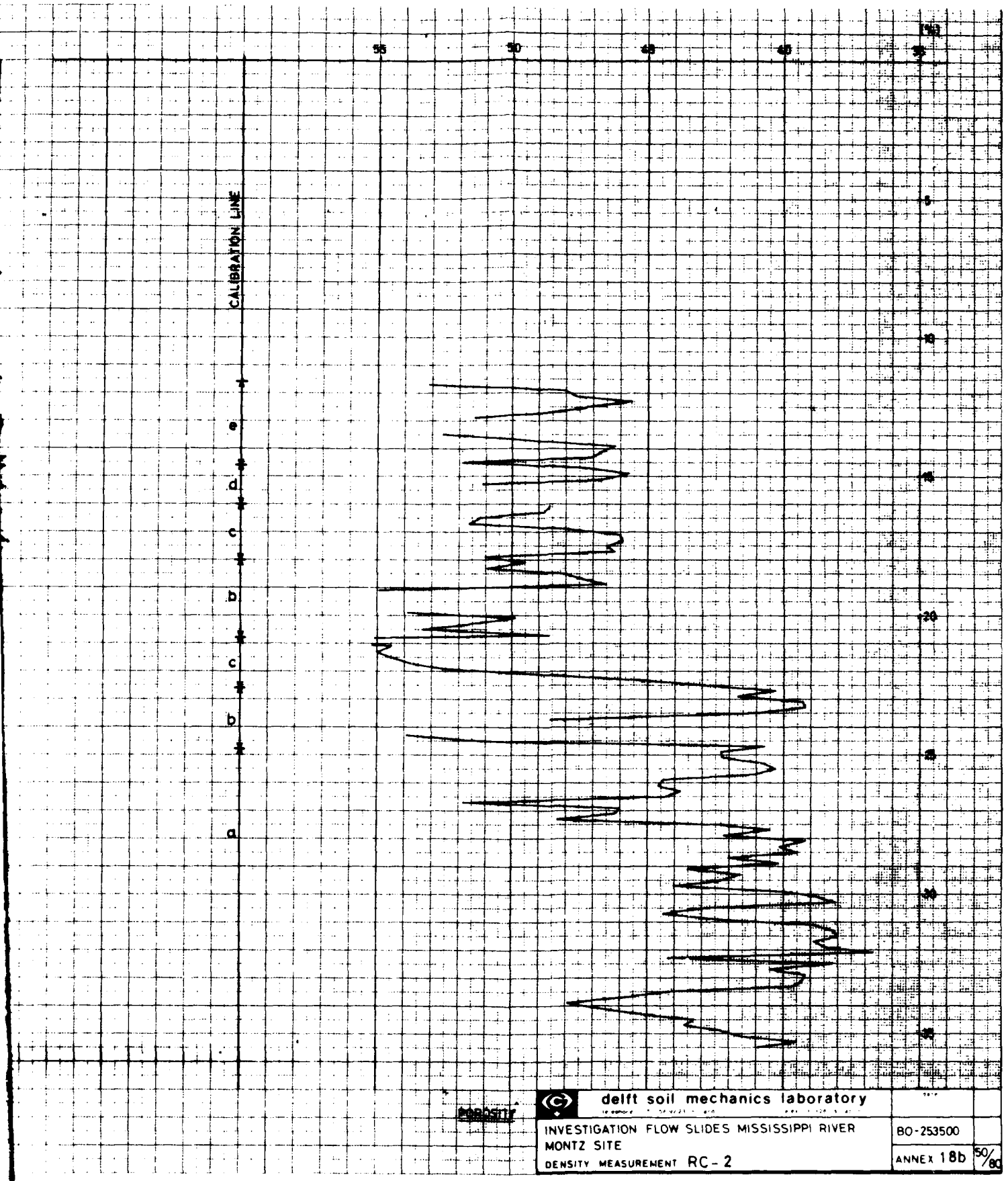
80-253500

ANNEX 18 a

90/80



SPECIFIC ELECTRICAL RESISTIVITIES SOIL (ρ_s) AND POREWATER (ρ_w)



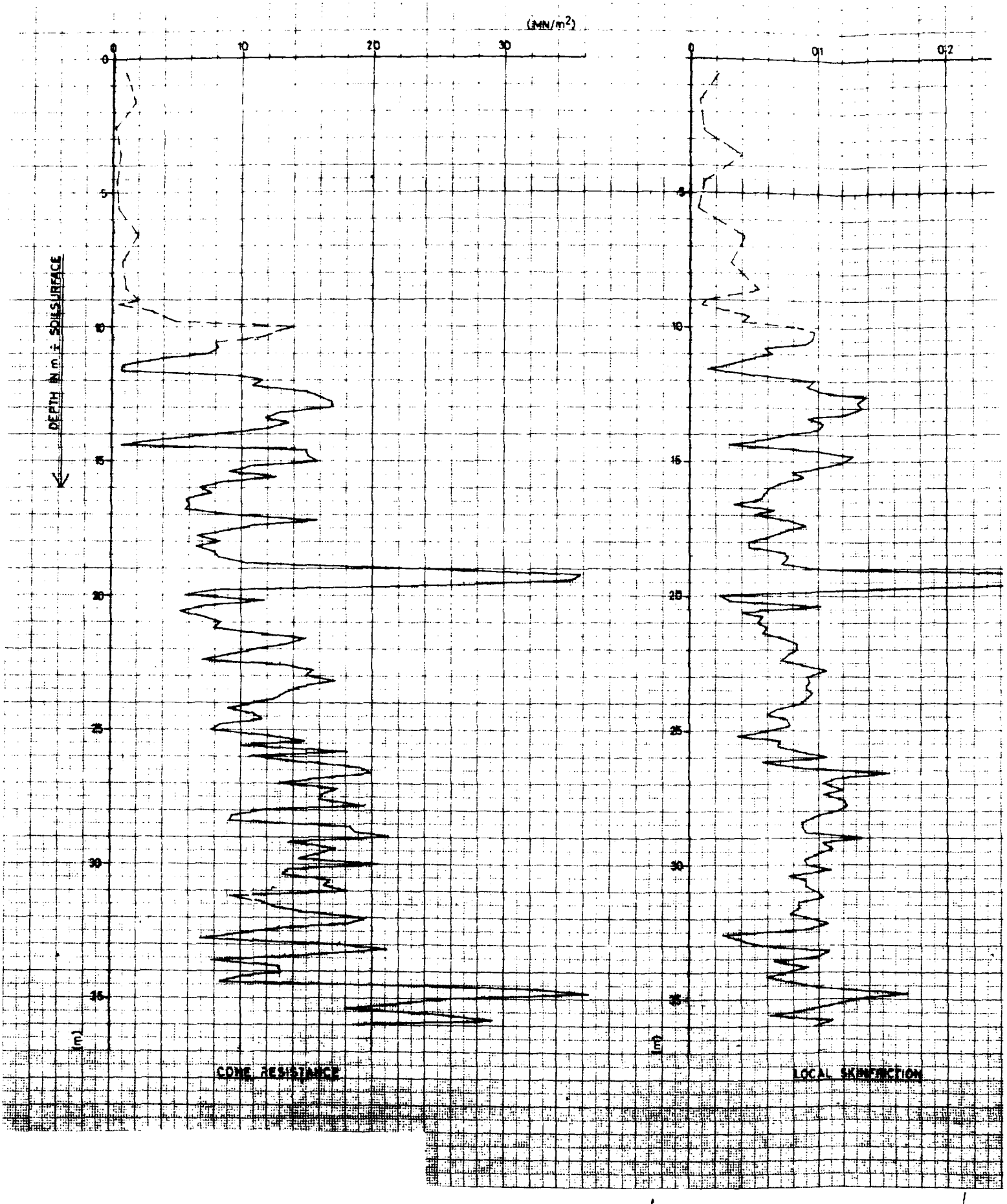
delft soil mechanics laboratory

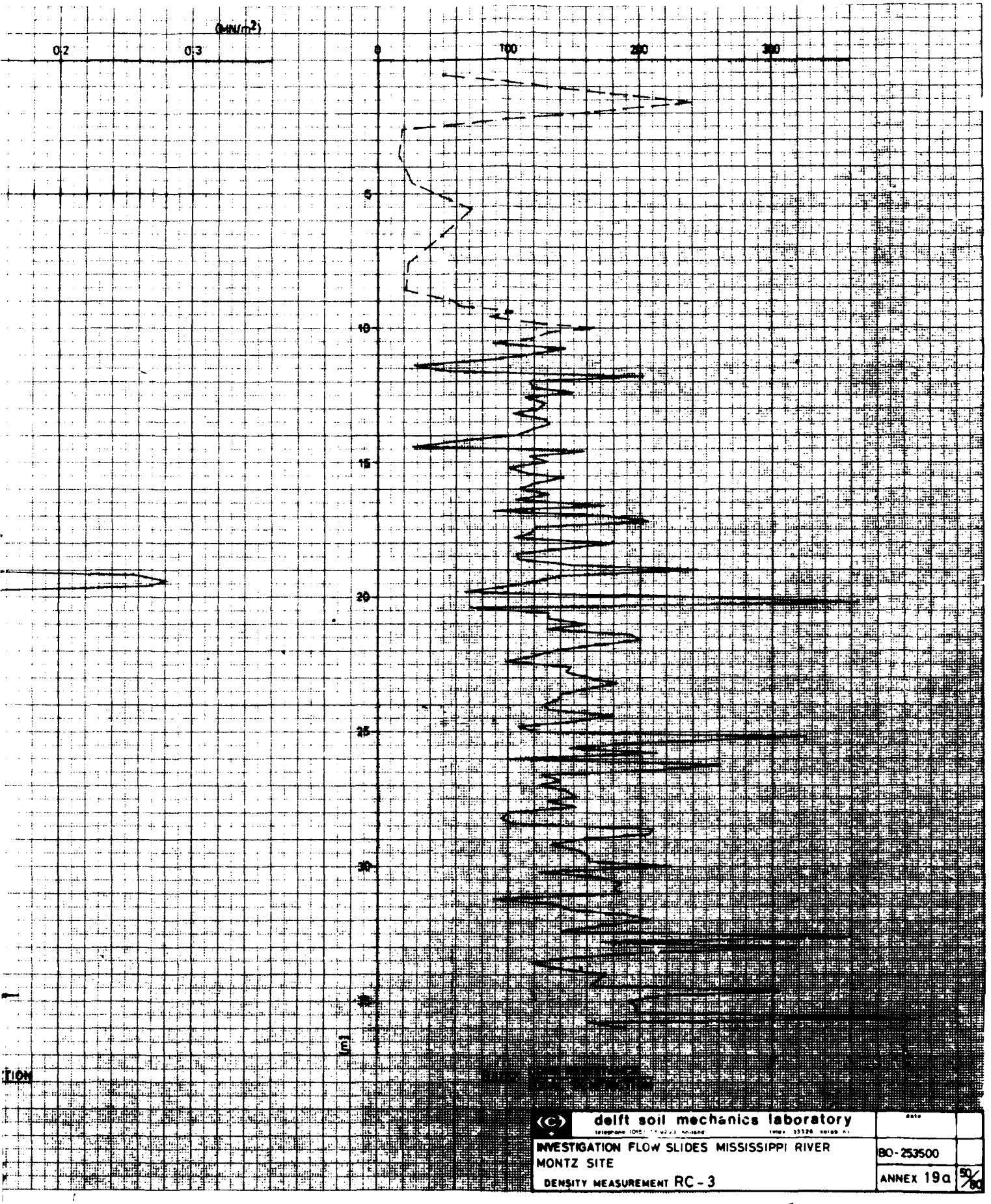
INVESTIGATION FLOW SLIDES MISSISSIPPI RIVER
MONTZ SITE
DENSITY MEASUREMENT RC-2

BO-253500

ANNEX 18b 50/80

2


(MN/m²)
0
10
20
30
0
0.1
0.2
DEPTH IN m ± SOILSURFACE
5
10
15
20
25
30
35
CONE RESISTANCE
LOCAL SKINFRICTION



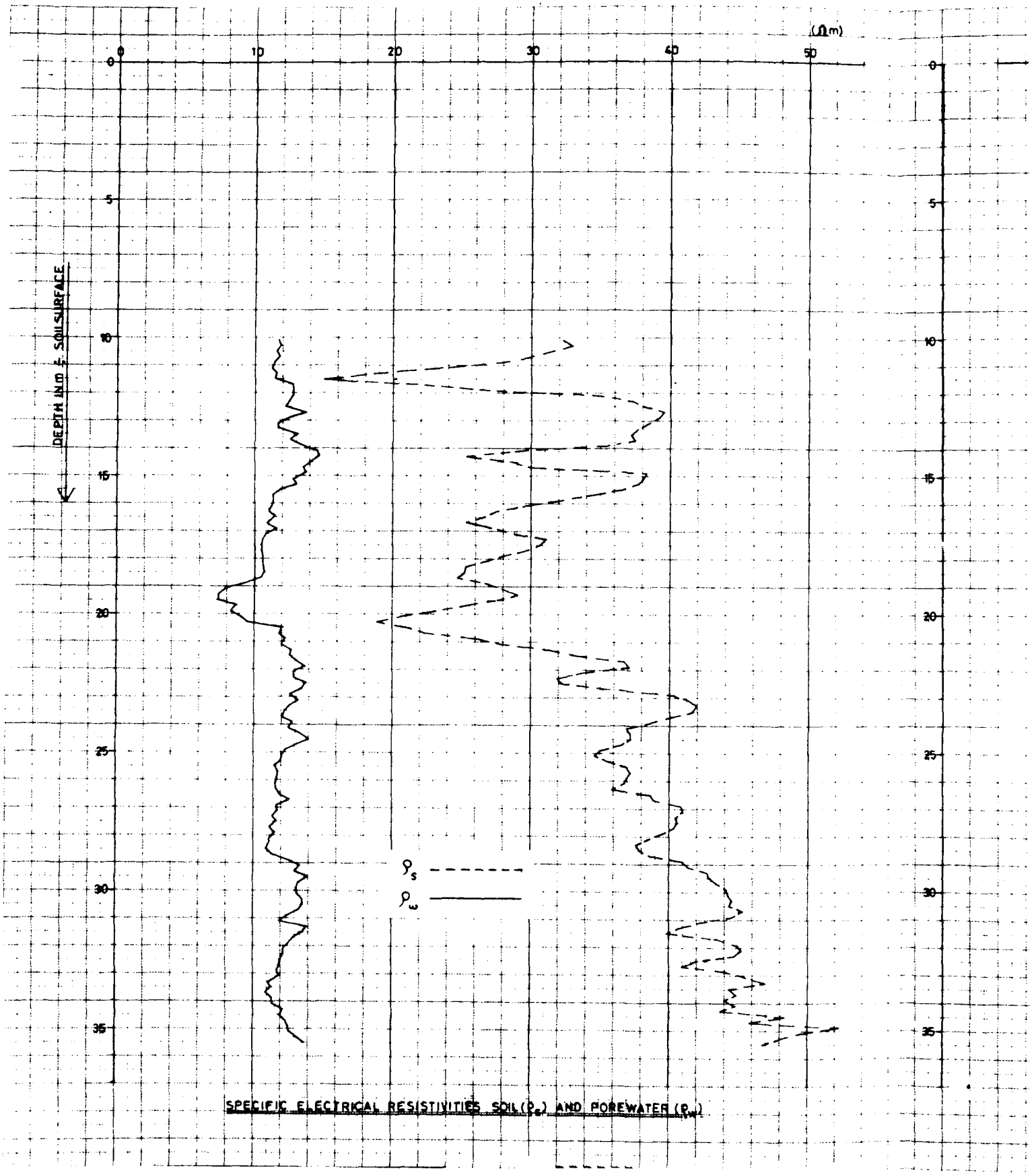
(C) delft soil mechanics laboratory

INVESTIGATION FLOW SLIDES MISSISSIPPI RIVER
MONTZ SITE
DENSITY MEASUREMENT RC - 3

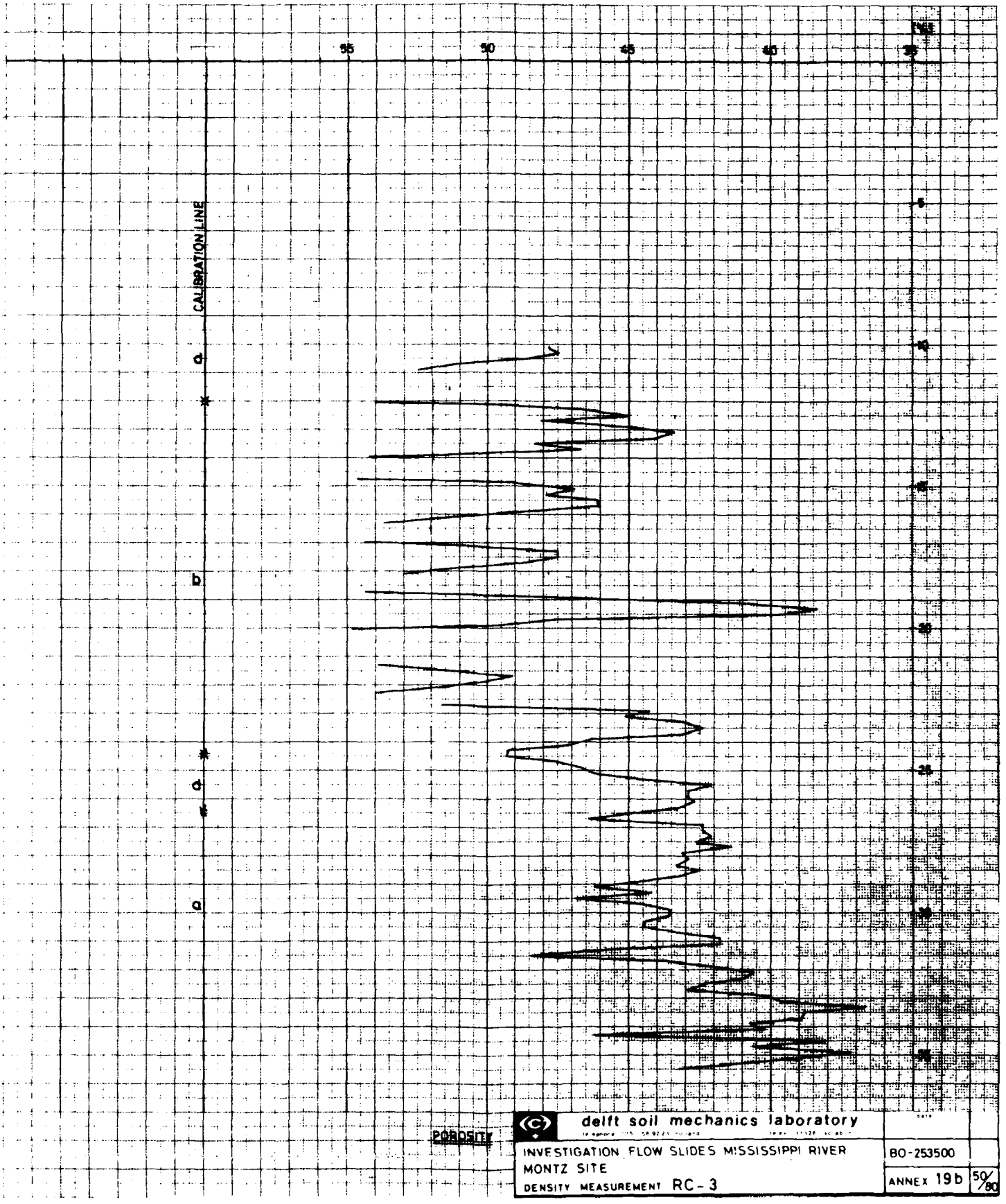
80-253500

ANNEX 19a

2



SPECIFIC ELECTRICAL RESISTIVITIES SOIL (ρ_s) AND POREWATER (ρ_w)

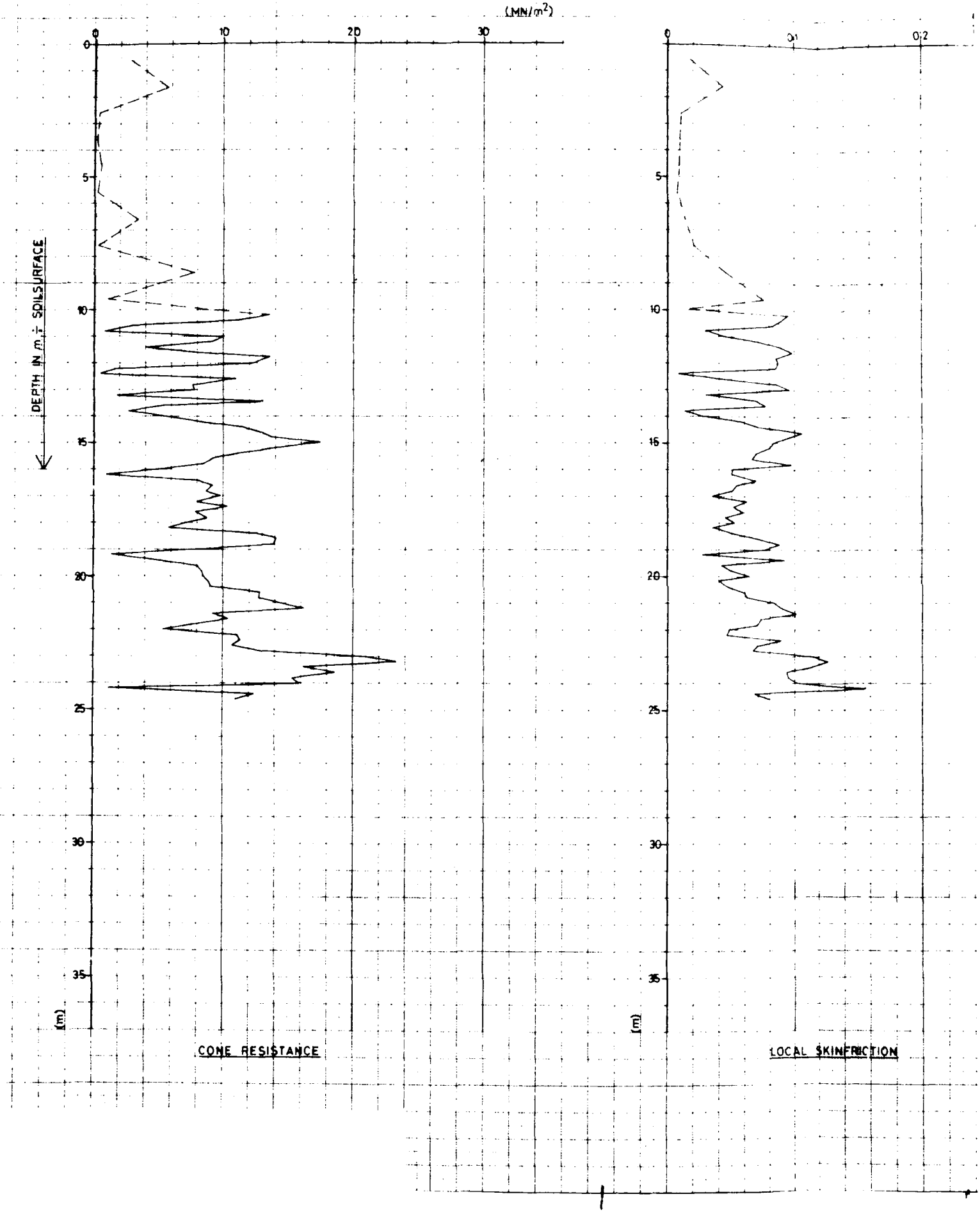


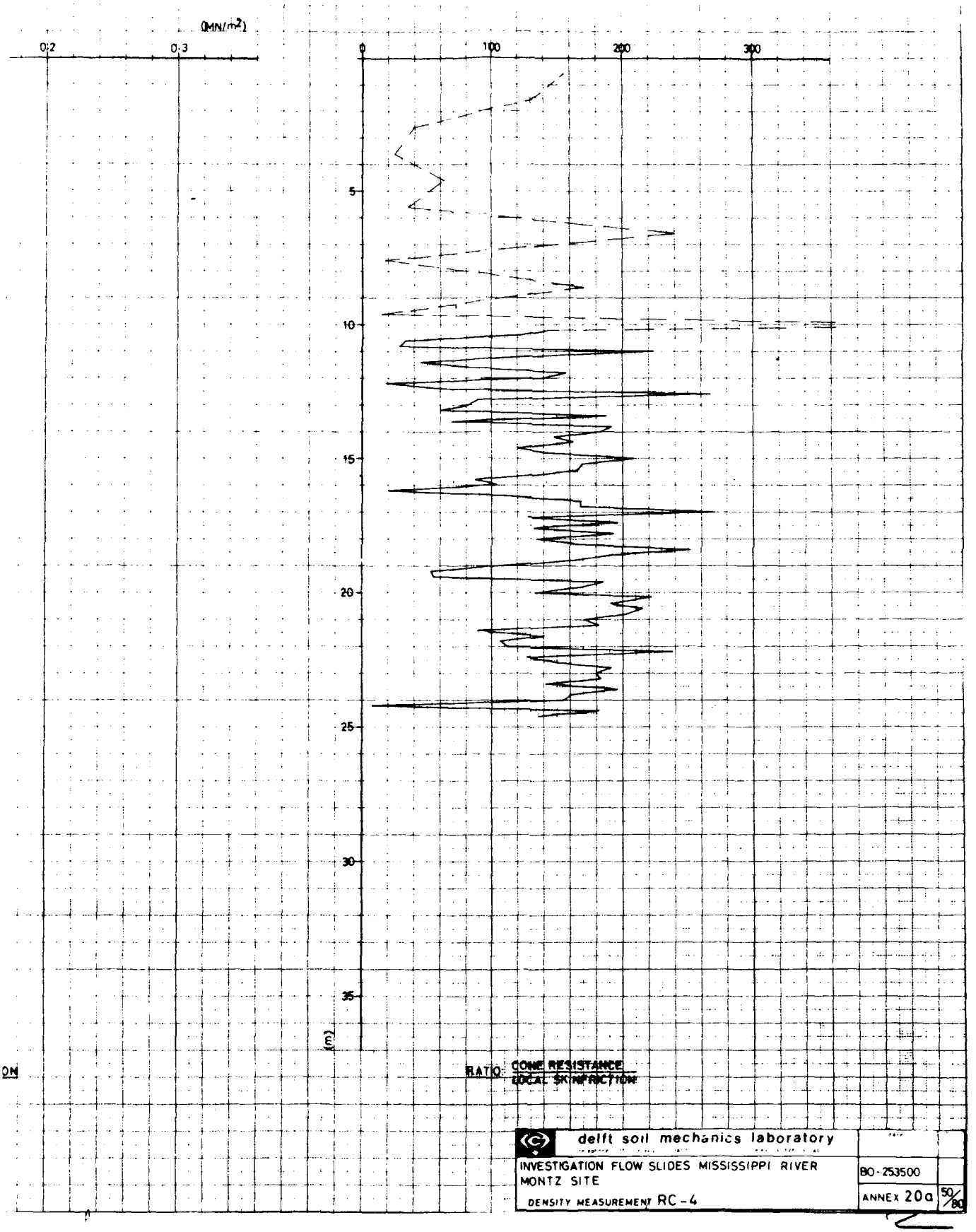
delft soil mechanics laboratory

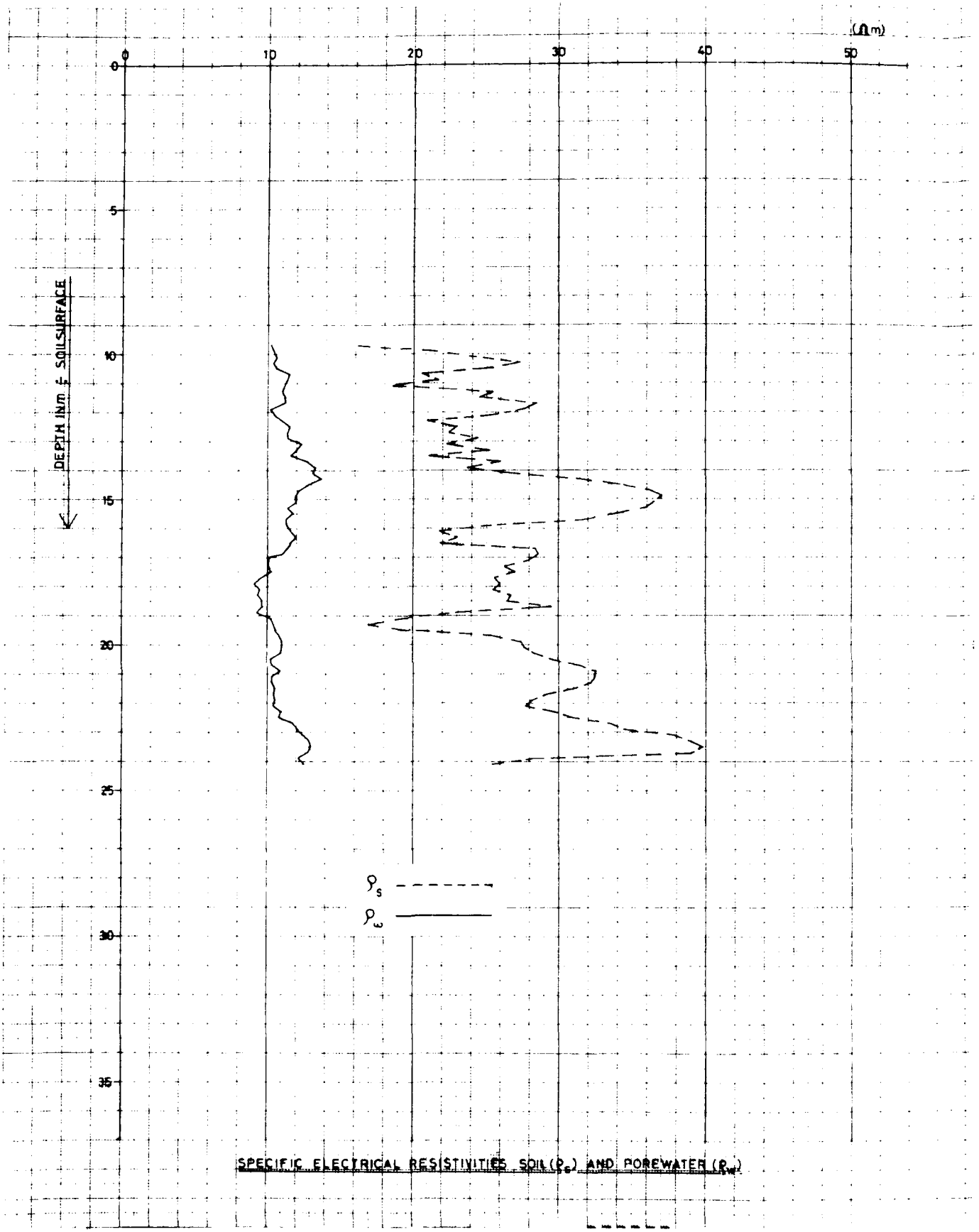
INVESTIGATION FLOW SLIDES MISSISSIPPI RIVER
MONTZ SITE
DENSITY MEASUREMENT RC-3

BO-253500

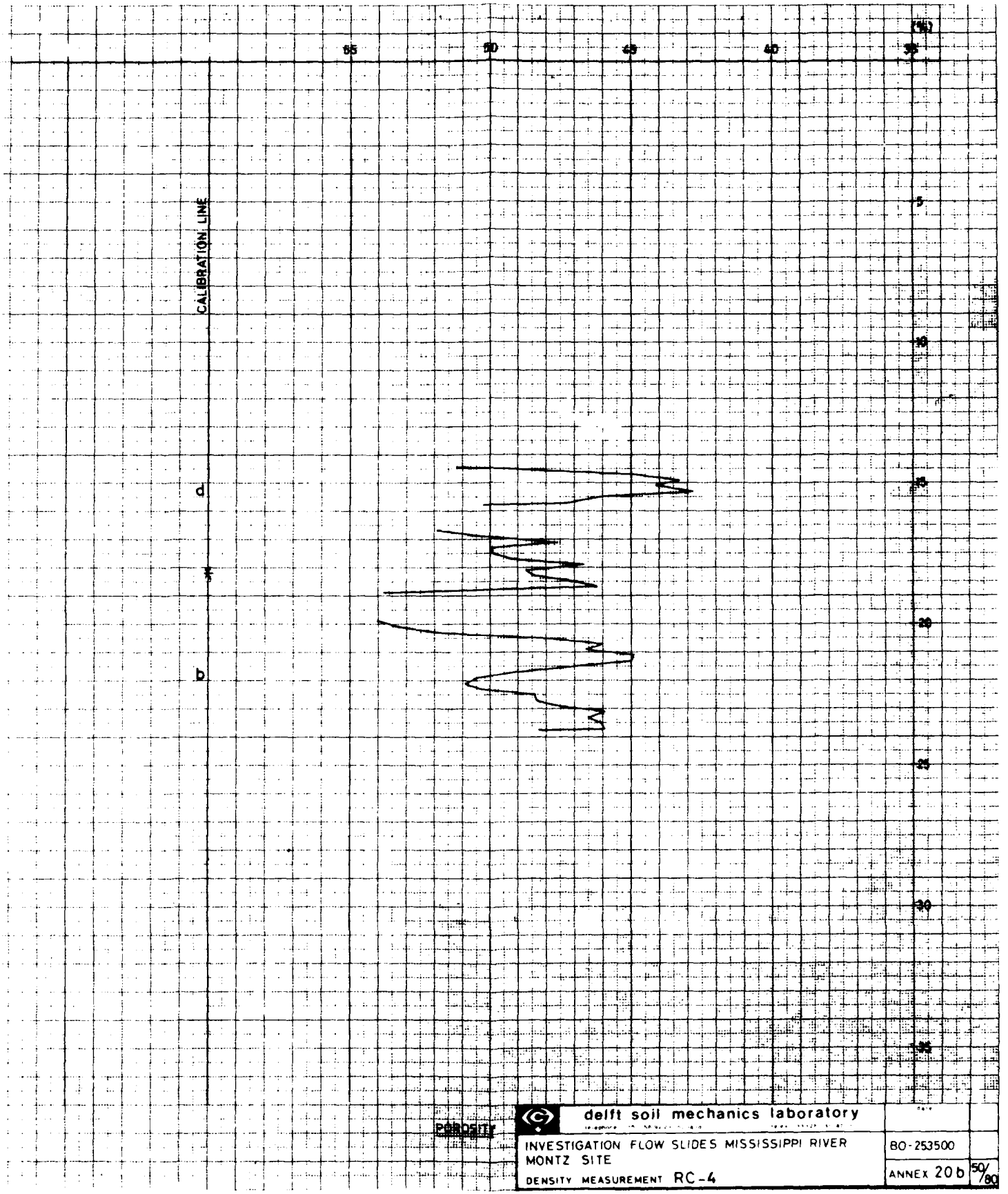
ANNEX 19b 50/80


(MN/m²)
0
10
20
30
0
0,1
0,2
5
10
15
20
25
30
35
DEPTH IN m ↓ SOILSURFACE
(m)
CONE RESISTANCE
LOCAL SKINFRICTION


(MN/m²)
0·2
0·3
0
100
200
300
5
10
15
20
25
30
35
(m)
RATIO: CONE RESISTANCE / LOCAL SKIN FRICTION
delft soil mechanics laboratory
INVESTIGATION FLOW SLIDES MISSISSIPPI RIVER
MONTZ SITE
DENSITY MEASUREMENT RC-4
80-253500
ANNEX 20a
50/80



SPECIFIC ELECTRICAL RESISTIVITIES SOIL (ρ_s) AND POREWATER (ρ_w)



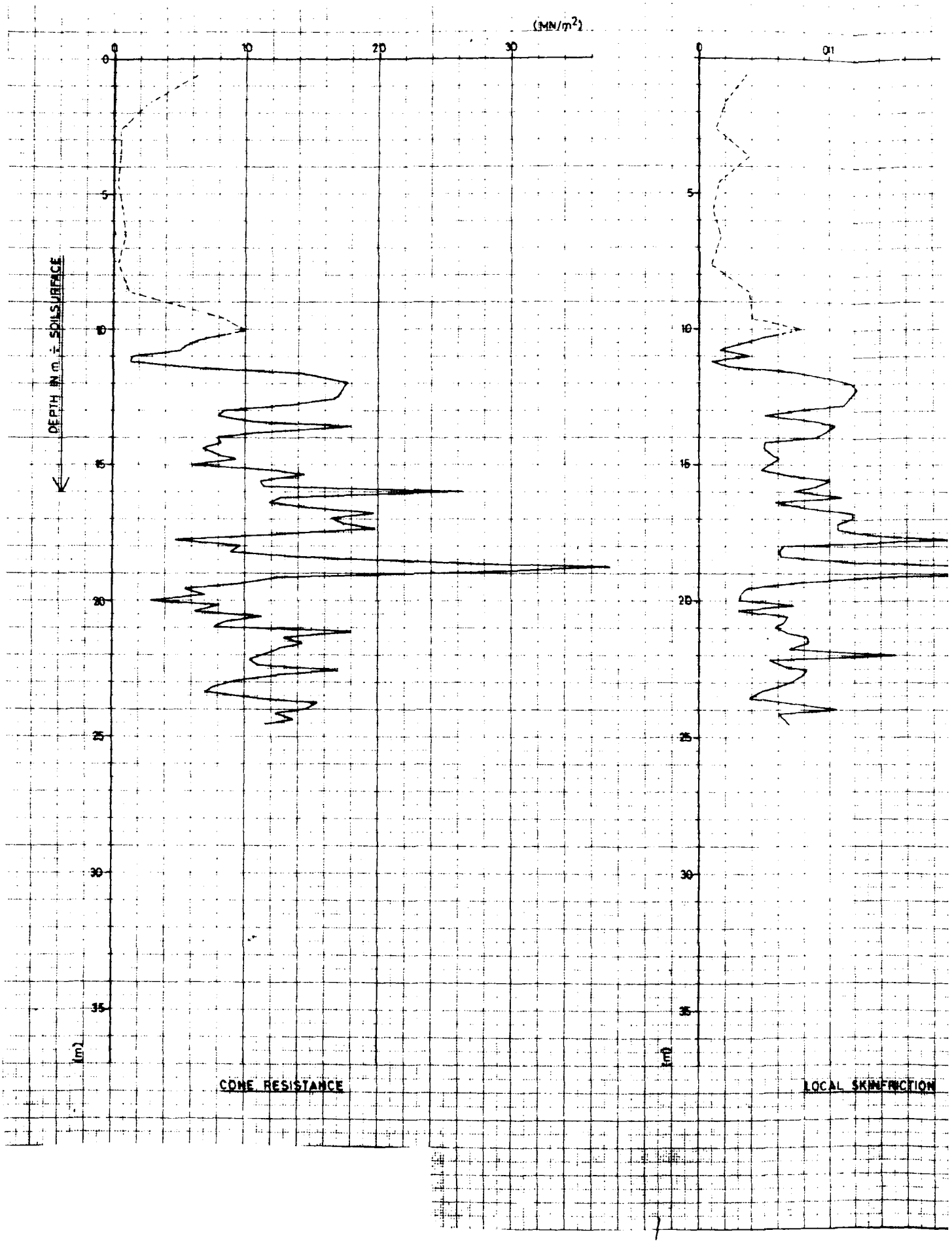
delft soil mechanics laboratory

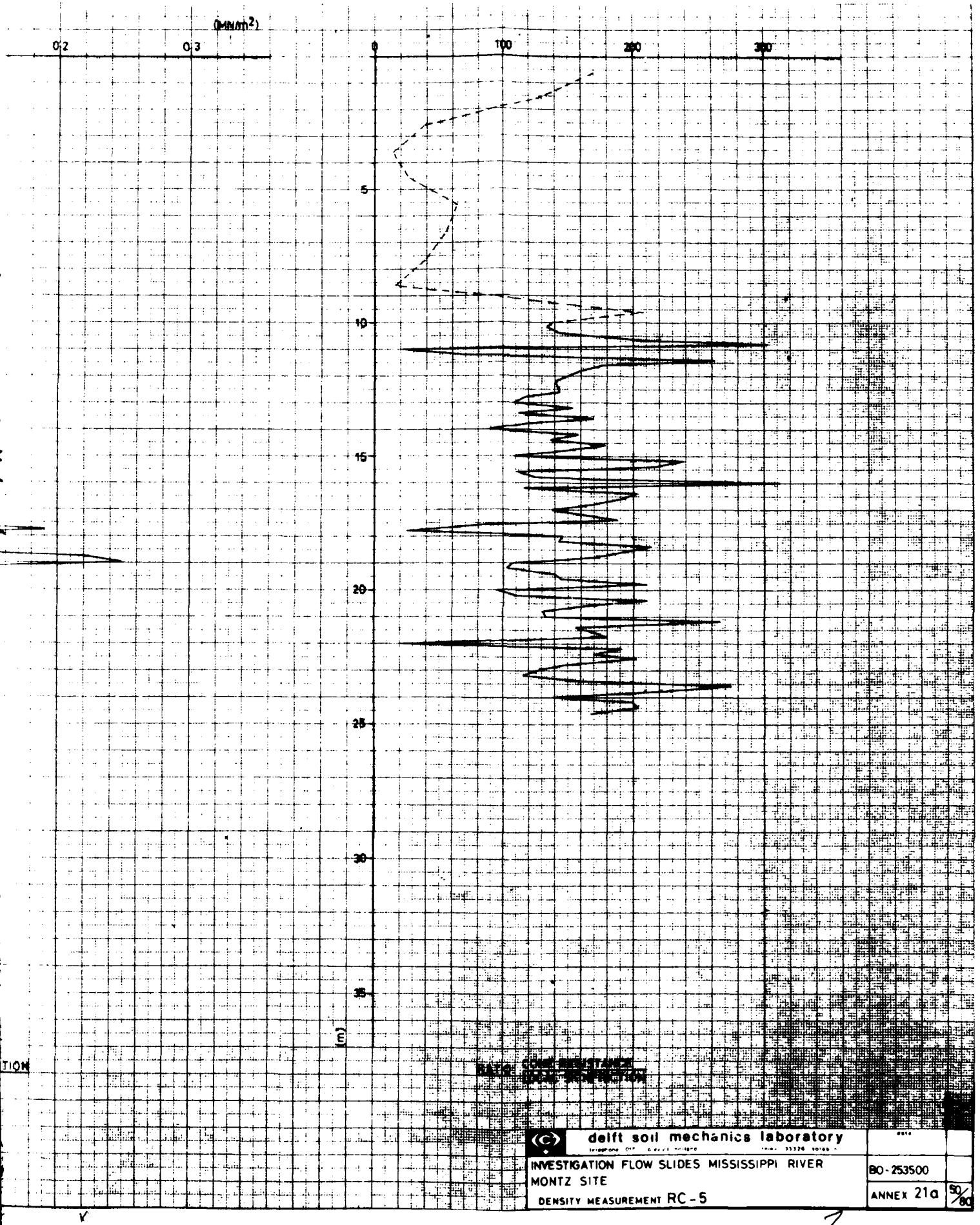
INVESTIGATION FLOW SLIDES MISSISSIPPI RIVER
MONTZ SITE

DENSITY MEASUREMENT RC-4

80-253500

ANNEX 20b 50/80

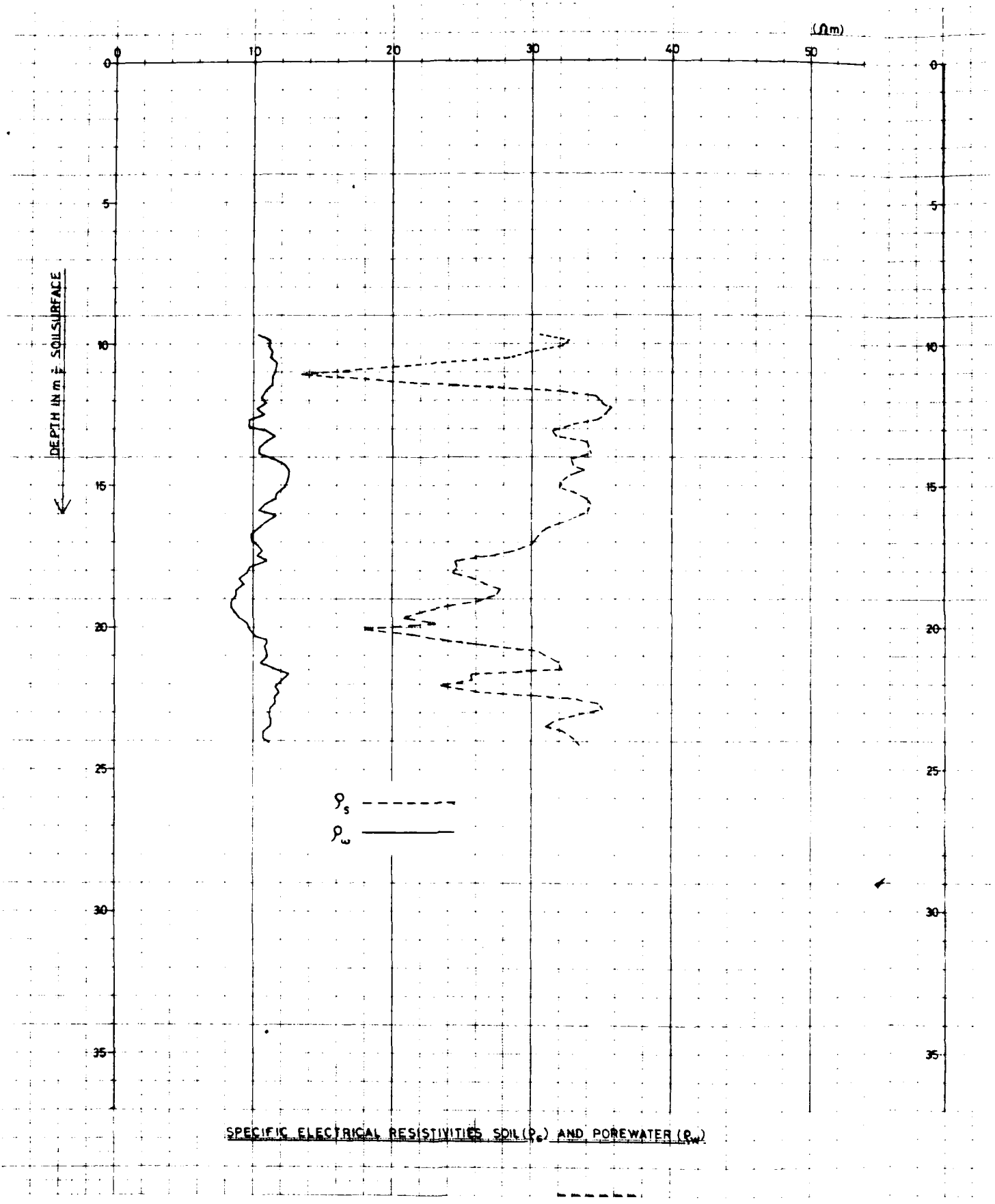

(MN/m²)
0
10
20
30
0
5
10
15
20
25
30
35
DEPTH IN m ± SOILSURFACE
(m)
CONE RESISTANCE
0
0.1
5
10
15
20
25
30
35
(m)
LOCAL SKINFRICTION



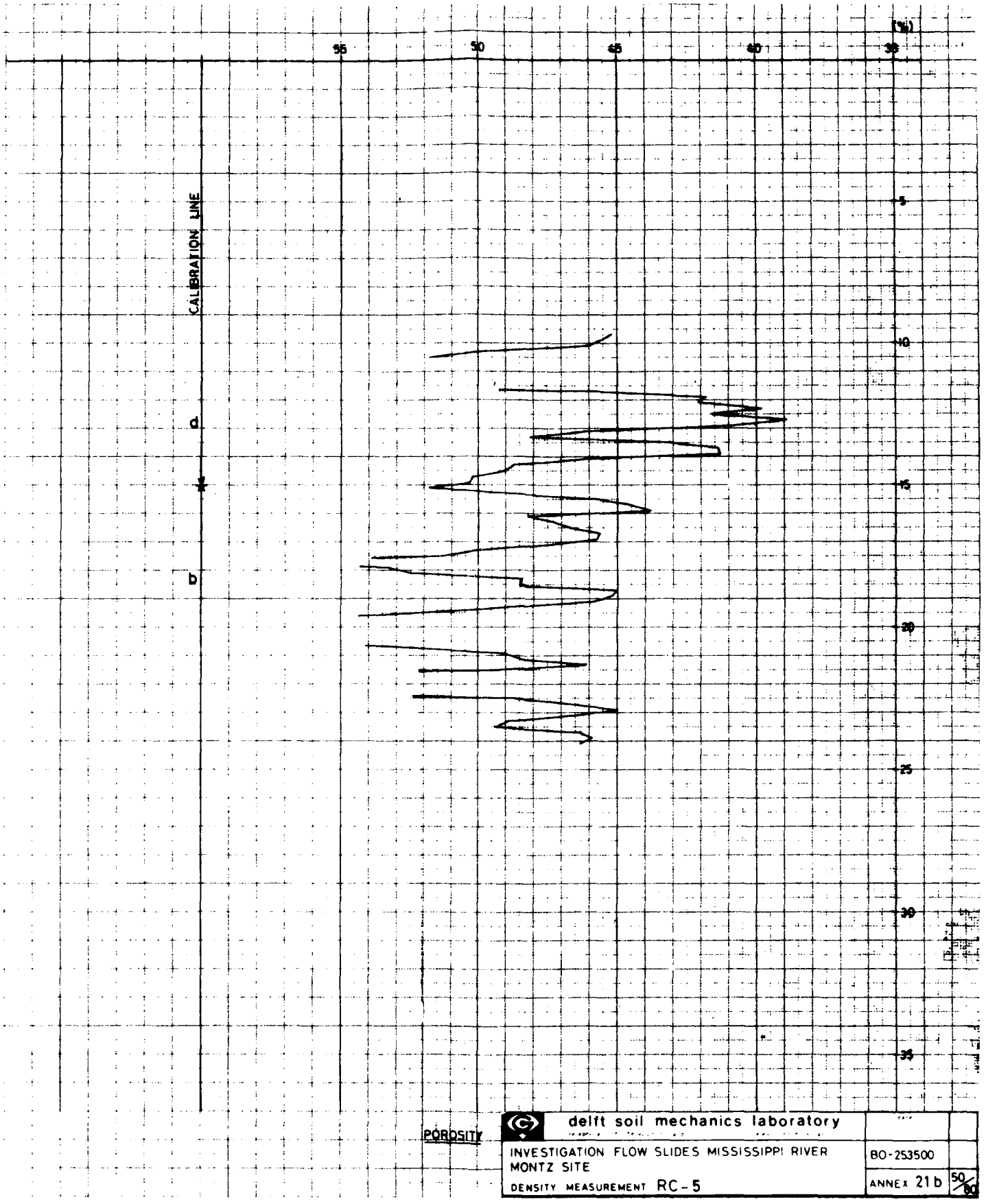
delft soil mechanics laboratory

INVESTIGATION FLOW SLIDES MISSISSIPPI RIVER
MONTZ SITE
DENSITY MEASUREMENT RC - 5

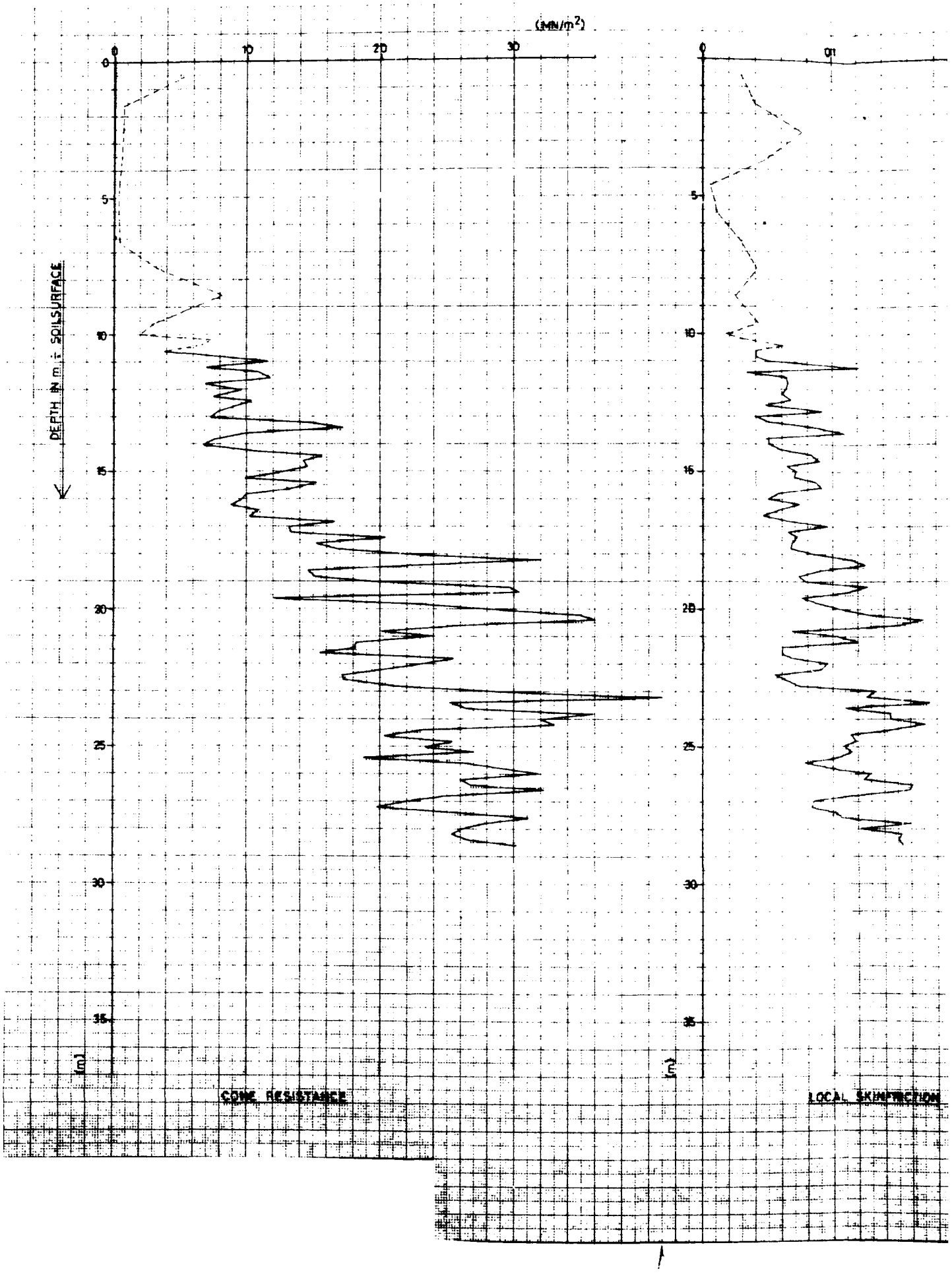
B0-253500
ANNEX 21a

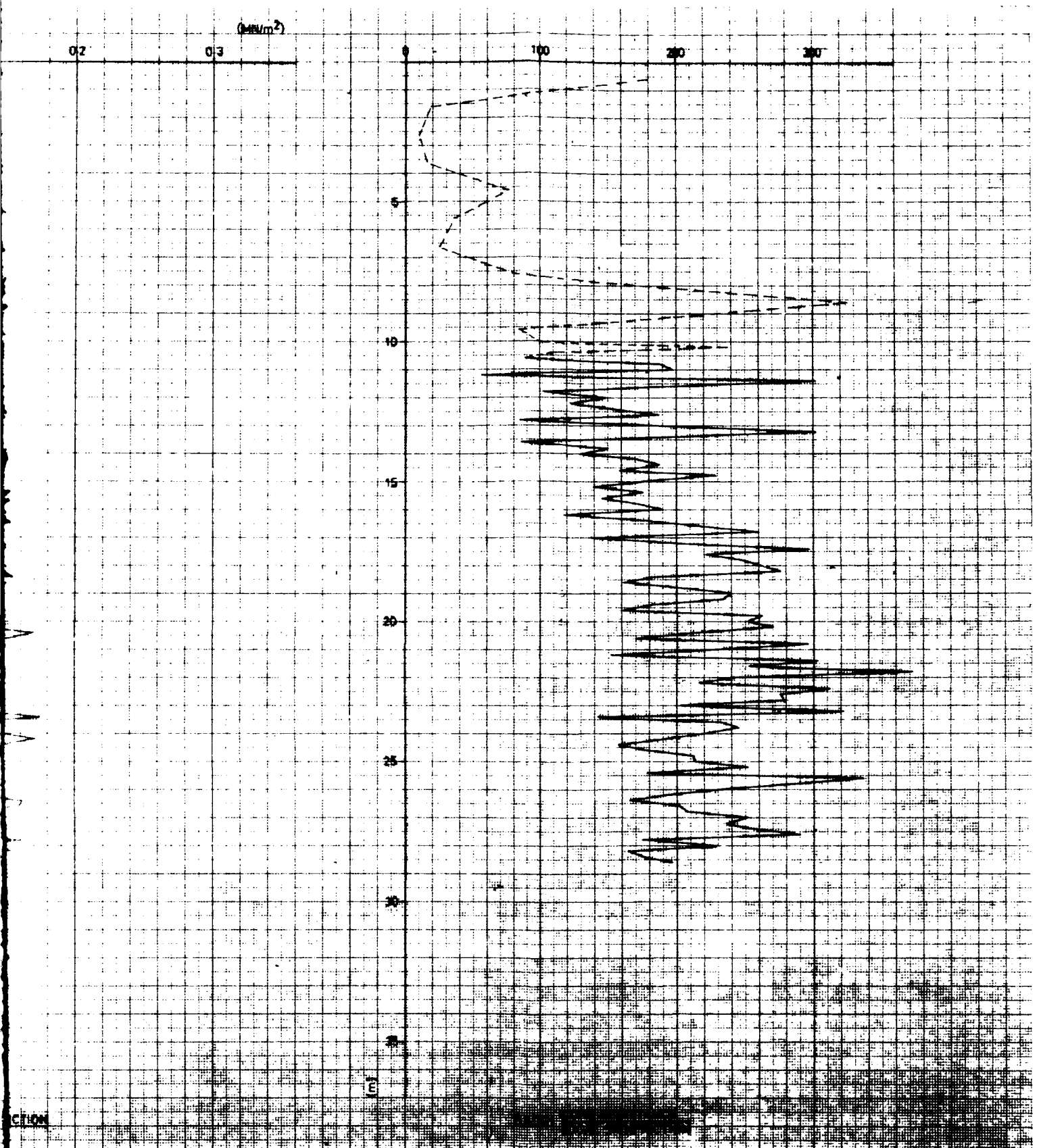


SPECIFIC ELECTRICAL RESISTIVITIES SOIL (ρ_s) AND POREWATER (ρ_w)



delft soil mechanics laboratory		
INVESTIGATION FLOW SLIDES MISSISSIPPI RIVER MONTZ SITE	BO-253500	
DENSITY MEASUREMENT RC-5	ANNEX 21b	50/80


(MN/m²)
0
10
20
30
0
0,1
5
10
15
20
25
30
35
DEPTH IN m ± SOILSURFACE
(m)
CONE RESISTANCE
(m)
LOCAL SKINFRICTION

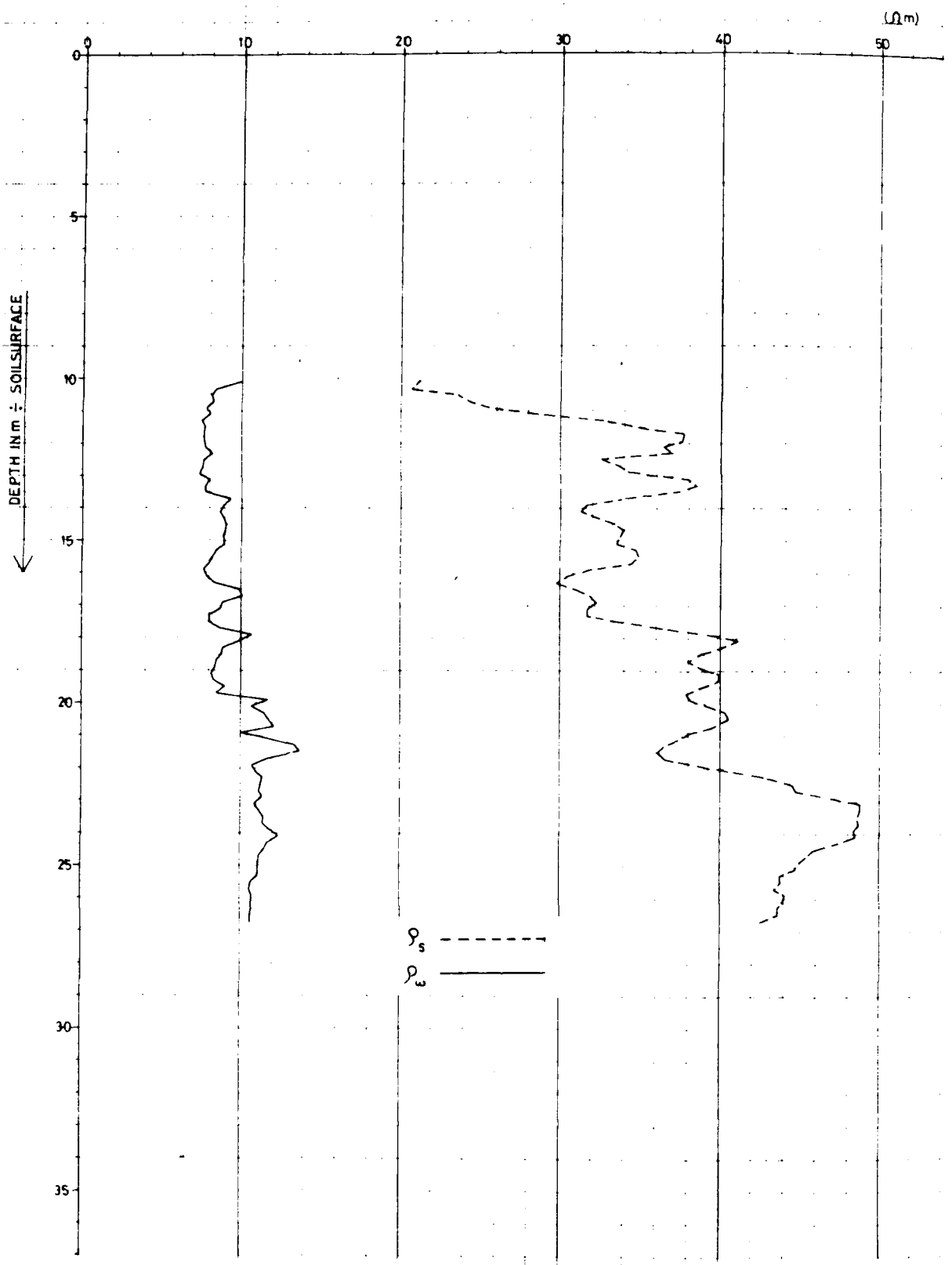


delft soil mechanics laboratory

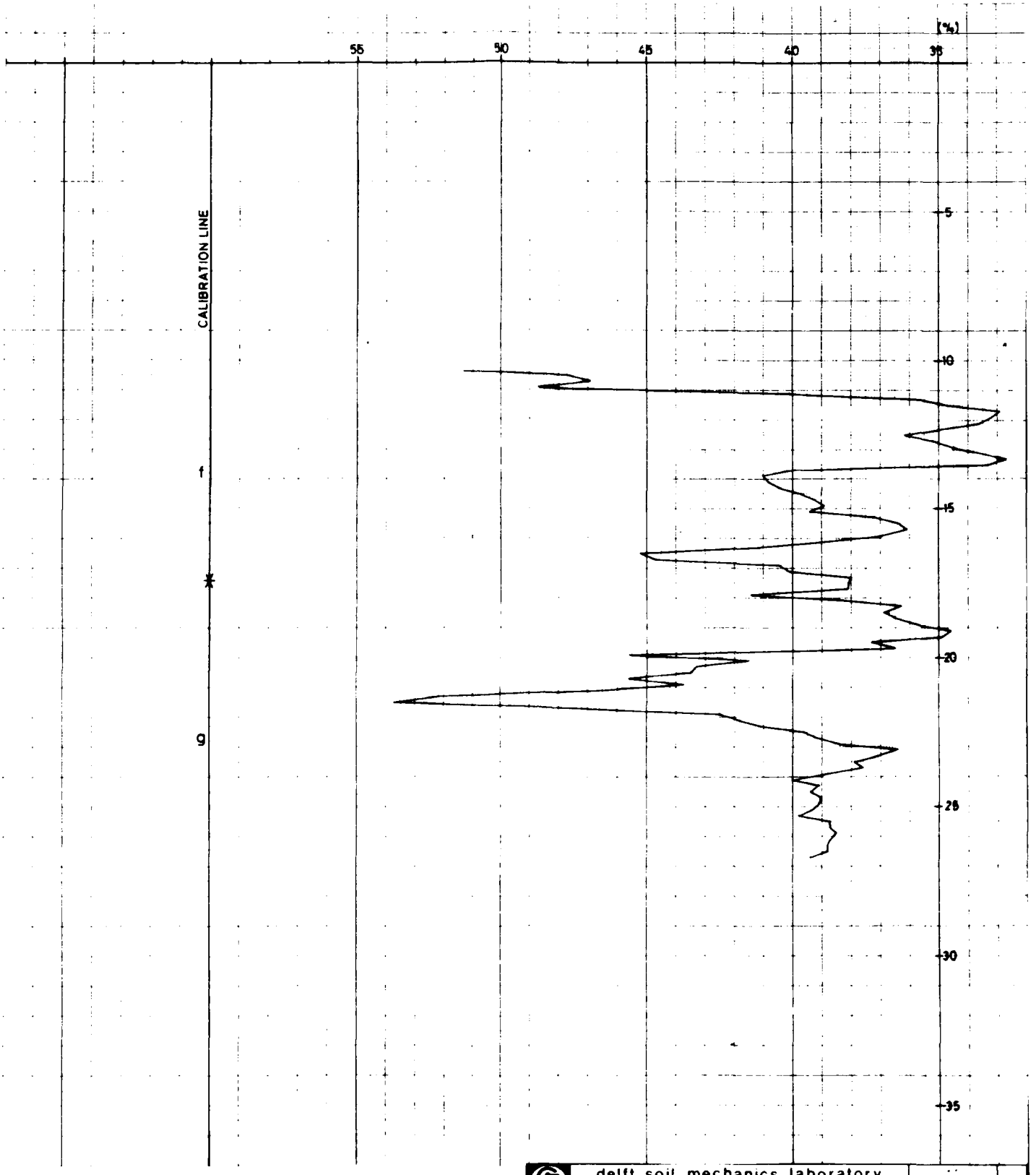
INVESTIGATION FLOW SLIDES MISSISSIPPI RIVER
BONNET CARRE SITE
DENSITY MEASUREMENT BRC-1

BO-253500

ANNEX 22a 50/80



SPECIFIC ELECTRICAL RESISTIVITIES SOIL (ρ_s) AND POREWATER (ρ_w)



delft soil mechanics laboratory

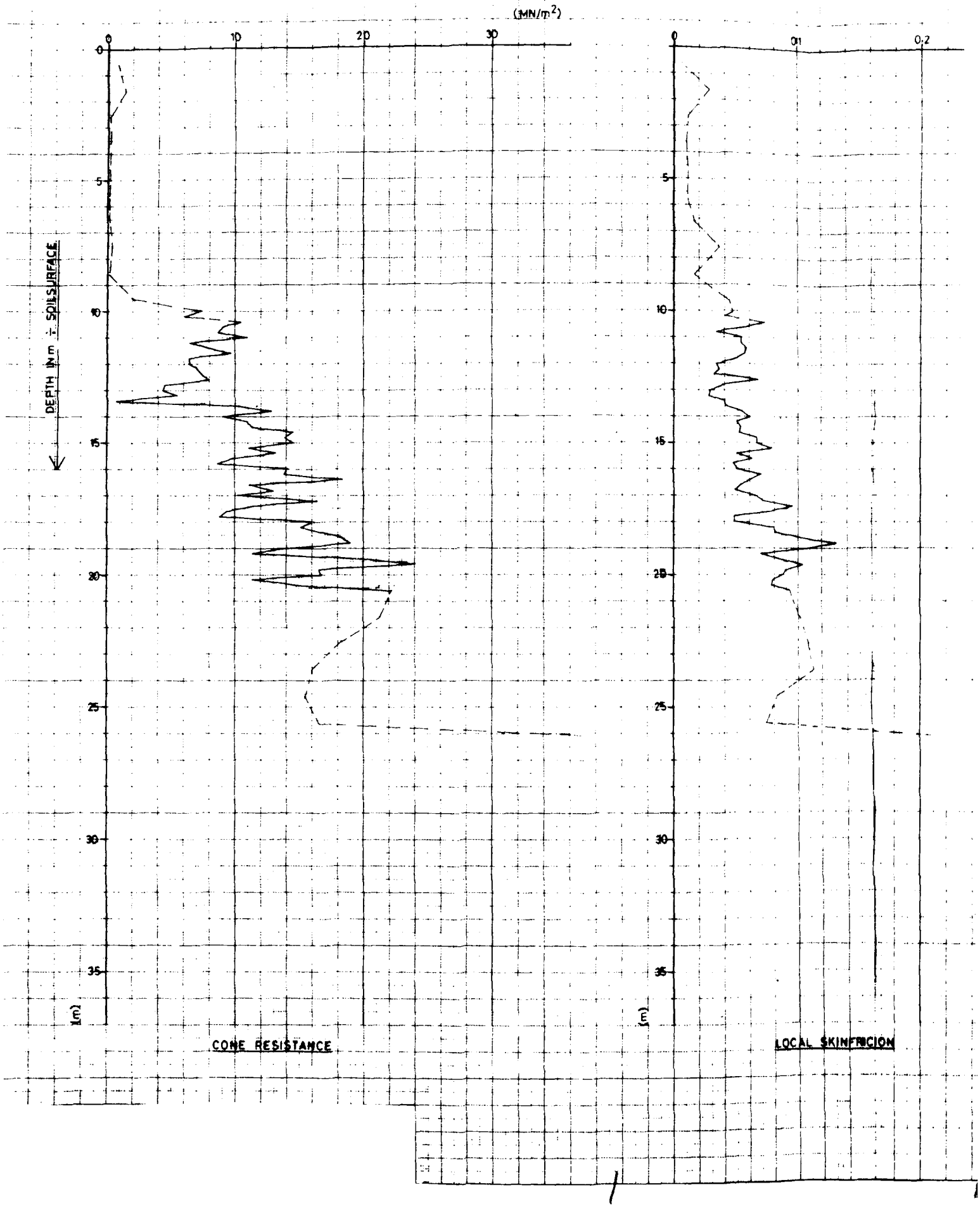
INVESTIGATION FLOW SLIDES MISSISSIPPI RIVER
BONNET CARRE SITE

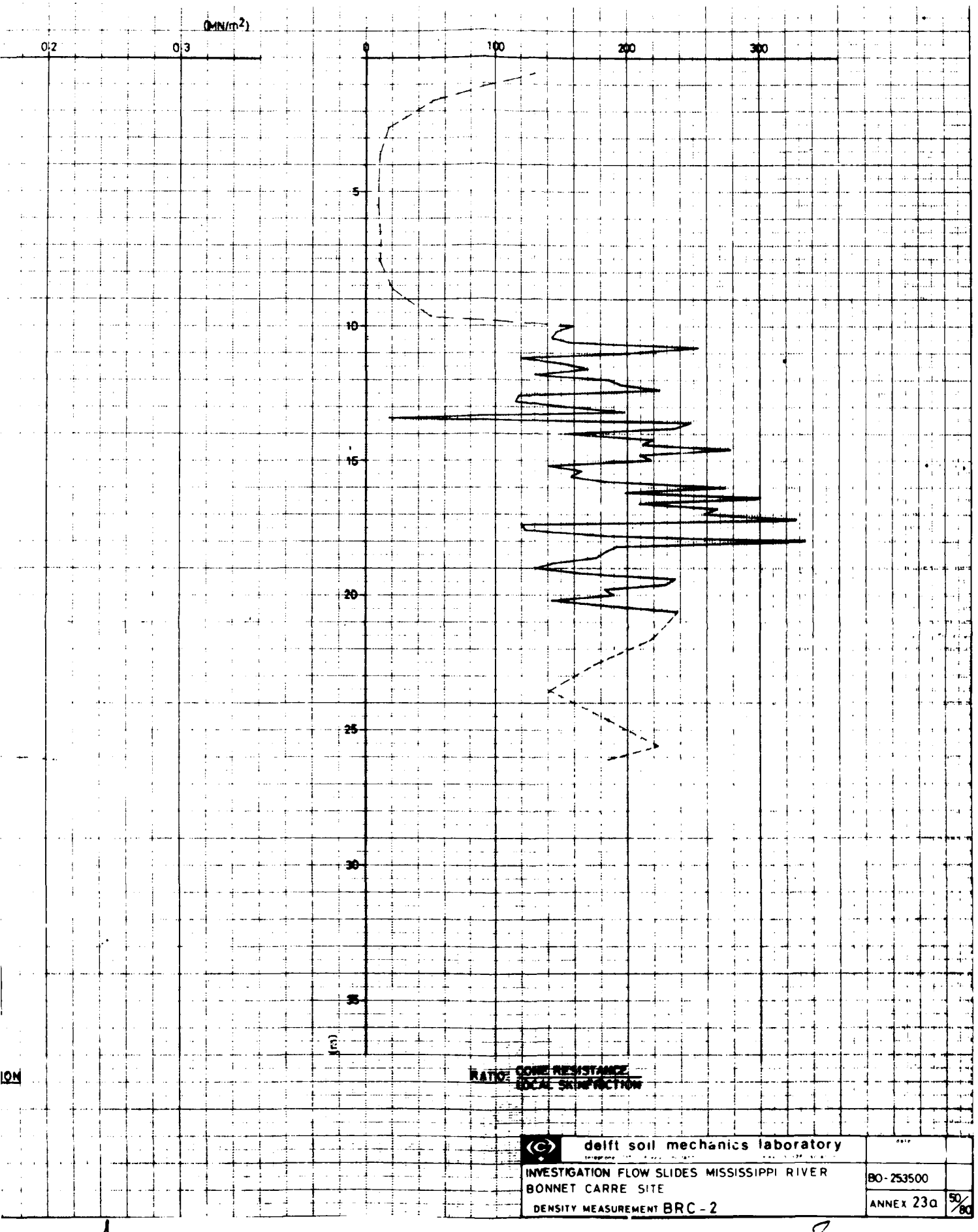
DENSITY MEASUREMENT BRC-1

BO-253500

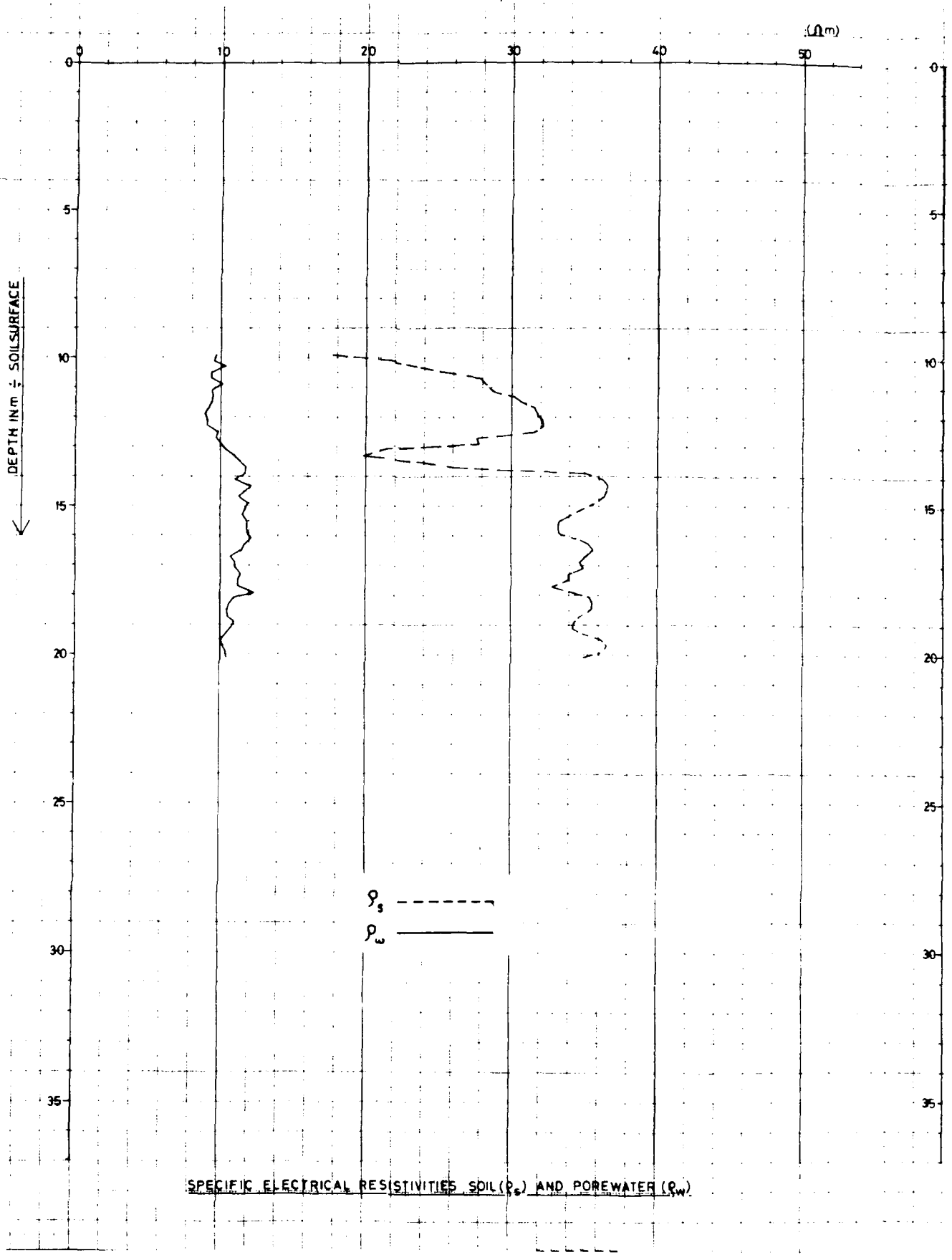
ANNEX 22b

50/80

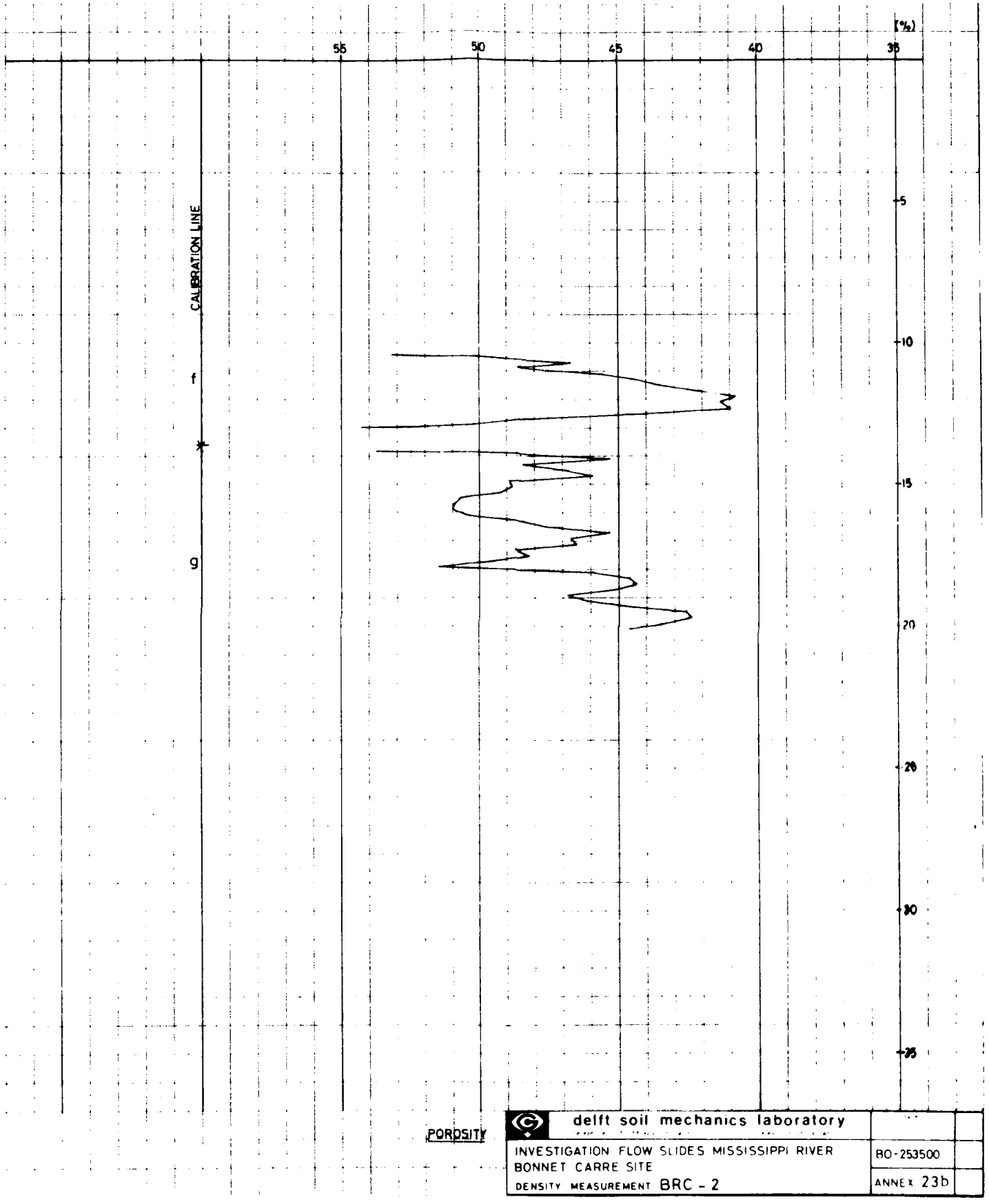

(MN/m²)
0
10
20
30
0
0,1
0,2
DEPTH IN m ÷ SOILSURFACE
0
5
10
15
20
25
30
35
(m)
CONE RESISTANCE
LOCAL SKINFRICION



delft soil mechanics laboratory		
INVESTIGATION FLOW SLIDES MISSISSIPPI RIVER BONNET CARRE SITE	BO-253500	
DENSITY MEASUREMENT BRC-2	ANNEX 23a	50/80



SPECIFIC ELECTRICAL RESISTIVITIES SOIL (ρ_s) AND POREWATER (ρ_w)



delft soil mechanics laboratory		
INVESTIGATION FLOW SLIDES MISSISSIPPI RIVER BONNET CARRE SITE	BO-253500	
DENSITY MEASUREMENT BRC - 2	ANNEX 23b	

2

APPENDIX H

ELECTRICAL PIEZOCONE PENETRATION TESTS; ARDAMAN AND ASSOCIATES, CONTRACT REPORT

FIELD INVESTIGATION
MONTZ AND BONNE CARRE POINT
CORPS OF ENGINEERS WES



Ardaman & Associates, Inc.

OFFICES

Orlando, 6015 Randolph Street, P.O. Box 13003, Orlando, Florida 32809, Phone (305) 855-3860
Bartow, 1987 S. Holland Parkway, Bartow, Florida 33830, Phone (813) 533-3893
Cocoa, 1300 N. Cocoa Blvd., P.O. Box 3557, Cocoa, Florida 32922, Phone (305) 632-2503
Fort Myers, 6522 Northside Circle, Suite 4, North Fort Myers, Florida 33903, Phone (813) 997-1688
Ocala, 101 N.E. First Avenue, Ocala, Florida 32670, Phone (904) 732-8049
Sarasota, 2500 Bee Ridge Road, P.O. Box 15008, Sarasota, Florida 33579, Phone (813) 922-3526
Tallahassee, 3175 West Tharpe Street, Tallahassee, Florida 32303, Phone (904) 576-6131

MEMBERS:
American Concrete Institute
American Society for Testing and Materials
American Consulting Engineers Council
Association of Soil and Foundation Engineers
Florida Institute of Consulting Engineers
Professional Engineers in Private Practice

Ardaman & Associates, Inc.

Consulting Engineers in Soil Mechanics,
Foundations, and Materials Testing

February 24, 1981
File Number 78-039

Department of the Army .
Waterways Experiment Station
Corps of Engineers
P. O. Box 631
Vicksburg, Mississippi 39180

Attention: Mr. Vic Torrey, III

Subject: Field Study of Liquifaction Potential of Sand Deposits near New Orleans.

Gentlemen:

This report presents the results of the field investigation program at two sites, Montz and Bonnet Carre Point, Louisiana, using our electric piezometer and piezocone. The purpose of this program was to measure soil parameters in regards to the potential to undergo liquifaction. Recent earth displacements into the Mississippi River at each site had been attributed to soil liquifaction.

It has been a pleasure assisting you with this project and we hope we can be of assistance in some future projects. If you have any questions, please do not hesitate to contact us.

Very truly yours,
ARDAMAN & ASSOCIATES, INC.

James P. Handley
Instrumentation Engineer

Anwar E. Z. Wissa
President

JPH:AEZW:ed

1.1 INTRODUCTION AND SCOPE

An ongoing problem along the lower Mississippi River in river bank deposits of silty and clayey sands is the frequent and sudden displacement of large amounts of soil from the banks out into the river. This condition has been attributed to soil liquifaction. Our firm, using the Geotechniques International, Inc. electronic piezometer probe and newly developed piezocone was retained under your Contract No. DACW39-80-C-102 (Neg.) to perform a site investigation program to measure excess pore water pressures generated during penetration at constant rates. In addition, when using the piezocone, point pressure and local sleeve friction were also recorded. This data was then evaluated to determine the liquification potential of the soils at two sites, both of which had experienced recent liquification slides.

The location of the two sites, Montz and Bonnet Carre Point, Louisiana, are shown on Figure 1. Both sites have similar general soil profiles. Examples of the soil profiles at each site are shown on Figures 2 and 3 from borings SPT-3 at the Montz site and boring N.E. at the Bonnet Carre site. Shallow soils down to -22 feet below ground level are loose to medium dense clayey and silty sands with clay lenses. These clay lenses are easily seen on the piezocone logs located in Appendix A. Soils below 22 feet are generally medium to dense sands with silty sand and clay lenses. At approximately 80 feet below ground, deposits of clean sands exist. It was anticipated that each test hole would be advanced down to a depth of at least 100 feet below ground surface, but the cone in several holes could not be advanced below approximately 80 feet due to this layer of clean sand. The testing program consisted of nine test holes. Six of the holes were located at the Montz site and three at the Bonnet Carre Point site. Four of the six holes at Montz were performed using the electric piezometer probe. The remaining two at Montz and all three at the Bonnet Carre Point site were performed with the piezocone.

1.2 INSTRUMENTATION DESCRIPTION

Two types of instruments were used on this project. The first called the "Piezometer Probe" has been in use by our firm for more than eight years. It is designed to soley measure pore pressure.

As illustrated in Figure 4, the piezometer probe consists of a high air entry, stainless steel, porous tip, hydraulically connected to a flush diaphragm pressure transducer contained in a 18° cone shaped housing. This housing attaches to a cylindrical adapter, the upper end having a male thread to which standard drill rods can be attached to jack the probe into the soil. A four conductor, shielded, electrical cable, from the transducer, protected by polyethylene tubing, is threaded through the unassembled drill rod sections and connected to surface data collection instruments. The output signal is readily converted to water pressure head using the transducer calibration. Depending upon the application, the range and sensitivity of the piezometer probe can be selected by changing the pressure transducer in the probe.

The second instrument used was the "Piezocone". This instrument was recently developed by Geotechniques International and has been used by our firm for the last year. As illustrated in Figure 5, the piezocone, like the piezometer probe, has a porous tip hydraulically connected to a pressure transducer for pore pressure measurements but housed in a 60° cone rather than an 18° cone. In addition, load cells are included to measure point resistance and local sleeve friction. Instrument temperature is also monitored. A feature unique to this instrument is the ability to change point load cells depending on the soil strengths to be measured and to protect these lower range cells from overload by an internal overload protection device.

A 12 conductor shielded cable is used between the piezocone and the data collection instruments. This cable is protected inside a 1/2" polyethelene tubing. Total cable length is 170 feet.

Also of importance in the design of this instrument is the ratio of the areas of cone face to the area of cone back side as illustrated in Figure 6. In doing any analysis using generated pore pressure, the value of pore pressures existing on the back side cannot be accurately established, thus the net contribution of pore pressure to total point load cannot be determined. The piezocone used has a ratio of back area to front area of less than 15% and therefore no correction to point load is made.

To measure the rate of penetration and the distance the cone was below ground, a depth transducer was utilized. This instrument outputs two signals. The first signal, when connected to a strip chart recorder displays rate and distance information in the form of a square wave output. The second signal is an analog signal of the actual depth below ground where the instrument is presently located. This signal is inputed to the data acquisition system and stored along with the probe or piezocone outputs on magnetic tape for later computer data reduction.

Support equipment at the surface consisted of: power supply, digital voltmeter, two-dual channel strip chart recorders, 10 channel data acquisition system with built-in voltmeter and magnetic tape storage.

1.3 TESTING PROCEDURES

The testing began at the Montz site. Thirty-one meters of Gouda cone rods were prestrung with the instrument cable and the system given an initial check out.

Actual pushing began using a W.E.S. Failing 1500 drill rig. This proved unsatisfactory due to the rods being unsupported during pushing causing rod buckling and the fact that the rig had a maximum strike of 36" which is very difficult to use with 1 meter rods. Our 10 ton Gouda cone rig was then contracted to complete the project.

The first operation consisted of pushing a pilot hole from the surface down to the ground water table and filling this hole with water. This pilot hole was easily made using a mechanical cone carried on the rig. By lowering the probe through this water filled hole, tip saturation was continuously insured. An extremely important operation prior to lowering the instrument into the pilot hole was to check the pore pressure system response, which is critical in sandy soils. By rapidly changing the water pressure at the tip and measuring the pore pressure transducer output on a high speed strip chart recorder, system response was verified. Typically, a response of less than .1 seconds was considered acceptable and the instrument lowered into the hole.

Upon reaching the bottom of the pilot hole, advancing the instrument was done in one meter strokes. Approximately 30 seconds was required to place each additional rod in the load frame in preparation for the next 1 meter push. On occasion, the time delay between pushes was increased to measure the rate of excess pore pressure dissipation and equilibrium pore pressures. The rate of dissipation is a measure of the relative permeability of the soil surrounding the tip. Pore pressure response measured before and after completing each hole remained high allowing several holes to be performed using the same sensing tip. In general, the rate of advancement was set at 2 cm/sec., which is the standard rate for Dutch cone testing.

Several changes to this procedure were used in an effort to obtain more significant pore pressure data. On several holes, various pushes were made at the full penetration speed of the load frame, typically 1 and 12 cm/sec, in an effect to generate excessive pore pressure.

The hole was advanced until the pushing limit of the cone rig was reached. It is of interest to note that even though a friction breaker was used on the drill rod string, the resistance due to rod friction together with load bearings on the point and friction breaker exceeded the cone rig limits rather than the capacity of the point load cell which was 500 kg/cm^2.

Data during pushing and during the stop times required for pore pressure decay were recorded continuously for all holes. Selected examples of pore pressure decay between pushes are shown in Figure 7.

CONCLUSIONS

At the Montz site, the first 10 ± 2 feet below ground level are loose to medium dense silty and sandy soils with numerous clay and silt lenses.

Between 12 and 20 feet below ground level, the soils are generally medium dense to dense sands with up to eight distinct lenses of fine grained soils. These lenses are not thought to be continuous as they vary in elevation between test holes.

At the Bonnie Carrie Site, soils in the first 8 feet below ground level are loose to medium dense silty sands with lenses of fine grained soils.

Between 8 and 20 feet below ground level are silty sands with as many as four fine grained soil lenses one foot or more thick but not necessarily continuous since they are encountered at different elevations.

At both sites, soils from 20 feet below ground level to hole refusal, are uniform sandy soils with friction ratio less than 2%.

At both sites the measured pore pressure generated during penetration indicated medium to dense deposits. When using the piezocone and its 60° point, dense soils will generate slight excess pore pressures. However, when using the piezometer probe with its 18° point in the same soils, very little excess or even negative pore pressures are generated. Both these effects can be seen on the attached cone logs.

The hydrostatic pressures measured at both sites indicate that no aquacludes exist. Static pore pressures measured indicated hydrostatic valves in all cases.

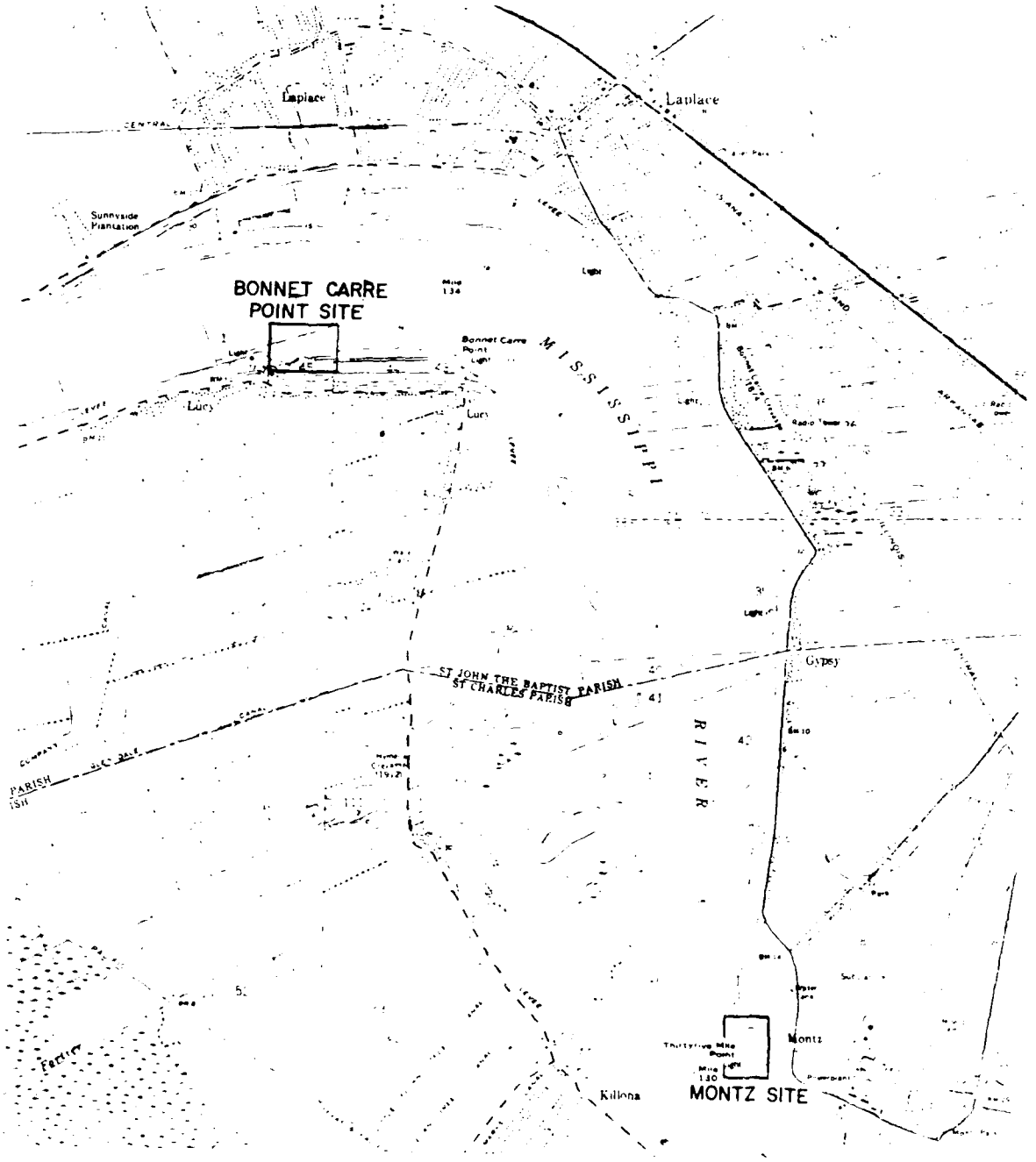


Figure H1. Site location plan

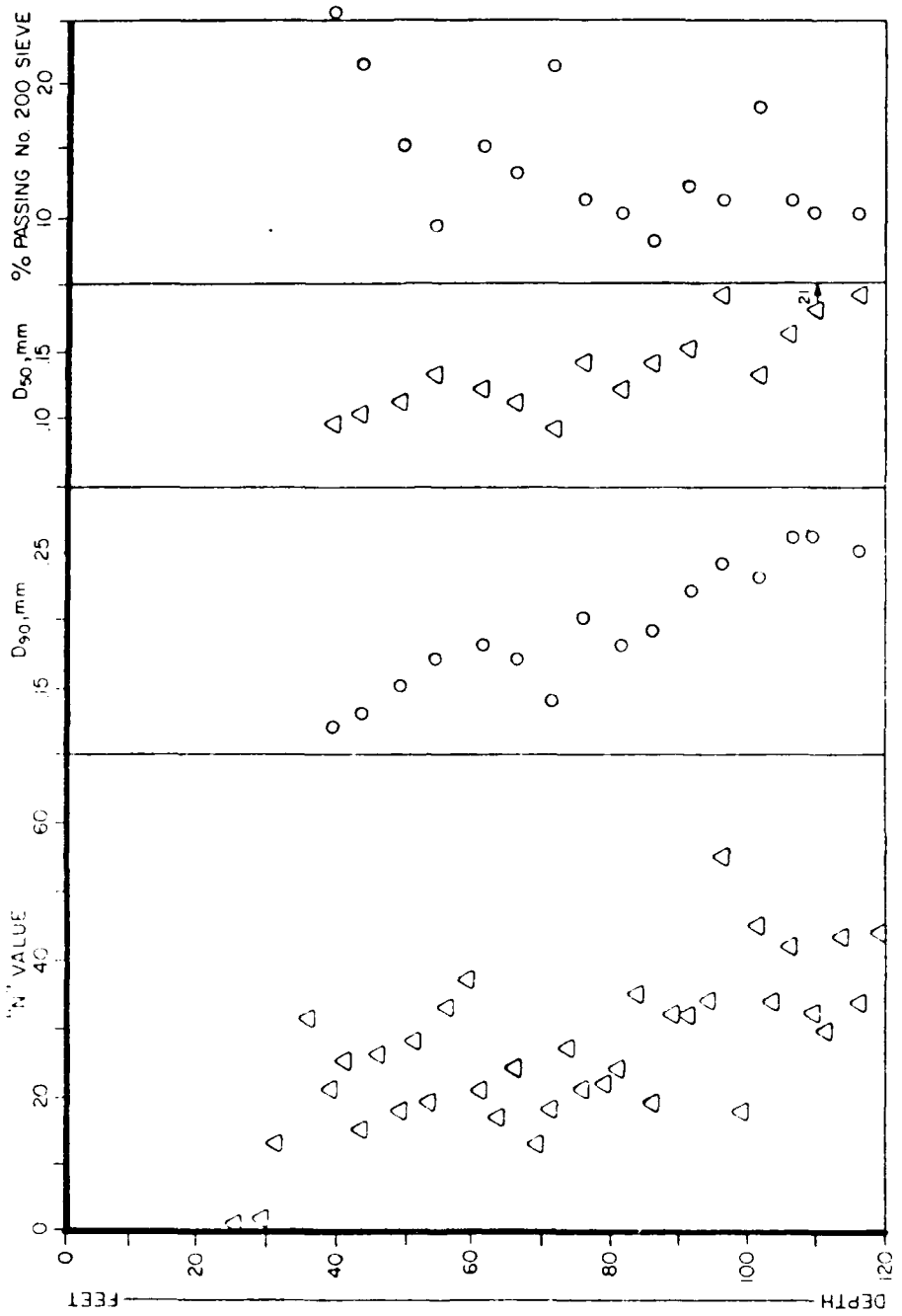


Figure H2. Typical soils profile Montz - SPT-3

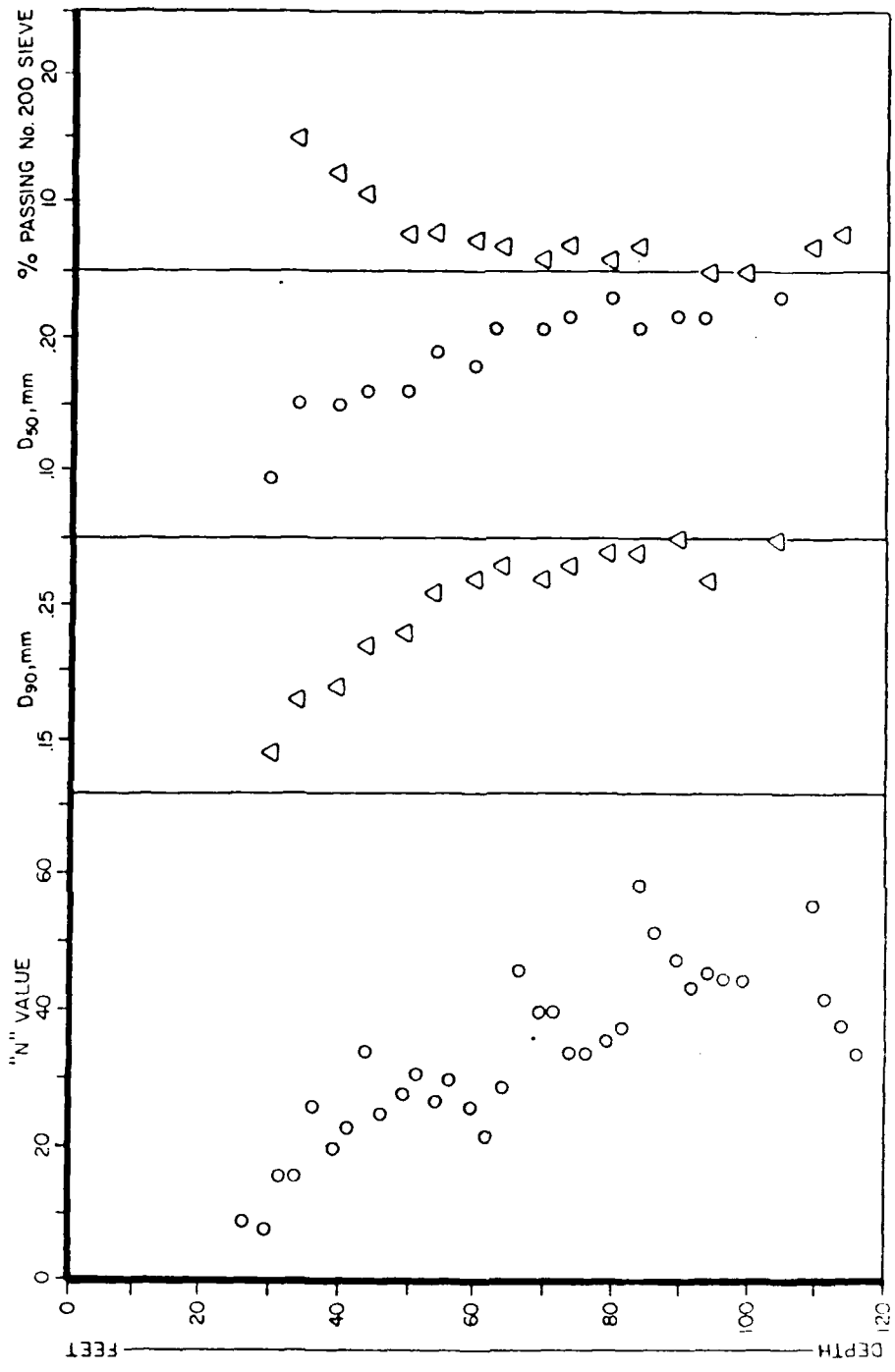


Figure H3. Typical soils profile Bonnet Carre Point N.E.

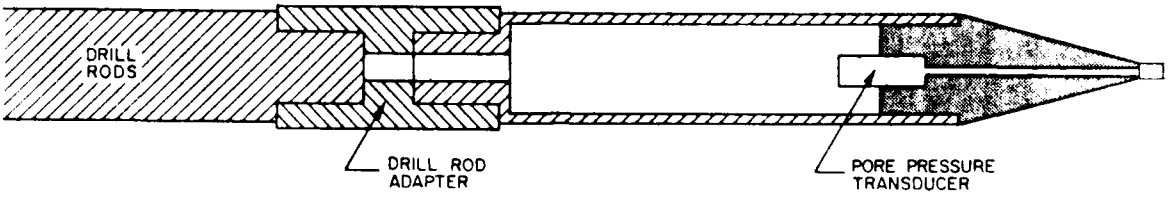


Figure H4. Piezometer probe schematic

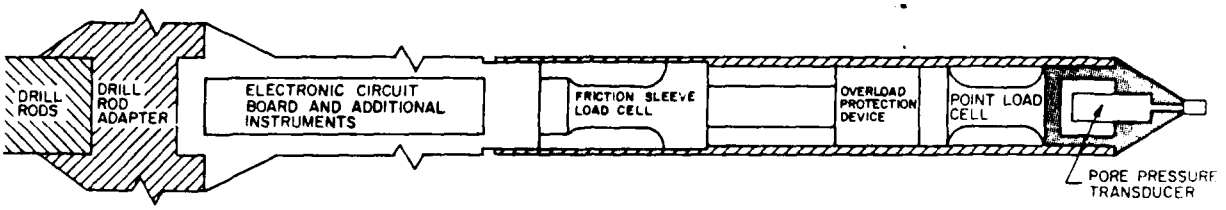


Figure H5. Piezocone schematic

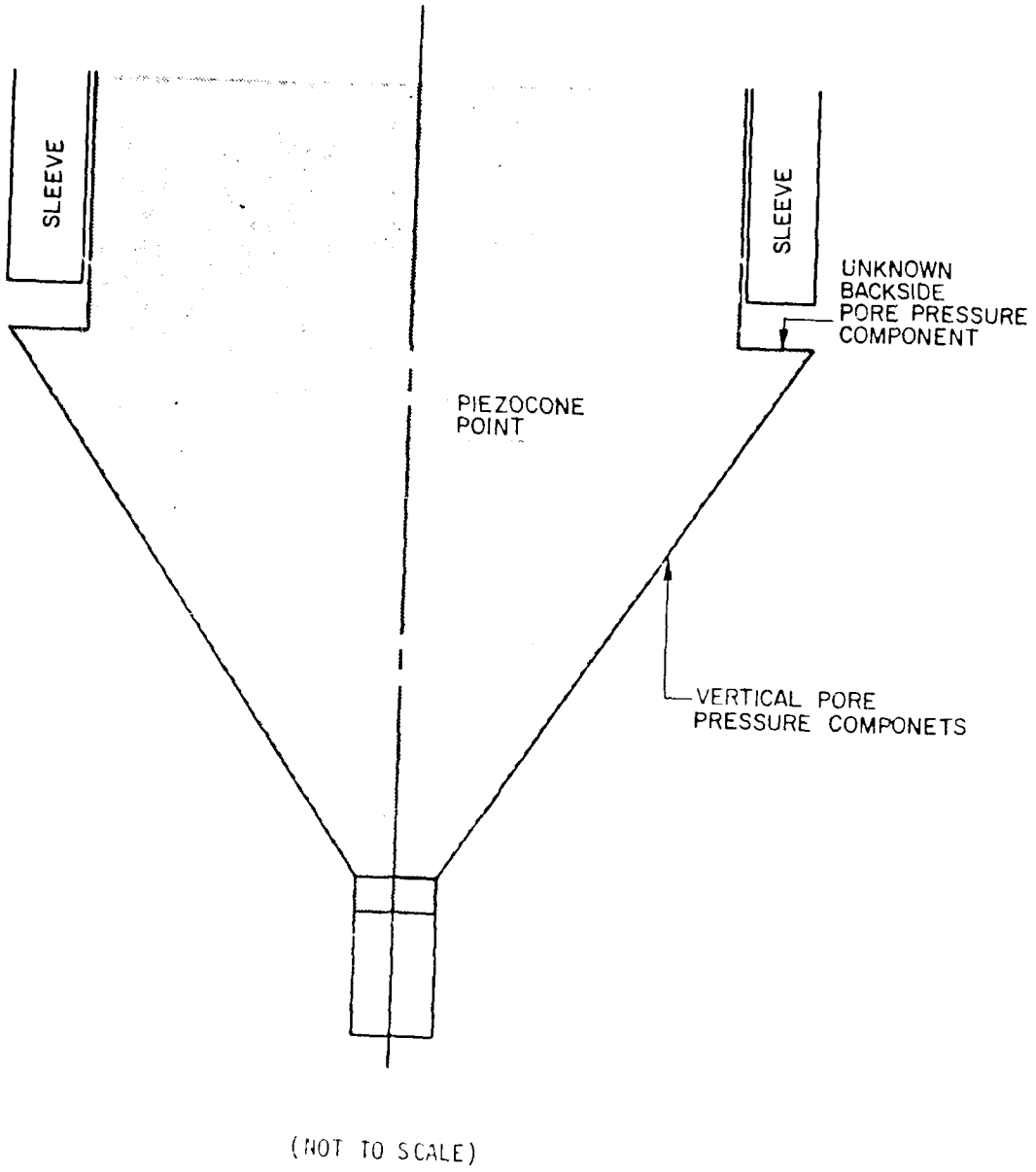


Figure H6. Field investigation

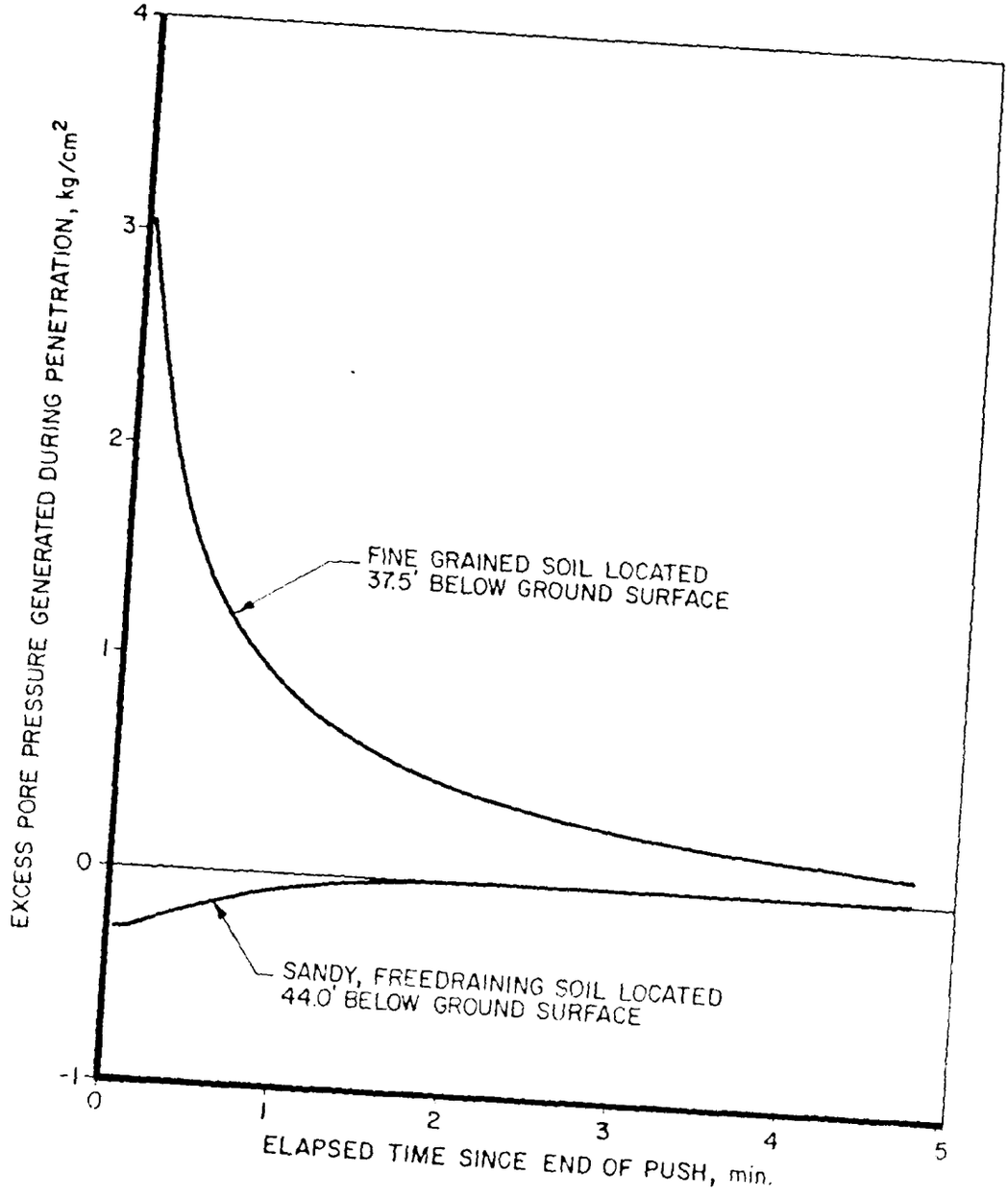
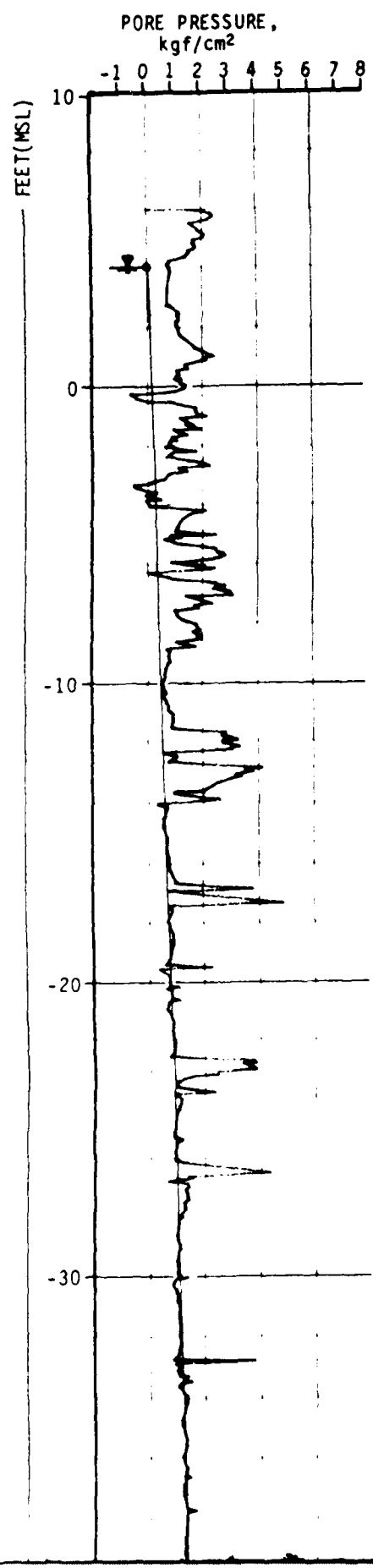
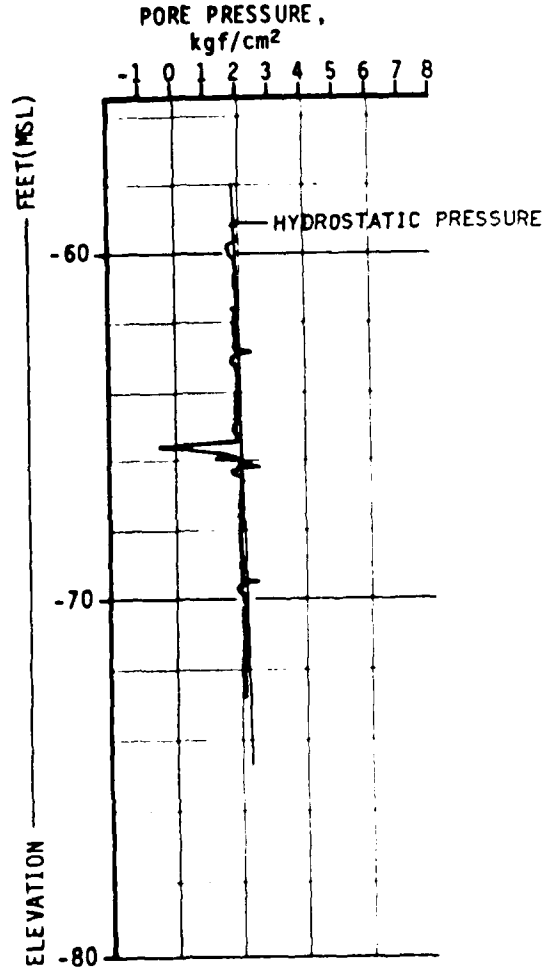
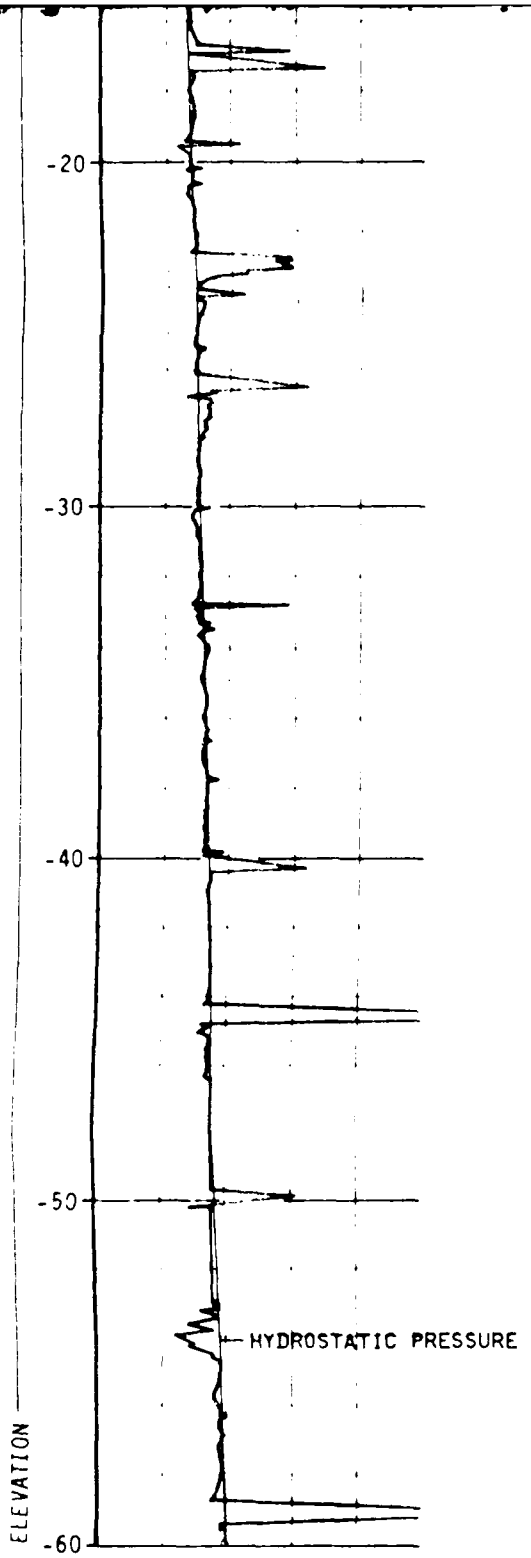


Figure H7. Static pore pressure decay piezocone hole No. W-6


PORE PRESSURE,
kgf/cm²
-1 0 1 2 3 4 5 6 7 8
FEET(MSL)
10
0
-10
-20
-30


PORE PRESSURE,
kgf/cm²
-1 0 1 2 3 4 5 6 7 8
FEET(MSL)
HYDROSTATIC PRESSURE
-60
-70
-80
ELEVATION



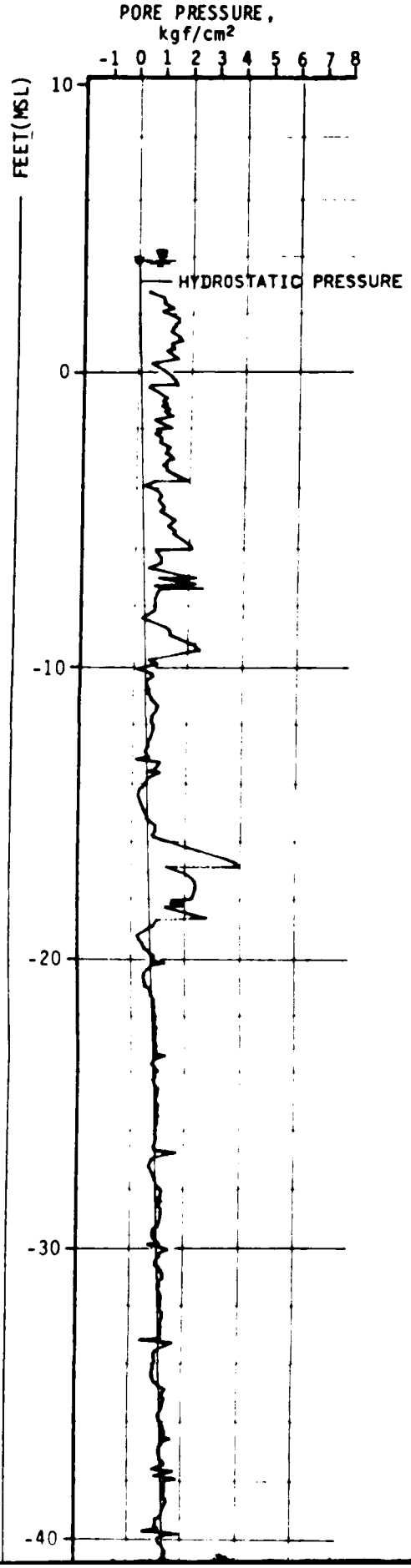
PIEZOPROBE HOLE NO. W-1

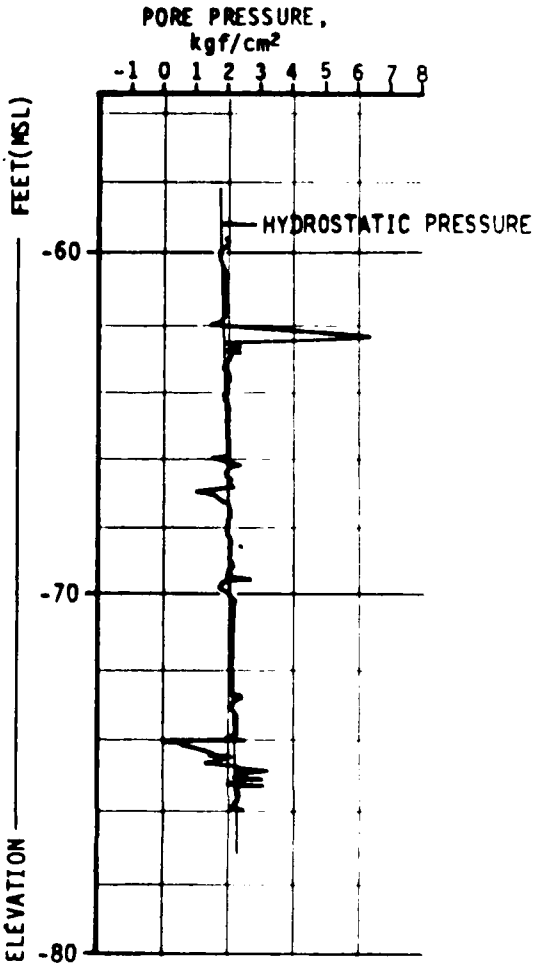
MONTZ, LA.

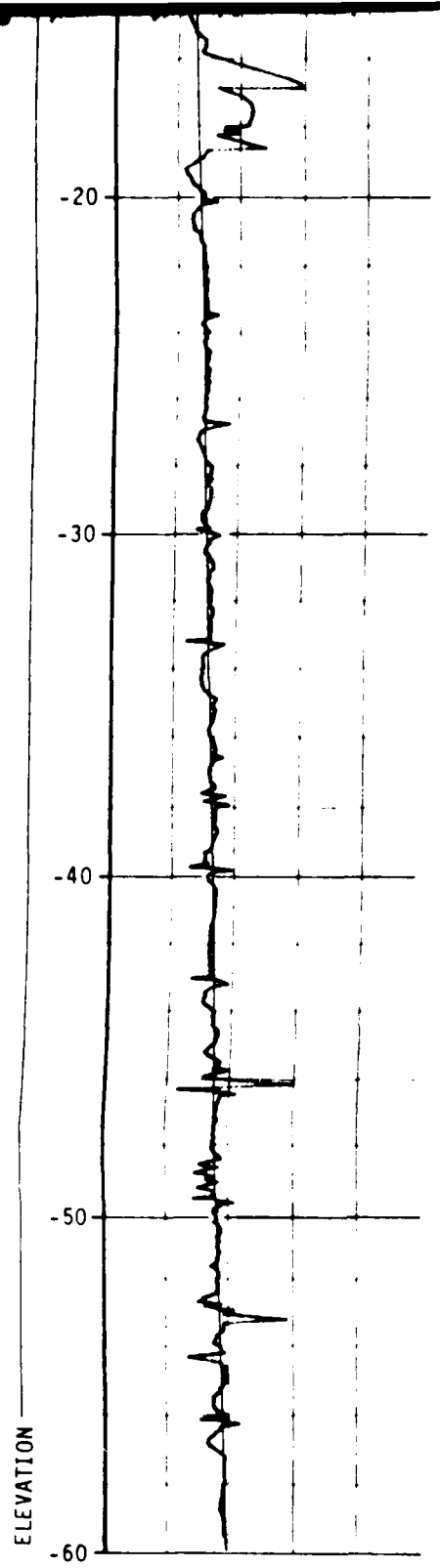
Ardaman & Associates, Inc.
Consulting Engineers in Soil Mechanics, Foundations, and Material Testing

FIELD INVESTIGATION
MONTZ AND BONNE CARRE POINT
CORPS OF ENGINEERS WES

DRAWN BY: GSW	CHECKED BY:	DATE:
FILE NO. 78-039	APPROVED BY:	


PORE PRESSURE,
kgf/cm²
-1 0 1 2 3 4 5 6 7 8
FEET(MSL)
10
0
-10
-20
-30
-40
HYDROSTATIC PRESSURE


PORE PRESSURE,
kgf/cm²
-1 0 1 2 3 4 5 6 7 8
FEET(MSL)
-60
-70
-80
ELEVATION
HYDROSTATIC PRESSURE



PIEZOPROBE HOLE NO. W-2

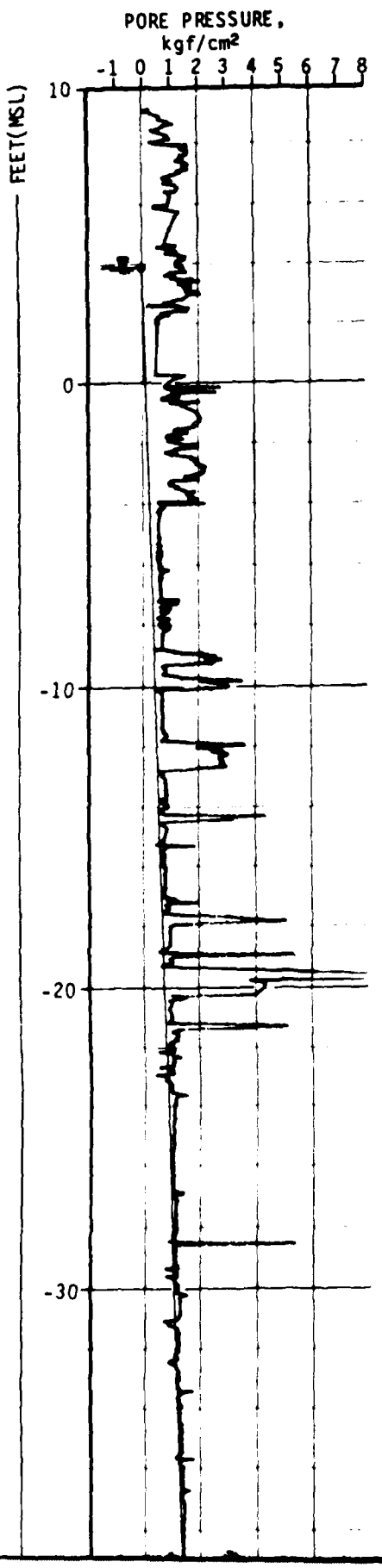
MONTZ, LA.

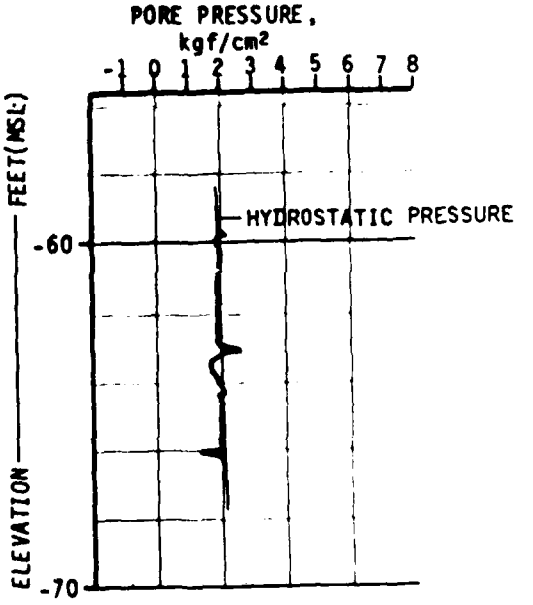
Ardaman & Associates, Inc.
Consulting Engineers in Soil Mechanics, Foundations, and Material Testing

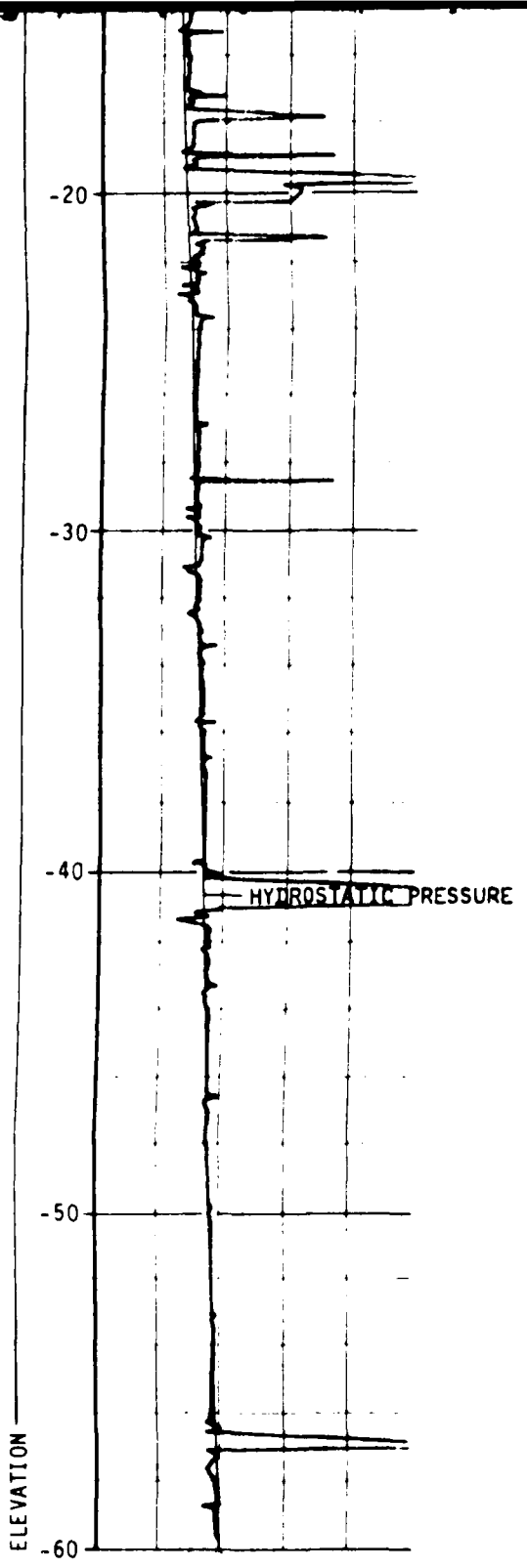
FIELD INVESTIGATION
MONTZ AND BONNE CARRE POINT
CORPS OF ENGINEERS WES

DRAWN BY: GSW | CHECKED BY: | APP

FILE NO. 78-039 | APPROVED BY:


PORE PRESSURE,
kgf/cm²
-1 0 1 2 3 4 5 6 7 8
FEET(MSL)
10
0
-10
-20
-30


PORE PRESSURE,
kgf/cm²
-1 0 1 2 3 4 5 6 7 8
FEET(MSL)
HYDROSTATIC PRESSURE
-60
-70
ELEVATION



PIEZOPROBE HOLE NO. W-3

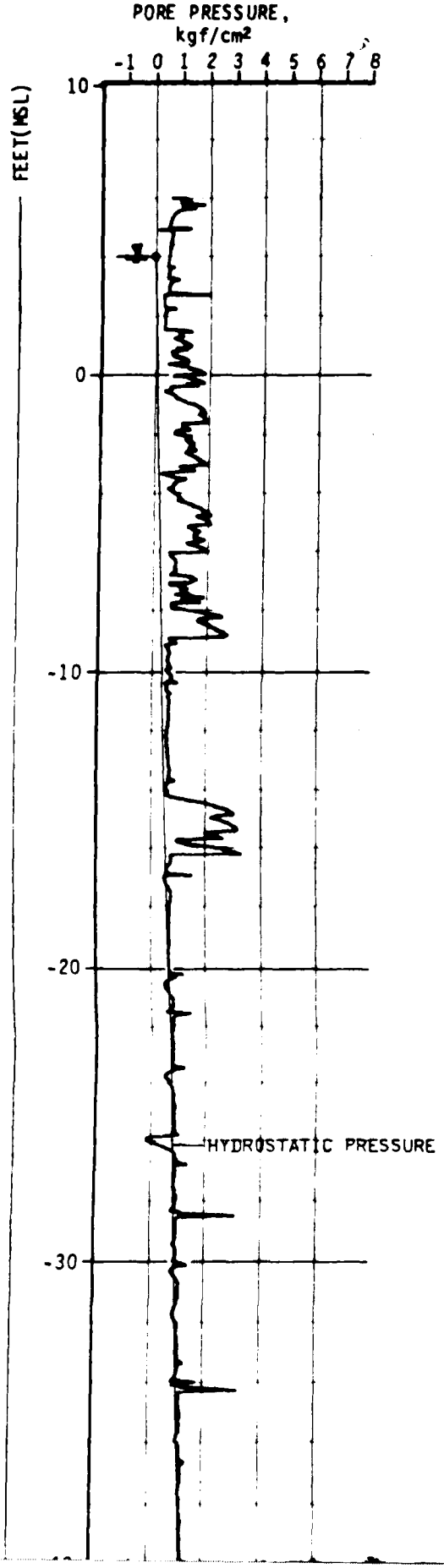
MONTZ, LA.

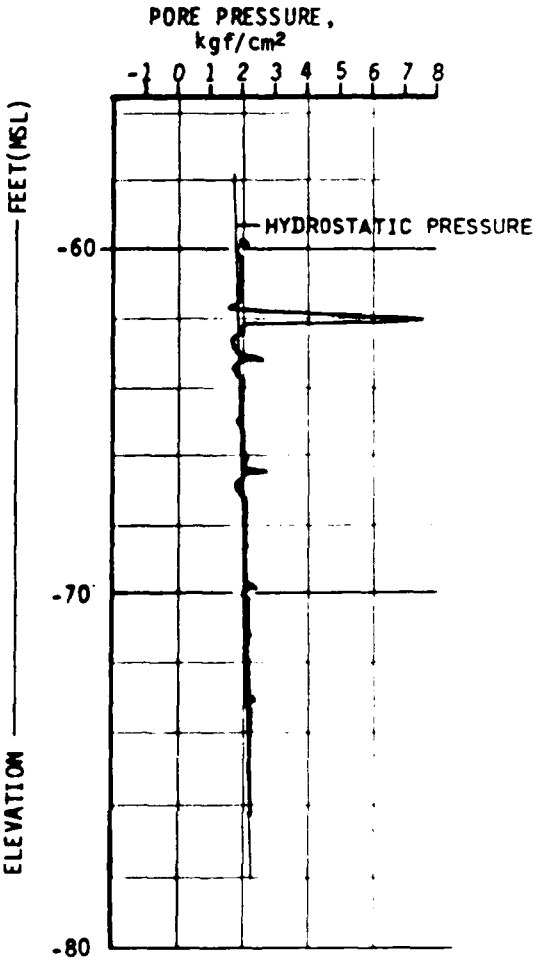
2

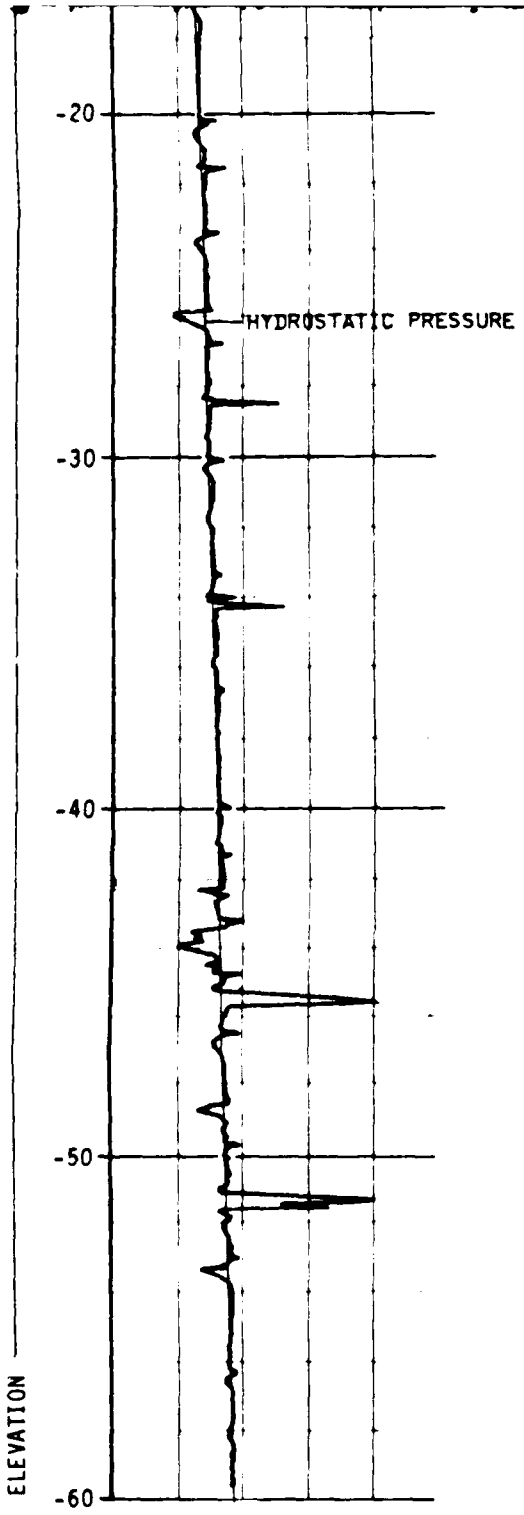
Ardaman & Associates, Inc.
Consulting Engineers in Soil Mechanics, Foundations, and Material Testing

FIELD INVESTIGATION
MONTZ AND BONNE CARRE POINT
CORPS OF ENGINEERS WES

DRAWN BY: GSN	CHECKED BY:	
FILE NO. 78-039	APPROVED BY:	


PORE PRESSURE,
kgf/cm²
-1 0 1 2 3 4 5 6 7 8
FEET(MSL)
10
0
-10
-20
-30
HYDROSTATIC PRESSURE


PORE PRESSURE,
kgf/cm²
-1 0 1 2 3 4 5 6 7 8
FEET(MSL)
ELEVATION
-60
-70
-80
HYDROSTATIC PRESSURE



PIEZOPROBE HOLE NO. W-4

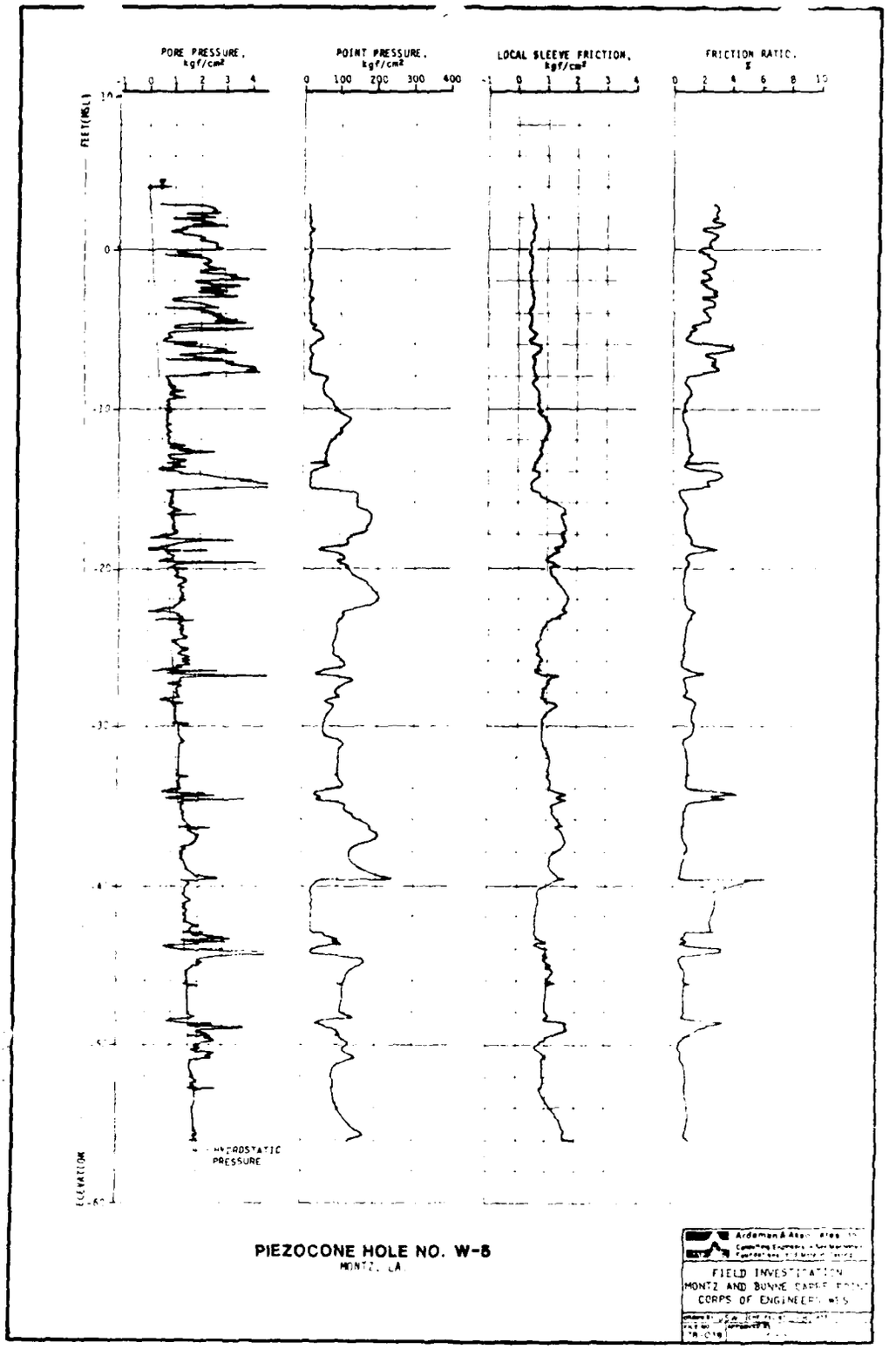
MONTZ, LA.

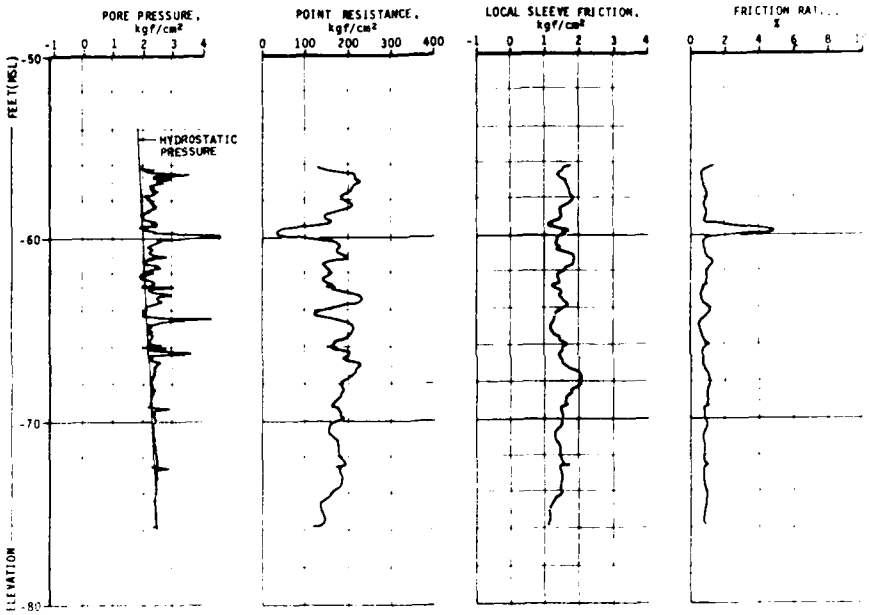
Ardaman & Associates, Inc.
Consulting Engineers in Soil Mechanics, Foundations, and Materials Testing

FIELD INVESTIGATION
MONTZ AND BONNE CARRE POINT
CORPS OF ENGINEERS WES

DRAWN BY: GSW	CHECKED BY:	DATE:
FILE NO. 78-039	APPROVED BY:	

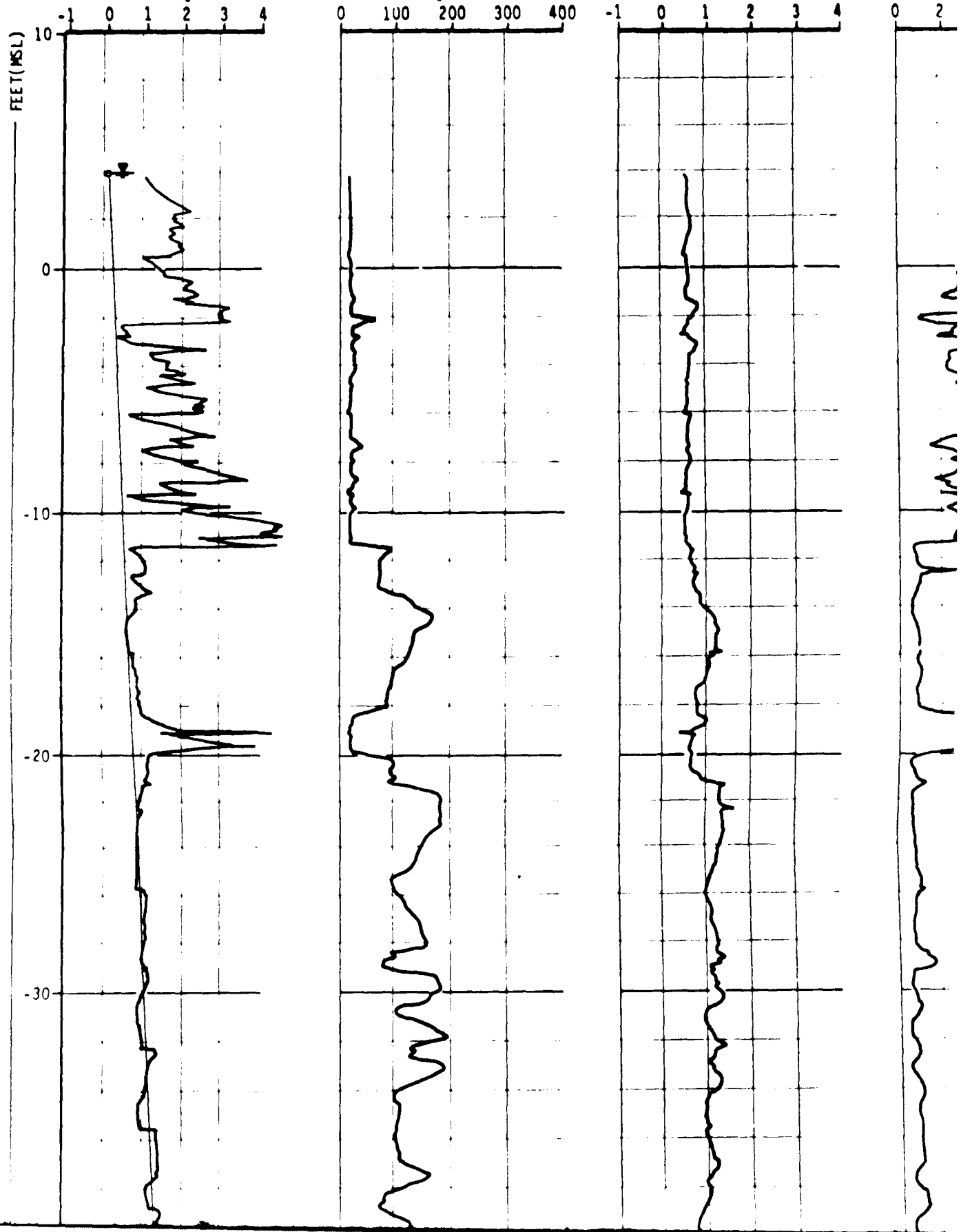
2


PORE PRESSURE, kgf/cm²
POINT PRESSURE, kgf/cm²
LOCAL SLEEVE FRICTION, kgf/cm²
FRICTION RATIO, %
FEET(MSL)
ELEVATION
HYDROSTATIC PRESSURE
PIEZOCONE HOLE NO. W-5
MONTZ, LA.
FIELD INVESTIGATION
MONTZ AND BUNNE CORPS OF ENGINEERS



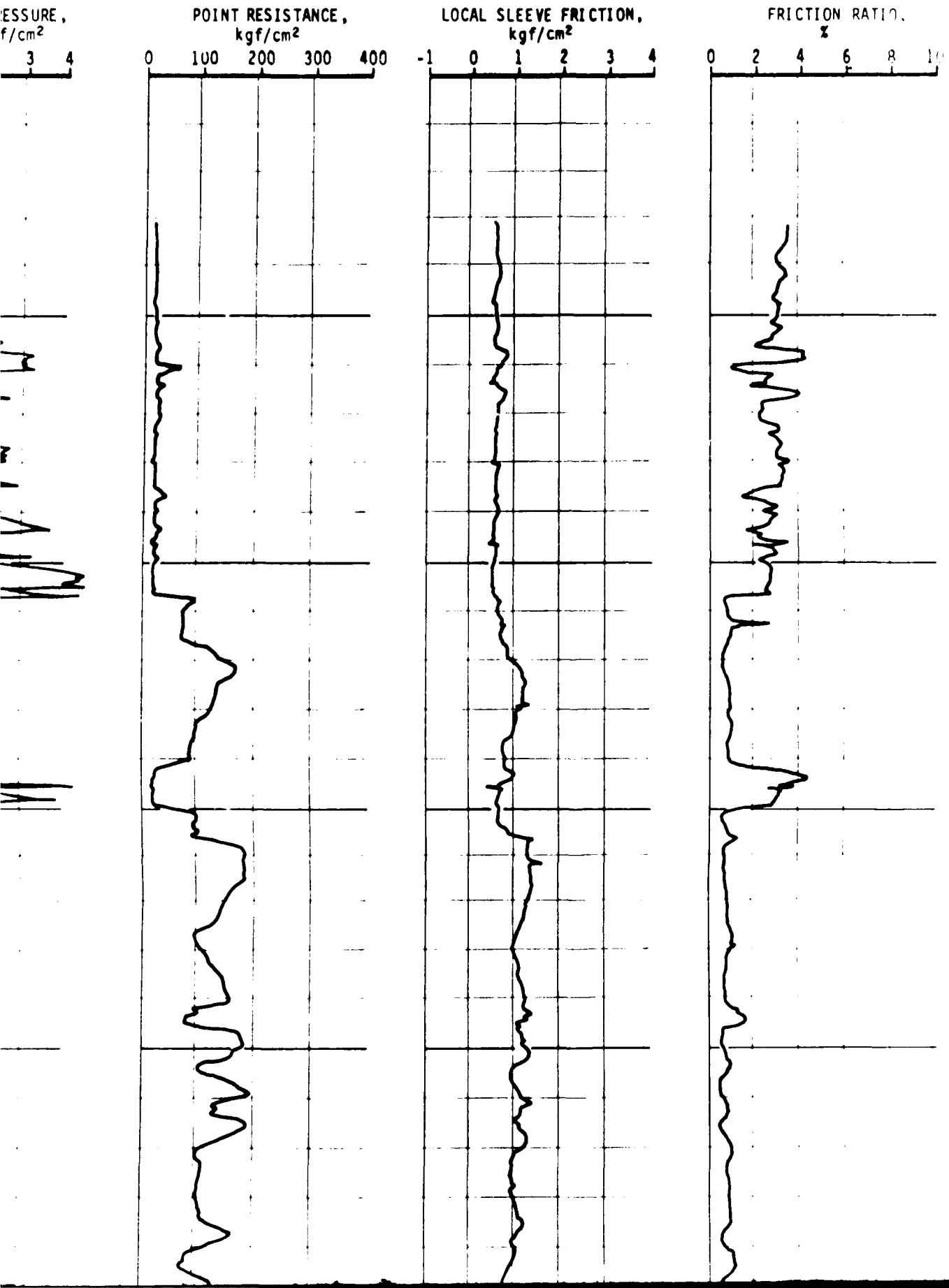
PIEZOCONE HOLE NO. W-5 (CONT'D)
MONTZ, LA.

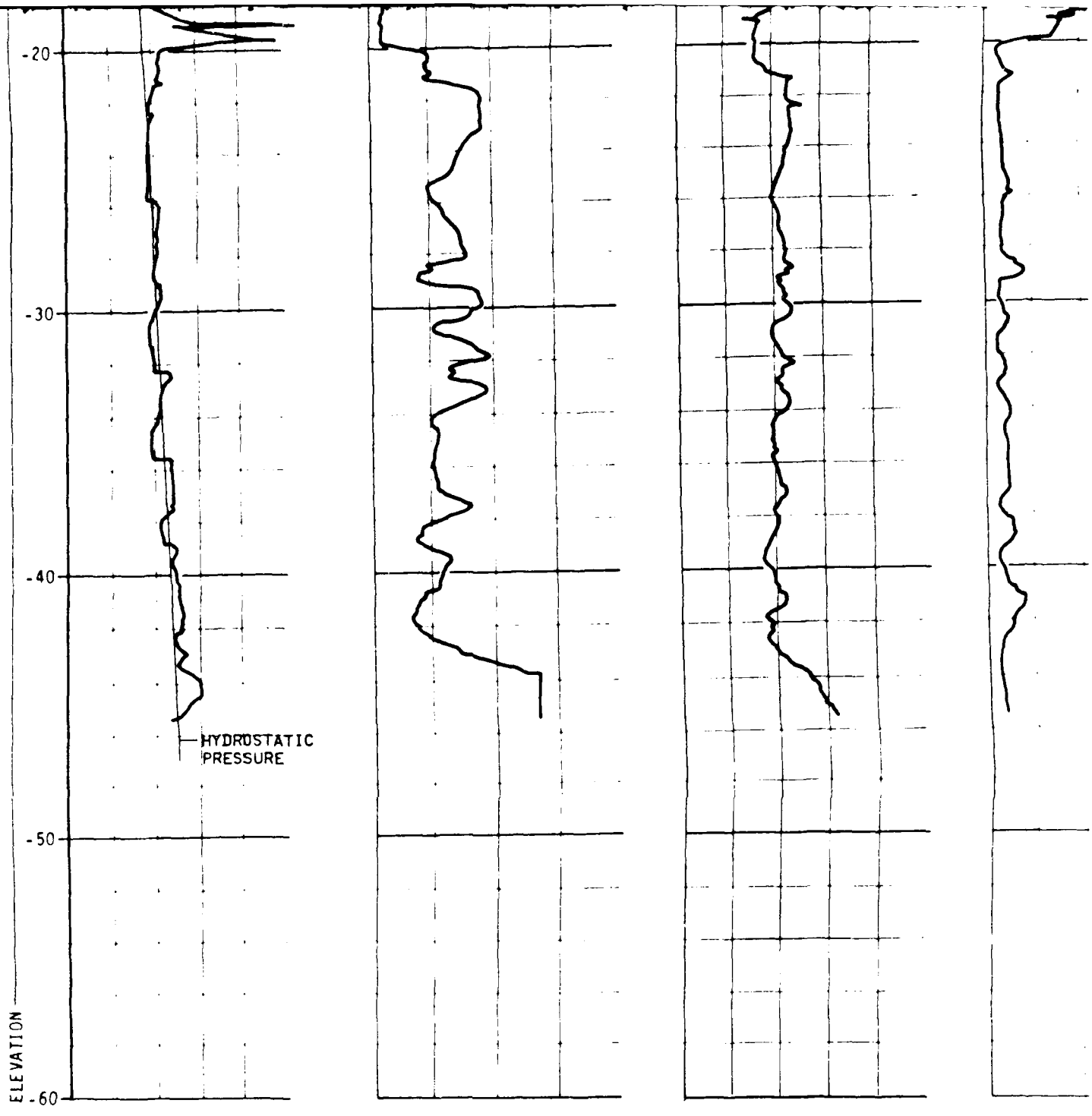
Ardaman & Associates
FIELD INVESTIGATION
MONTZ AND BONNE CARRE POINT
CORPS OF ENGINEERS
78-039


PORE PRESSURE, kgf/cm²
POINT RESISTANCE, kgf/cm²
LOCAL SLEEVE FRICTION, kgf/cm²
FEET(MSL)
-1 0 1 2 3 4
0 100 200 300 400
-1 0 1 2 3 4
10
0
-10
-20
-30

1

2

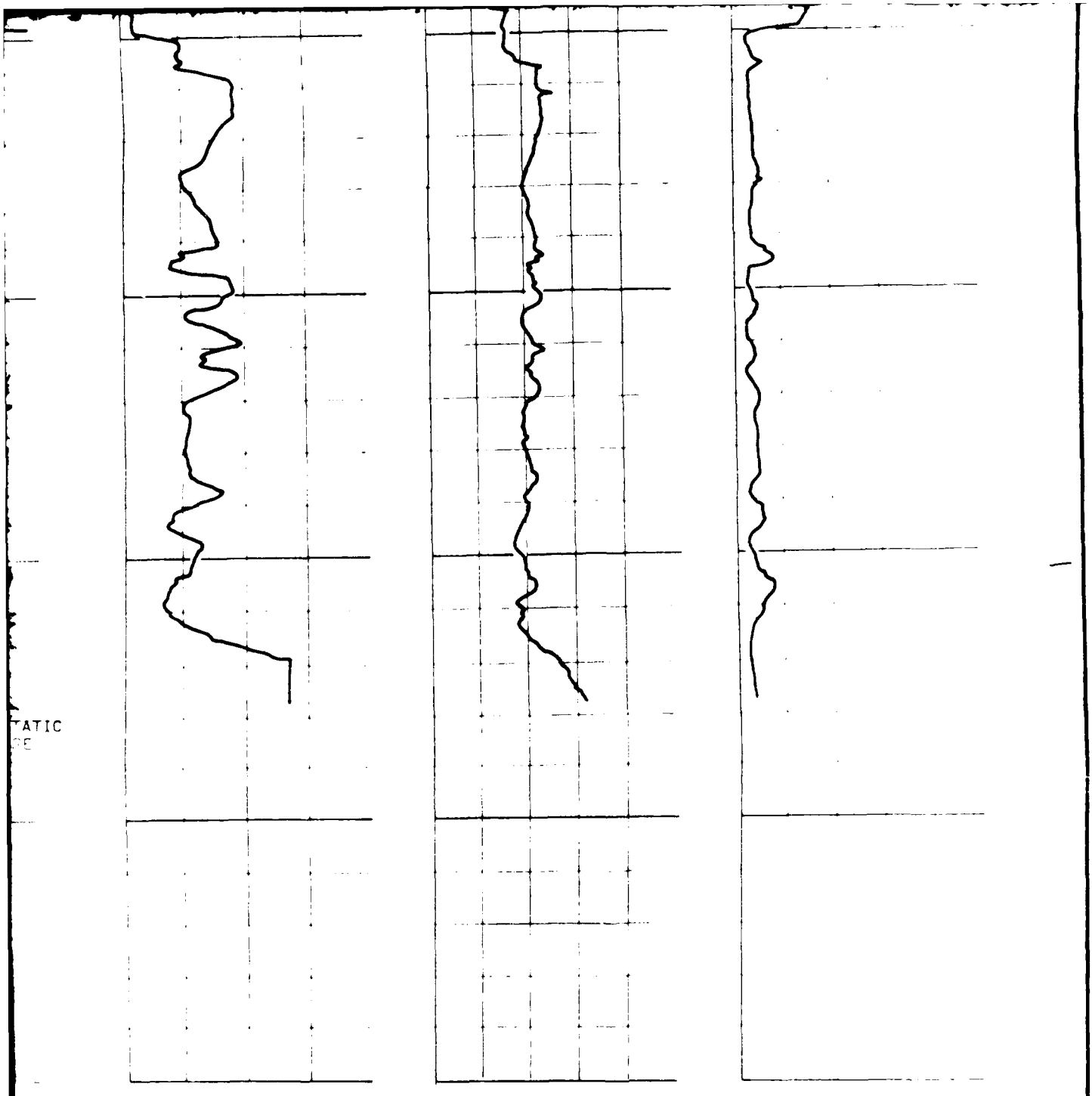

ESSURE,
f/cm²
3 4
POINT RESISTANCE,
kgf/cm²
0 100 200 300 400
LOCAL SLEEVE FRICTION,
kgf/cm²
-1 0 1 2 3 4
FRICTION RATIO,
%
0 2 4 6 8



PIEZOCONE HOLE NO. W-6

MONTZ, LA.

F
MONTZ
CORI
DRAWN BY: C
FILE NO.
78-039



TATIC
E

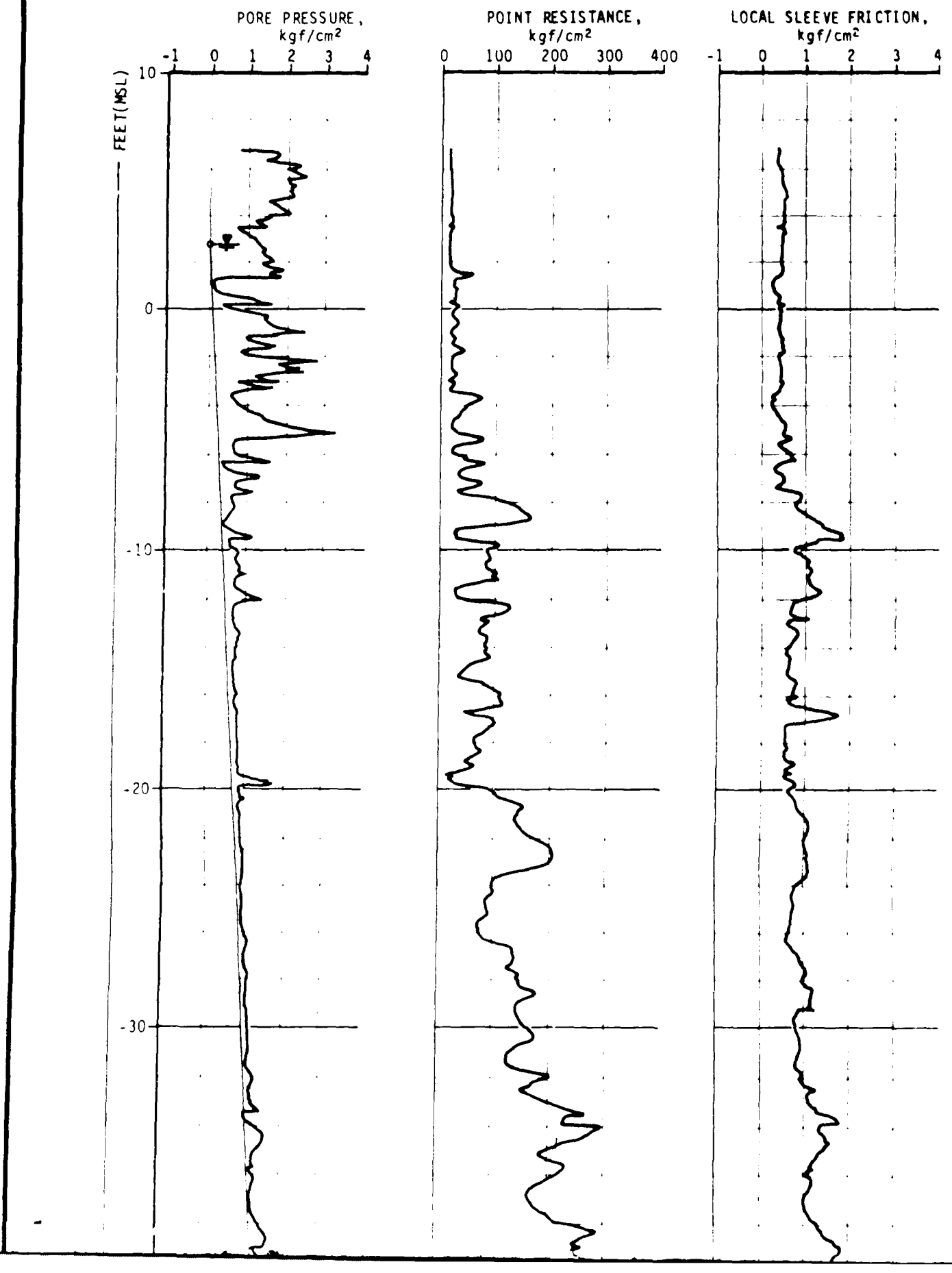
PIEZOCONE HOLE NO. W-6

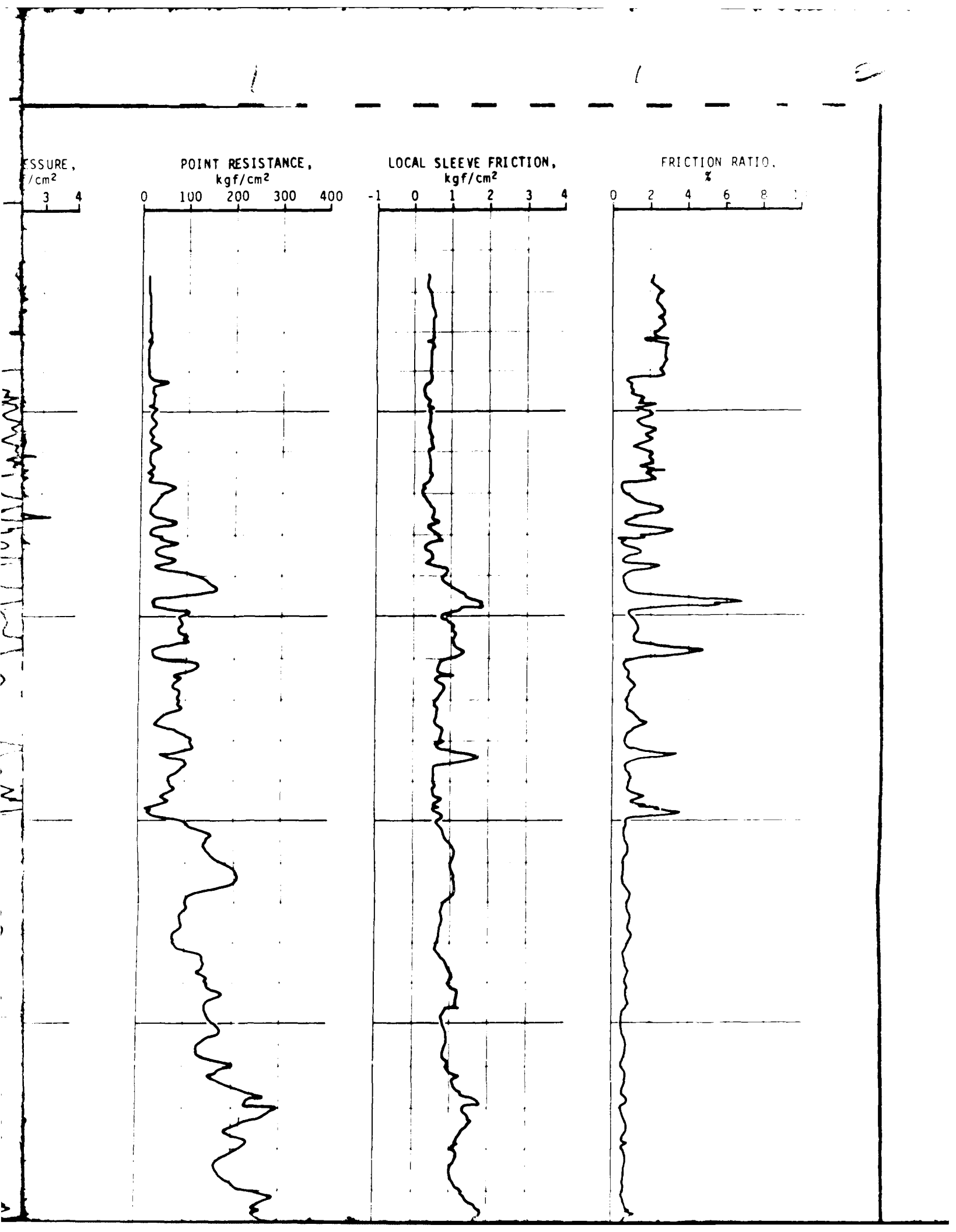
MONTZ, LA.

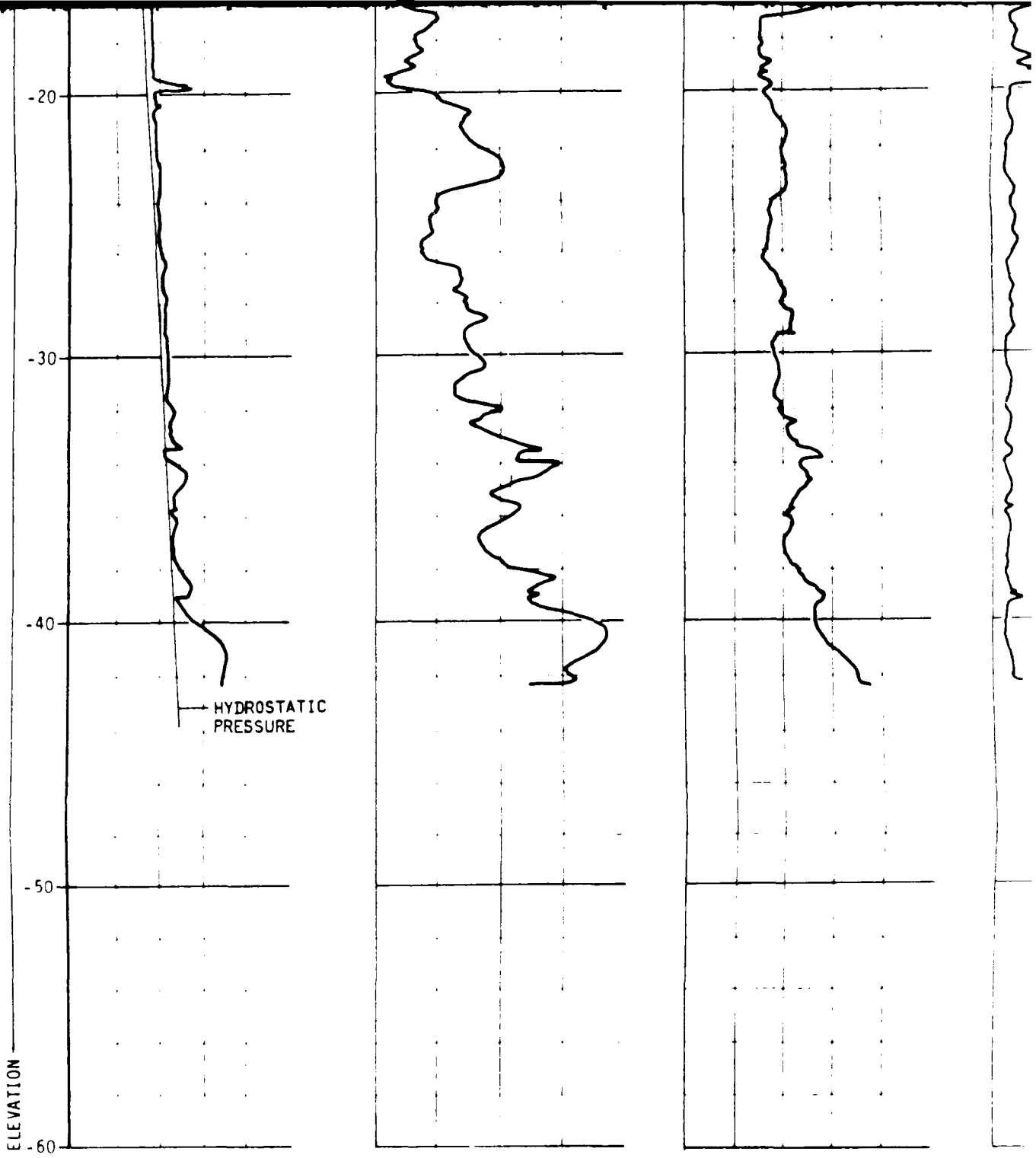
Ardaman & Associates, Inc.
Consulting Engineers in Soil Mechanics, Foundations, and Materials Testing

FIELD INVESTIGATION
MONTZ AND BONNE CARRE POINT
CORPS OF ENGINEERS WES

DRAWN BY: GSW	CHECKED BY:	DATE:
FILE NO. 78-039	APPROVED BY:	

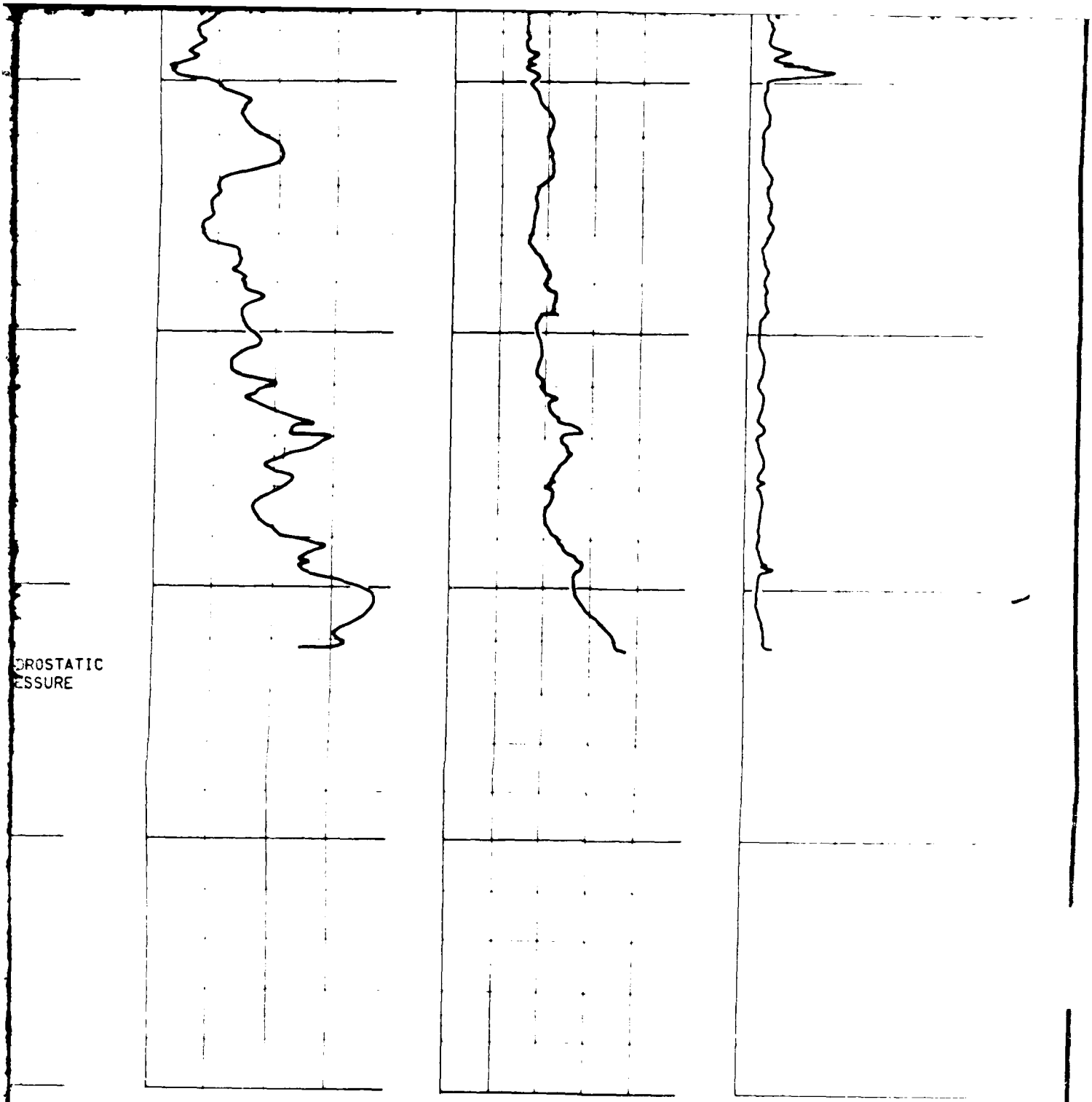

PORE PRESSURE, kgf/cm²
POINT RESISTANCE, kgf/cm²
LOCAL SLEEVE FRICTION, kgf/cm²
FEET(MSL)
-1 0 1 2 3 4
0 100 200 300 400
-1 0 1 2 3 4
10
0
-10
-20
-30


ESSURE,
/cm²
3 4
POINT RESISTANCE,
kgf/cm²
0 100 200 300 400
LOCAL SLEEVE FRICTION,
kgf/cm²
-1 0 1 2 3 4
FRICTION RATIO,
%
0 2 4 6 8



PIEZOCONE HOLE NO. BW-1

BONNE CARRE POINT, LA.



PIEZOCONE HOLE NO. BW-1

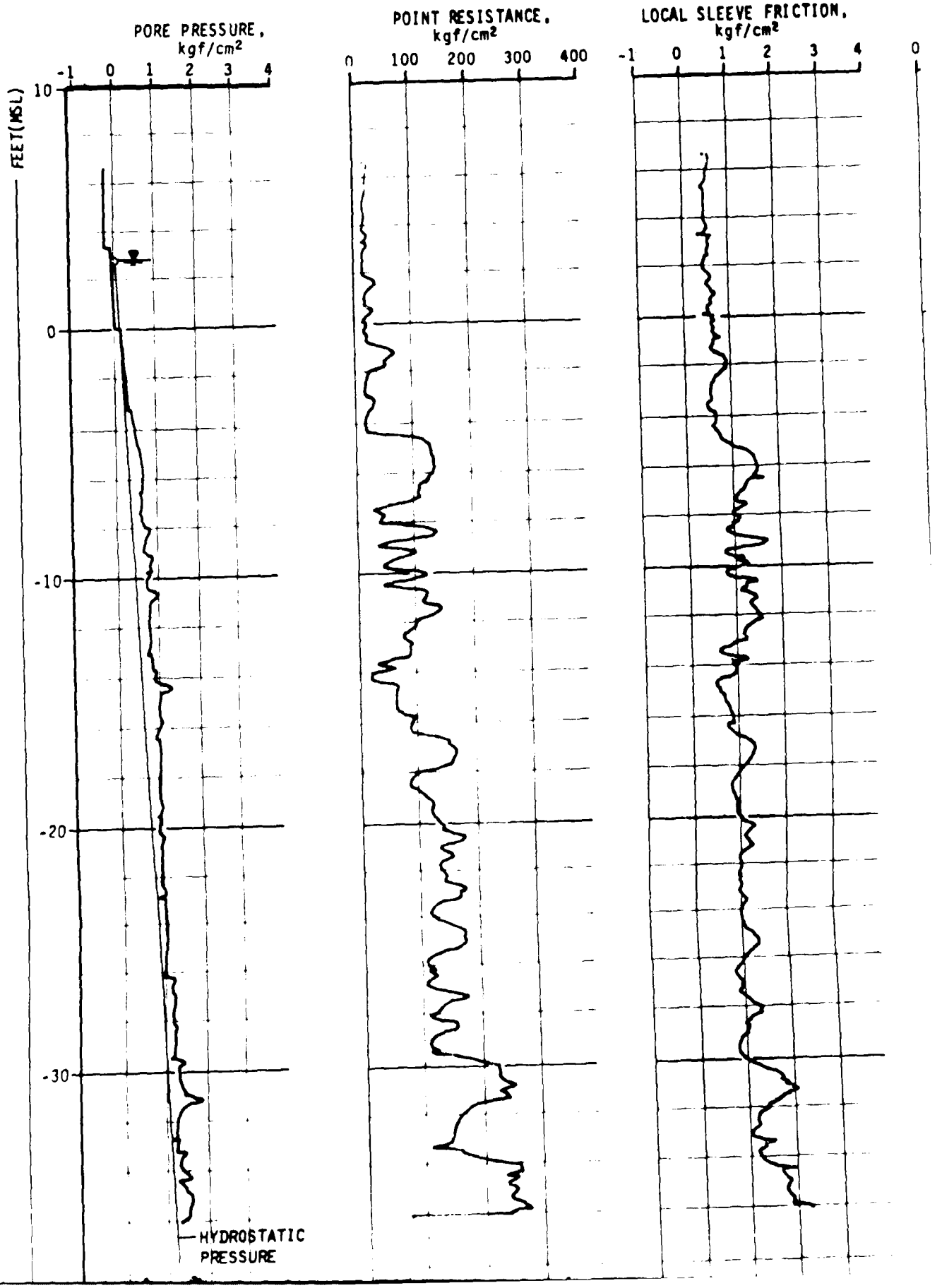
BONNE CARRE POINT, LA.

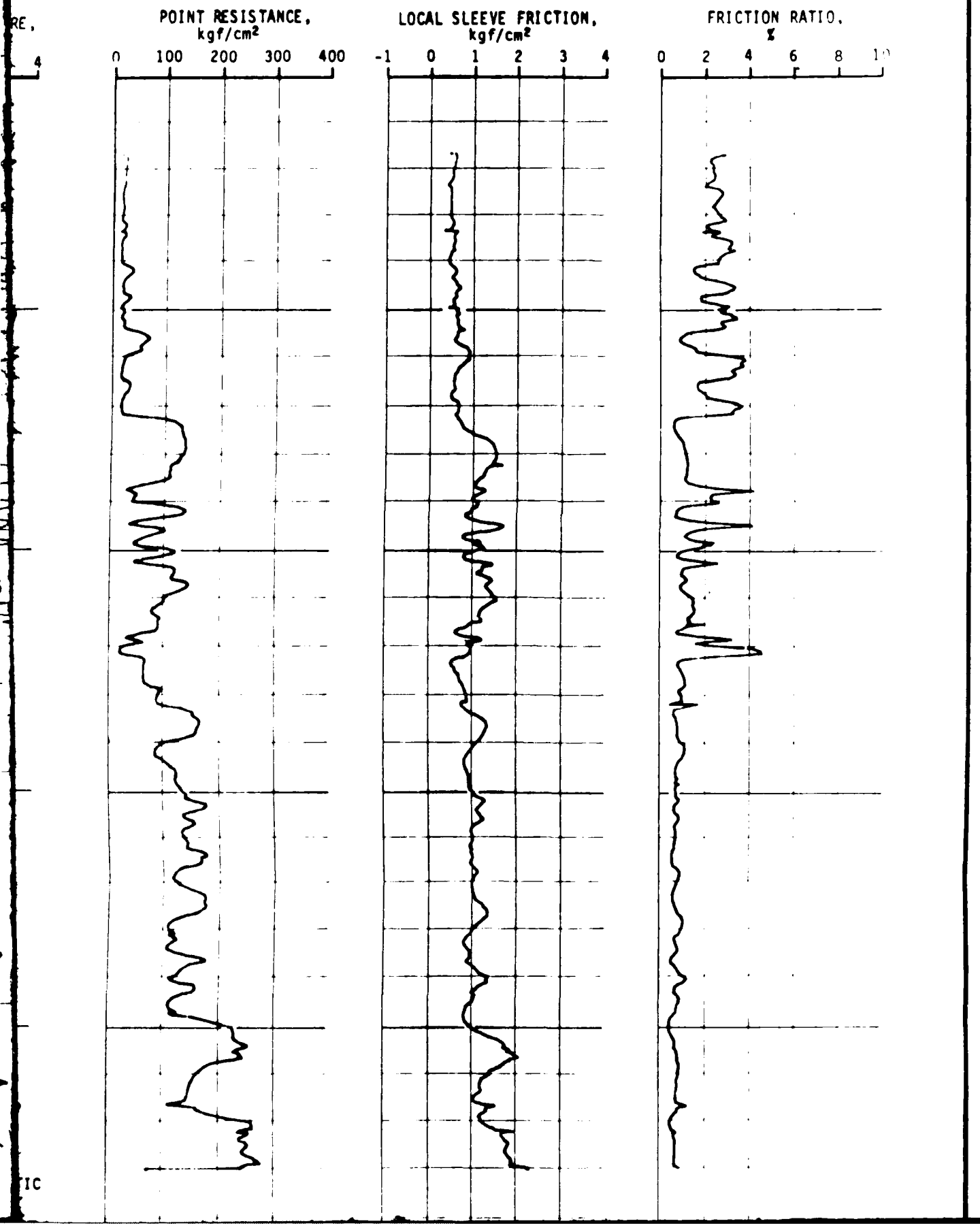
Ardaman & Associates, Inc.
Consulting Engineers in Soil Mechanics, Foundations, and Materials

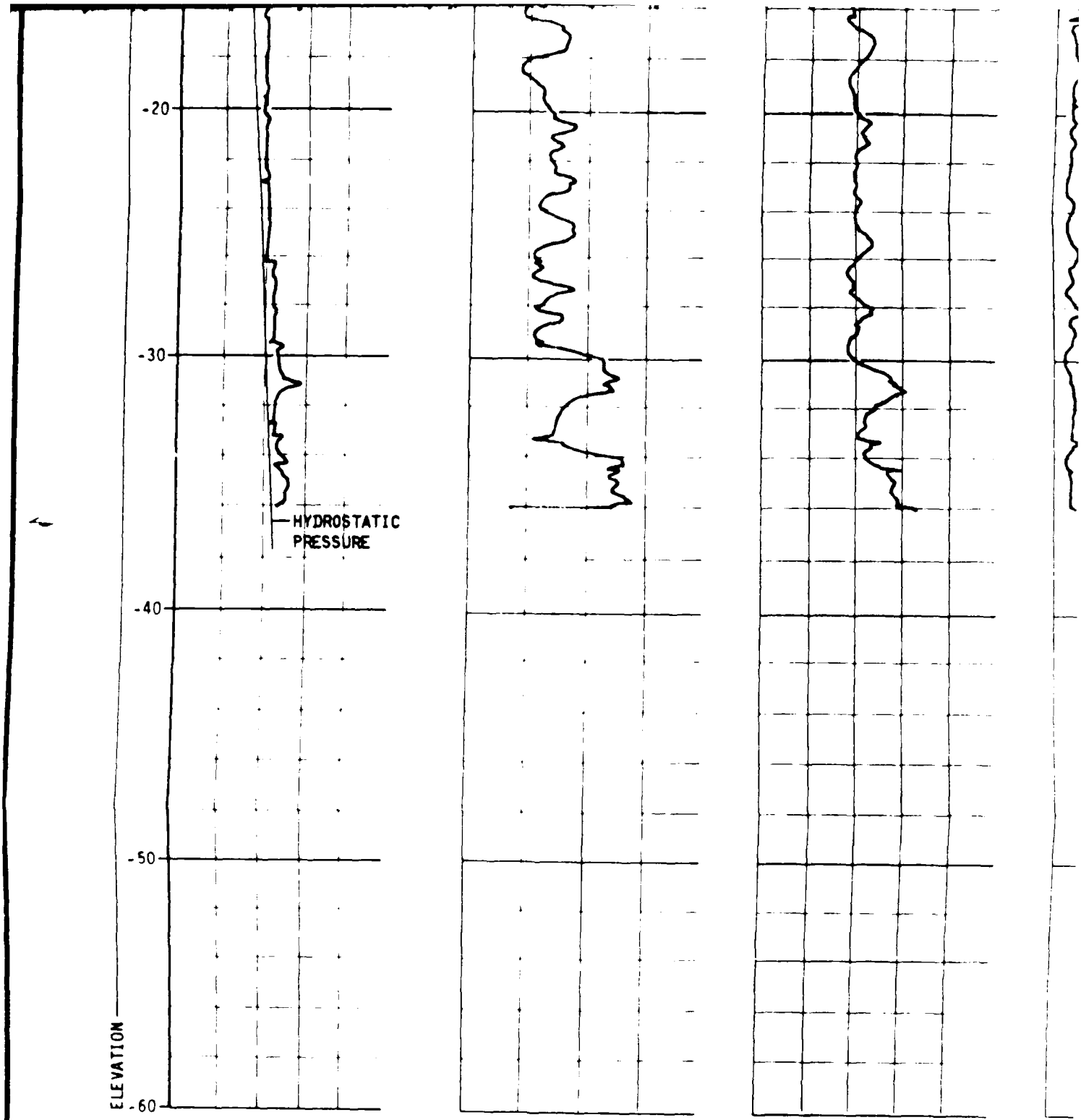
FIELD INVESTIGATION
MONTZ AND BONNE CARRE POINT
CORPS OF ENGINEERS WES

DRAWN BY GSW | CHECKED BY
FILE NO. 78-039 | APPROVED BY

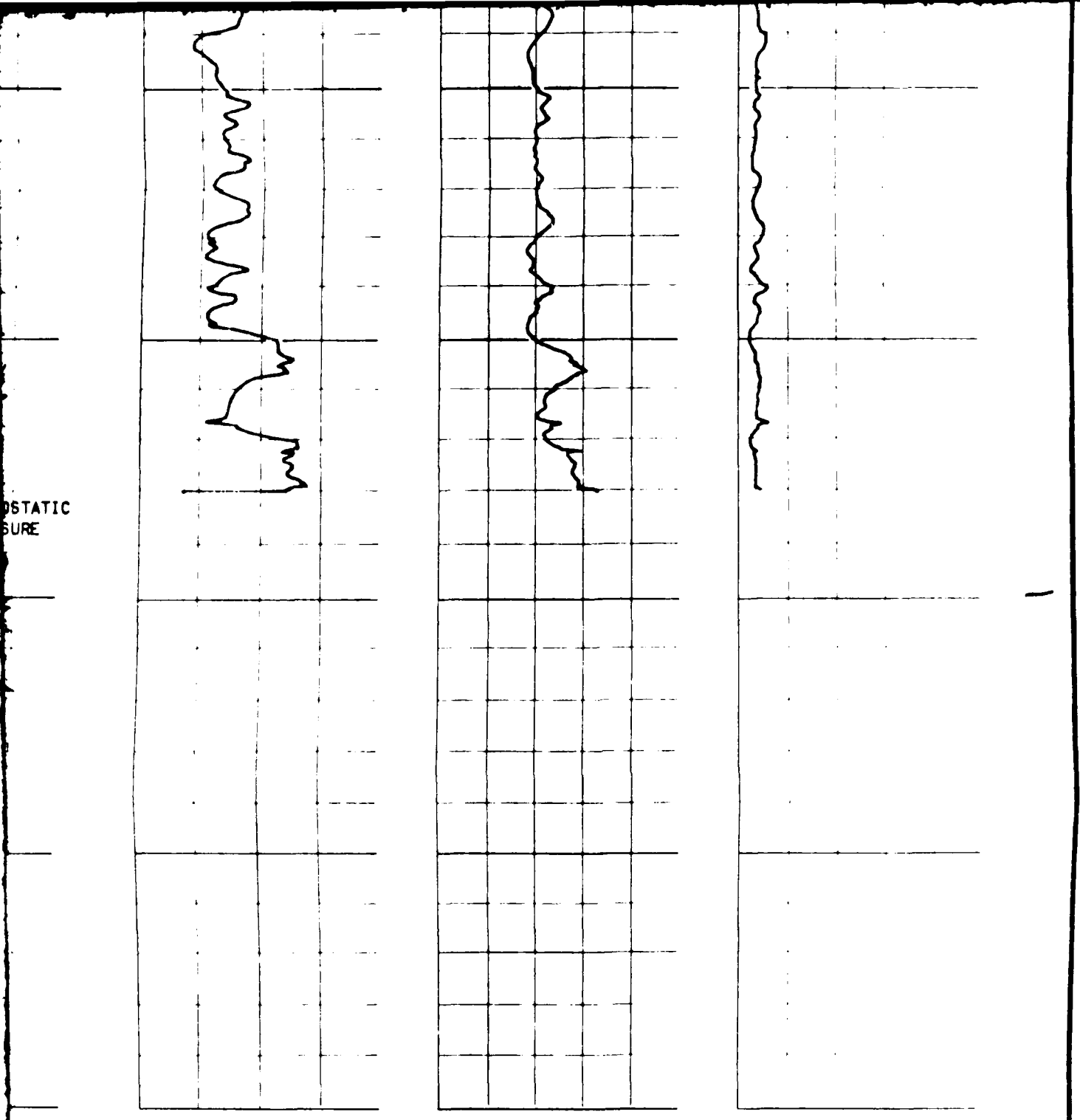
2


PORE PRESSURE, kgf/cm²
-1 0 1 2 3 4
POINT RESISTANCE, kgf/cm²
0 100 200 300 400
LOCAL SLEEVE FRICTION, kgf/cm²
-1 0 1 2 3 4
FEET(MSL)
10
0
-10
-20
-30
HYDROSTATIC PRESSURE


POINT RESISTANCE,
kgf/cm²
0
100
200
300
400
LOCAL SLEEVE FRICTION,
kgf/cm²
-1
0
1
2
3
4
FRICTION RATIO,
%
0
2
4
6
8



PIEZOCONE HOLE NO. BW-2
BONNE CARRE POINT, LA.



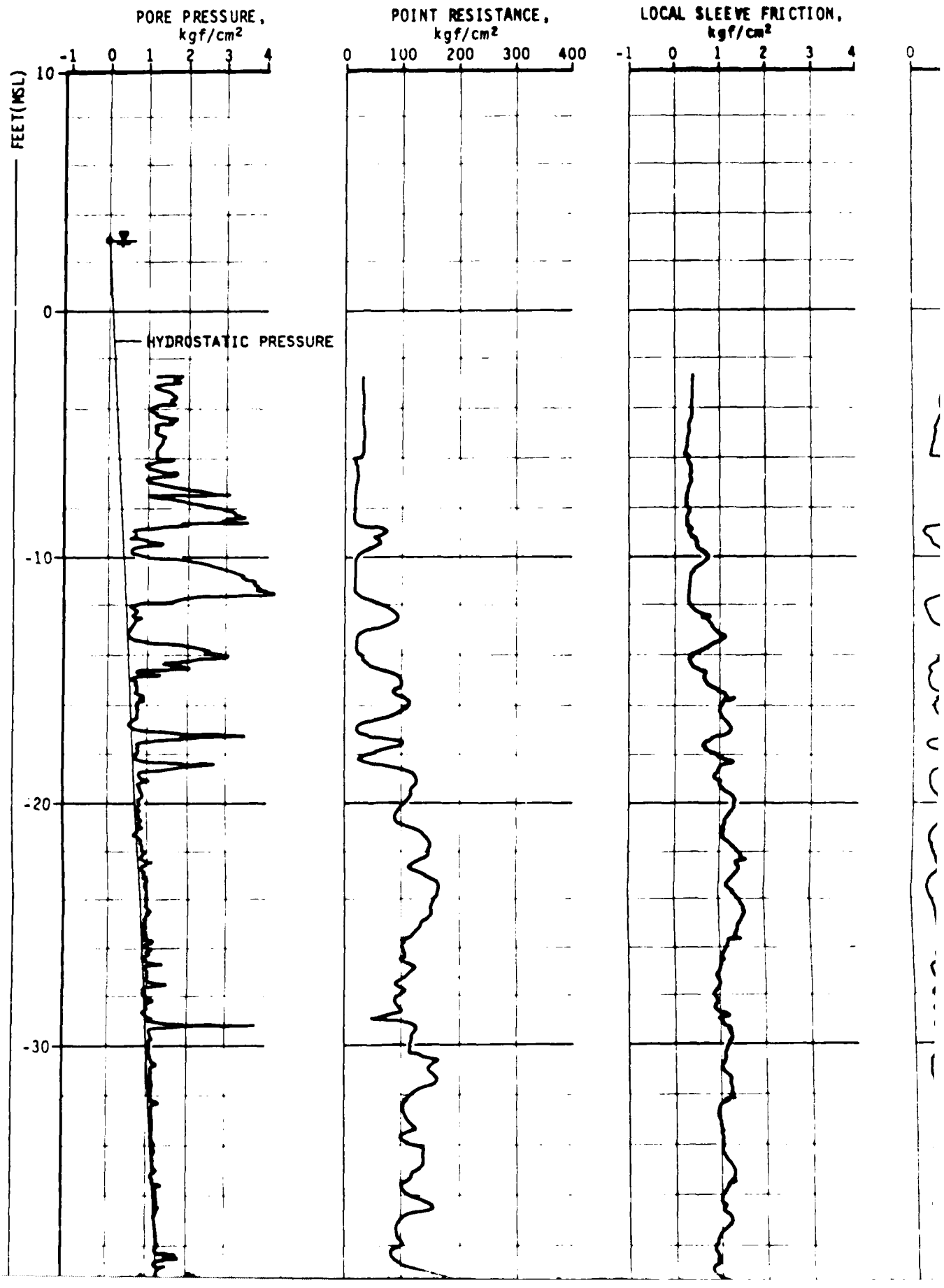
PIEZOCONE HOLE NO. BW-2

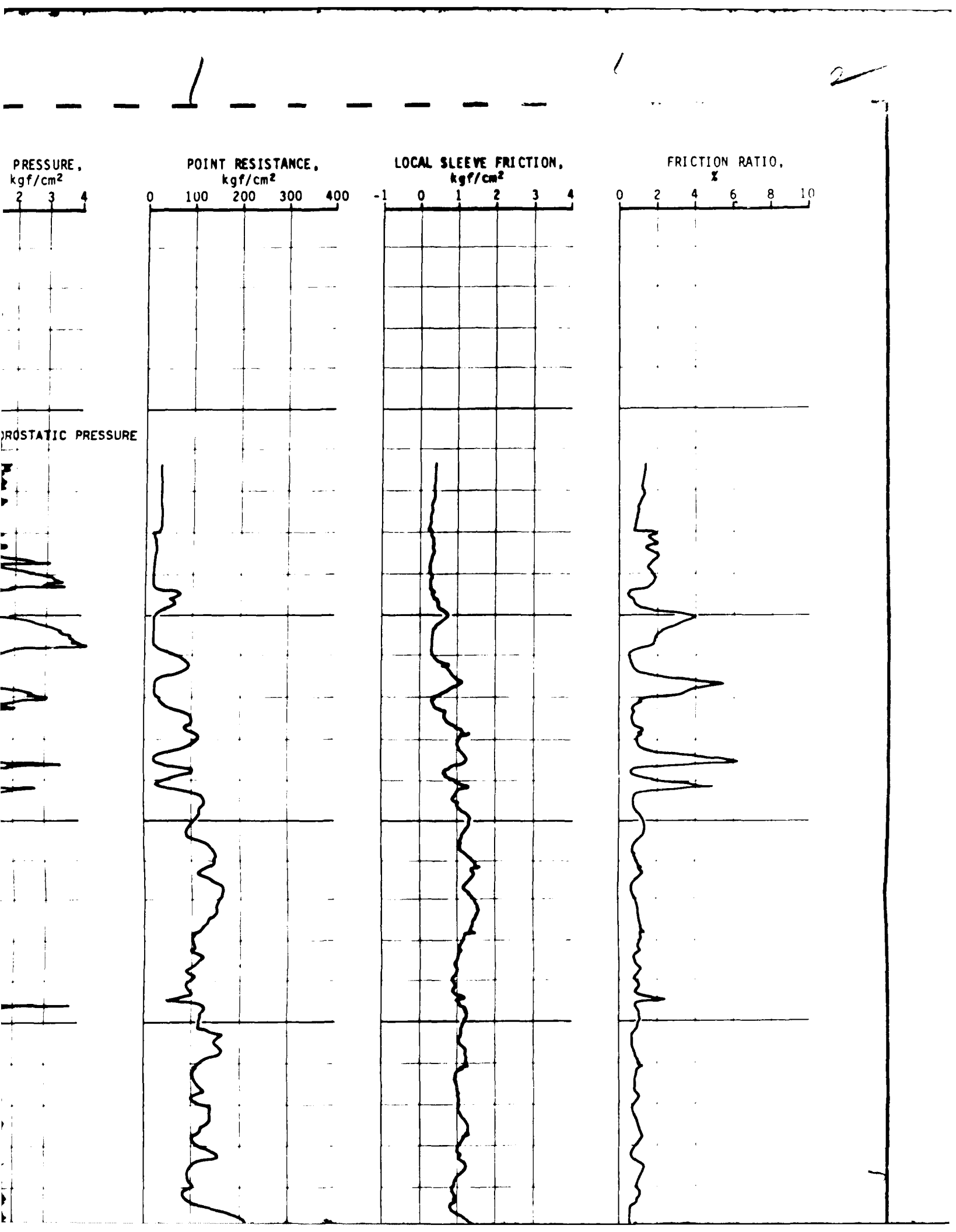
BONNE CARRE POINT, LA.

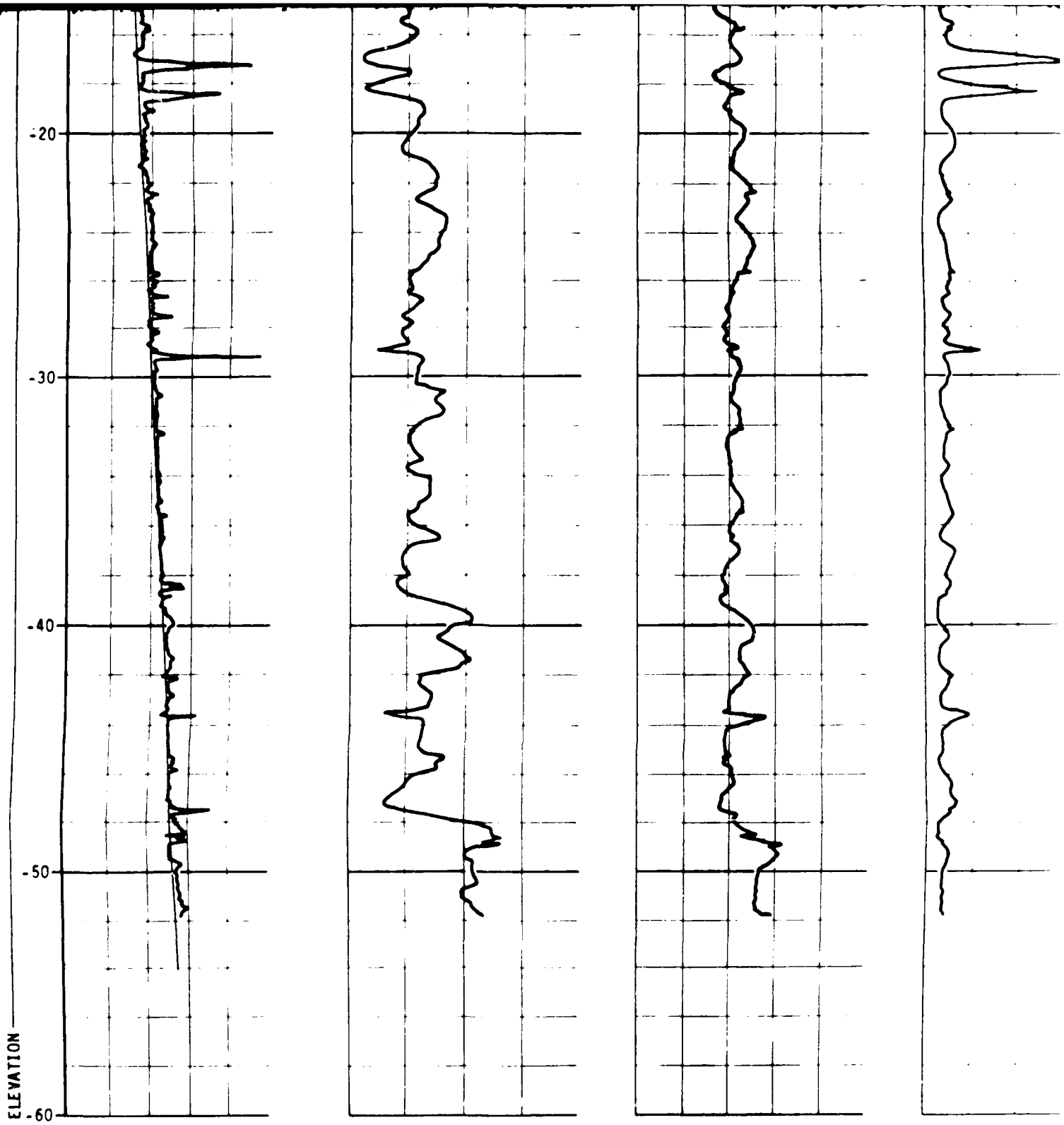
Ardaman & Associates, Inc.
Consulting Engineers in Soil Mechanics, Foundations, and Material Testing

FIELD INVESTIGATION
MONTZ AND BONNE CARRE POINT
CORPS OF ENGINEERS WES

DRAWN BY: GSW	CHECKED BY:	DATE: 1-23-91
FILE NO. 78-039	APPROVED BY:	


PORE PRESSURE, kgf/cm²
POINT RESISTANCE, kgf/cm²
LOCAL SLEEVE FRICTION, kgf/cm²
FEET(MSL)
HYDROSTATIC PRESSURE
-1 0 1 2 3 4
0 100 200 300 400
10
0
-10
-20
-30


PRESSURE,
kgf/cm²
2 3 4
ROSTATIC PRESSURE
POINT RESISTANCE,
kgf/cm²
0 100 200 300 400
LOCAL SLEEVE FRICTION,
kgf/cm²
-1 0 1 2 3 4
FRICTION RATIO,
%
0 2 4 6 8 10



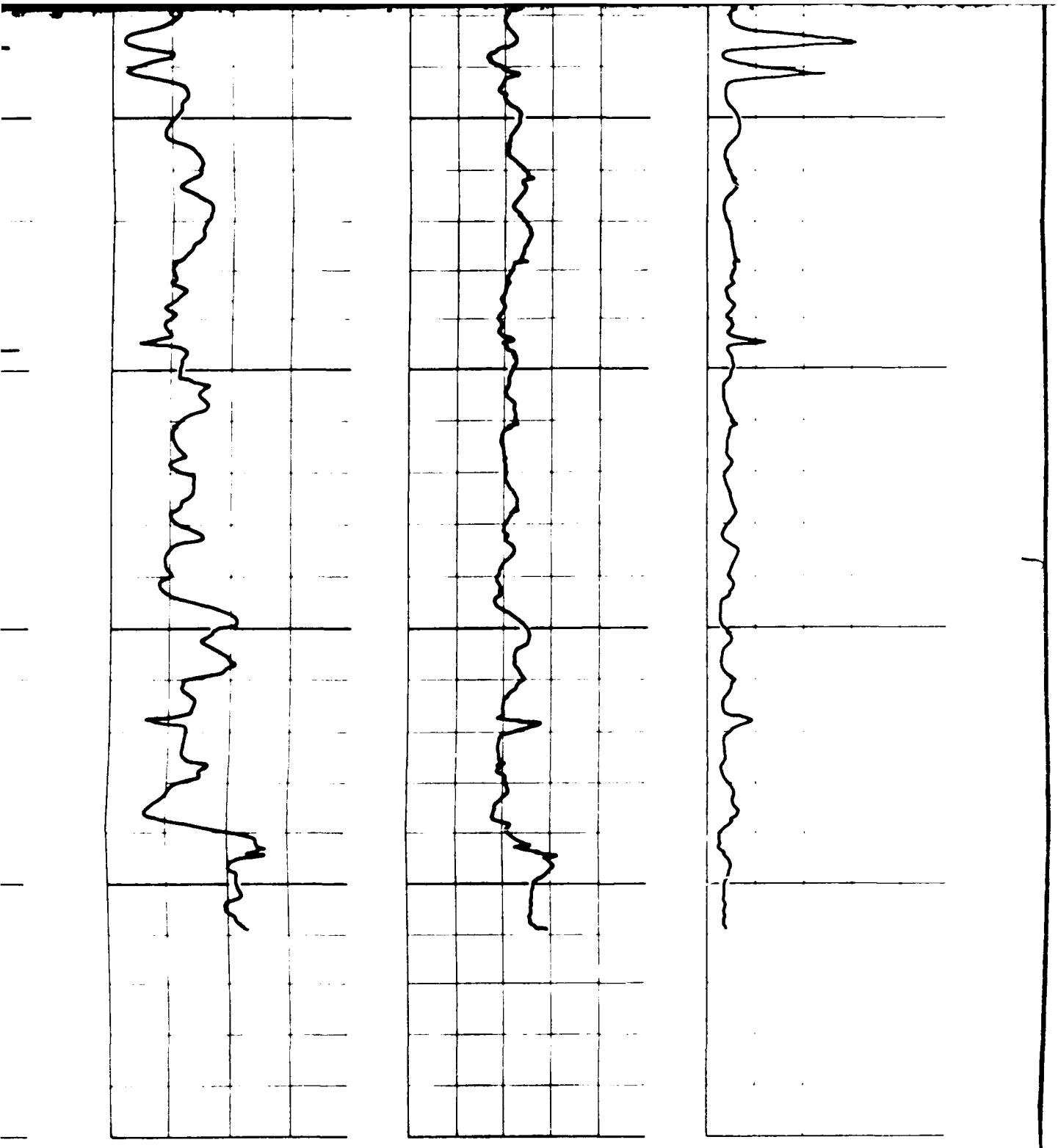
PIEZOCONE HOLE NO. BW-3

BONNE CARRE POINT, LA.

Ard
Cons
Foun

FIELD
MONTZ AND
CORPS OF

DRAWN BY: GSW
FILE NO. 78-039



PIEZOCONE HOLE NO. BW-3

BONNE CARRE POINT, LA.

Ardaman & Associates, Inc.
Consulting Engineers in Soil Mechanics, Foundations, and Materials Testing

FIELD INVESTIGATION
MONTZ AND BONNE CARRE POINT
CORPS OF ENGINEERS WES

DRAWN BY: GSW	CHECKED BY:	DATE:
FILE NO. 78-039	APPROVED BY:	

APPENDIX I

FRESH DEPOSITS, IN SITU DENSITIES BY NUCLEAR GAGE

MONTZ SITE NUCLEAR GAGE READINGS

Surface Reading No.	Dry Density pcf	Visual Classification
1	90.5	(SP-SM)
2	88.0	(SP-SM)
3	77.2	(ML)
4	84.1	(SM)
5	88.2	(SP-SM)
6	91.0	(SP-SM)
7	88.1	(SP-SM)
8	87.6	(SM)
9	87.6	(SM)
10	86.6	(SM)
11	92.6	(SP-SM)
12	--	Clay
13	89.5	(SP-SM)
14	92.3	(SP-SM)
15	82.9	(SM)
16	91.3	(SP-SM)
17	91.1	(SP-SM)
18	93.3	(SP-SM)
19	93.4	(SP-SM)
20	95.4	(SP-SM)
21	93.4	(SP-SM)
22	90.4	(SP-SM)
23	98.5	(SP-SM)
24	93.0	(SP-SM)
25	92.1	(SP-SM)
26	73.9	(ML)
Bench Reading No.		
1	95.3	(SP-SM)
2	92.4	(SP-SM)
3	88.5	(SP-SM)
4	91.9	(SP-SM)
5	88.9	(SP-SM)
6	90.3	(SP-SM)
7	88.2	(SP-SM)

Note: For location of readings see Figure 22.

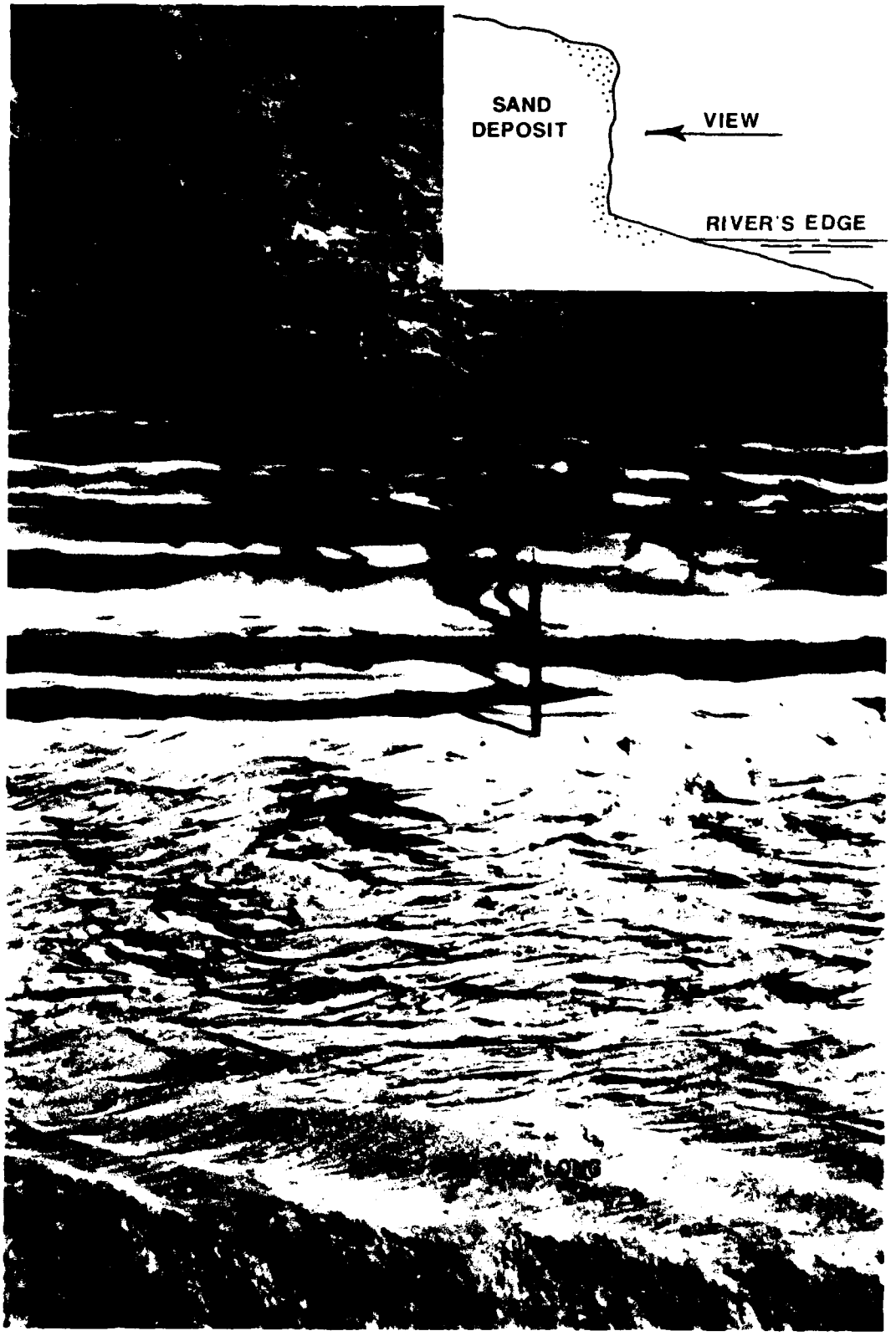
BONNET CARRE SITE NUCLEAR GAGE READINGS

Surface Reading No.	Dry Density pcf	Visual Classification
1	88.4	(SP-SM)
2	88.9	(SP-SM)
3	82.2	(SM)
4	86.7	(SM)
5	84.3	(SM)
6	90.6	(SP-SM)
7	98.7	(SP)
8	89.8	(SP-SM)
9	86.6	(SM)
10	97.5	(SP)
11	92.4	(SP-SM)
Bench Reading No.		
1	96.4	(SP-SM)
2	91.0	(SP-SM)
3	91.7	(SP-SM)
4	79.7	(ML)
5	84.8	(SM)
6	81.4	(SM)

NOTE: For location of readings see Figure 22 of main text.

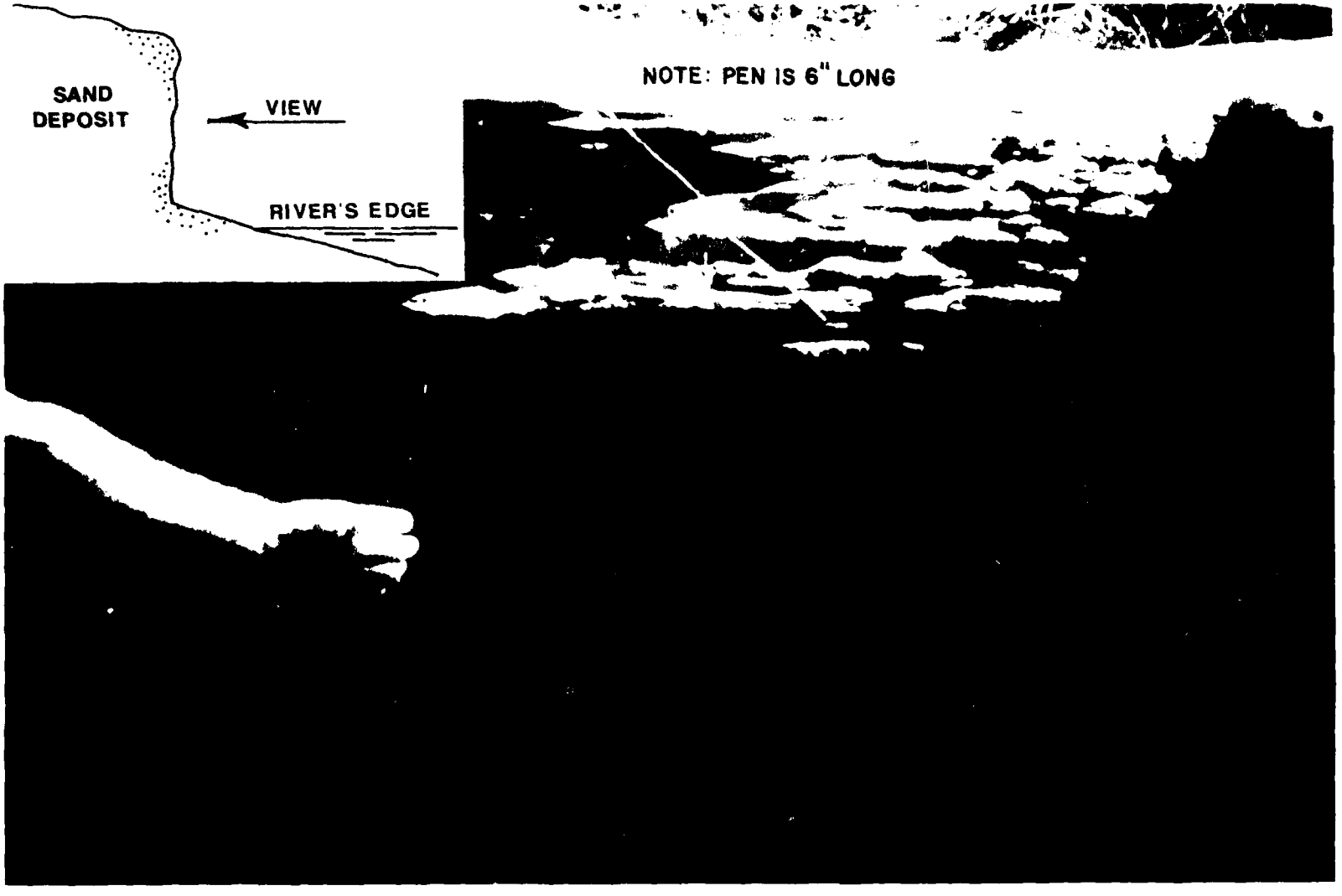
APPENDIX J

PHOTOGRAPHS OF DEPOSITIONAL FABRICS IN SANDS AND SILTY SANDS, FRESH DEPOSIT, AND MONTZ SITE


SAND
DEPOSIT
VIEW
RIVER'S EDGE


SAND
DEPOSIT
VIEW
RIVER'S EDGE


SAND
DEPOSIT
VIEW
RIVER'S EDGE


SAND
DEPOSIT
VIEW
RIVER'S EDGE
NOTE: PEN IS 6" LONG




RIVER
VIEW
RIVER S EDGE
SAND DEPOSIT
APPROXIMATELY 1 FT.

APPENDIX K

TRIAXIAL TEST RESULTS ON UNDISTURBED SAMPLES, MONTZ AND BONNET CARRE POINT SITES

DEFINITION OF TERMS

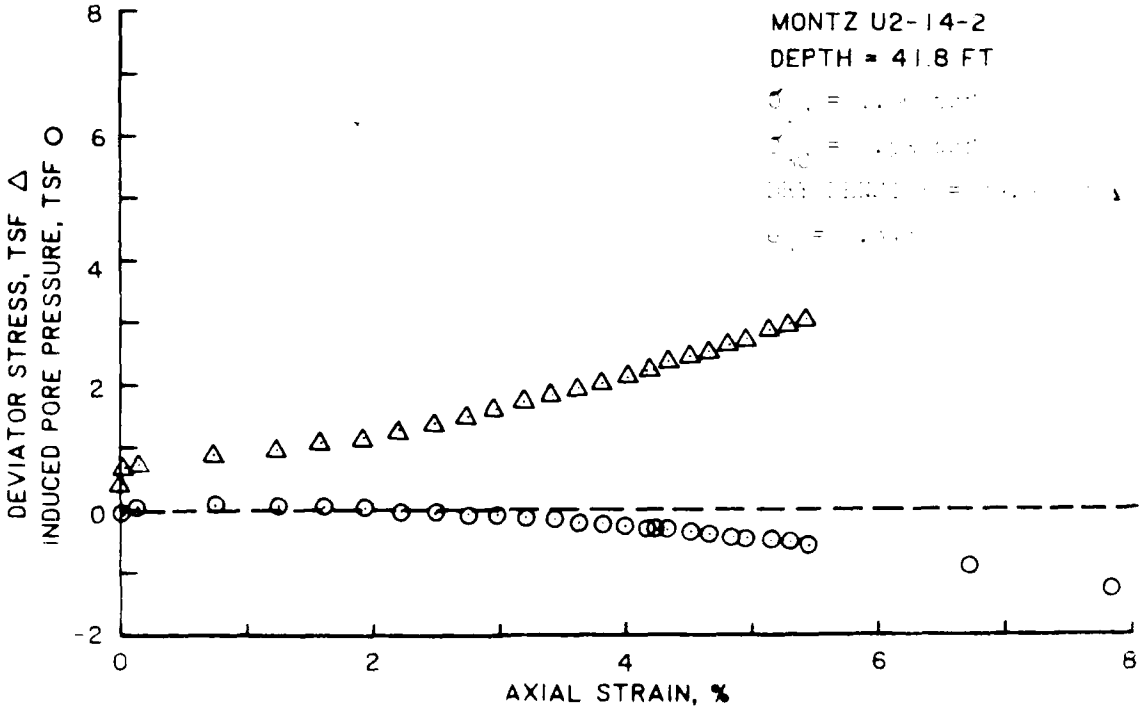
σ_{1C} = Vertical consolidation stress
σ_{3C} = Horizontal consolidation stress
e_c = Void ratio after consolidation

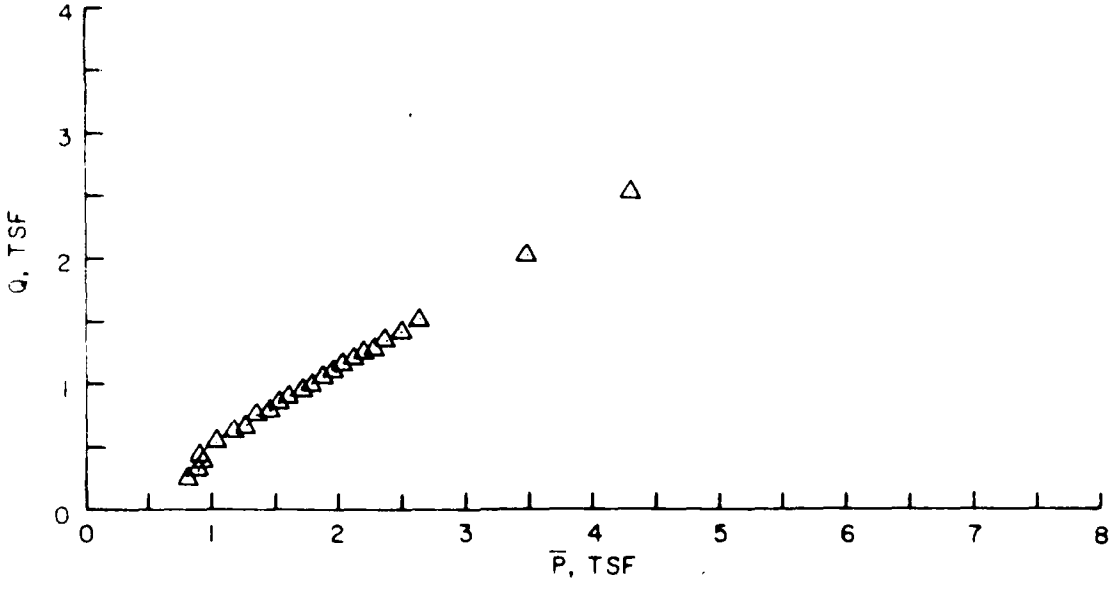
FOR THE EFFECTIVE STRESS PATH:

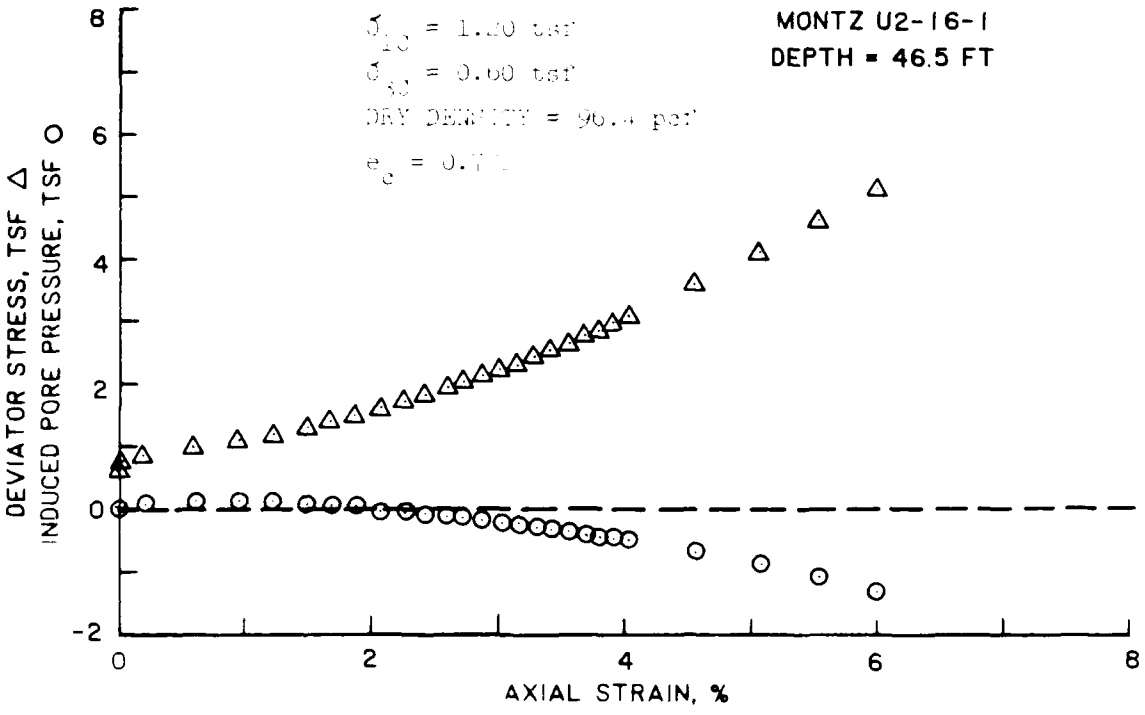
$$Q = \frac{(\sigma_1 - \sigma_3)}{2}$$

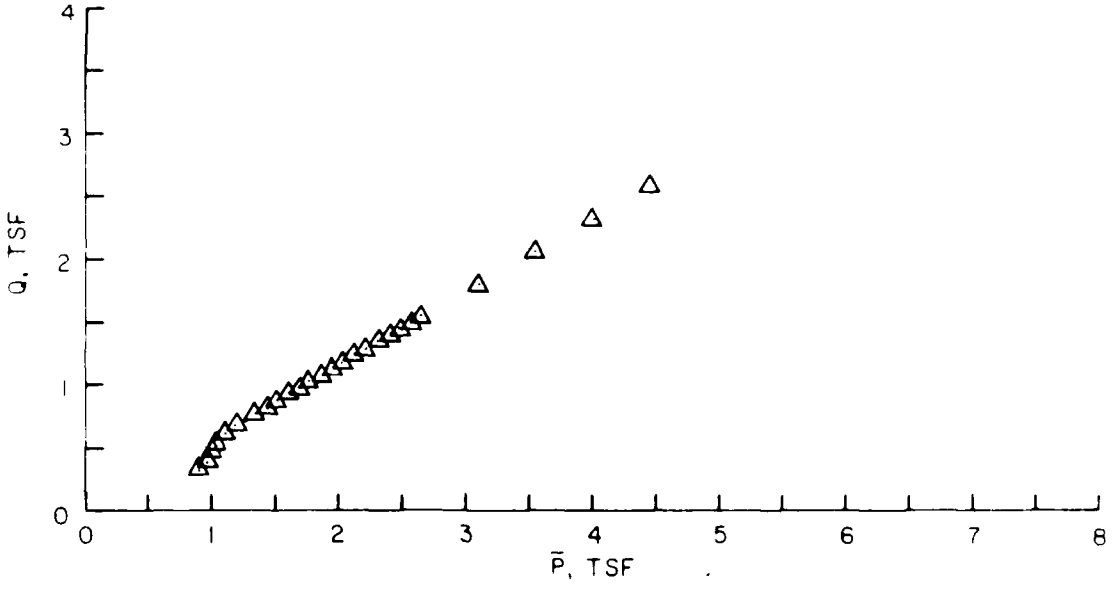
$$\bar{P} = \frac{\bar{\sigma}_1 + \bar{\sigma}_3}{2}$$

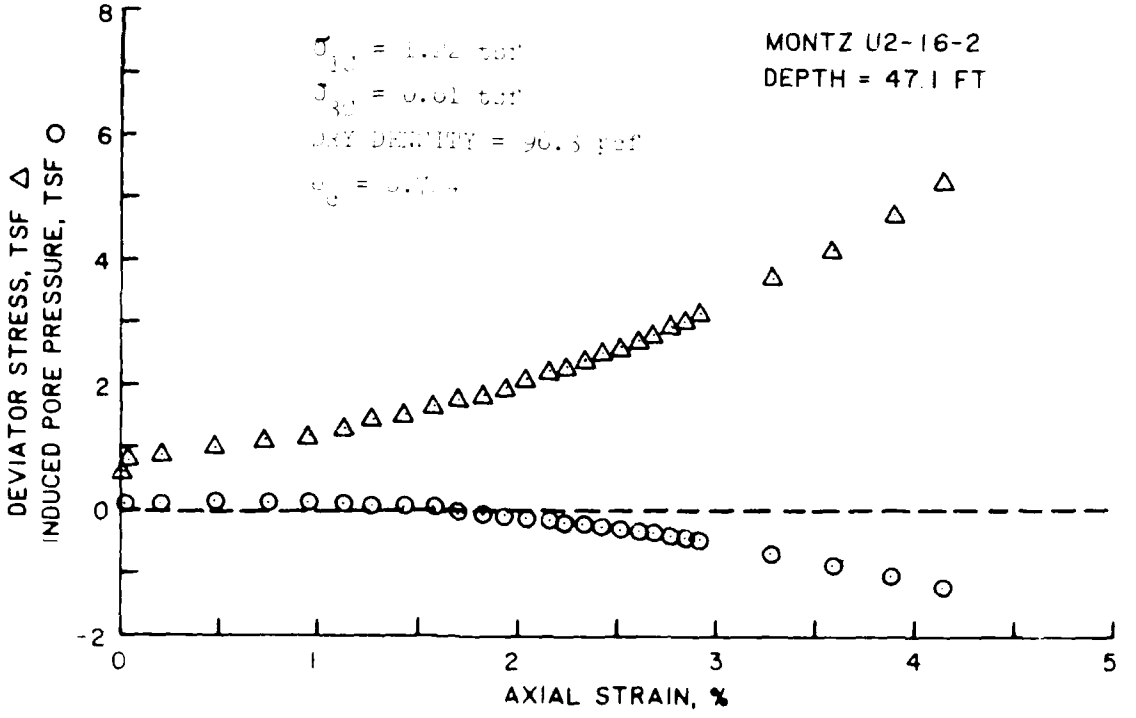
The following undisturbed specimens, (Montz U1-20, Bonnet Carre U1B-24, and Bonnet Carre U3B-5A), were deliberately consolidated to stresses from four to seven times their approximate in situ values to see if they would exhibit liquefaction/partial liquefaction. As shown, they still tended to dilate.

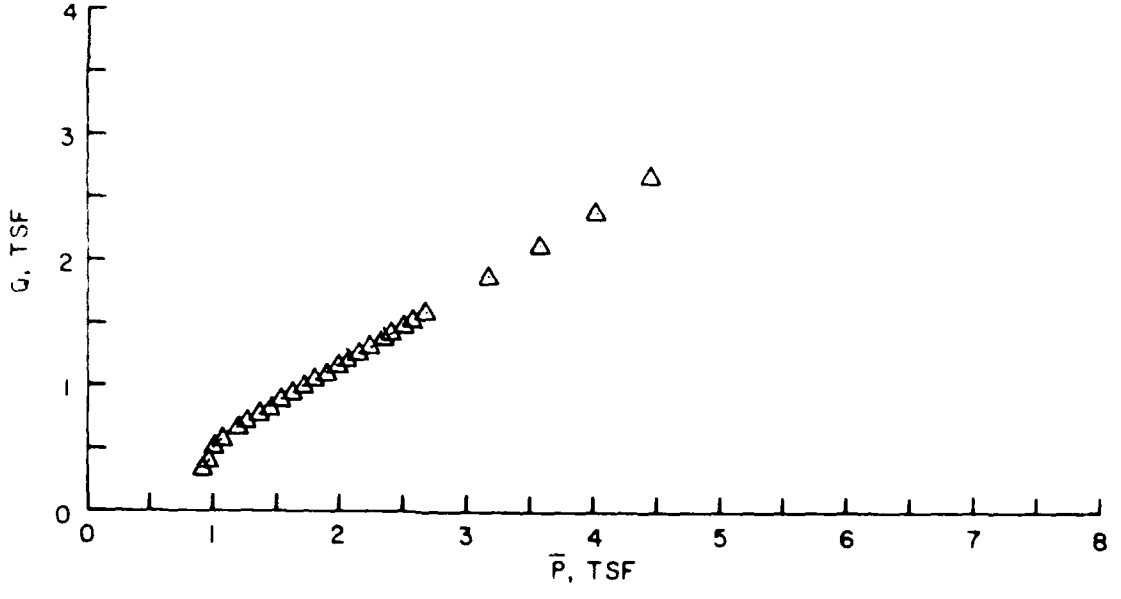

MONTZ U2-14-2
DEPTH = 41.8 FT
DEVIATOR STRESS, TSF Δ
INDUCED PORE PRESSURE, TSF O
8
6
4
2
0
-2
0
2
4
6
8
AXIAL STRAIN, %

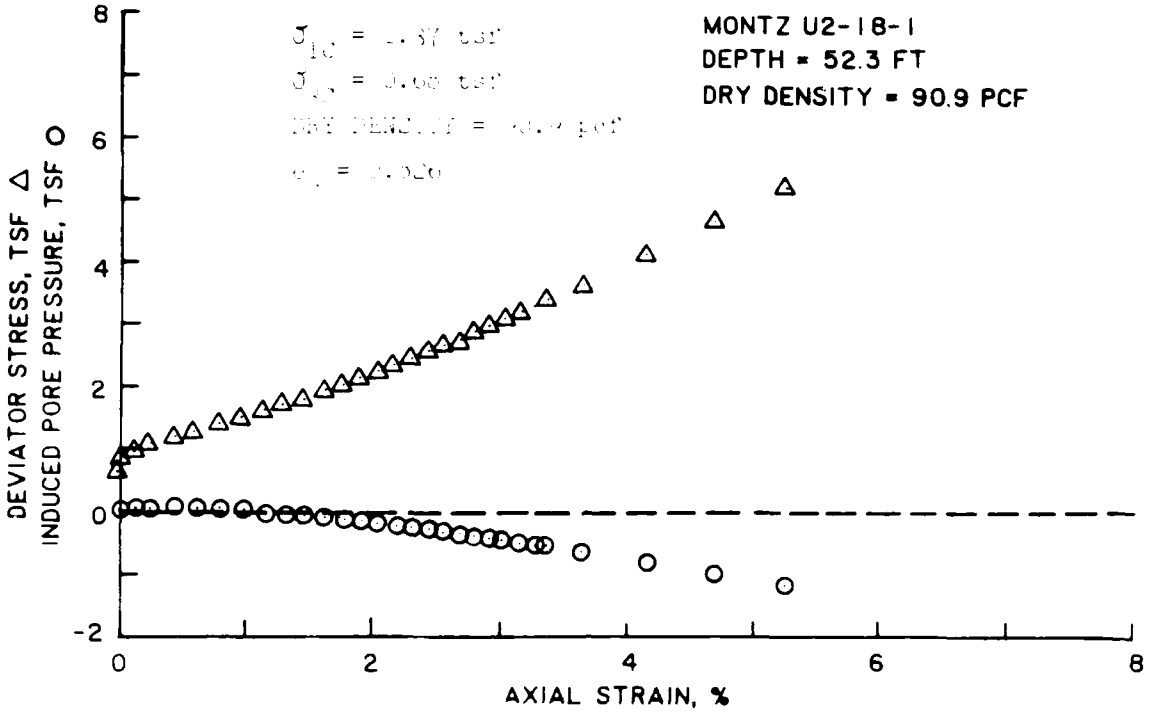

Q, TSF
4
3
2
1
0
0
1
2
3
4
5
6
7
8
P̄, TSF

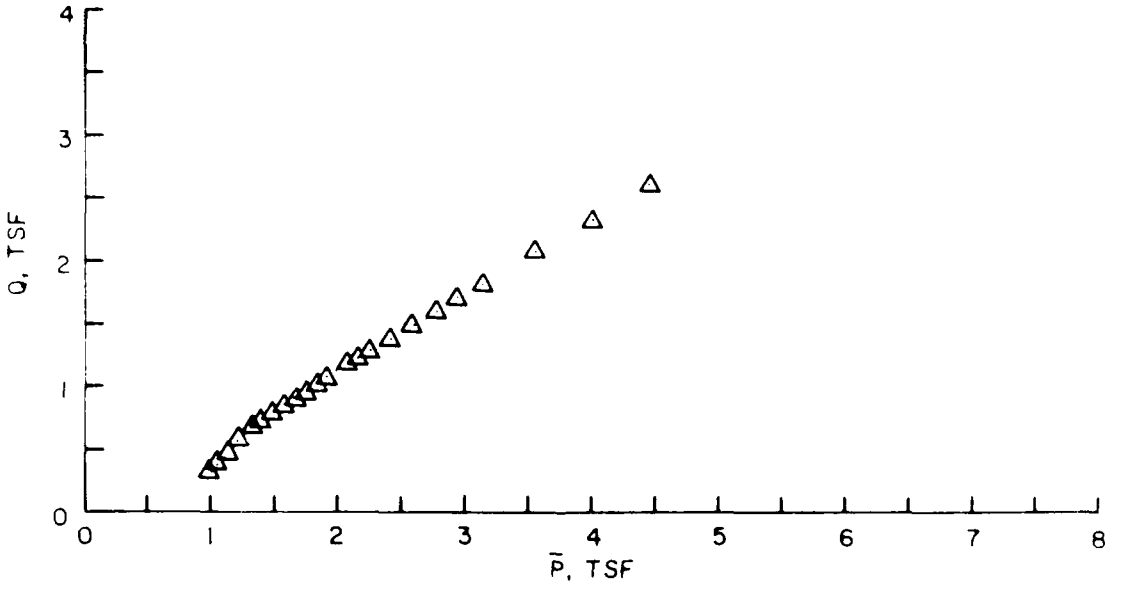

MONTZ U2-16-1
DEPTH = 46.5 FT
DEVIATOR STRESS, TSF Δ
INDUCED PORE PRESSURE, TSF O
AXIAL STRAIN, %

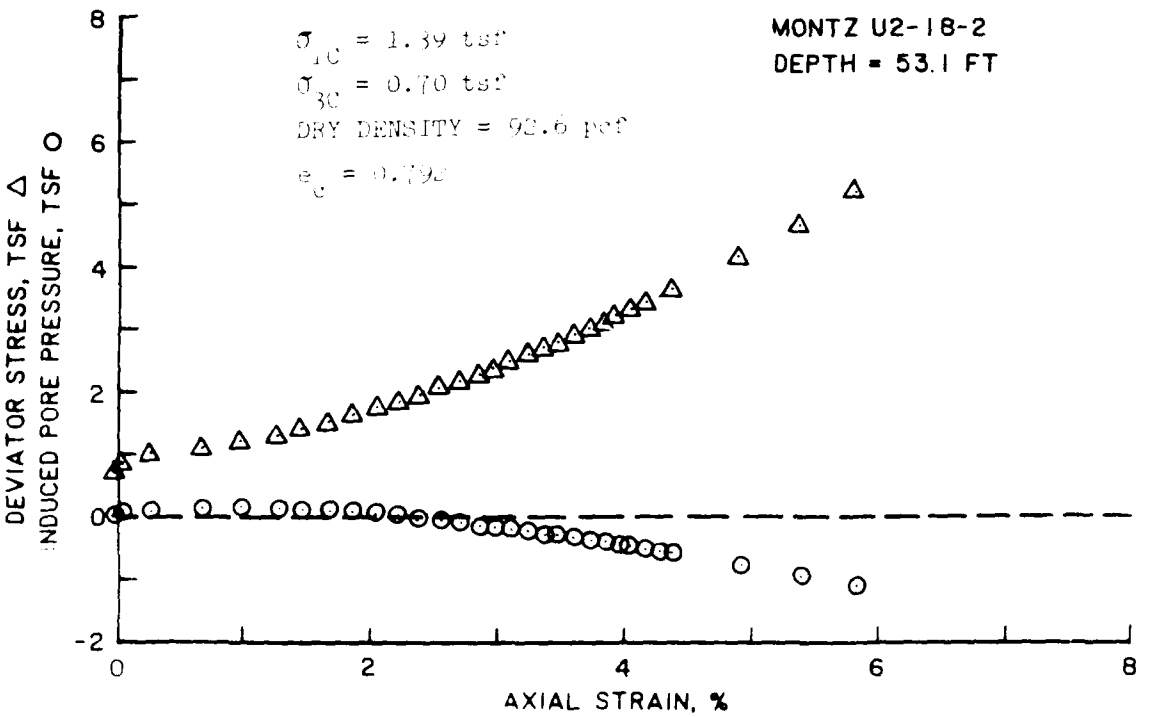

Q, TSF
P̄, TSF

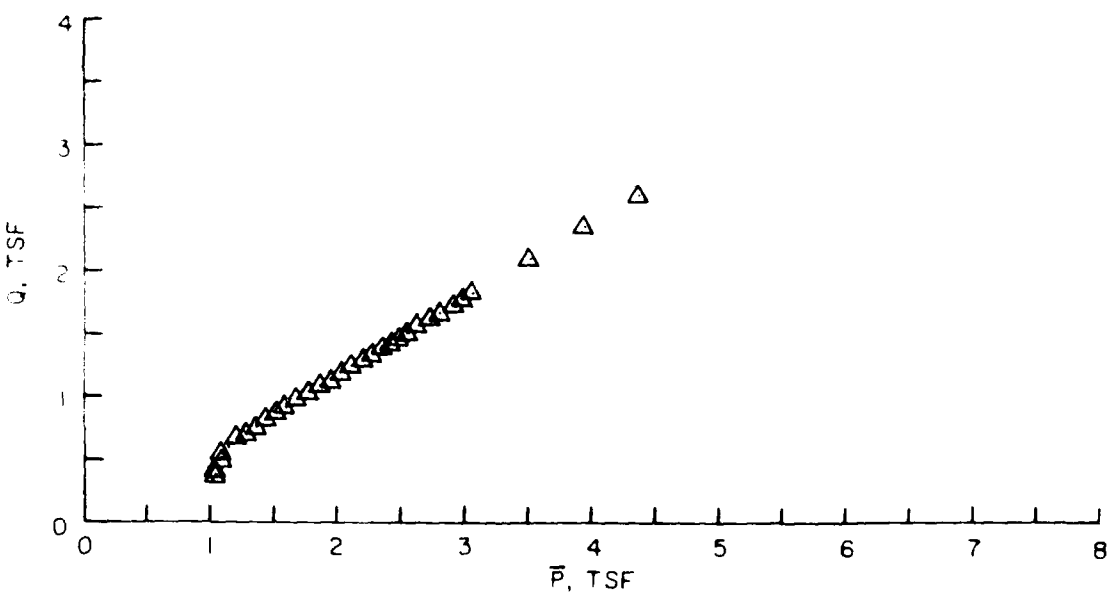

MONTZ U2-16-2
DEPTH = 47.1 FT
DEVIATOR STRESS, TSF Δ
INDUCED PORE PRESSURE, TSF O
AXIAL STRAIN, %

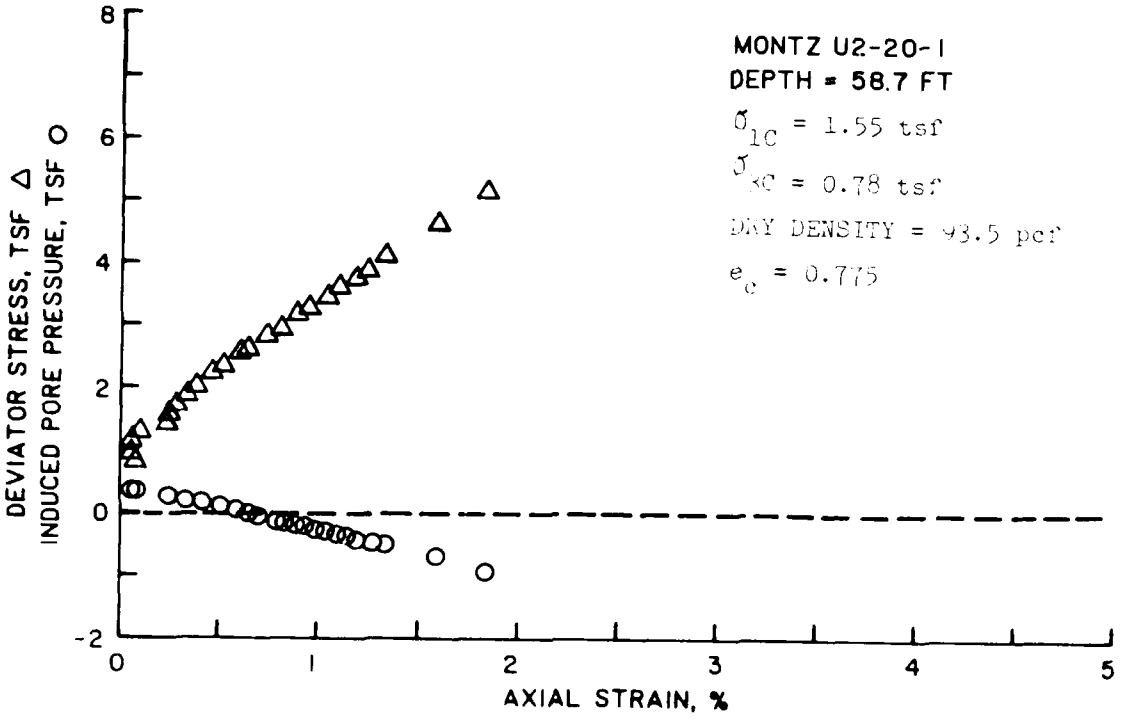

Q, TSF
P̄, TSF

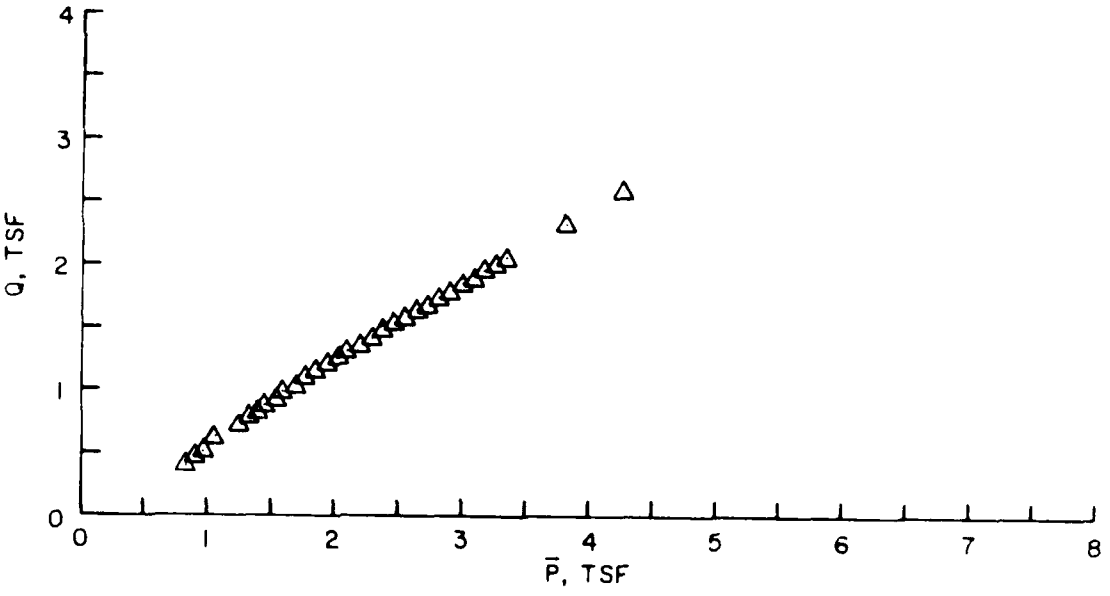

MONTZ U2-18-1
DEPTH = 52.3 FT
DRY DENSITY = 90.9 PCF
DEVIATOR STRESS, TSF Δ
INDUCED PORE PRESSURE, TSF O
AXIAL STRAIN, %
8
6
4
2
0
-2
0
2
4
6
8

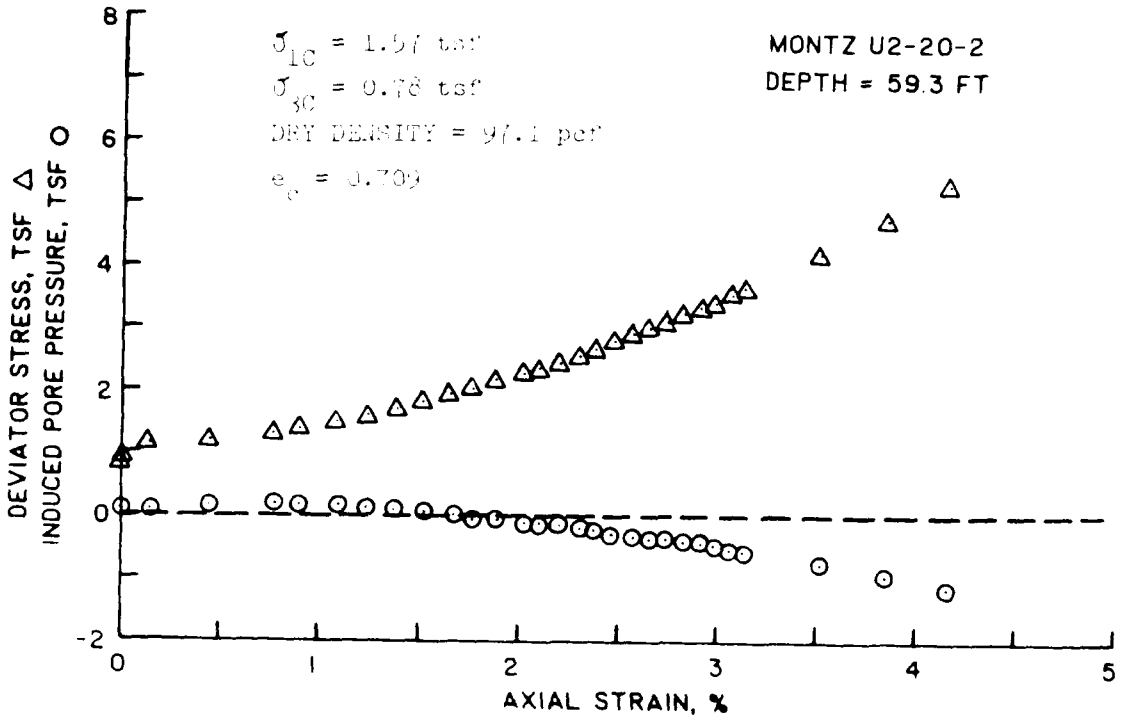

Q, TSF
P̄, TSF
4
3
2
1
0
0
1
2
3
4
5
6
7
8

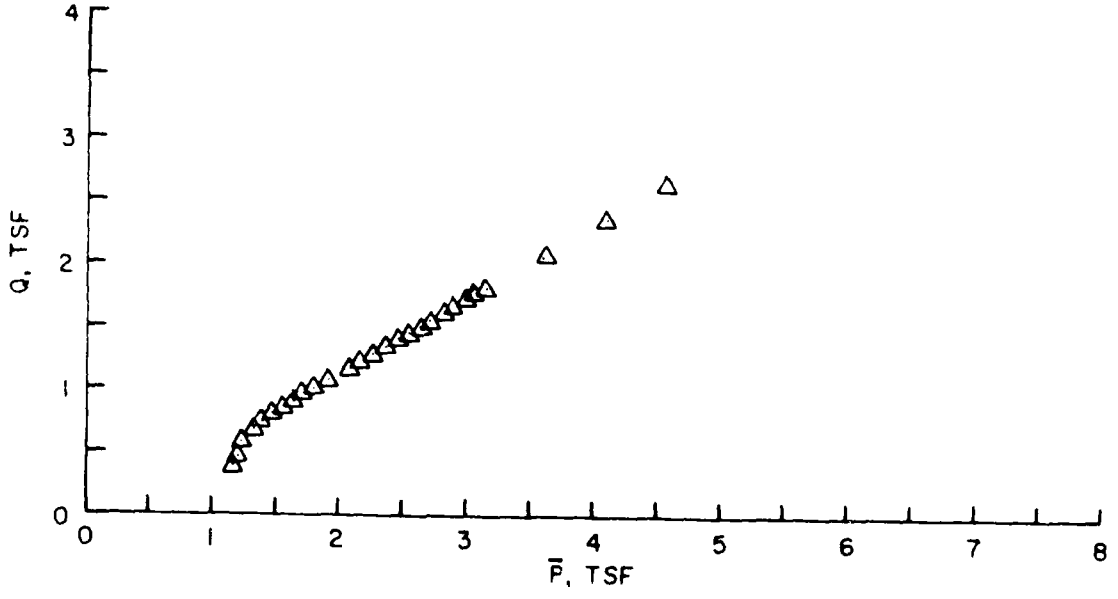

MONTZ U2-18-2
DEPTH = 53.1 FT
σ_{1C} = 1.39 tsf
σ_{3C} = 0.70 tsf
DRY DENSITY = 92.6 pcf
e_c = 0.79
DEVIATOR STRESS, TSF Δ
INDUCED PORE PRESSURE, TSF O
AXIAL STRAIN, %

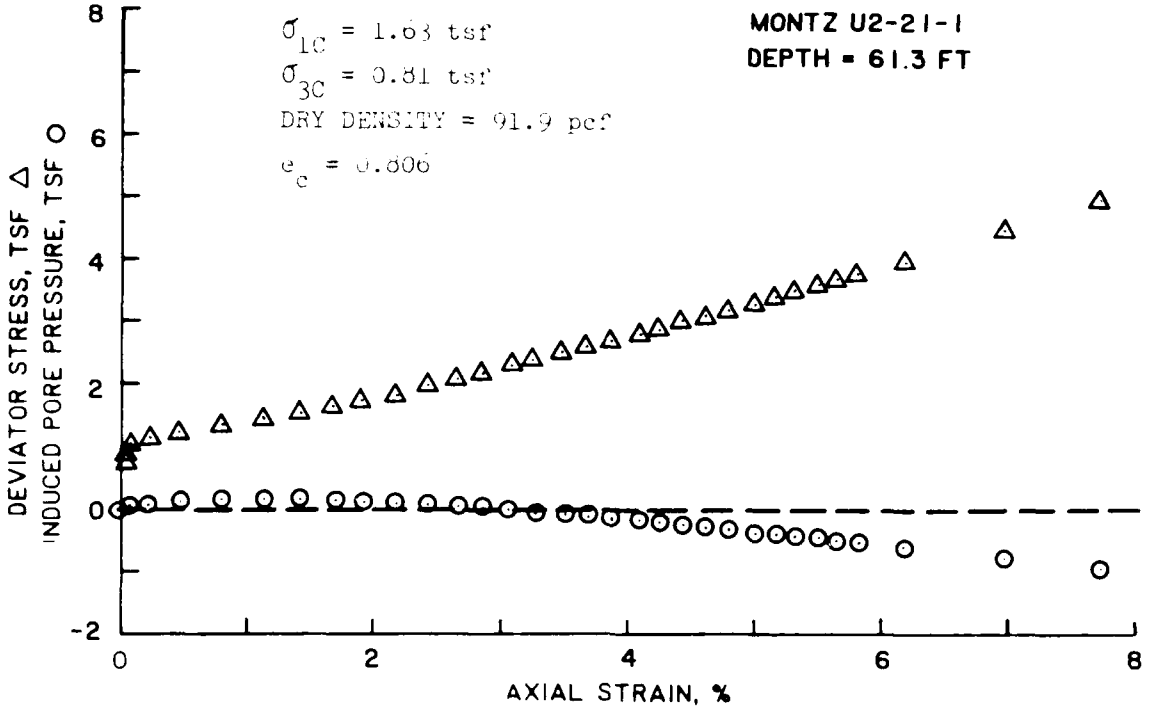

Q, TSF
$\bar{P}$, TSF

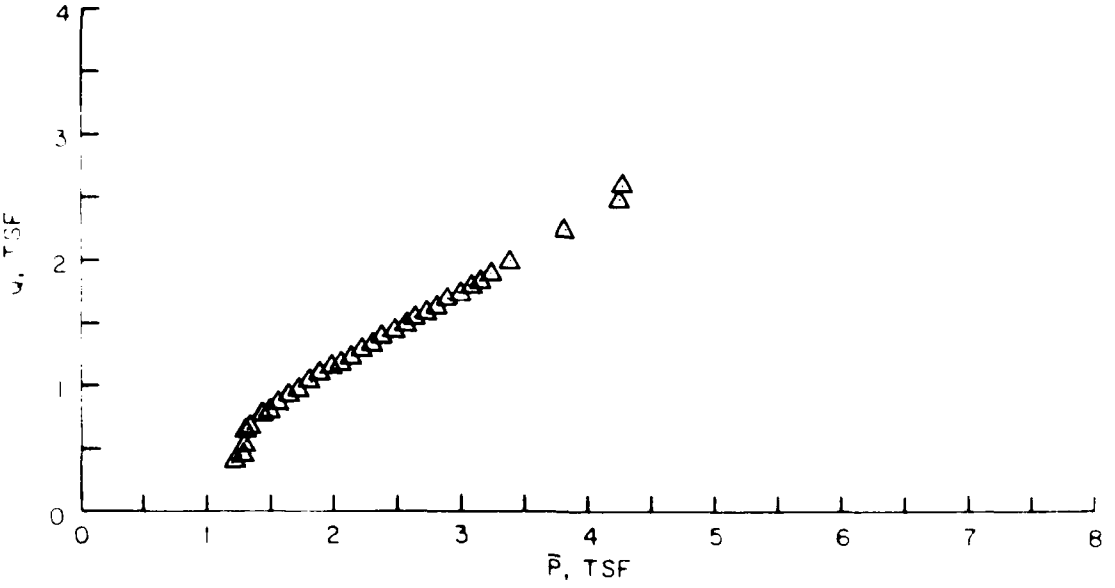

MONTZ U2-20-1
DEPTH = 58.7 FT
σ_{1C} = 1.55 tsf
σ_{3C} = 0.78 tsf
DRY DENSITY = 93.5 pcf
e_c = 0.775
DEVIATOR STRESS, TSF Δ
INDUCED PORE PRESSURE, TSF O
AXIAL STRAIN, %

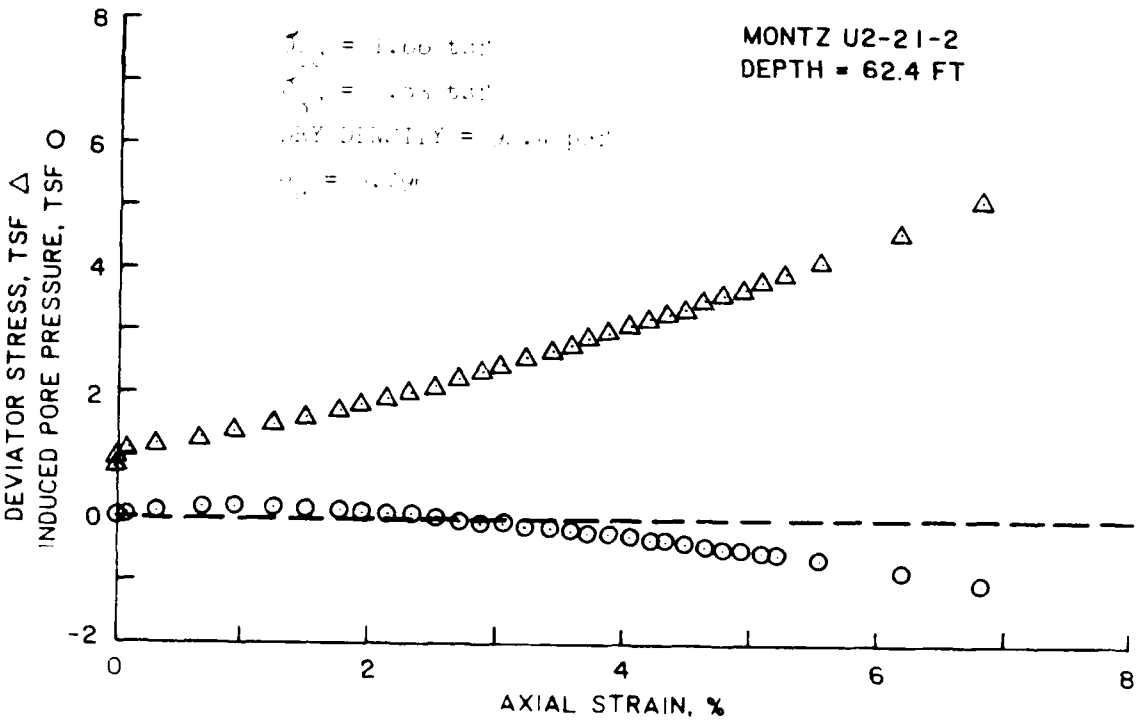

Q, TSF
$\bar{P}$, TSF

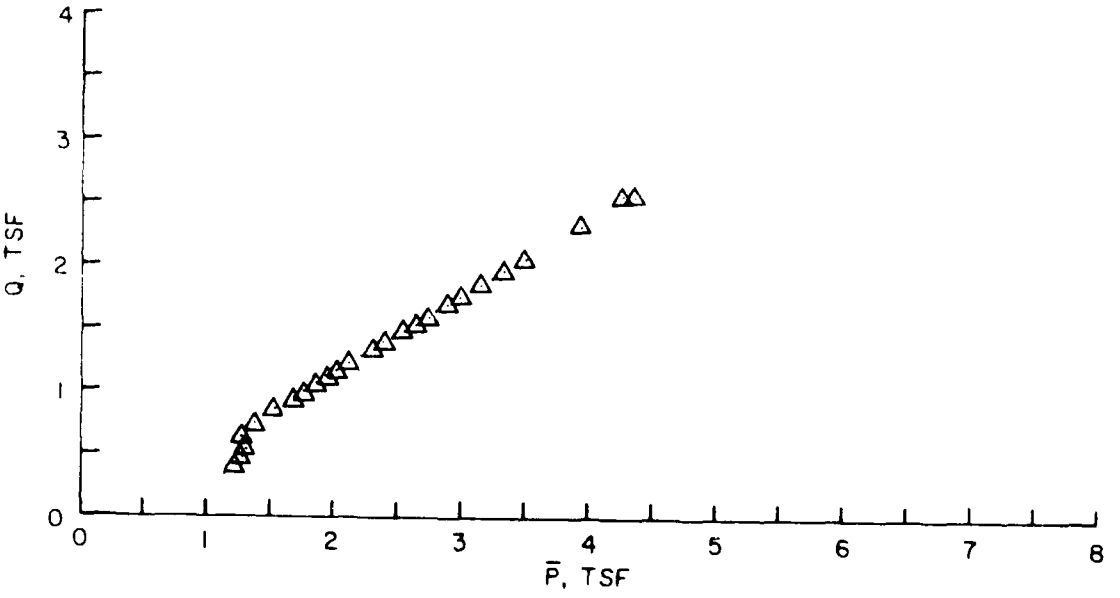

σ_{1c} = 1.57 tsf
σ_{3c} = 0.78 tsf
DRY DENSITY = 97.1 pcf
e_c = 0.709
MONTZ U2-20-2
DEPTH = 59.3 FT
DEVIATOR STRESS, TSF Δ
INDUCED PORE PRESSURE, TSF O
AXIAL STRAIN, %

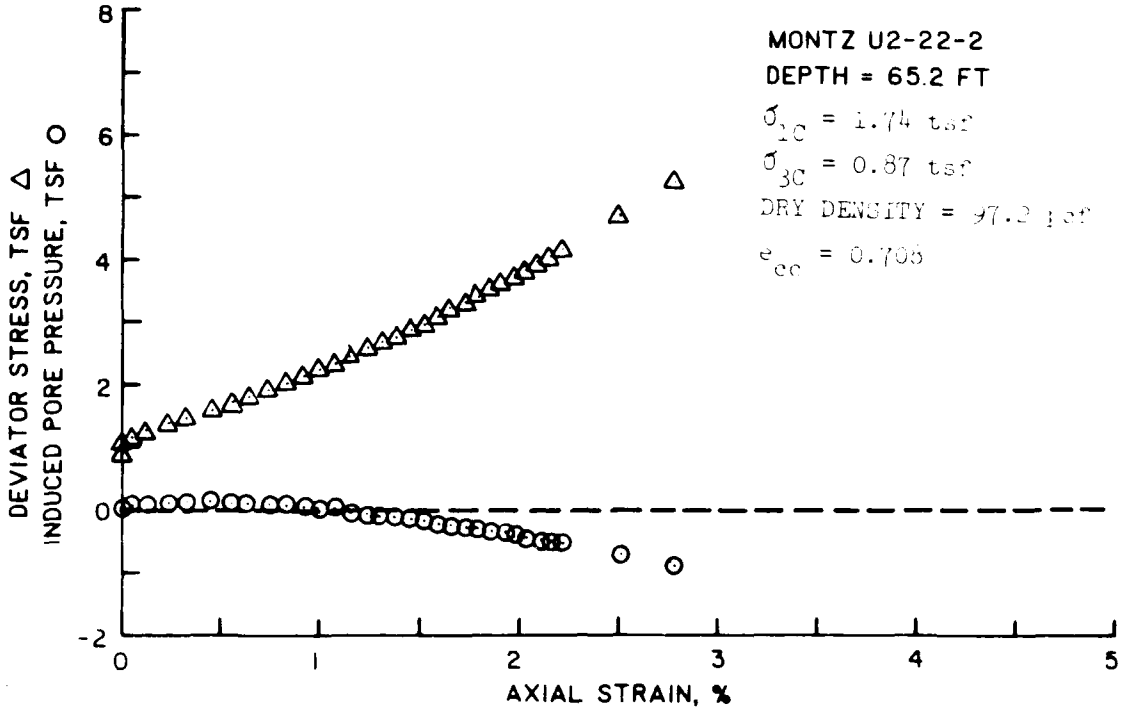

Q, TSF
$\bar{P}$, TSF

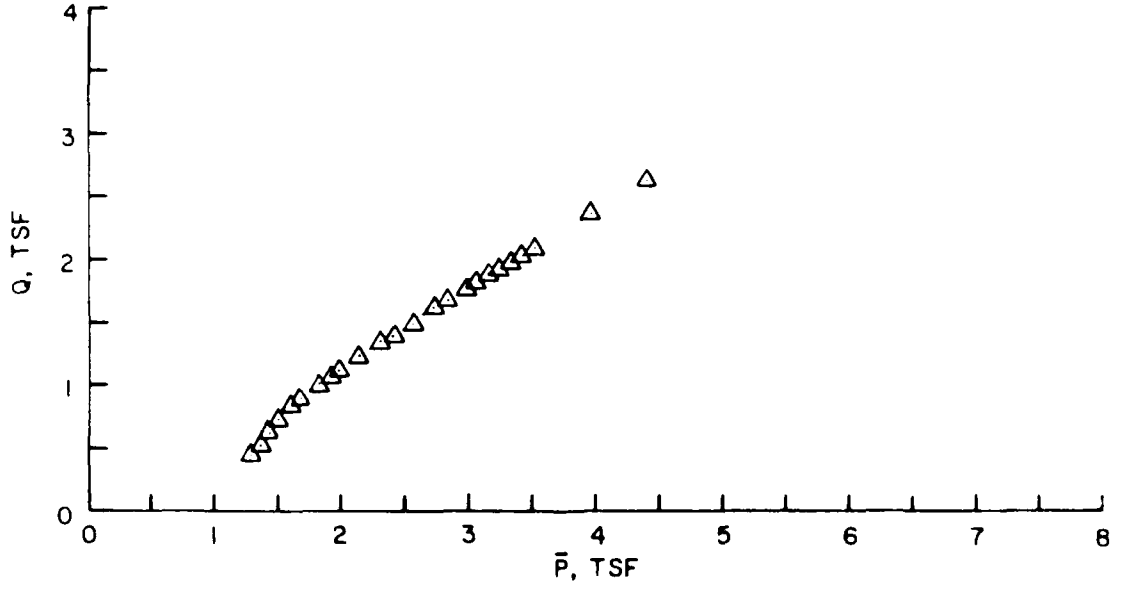

σ_{1C} = 1.63 tsf
σ_{3C} = 0.81 tsf
DRY DENSITY = 91.9 pcf
e_c = 0.806
MONTZ U2-21-1
DEPTH = 61.3 FT
DEVIATOR STRESS, TSF △
INDUCED PORE PRESSURE, TSF O
AXIAL STRAIN, %

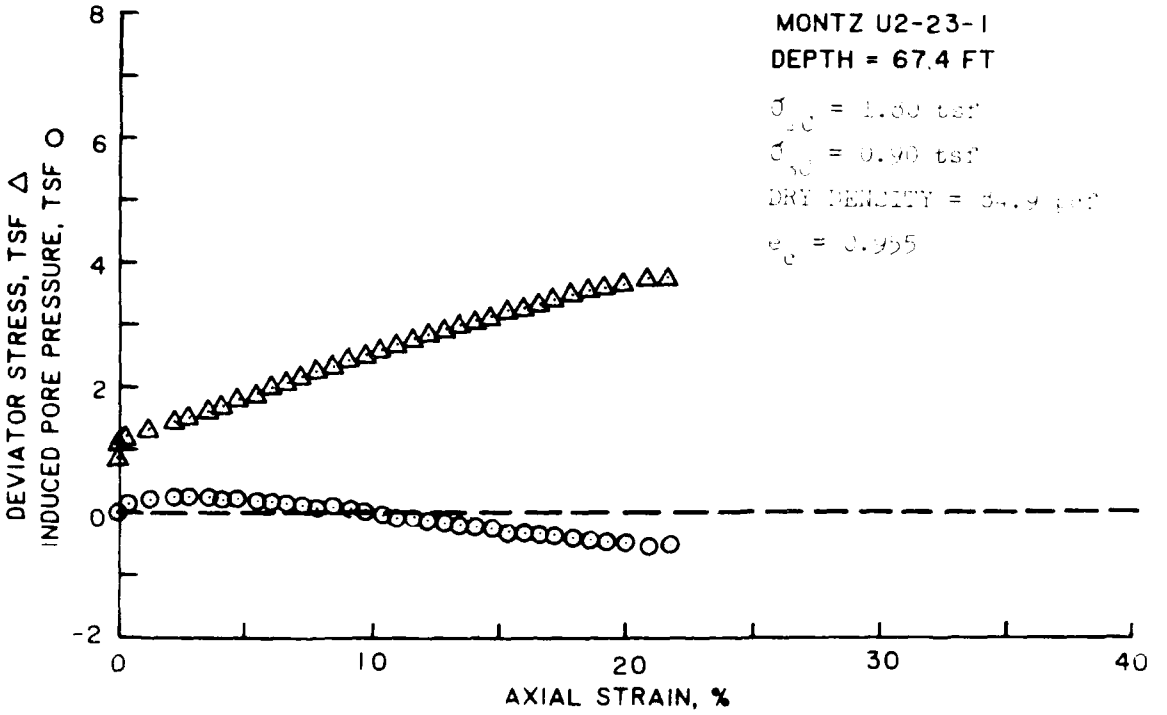

$\bar{P}$, TSF

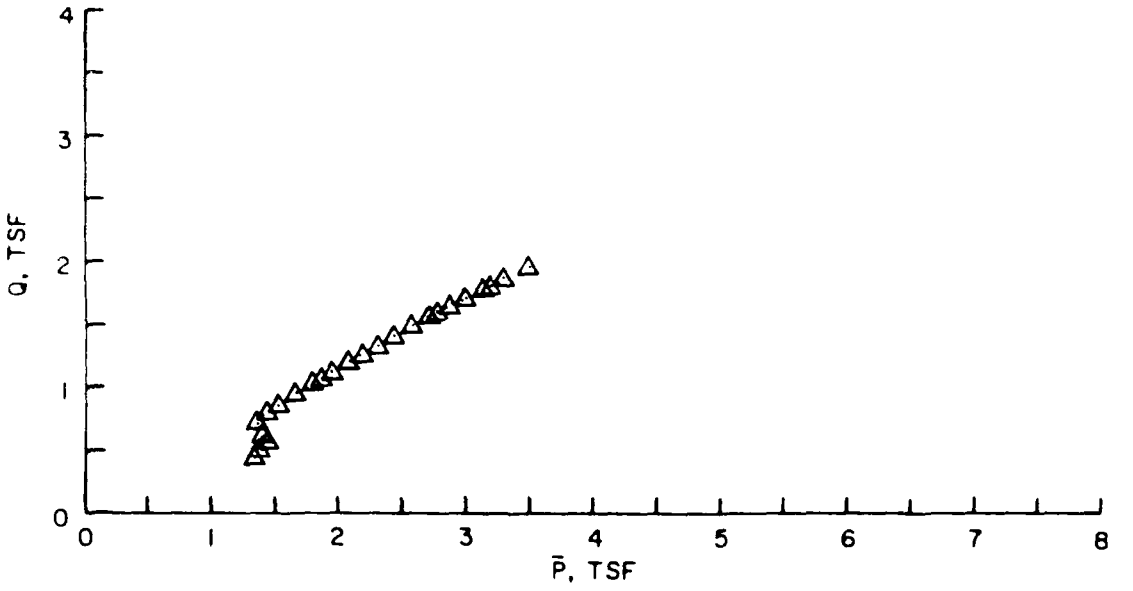

MONTZ U2-21-2
DEPTH = 62.4 FT
DEVIATOR STRESS, TSF Δ
INDUCED PORE PRESSURE, TSF O
AXIAL STRAIN, %

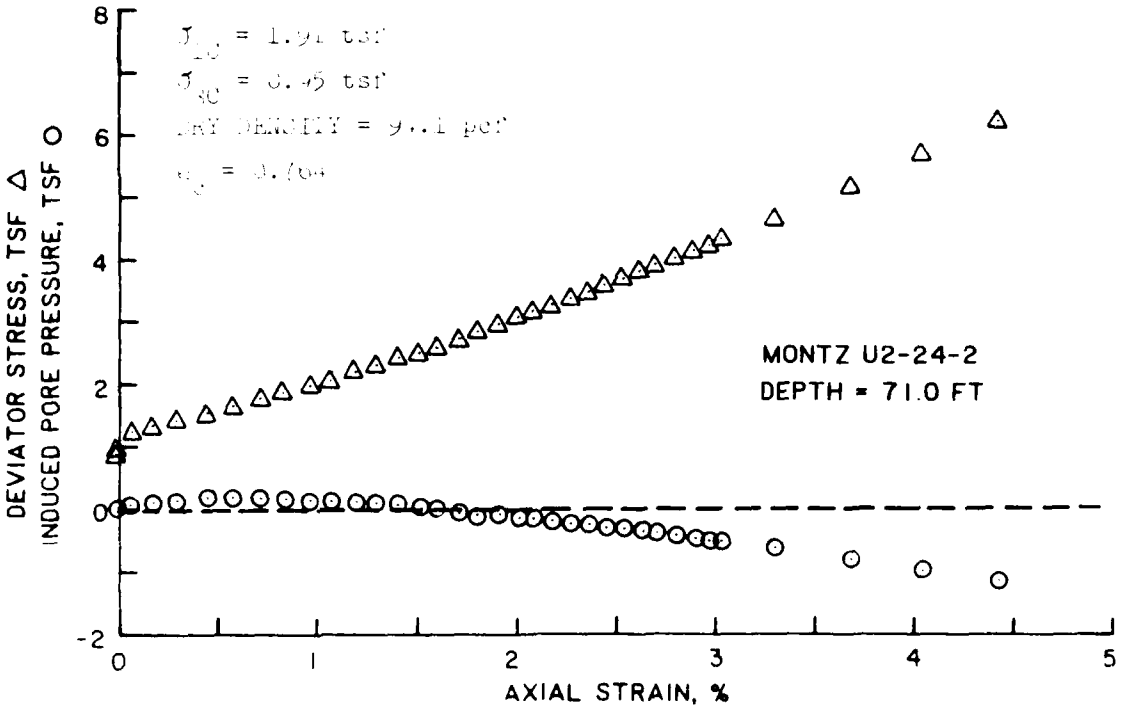

Q, TSF
$\bar{P}$, TSF

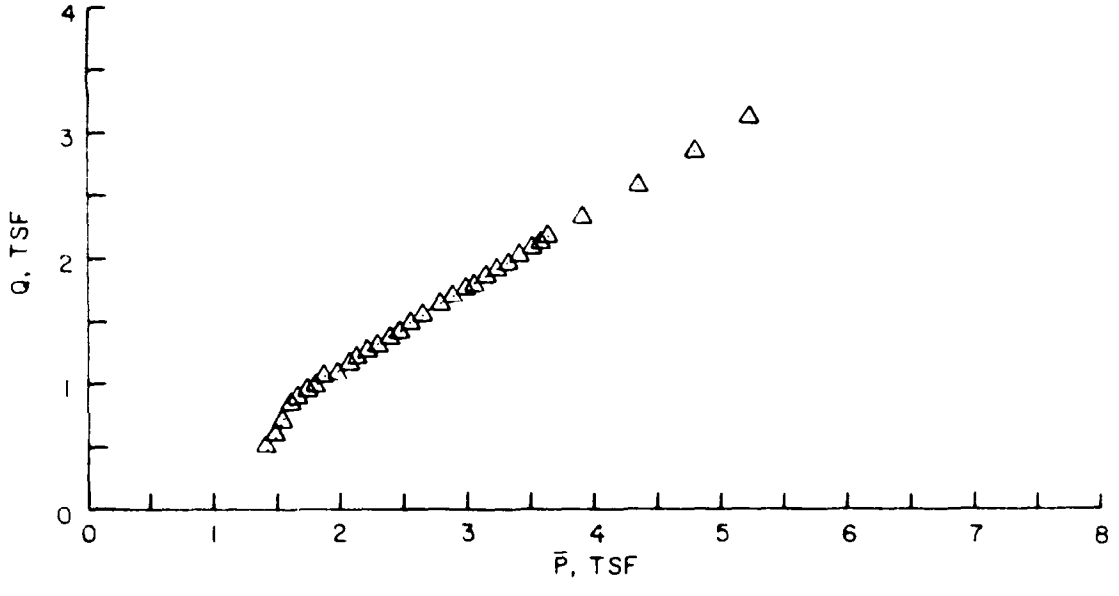

MONTZ U2-22-2
DEPTH = 65.2 FT
σ_{1C} = 1.74 tsf
σ_{3C} = 0.87 tsf
DRY DENSITY = 97.2 pcf
e_{cc} = 0.703
DEVIATOR STRESS, TSF Δ
INDUCED PORE PRESSURE, TSF O
AXIAL STRAIN, %

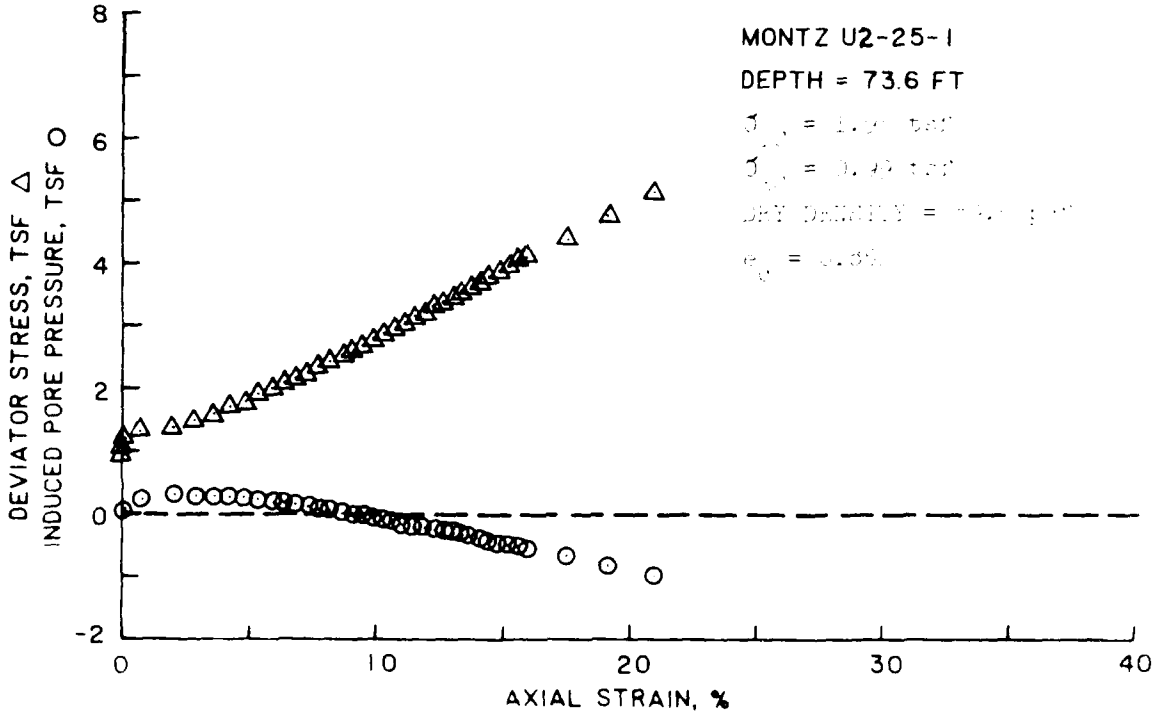

Q, TSF
$\bar{P}$, TSF

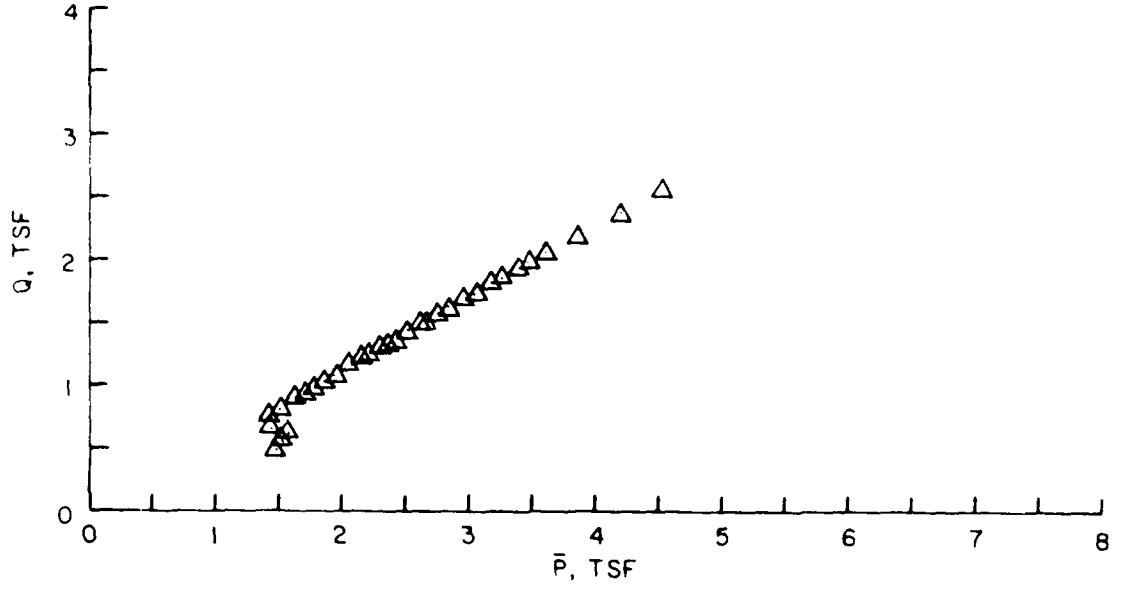

MONTZ U2-23-1
DEPTH = 67.4 FT
σ_{3c} = 1.50 tsf
σ_{3c} = 0.90 tsf
DRY DENSITY = 84.9 pcf
e_c = 0.985
DEVIATOR STRESS, TSF Δ
INDUCED PORE PRESSURE, TSF O
8
6
4
2
0
-2
0
10
20
30
40
AXIAL STRAIN, %

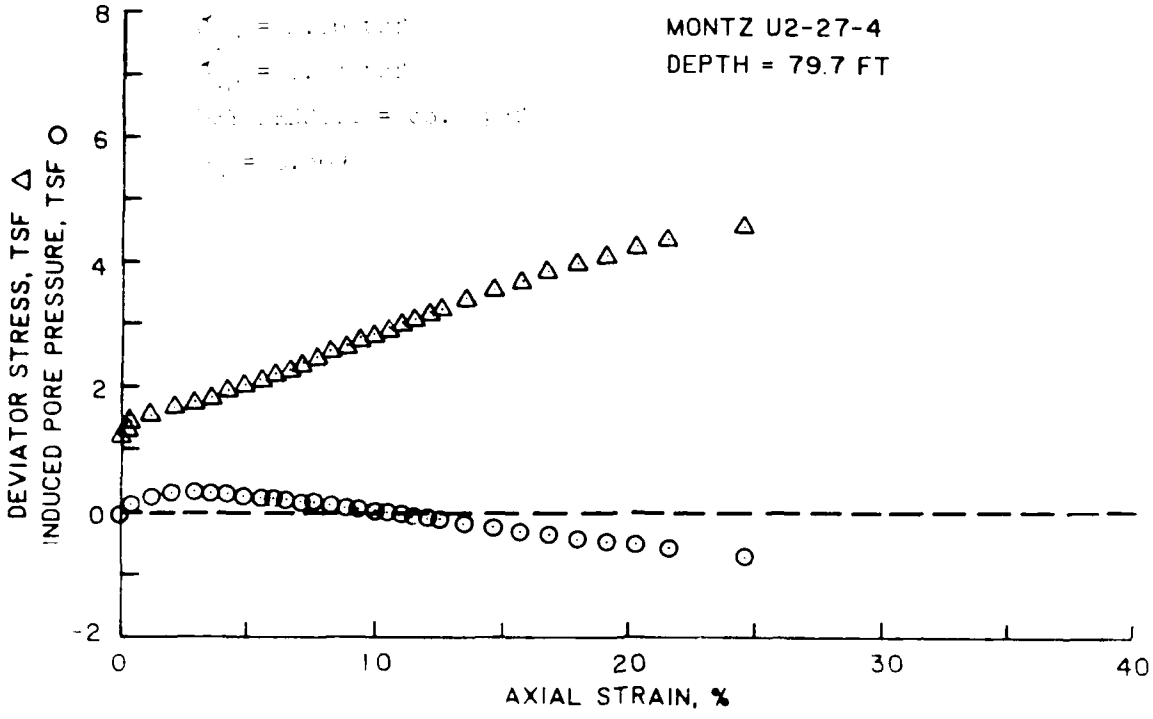

Q, TSF
4
3
2
1
0
0
1
2
3
4
5
6
7
8
$\bar{P}$, TSF

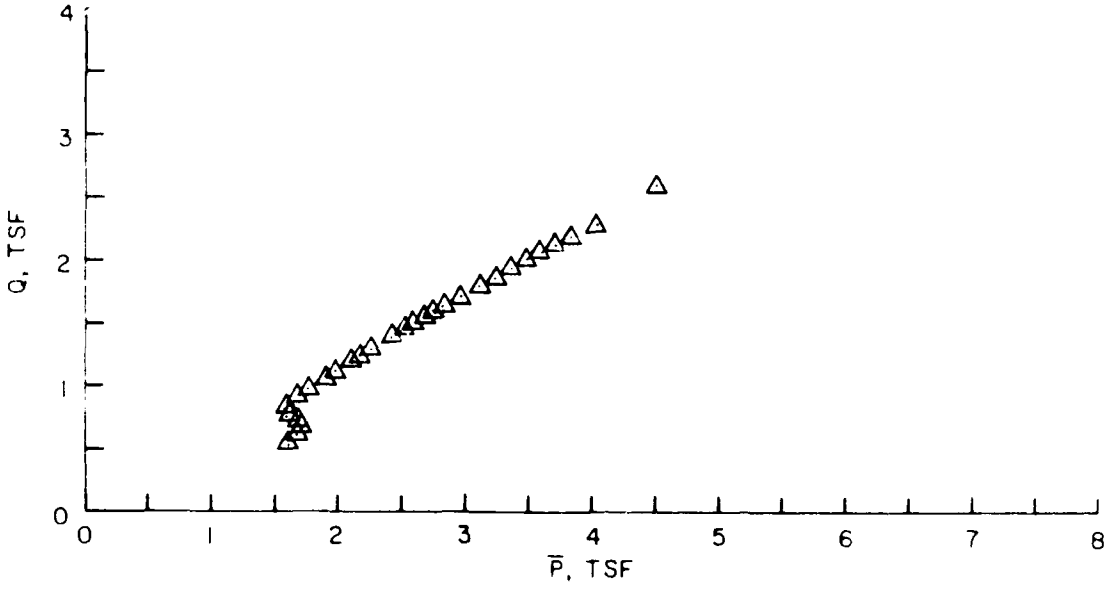

DEVIATOR STRESS, TSF Δ
INDUCED PORE PRESSURE, TSF O
AXIAL STRAIN, %
MONTZ U2-24-2
DEPTH = 71.0 FT

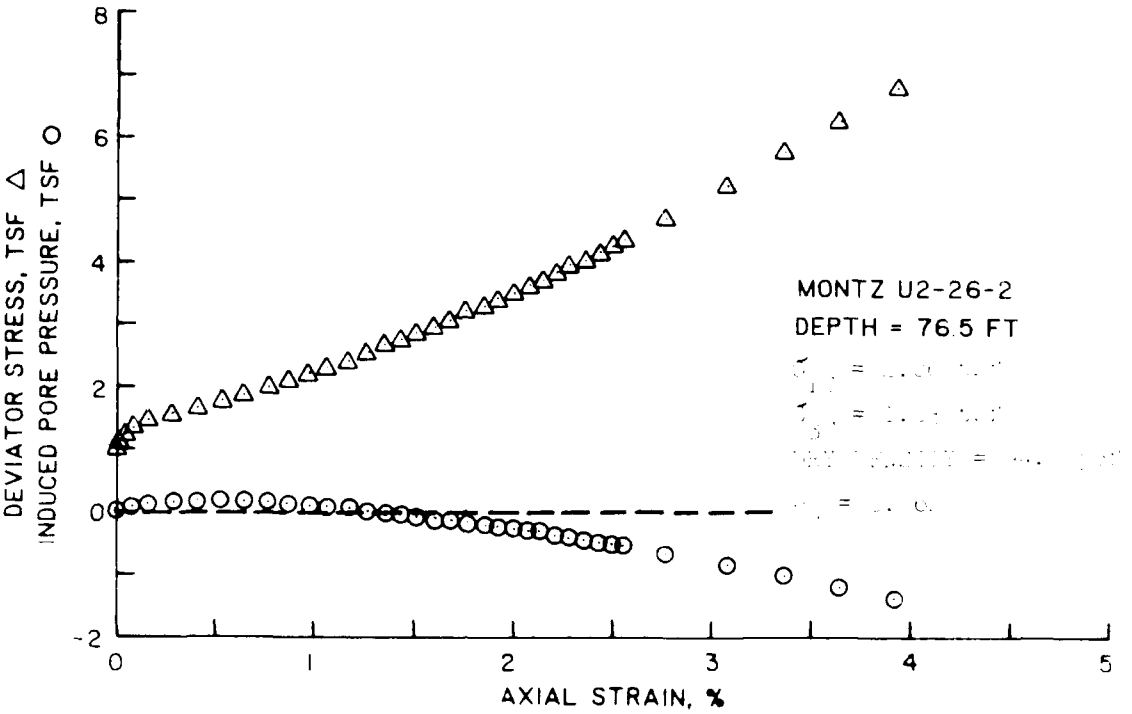

Q, TSF
P̄, TSF

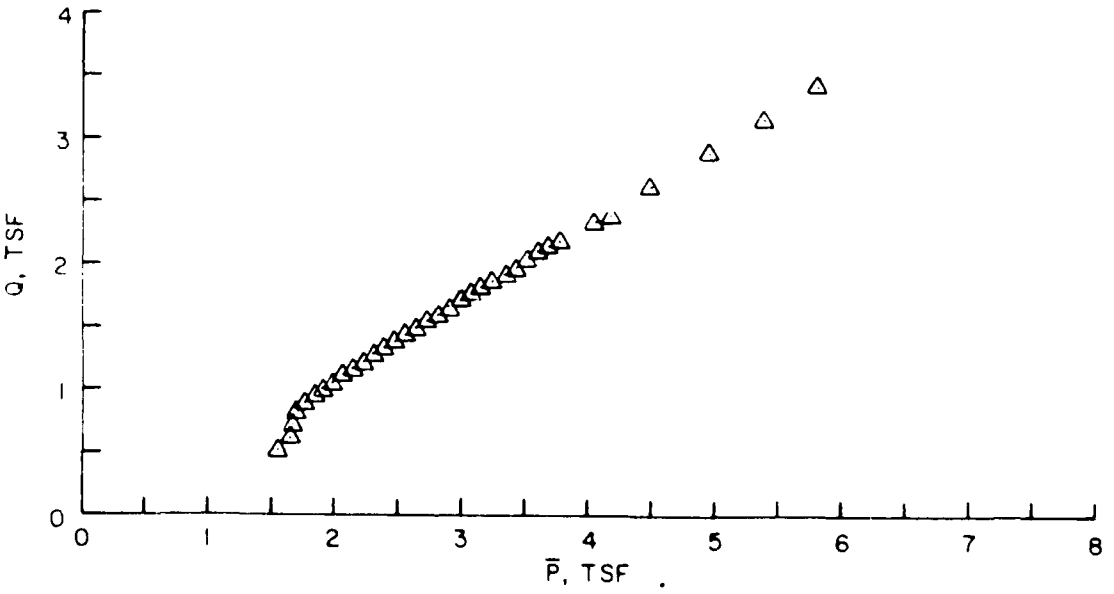

MONTZ U2-25-1
DEPTH = 73.6 FT
DEVIATOR STRESS, TSF Δ
INDUCED PORE PRESSURE, TSF O
AXIAL STRAIN, %

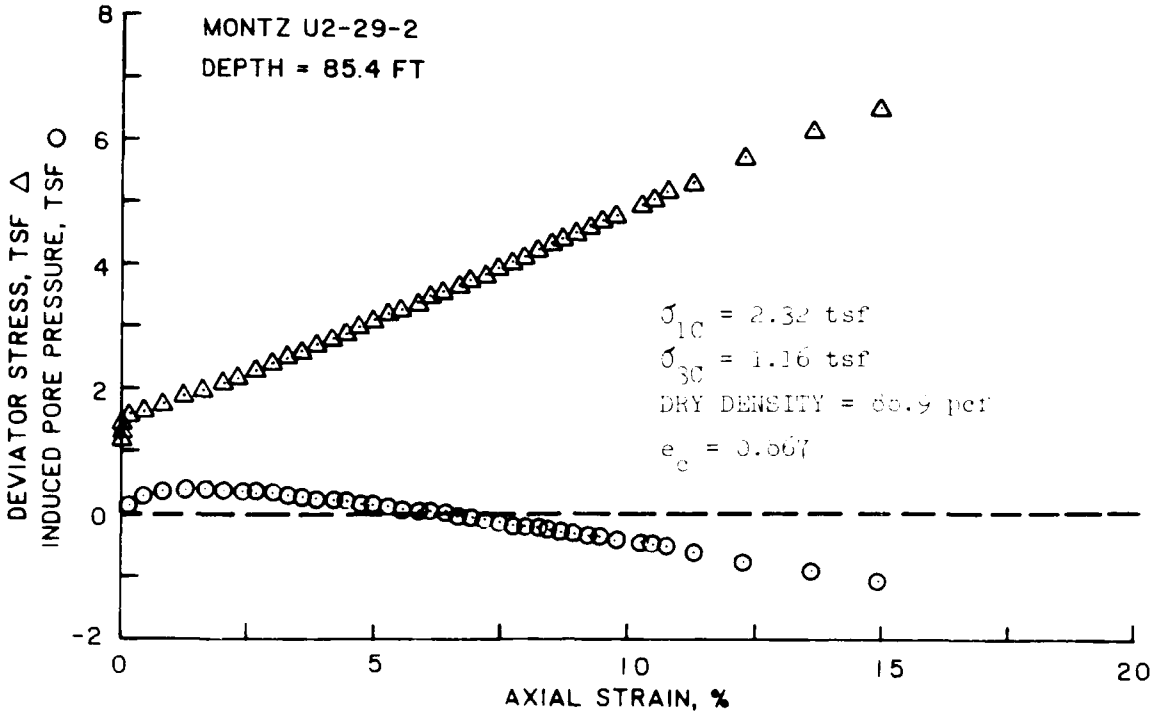

Q, TSF
P̄, TSF

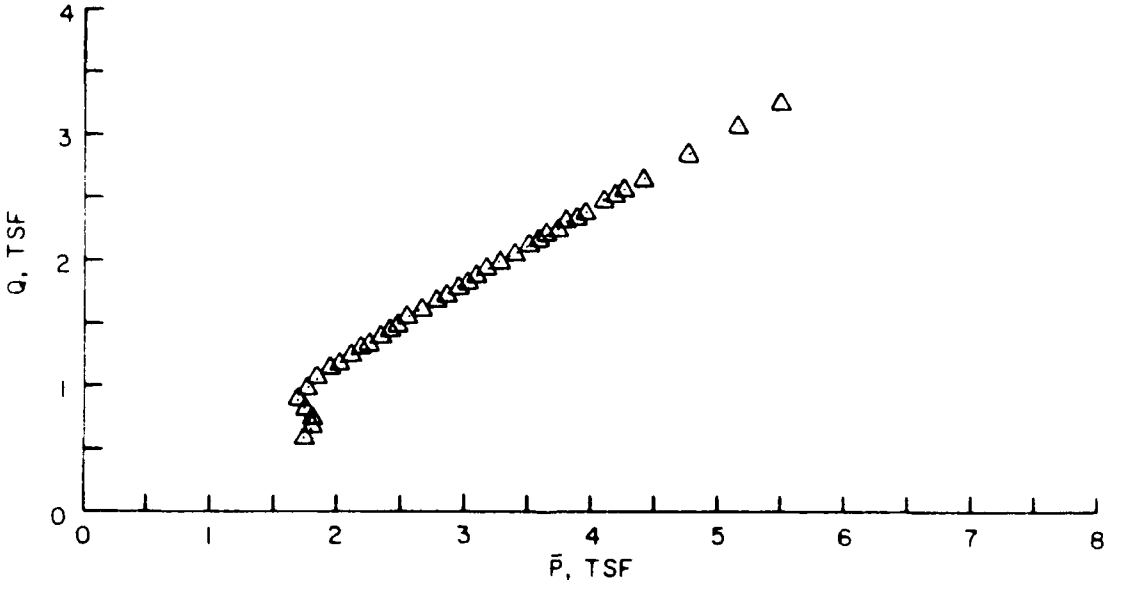

MONTZ U2-27-4
DEPTH = 79.7 FT
DEVIATOR STRESS, TSF Δ
INDUCED PORE PRESSURE, TSF O
8
6
4
2
0
-2
0
10
20
30
40
AXIAL STRAIN, %

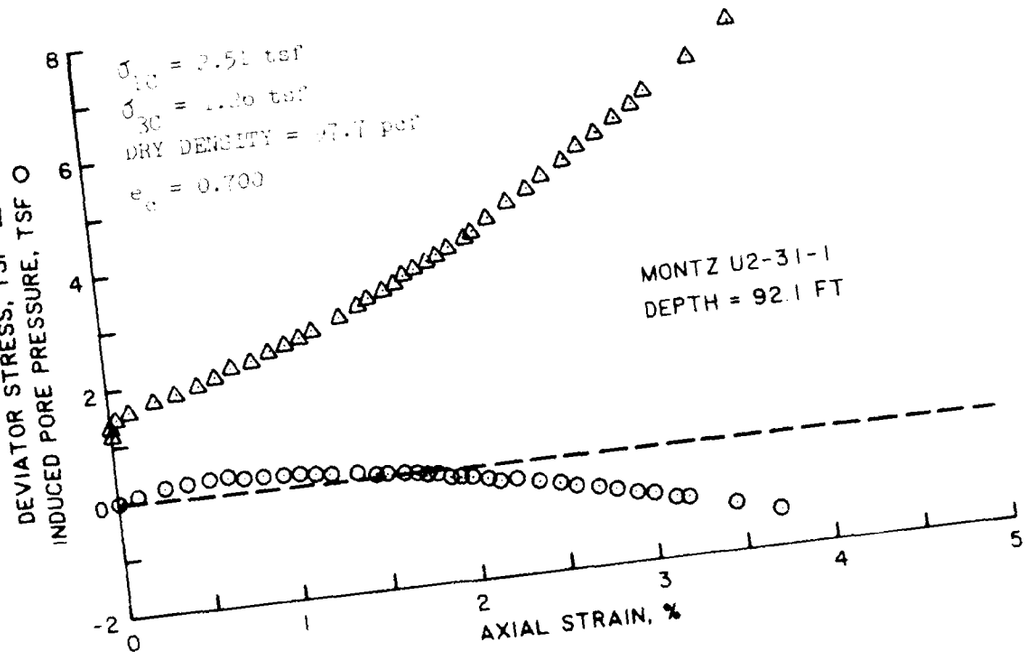

Q, TSF
4
3
2
1
0
0
1
2
3
4
5
6
7
8
P̄, TSF

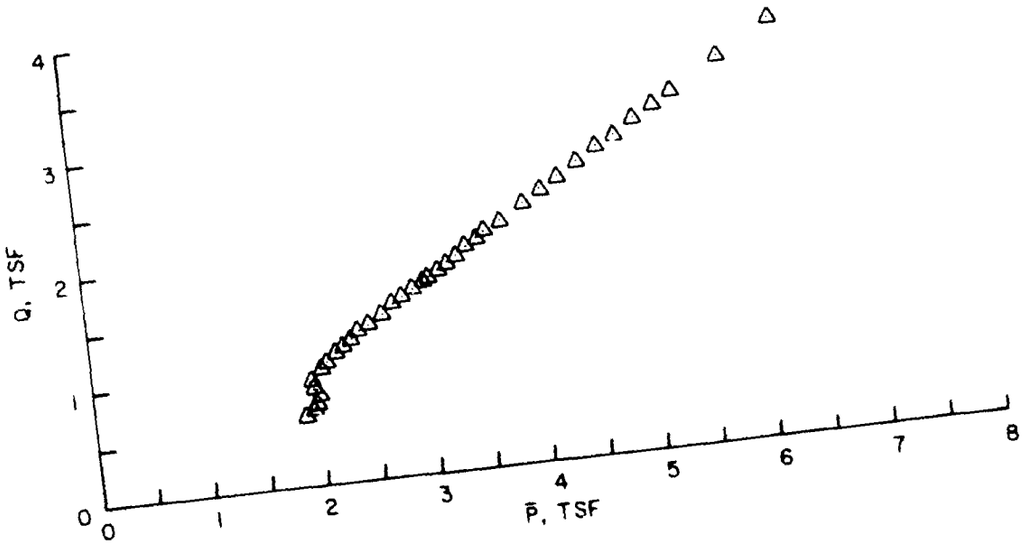

DEVIATOR STRESS, TSF △
INDUCED PORE PRESSURE, TSF ○
8
6
4
2
0
-2
0
1
2
3
4
5
AXIAL STRAIN, %
MONTZ U2-26-2
DEPTH = 76.5 FT

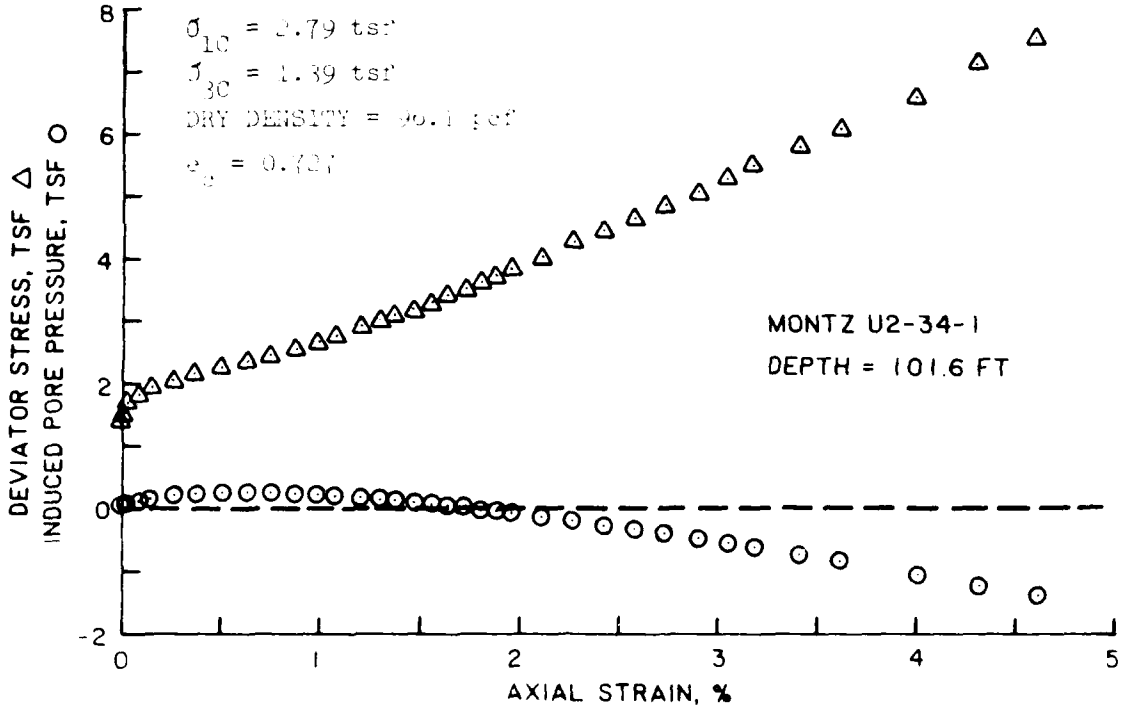

Q, TSF
4
3
2
1
0
0
1
2
3
4
5
6
7
8
P̄, TSF

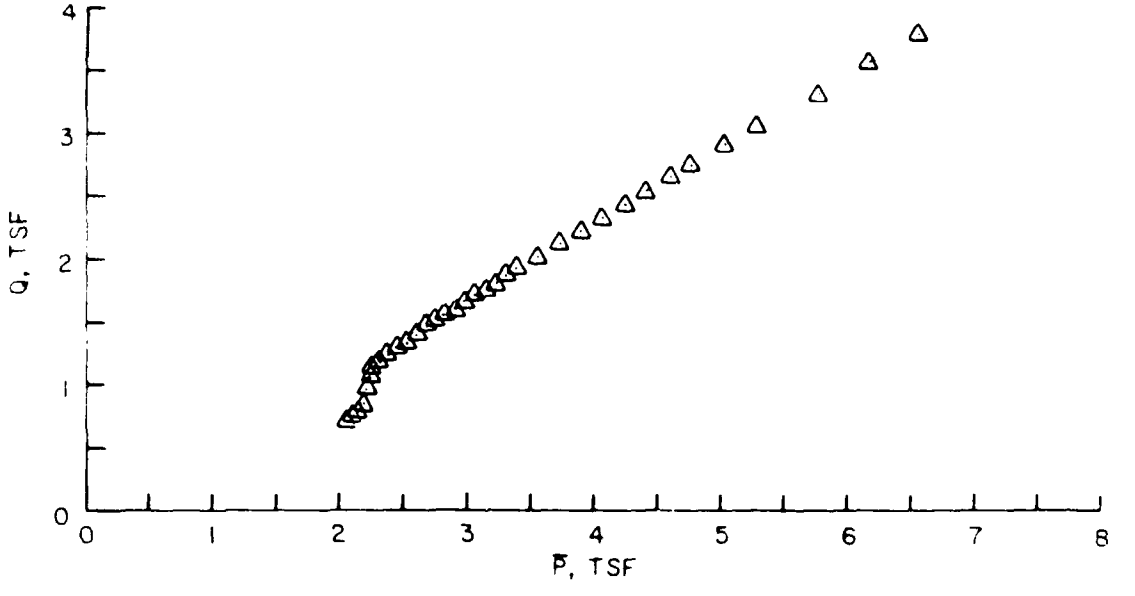

MONTZ U2-29-2
DEPTH = 85.4 FT
σ_{1C} = 2.32 tsf
σ_{3C} = 1.16 tsf
DRY DENSITY = 88.9 pcf
e_c = 0.867
DEVIATOR STRESS, TSF △
INDUCED PORE PRESSURE, TSF ○
AXIAL STRAIN, %
8
6
4
2
0
-2
0
5
10
15
20

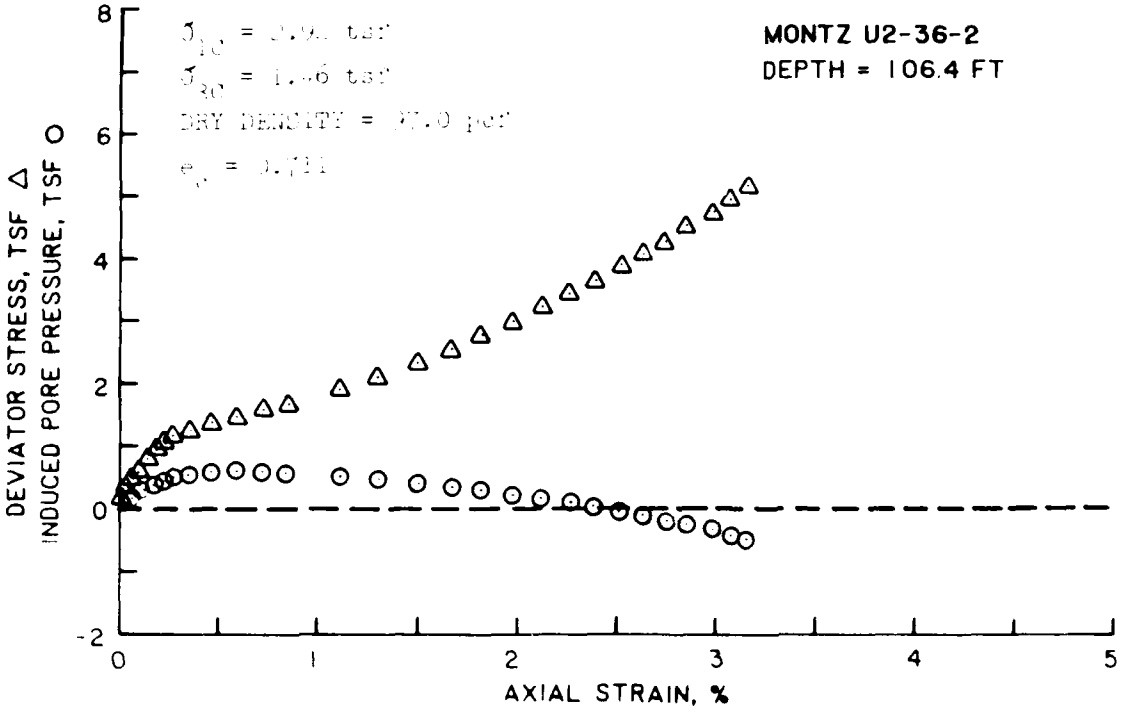

Q, TSF
$\bar{P}$, TSF
4
3
2
1
0
0
1
2
3
4
5
6
7
8

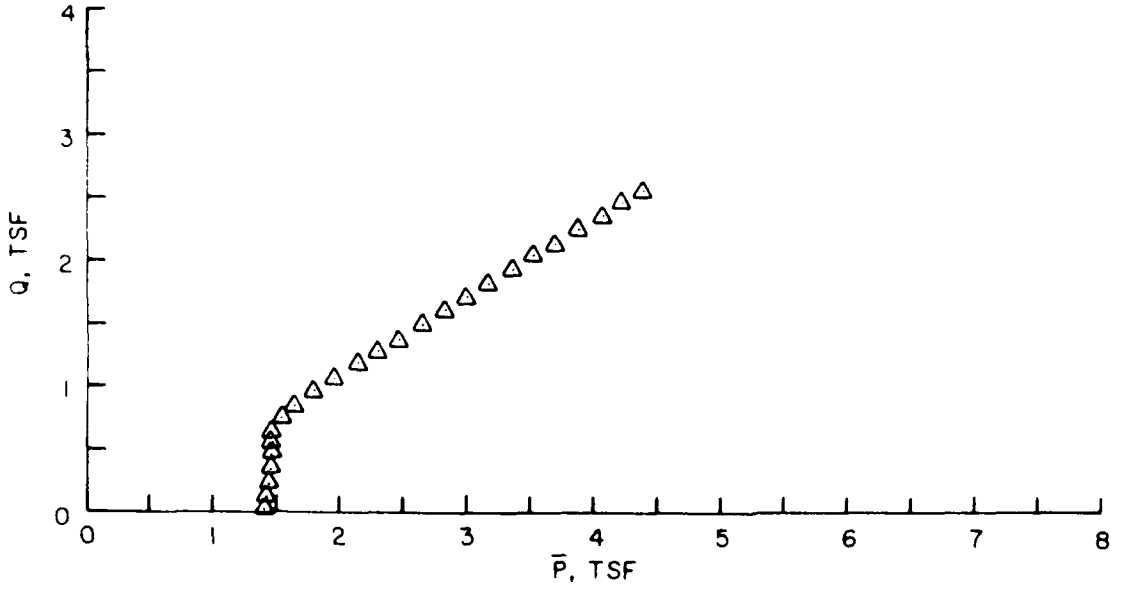

DEVIATOR STRESS, TSF △
INDUCED PORE PRESSURE, TSF O
DRY DENSITY = 97.7 pcf
MONTZ U2-31-1
DEPTH = 92.1 FT
AXIAL STRAIN, %

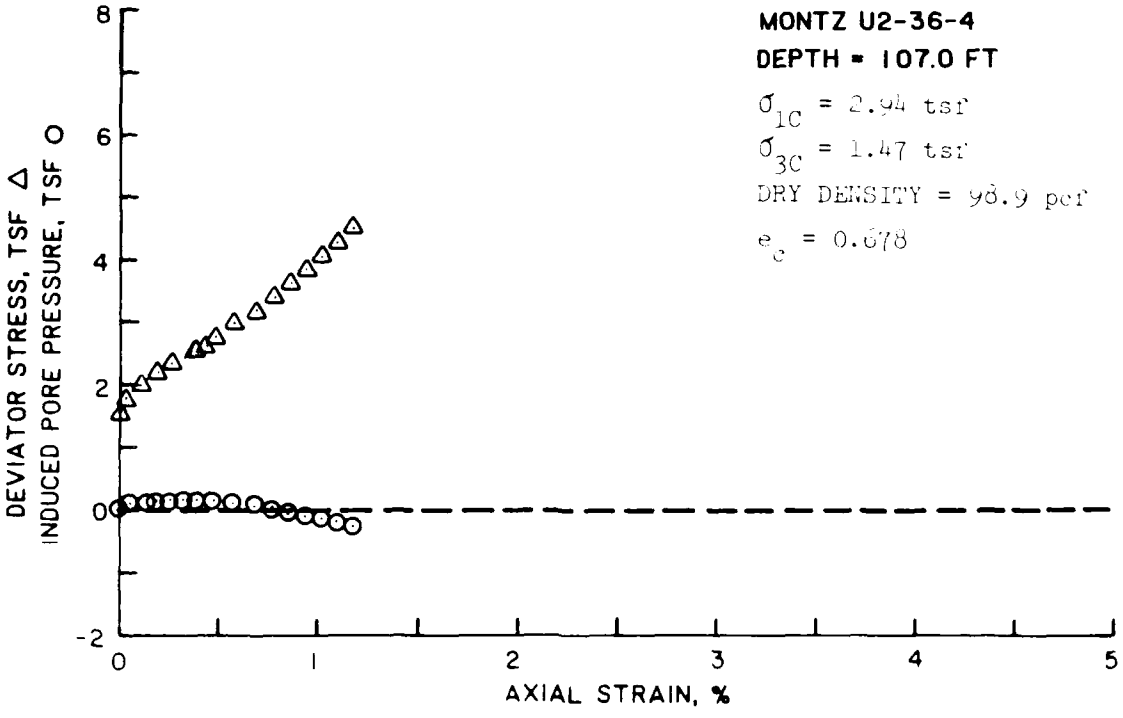

Q, TSF
P̄, TSF

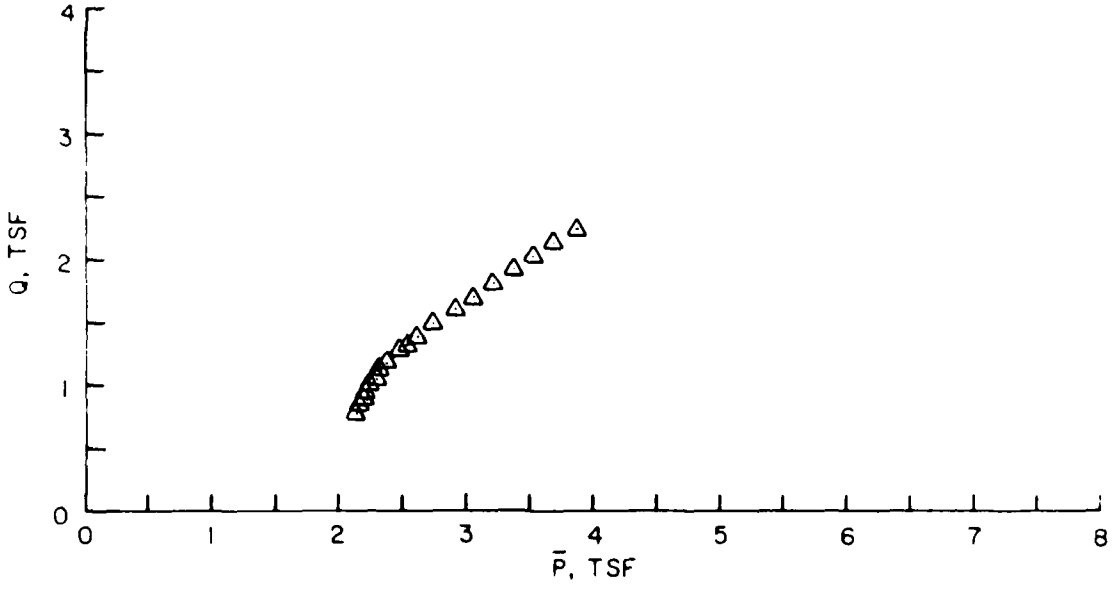

σ_{1C} = 3.79 tsf
σ_{3C} = 1.39 tsf
DRY DENSITY = 96.1 pcf
e_o = 0.721
MONTZ U2-34-1
DEPTH = 101.6 FT
DEVIATOR STRESS, TSF Δ
INDUCED PORE PRESSURE, TSF O
AXIAL STRAIN, %

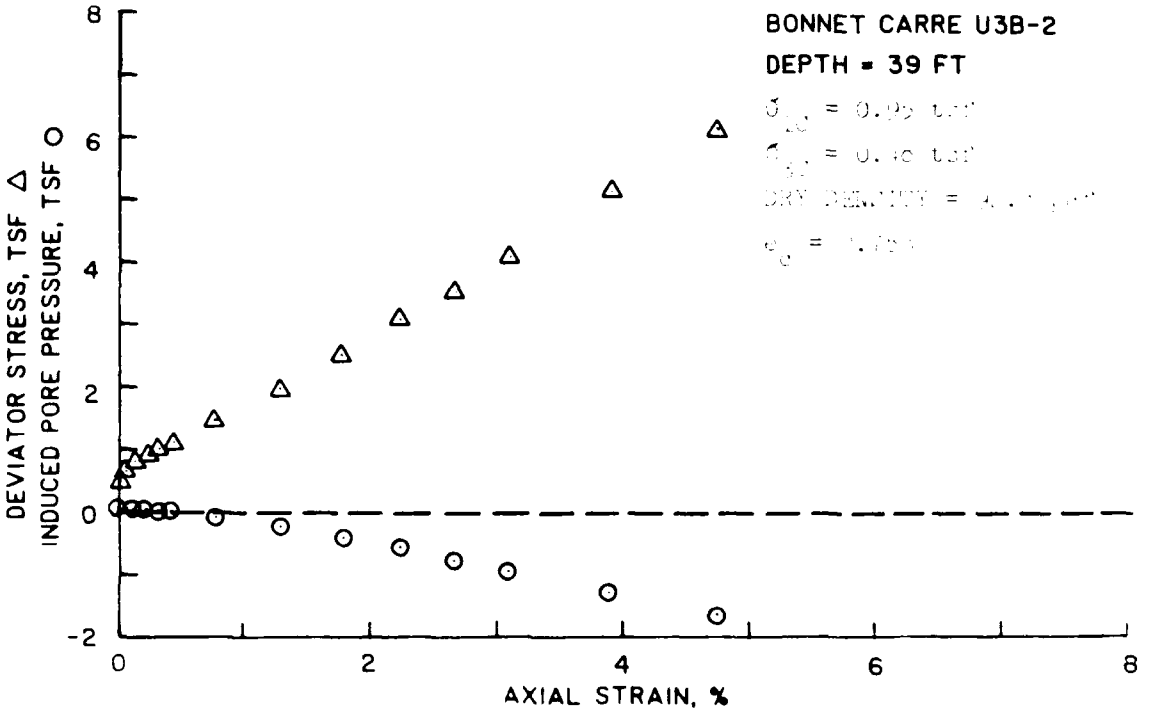

Q, TSF
P̄, TSF

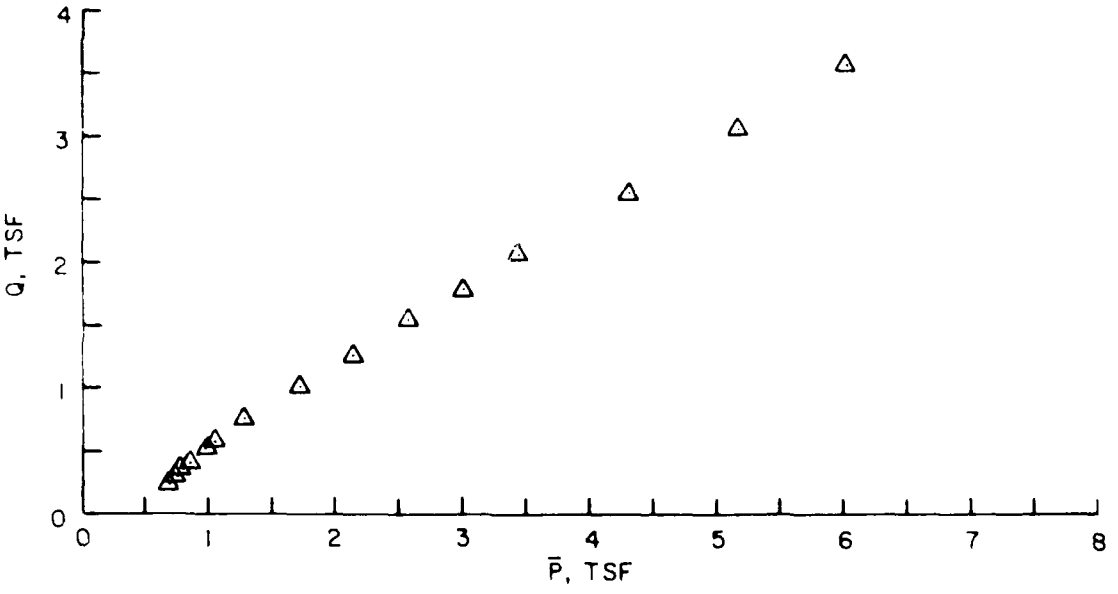

MONTZ U2-36-2
DEPTH = 106.4 FT
DRY DENSITY = 97.0 pcf
DEVIATOR STRESS, TSF Δ
INDUCED PORE PRESSURE, TSF O
AXIAL STRAIN, %

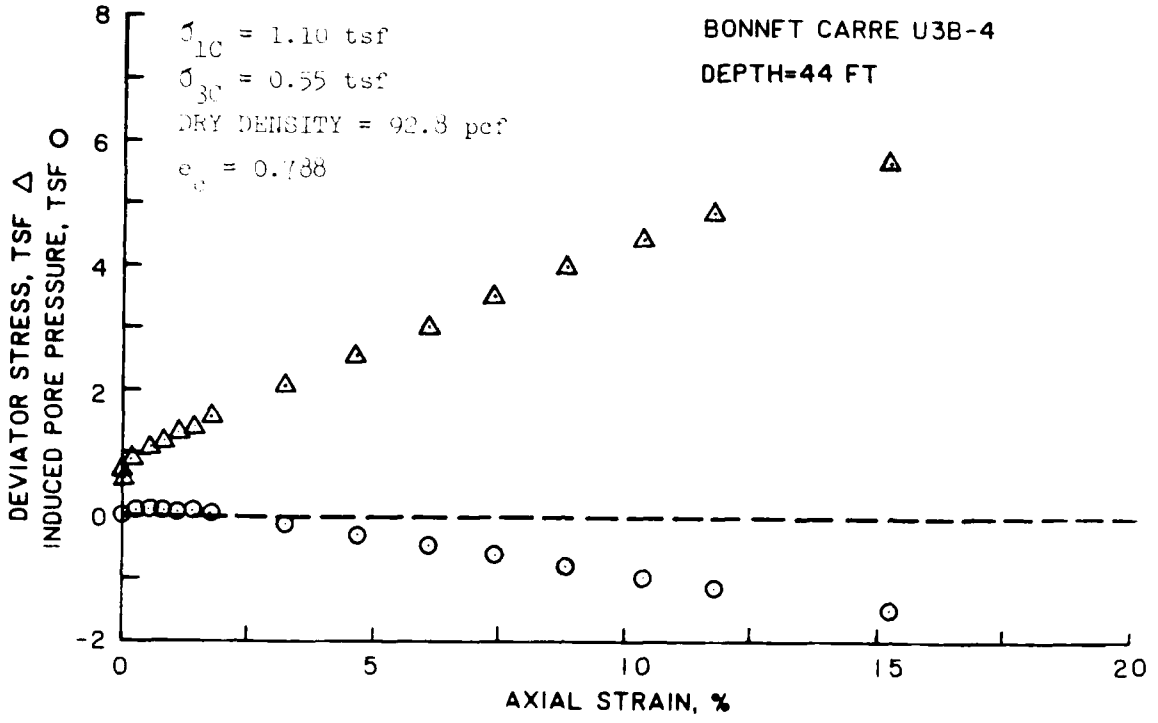

Q, TSF
P̄, TSF

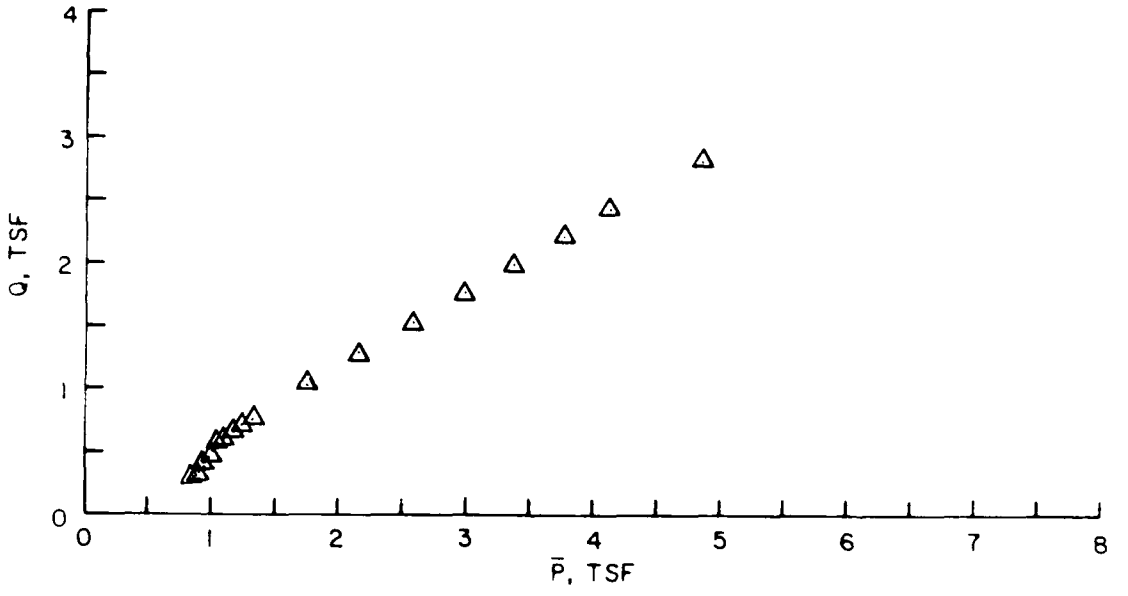

MONTZ U2-36-4
DEPTH = 107.0 FT
σ_{1C} = 2.94 tsf
σ_{3C} = 1.47 tsf
DRY DENSITY = 98.9 pcf
e_c = 0.678
DEVIATOR STRESS, TSF Δ
INDUCED PORE PRESSURE, TSF O
AXIAL STRAIN, %

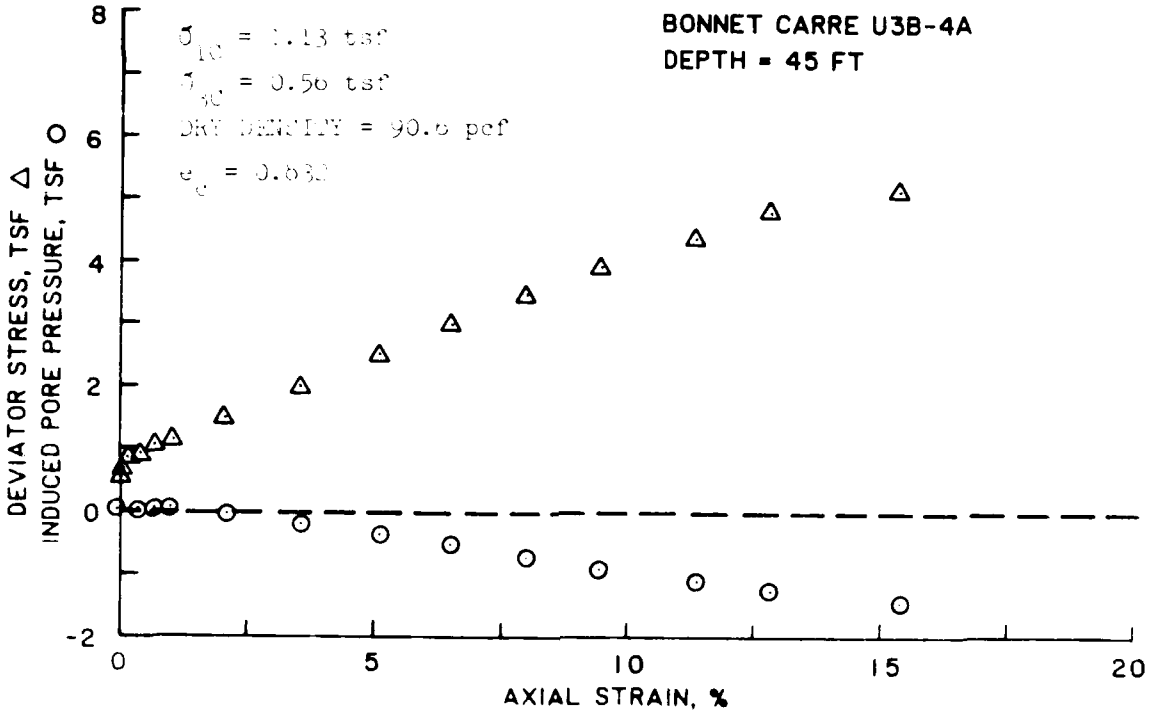

Q, TSF
$\bar{P}$, TSF

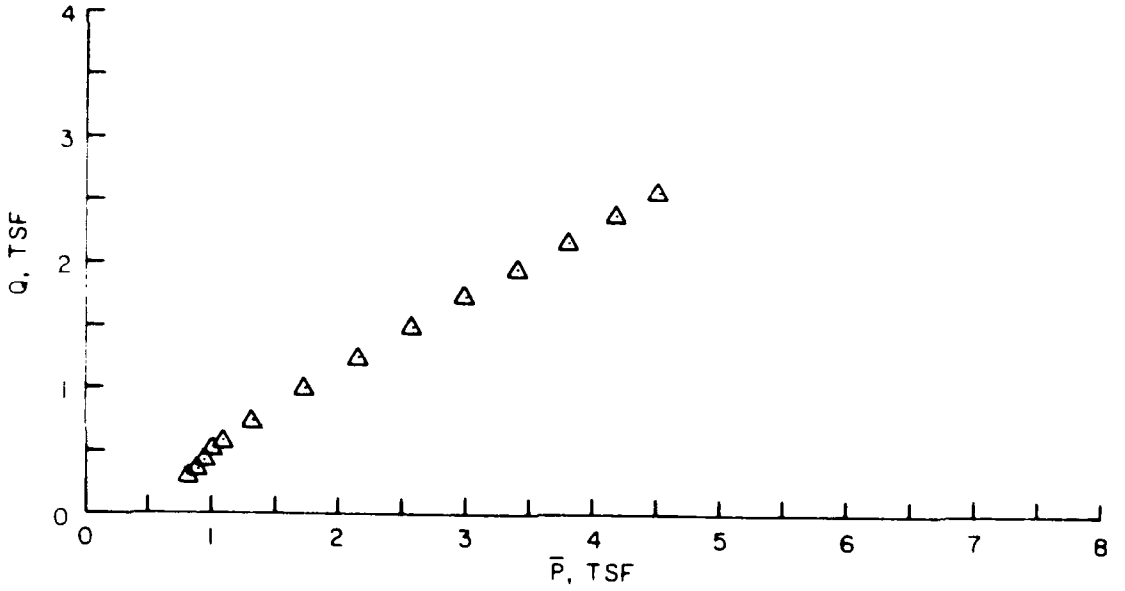

BONNET CARRE U3B-2
DEPTH = 39 FT
DEVIATOR STRESS, TSF Δ
INDUCED PORE PRESSURE, TSF O
AXIAL STRAIN, %

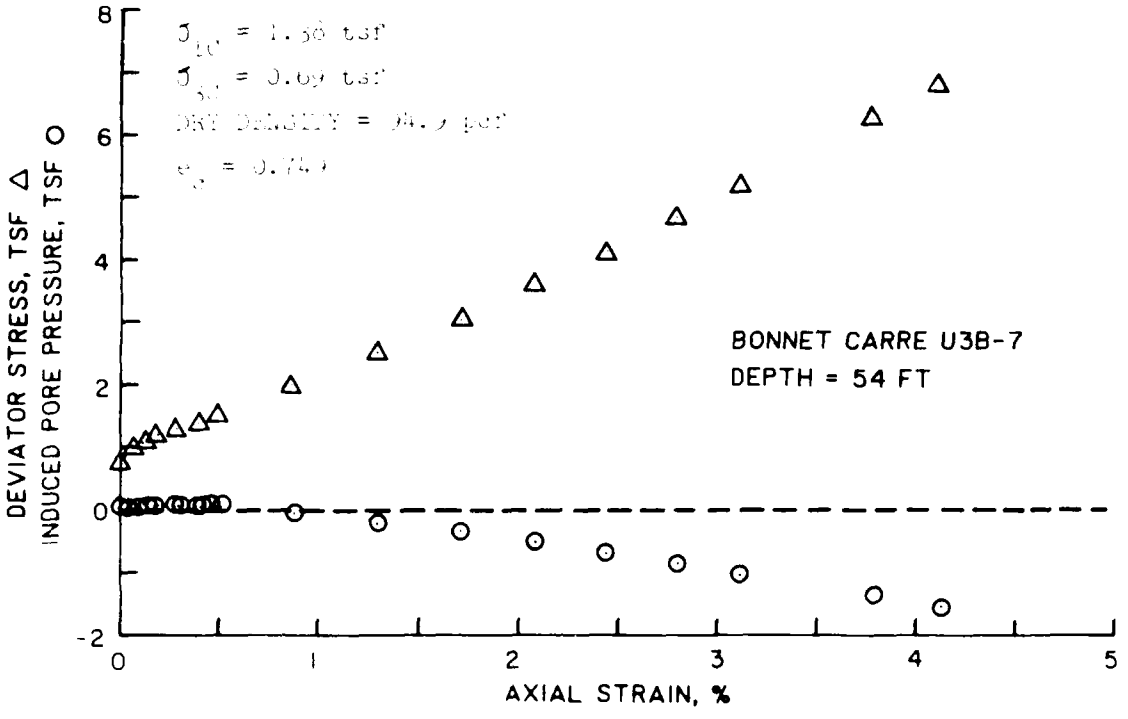

Q, TSF
P̄, TSF

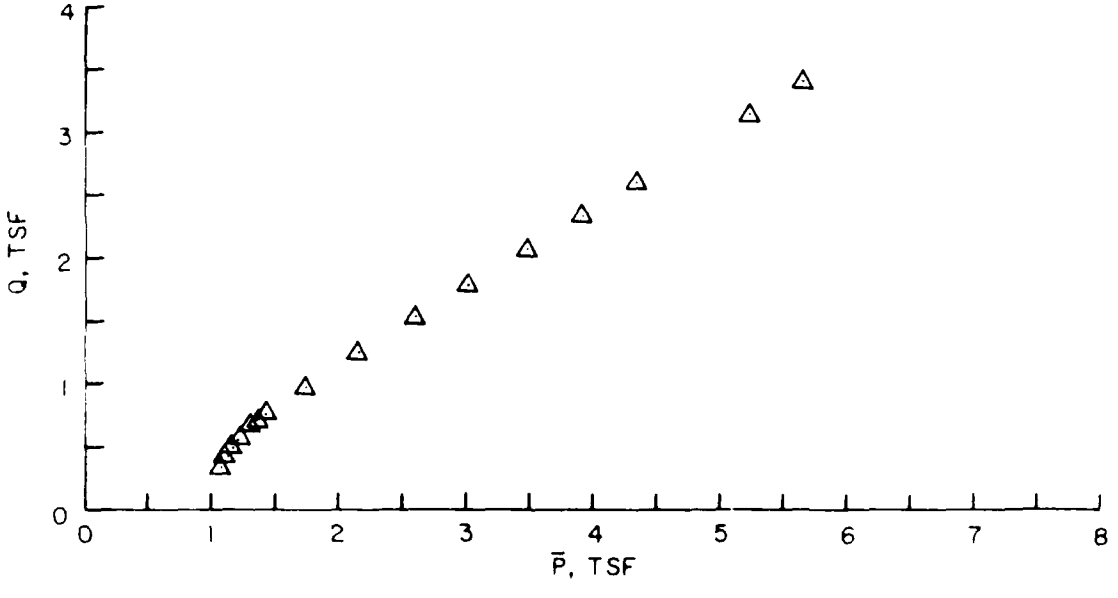

σ_{1C} = 1.10 tsf
σ_{3C} = 0.55 tsf
DRY DENSITY = 92.8 pcf
e_c = 0.788
BONNET CARRE U3B-4
DEPTH=44 FT
DEVIATOR STRESS, TSF Δ
INDUCED PORE PRESSURE, TSF O
AXIAL STRAIN, %

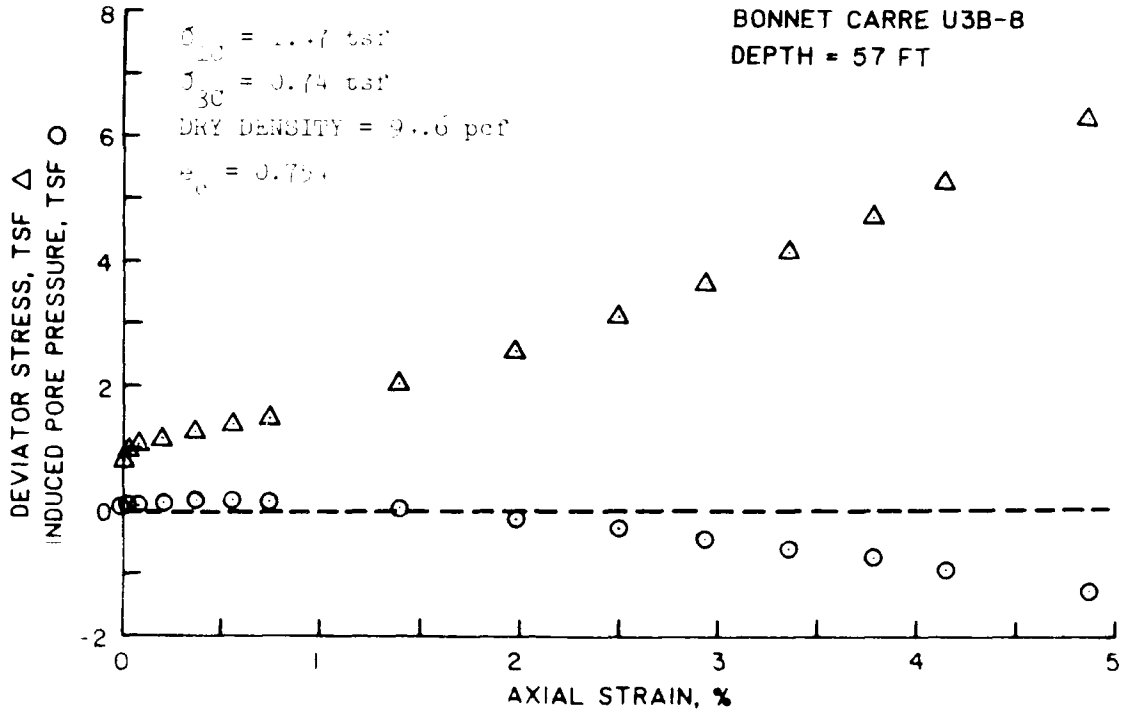

Q, TSF
$\bar{P}$, TSF

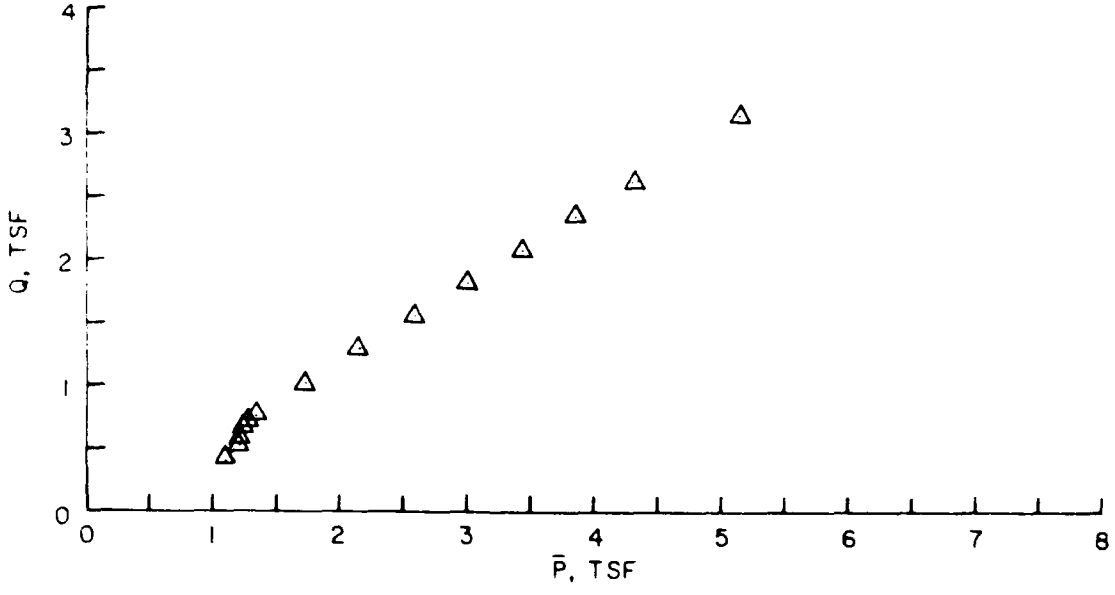

BONNET CARRE U3B-4A
DEPTH = 45 FT
σ_{3c} = 1.13 tsf
σ_{3c} = 0.56 tsf
DRY DENSITY = 90.6 pcf
e_c = 0.632
DEVIATOR STRESS, TSF Δ
INDUCED PORE PRESSURE, TSF O
AXIAL STRAIN, %

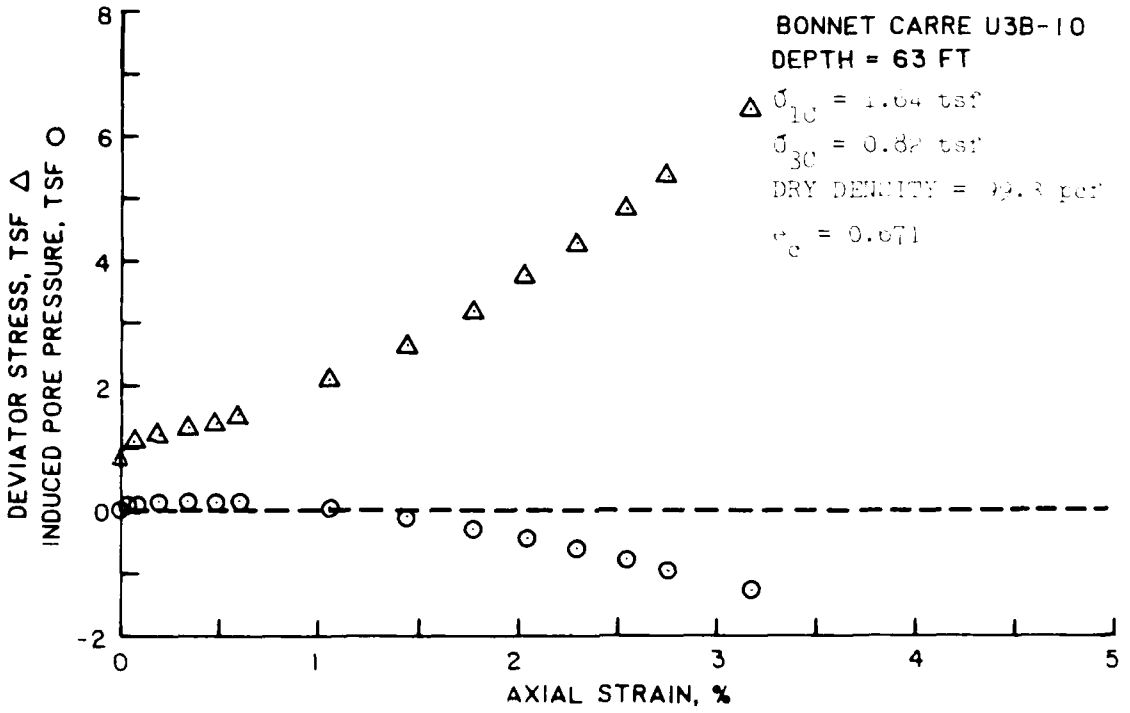

Q, TSF
$\bar{P}$, TSF

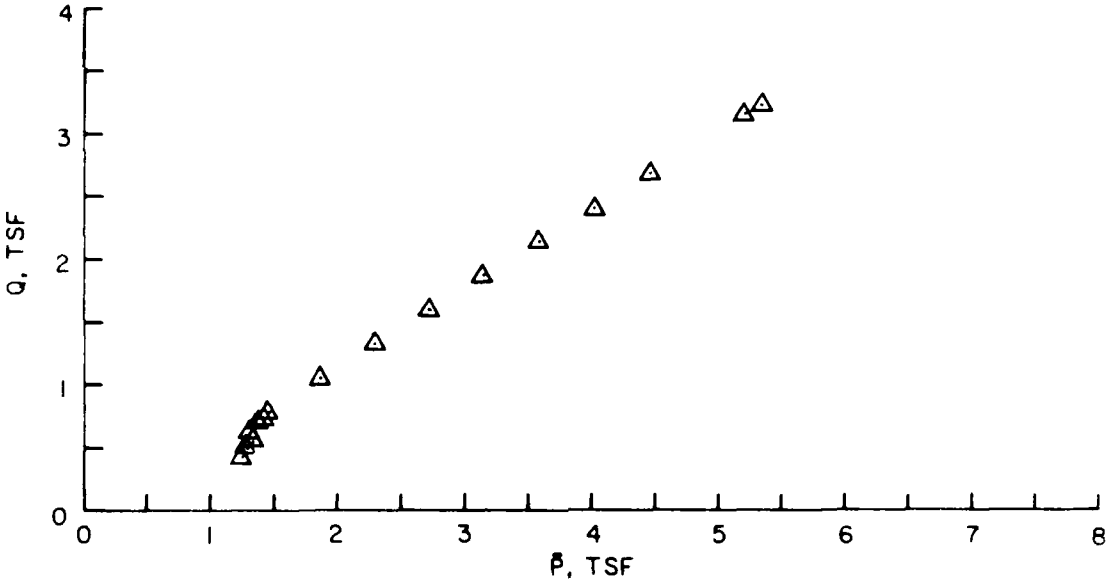

DEVIATOR STRESS, TSF △
INDUCED PORE PRESSURE, TSF O
AXIAL STRAIN, %
BONNET CARRE U3B-7
DEPTH = 54 FT

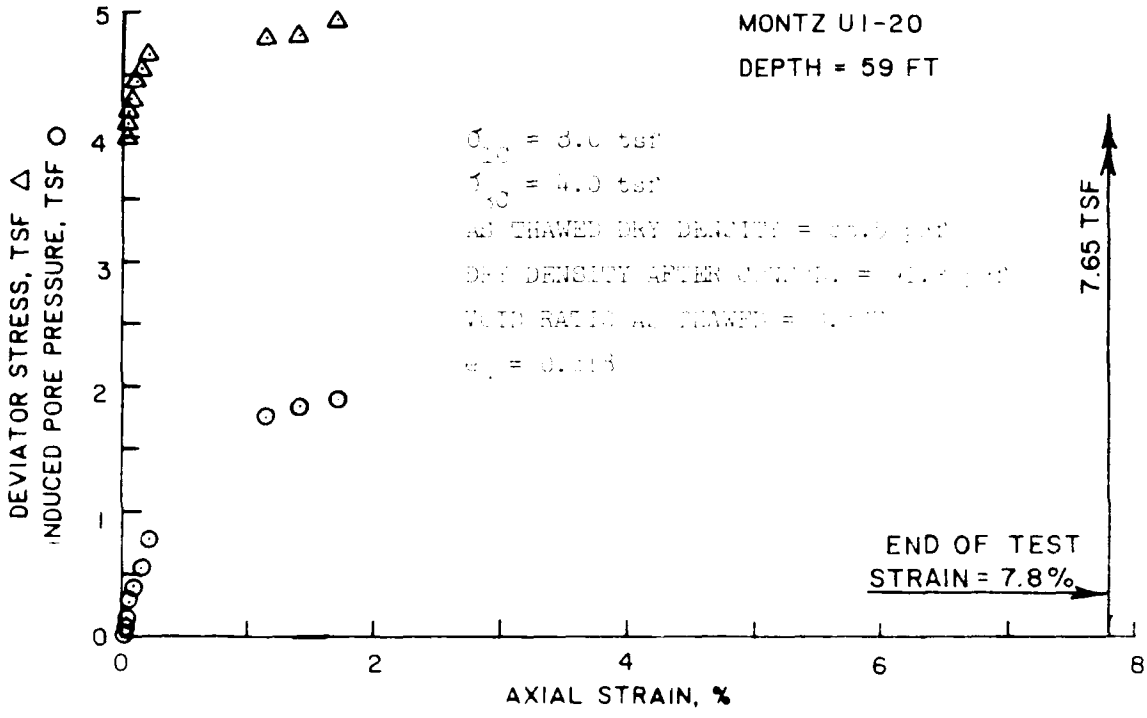

Q, TSF
P̄, TSF

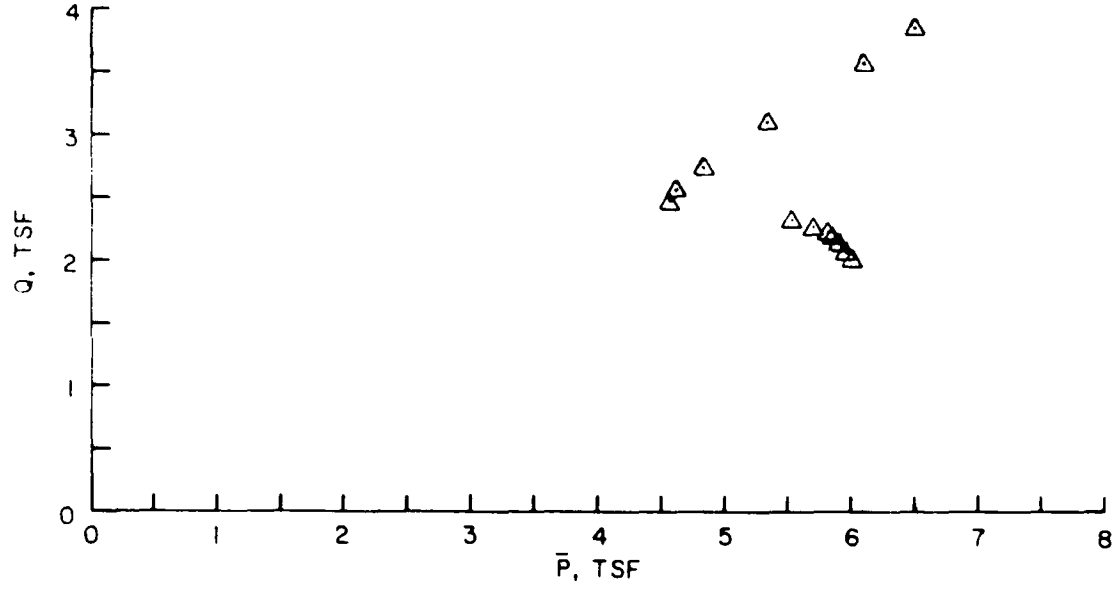

BONNET CARRE U3B-8
DEPTH = 57 FT
σ_{3C} = 0.74 tsf
DRY DENSITY = 9..6 pcf
DEVIATOR STRESS, TSF Δ
INDUCED PORE PRESSURE, TSF O
AXIAL STRAIN, %

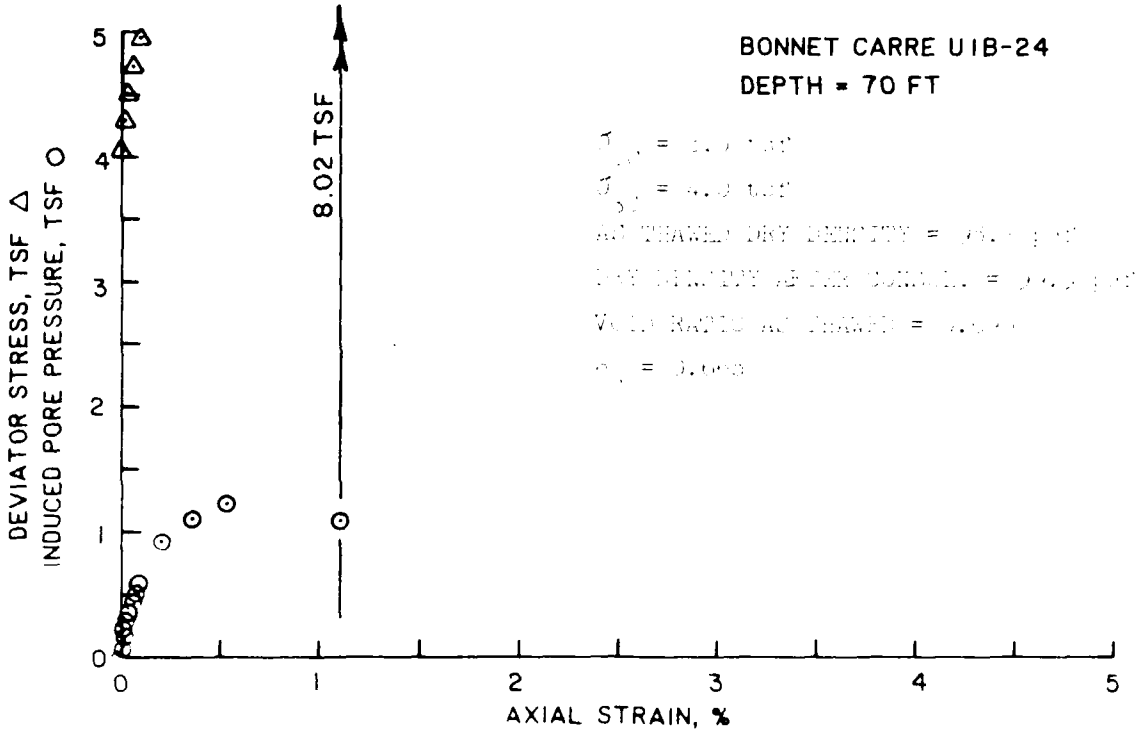

Q, TSF
$\bar{P}$, TSF

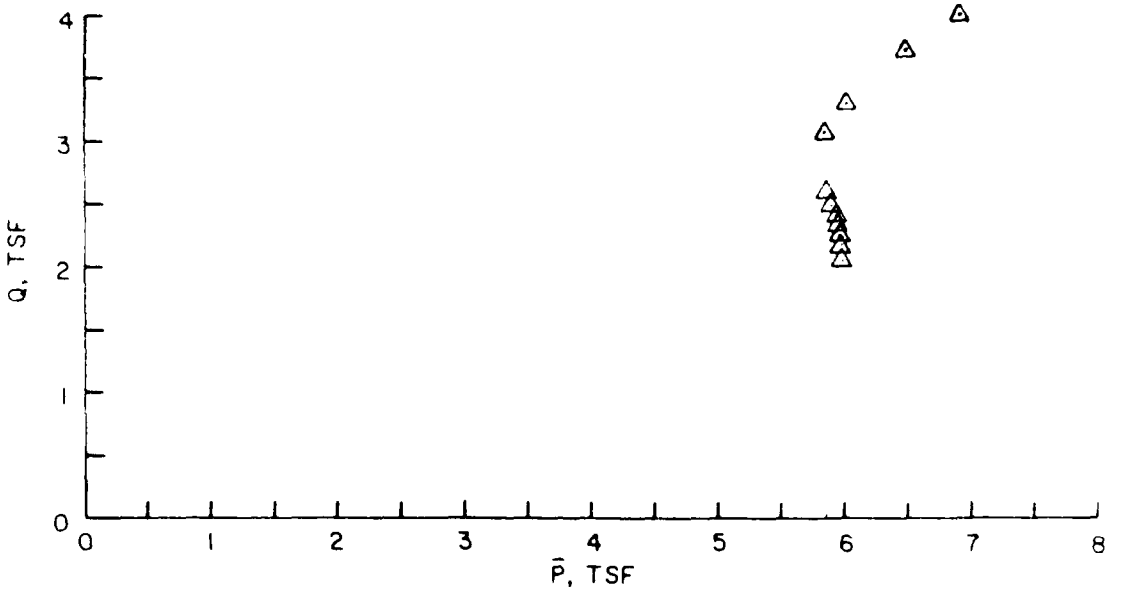

BONNET CARRE U3B-10
DEPTH = 63 FT
σ_{1c} = 1.64 tsf
σ_{3c} = 0.82 tsf
DRY DENSITY = 99.3 pcf
e_c = 0.671
DEVIATOR STRESS, TSF Δ
INDUCED PORE PRESSURE, TSF O
AXIAL STRAIN, %

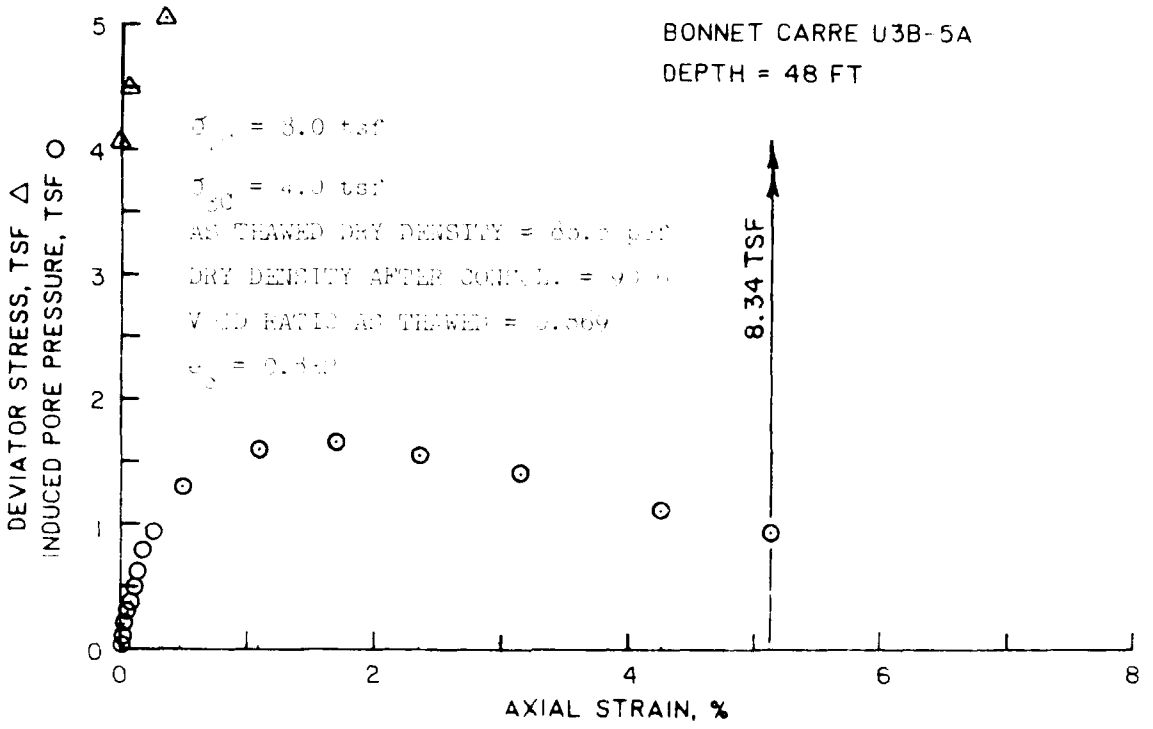

Q, TSF
p, TSF

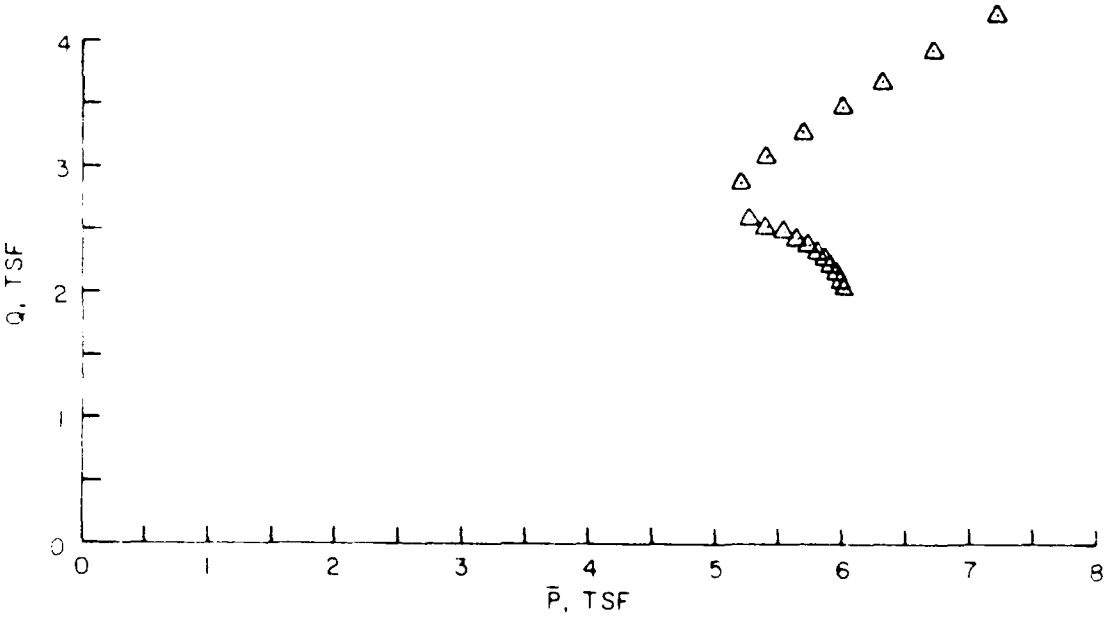

MONTZ U1-20
DEPTH = 59 FT
7.65 TSF
END OF TEST
STRAIN = 7.8%
DEVIATOR STRESS, TSF Δ
INDUCED PORE PRESSURE, TSF O
AXIAL STRAIN, %

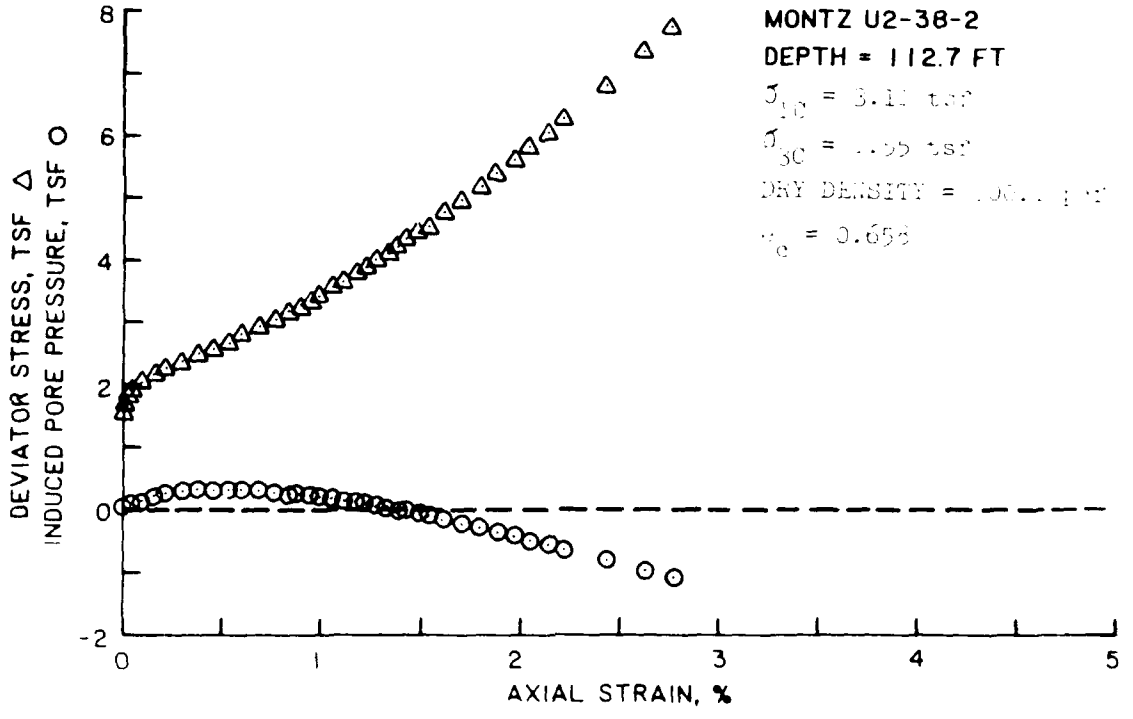

Q, TSF
P̄, TSF

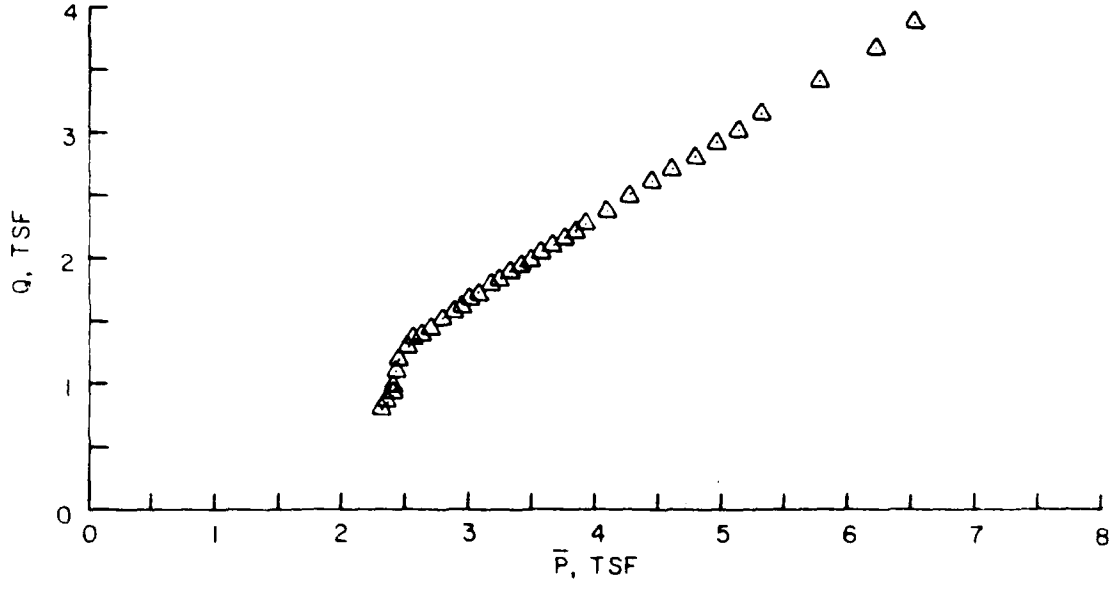

BONNET CARRE U1B-24
DEPTH = 70 FT
8.02 TSF
DEVIATOR STRESS, TSF Δ
INDUCED PORE PRESSURE, TSF O
AXIAL STRAIN, %
0
1
2
3
4
5

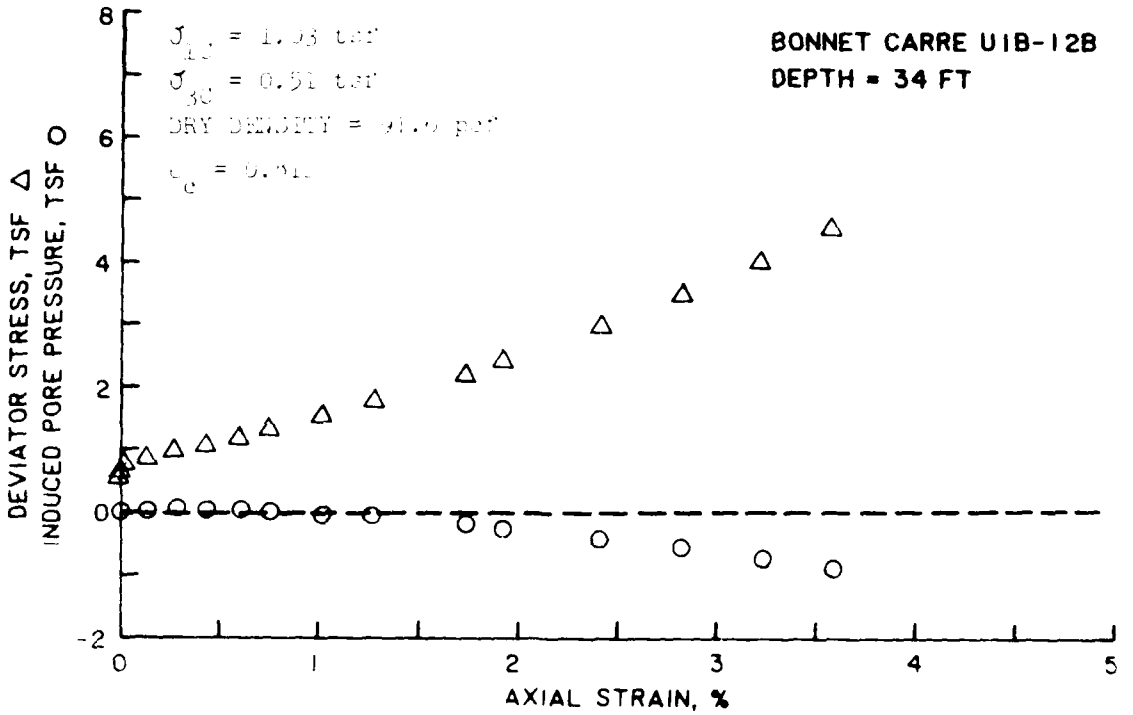

Q, TSF
P̄, TSF
0
1
2
3
4
5
6
7
8

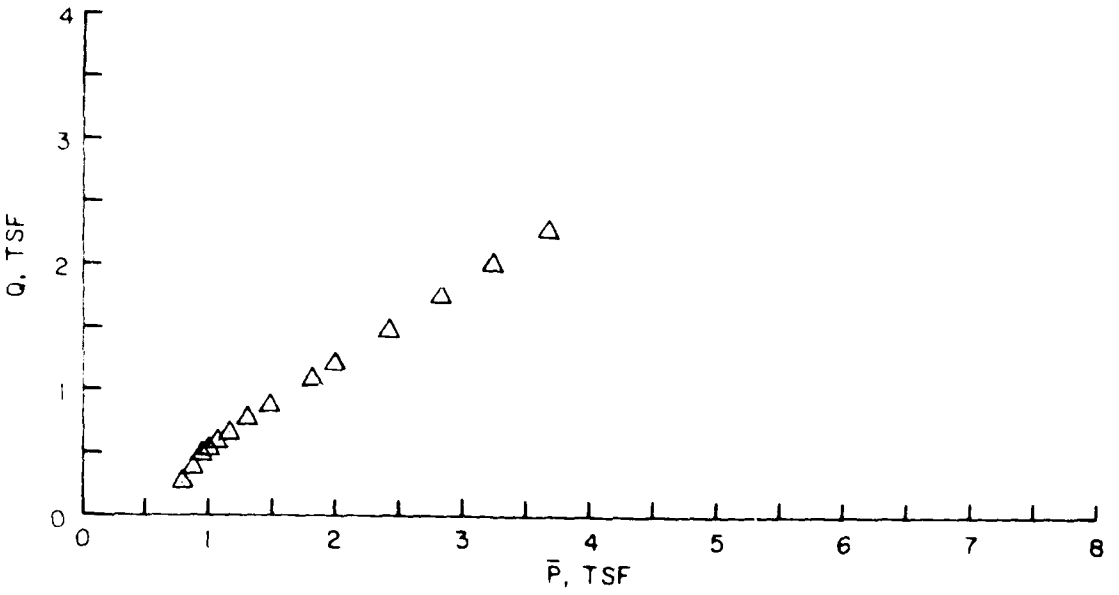

BONNET CARRE U3B-5A
DEPTH = 48 FT
8.34 TSF
DEVIATOR STRESS, TSF Δ
INDUCED PORE PRESSURE, TSF O
AXIAL STRAIN, %

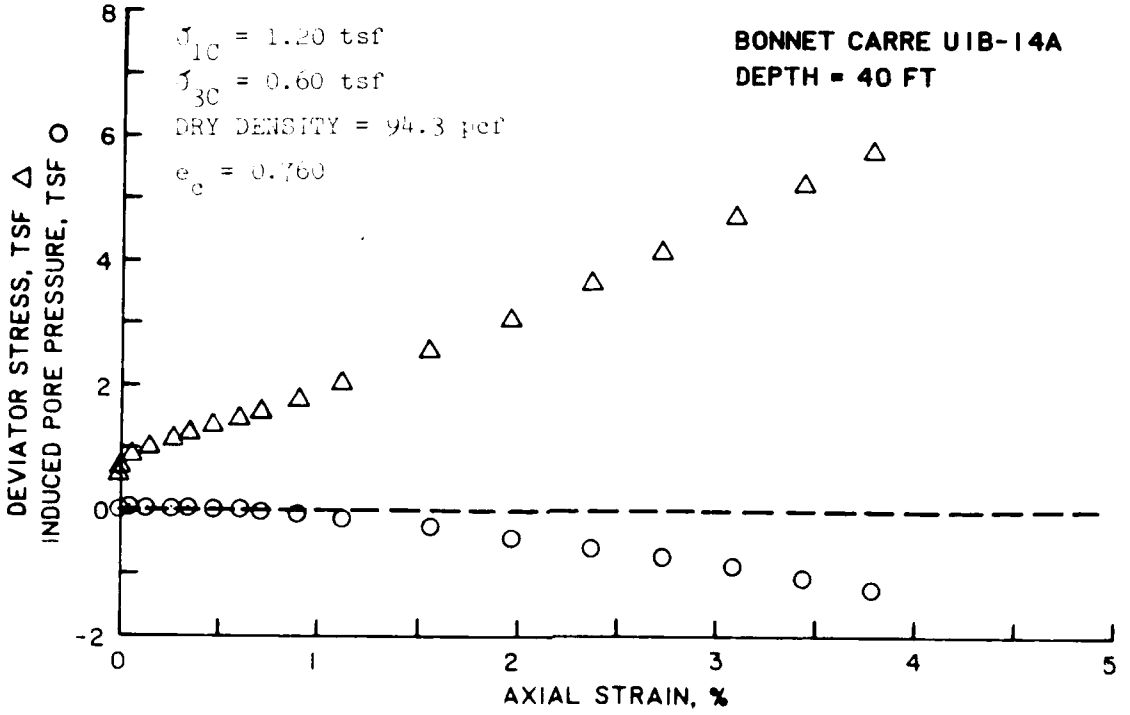

Q, TSF
P̄, TSF

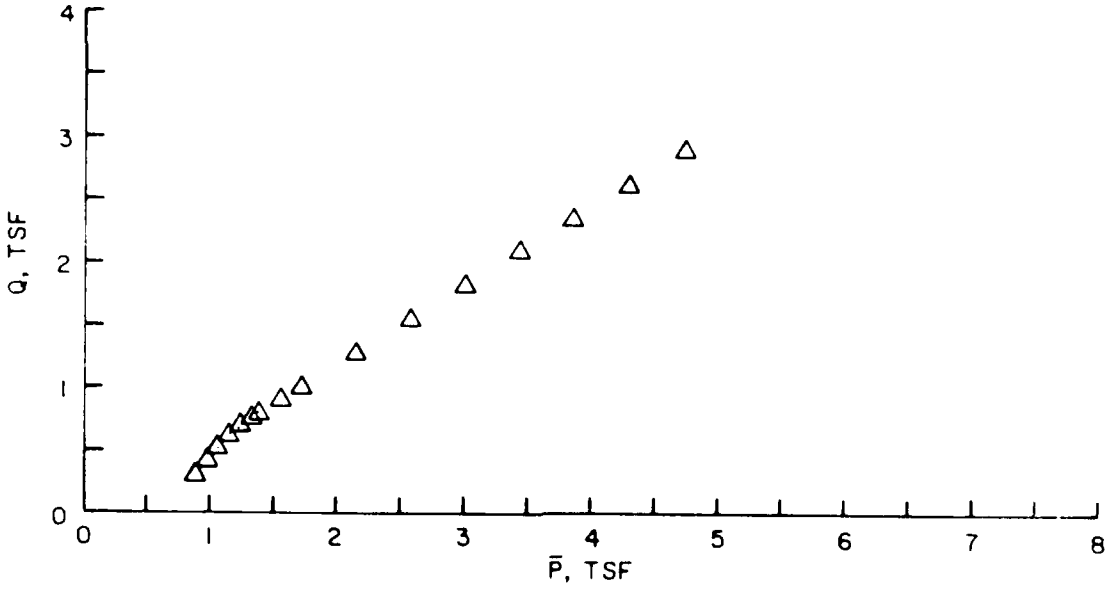

MONTZ U2-38-2
DEPTH = 112.7 FT
σ_{3c} = 3.11 tsf
σ_{3c} = [illegible] tsf
DRY DENSITY = [illegible] pcf
ϵ_c = 0.658
DEVIATOR STRESS, TSF Δ
INDUCED PORE PRESSURE, TSF O
AXIAL STRAIN, %

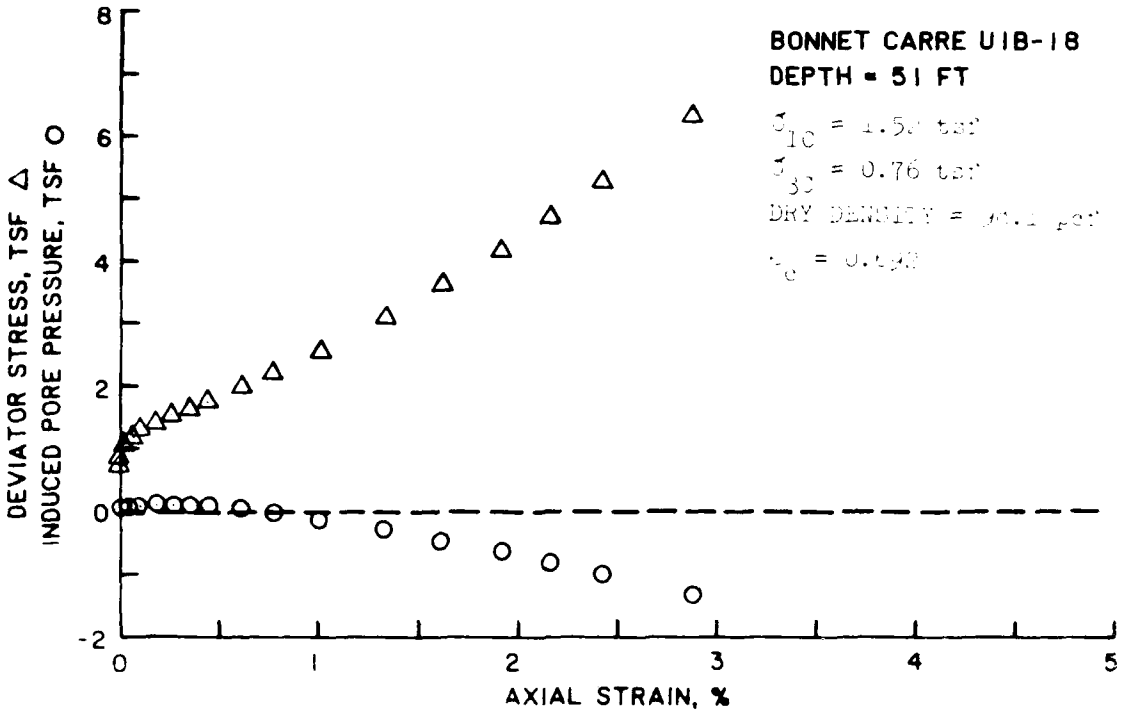

Q, TSF
$\bar{P}$, TSF

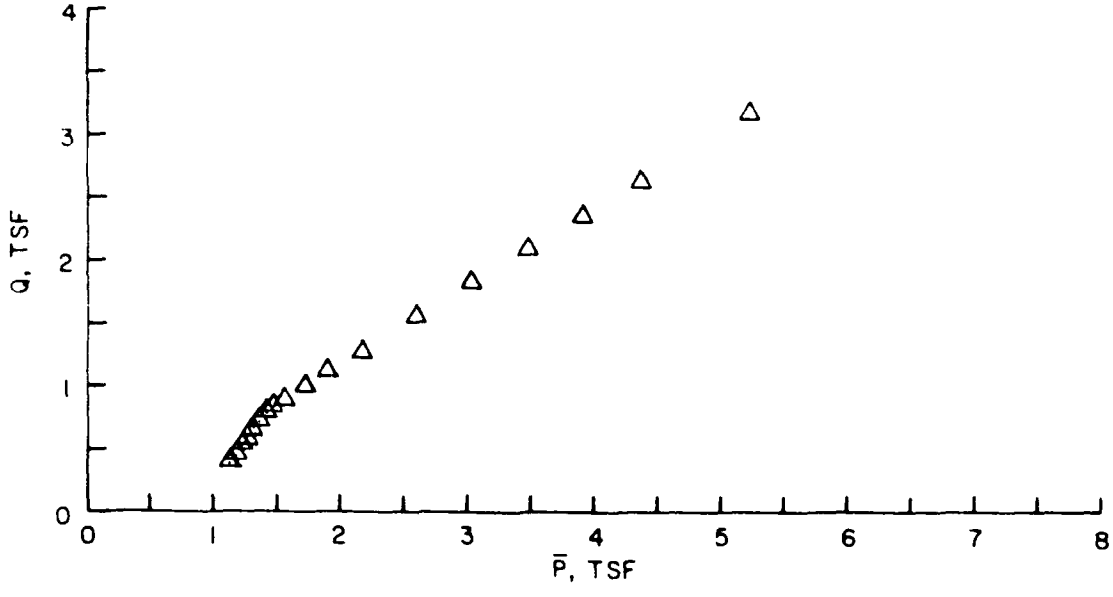

BONNET CARRE U1B-12B
DEPTH = 34 FT
DEVIATOR STRESS, TSF Δ
INDUCED PORE PRESSURE, TSF O
AXIAL STRAIN, %

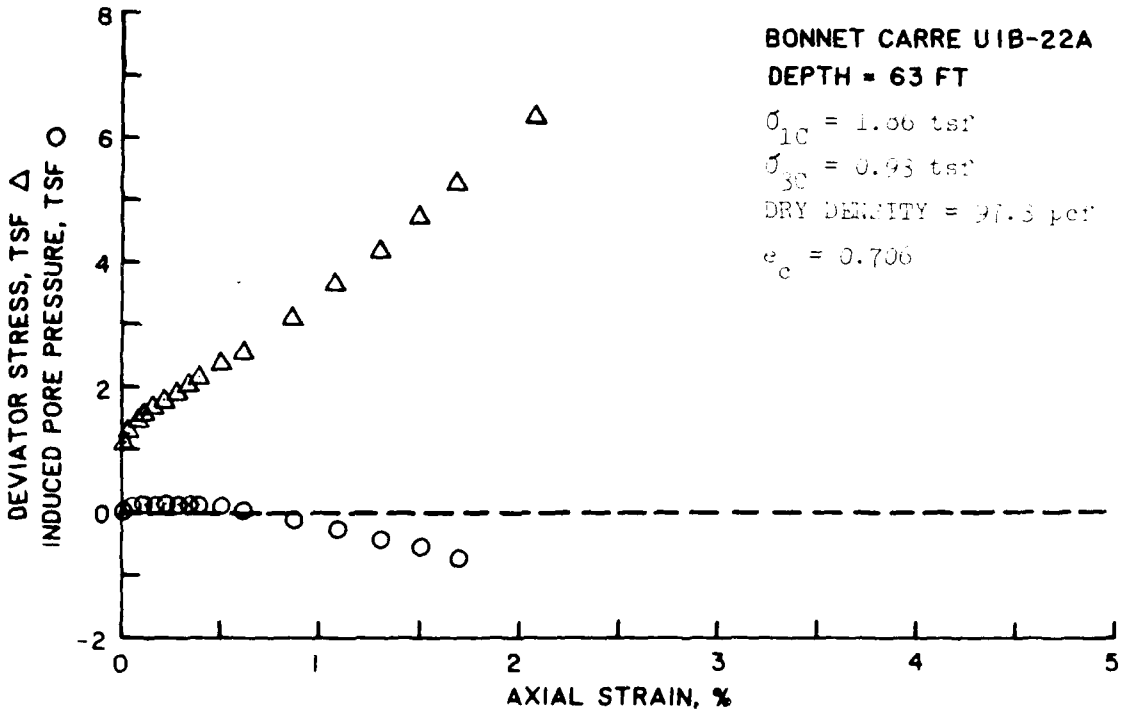

Q, TSF
P̄, TSF

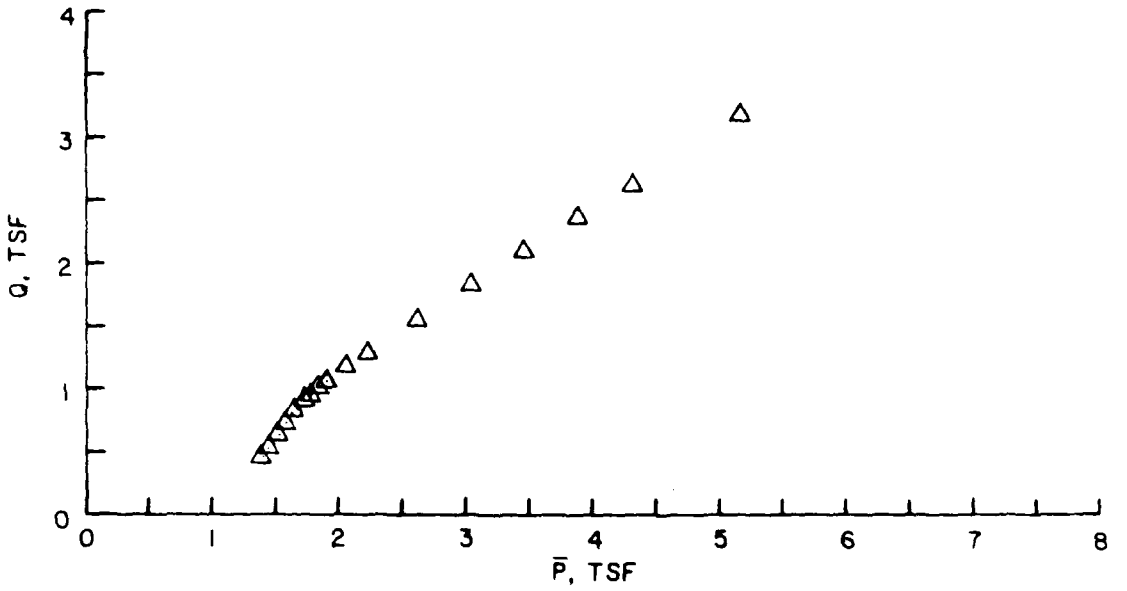

σ_{1C} = 1.20 tsf
σ_{3C} = 0.60 tsf
DRY DENSITY = 94.3 pcf
e_c = 0.760
BONNET CARRE U1B-14A
DEPTH = 40 FT
DEVIATOR STRESS, TSF Δ
INDUCED PORE PRESSURE, TSF O
AXIAL STRAIN, %

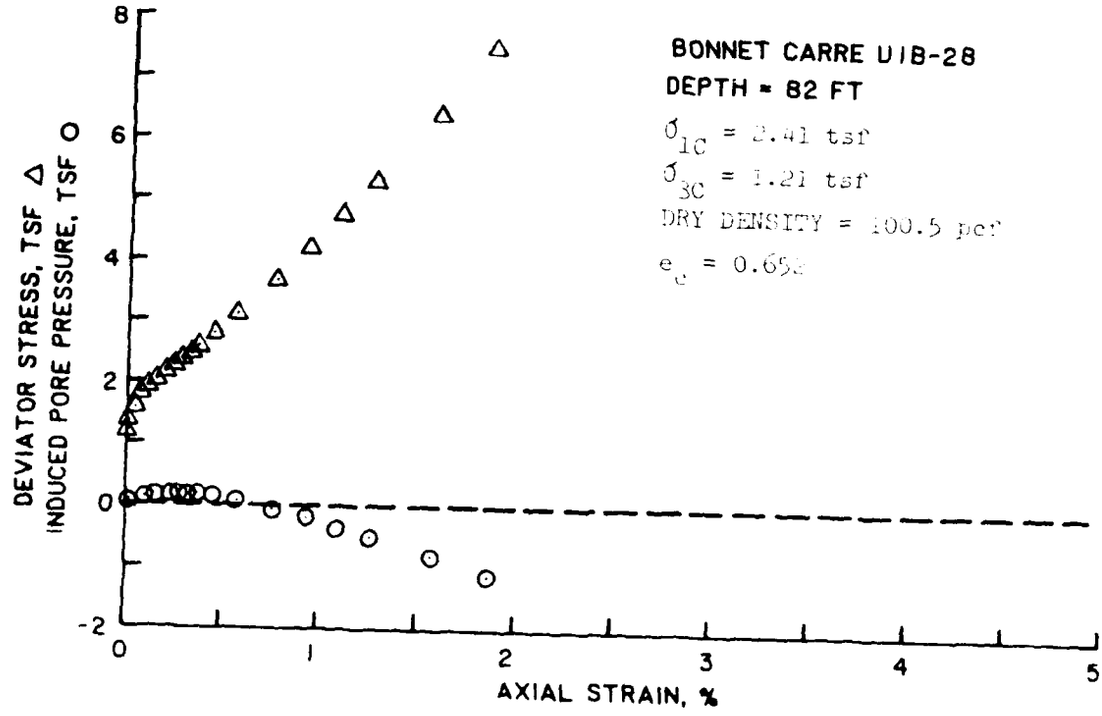

Q, TSF
$\bar{P}$, TSF

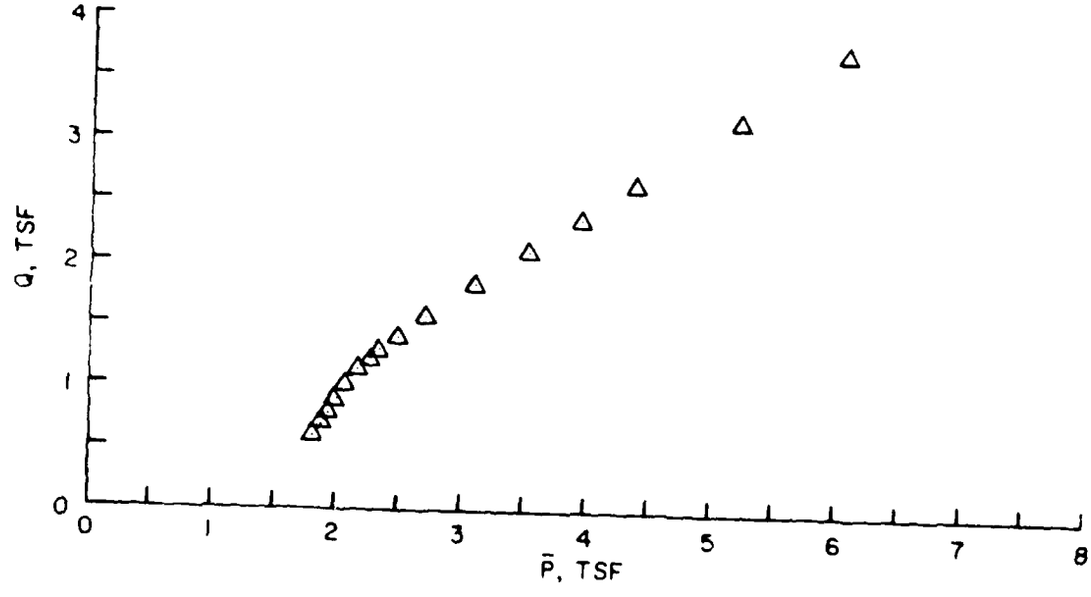

BONNET CARRE U1B-18
DEPTH = 51 FT
σ_{1c} = 1.5[illegible] tsf
σ_{3c} = 0.76 tsf
DRY DENSITY = [illegible] pcf
w_c = 0.[illegible]%
DEVIATOR STRESS, TSF Δ
INDUCED PORE PRESSURE, TSF O
AXIAL STRAIN, %

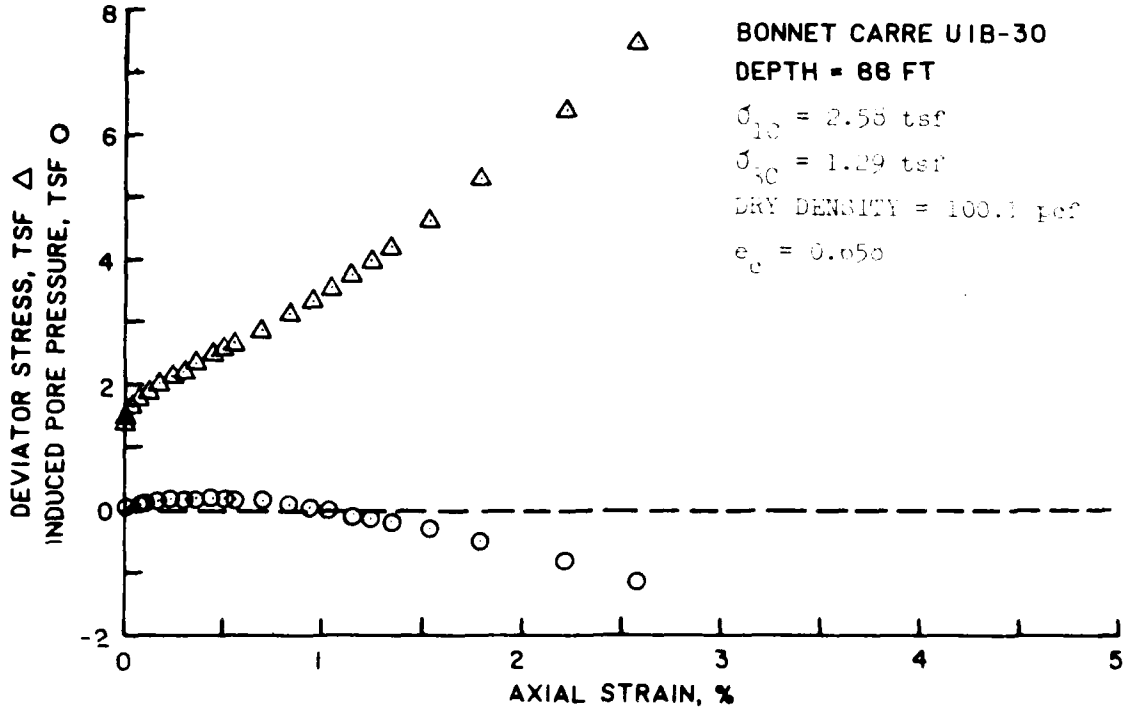

Q, TSF
$\bar{P}$, TSF

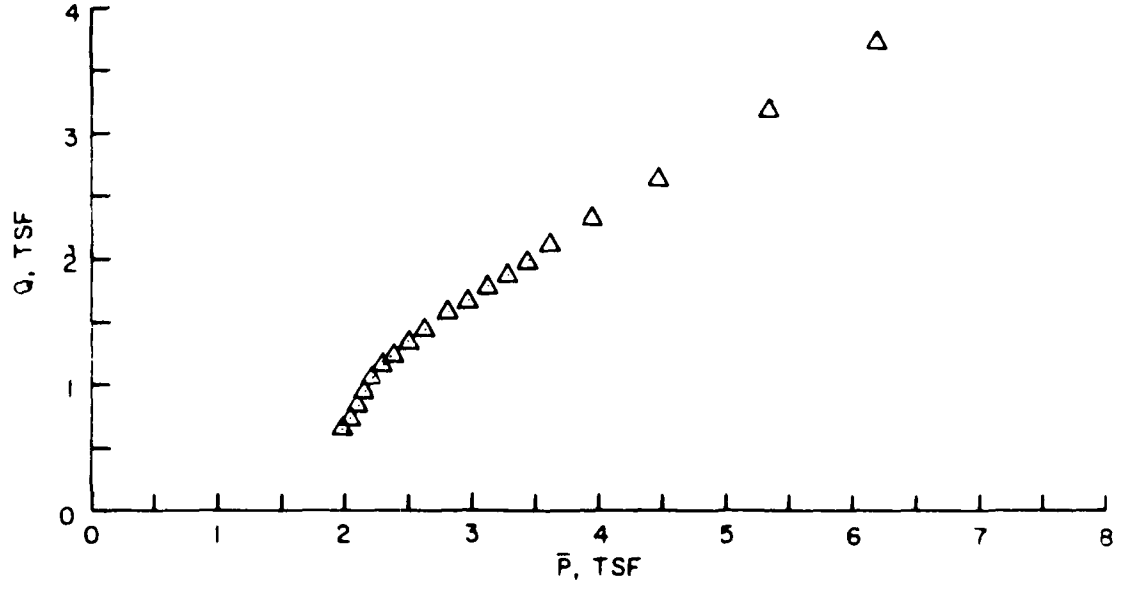

BONNET CARRE U1B-22A
DEPTH = 63 FT
σ_{1c} = 1.86 tsf
σ_{3c} = 0.93 tsf
DRY DENSITY = 97.3 pcf
e_c = 0.706
DEVIATOR STRESS, TSF Δ
INDUCED PORE PRESSURE, TSF O
AXIAL STRAIN, %

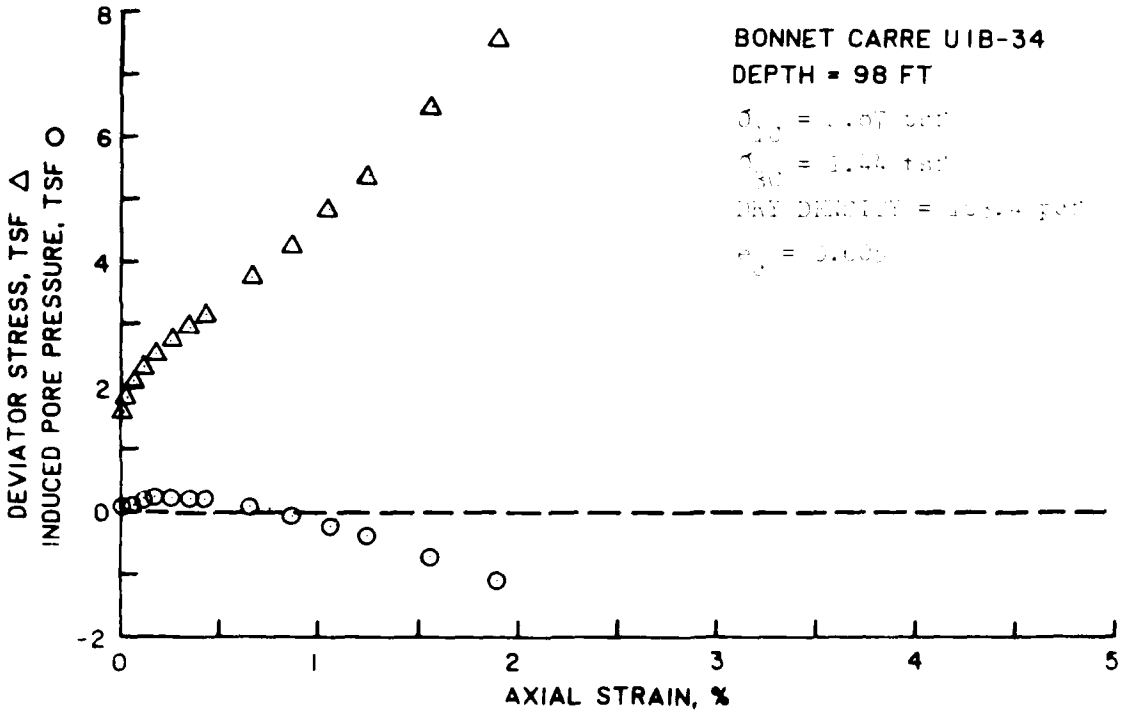

Q, TSF
$\bar{P}$, TSF

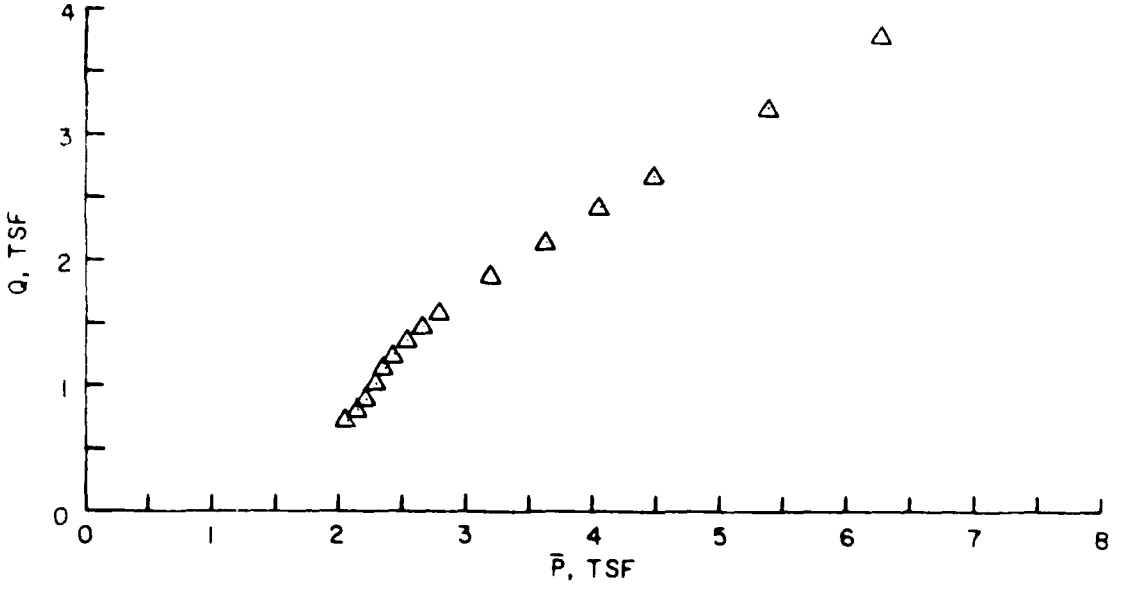

BONNET CARRE U1B-28
DEPTH = 82 FT
σ_{1C} = 2.41 tsf
σ_{3C} = 1.21 tsf
DRY DENSITY = 100.5 pcf
e_c = 0.65
DEVIATOR STRESS, TSF Δ
INDUCED PORE PRESSURE, TSF O
AXIAL STRAIN, %

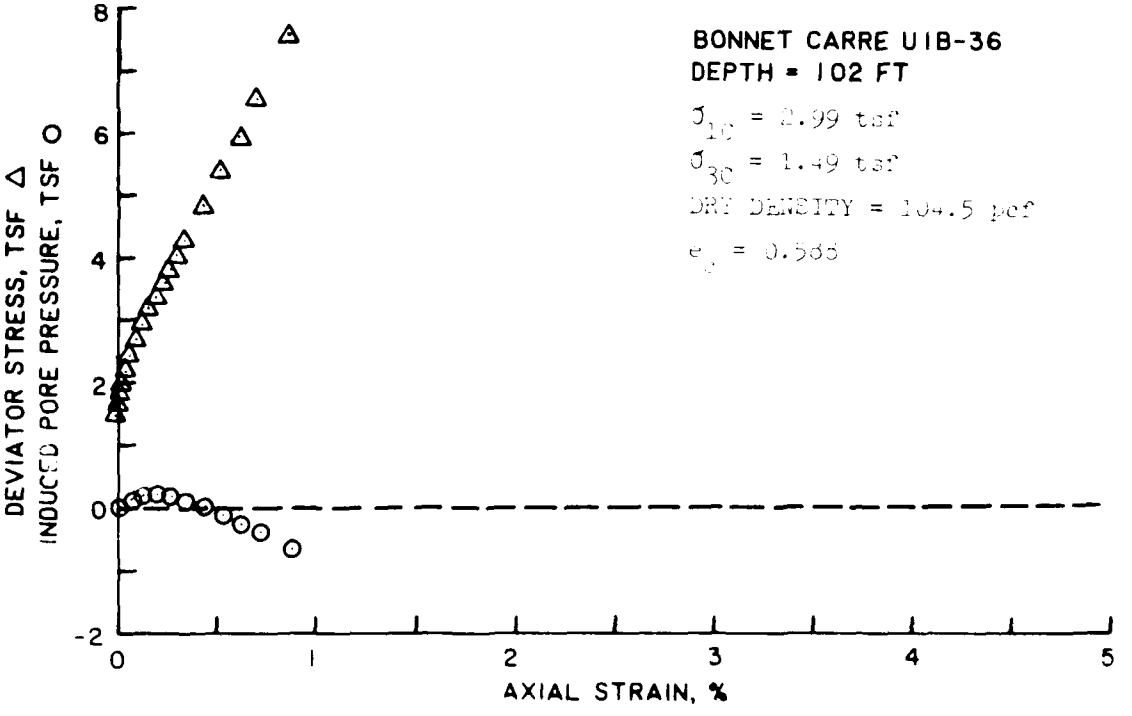

Q, TSF
$\bar{P}$, TSF

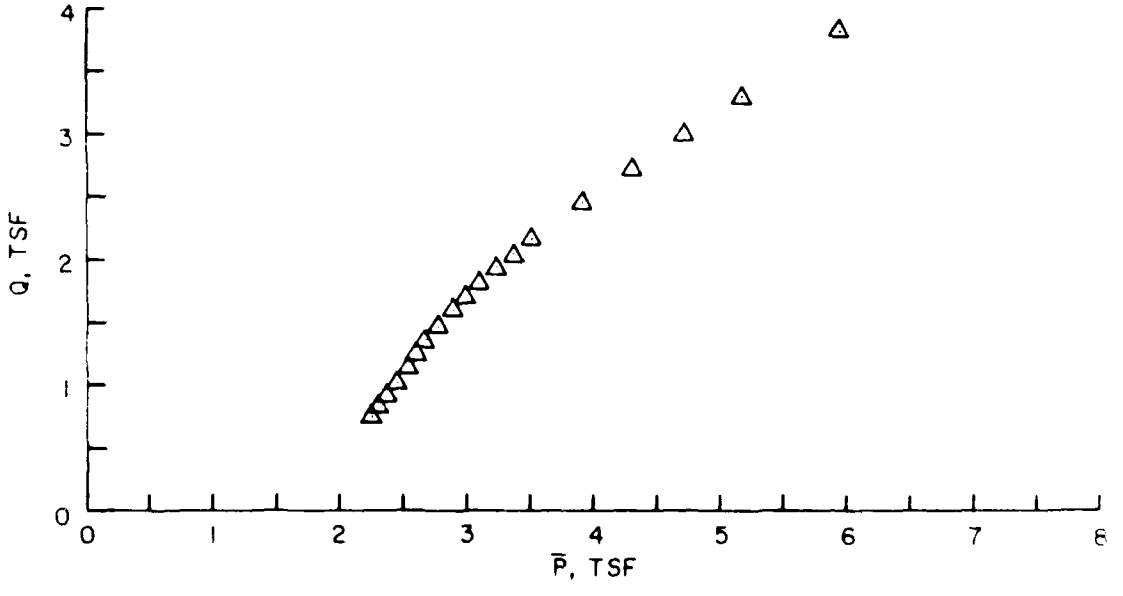

BONNET CARRE U1B-30
DEPTH = 88 FT
σ_{1c} = 2.58 tsf
σ_{3c} = 1.29 tsf
DRY DENSITY = 100.1 pcf
e_c = 0.656
DEVIATOR STRESS, TSF △
INDUCED PORE PRESSURE, TSF O
AXIAL STRAIN, %

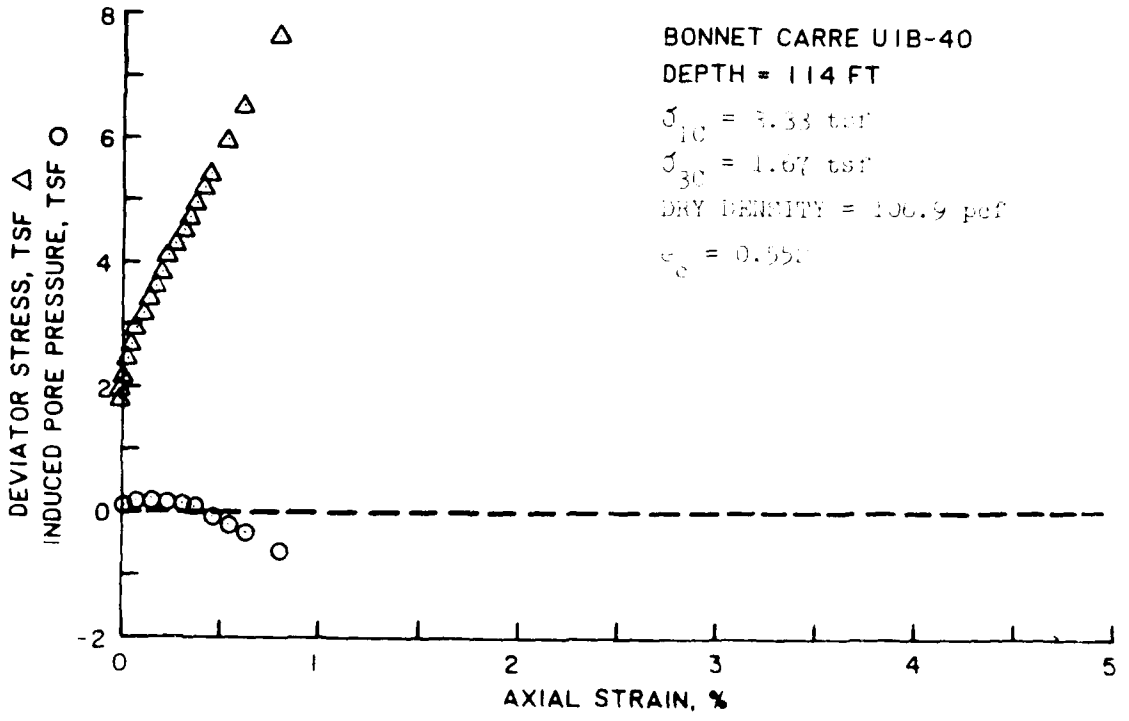

Q, TSF
$\bar{P}$, TSF

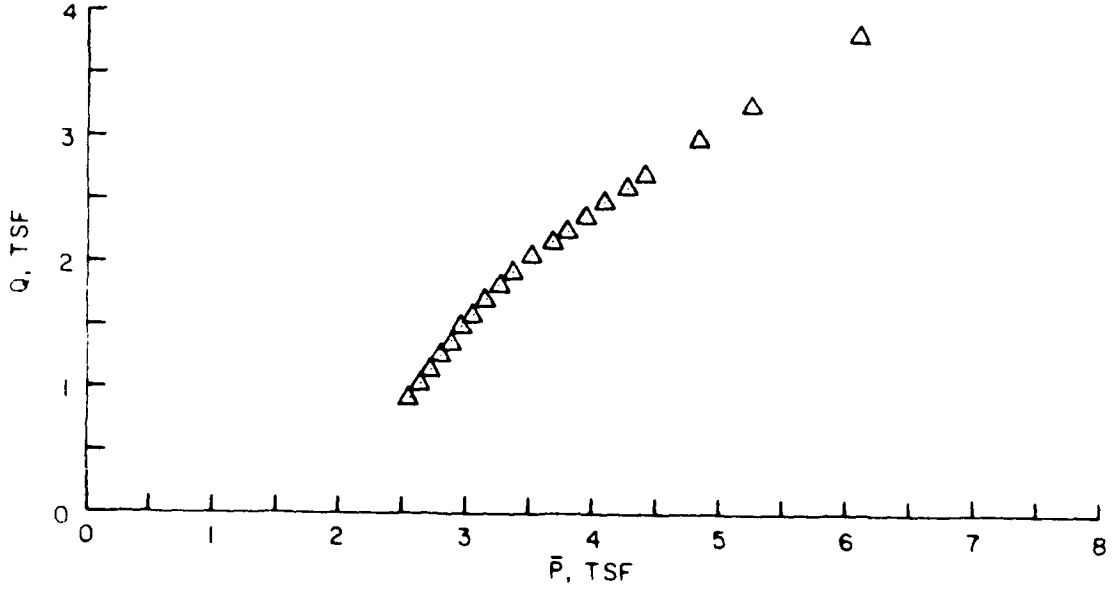

BONNET CARRE U1B-34
DEPTH = 98 FT
DEVIATOR STRESS, TSF Δ
INDUCED PORE PRESSURE, TSF O
AXIAL STRAIN, %


Q, TSF
P̄, TSF


BONNET CARRE U1B-36
DEPTH = 102 FT
σ_{1c} = 2.99 tsf
σ_{3c} = 1.49 tsf
DRY DENSITY = 104.5 pcf
e_c = 0.588
DEVIATOR STRESS, TSF Δ
INDUCED PORE PRESSURE, TSF O
AXIAL STRAIN, %

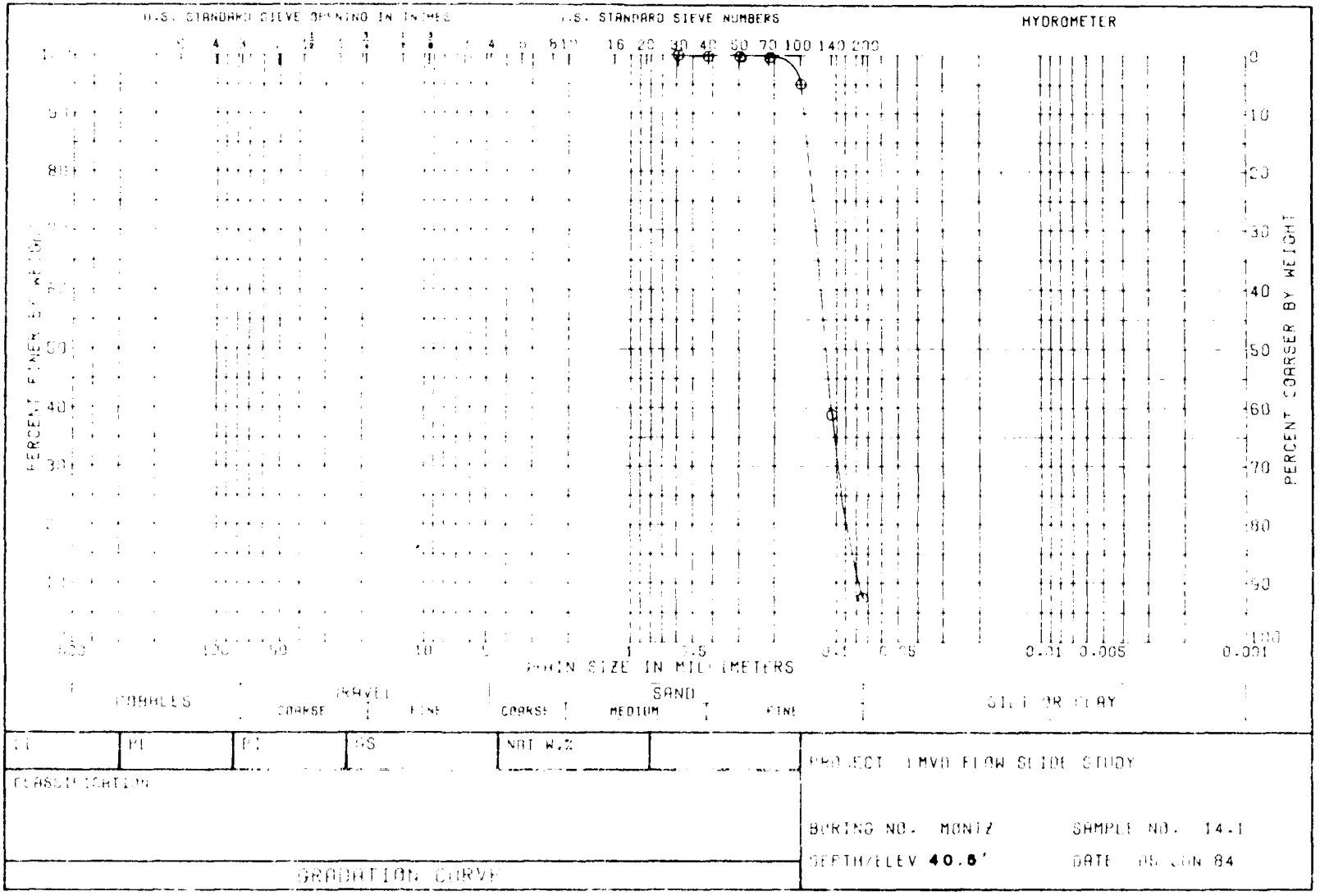

Q, TSF
$\bar{P}$, TSF

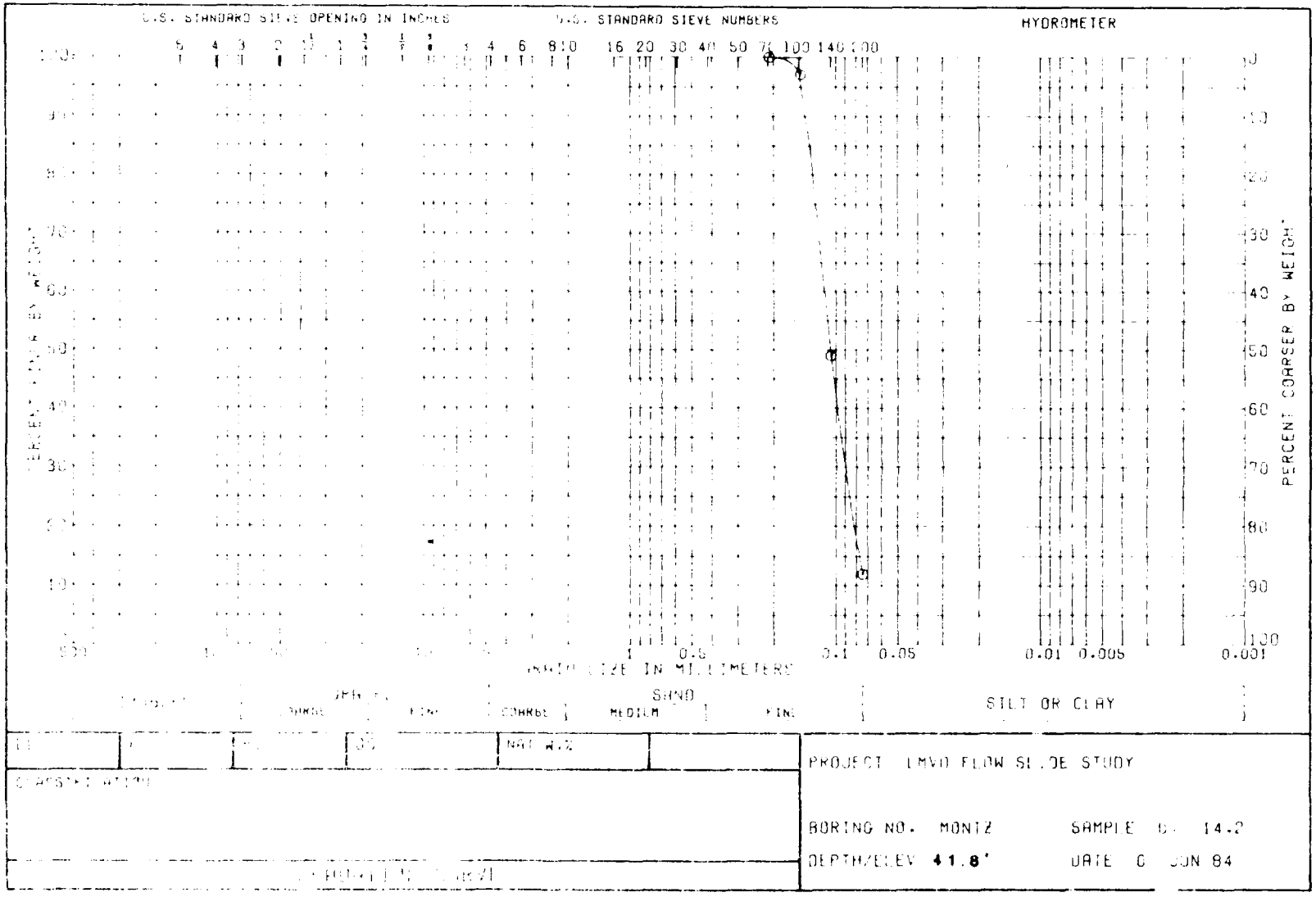

BONNET CARRE U1B-40
DEPTH = 114 FT
σ_{1c} = 3.33 tsf
σ_{3c} = 1.67 tsf
DRY DENSITY = 100.9 pcf
ε_c = 0.55%
DEVIATOR STRESS, TSF Δ
INDUCED PORE PRESSURE, TSF O
AXIAL STRAIN, %

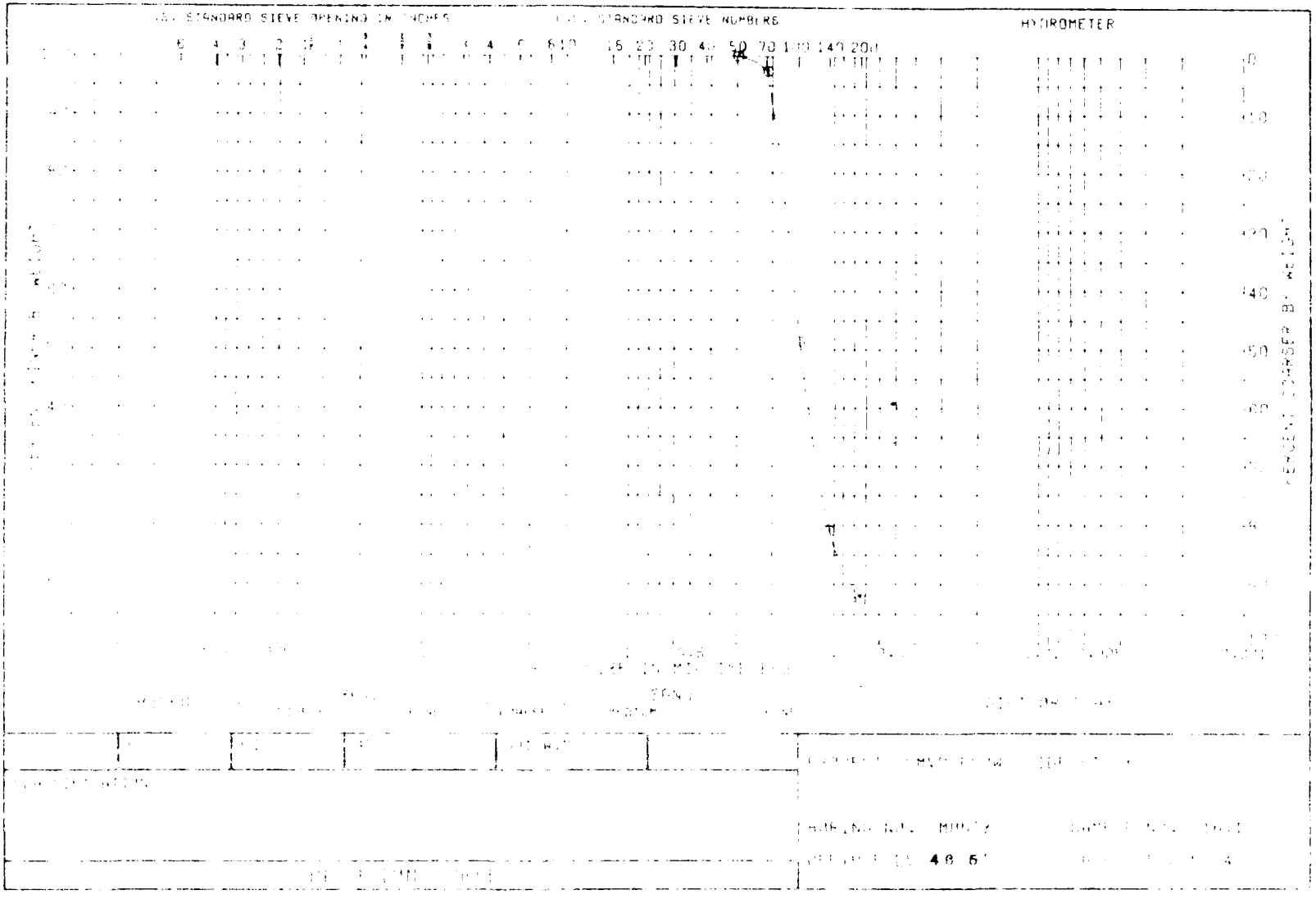

Q, TSF
$\bar{P}$, TSF

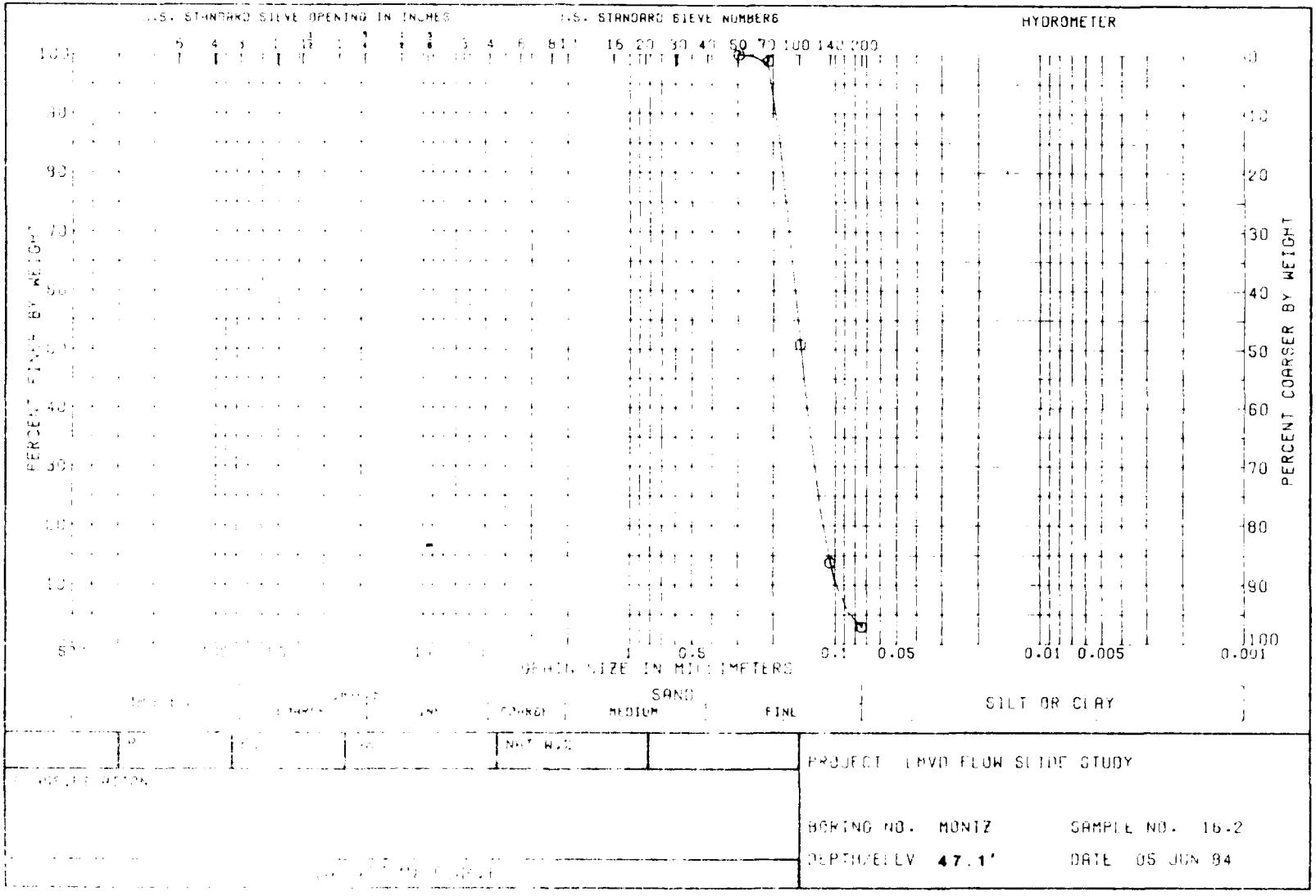
APPENDIX L

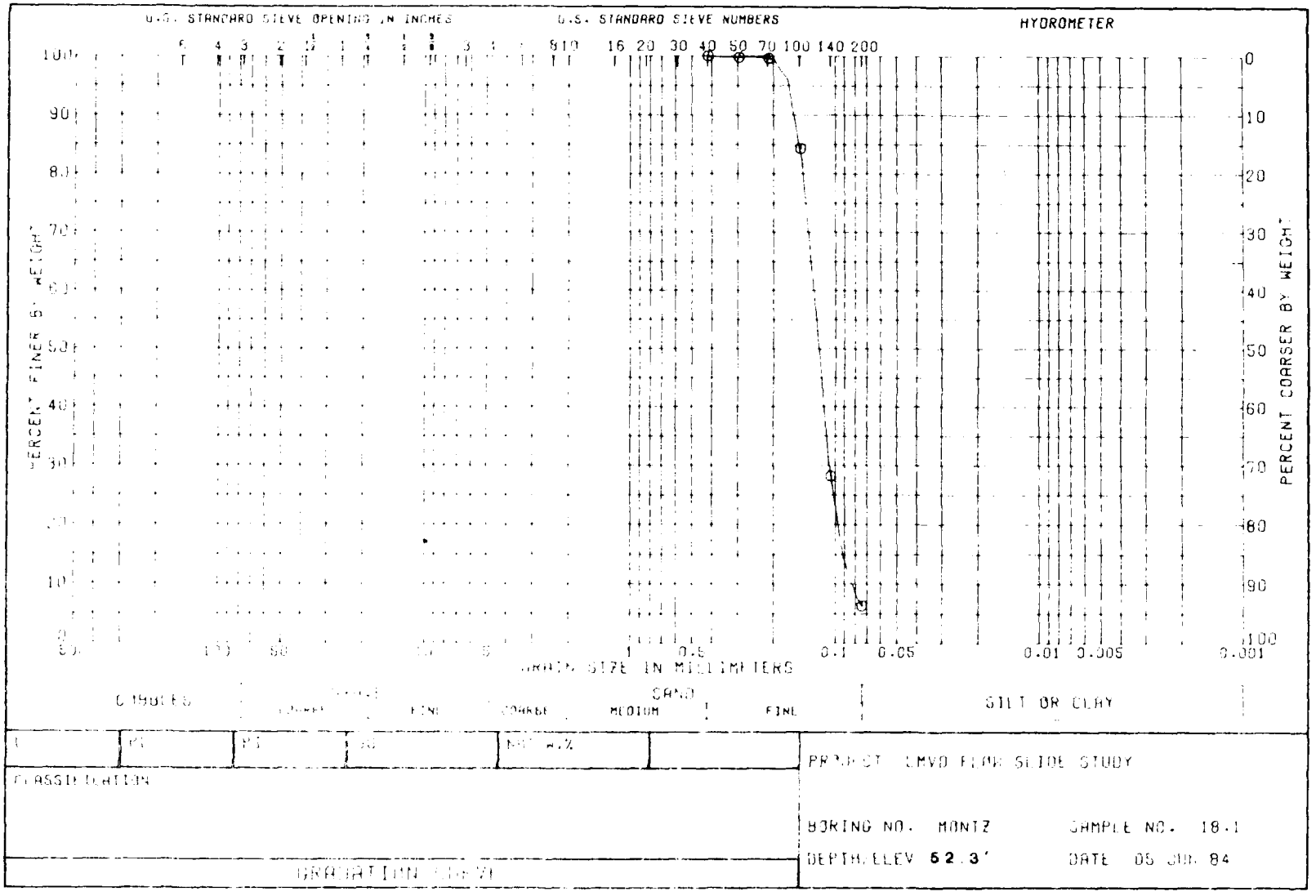
GRADATION CURVES FOR TESTED UNDISTURBED SAMPLES, MONTZ AND BONNET CARRE POINT SITES

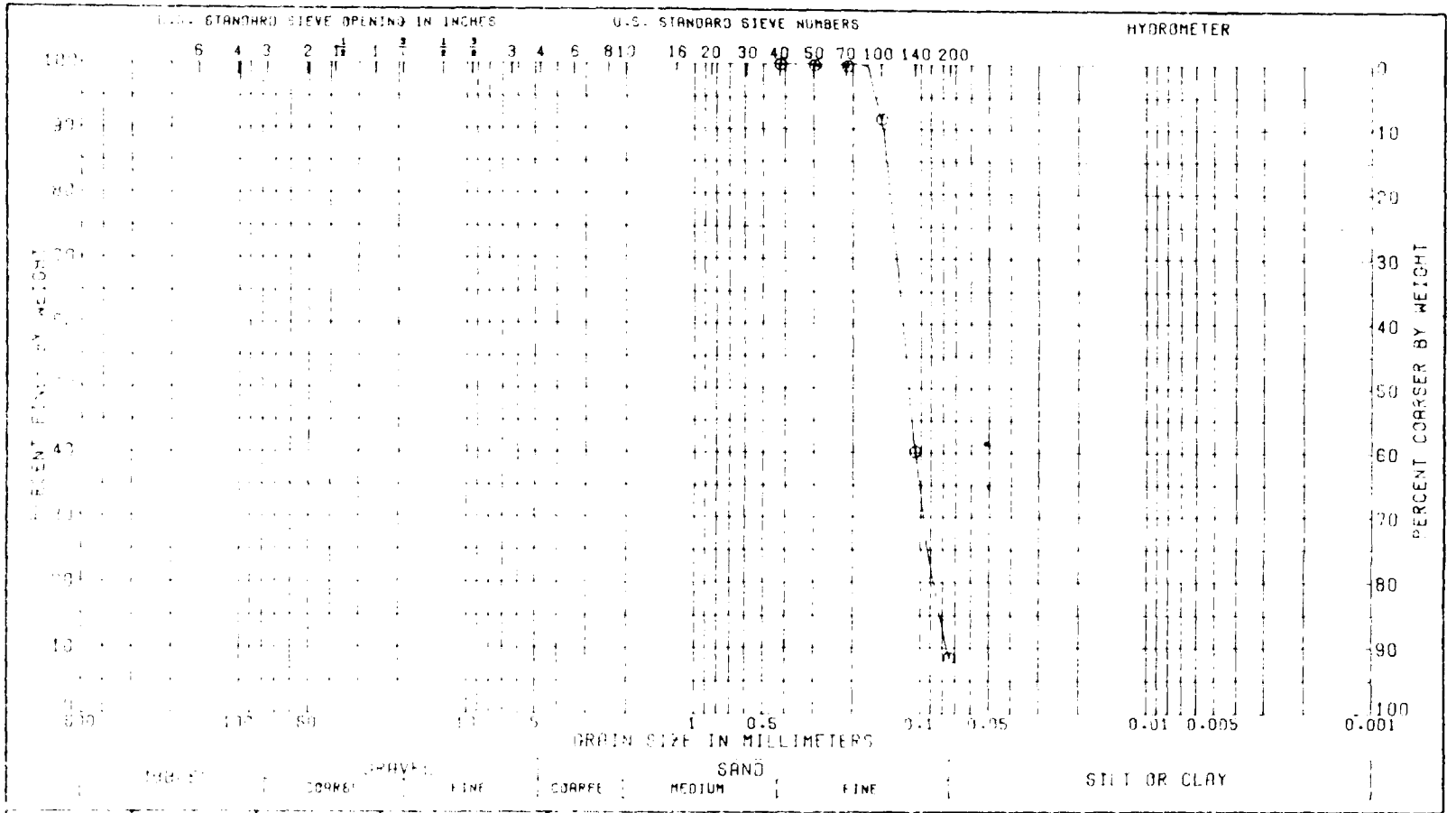

U.S. STANDARD SIEVE OPENING IN INCHES
U.S. STANDARD SIEVE NUMBERS
HYDROMETER
PERCENT FINER BY WEIGHT
PERCENT COARSER BY WEIGHT
GRAIN SIZE IN MILLIMETERS
COBBLES
GRAVEL
COARSE
FINE
SAND
COARSE
MEDIUM
FINE
SILT OR CLAY
LL
PL
PI
GS
NAT W.%
CLASSIFICATION
PROJECT LMVD FLOW SLIDE STUDY
BORING NO. MONTZ
SAMPLE NO. 14.1
DEPTH/ELEV 40.8'
DATE 05 JUN 84
GRADATION CURVE

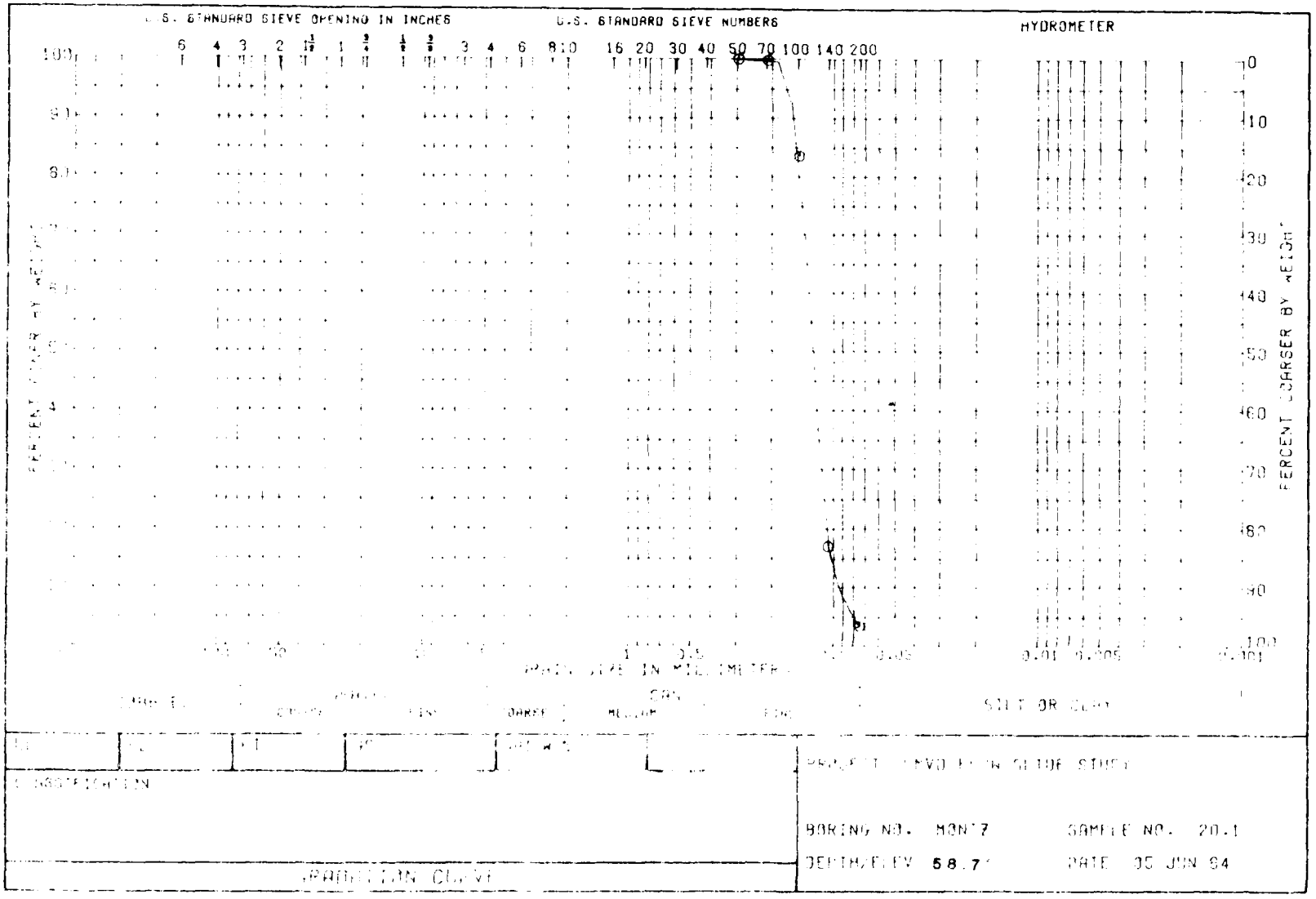

U.S. STANDARD SIEVE OPENING IN INCHES
U.S. STANDARD SIEVE NUMBERS
HYDROMETER
5 4 3 2 1 3/4 1/2 3/8 1/4 4 6 8 10 16 20 30 40 50 70 100 140 200
PERCENT FINER BY WEIGHT
PERCENT COARSER BY WEIGHT
GRAIN SIZE IN MILLIMETERS
1 0.5 0.1 0.05 0.01 0.005 0.001
COBBLES
GRAVEL
COARSE
FINE
SAND
COARSE
MEDIUM
FINE
SILT OR CLAY
NAT W.C.
PROJECT LMVD FLOW SLIDE STUDY
BORING NO. MONTZ
SAMPLE NO. 14.2
DEPTH/ELEV 41.8'
DATE C JUN 84

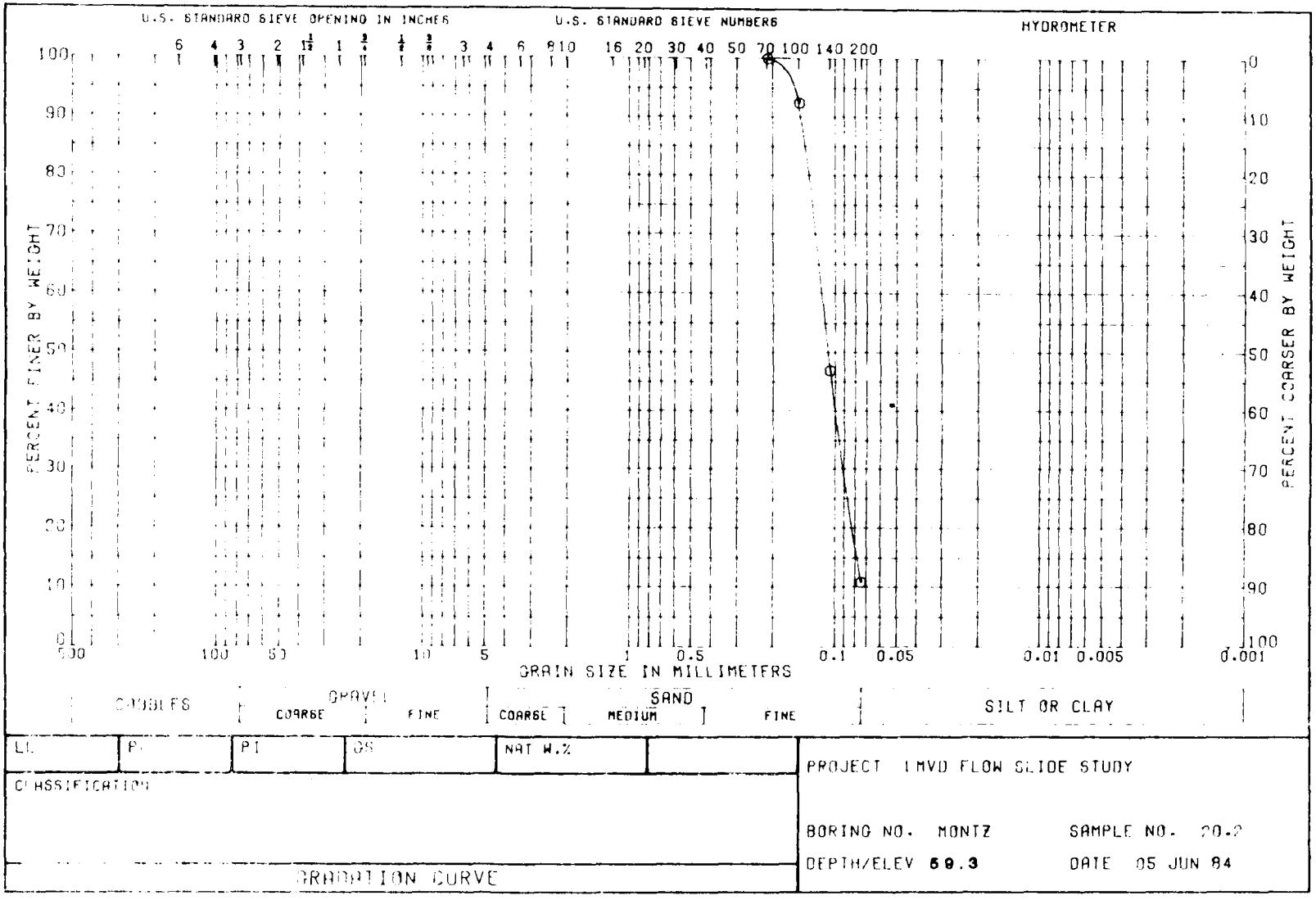

HYDROMETER


U.S. STANDARD SIEVE OPENING IN INCHES
U.S. STANDARD SIEVE NUMBERS
HYDROMETER
PERCENT FINER BY WEIGHT
PERCENT COARSER BY WEIGHT
GRAIN SIZE IN MILLIMETERS
SAND
COARSE
MEDIUM
FINE
SILT OR CLAY
PROJECT LMVD FLOW SLIDE STUDY
BORING NO. MONTZ
SAMPLE NO. 16-2
DEPTH/ELEV 47.1'
DATE 05 JUN 84


U.S. STANDARD SIEVE OPENING IN INCHES
U.S. STANDARD SIEVE NUMBERS
HYDROMETER
6 4 3 2 1½ 1 ¾ ½ ⅜ ¼ 3 4 8 10 16 20 30 40 50 70 100 140 200
PERCENT FINER BY WEIGHT
PERCENT COARSER BY WEIGHT
100 90 80 70 60 50 40 30 20 10 0
0 10 20 30 40 50 60 70 80 90 100
GRAIN SIZE IN MILLIMETERS
150 75 50 25 9.5 4.75 2 1 0.5 0.25 0.1 0.05 0.01 0.005 0.001
COBBLES
GRAVEL
COARSE
FINE
SAND
COARSE
MEDIUM
FINE
SILT OR CLAY
CLASSIFICATION
PROJECT LMVD FLOW SLIDE STUDY
BORING NO. MONTZ
SAMPLE NO. 18-1
DEPTH/ELEV 52.3'
DATE 05 JUN 84


U.S. STANDARD SIEVE OPENING IN INCHES
U.S. STANDARD SIEVE NUMBERS
HYDROMETER
6 4 3 2 1½ 1 ¾ ½ ⅜ ¾ 4 6 8 10 16 20 30 40 50 70 100 140 200
PERCENT FINER BY WEIGHT
PERCENT COARSER BY WEIGHT
GRAIN SIZE IN MILLIMETERS
COBBLES
GRAVEL
COARSE
FINE
SAND
COARSE
MEDIUM
FINE
SILT OR CLAY
PROJECT CMVD FLOW SLIDE STUDY
BORING NO. MON12
SAMPLE NO. 18-2
DEPTH/ELEV 53.1'
DATE 05 JUN 84
GRADATION CURVE


U.S. STANDARD SIEVE OPENING IN INCHES
U.S. STANDARD SIEVE NUMBERS
HYDROMETER
6 4 3 2 1½ 1 ¾ ½ ⅜ 3 4 6 8 10 16 20 30 40 50 70 100 140 200
PERCENT FINER BY WEIGHT
PERCENT COARSER BY WEIGHT
GRAIN SIZE IN MILLIMETERS
SILT OR CLAY
CLASSIFICATION
PROJECT REVOLUTION CLOVE
BORING NO. MON'7
SAMPLE NO. 20.1
DEPTH/ELEV 58.7'
DATE 05 JUN 84



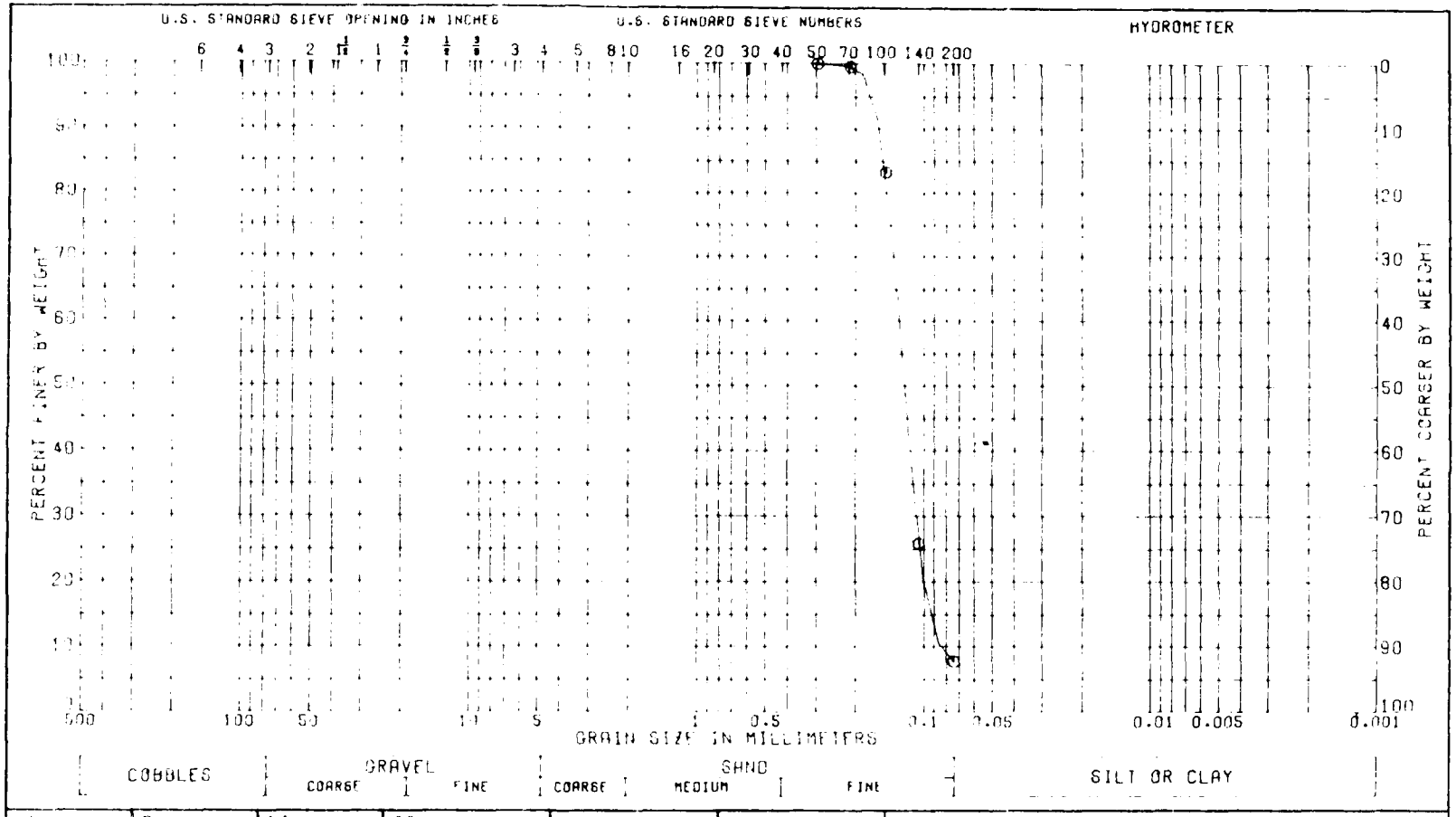
LL	PL	PI	GS	NAT W.%	
CLASSIFICATION					

GRADATION CURVE

PROJECT MVD FLOW SLIDE STUDY

BORING NO. MONTZ SAMPLE NO. 20-2

DEPTH/ELEV 59.3 DATE 05 JUN 84



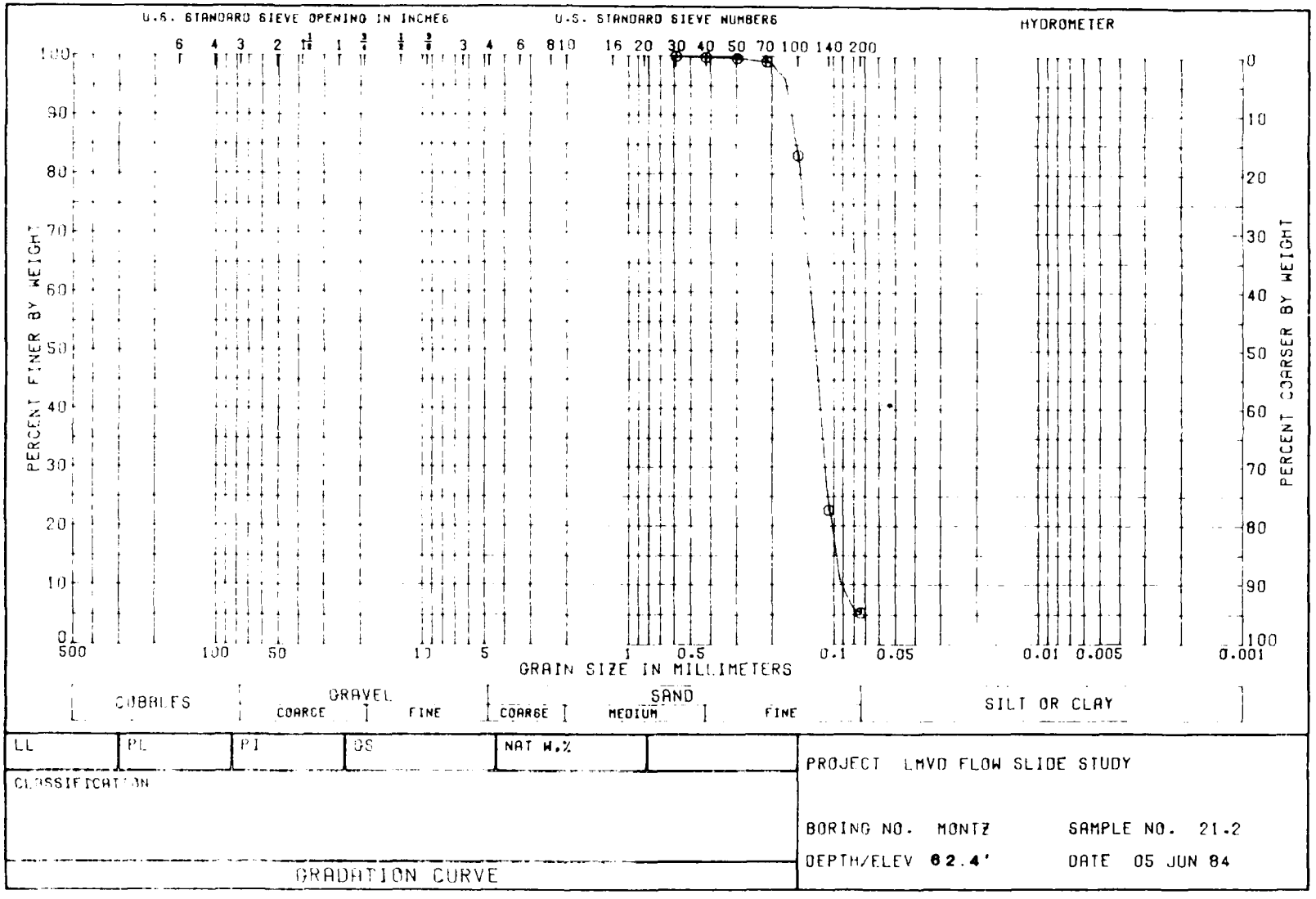
LL	PL	PI	GS	NAT W.%	
CLASSIFICATION					

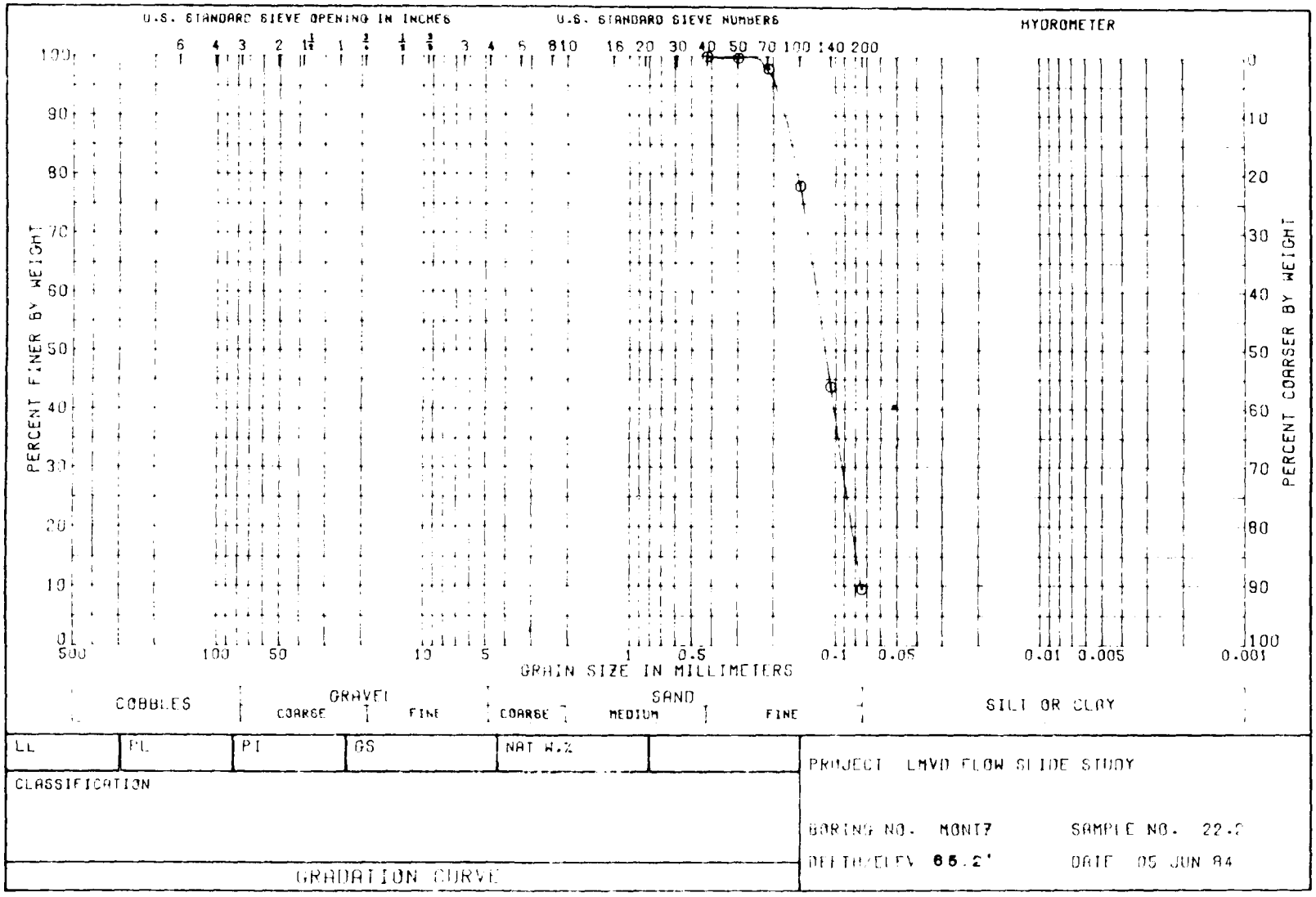
GRADATION CURVE

PROJECT LMVD FLOW SLIDE STUDY

BORING NO. MON17 SAMPLE NO. 21.1

DEPTH/ELEV 61.3' DATE 05 JUN 94


U.S. STANDARD SIEVE OPENING IN INCHES
U.S. STANDARD SIEVE NUMBERS
HYDROMETER
6 4 3 2 1½ 1 ¾ ½ ⅜ 3 4 6 8 10 16 20 30 40 50 70 100 140 200
PERCENT FINER BY WEIGHT
PERCENT COARSER BY WEIGHT
100 90 80 70 60 50 40 30 20 10 0
0 10 20 30 40 50 60 70 80 90 100
500 100 50 10 5 1 0.5 0.1 0.05 0.01 0.005 0.001
GRAIN SIZE IN MILLIMETERS
COBBLES
GRAVEL
COARSE
FINE
SAND
COARSE
MEDIUM
FINE
SILT OR CLAY
LL
PL
PI
GS
NAT W.%
CLASSIFICATION
GRADATION CURVE
PROJECT LMVD FLOW SLIDE STUDY
BORING NO. MONTZ
SAMPLE NO. 21.2
DEPTH/ELEV 62.4'
DATE 05 JUN 84



LL	PL	PI	GS	NAT W.%	

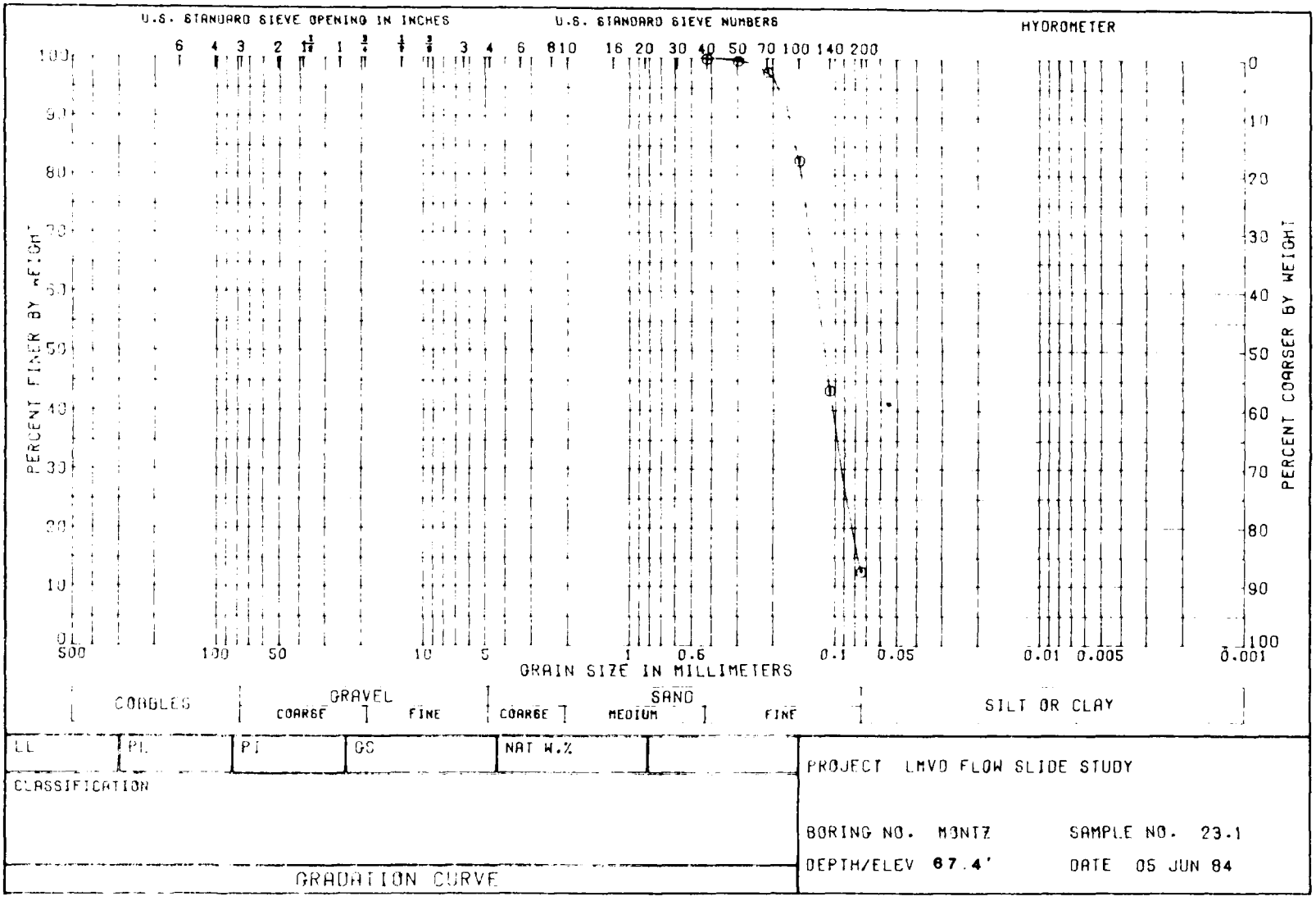
CLASSIFICATION

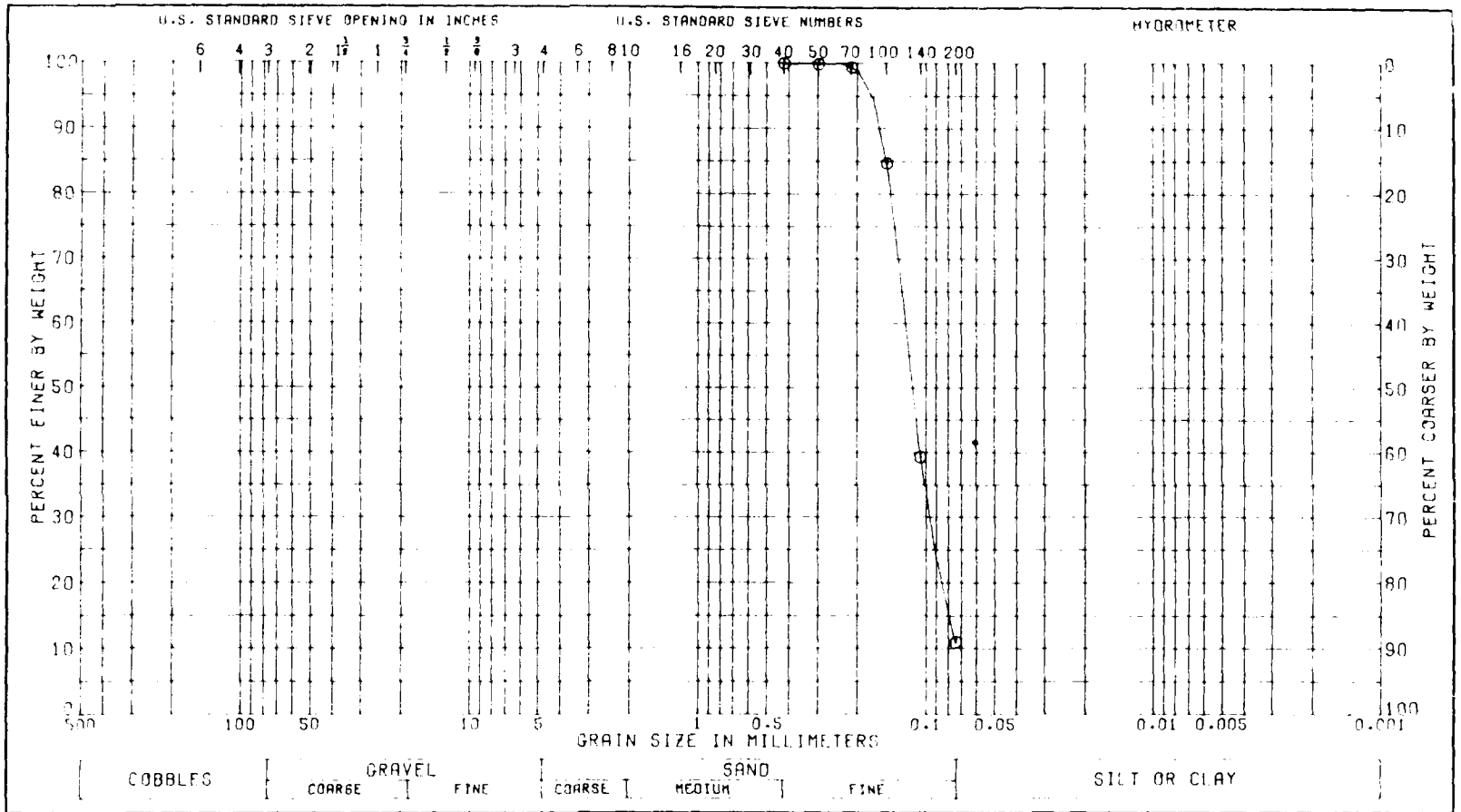
GRADATION CURVE

PROJECT LMVD FLOW SLIDE STUDY

BORING NO. MONI7 SAMPLE NO. 22.2

DEPTH/ELEV 66.2' DATE 05 JUN 84


U.S. STANDARD SIEVE OPENING IN INCHES
U.S. STANDARD SIEVE NUMBERS
HYDROMETER
6 4 3 2 1½ 1 ¾ ½ ⅜ 3 4 6 8 10 16 20 30 40 50 70 100 140 200
PERCENT FINER BY WEIGHT
PERCENT COARSER BY WEIGHT
100 90 80 70 60 50 40 30 20 10 0
0 10 20 30 40 50 60 70 80 90 100
500 100 50 10 5 1 0.6 0.1 0.05 0.01 0.005 0.001
GRAIN SIZE IN MILLIMETERS
COBBLES
GRAVEL
COARSE
FINE
SAND
COARSE
MEDIUM
FINE
SILT OR CLAY
LL
PL
PI
GS
NAT W.%
CLASSIFICATION
GRADATION CURVE
PROJECT LMVD FLOW SLIDE STUDY
BORING NO. MONTZ
SAMPLE NO. 23.1
DEPTH/ELEV 67.4'
DATE 05 JUN 84



LL	PL	PI	GS	NAT W.%	

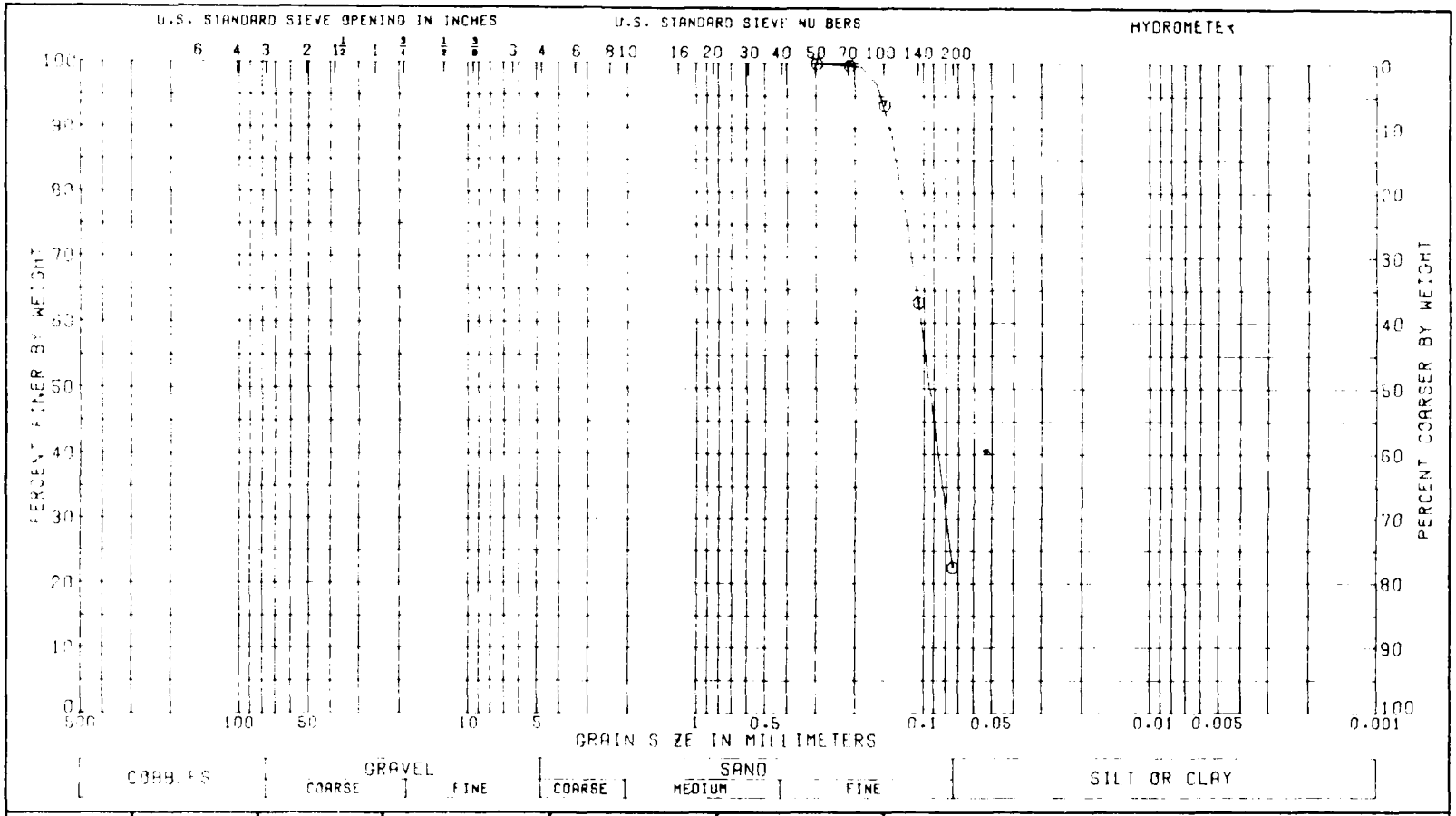
CLASSIFICATION

GRADATION CURVE

PROJECT LMVD FLOW SLIDE STUDY

BORING NO. MONTZ SAMPLE NO. 24.2

DEPTH/ELEV 71.0' DATE 05 JUN 84



LL	PL	PI	GS	NAT W.%	

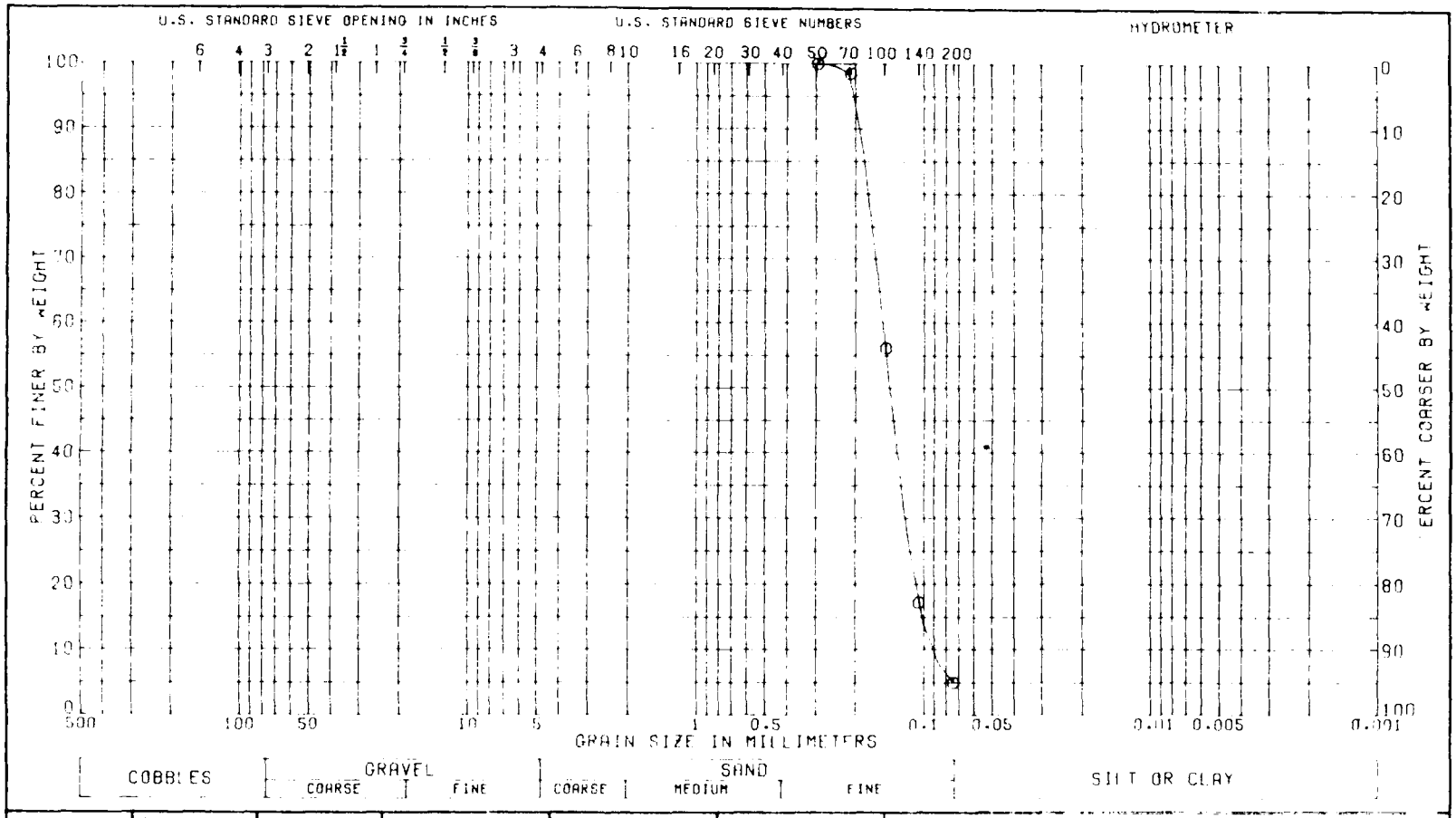
CLASSIFICATION

GRADATION CURVE

PROJECT LMVD FLOW SLIDE STUDY

BORING NO. MONTZ SAMPLE NO. 25.1

DEPTH/ELEV **73.6'** DATE 05 JUN 84



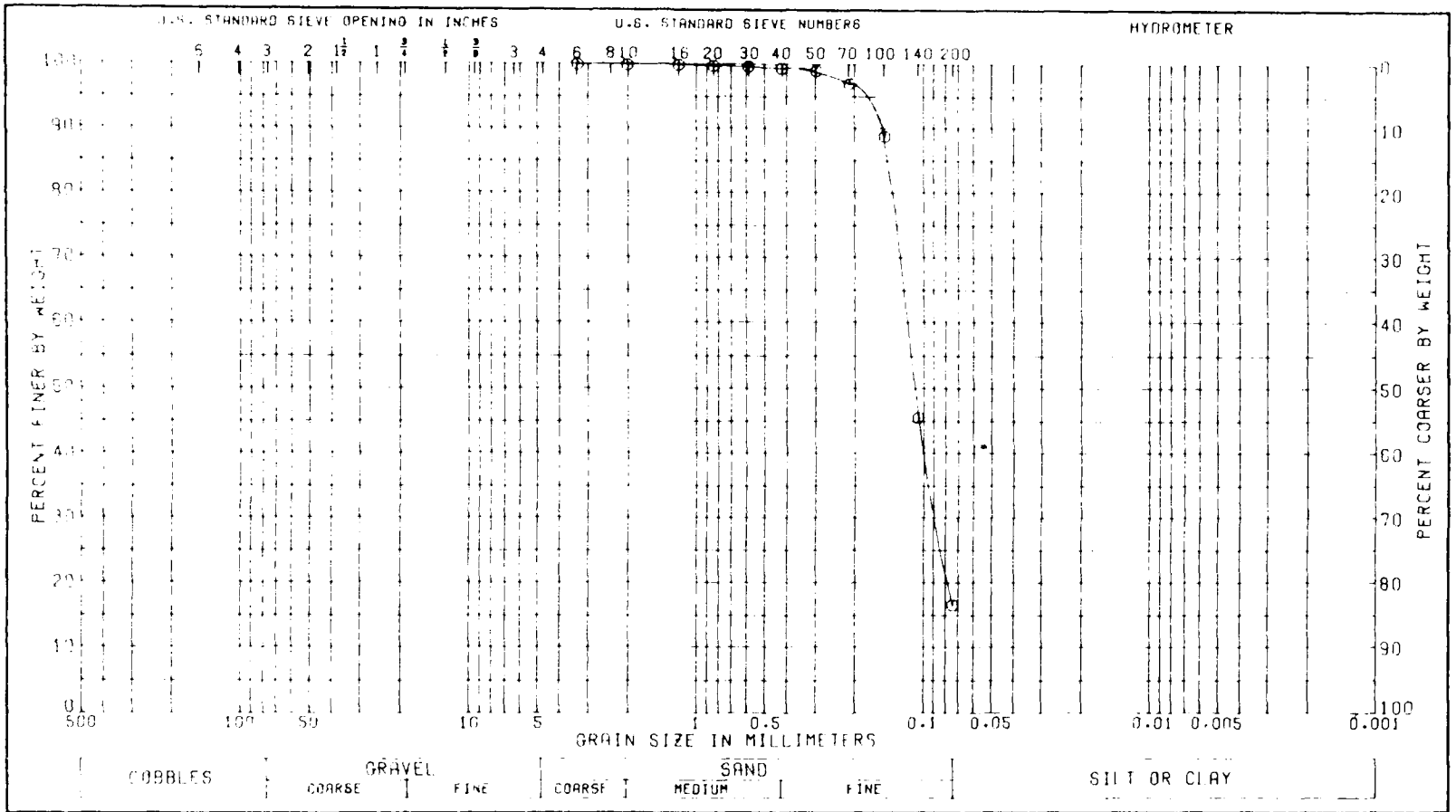
LL	PL	PI	GS	NAT W.%	
CLASSIFICATION					

GRADATION CURVE

PROJECT LMVD FLOW SLIDE STUDY

BORING NO. MONTZ SAMPLE NO. 26.2

DEPTH/ELEV 76.5' DATE 06 JUN 84



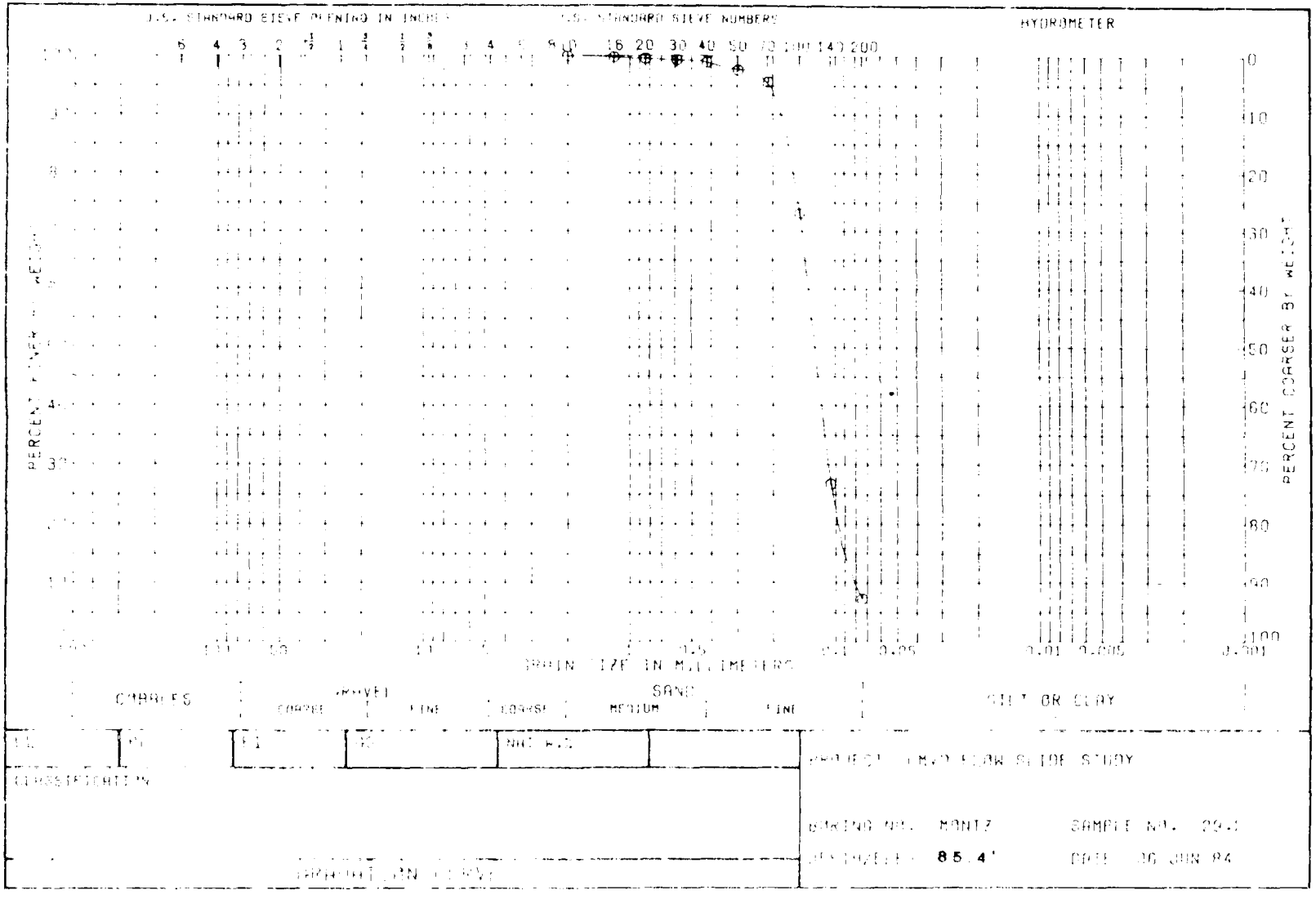
LL	PL	PI	GS	NAT W.%	
CLASSIFICATION					

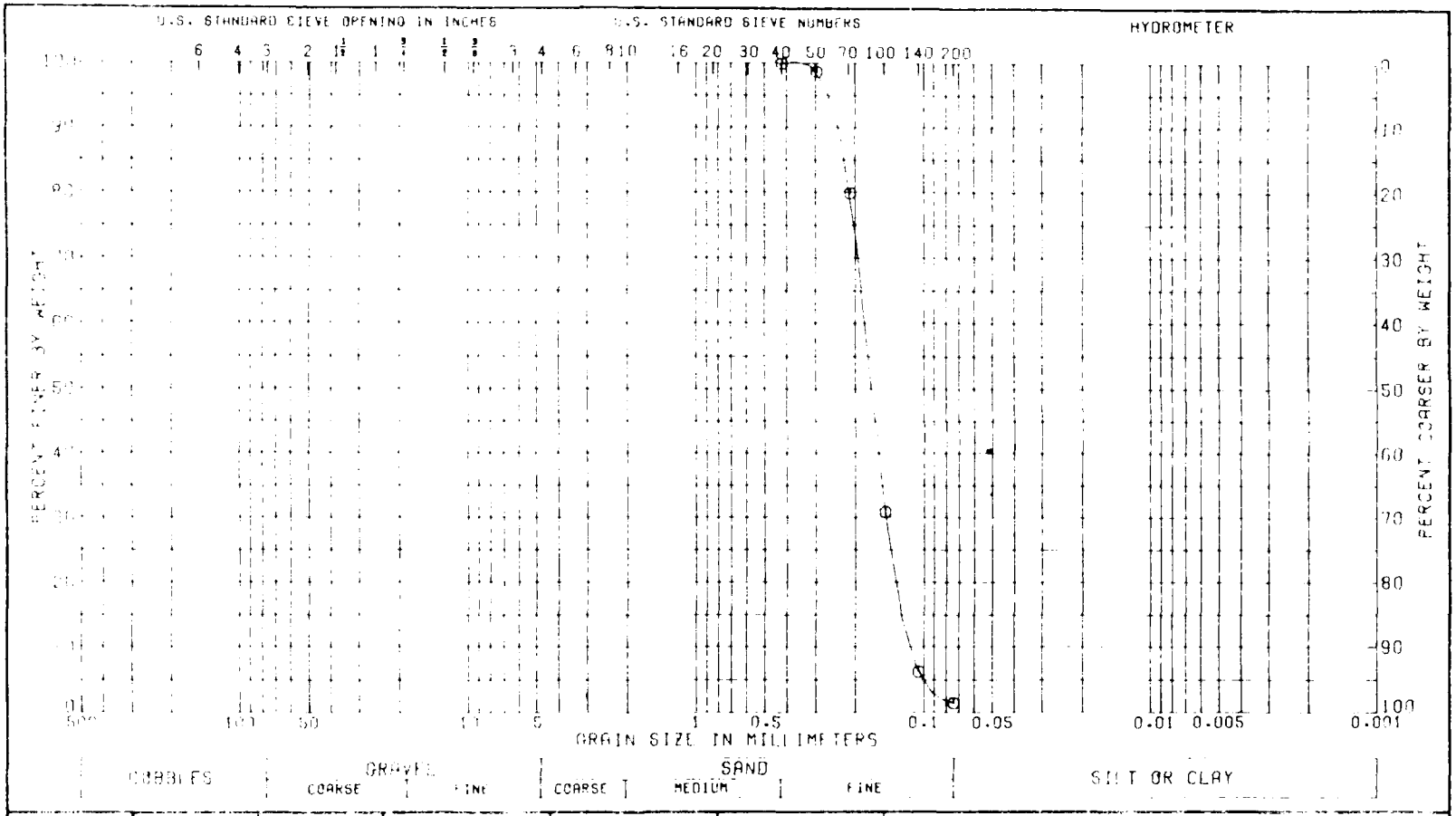
GRADATION CURVE

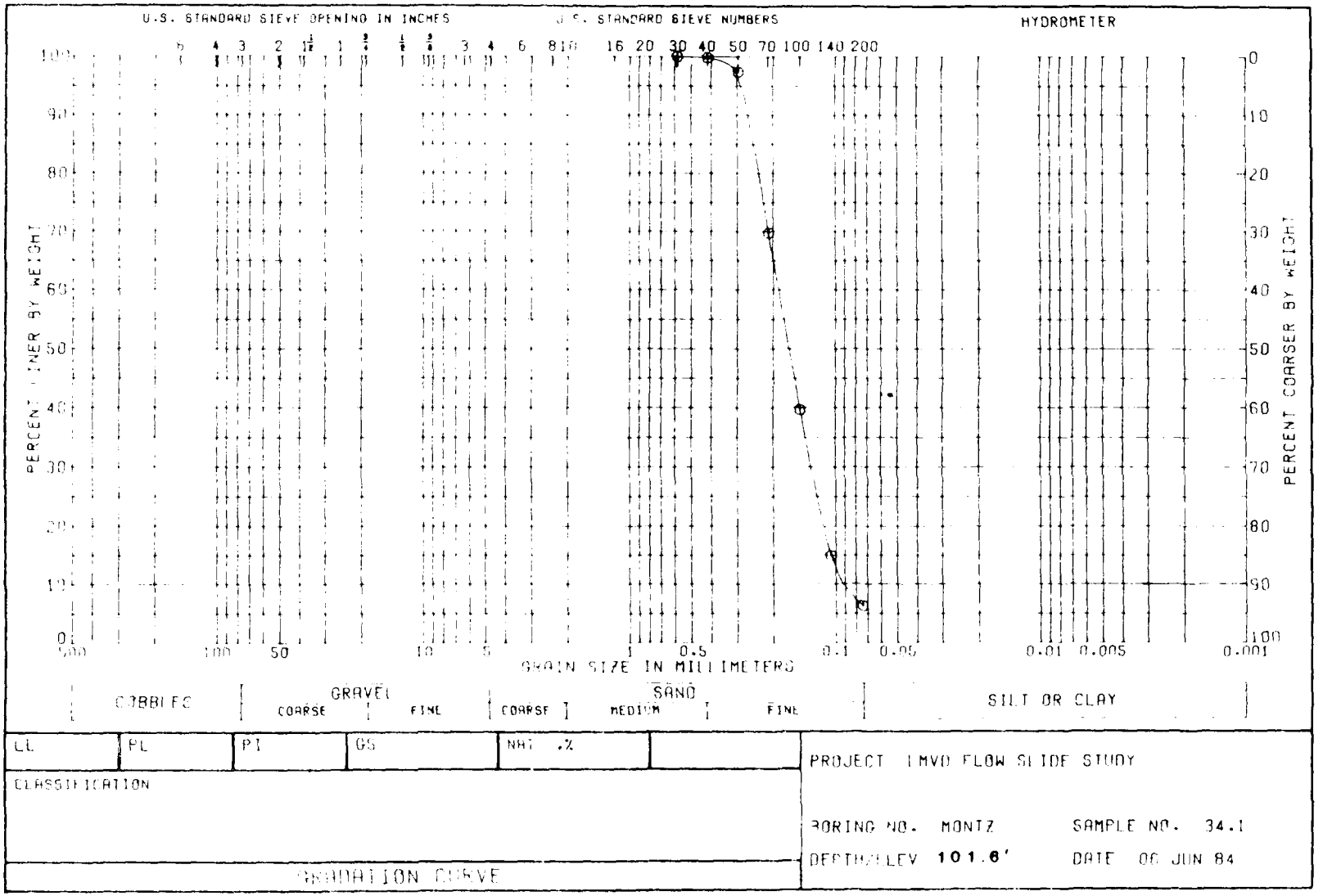
PROJECT LMVD FLOW SLIDE STUDY

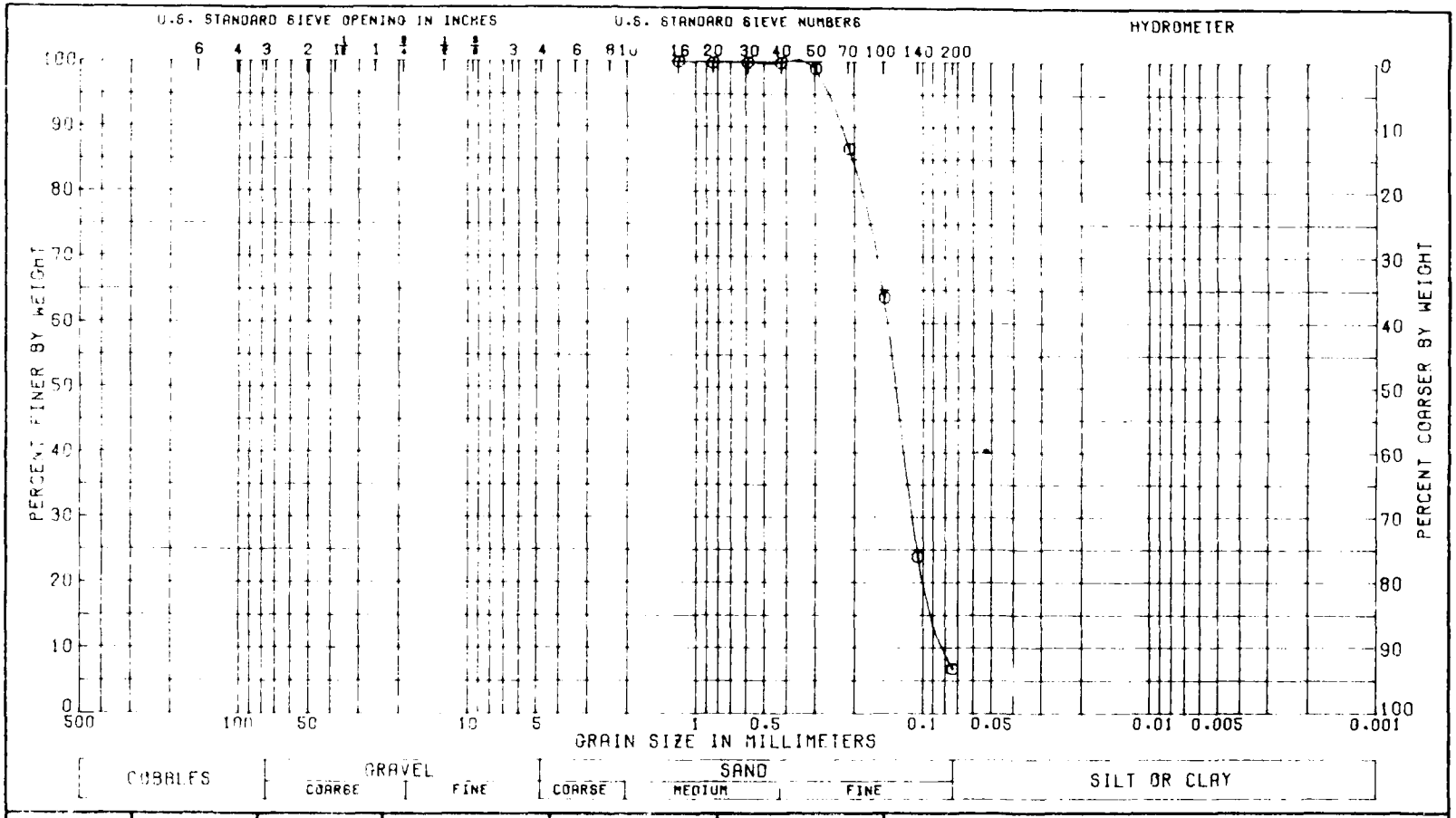
BORING NO. MONTZ SAMPLE NO. 27.4

DEPTH/ELEV 79.7' DATE 06 JUN 84


U.S. STANDARD SIEVE OPENING IN INCHES
U.S. STANDARD SIEVE NUMBERS
HYDROMETER
PERCENT FINER BY WEIGHT
PERCENT COARSER BY WEIGHT
GRAIN SIZE IN MILLIMETERS
COBBLES
GRAVEL
COARSE
FINE
SAND
COARSE
MEDIUM
FINE
SILT OR CLAY
CLASSIFICATION
PROJECT
BORING NO.
SAMPLE NO.
ELEVATION
DATE


U.S. STANDARD SIEVE OPENING IN INCHES
U.S. STANDARD SIEVE NUMBERS
HYDROMETER
6 4 3 2 1½ 1 ¾ ½ ⅜ ¼ 4 6 8 10 16 20 30 40 50 70 100 140 200
PERCENT FINER BY WEIGHT
PERCENT COARSER BY WEIGHT
GRAIN SIZE IN MILLIMETERS
0.01 0.005 0.001
COBBLES
GRAVEL
COARSE
FINE
SAND
COARSE
MEDIUM
FINE
SILT OR CLAY
NAT W.%
CLASSIFICATION
GRADATION CURVE
PROJECT LMVD FLOW SLIDE STUDY
BORING NO. MONTZ
SAMPLE NO. 31.1
DEPTH/ELEV 92.1'
DATE 06 JUN 84


U.S. STANDARD SIEVE OPENING IN INCHES
U.S. STANDARD SIEVE NUMBERS
HYDROMETER
PERCENT FINER BY WEIGHT
PERCENT COARSER BY WEIGHT
GRAIN SIZE IN MILLIMETERS
COBBLES
GRAVEL
COARSE
FINE
SAND
COARSE
MEDIUM
FINE
SILT OR CLAY
LL
PL
PI
GS
NAT .%
CLASSIFICATION
GRADATION CURVE
PROJECT IMVD FLOW SLIDE STUDY
BORING NO. MONTZ
SAMPLE NO. 34.1
DEPTH/ELEV 101.6'
DATE 06 JUN 84



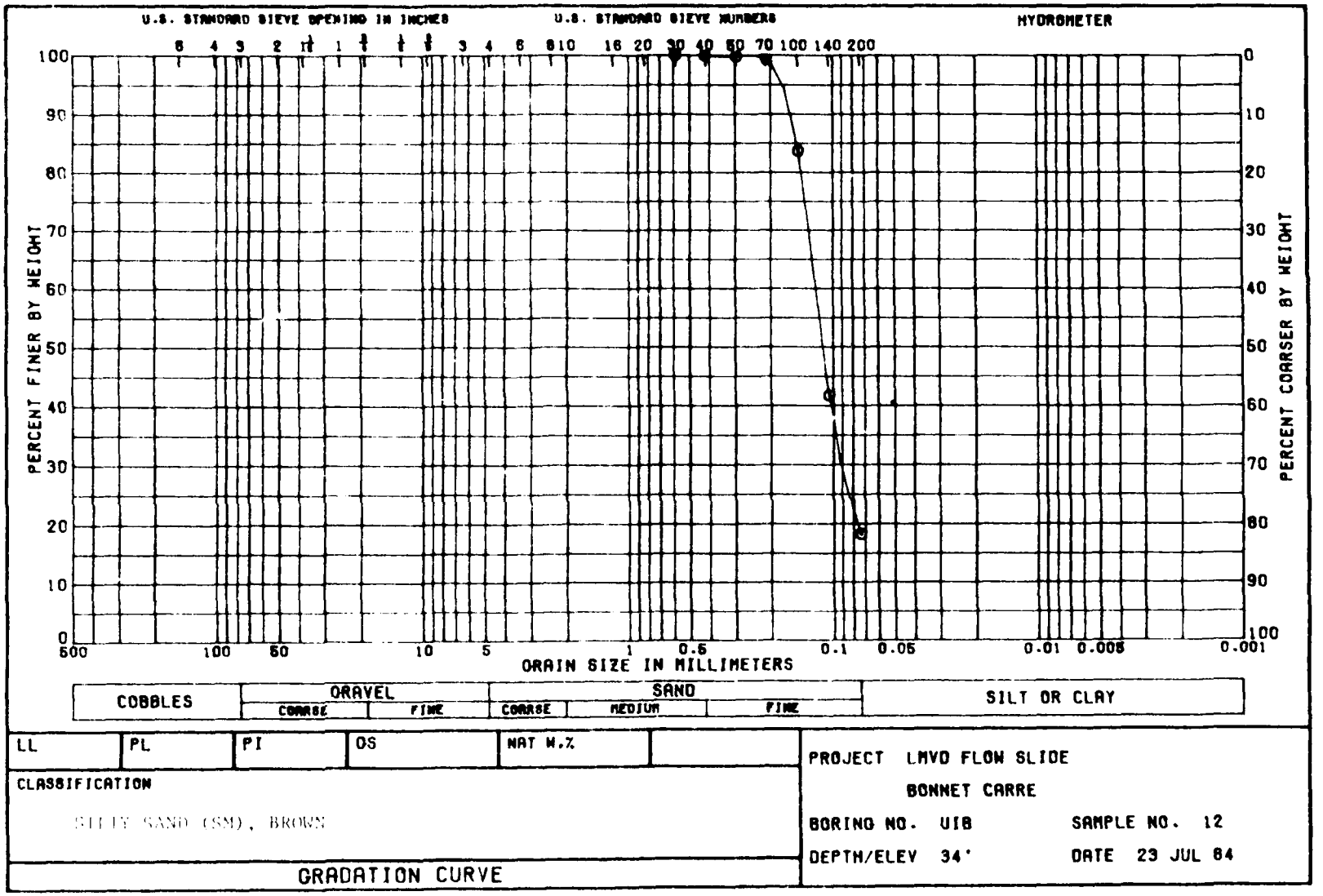
LL	PI	PI	GS	NAT W.%	
CLASSIFICATION					

GRADATION CURVE

PROJECT LMVD FLOW SLIDE STUDY

BORING NO. MONTZ SAMPLE NO. 38.2

DEPTH/ELEV 112.7' DATE 06 JUN 84



LL	PL	PI	OS	NAT W.%	

CLASSIFICATION

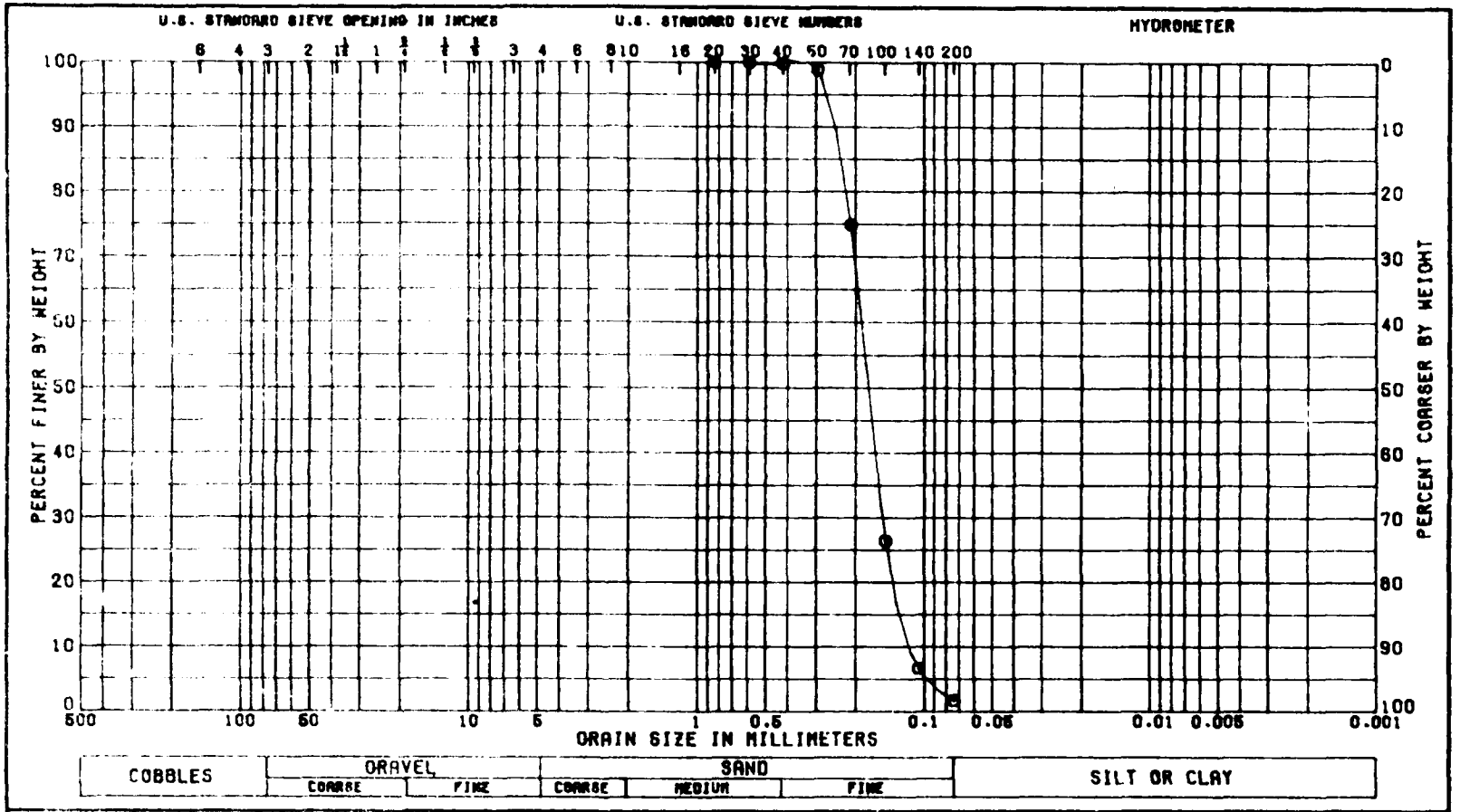
SILTY SAND (SM), BROWN

GRADATION CURVE

PROJECT LMVD FLOW SLIDE
BONNET CARRE

BORING NO. U1B SAMPLE NO. 12

DEPTH/ELEV 34' DATE 23 JUL 84

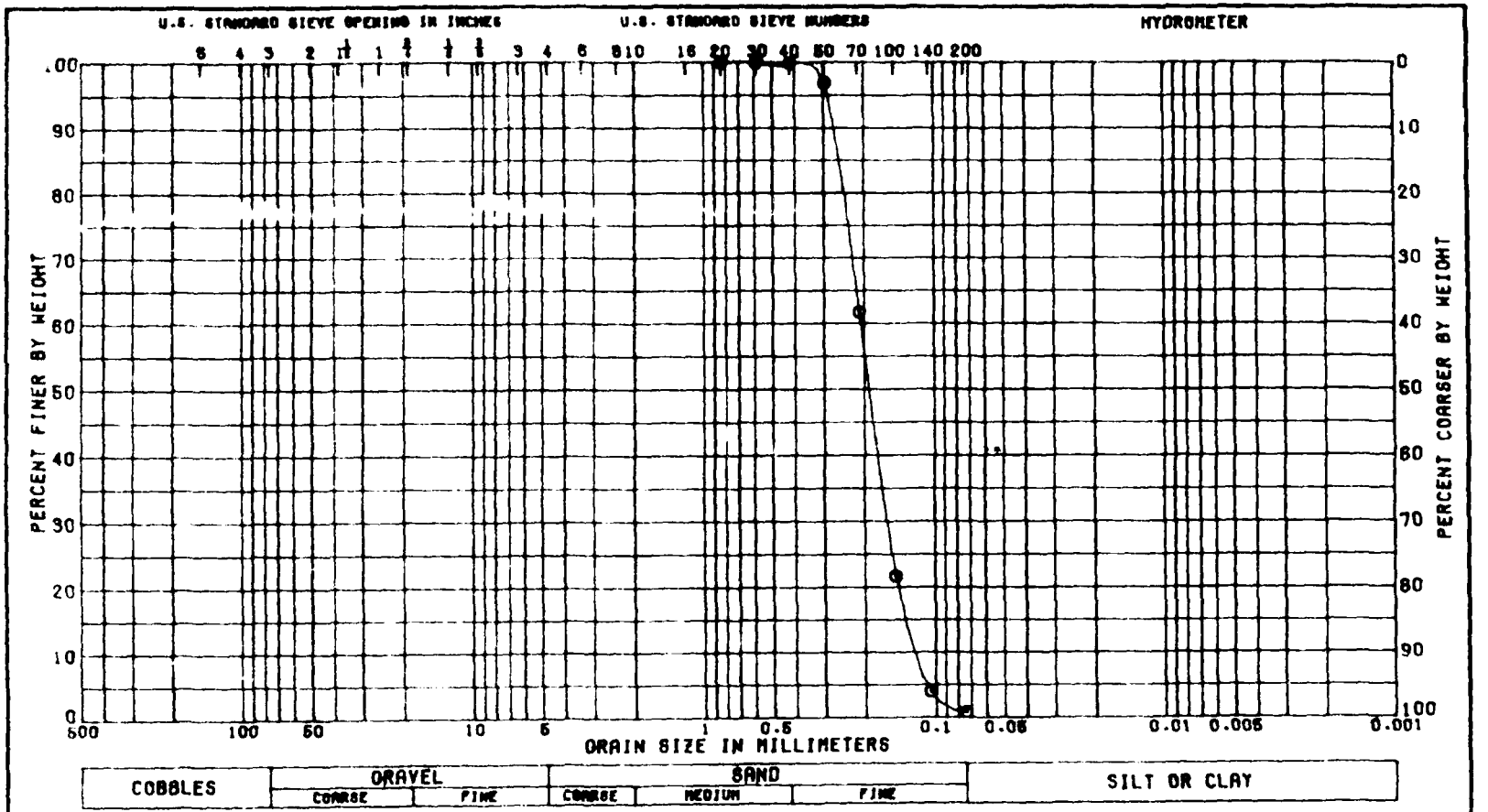


LL	PL	PI	GS	NAT W.%	

CLASSIFICATION

GRADATION CURVE

PROJECT LMVD FLOW SLIDE
BONNET CARRE
BORING NO. U1B SAMPLE NO. 18
DEPTH/ELEV 51' DATE 23 JUL 84



LL	PL	PI	OS	NAT W.%	

CLASSIFICATION

SAND (SP), BROWN

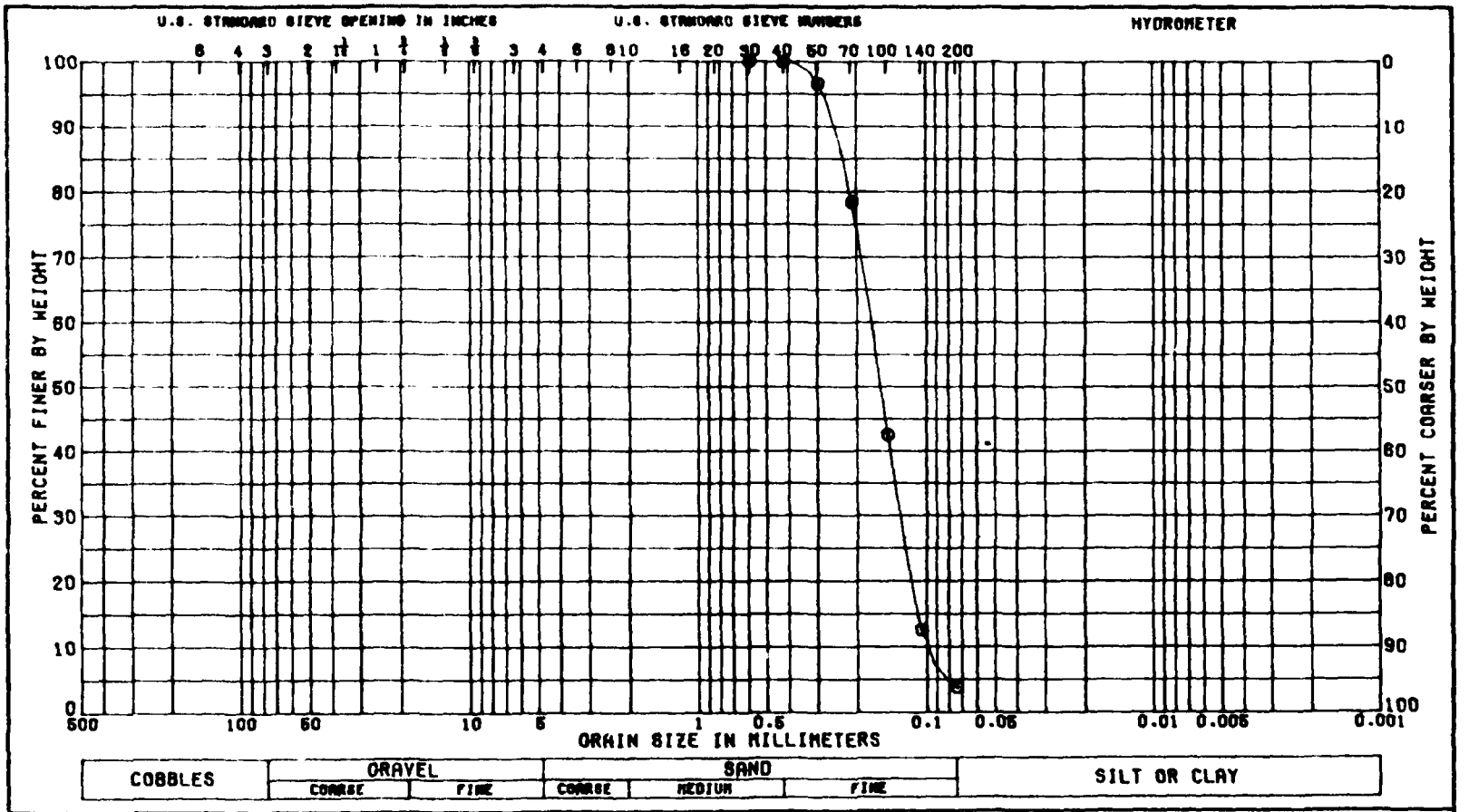
GRADATION CURVE

PROJECT LMVD FLOW SLIDE

BONNET CARRE

BORING NO. U18 SAMPLE NO. 22

DEPTH/ELEV 69' DATE 23 JUL 84



LL	PL	PI	OS	NAT M.C	

CLASSIFICATION

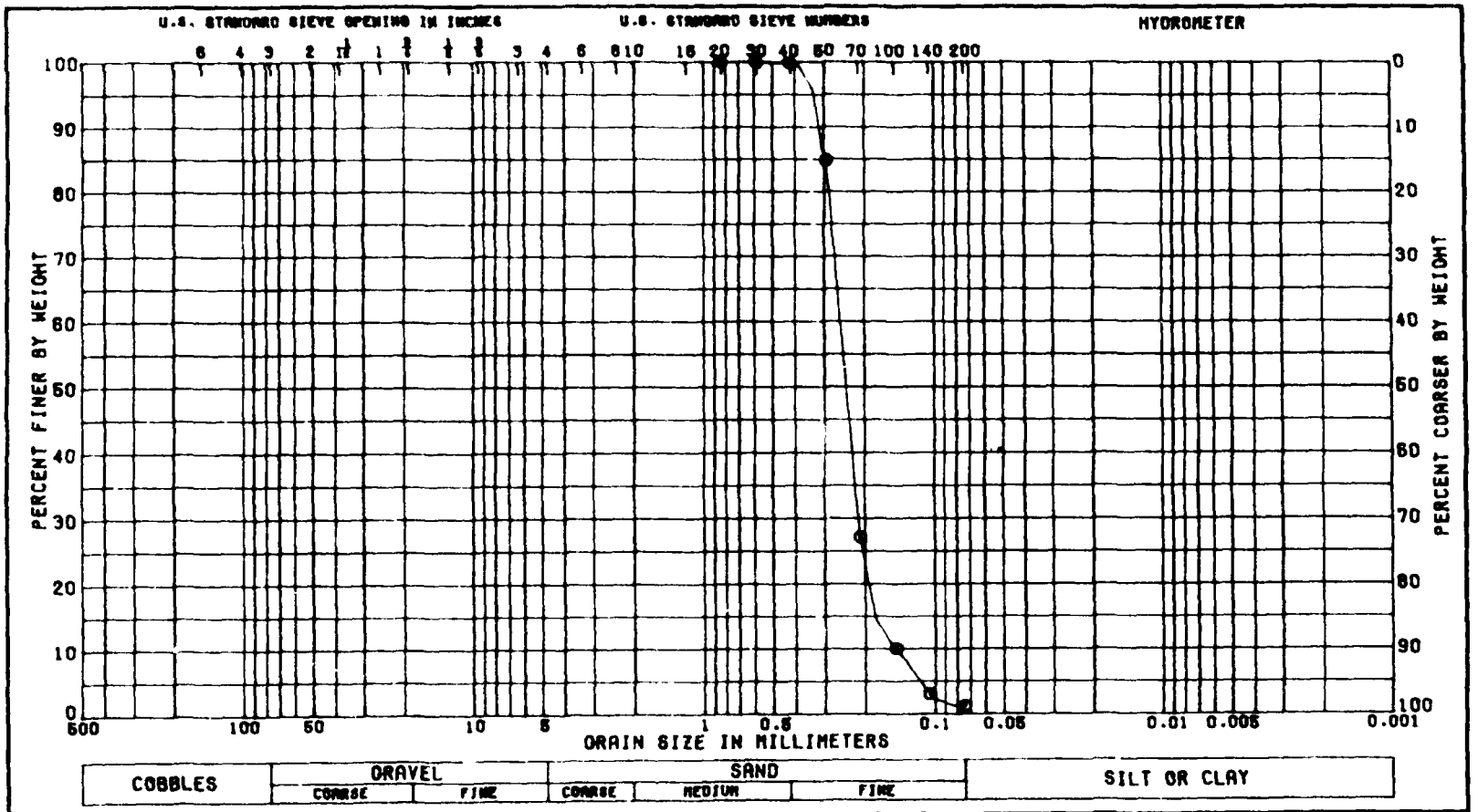
SAND (SP), BROWN

GRADATION CURVE

PROJECT LMVD FLOW SLIDE
BONNET CARRE

BORING NO. U1B SAMPLE NO. 24

DEPTH/ELEV 70' DATE 23 JUL 84



LL	PL	PI	OS	NAT W.%	

CLASSIFICATION

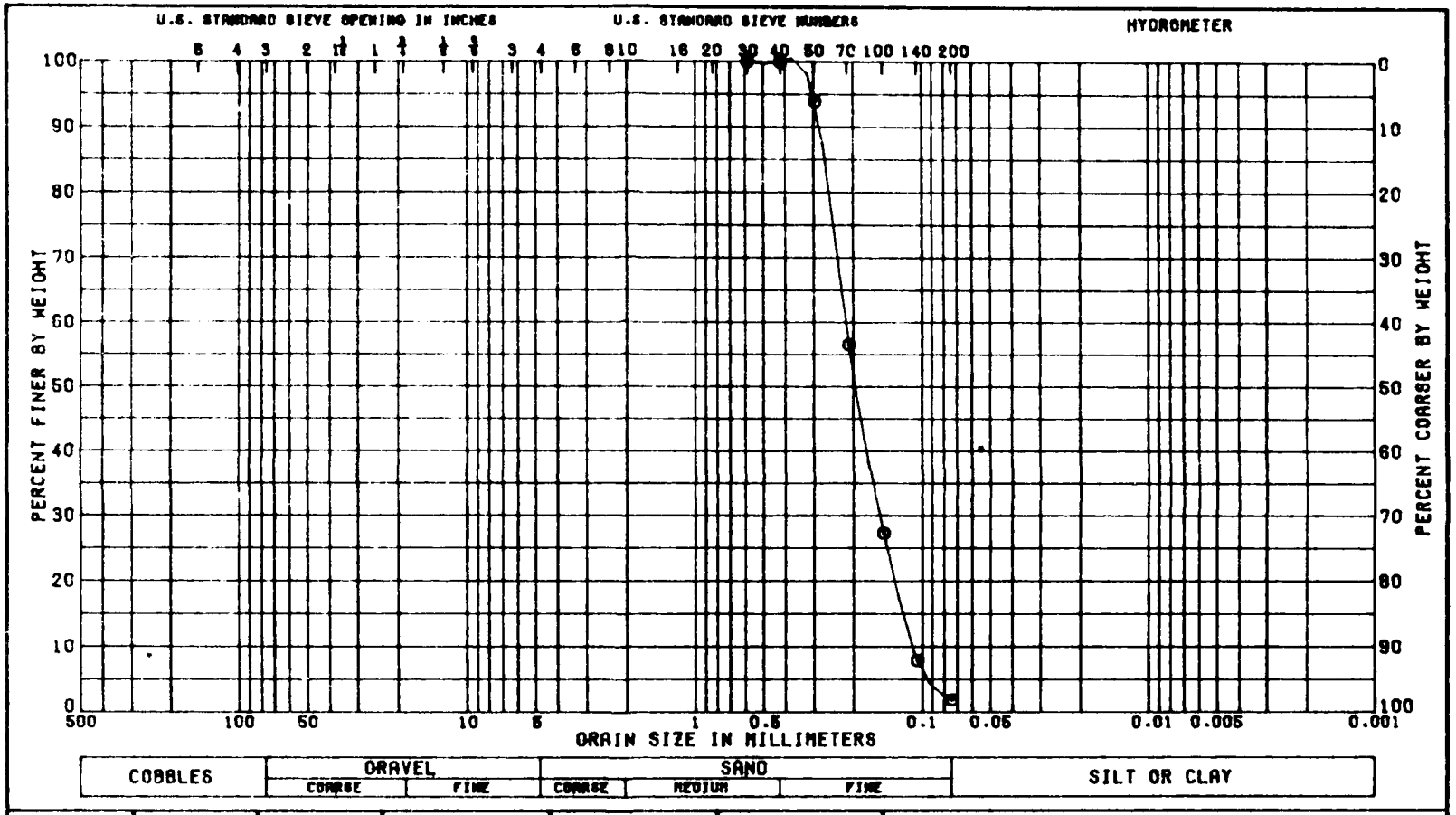
SAND (SP), BROWN

GRADATION CURVE

PROJECT LMVD FLOW SLIDE
BONNET CARRE

BORING NO. UIB SAMPLE NO. 28

DEPTH/ELEV 82' DATE 23 JUL 84



LL	PL	PI	OS	NAT W.%	

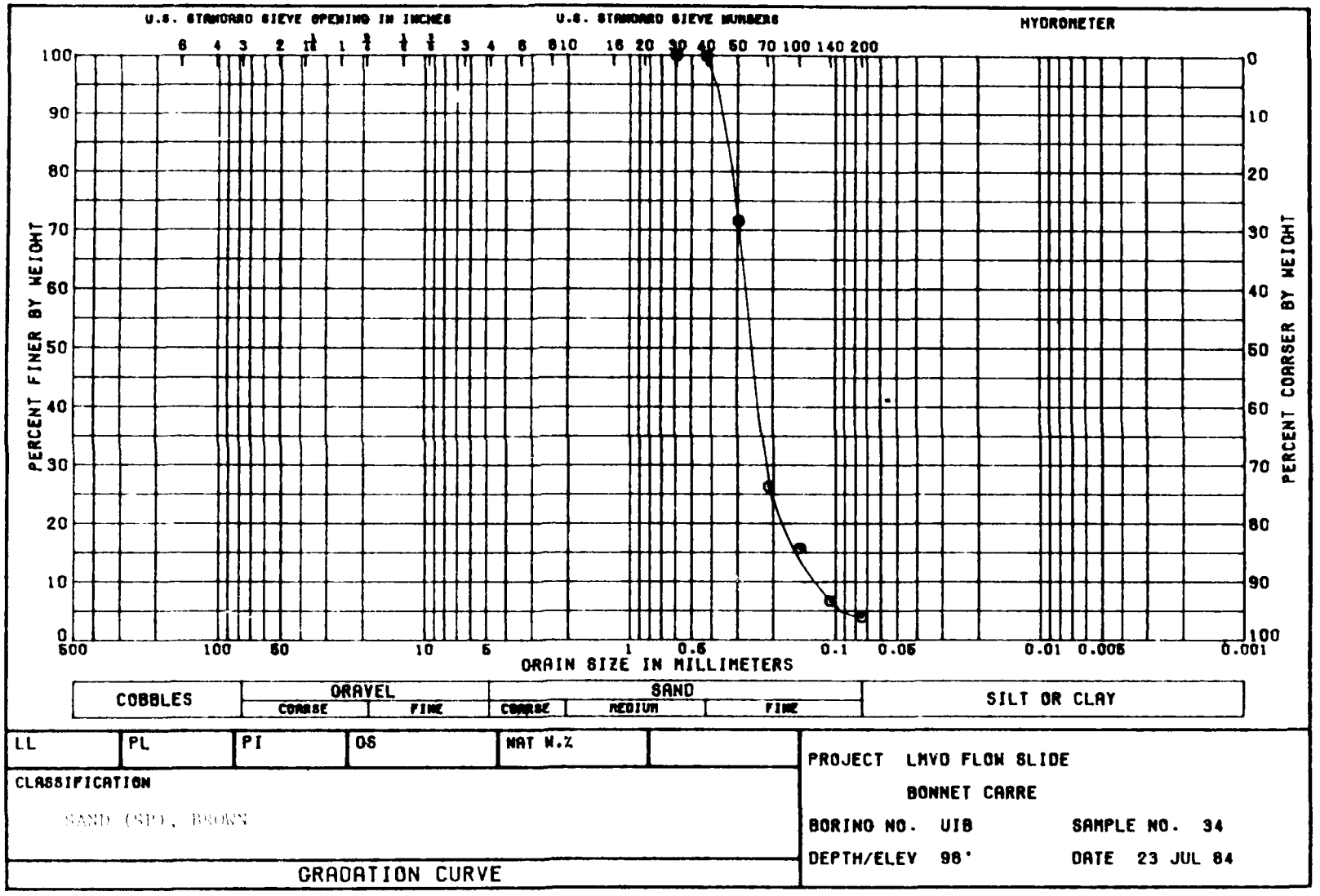
CLASSIFICATION

GRADATION CURVE

PROJECT LMVD FLOW SLIDE
BONNET CARRE

BORING NO. UIB SAMPLE NO. 30

DEPTH/ELEV 88' DATE 23 JUL 84



LL	PL	PI	OS	NAT W.%	

CLASSIFICATION

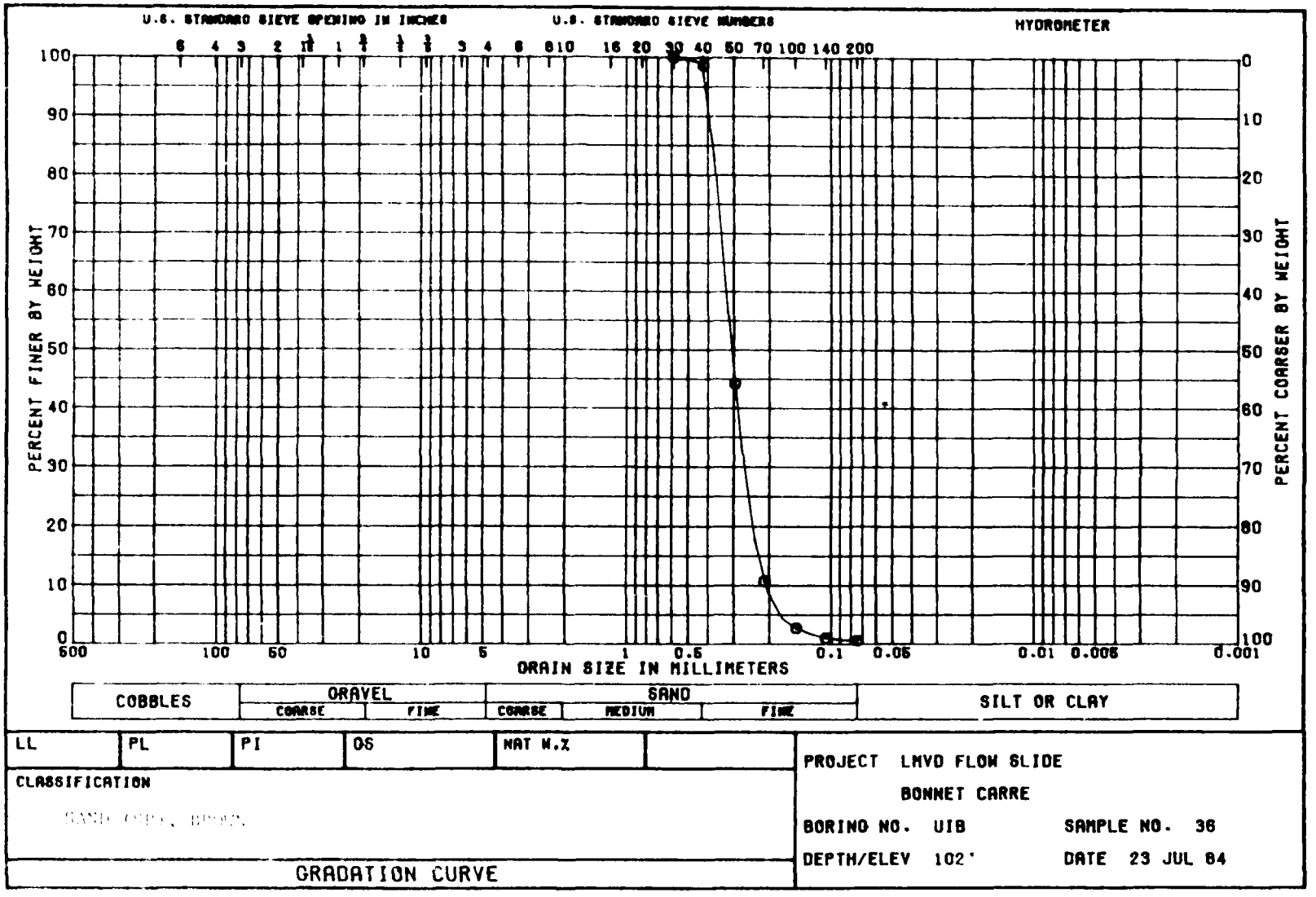
SAND (SP), BROWN

GRADATION CURVE

PROJECT LMVD FLOW SLIDE
BONNET CARRE

BORING NO. UIB SAMPLE NO. 34

DEPTH/ELEV 98' DATE 23 JUL 84



LL	PL	PI	OS	NAT W.%	

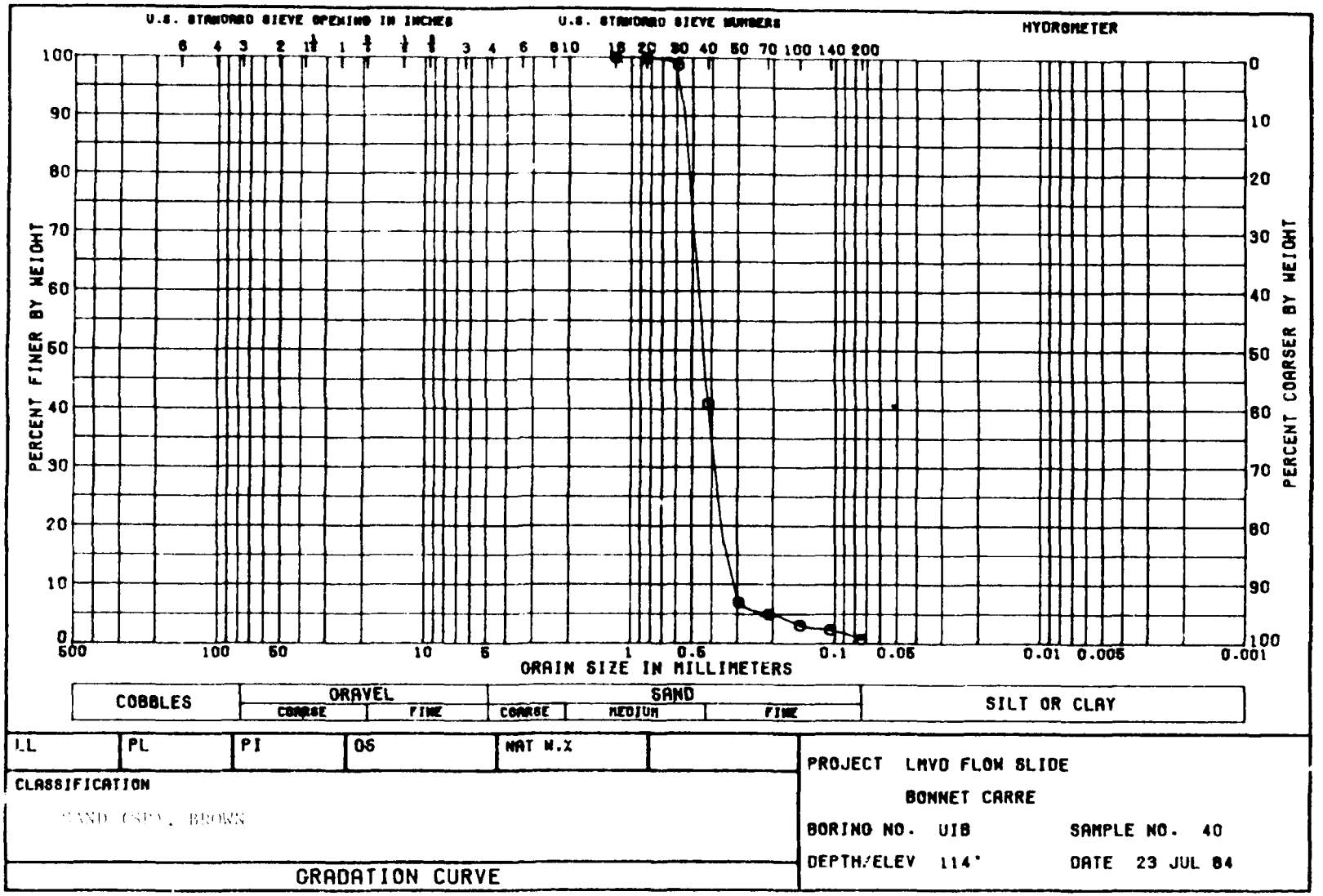
CLASSIFICATION

GRADATION CURVE

PROJECT LMVD FLOW SLIDE
BONNET CARRE

BORING NO. UIB SAMPLE NO. 36

DEPTH/ELEV 102' DATE 23 JUL 84



LL	PL	PI	OS	NAT W.%	

CLASSIFICATION

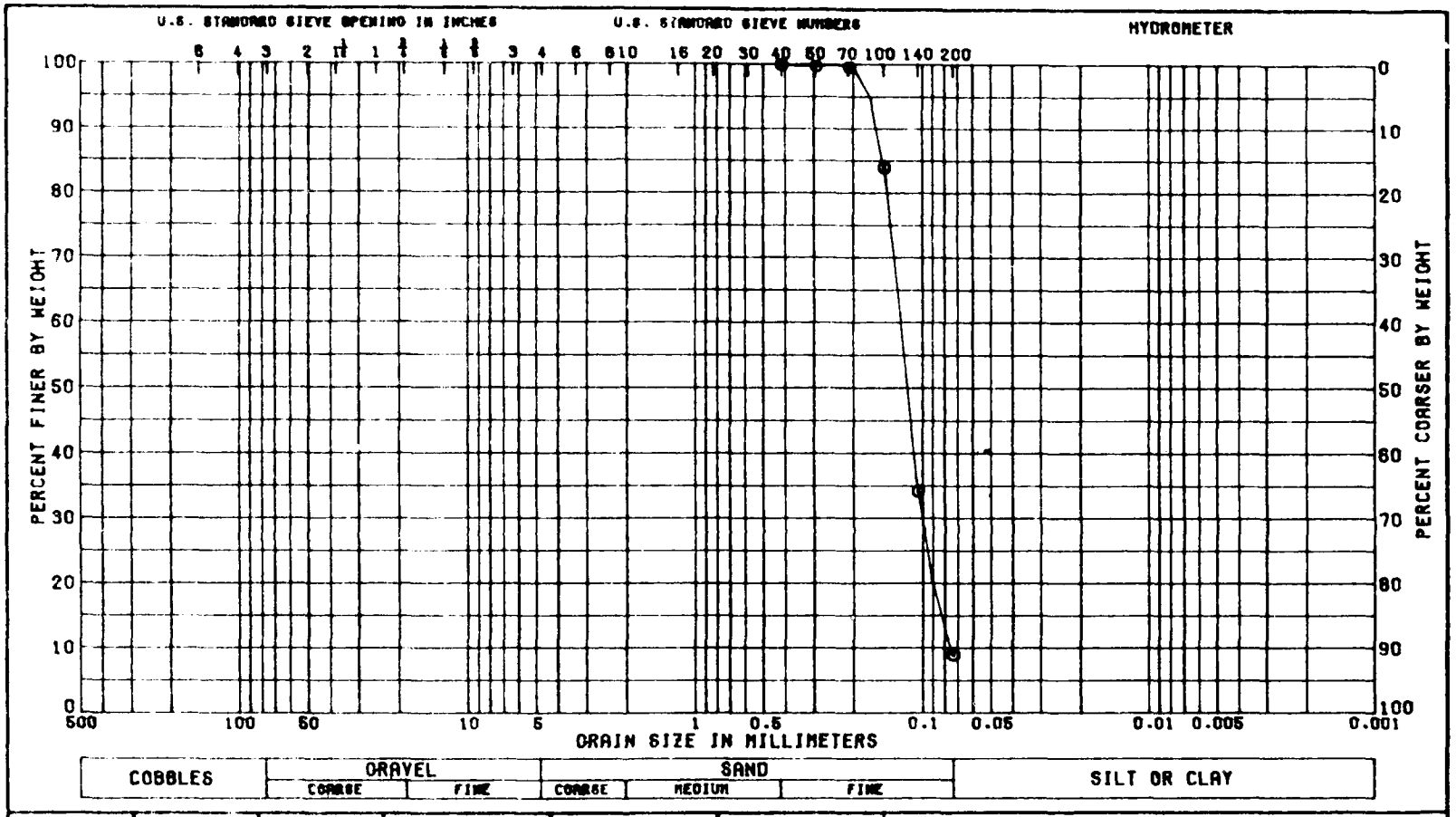
SAND (SP), BROWN

GRADATION CURVE

PROJECT LMVD FLOW SLIDE
BONNET CARRE

BORING NO. UIB SAMPLE NO. 40

DEPTH/ELEV 114' DATE 23 JUL 84



LL	PL	PI	OS	NAT W.%	

CLASSIFICATION

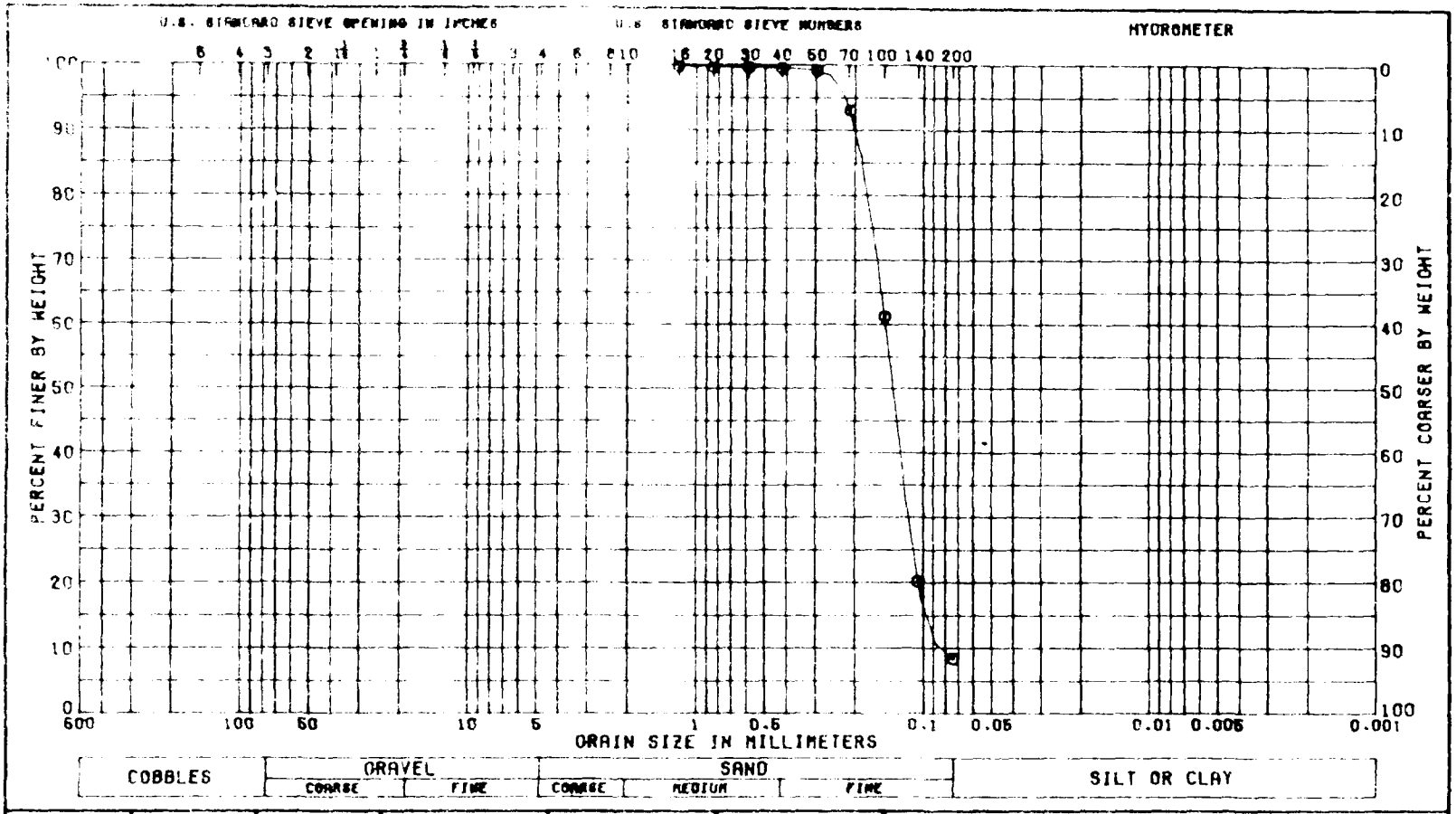
[illegible]

GRADATION CURVE

PROJECT LMVD FLOW SLIDE
BONNET CARRE

BORING NO. U3B SAMPLE NO. 2

DEPTH/ELEV 39' DATE 23 JUL 84



LL	PL	PI	OS	NAT M.%	

CLASSIFICATION

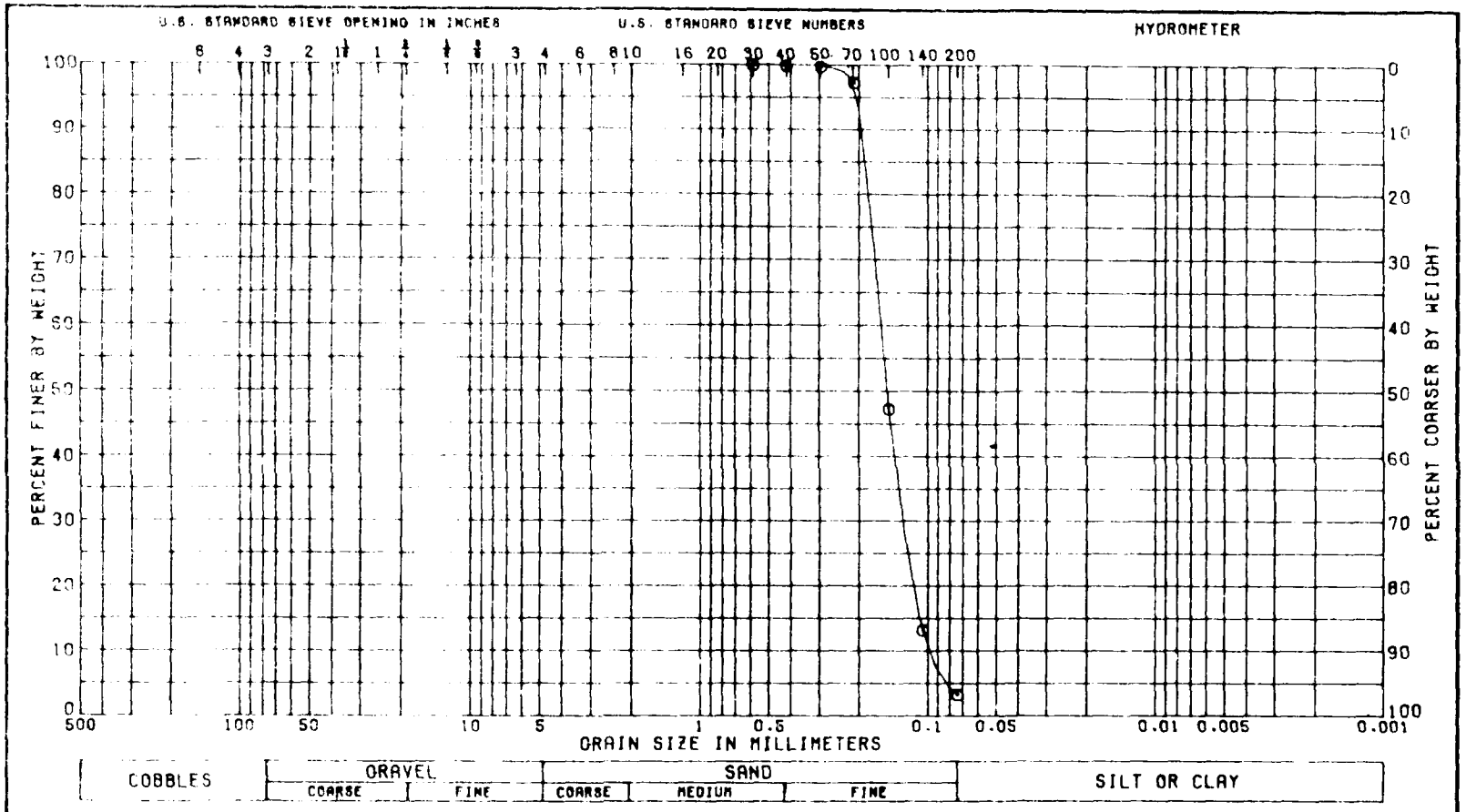
GRADATION CURVE

PROJECT LMVD FLOW SLIDE

BONNET CARRE

BORING NO. U3B SAMPLE NO. 4

DEPTH/ELEV 44' DATE 23 JUL 84



LL	PL	PI	OS	NAT W.%	

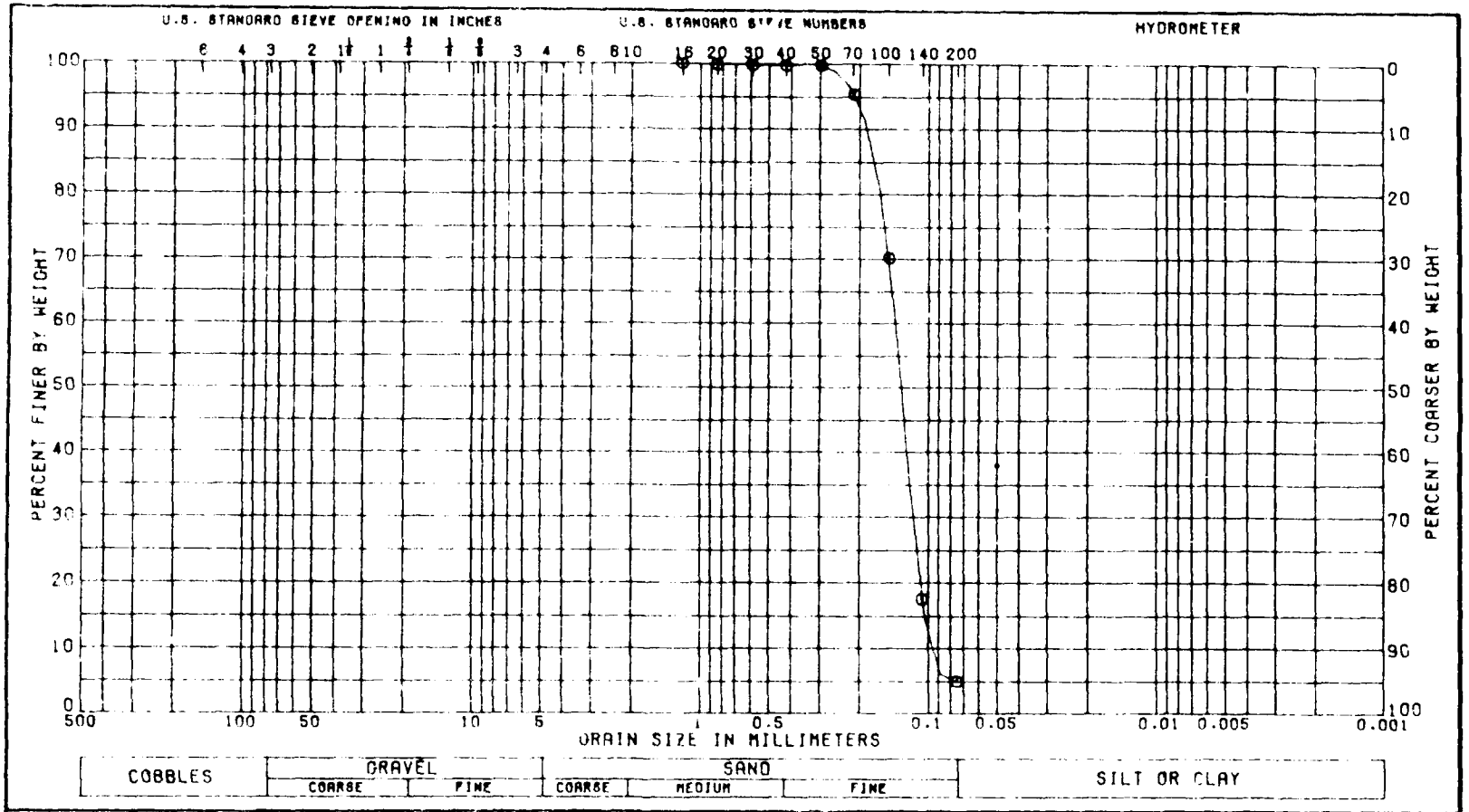
CLASSIFICATION

GRADATION CURVE

PROJECT LMVD FLOW SLIDE
BONNET CARRE

BORING NO. U38 SAMPLE NO. 5

DEPTH/ELEV 48' DATE 23 JUL 84



LL	PL	PI	OS	NAT W.%	

CLASSIFICATION

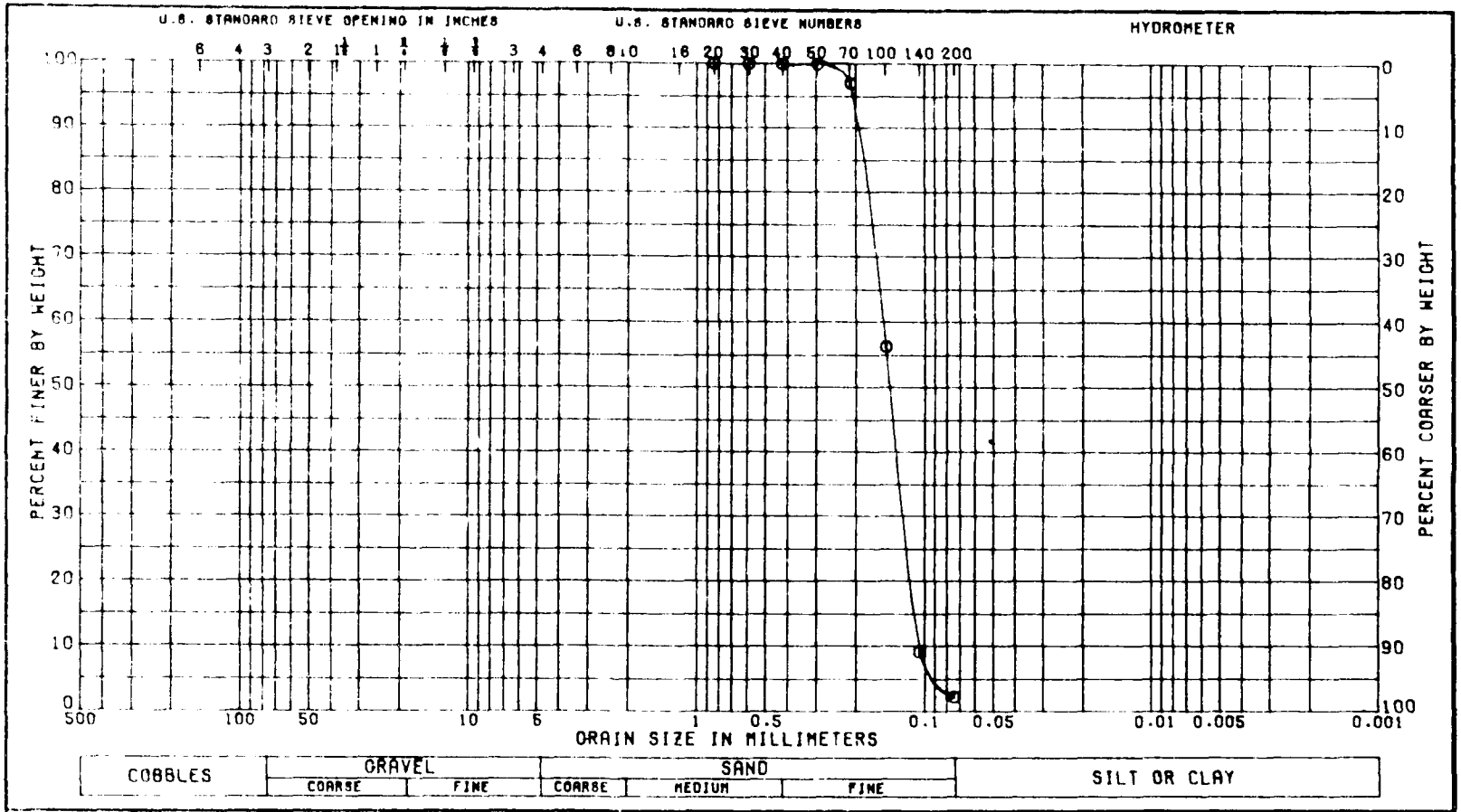
GRADATION CURVE

PROJECT LMVD FLOW SLIDE

BONNET CARRE

BORING NO. U3B SAMPLE NO. 7

DEPTH/ELEV 54' DATE 23 JUL 84



LL	PL	PI	GS	NAT W,%	

CLASSIFICATION

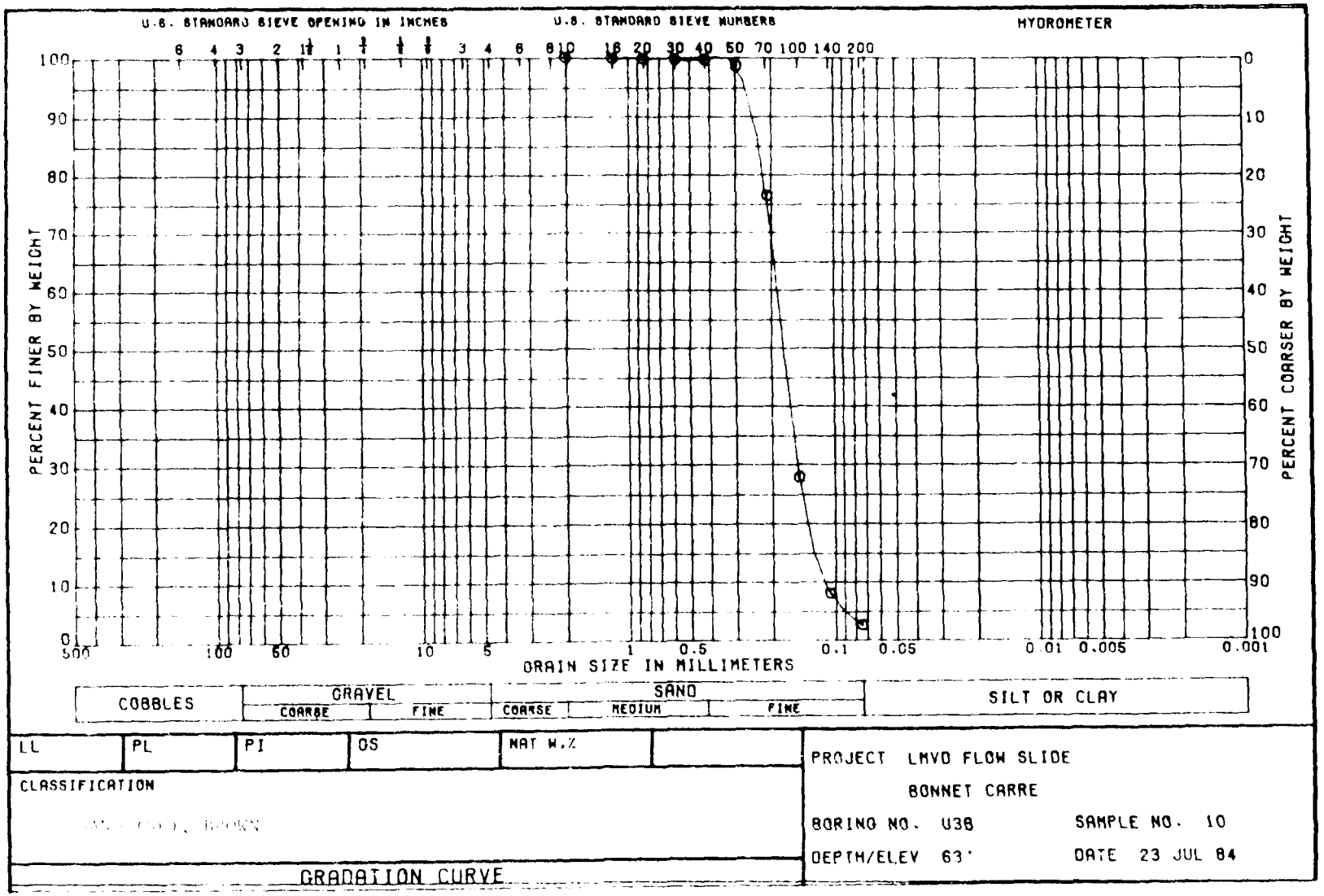
GRADATION CURVE

PROJECT LMVD FLOW SLIDE

BONNET CARRE

BORING NO. U3B SAMPLE NO. 8

DEPTH/ELEV 57' DATE 23 JUL 84



LL	PL	PI	OS	NAT W.%	

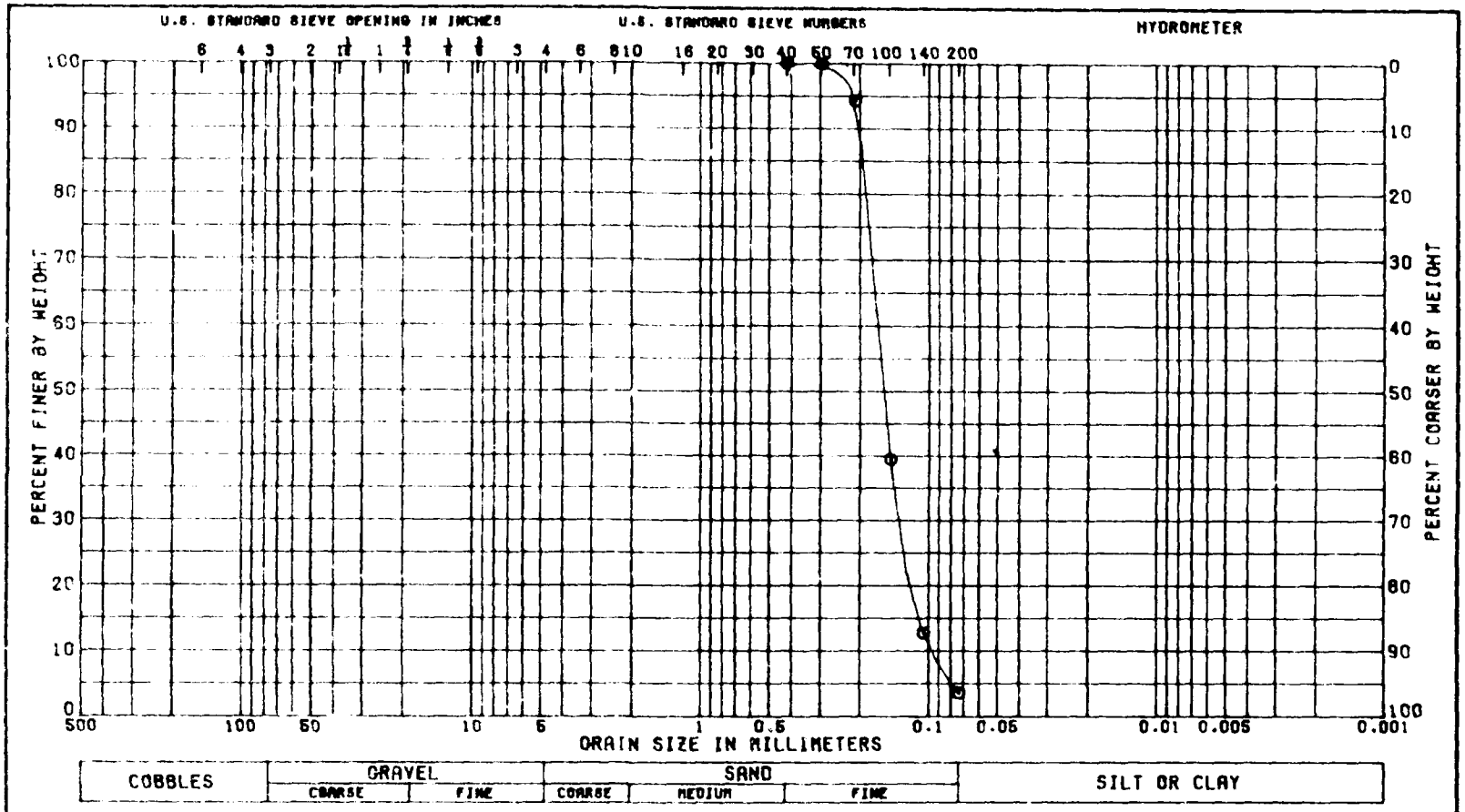
CLASSIFICATION

GRADATION CURVE

PROJECT LMVD FLOW SLIDE
BONNET CARRE

BORING NO. U38 SAMPLE NO. 10

DEPTH/ELEV 63' DATE 23 JUL 84



LL	PL	PI	OS	NAT W,%	

CLASSIFICATION

GRADATION CURVE

PROJECT LMVD FLOW SLIDE
BONNET CARRE

BORING NO. UIB SAMPLE NO. 14

DEPTH/ELEV 40' DATE 23 JUL 84

APPENDIX M

POTAMOLOGY METHODS FOR OBTAINING LABORATORY MAXIMUM AND MINIMUM DENSITIES

The standard procedures used in the Waterways Experiment Station soils laboratory to determine maximum and minimum densities at the beginning of the potamology investigations were as follows:

a. Maximum density. Oven-dry sand was compacted in a 2-in.-diam by 4-in.-high mold with a 2-in.-high detachable collar in four 100-g layers by 25 blows per layer of a 4-lb hammer falling 12 in. The diameter of the face of the hammer was 1-3/4 in. Then the collar was removed, the excess material struck off with a steel straightedge, and the density computed on the basis of the volume of the mold and weight of dry material.

b. Minimum density. Oven-dry sand was poured into the same mold (without the collar) from a constant height; the height was controlled by pouring into a small funnel with a 6-in. plastic tube attached to the stem. The bottom of the tube was held 1/2 in. above the surface of the sand in the mold. The intensity of deposition was controlled by keeping the funnel filled to a constant level. The surface was struck off and the density computed as in the case of the maximum density.

APPENDIX N

CRITICAL VOID RATIO TRIAXIAL TEST SERIES, MONTZ COMPOSITE SAND

DEFINITION OF TERMS

σ_{1c} = Vertical consolidation stress, tsf

σ_{3c} = Horizontal consolidation stress, tsf

$\bar{\sigma}$ = Minimum effective confining stress during liquefaction of a specimen

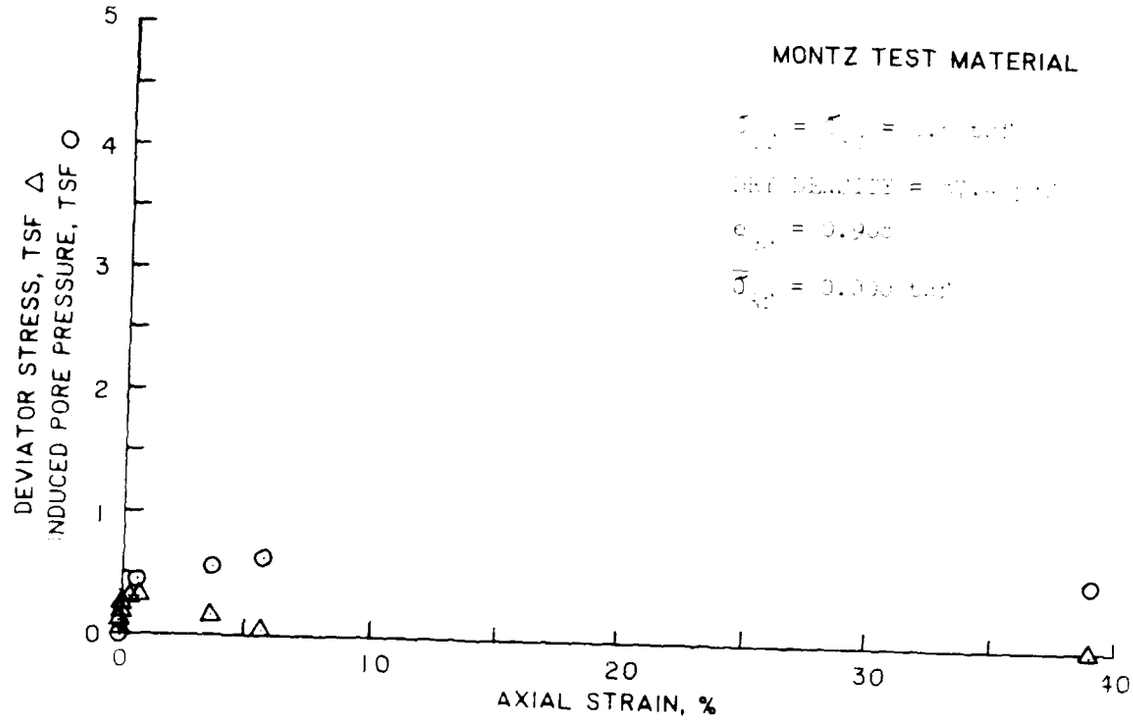
σ_{df} = Minimum deviator stress corresponding to σ_{3f}

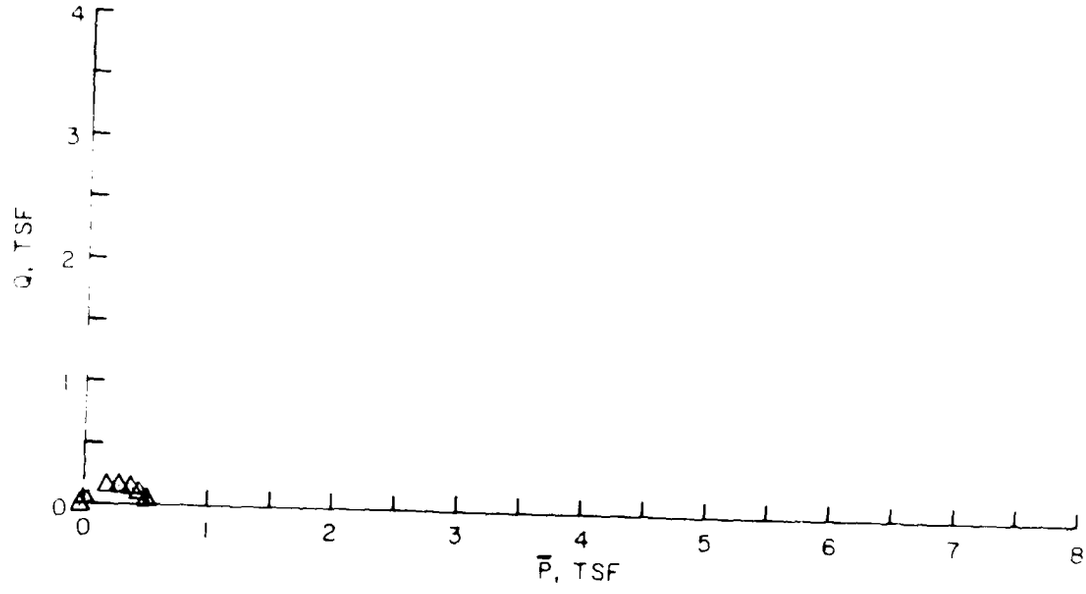
e_{cc} = Corrected void ratio after consolidation. Since specimens were reconstituted in 6 layers, the measured void ratio after consolidation is a gross value which may or may not be consistent with observed values of $\bar{\sigma}_{3f}$ and σ_{df}. e_{cc} is determined by using the results of all tests in the critical void ratio series to adjust measured values of void ratio after consolidation to produce a consistent trend among e_{cc}, $\bar{\sigma}_{3f}$ and $\bar{\sigma}_{df}$. This data smoothing procedure is particularly necessary when the critical void ratio curve is so flat in slope that very small differences in void ratio produce relatively large differences in $\bar{\sigma}_{3f}$ and σ_{df}

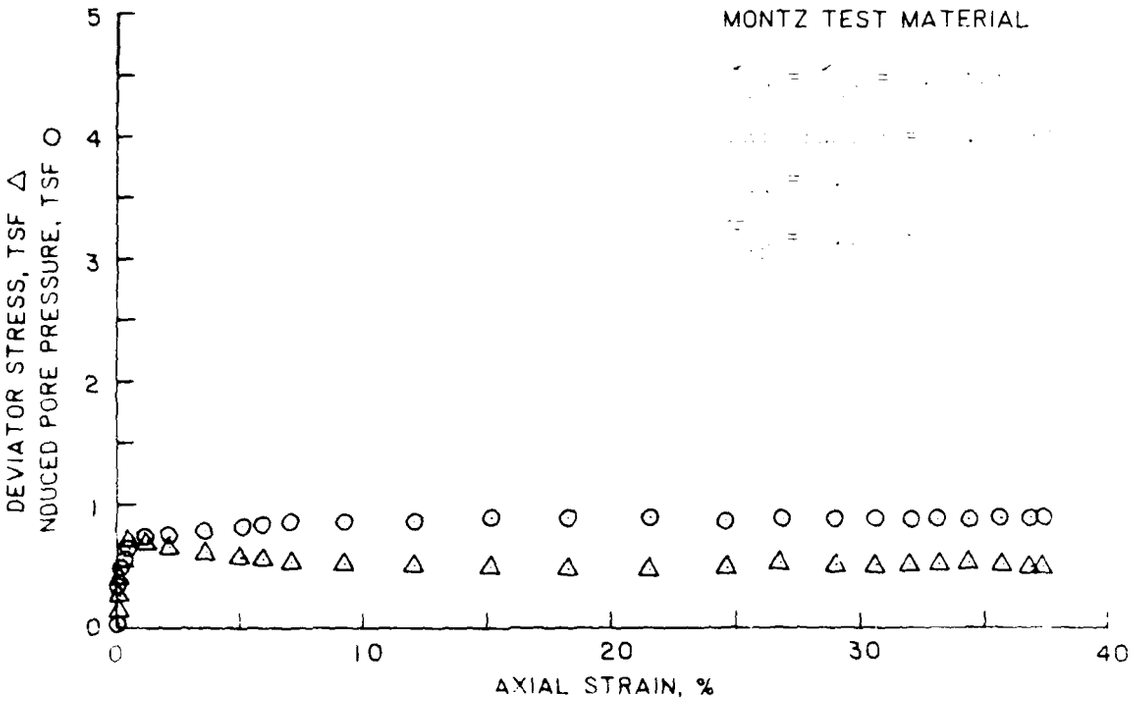
FOR THE EFFECTIVE STRESS PATH:

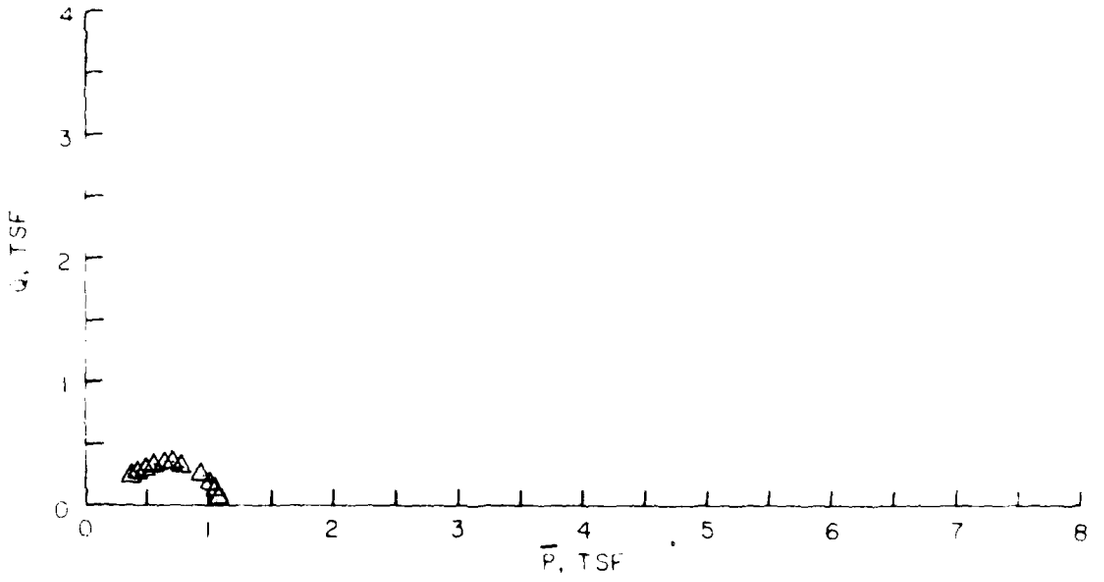
$$Q = \frac{(\sigma_1 - \sigma_3)}{2}$$

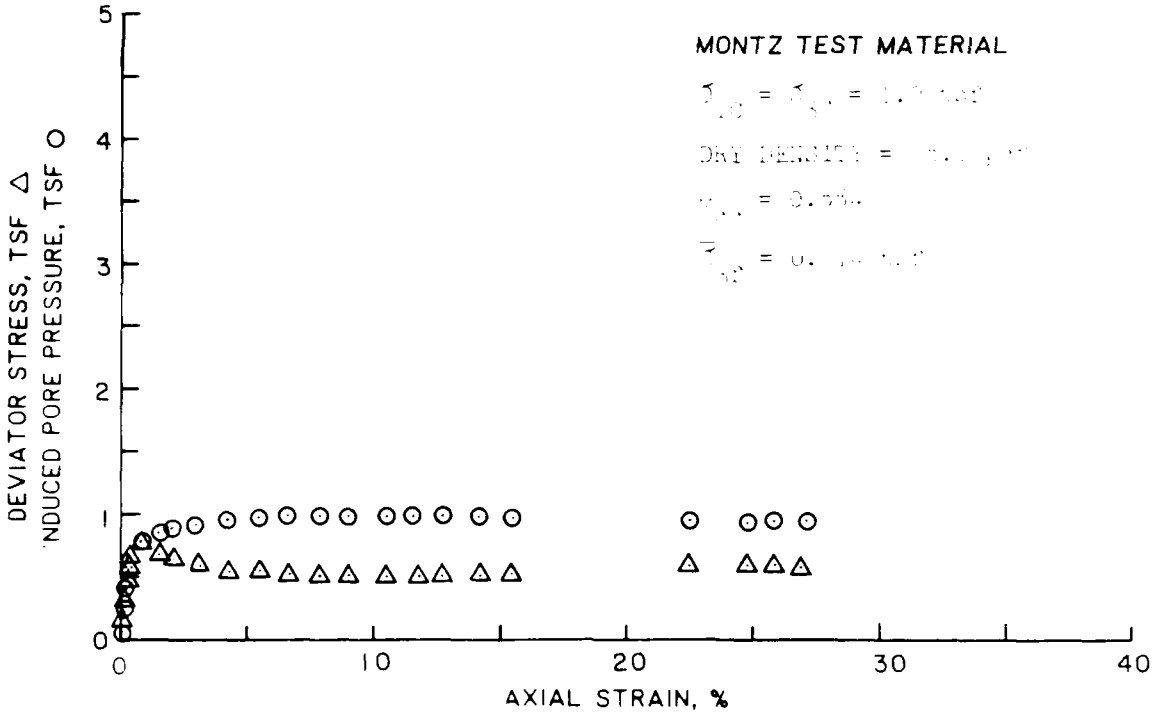
$$\bar{P} = \frac{(\bar{\sigma}_1 + \bar{\sigma}_3)}{2}$$

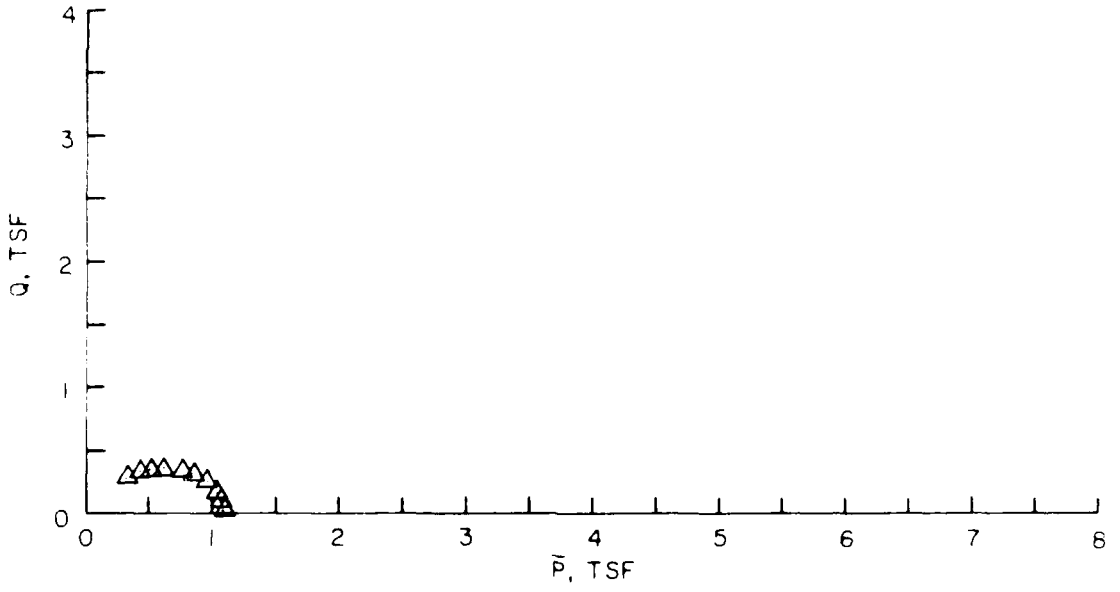

MONTZ TEST MATERIAL
DEVIATOR STRESS, TSF Δ
INDUCED PORE PRESSURE, TSF O
AXIAL STRAIN, %
0
10
20
30
40
1
2
3
4
5

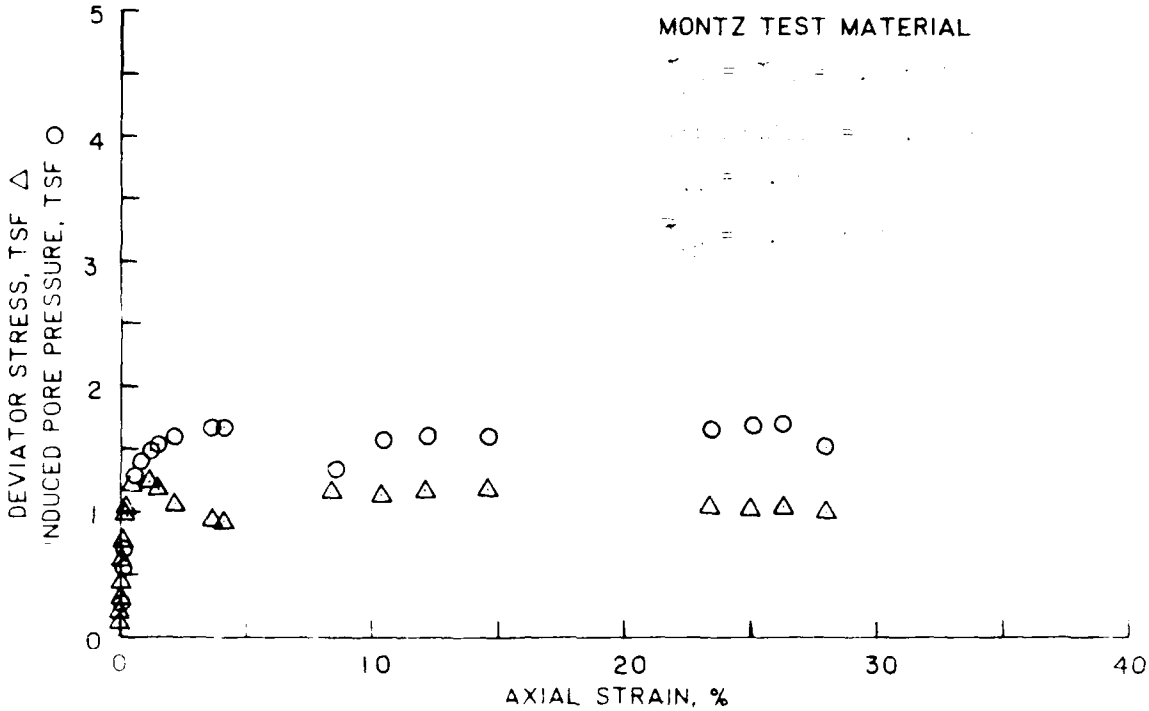

Q, TSF
P̄, TSF
0
1
2
3
4
5
6
7
8

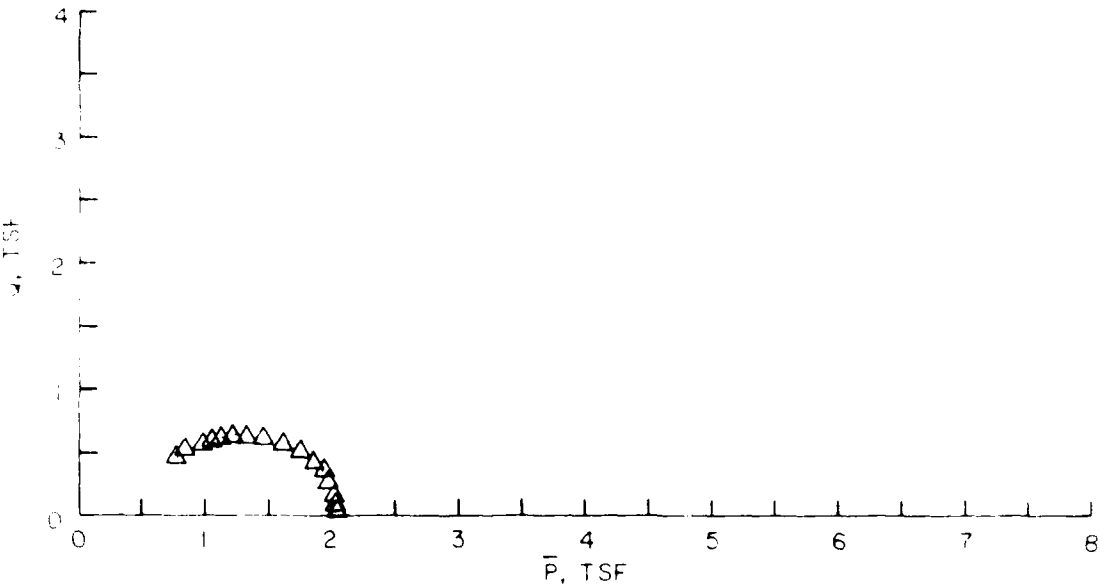

MONTZ TEST MATERIAL
DEVIATOR STRESS, TSF Δ
NDUCED PORE PRESSURE, TSF O
0
1
2
3
4
5
0
10
20
30
40
AXIAL STRAIN, %

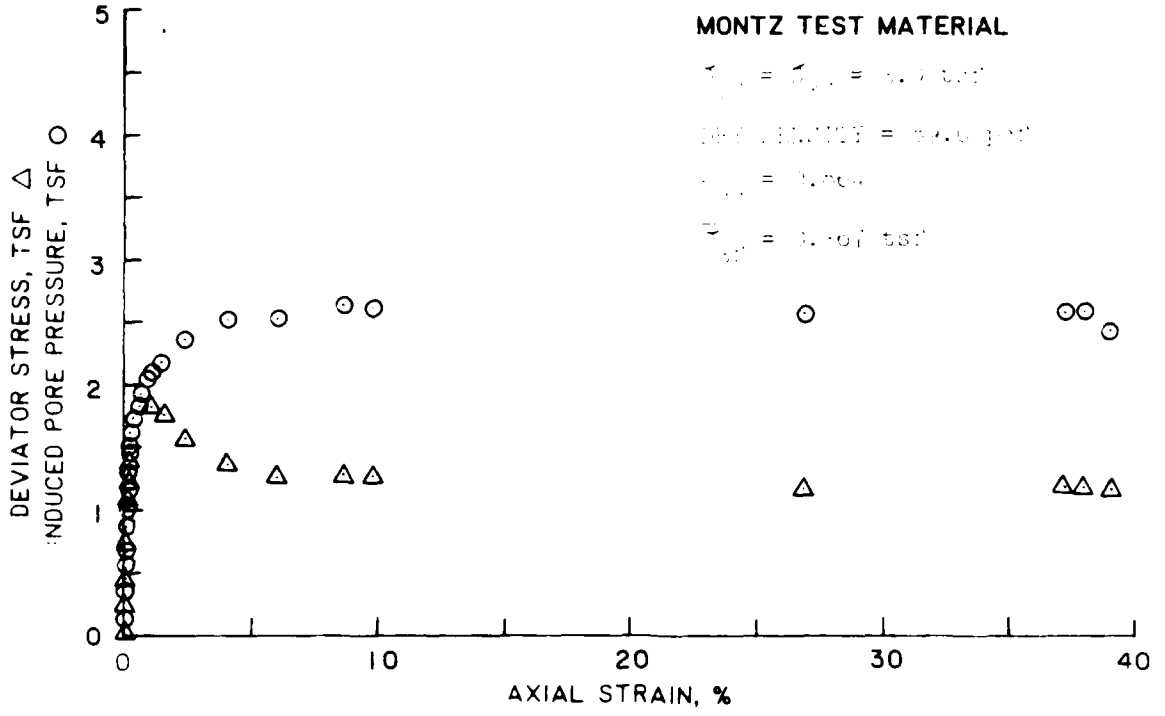

4
3
2
1
0
0
1
2
3
4
5
6
7
8
P, TSF

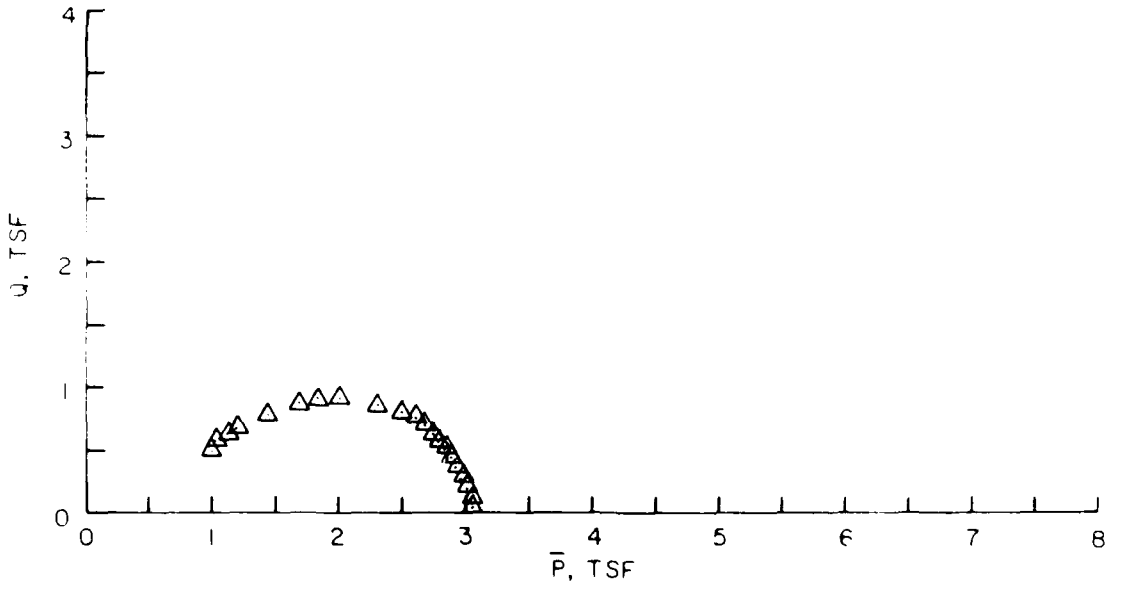

MONTZ TEST MATERIAL
DEVIATOR STRESS, TSF Δ
INDUCED PORE PRESSURE, TSF O
AXIAL STRAIN, %
0
10
20
30
40
1
2
3
4
5

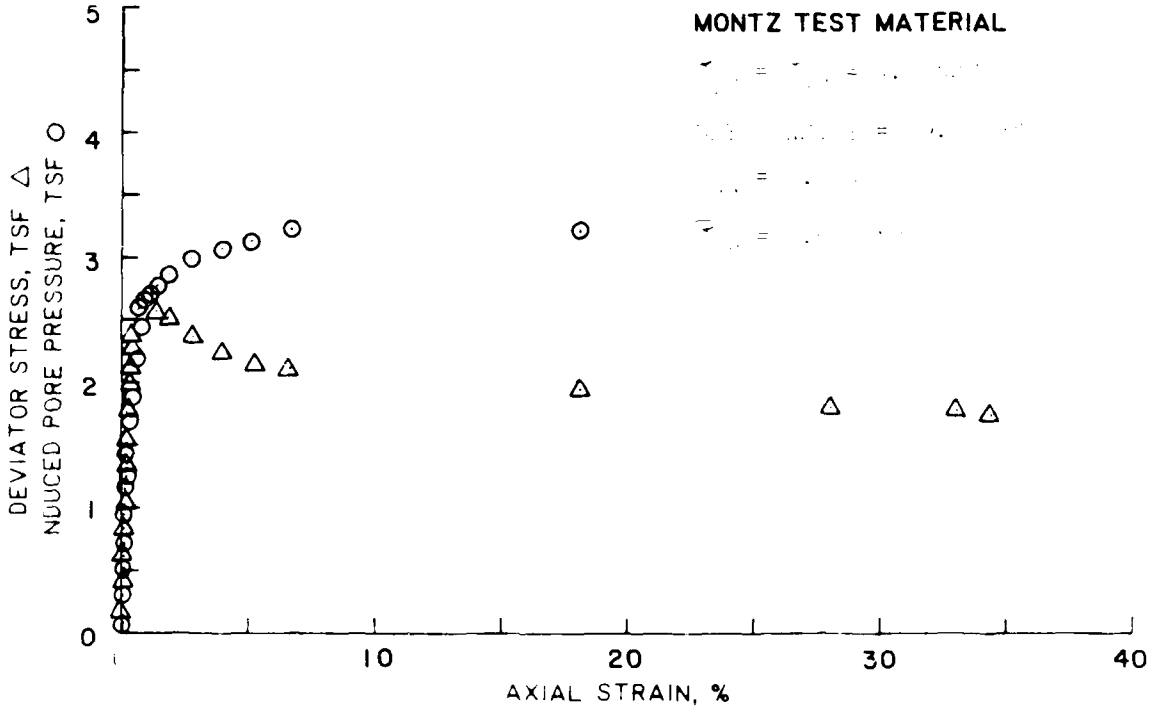

Q, TSF
P̃, TSF
0
1
2
3
4
5
6
7
8

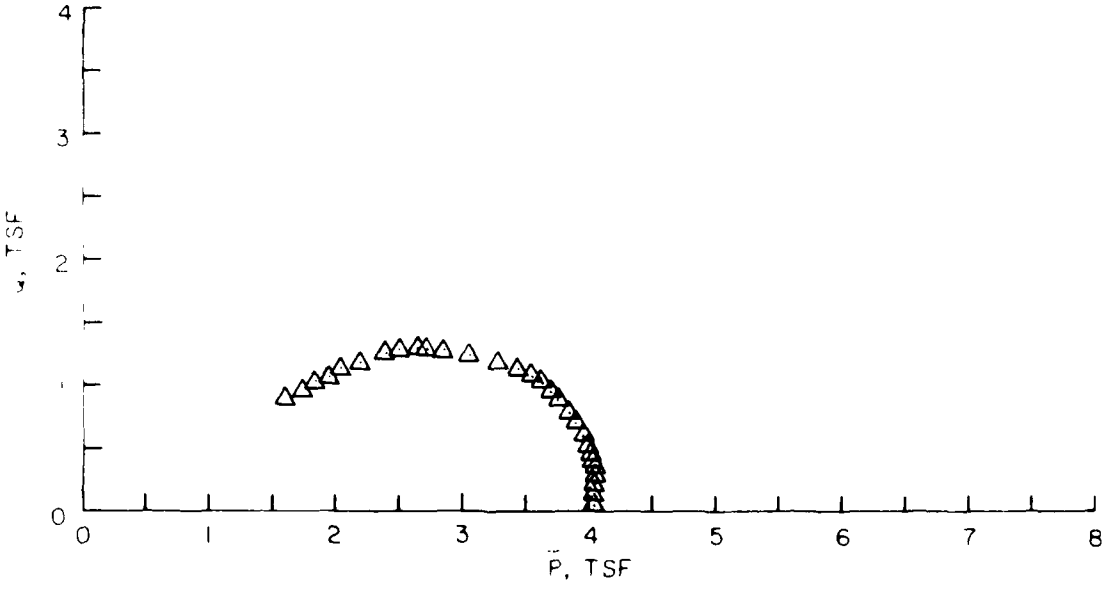

MONTZ TEST MATERIAL
DEVIATOR STRESS, TSF △
INDUCED PORE PRESSURE, TSF ○
0
1
2
3
4
5
0
10
20
30
40
AXIAL STRAIN, %

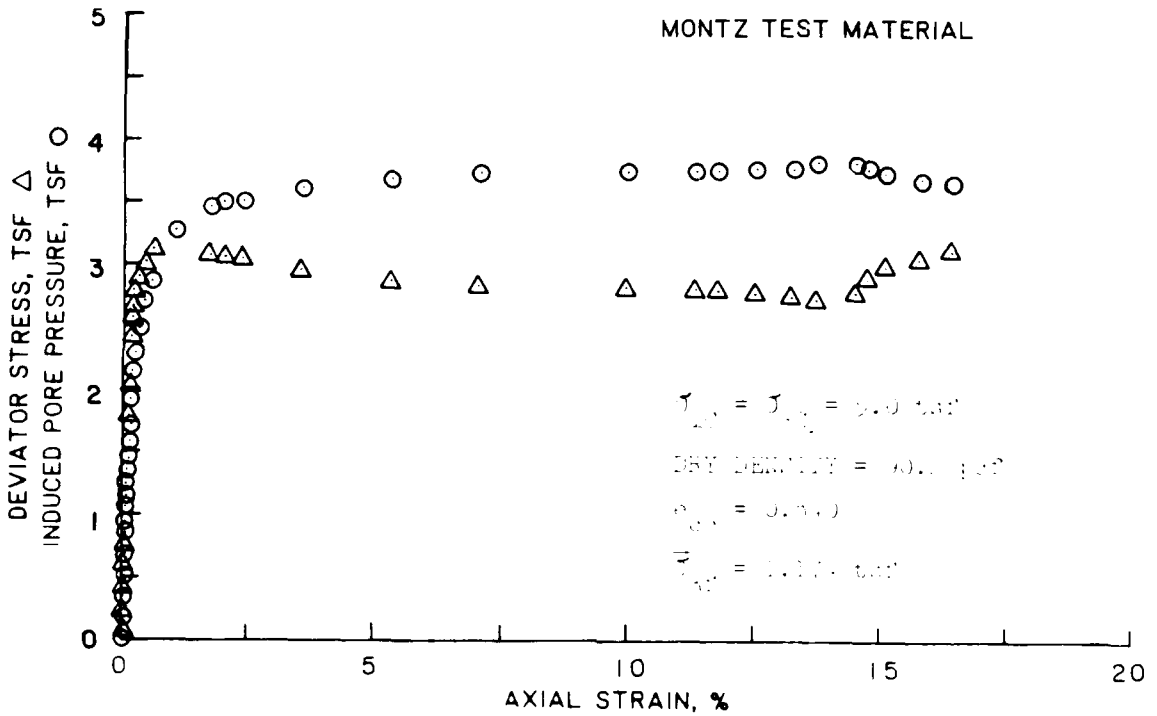

0
1
2
3
4
0
1
2
3
4
5
6
7
8
P̄, TSF

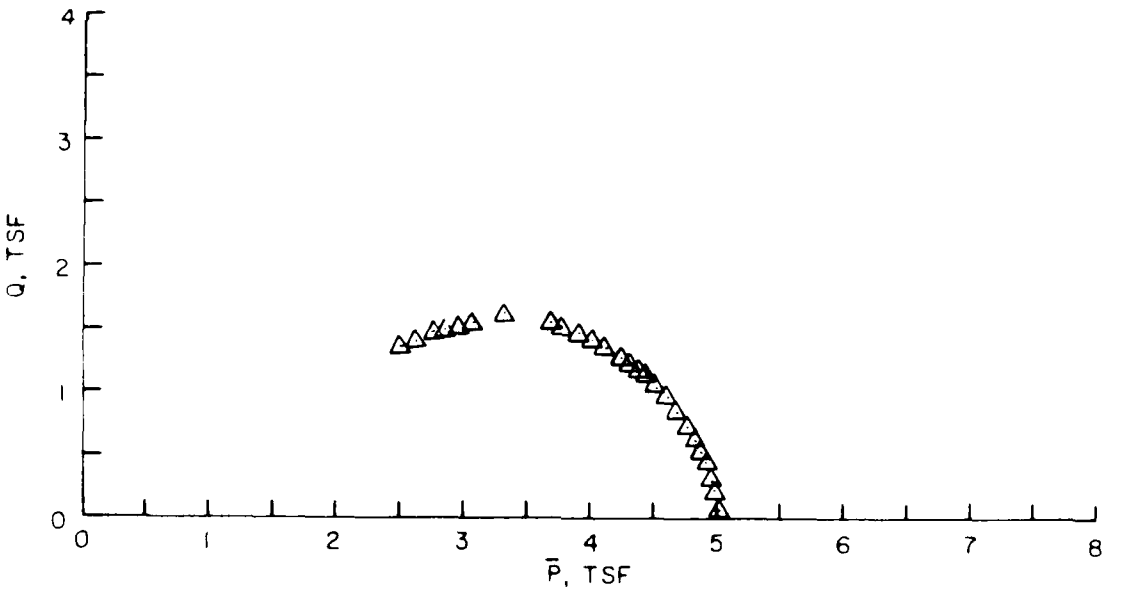

MONTZ TEST MATERIAL
DEVIATOR STRESS, TSF △
INDUCED PORE PRESSURE, TSF ○
AXIAL STRAIN, %
0
10
20
30
40
1
2
3
4
5


q, TSF
P̄, TSF
0
1
2
3
4
5
6
7
8


MONTZ TEST MATERIAL
DEVIATOR STRESS, TSF △
NUUCED PORE PRESSURE, TSF O
0
1
2
3
4
5
10
20
30
40
AXIAL STRAIN, %

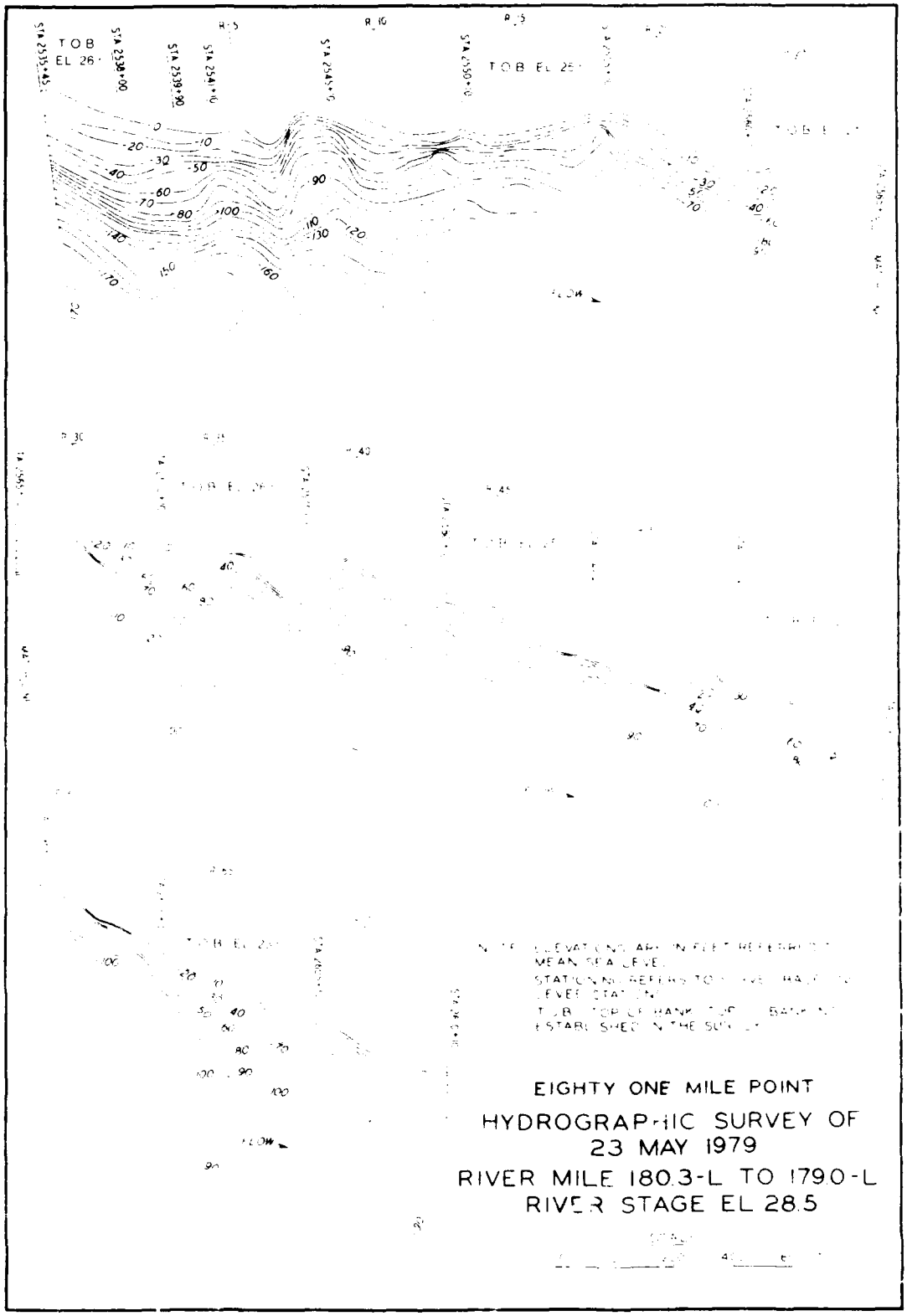

0
1
2
3
4
5
6
7
8
P, TSF

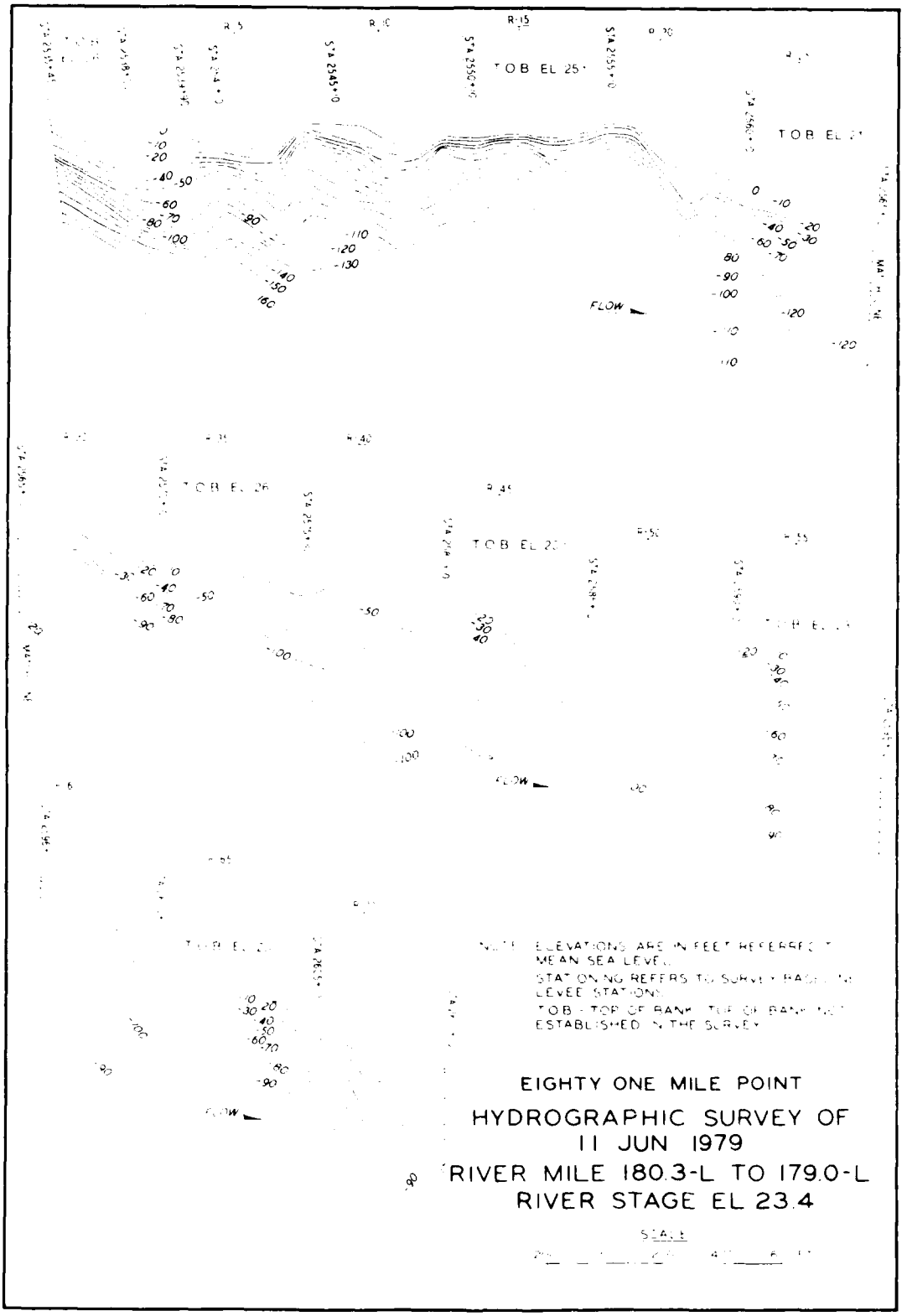

MONTZ TEST MATERIAL
DEVIATOR STRESS, TSF △
INDUCED PORE PRESSURE, TSF ○
AXIAL STRAIN, %
0
5
10
15
20
1
2
3
4
5

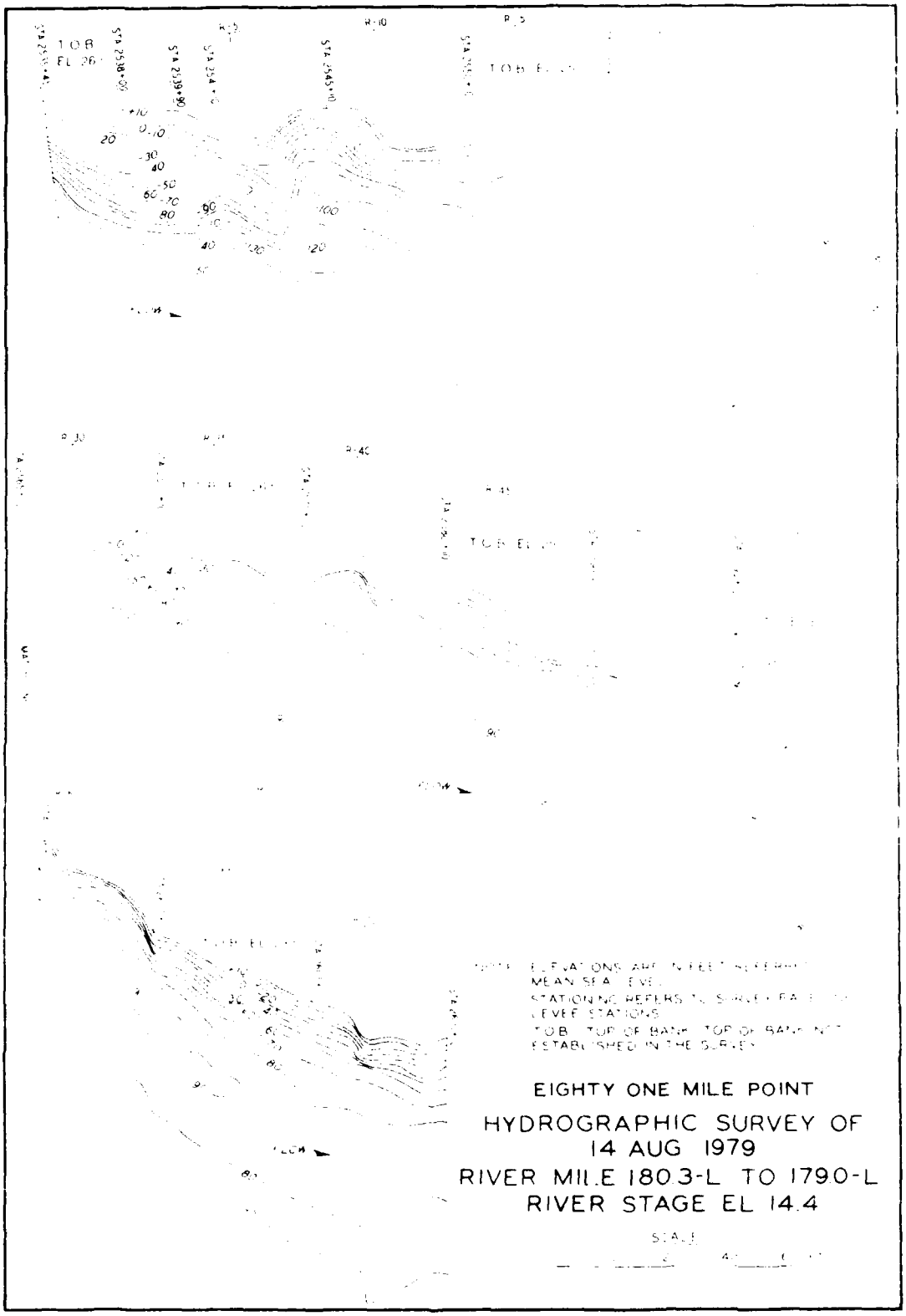

Q, TSF
$\bar{P}$, TSF
0
1
2
3
4
5
6
7
8

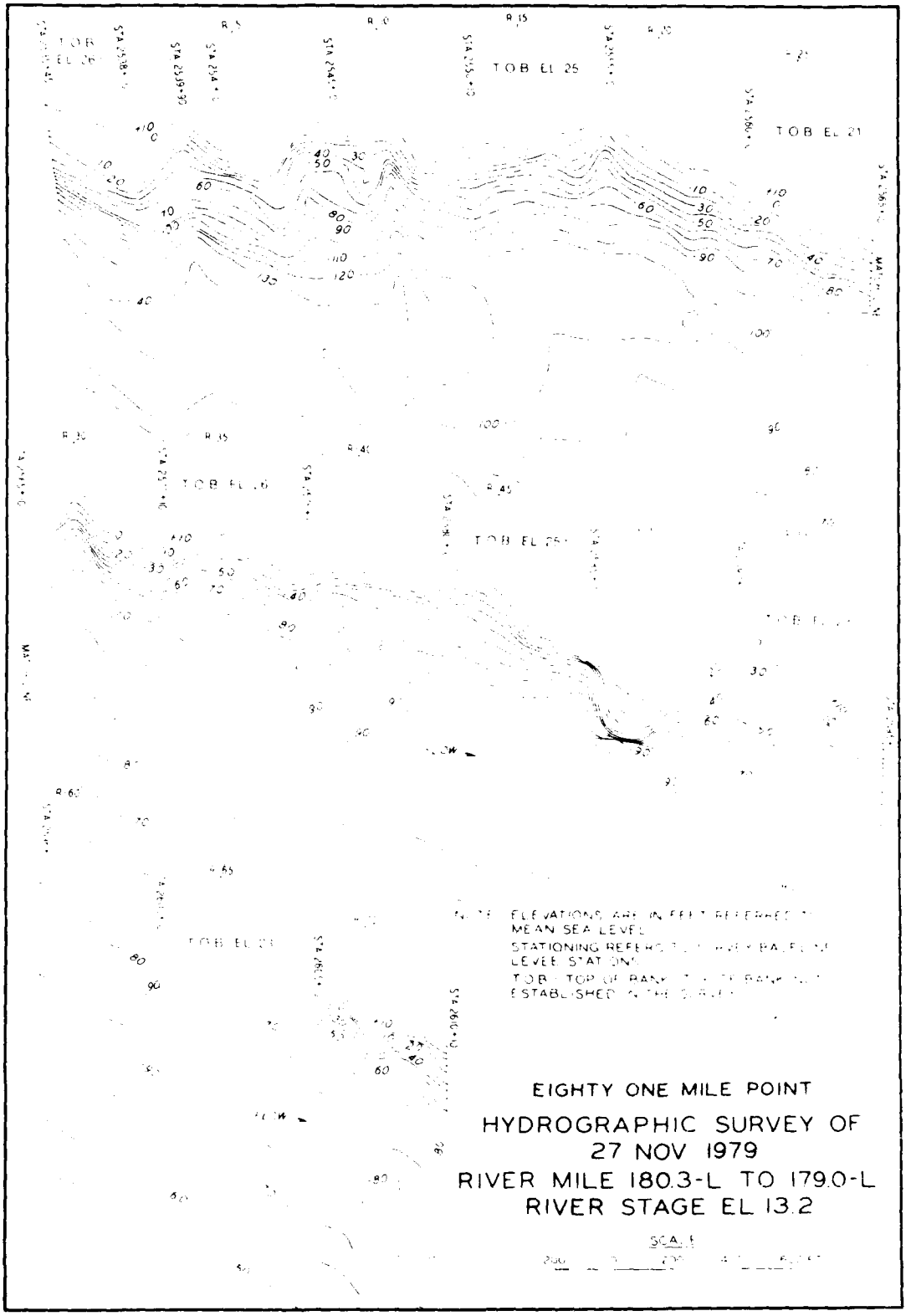
APPENDIX O

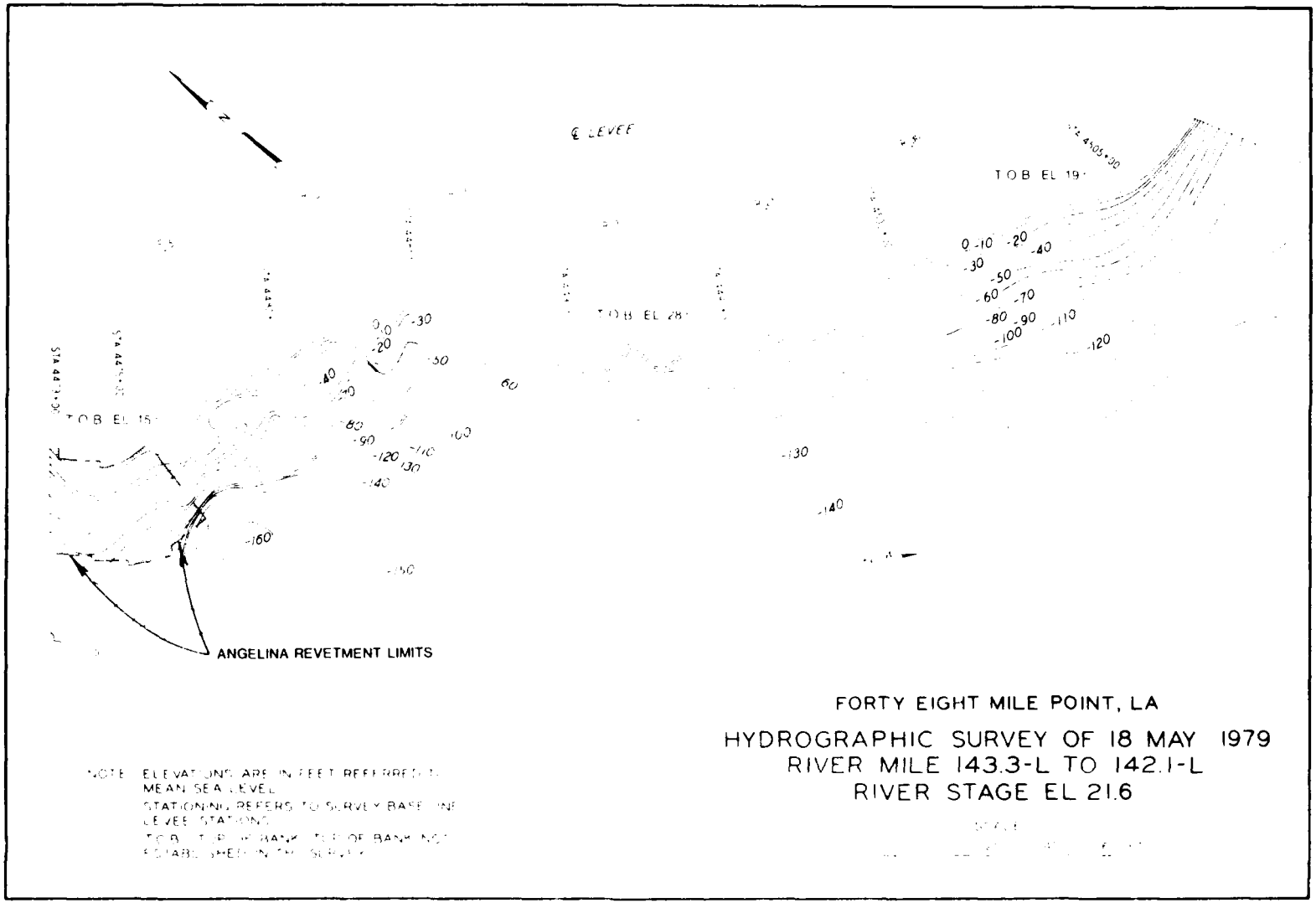
BANK CONTOURS FROM 1979 HYDROGRAPHIC SURVEYS ALONG FOUR BANK REACHES BELOW BATON ROUGE, LA


TOB EL 26
TOB EL 25
EIGHTY ONE MILE POINT
HYDROGRAPHIC SURVEY OF
23 MAY 1979
RIVER MILE 180.3-L TO 179.0-L
RIVER STAGE EL 28.5


TOB EL 25
TOB EL 26
TOB EL 23
FLOW
FLOW
FLOW
NOTE: ELEVATIONS ARE IN FEET REFERRED TO MEAN SEA LEVEL.
STATIONING REFERS TO SURVEY BASELINE LEVEE STATIONS.
TOB - TOP OF BANK. TOP OF BANK NOT ESTABLISHED IN THE SURVEY.
EIGHTY ONE MILE POINT
HYDROGRAPHIC SURVEY OF
11 JUN 1979
RIVER MILE 180.3-L TO 179.0-L
RIVER STAGE EL 23.4
SCALE

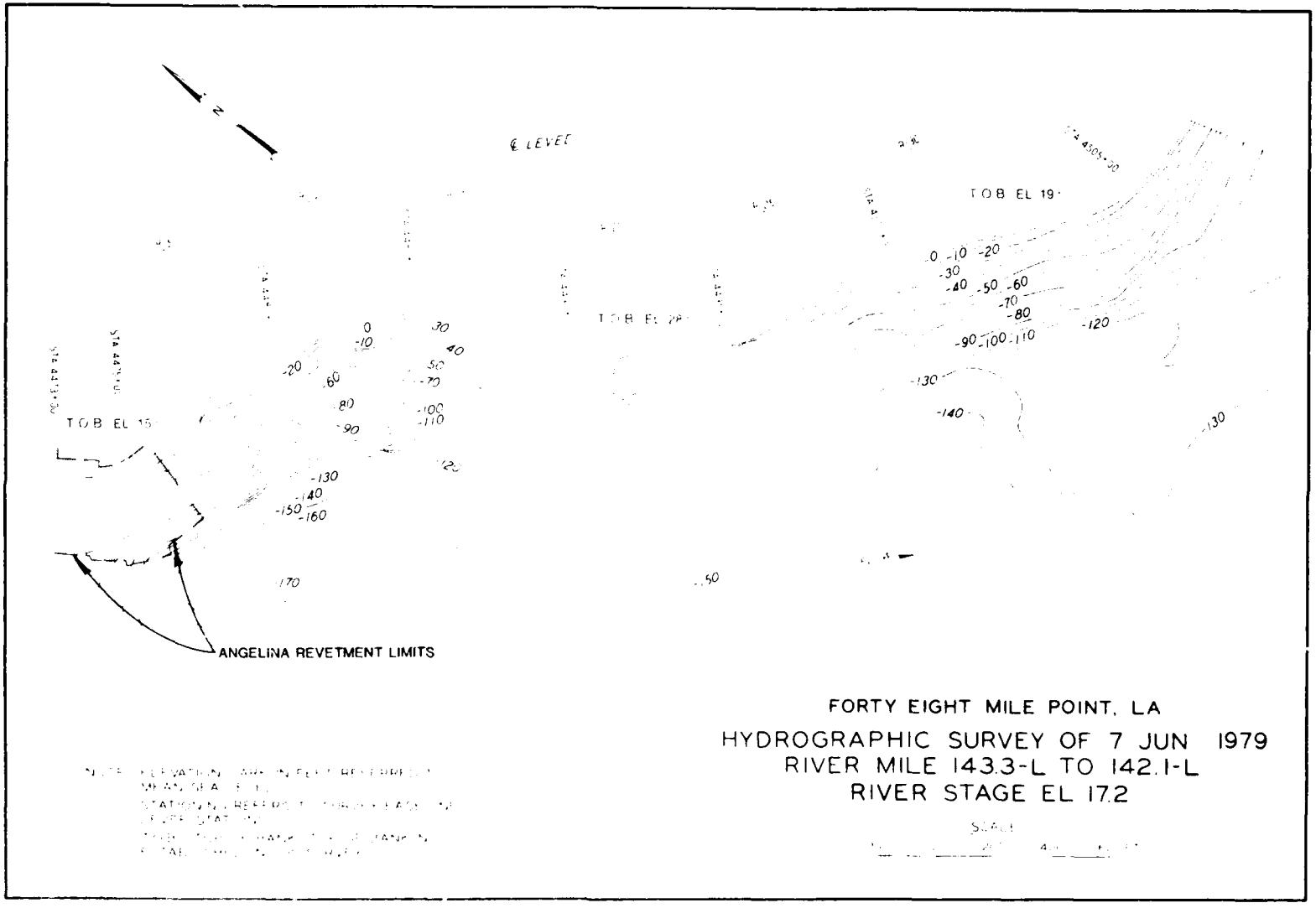

EIGHTY ONE MILE POINT
HYDROGRAPHIC SURVEY OF
14 AUG 1979
RIVER MILE 180.3-L TO 179.0-L
RIVER STAGE EL 14.4

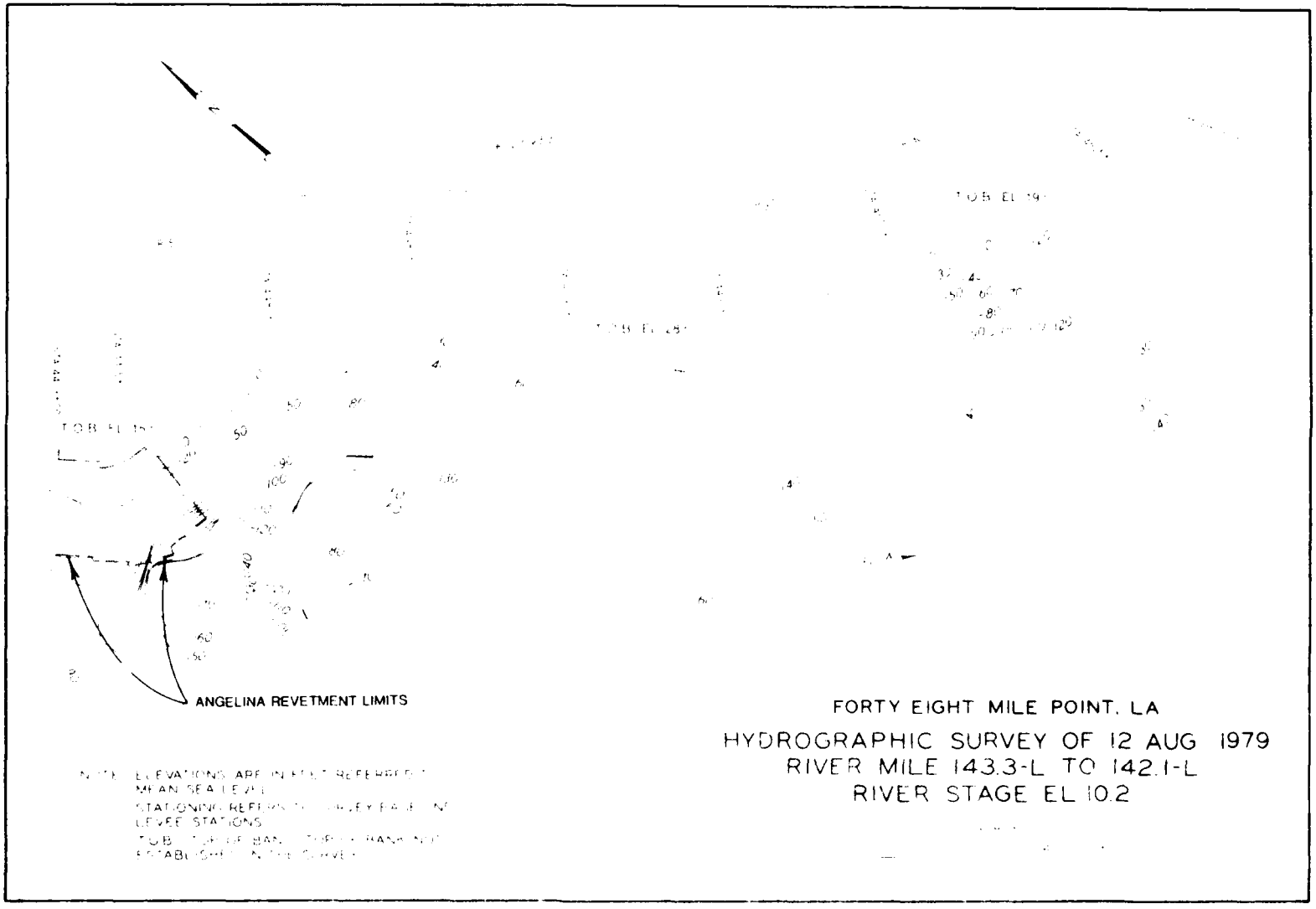

TOB EL 25
TOB EL 21
TOB EL 25
MEAN SEA LEVEL
EIGHTY ONE MILE POINT
HYDROGRAPHIC SURVEY OF
27 NOV 1979
RIVER MILE 180.3-L TO 179.0-L
RIVER STAGE EL 13.2

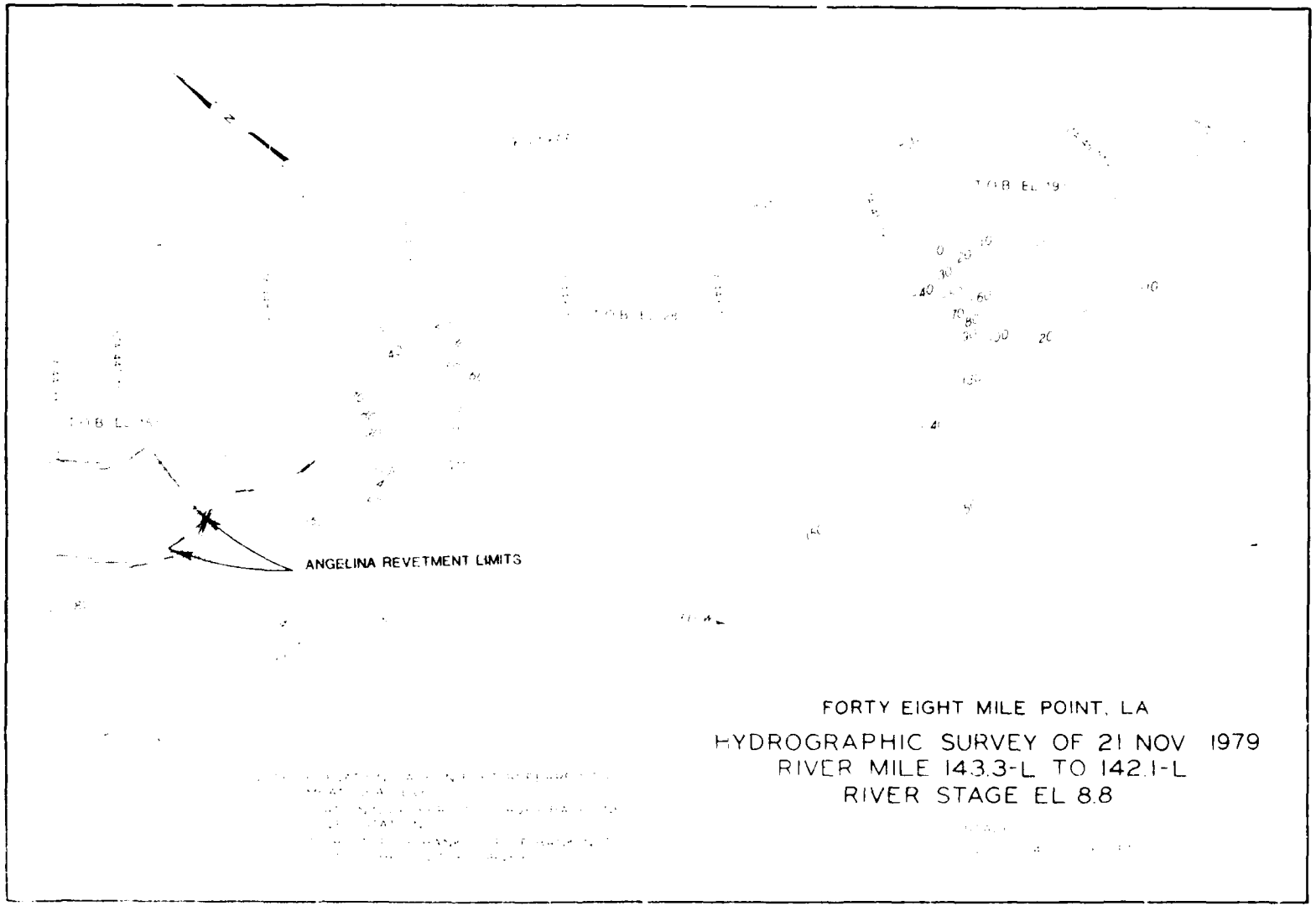


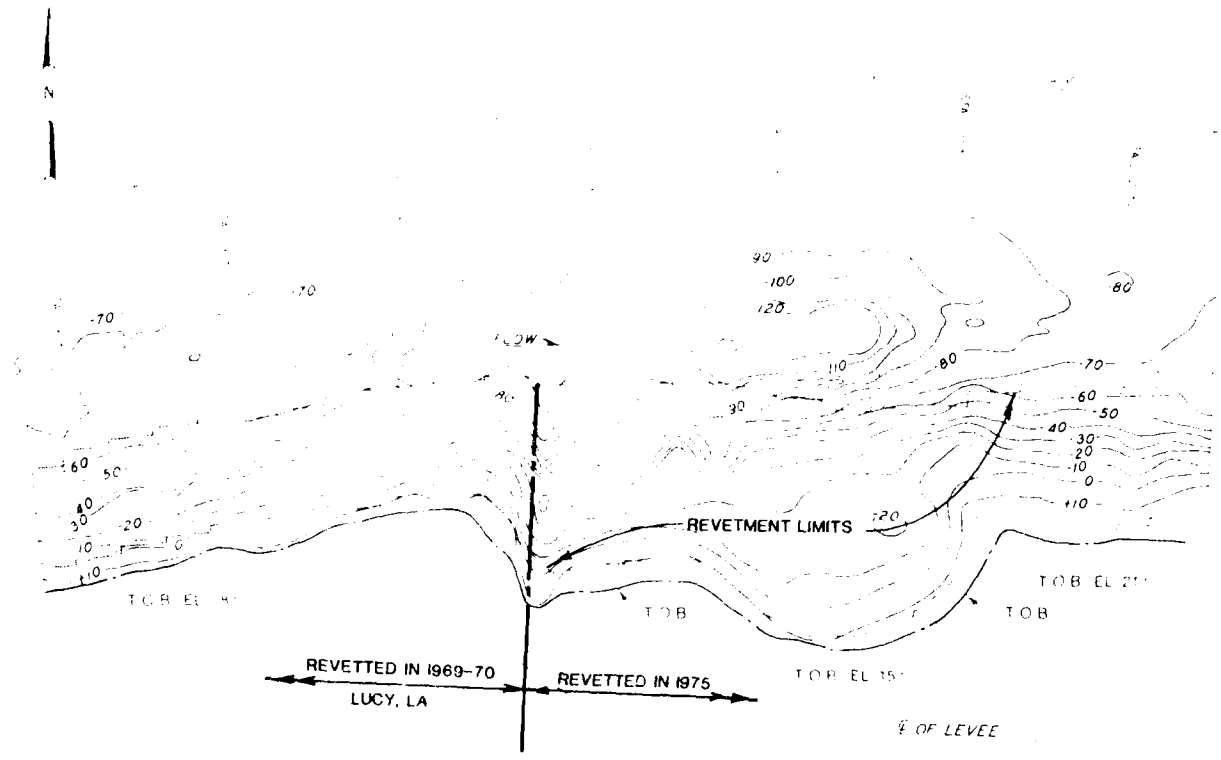
FORTY EIGHT MILE POINT, LA

HYDROGRAPHIC SURVEY OF 18 MAY 1979
RIVER MILE 143.3-L TO 142.1-L
RIVER STAGE EL 21.6


TOB EL 15
TOB EL 19
ANGELINA REVETMENT LIMITS
FORTY EIGHT MILE POINT, LA
HYDROGRAPHIC SURVEY OF 7 JUN 1979
RIVER MILE 143.3-L TO 142.1-L
RIVER STAGE EL 17.2


ANGELINA REVETMENT LIMITS
FORTY EIGHT MILE POINT, LA
HYDROGRAPHIC SURVEY OF 12 AUG 1979
RIVER MILE 143.3-L TO 142.1-L
RIVER STAGE EL 10.2

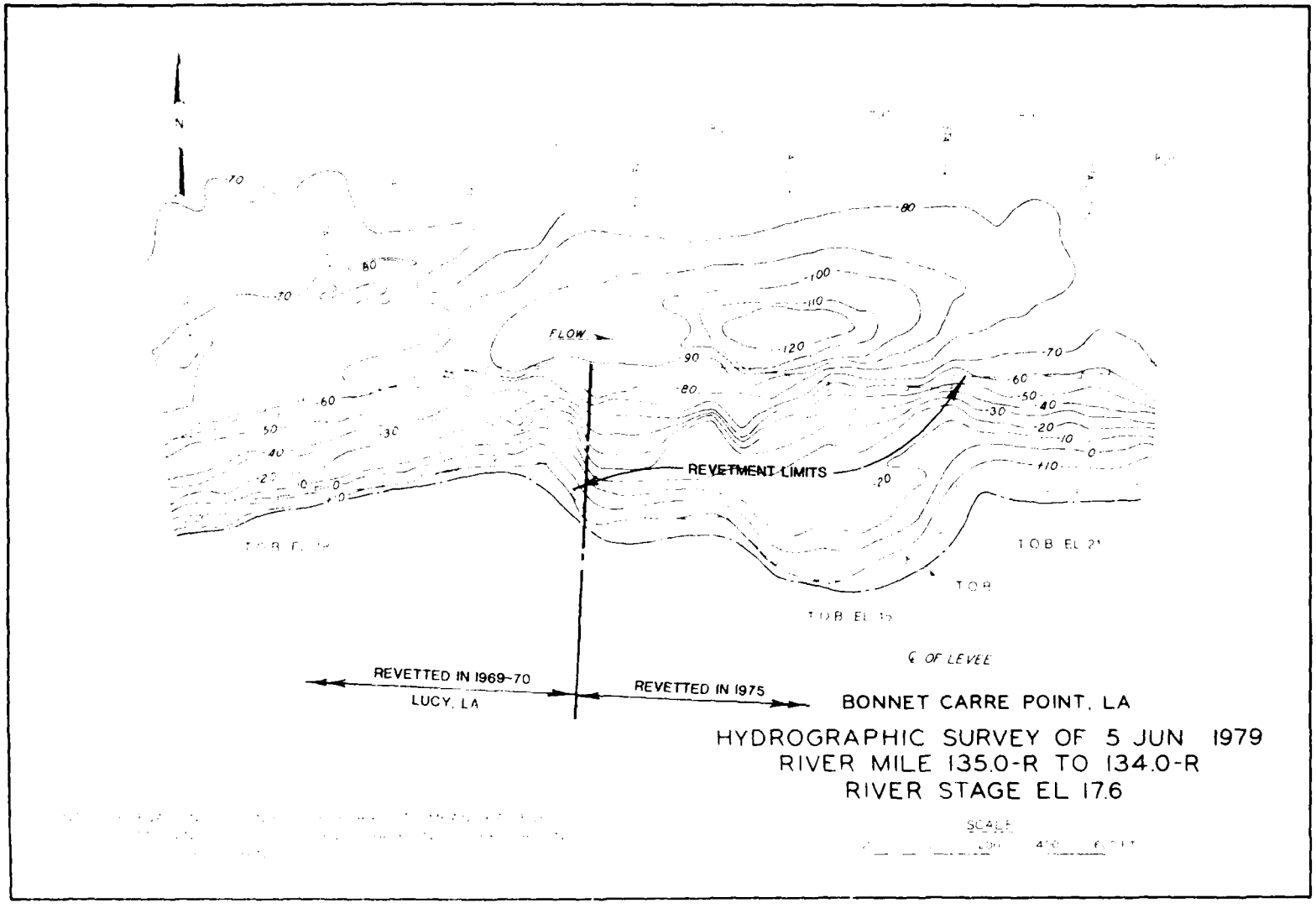

ANGELINA REVETMENT LIMITS
FORTY EIGHT MILE POINT, LA
HYDROGRAPHIC SURVEY OF 21 NOV 1979
RIVER MILE 143.3-L TO 142.1-L
RIVER STAGE EL 8.8

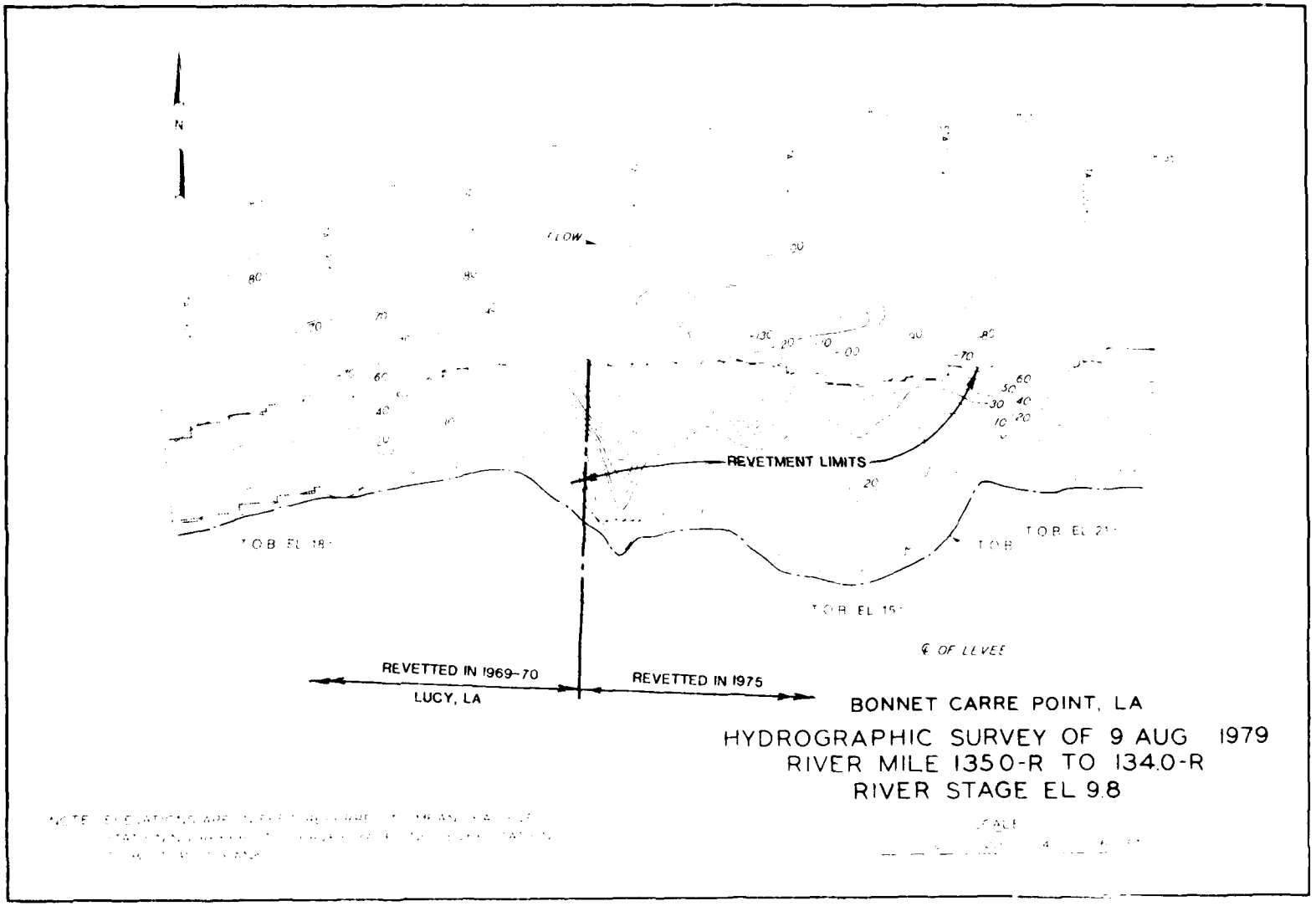


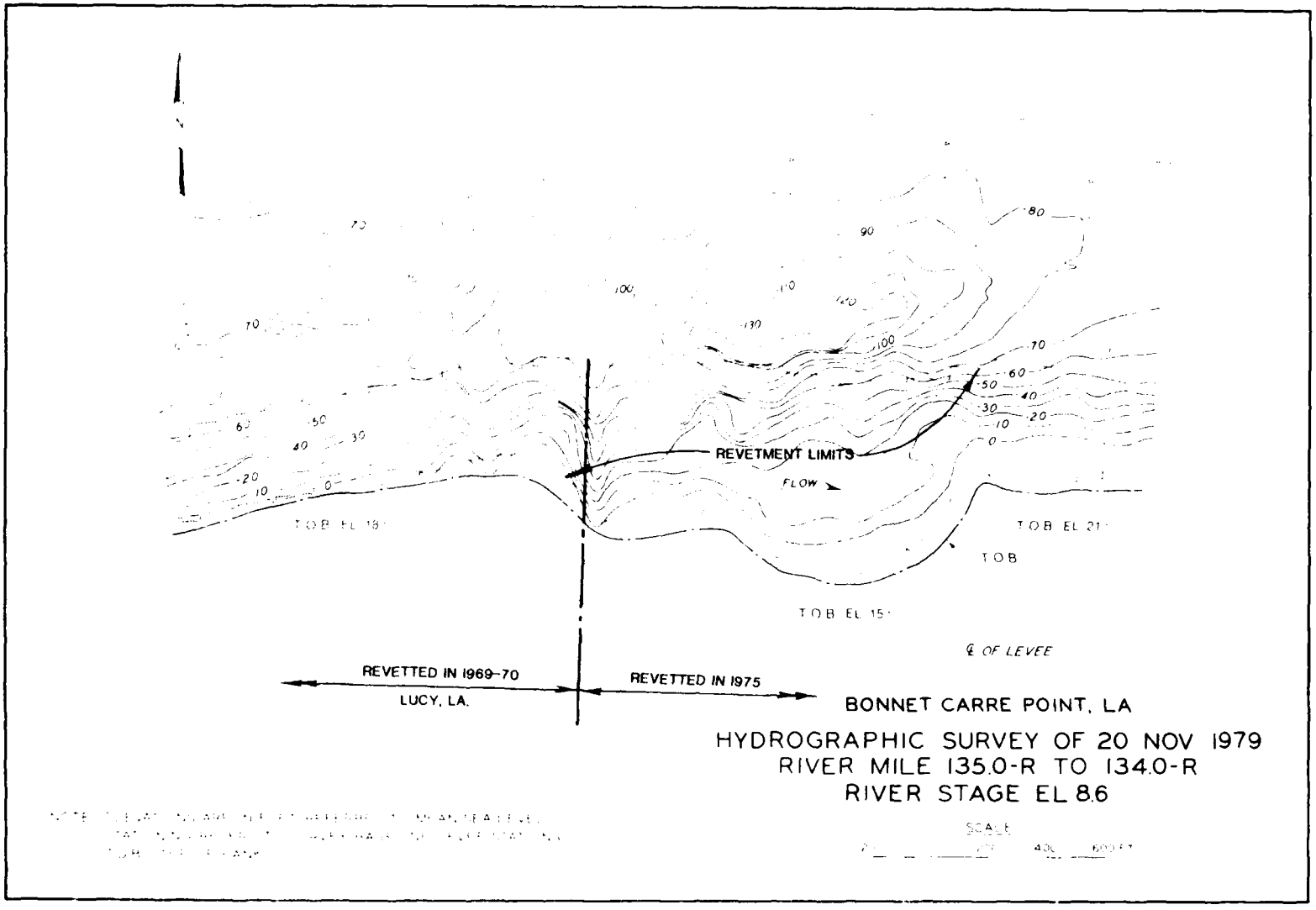
BONNET CARRE POINT, LA

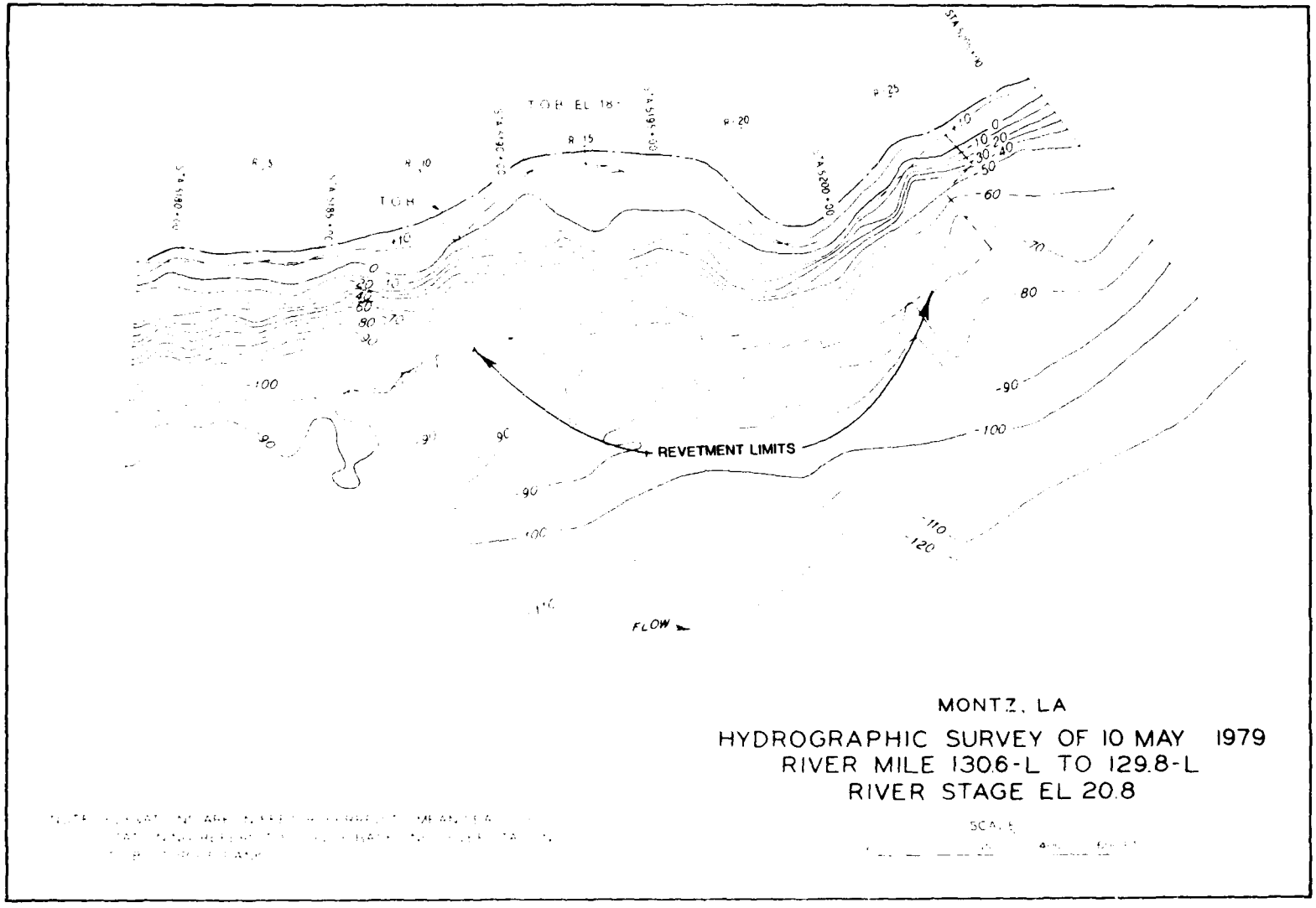
HYDROGRAPHIC SURVEY OF 15 MAY 1979
RIVER MILE 135.0-R TO 134.0-R
RIVER STAGE EL 21.8

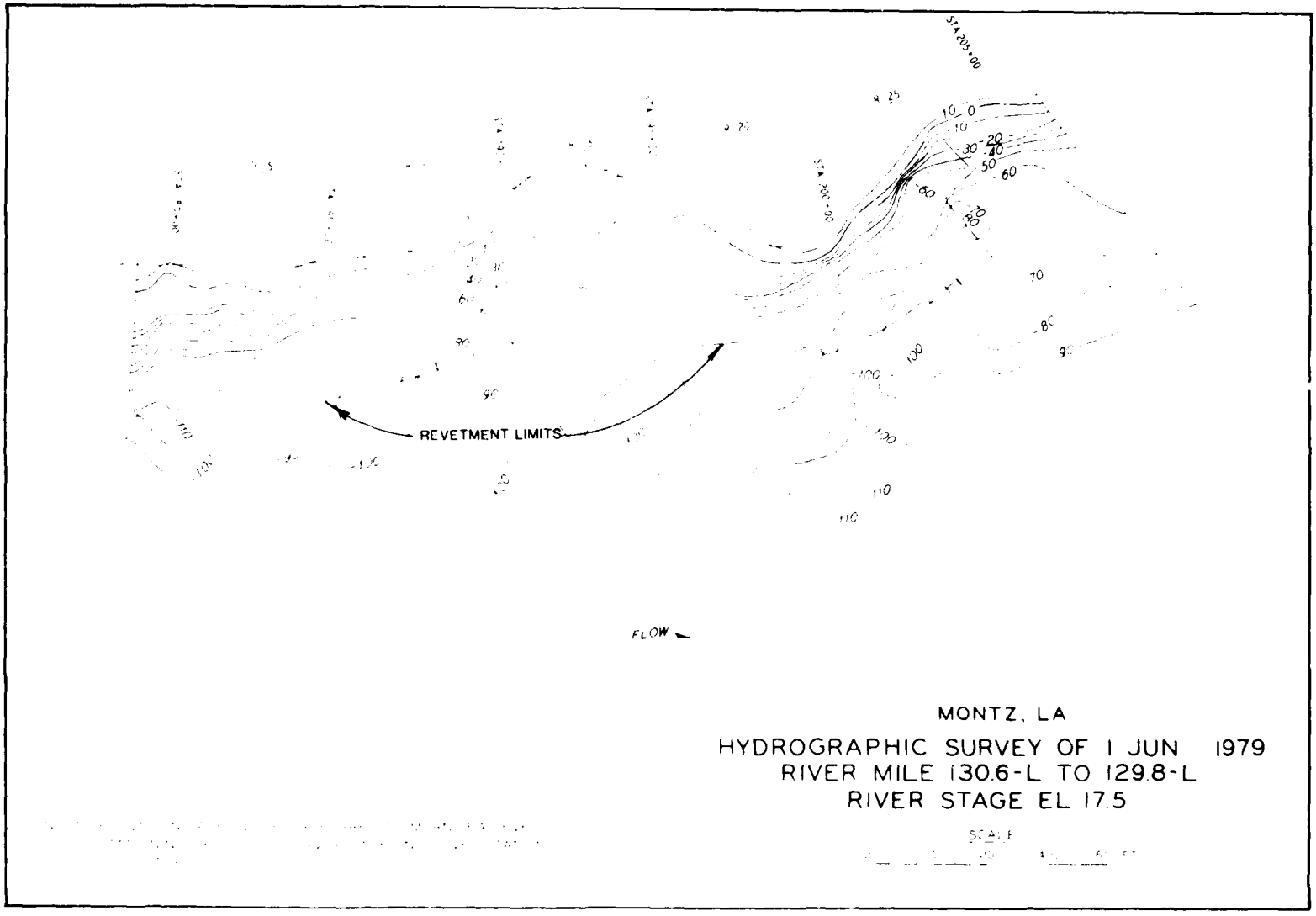
SCALE

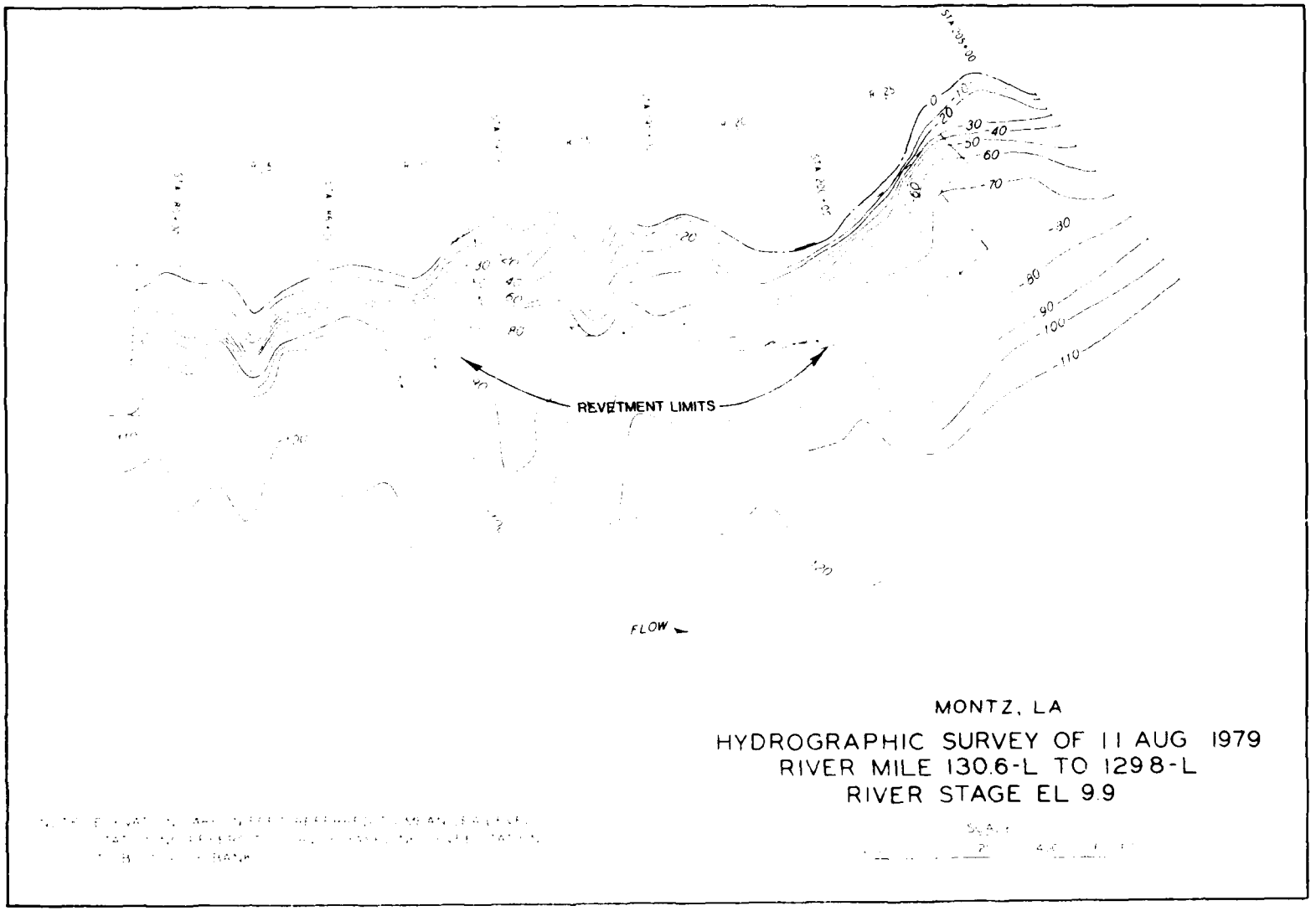

N
FLOW
REVETMENT LIMITS
T.O.B.
T.O.B EL 21
T.O.B EL 12
℄ OF LEVEE
REVETTED IN 1969-70
LUCY, LA
REVETTED IN 1975
BONNET CARRE POINT, LA
HYDROGRAPHIC SURVEY OF 5 JUN 1979
RIVER MILE 135.0-R TO 134.0-R
RIVER STAGE EL 17.6
SCALE

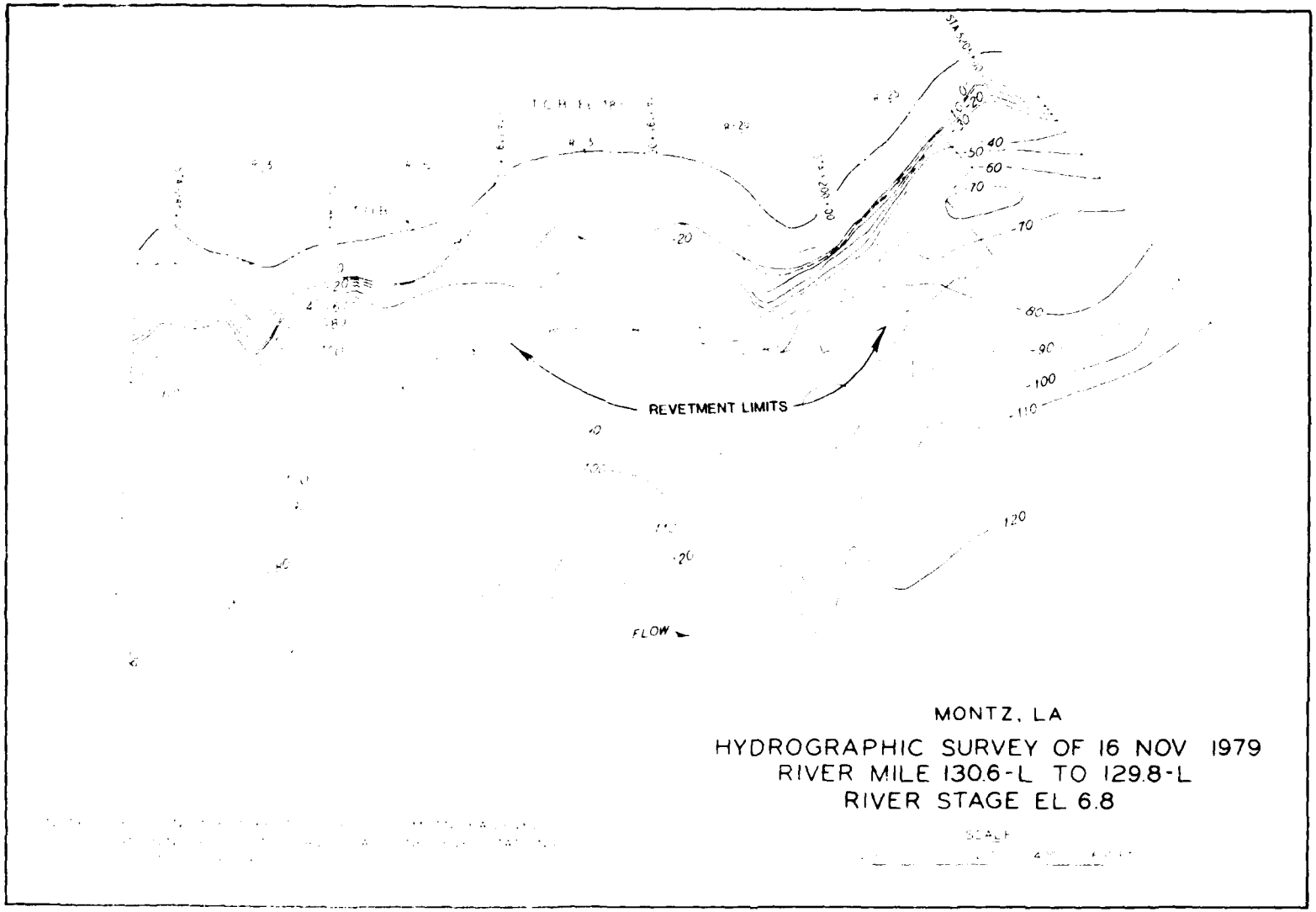

N
FLOW
REVETMENT LIMITS
TOB EL 18
TOB EL 15
TOB EL 21
℄ OF LEVEE
REVETTED IN 1969-70
REVETTED IN 1975
LUCY, LA
BONNET CARRE POINT, LA
HYDROGRAPHIC SURVEY OF 9 AUG 1979
RIVER MILE 135.0-R TO 134.0-R
RIVER STAGE EL 9.8

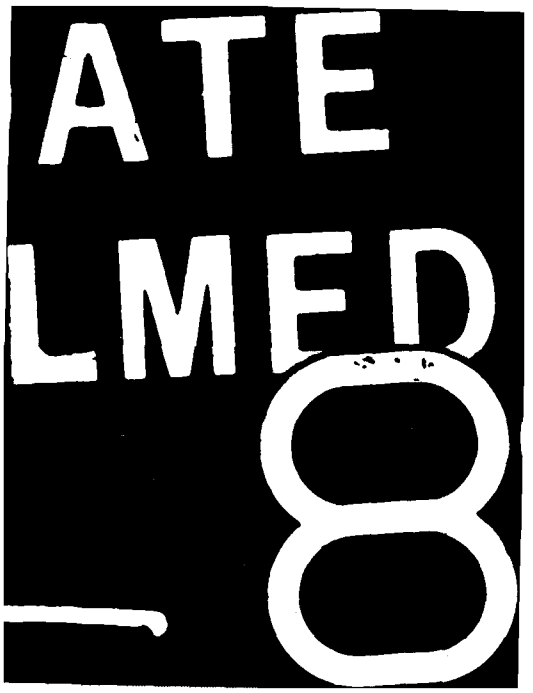

REVETMENT LIMITS
FLOW
TOB EL 18'
TOB EL 21'
TOB
TOB EL 15'
℄ OF LEVEE
REVETTED IN 1969-70
REVETTED IN 1975
LUCY, LA.
BONNET CARRE POINT, LA
HYDROGRAPHIC SURVEY OF 20 NOV 1979
RIVER MILE 135.0-R TO 134.0-R
RIVER STAGE EL 8.6
SCALE


TOH EL 18
TOH
R 5
R 10
R 15
R 20
R 25
REVETMENT LIMITS
FLOW
MONTZ, LA
HYDROGRAPHIC SURVEY OF 10 MAY 1979
RIVER MILE 130.6-L TO 129.8-L
RIVER STAGE EL 20.8


REVETMENT LIMITS
FLOW
MONTZ, LA
HYDROGRAPHIC SURVEY OF 1 JUN 1979
RIVER MILE 130.6-L TO 129.8-L
RIVER STAGE EL 17.5
SCALE


REVETMENT LIMITS
FLOW
MONTZ, LA
HYDROGRAPHIC SURVEY OF 11 AUG 1979
RIVER MILE 130.6-L TO 129.8-L
RIVER STAGE EL 9.9


REVETMENT LIMITS
FLOW
MONTZ, LA
HYDROGRAPHIC SURVEY OF 16 NOV 1979
RIVER MILE 130.6-L TO 129.8-L
RIVER STAGE EL 6.8


ATE
LMED
8

[redacted]